Intelligent Pattern Analysis of the Foetal Electrocardiogram

By

Nicholas John Outram

A thesis submitted to the University of Plymouth
in partial fulfilment for the degree of

DOCTOR OF PHILOSOPHY

School of Electronic, Communication and
Electrical Engineering

Intelligent Pattern Analysis of the Foetal Electrocardiogram

Nicholas John Outram

Abstract

The aim of the project on which this thesis is based is to develop reliable techniques for foetal electrocardiogram (ECG) based monitoring, to reduce incidents of unnecessary medical intervention and foetal injury during labour. World-wide electronic foetal monitoring is based almost entirely on the cardiotocogram (CTG), which is a continuous display of the foetal heart rate (FHR) pattern together with the contraction of the womb. Despite the widespread use of the CTG, there is no significant improvement in foetal outcome. In the UK alone it is estimated that birth related negligence claims cost the health authorities over £400M per-annum. An expert system, known as INFANT, has recently been developed to assist CTG interpretation. However, the CTG alone does not always provide all the information required to improve the outcome of labour. The widespread use of ECG analysis has been hindered by the difficulties with poor signal quality and the difficulties in applying the specialised knowledge required for interpreting ECG patterns, in association with other events in labour, in an objective way.

A fundamental investigation and development of optimal signal enhancement techniques that maximise the available information in the ECG signal, along with different techniques for detecting individual waveforms from poor quality signals, has been carried out. To automate the visual interpretation of the ECG waveform, novel techniques have been developed that allow reliable extraction of key features and hence allow a detailed ECG waveform analysis. Fuzzy logic is used to automatically classify the ECG waveform shape using these features by using knowledge that was elicited from expert sources and derived from example data. This allows the subtle changes in the ECG waveform to be automatically detected in relation to other events in labour, and thus improve the clinicians position for making an accurate diagnosis. To ensure the interpretation is based on reliable

information and takes place in the proper context, a new and sensitive index for assessing the quality of the ECG has been developed.

New techniques to capture, for the first time in machine form, the clinical expertise / guidelines for electronic foetal monitoring have been developed based on fuzzy logic and finite state machines. The software model provides a flexible framework to further develop and optimise rules for ECG pattern analysis. The signal enhancement, QRS detection and pattern recognition of important ECG waveform shapes have had extensive testing and results are presented. Results show that no significant loss of information is incurred as a result of the signal enhancement and feature extraction techniques.

Author's Declaration

At no time during the registration for the degree of Doctor of Philosophy has the author been registered for any other University award.

This study was financed with the aid of the Polytechnic Central Funding Council (PCFC), and carried out in collaboration with Derriford Hospital, Gothenburg Central Hospital and the Plymouth Health Trust.

Relevant scientific and engineering seminars and conferences were regularly attended at which work was always presented; clinical experts in Plymouth and Sweden were visited for consultation purposes, and several papers prepared for publication.

Publications.

Six conference papers and one major journal paper have been published during the course of this study.

Awards

IEE Dr V.K. Zworykin Premium (1997)

External contacts

Professor Karl Gustav Rosén, Chalmers University, Goteborg, Sweden.

Professor Keith Greene & Dr Roberto Luzietti, Plymouth Postgraduate Medical School, Plymouth, UK

Mr John Curnow, Biomedical Engineering, Derriford Hospital, Plymouth.

Nicholas John Outram 15th October 1997

Acknowledgements

The author gratefully acknowledges the assistance of Dr. Phil Culverhouse and Prof. Martin Tomlinson for their supervision; Prof. Karl Rosén, Dr. Jenny Westgate, Prof. Keith Greene, Dr. Rob Keith, Dr. Roberto Luzietti and Dr. Mark Davies for clinical assistance; the labour ward staff at Plymouth General Hospital for their help and co-operation; the P.C.F.C. and South-West Regional Health Authority for the financial support of for this work; all the administrative personnel at the University of Plymouth who are involved in this project.

I would especially like to thank my first supervisor and director of studies Prof. Emmanuel Ifeachor for his supervision, tremendous patience, active involvement and guidance throughout this project and for the benefit of his wide knowledge and vision for this project; I would also like to make a special acknowledgement and thanks to the following people; Mr. John Curnow for the benefit of his wide engineering experience, knowledge of this work, technical support and friendship; Peter VanEetvelt for his unlimited enthusiasm, friendship and tremendous mathematical versatility and experience, from which I and many others have greatly benefited.

Table of Contents

AUTHOR'S DECLARATION i

ACKNOWLEDGEMENTS ii

TABLE OF CONTENTS iii

TABLE OF FIGURES ix

TABLES xiv

CHAPTER 1 1

1. INTRODUCTION 2

1.1 BACKGROUND TO ELECTRONIC FOETAL ELECTROCARDIOGRAM (ECG) MONITORING 3

1.1.1 CTG Monitoring *4*

1.1.2 ECG Monitoring *5*

1.2 BASIC PHYSIOLOGY OF ST WAVEFORM CHANGES 6

1.3 CLINICAL EVIDENCE 8

1.4 BENEFITS OF ST WAVEFORM MONITORING 8

1.5 PROBLEMS IN FOETAL ECG MONITORING 9

1.6 CURRENT SCOPE OF ELECTRONIC ST WAVEFORM MONITORING. 10

1.7 AIMS AND OBJECTIVES OF THE PROJECT 11

1.8 OVERVIEW OF THE THESIS. 12

CHAPTER 2 15

2. SIGNAL ENHANCEMENT 16

2.1 INTRODUCTION 16

2.2 SOURCES OF NOISE 17

2.2.1 Baseline shift *17*

2.2.2 Muscle noise *19*

2.2.3 Power-line noise *20*

2.3 SIGNAL ENHANCEMENT TECHNIQUES 21

2.3.1 Filter Design for Foetal ECG Analysis *23*

2.3.2 New filter design method *26*

2.3.3 Theory 32
2.4 DESIGN OF A NARROW-BAND NOTCH FILTER FOR REMOVING POWER-LINE NOISE 34
2.5 DESIGN OF A LINEAR LOW-PASS FILTER 37
2.5.1 Optimal Filtering 40
2.5.2 SNR enhancement using fixed linear filtering 42
2.5.3 Signal Averaging 44
2.5.4 Averaging and signal-to-noise ratio improvement 45
2.5.5 Time Coherent Filtering 47
2.6 QUALITY ASSESSMENT 53
2.6.1 Approximation and Assessment of Baseline Shift Noise 54
2.6.2 Chebyshev Polynomial Approximation 55
2.6.3 Evaluation of Chebyshev Polynomials 57
2.6.4 Determining the degree of approximation 59
2.6.5 Assessment of baseline shift using Fuzzy Logic 62
2.6.6 Assessing random noise and short-term transients 62
2.6.7 Estimating the Signal-To-Noise Ratio for an Ensemble of ECG Waveforms Using Eigenvalue Analysis 63
2.6.8 Estimating the signal-to-Noise ratio for an ensemble of ECG waveforms using cross-correlation. 65
2.6.9 Comparative results for signal-to-noise estimation accuracy 67
2.7 VALIDATION OF DIFFERENT SIGNAL ENHANCEMENT TECHNIQUES 68
2.8 ASSESSING THE EFFECTS OF DIFFERENT COMB FILTERS ON SENSITIVE FOETAL ECG WAVEFORM SHAPES 69
2.8.1 Validating the effects of the different comb filters on measured features in the foetal ECG waveform 70
2.9 DISCUSSION AND CONCLUSION 74
2.10 NOVELTY AND CONTRIBUTION TO KNOWLEDGE 79

CHAPTER 3 ..... **81**

3. QRS DETECTION **82**

3.1 INTRODUCTION 82
3.2 PRE-PROCESSING : THE SIGNAL ENHANCEMENT SCHEME FOR QRS DETECTION 82
3.2.1 Differentiation 83
3.2.2 Non-linear prediction filter 84
3.2.3 Linear filtering design by least-squares approximation 86
3.2.4 Comb filtering 89
3.2.5 Comparison of pre-processing techniques 92
3.3 DESIGN OF A PATTERN RECOGNITION TECHNIQUE FOR QRS DETECTION 93
3.4 DESIGN OF A QRS DETECTOR USING A SIMPLE CORRELATION TECHNIQUE 95
3.4.1 Adapting the template vector online 97

3.4.2 On-line estimation of the QRS pattern 97
3.4.3 Efficient implementation of the correlation algorithm 99
3.5 DESIGN OF A QRS DETECTOR USING OFF-LINE ESTIMATION 101
3.5.1 Using the Multi-Layered Perceptron to represent a complex pattern space 102
3.5.2 Theoretical discussion of the Multi-Layered Perceptron 104
3.5.3 Novelty detection 107
3.5.4 Supervised training of the Multi-Layered Perceptron for QRS detection 108
3.6 COMPARING AND OPTIMISING THE PERFORMANCE OF THE QRS DETECTION TECHNIQUES 112
3.6.1 Receiver Operator Characteristic (ROC) Analysis 112
3.6.2 Validation methodology 114
3.6.3 Results for the correlation algorithm 115
3.6.4 Results for the MLP 117
3.7 DISCUSSION AND CONCLUSION 119

CHAPTER 4 ..... **121**

4.1 INTRODUCTION 122
4.2 USING CHEBYSHEV POLYNOMIALS TO SIMPLIFY FEATURE EXTRACTION 124
4.3 DESCRIBING THE ST SHAPE BY QUANTITATIVE FEATURE EXTRACTION 125
4.3.1 Locating the reference points 128
4.3.2 Location of the Q and S peaks 128
4.3.3 Locating the J-point 128
4.3.4 Iso-electric level 129
4.3.5 Locating the T complex peak 129
4.3.6 Locating the T-wave onset. 131
4.4 CALCULATING AREAS AND DERIVATIVES OF CHEBYSHEV POLYMONIALS 132
4.4.1 Computing the indefinite integral of the Chebyshev polynomials 133
4.4.2 Computing the derivative of Chebyshev polynomials 135
4.5 DESCRIBING THE PR SEGMENT SHAPE. 136
4.5.1 The centroid 136
4.6 EXTRACTION OF TRENDS IN FEATURES 138
4.7 DECIMATION TECHNIQUES TO ENHANCE TRENDS IN THE FOETAL ECG FEATURES 139
4.8 DISCUSSION AND CONCLUSION 144

CHAPTER 5 ..... **147**

5. FUZZY LOGIC CONCEPTS **148**

5.1 INTRODUCTION 148
5.2 UNCERTAINTY AND IMPRECISION IN MANAGEMENT OF LABOUR 148

5.3 DEVELOPMENT CYCLE OF A FUZZY EXPERT SYSTEM 149
5.4 DEFINITION OF THE PROBLEM 150
5.5 DEFINITION OF LINGUISTIC AND FUZZY VARIABLES 150
5.6 MODELLING LINGUISTIC TERMS WITH FUZZY SETS 150
5.7 FUZZY SET OPERATORS 154
5.7.1 Zadeh *155*
5.7.2 Product *156*
5.7.3 Mean *157*
5.7.4 Yager *158*
5.7.5 Comparison of different operators *159*
5.7.6 Compliment operators *161*
5.8 HEDGES 162
5.9 INFERENCE 163
5.10 FUZZY COMPOSITIONAL RULES OF INFERENCE 165
5.11 INTERPRETATION OF FUZZY SET OUTPUTS 168
5.11.1 Interpreting fuzzy sets by de-fuzzification *168*
5.11.2 Interpretation of fuzzy set outputs by linguistic approximation *170*
5.12 DISCUSSION AND CONCLUSION 174

CHAPTER 6 ..... **176**

6. DESIGN OF THE FUZZY EXPERT MODEL **177**

6.1 INTRODUCTION 177
6.2 DEVELOPMENT CYCLE OF A FUZZY EXPERT SYSTEM 177
6.3 KNOWLEDGE ELICITATION 178
6.4 DESIGNING THE FUZZY SETS AND VARIABLES 180
6.5 DESIGNING THE FUZZY SETS 181
6.5.1 Managing unknown scenarios *182*
6.6 DESIGNING THE FUZZY RULES 183
6.7 RULES AND FUZZY SETS FOR ASSESSING THE QUALITY OF ECG DATA 184
6.7.1 Elicitation of the rules *185*
6.7.2 Define the linguistic terms, fuzzy variables and relevant adjectives *185*
6.7.3 Define the fuzzy sets *185*
6.7.4 Define the rules *186*
6.8 STATIC PATTERN RECOGNITION OF THE ST SEGMENT SHAPE 187
6.8.1 Technique 1: Linear regression *189*
6.8.2 Technique 2: Minimum gradient *190*
6.8.3 Technique 3: New Fuzzy Logic Method *190*
6.8.4 Designing the rules to classify the ST segment shape *194*
6.8.5 Derivation of the fuzzy sets using frequency distribution data *195*

6.9 VALIDATING THE DETECTION RATE OF BI-PHASIC WAVEFORMS 195
6.9.1 The minimum gradient technique *197*
6.9.2 The linear-regression technique *199*
6.9.3 The fuzzy logic technique *200*
6.10 SUMMARY OF RESULTS 204
6.11 PATTERN RECOGNITION OF ST WAVEFORM SHAPE CHANGES OVER TIME 204
6.12 ADDING MEMORY 205
6.13 USING STATE MACHINES TO ADD MEMORY TO INTELLIGENT SYSTEMS 207
6.14 FUZZY STATE MODEL FOR MANAGING COMPLEX PATTERNS IN TIME. 210
6.15 STATE TRANSITION USING AN ACCUMULATED TRUTH MODEL 211
6.15.1 Fuzzy filter structures *212*
6.15.2 Fuzzy intersection operator *213*
6.16 CHAINING STATE TRANSITIONS 216
6.17 PROTOTYPE STATE MODEL FOR ST WAVEFORM ANALYSIS 218
6.18 FOETAL CONDITION MATRIX (FCM) 219
6.19 EXAMPLES 221
6.19.1 Current limitations *222*
6.20 LINGUISTIC APPROXIMATION 223
6.21 DISCUSSION AND CONCLUSION 223

CHAPTER 7 ..... **226**

7. DISCUSSION, CONCLUSION AND FUTURE WORK **227**

7.1 INTRODUCTION 227
7.2 SIGNAL ENHANCEMENT AND QUALITY ASSESSMENT 227
7.3 INTELLIGENT FOETAL ECG INTERPRETATION AND ASSESSMENT 230
7.3.1 Automatic monitoring of the ECG waveform *231*
7.4 LIMITATIONS OF THE CURRENT WORK 231
7.5 FUTURE WORK 232
7.5.1 Data collection and archiving *232*
7.5.2 Develop a medical data database *234*
7.5.3 Foetal ECG Simulator *236*
7.5.4 Further investigation into Fuzzy State Machines *236*
7.5.5 Graphical User Interface *236*
7.5.6 Integrating into the STAN® (Cinventa AB) system *238*
7.5.7 Integrating CTG, ECG and Blood-Gas *240*
7.6 PUBLICATIONS 241
7.7 CONCLUSION 242

REFERENCES **243**

APPENDIX A 247

APPENDIX B 254

APPENDIX C 271

APPENDIX D 277

APPENDIX E 280

APPENDIX F 282

APPENDIX G 285

PUBLICATIONS 287

Table of Figures

FIGURE 1 THE DECOMPOSITION OF THE FOETAL ECG WAVEFORM 3

FIGURE 2 INTERNAL MONITORING OF THE FOETUS 4

FIGURE 3 THE CARDIAC VECTOR 4

FIGURE 4 THE CARDIOTOCOGRAM (CTG) 5

FIGURE 5 THE DIFFERENT CONFIGURATIONS OF THE FOETAL ECG ST WAVEFORM. (A) ELEVATED ST WAVEFORM, (B) BI-PHASIC ST WAVEFORM, (C) NEGATIVE ST WAVEFORM AND (D) DEPRESSED ST WAVEFORM 7

FIGURE 6 A SAMPLE OF THE PAPER TRACE PRODUCED BY THE STAN® MONITOR 11

FIGURE 7 DATA ACQUISITION SYSTEM 16

FIGURE 8 BASELINE SHIFT IN FOETAL ECG DATA. (A) TYPE 1 - LOW BASELINE SHIFT FROM A GOOD QUALITY SIGNAL, (B) TYPE 2 - MEDIUM BASELINE SHIFT AND (C) TYPE 3 - ACUTE BASELINE SHIFT WHICH RENDERS THE SIGNAL UNUSABLE FOR ECG SHAPE ANALYSIS 19

FIGURE 9 FOETAL ECG SHOWING MUSCLE NOISE AND MATERNAL ECG INTERFERENCE 20

FIGURE 10 (A) ECG WAVEFORM CORRUPTED WITH POWER-LINE NOISE AND (B) THE RESPECTIVE POWER-SPECTRUM 21

FIGURE 11 A SUMMARY OF THE CTG FEATURE SIGNAL ENHANCEMENT USED TO HELP DETECT THE QRS COMPLEX FROM THE RAW ECG SIGNAL 22

FIGURE 12 A SUMMARY OF THE SENSITIVE SIGNAL ENHANCEMENT USED IN THIS WORK TO MINIMISE THE EFFECTS OF NOISE IN THE FOETAL SCALP ECG AND PRESERVE THE ECG SIGNAL SHAPE 22

FIGURE 13 MAGNITUDE RESPONSE FOR REMOVING BASELINE SHIFT ENERGY 23

FIGURE 14 THE RINGING EFFECTS OF IIR FILTERS ON THE FOETAL ECG WAVEFORM 24

FIGURE 15 SPECIFICATION OF A REPEATING FREQUENCY SPECTRUM FILTER. 26

FIGURE 16 LOW-PASS FILTER SPECIFICATION 27

FIGURE 17 LOW PASS FILTER SPECIFICATION AT A LOWER SAMPLING FREQUENCY 27

FIGURE 18 LOW-PASS FILTER DESIGNED DIRECTLY WITH THE REMEZ EXCHANGE ALGORITHM 28

FIGURE 19 MAGNITUDE RESPONSE AND FILTER COEFFICIENTS OF A REPEATING FREQUENCY SPECTRUM FILTER 29

FIGURE 20 (A) REPEATING FREQUENCY SPECTRUM FILTER, (B) ANTI-IMAGE FILTER & (C) RESULTING LOW-PASS FILTER 30

FIGURE 21 ANTI-IMAGE FILTER 30

FIGURE 22 RESULTING MAGNITUDE RESPONSE OF THE CASCADED FILTERS 31

FIGURE 23 (A) REPEATING FREQUENCY SPECTRUM FILTER, (B) ANTI-IMAGE FILTER & (C) RESULTING BAND-PASS FILTER 31

FIGURE 24 ANTI-IMAGE FILTER FOR THE BAND-PASS FILTER 32

FIGURE 25 OVERALL MAGNITUDE RESPONSE OF THE BAND-PASS FILTER DESIGN 32

FIGURE 26 (A) ECG WAVEFORM CORRUPTED WITH POWER-LINE NOISE AND (B) THE RESPECTIVE POWER SPECTRUM 34

FIGURE 27 DESIGN OF THE TWO STAGE NARROW BAND NOTCH FILTER 35

FIGURE 28 MAGNITUDE RESPONSE OF THE FIRST MULTI-BAND PASS FILTER. 35
FIGURE 29 THE MAGNITUDE RESPONSE OF THE SECOND MULTI-BAND PASS FILTER. 36
FIGURE 30 THE COMBINED MAGNITUDE RESPONSE FOR REMOVING NARROW BAND 50HZ HARMONICS. 37
FIGURE 31 REPEATING FREQUENCY SPECTRUM FILTER DESIGNED FOR EXTRACTING BASELINE SHIFT 38
FIGURE 32 ADDITIONAL ANTI-IMAGE FILTER. 39
FIGURE 33 A FILTER FOR EXCLUSIVELY REMOVING THE LOW-FREQUENCY NOISE FROM ECG SIGNALS 39
FIGURE 34 (A) RAW ECG (B) RAW DATA FILTERED TO REMOVE POWER-LINE NOISE AND BASELINE SHIFTS. 40
FIGURE 35 THE SMOOTH APPROXIMATION H(K) OF THE AVERAGE SIGNAL SPECTRUM |X(K)| 41
FIGURE 36 RAW ECG DATA CORRUPTED WITH RANDOM NOISE 42
FIGURE 37 FIXED LOW-PASS FILTER DESIGNED TO ATTENUATE MUSCLE NOISE. 43
FIGURE 38 ILLUSTRATION OF TIME COHERENT SAMPLING 48
FIGURE 39 MAGNITUDE RESPONSE OF EVENLY WEIGHTED AVERAGE (HR=120 BPM) (A) N=10, (B) N=20, (C) N=30 & (D) N=50 50
FIGURE 40 CHANGING TIME INTERVALS BETWEEN CONSECUTIVE HEART BEATS 51
FIGURE 41 LINEAR INTERPOLATION AND RE-SAMPLING 51
FIGURE 42 MAGNITUDE RESPONSE OF (A) A 30 BEAT AVERAGE AND (B) A TIME-COHERENT IIR FILTER 52
FIGURE 43 FOURTH ORDER RECURSIVE FILTER STRUCTURE 52
FIGURE 44 A COMPARISON OF THE (A)RAW, (B) 30-BEAT-AVERAGE WAVEFORM AND (C) TIME-COHERENT FILTERED WAVEFORM 53
FIGURE 45 BASELINE SHIFT IN FOETAL ECG DATA 54
FIGURE 46 APPROXIMATION OF THE BASELINE SHIFT IN RAW FOETAL ECG DATA 58
FIGURE 47 ENHANCED BASELINE APPROXIMATION USING MULTI-RATE FILTER TECHNIQUE 59
FIGURE 48 MAGNITUDE AND PHASE RESPONSE OF THE SIXTH ORDER RECURSIVE FILTER USED FOR BASELINE SHIFT APPROXIMATION 60
FIGURE 49 POOR QUALITY RAW ECG DATA AND THE OUTPUT OF THE DECIMATION FILTER 61
FIGURE 50 DIFFERENT FILTER SPECIFICATIONS FOR THE ECG ST WAVEFORM COMB FILTER 69
FIGURE 51 CASE OE102: PLOT OF T/QRS TROUGH RATIO WITH NO FILTERING AND WITH FILTER TYPE 1 72
FIGURE 52 CASE OE102: PLOT OF T/QRS TROUGH RATIO FOR FILTERS TYPE 2,3 & 4 72
FIGURE 53 CASE OE111: PLOT OF T/QRS PEAK RATIO WITH NO FILTERING AND WITH FILTER TYPE1 73
FIGURE 54 CASE OE111: PLOT OF T/QRS PEAK RATIO FOR FILTERS TYPE 2,3 & 4 73
FIGURE 55 LOCATING THE CANDIDATE QRS COMPLEX BY DIFFERENTIATION 83
FIGURE 56 NON-LINEAR PREDICTION FILTER USING A MLP 85
FIGURE 57 LOCATING THE CANDIDATE QRS COMPLEX BY NON-LINEAR PREDICTION 86
FIGURE 58 APPROXIMATION F(T) OF THE LOW-FREQUENCY NOISE CONTENT FOR AN INDIVIDUAL ECG WAVEFORM 87
FIGURE 59 MAGNITUDE RESPONSE OF SAVITZKY-GOLAY FILTER 88
FIGURE 60 RESULTS OF THE SAVITZKY-GOLAY SMOOTHING FILTER 88
FIGURE 61 PROTOTYPE FILTER FOR QRS DETECTION PRE-PROCESSING 89
FIGURE 62 MULTIPLE NOTCH FILTER FOR REMOVING BASELINE SHIFTS AND POWER-LINE HARMONICS 90
FIGURE 63 (A)BAND SELECTION FILTER DESIGNED AT FS=250HZ AND (B) MAGNITUDE RESPONSE AFTER RESTORING THE SAMPLING RATE TO 500HZ 91

FIGURE 64 COMBINED MAGNITUDE RESPONSE FOR THE QRS ENHANCEMENT FILTER 91
FIGURE 65 FILTERING RAW ECG DATA WITH HIGH ENERGY BASELINE SHIFT, POWER-LINE AND RANDOM NOISE (TOP) TO PRODUCE FLAT ECG DATA (BOTTOM) WITH MINIMAL BASELINE SHIFT AND POWER-LINE NOISE REMAINING 92
FIGURE 66 VECTOR PATTERN CLASSIFIER WITH A SIMPLE VECTOR X AS AN INPUT AND A SINGLE SCALAR OUTPUT Y(X) 94
FIGURE 67 CONCEPTUAL DIAGRAM ILLUSTRATING THE SIMPLE PATTERN SPACE OF THE QRS COMPLEX & NOISE96
FIGURE 68 A COMPARISON OF THE STATIC AND ADAPTIVE QRS COMPLEX DETECTOR 97
FIGURE 69 QRS DETECTOR BASED ON LINEAR CORRELATION 99
FIGURE 70 CONCEPTUAL DIAGRAM OF THE COMPLEX PATTERN SPACE OF THE QRS PATTERN 101
FIGURE 71 MULTI-LAYERED PERCEPTRON (MLP) 102
FIGURE 72 ARTIFICIAL NEURON 103
FIGURE 73 SIGMOIDAL ACTIVATION FUNCTION USED AT THE HIDDEN LAYER OF THE MLP 103
FIGURE 74 GENERALISED NETWORK STRUCTURE FOR A NON-LINEAR MAPPING FOR TWO VARIABLES 105
FIGURE 75 CONCEPTUAL DIAGRAM ILLUSTRATING THE NEED FOR NOVELTY DETECTION 108
FIGURE 76 (A) CORRECT APPROXIMATION FOUND BY FITTING TO THE OVERALL TREND IN THE DATA AND (B) INCORRECT APPROXIMATION FOUND BY FITTING EVERY POINT IN THE DATA 111
FIGURE 77 RMS ERROR OF 20-5-1 MLP TRAINED ON ECG QRS PATTERNS 111
FIGURE 78 IDEALISED ROC CURVES FOR PERFECT AND NO DISCRIMINATION 114
FIGURE 79 EXAMPLES OF TRUE POSITIVE, TRUE NEGATIVE, FALSE POSITIVE AND FALSE NEGATIVE EVENTS . 115
FIGURE 80 ROC CURVE FOR THE CORRELATION TECHNIQUE 116
FIGURE 81 ROC CURVE FOR THE MLP 119
FIGURE 82 DECOMPOSITION OF THE FOETAL ECG WAVEFORM 122
FIGURE 83. SMOOTH CHEBYSHEV APPROXIMATION OF THE FOETAL ECG ST WAVEFORM 124
FIGURE 84 CLASSIFICATION OF THE ST SEGMENT AS (A) NORMAL ELEVATED T, (B) NEGATIVE T, (C) BI-PHASIC ST WITH NORMAL ELEVATED T AND (D) DEPRESSED ST WITH NORMAL T 125
FIGURE 85 LOCATION OF THE ISO-ELECTRIC REGION 126
FIGURE 86 NEW FEATURES USED TO QUANTIFY THE ST WAVEFORM SHAPE 127
FIGURE 87 DEFINING THE ONSET OF THE T WAVE 132
FIGURE 88 USING THE CENTROID TO LOCATE THE P WAVE 137
FIGURE 89 T/QRS RATIO MEASURED ON A BEAT-BY-BEAT BASIS AND SMOOTHED. 138
FIGURE 90 INTERPOLATION OF ECG FEATURES 139
FIGURE 91 OVER-SAMPLING THE FEATURES AT 3HZ 140
FIGURE 92 PROTOTYPE FILTER FOR SAMPLING RATE CONVERSION 141
FIGURE 93 FEATURE DECIMATION AND SMOOTHING SCHEME 141
FIGURE 94 THREE FILTER STAGES USED TO DECIMATE THE FEATURE SAMPLING RATE FROM 3HZ TO 1/15 HZ . 142
FIGURE 95 EVENLY SAMPLING AND DECIMATING THE T/QRS RATIO FEATURES USING MULTI-RATE TECHNIQUES 143
FIGURE 96 A SIMPLIFIED CLASSIFICATION OF THE CTG INTO ITS SUBTYPES 149
FIGURE 97 DEVELOPMENT OF THE FUZZY EXPERT SYSTEM 150
FIGURE 98 CRISP SUB-SETS OF THE T/QRS SET 151
FIGURE 99 CRISP MEMBERSHIP FUNCTIONS FOR THE T/QRS SUB-SETS WITH ADDED HYSTERESIS 152

FIGURE 100 FUZZY SETS 153
FIGURE 101 ZAHEH'S INTERSECTION AND FUZZY UNION OPERATORS 156
FIGURE 102 PRODUCT INTERSECTION AND FUZZY UNION OPERATORS 157
FIGURE 103 MEAN INTERSECTION AND FUZZY UNION OPERATORS 158
FIGURE 104 YAGER'S INTERSECTION AND UNION FUZZY OPERATORS (K=1) 159
FIGURE 105 YAGER'S INTERSECTION AND UNION FUZZY OPERATORS (K=60) 159
FIGURE 106 YAGER COMPLIMENT OPERATOR 162
FIGURE 107 SUGENO COMPLIMENT OPERATOR 162
FIGURE 108 FUZZY SETS FOR T/QRS MODIFIED BY THE 'VERY' HEDGE 163
FIGURE 109 (A) T/QRS SET AND (B) CONSEQUENT ST WAVEFORM SET 165
FIGURE 110 FUZZY INFERENCE USING THE AND OPERATOR 167
FIGURE 111 DE-FUZZIFICATION USING THE CENTROID ALGORITHM 169
FIGURE 112 CONSEQUENT FUZZY SET Y 170
FIGURE 113 RELATING SIMILARITY MEASURES TO FUZZY HEDGES 171
FIGURE 114 MOST LIKELY NORMAL 172
FIGURE 115 SLIGHTLY NORMAL 172
FIGURE 116 SLIGHTLY ABNORMAL 172
FIGURE 117 SLIGHTLY INTERMEDIATE 172
FIGURE 118 DEVELOPMENT CYCLE OF THE FUZZY EXPERT MODEL 178
FIGURE 119 KNOWLEDGE ELICITATION SOURCES 178
FIGURE 120 EXTENDING THE FUZZY UNIVERSE OF DISCOURSE AS ERROR CHECKING 182
FIGURE 121 STRUCTURE OF THE FUZZY EXPERT MODEL 183
FIGURE 122 FUZZY SETS FOR BASELINE SHIFT SPAN 186
FIGURE 123 FUZZY SETS FOR SIGNAL-TO-NOISE RATIO (DB) 186
FIGURE 124 FUZZY OUTPUT SET FOR OVERALL QUALITY INDEX OF THE DATA 186
FIGURE 125 FUZZY SET FOR ST WAVEFORM IS ABNORMAL 188
FIGURE 126 (A) NORMAL, (B) ABNORMAL (NEGATIVE T), (C) ABNORMAL (BI-PHASIC ST, POSITIVE T), (D) ABNORMAL (DEPRESSED ST, NORMAL T), (E) SUSPICIOUS (NEGATIVE ST SLOPE, NORMAL T, POSITIVE ST), (F) SUSPICIOUS (NEGATIVE ST SLOPE, NORMAL T, POSITIVE ST) 189
FIGURE 127 DETERMINING THE ST SLOPE 191
FIGURE 128 SCATTER PLOT OF ST PEAK 1 AND ST PEAK 2 FOR A POSITIVE ST WITH A NEGATIVE ST SEGMENT SLOPE 193
FIGURE 129 POSITIVE ST WITH NEGATIVE SLOPE 194
FIGURE 130 FUZZY SETS USED FOR INTERPRETING THE ST SEGMENT SHAPE. (A) PEAK 1, (B) PEAK 2, (C) PEAK DIFFERENCE ΔPEAK AND (D) DISTANCE BETWEEN THE PEAKS 196
FIGURE 131 ROC CURVE FOR BI-PHASIC ST DETECTION USING THE MINIMUM GRADIENT METHOD 198
FIGURE 132 ROC CURVE FOR BI-PHASIC ST DETECTION USING THE LINEAR REGRESSION METHOD 200
FIGURE 133 ROC CURVE FOR NORMAL 203
FIGURE 134 ROC CURVE FOR BI-PHASIC 1 203
FIGURE 135 ROC CURVE FOR BI-PHASIC 2 203
FIGURE 136 ROC CURVE FOR BI-PHASIC 3 203

FIGURE 137 FINITE STATE MACHINE 207
FIGURE 138 CONCEPTUAL STATE MACHINE 208
FIGURE 139 FUZZY-STATE MACHINE USED TO REPRESENT AND RECALL EVENTS DURING LABOUR 210
FIGURE 140 THE OUTPUT TRUTH FOR "ABNORMAL ST WAVEFORM" 212
FIGURE 141 SCHEMATIC STRUCTURE OF THE FUZZY FILTER 213
FIGURE 142 OUTPUT TRUTH OF THE RULE "ST WAVEFORM IS ABNORMAL FOR 20 MINUTES OR MORE" 215
FIGURE 143 ACCUMULATED TRUTH FOR "STATE B" 216
FIGURE 144 ACCUMULATED TRUTH FOR STATE C 218
FIGURE 145 STATE MODEL FOR ST WAVEFORM ANALYSIS 218
FIGURE 146 EXAMPLES OF THE FOETAL CONDITION MATRIX 222
FIGURE 147 FUZZY SETS DESCRIBING THE ST SEGMENT 223
FIGURE 148 DATA ACQUISITION SYSTEM 233
FIGURE 149 OUTLINE SOLUTION FOR SIMPLIFYING ECG DATA AQUISITION 234
FIGURE 150 TYPICAL OUTLINE FOR THE RESEARCH DATA FILE SERVER 235
FIGURE 151 RECOMMENDED MULTI CENTRE DATA COLLECTION 237
FIGURE 152 CHAIN OF EXPERTISE 239

Tables

TABLE 1 FILTER COEFFICIENTS FOR THE TIME-COHERENT FILTER 52

TABLE 2 SPECIFICATION FOR THE DECIMATION FILTER 60

TABLE 3 BASELINE QUALITY DECISION MATRIX 62

TABLE 4 COMPARISON OF SNR ESTIMATION USING DIFFERENT TECHNIQUES 67

TABLE 5 QUANTIFYING THE EFFECTS OF DIFFERENT COMB FILTERS ON THE T/QRS RATIO PEAK (SHOWN TO 4 SIGNIFICANT DIGITS) 71

TABLE 6 QUANTIFYING THE EFFECTS OF DIFFERENT COMB FILTERS ON THE T/QRS RATIO TROUGH (SHOWN TO 4 SIGNIFICANT DIGITS) 71

TABLE 7 TWO-BY-TWO CONTINGENCY TABLE 113

TABLE 8 CONTINGENCY TABLE FOR THE CORRELATION ALGORITHM (WITH ON-LINE LEARNING) 116

TABLE 9 CONTINGENCY TABLE FOR CASE OE102 USING AN MLP 117

TABLE 10 CONTINGENCY TABLE FOR CASE OE108 USING AN MLP 117

TABLE 11 CONTINGENCY TABLE FOR CASE OE102 USING AN MLP BY ADDING RANDOM NOISE 118

TABLE 12 CONTINGENCY TABLE FOR THE MULTI-LAYERED PERCEPTRON 119

TABLE 13 EXPECTED LOCATIONS OF PEAKS WITHIN THE FETAL ECG RELATIVE TO THE R WAVE 130

TABLE 14 LOGICAL OPERATORS 154

TABLE 15 TABLE OF KEY FUZZY SETS. 181

TABLE 16 VARIABLES AND ADJECTIVES FOR BASELINE QUALITY ASSESSMENT 185

TABLE 17 MATRIX FOR ASSESSING SIGNAL QUALITY 187

TABLE 18 CONTINGENCY TABLE FOR THE MINIMUM ST GRADIENT METHOD 197

TABLE 19 CONTINGENCY TABLE FOR THE LINEAR REGRESSION METHOD 199

TABLE 20 CONTINGENCY TABLE FOR A NORMAL ST SEGMENT 200

TABLE 21 CONTINGENCY TABLE FOR A BI-PHASIC 1 ST SEGMENT 201

TABLE 22 CONTINGENCY TABLE FOR A BI-PHASIC 2 ST SEGMENT 201

TABLE 23 CONTINGENCY TABLE FOR A BI-PHASIC 3 ST SEGMENT 202

TABLE 24 SUMMARY OF PERFORMANCE METRICS FOR EACH BI-PHASIC WAVEFORM CLASSIFICIATION TECHNIQUE. 204

TABLE 25 FOETAL CONDITION MATRIX USED TO GUIDE THE CLINICIAN. 219

TABLE 26 SUMMARY OF THE CLINICAL GUIDELINES GIVEN TO CLINICIANS 220

TABLE 27 FUZZY TRUTH VALUES 220

Chapter 1

Introduction

1. Introduction

The injury or death of a child during labour, which could have been prevented, is deeply traumatic. It is particularly unfortunate when a foetus survives through a term of a perfectly normal pregnancy, only to lose its life or become permanently brain damaged during the final stages of labour.

Injury or death at birth is also economically costly, both in the short and long term. It is impossible to determine the long-term emotional and financial costs of supporting a person throughout life who is permanently brain damaged at birth. In the United Kingdom alone, it is estimated that over £400,000,000 is spent each year on birth related negligence claims, much of which can be attributed to uncertainty during the management of labour. In the event of foetal injury or death, there is an increasing trend for the parents to litigate, which has put additional pressure on clinicians to become increasingly defensive and has lead to an increasing trend in defensive clinical intervention (such as increased caesarean section rates).

During labour, a critical problem often faced by clinicians is how to accurately discriminate between a foetus that is coping well with the normal stresses of labour, and one which is not coping with labour and has become distressed. It is desirable that clinical intervention, such as foetal blood sampling or vaginal examinations, is avoided where possible because it imposes a small risk to the mother and baby and can cause discomfort. More serious intervention, such as caesarean sections or forceps deliveries, pose a greater threat to the health of the mother and baby. In cases where the foetus is suspected to be distressed, there is increasing pressure for the clinician to intervene and either deliver by forceps or caesarean section. Many of these cases often turn out to be false alarms. A misjudgement either way can result in a damaged baby and/or litigation.

A major difficulty is that there are many natural sources of stress on the foetus during labour, such as the squeezing effect of uterine contractions which cause a temporary reduction in blood supply and oxygen deficiency. The foetus has many defence mechanisms that enable it to cope well with stressful events during labour such as redirecting valuable blood flow from the non-vital organs to the vital organs, adjusting its metabolic needs and utilising stored energy to maintain its heart

function (anaerobic metabolism). Foetal distress occurs when a foetus can no longer compensate for the effects of stress in labour, which can quickly lead to foetal injury or even a stillbirth. If continuous information on the foetal condition is available then the clinician is in a position to improve the level of care by making more accurate and timely decisions. Thus the clinician could respond to appropriate signs of foetal distress to prevent foetal injury and at the same time prevent unnecessary intervention. A primary aim of this project is to provide the basis for computer assisted management of labour to help clinicians discriminate between a healthy foetus which can compensate for labour induced stress and one which is not able to compensate. This is achieved by using electronic foetal electrocardiogram (ECG) monitoring.

1.1 Background to Electronic Foetal Electrocardiogram (ECG) Monitoring

Electronic foetal ECG monitoring is a technique of obtaining important information about the condition of the foetus during labour by measuring the electrical signals generated by the foetal heart as measured from the body surface. The idealised ECG is illustrated in Figure 1.

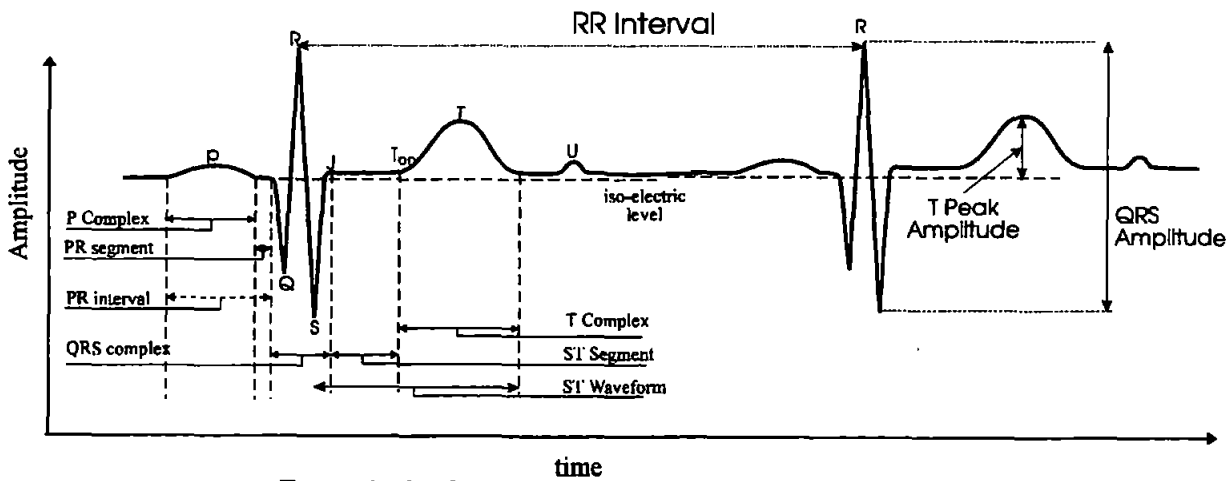

Figure 1 The decomposition of the foetal ECG waveform

The ECG signals are obtained from a spiral scalp electrode which is attached to the foetal scalp (Figure 2) or buttock (in the case of a breach delivery). These electrodes are routinely used in modern obstetric care. In this work, the single spiral foetal scalp electrode *(Curnow et al. 1995)* is used throughout to acquire the foetal ECG data. The shape or configuration of the ECG waveform is determined by the angle of measurement across the heart. There are two configurations potentially available

to the clinician. The preferred configuration for ECG waveform analysis is the scalp/maternal thigh configuration, or the uni-polar configuration, which measures the cardiac vector longitudinally across the foetal heart (seeFigure 3). The alternative is the bi-polar configuration, which measures the signal from the scalp with respect to an internal vaginal reference.

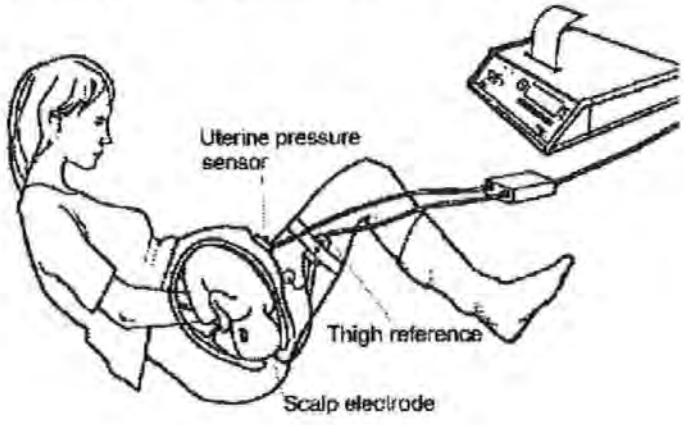

Figure 2 Internal monitoring of the foetus

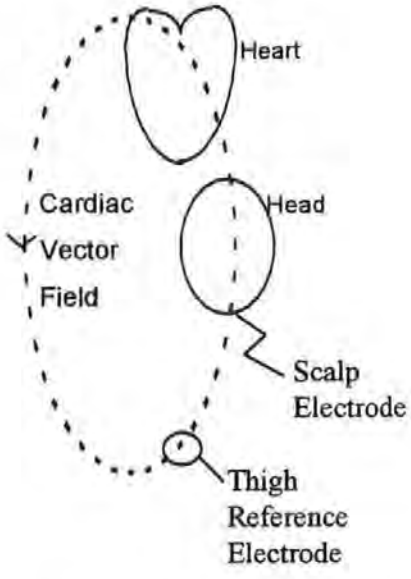

Figure 3 The cardiac vector

The uni-polar lead configuration, with the reference thigh electrode placed far away from the signal source, is less sensitive than the bi-polar configuration to movements of the foetal heart as the foetus rotates in the birth channel (*Luzietti & Rosén 1994*) and gives a better signal quality. Furthermore the longitudinal axis has been shown to be more sensitive to changes in the foetal ECG waveform occurring with oxygen deficiency.

1.1.1 CTG Monitoring

The normal foetal ECG signal obtained using a uni-polar lead configuration is characterised by five peaks and valleys labelled P, Q, R, S and T (see Figure 1). The reciprocal of the time interval between two consecutive R peaks (in seconds), known as the RR interval, is multiplied by 60 and gives the instantaneous foetal heart rate (FHR) in beats per minute (see Figure 4). A plot of successive instantaneous heart rates gives the FHR pattern. A continuous display of the FHR pattern together with the contraction of the womb (uterine activity) is known as the cardiotocogram (CTG) (see Figure 4). Despite the widespread introduction of CTG monitoring into routine clinical practice in recent years, there has been no

significant improvement in foetal outcome *(Lilja et al. 1985)*. This has coincided and is thought to relate in part to a marked increase in clinical intervention rates. This is mostly because the CTG is very difficult to interpret and does not provide all the information required. Foetal heart monitoring has therefore become increasingly controversial.

At present, only the CTG is routinely used to monitor the foetus during labour. Although simple to measure and record, the CTG pattern is subjective and difficult to interpret, and correct interpretation demands a high level of expertise which is rarely available at all times in a labour ward. It is recognised that a normal heart-rate pattern is a good predictor of foetal outcome but an abnormal heart-rate pattern is a poor predictor of foetal outcome *(Newbold et al. 1991)*. Difficulty and uncertainty in interpreting CTG patterns during labour can lead to unnecessary medical intervention (e.g. forceps, caesarean section, foetal blood sampling).

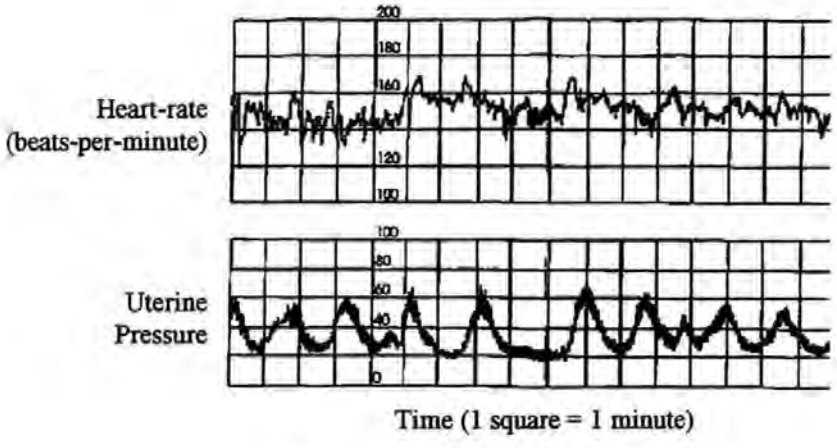

Figure 4 The Cardiotocogram (CTG)

The need for computer-assistance in the management of labour to improve the quality of obstetric care is widely recognised *(Krausse et al. 1991)*. An expert system, the INFANT *(Ifeachor et al. 1991; Keith et al. 1994)*, has been developed to analyse and interpret changes in the CTG, taking into account important events in labour, and to provide advice to clinicians.

1.1.2 ECG Monitoring

The CTG does contain important information which, if monitored and interpreted correctly, will detect many cases of foetal distress. However, the CTG alone does not always provide the information needed for accurate and timely assessment of

foetal condition *(Rosén & Luzietti 1994)*. Additional information about the condition of the foetus, such as myocardial workload *(Rosén & Luzietti 1994)*, may be obtained by a proper analysis of progressive changes in the foetal ECG waveform *(Westgate et al. 1993; Newbold 1991)*. This is obtained without altering current patient handling routines as the ECG is used to derive the FHR *(Rosén et al. 1992)* is already available from the scalp electrode. The physiology of the foetal ECG waveform is better understood than the CTG *(Rosén et al. 1992)* and it is proposed by *Rosén et al. 1992*, that by full analysis of the ECG, it should be possible to detect incidents of foetal distress before any tissue damage occurs in the foetus and often before any abnormal CTG changes are observed *(Rosén et al. 1992; Westgate et al. 1993)*. The evidence for this has been built up over many years and as knowledge of foetal physiology has developed. It has been shown how the analysis of the ST waveform, combined with the CTG, can be used to safely reduce clinical intervention without affecting the outcome of labour (*Westgate et al. 1993*). Furthermore, there is experimental, observational and theoretical evidence to suggest that changes in the ST waveform shape, such as those illustrated in Figure 5, convey important information that relate to how the foetus is compensating to the stresses of labour. This can be used to detect abnormalities before any tissue damage occurs *(Greene & Westgate 1993)*. To understand how this could be used, the basic physiology of ST waveform is discussed.

1.2 Basic physiology of ST waveform changes

The shape of the foetal ECG reflects the superposition of the electrical signals conducting within the myocardium (the muscular wall of the heart), as seen from the body surface. The ST waveform of the ECG is routinely used in adult cardiology during stress tests to detect heart damage. The ST waveform, which reflects the re-polarisation of the heart muscle cells of the myocardium, is very sensitive to coronary insufficiency such as ischemia in the adult ECG *(Rosén & Luzietti 1994)*. A hypothesis which has been undergoing investigation for more than 20 years is that the foetal heart should also show changes in the ST waveform as a response to stresses in labour, such as the natural squeezing effect of uterine contractions, temporary occlusions of the umbilical cord, maternal hypotension (low blood pressure) or placental haemorrhaging. These stresses can be intermittent,

resulting in slow and subtle changes in the foetal CTG and ECG. In extreme cases, these stresses can also be chronic and potentially fatal for the foetus, and show up as rapid changes in the CTG and ECG. The fully developed term foetus however is equipped to cope with the normal stresses of labour. Stresses such as uterine contractions can reduce blood-flow from the placenta and restrict oxygen supply. If there is an imbalance between oxygen consumption and supply, the foetus is normally able to compensate by diverting blood flow away from non-vital organs to the vital organs. It also has rich glycogen supplies which can be consumed to anaerobically maintain heart function. This latter process, known as anaerobic metabolism, produces lactic acid and potassium ions K^+ as products. The extra potassium ions are responsible for a change in heart muscle cell potentials and conduction properties of the myocardium. The sequence by which the muscle cells depolarise is disturbed, and this is reflected by changes in ST waveform shape (see Figure 5). This can be continuously monitored by examining the ECG and has been observed to show up abnormalities before any tissue damage has occurred. A compensating foetus will typically show an ST waveform with a permanently elevated T complex and an elevated ST segment (See Figure 5(a)). A foetus which is not fully compensating to a reduction in oxygen will show a changing T complex, negative T complex, bi-phasic ST waveform or depressed ST segment as illustrated in Figure 5(b), (c) and (d) *(Rosén & Luzietti 1994; Westgate et al. 1993).*

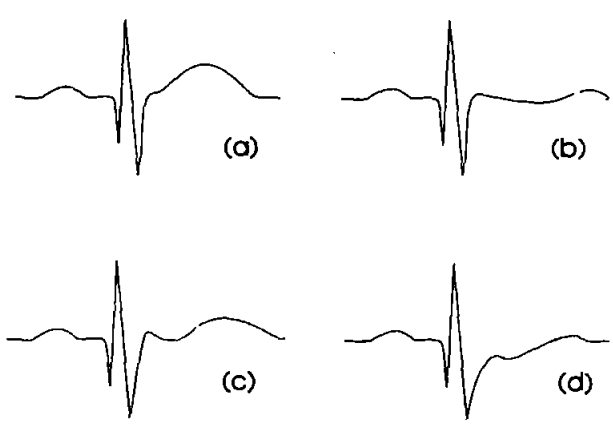

Figure 5 The different configurations of the foetal ECG ST Waveform. (a) Elevated ST waveform, (b) Bi-phasic ST waveform, (c) Negative ST waveform and (d) Depressed ST waveform

1.3 Clinical evidence

In a recent clinical trial of 2400 cases, the combination of the CTG and the ECG reduced clinical intervention by 46% with no adverse effect on neonatal outcome *(Westgate et al. 1993)*. The amplitude of the T peak divided by the height of the QRS amplitude (see Figure 1), known as the T/QRS ratio, was measured and monitored during labour. Guidelines were provided to clinicians to enable them to interpret T/QRS ratio changes in conjunction with CTG changes *(Rosén 1994)*. Although the T/QRS ratio is acknowledged as a crude quantifiable measure of ST waveform shape, this alone was able to redress some of the problems in foetal heart-monitoring *(Westgate et al. 1993)*. It is also reported, that in observations from human deliveries and from animal experiments, full analysis of the ST waveform shape could be used to detect foetal distress *before tissue damage occurs (Rosén et al. 1986)*.

1.4 Benefits of ST waveform monitoring

The benefits of ST waveform are summarised below.

- The ST waveform provides additional information to the CTG for the clinician to use without the need to change current patient handling routines.
- The ST waveform reflects changes in the foetal heart before any tissue damage occurs.
- Correct use of the combined ST waveform and CTG can significantly and safely reduce clinical intervention.
- The physiology of the ST waveform changes are better understood than foetal heart-rate changes.

Despite such positive findings, the foetal ECG is still not widely used and its use is still limited to a few centres in the world. There still remains controversy regarding the use of foetal monitors in health-care because of the many problems which hinder its use. These are summarised below.

1.5 Problems in foetal ECG monitoring

There are many problems which have hindered the widespread use of foetal ECG monitoring.

- ***Uncertainty.*** The major cause of clinical error is uncertainty. For the ECG (and CTG), the subjective and often heuristic nature of the clinical knowledge is a major source of uncertainty, and demands a high degree of expertise and experience for effective interpretation.

- ***Data quality.*** The quality of the raw foetal ECG signal can vary considerably throughout labour due to the presence of noise and artefact in the ECG signal *(Shield & Kirk 1981; Curnow et al. 1981)*. Measurements such as the T/QRS ratio which are taken from poor quality ECG data can become imprecise which, if unchecked, adds further uncertainty and can be dangerously misleading.

- ***Monitoring.*** The large amount of information produced by the foetal ECG, in addition to that of the CTG, would require continuous and vigilant monitoring by the clinician, but this is not always practical in a busy labour ward. Continuous monitoring is a very intensive process which could lead to fatigue and eventually mistakes. Computer assistance would help to provide constant monitoring.

- ***Too much emphasis on the T/QRS ratio.*** There is too much emphasis on the T/QRS ratio as it is only a crude quantification of ST waveform shape. Negative and bi-phasic ST waveform shapes (see Figure 5) are not detectable by observing the T/QRS ratio alone. One case reported by *Rosén & Luzietti et al., 1994* discusses a still birth delivery caused by a placental abruption. This case showed bi-phasic waveforms for eight minutes at the beginning of monitoring, followed by normal ECG and CTG until foetal death. This case was not detected as neither the T/QRS ratio or the CTG

showed any clear indication of there being any foetal distress *(Rosén & Luzietti et al. 1994).*

- ***Lack of abnormal cases.*** Examples of abnormal cases are essential to demonstrate the full diagnostic potential of the foetal ECG. However, it is very difficult to obtain recorded data from abnormal cases as very few centres in the world collect foetal ECG data and abnormal cases are (thankfully) very rare. To date, only one case has been collected for this project which clearly demonstrates abnormal ECG waveform shapes.

1.6 Current scope of electronic ST waveform monitoring.

At the time of writing, the only device available for foetal ST waveform monitoring is the STAN® (ST ANalyser) monitor produced by Cinventa AB (Sweden). This produces a paper trace such as that shown in Figure 6. The CTG is displayed alongside a plot of averaged ECG waveforms and a T/QRS ratio trace. This system is currently being used in a number of centres in Europe. The current STAN® monitor has very limited processor capacity and is therefore restricted to very simple signal processing and ECG interpretation. This project is currently being used as a basis for developing the future STAN® system.

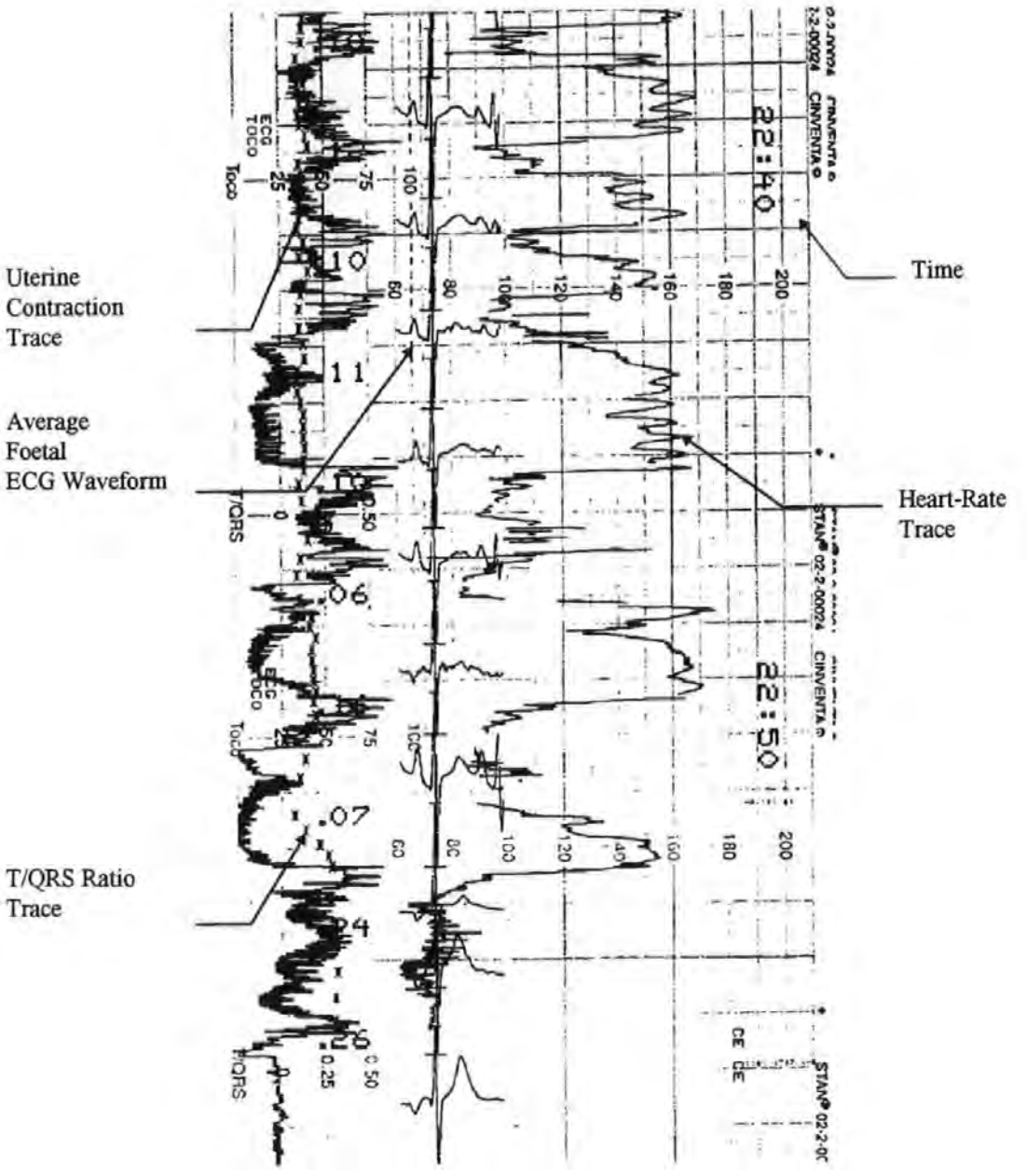

Figure 6 A sample of the paper trace produced by the STAN® monitor[1]

1.7 Aims and objectives of the project

The aims of this project are to develop techniques to overcome the problems that have hindered the widespread use of the foetal ECG and to use these techniques to develop an intelligent tool that can provide a non-expert clinician access with decision support and access to expert knowledge. This will help them make accurate, objective and timely decisions. Such a system would provide a unique

[1] Courtesy of Cinventa AB, Sweden.

platform from which to demonstrate the full clinical value of foetal ECG for the first time. To achieve these aims, the key objectives are to:

1. Obtain a variety of data including normal and abnormal cases.
2. Develop techniques to enhance ECG data online and assess quality of the signal.
3. Determine and extract key robust and quantifiable features from the ECG waveforms.
4. Develop techniques to extract salient features from the ECG to allow detailed waveform analysis.
5. Develop an intelligent system to automatically classify the shape of the ECG waveform and interpret shape changes throughout labour.
6. Validate the findings and show agreement between the system and human experts.

1.8 Overview of the thesis.

Throughout the duration of this project, an intelligent software system has been developed in the C++ programming language to simulate the on-line assessment of foetal ECG. The key stages of this project are summarised.

The first priority of this project is to collect and document raw digitised foetal ECG data. Ideally a set of data from clinically normal and abnormal cases, of differing quality, is required for testing and validation. Normal data is available but abnormal data is difficult to obtain because such cases are still quite rare. At the start of this work no abnormal human foetal ECG data was available on electronic media. It was not anticipated that a significant quantity of abnormal data could be collected from a single maternity ward in the three years of this study as not all cases are monitored. A single case with abnormal ECG has been collected, although this is a pre-term foetus (<36 weeks gestation) and therefore would not normally be considered for ECG monitoring.

To overcome the problems with poor signal quality, digital signal processing techniques have been developed to enhance the raw foetal ECG signal in order to optimise the signal-to-noise ratio, maximise the available information, and to

preserve important shape changes in the ECG waveform data. This is the subject matter of chapter 2 and is the basis of one IEE colloquium paper *(Outram & Ifeachor 1994)* and two journal papers *(Outram et al. 1995; Outram et al. 1997)*. Some of these techniques have now been implemented into the STAN® monitor.

As foetal monitoring is a life-critical procedure, a measure of signal quality is essential in order to prevent misleading information being presented either to the system or to the clinician. Sensitive techniques have been developed to estimate and interpret the signal quality which is discussed in chapters 2 and 6 respectively.

A critical component of the signal processing is to accurately locate each ECG waveform from the raw signal. This uses signal processing algorithms and pattern recognition techniques to discriminate between a true ECG waveform and noise. This is discussed in chapter 3 and has provided the basis of one workshop paper *(Ifeachor & Outram 1993)* and one IEE colloquium paper *(Outram et al. 1993)*.

Another key aspect of foetal ECG interpretation is pattern recognition of different ECG waveform shapes. This process is simplified by extracting new features, in addition to the T/QRS ratio. These are extracted to quantify the shape of the foetal ECG on a beat-by-beat basis using data quality measures to check for errors. Techniques to do this have been developed and are discussed in chapter 4. This work was developed in a way which provides enough flexibility for a clinician to explore other new features from the ECG waveform. Some of the results of this work are included in a journal paper *(Outram et al. 1995)*.

The clinician is provided with a written set of clinical guidelines to help recognise and interpret the pattern changes in the foetal ECG waveform. These rules and guidelines are formalised into rules suitable for implementing on a computer. These rules are elicited from human experts, medical research literature and from analysis of the data itself where necessary. The important variables, rules, patterns, contradictions, and sources of uncertainty are identified. These concepts and others are discussed in chapter 5 and in two conference papers *(Ifeachor & Outram 1994; Ifeachor & Outram 1995a)*.

A key task in the clinical guidelines is to classify the ECG waveform shape as one of the recognised shapes described in the clinical guidelines (see Figure 5). To automate this task a set of features are first identified which, when interpreted with

a new set of fuzzy rules, are shown to successfully classify each ECG waveform as one or more of these recognised shapes and is discussed in chapter 6.

The elicited fuzzy rules and guidelines are implemented into an intelligent system which can faithfully model the human experts thinking and methodology to a degree that clinicians would not need to constantly supervise the ECG data. This system uses expert knowledge to *provide clinicians with a clear objective assessment of the foetal condition* as well as the expert reasoning behind it.

Fuzzy logic is used to manage the imprecision and uncertainty in foetal assessment. The concepts behind fuzzy logic are discussed in chapter 5. New techniques to model the experts interpretation of *progressive changes through time* using fuzzy models are described in chapter 6 and in a conference paper *(Outram et al. 1996)*. A prototype fuzzy expert system has been developed to infer the quality of the signal and to interpret the *shape changes* using these new techniques.

The system has been tested on the available data and has demonstrated the ability to detect abnormal waveforms. It has also been demonstrated that the signal enhancement techniques described in chapter 2 and the feature extraction techniques described in chapter 4 do not introduce any significant distortion to the useful features.

This work provides a flexible tool to measure almost any feature from the foetal ECG waveform. It also provides a framework to investigate, develop and refine new rules for interpreting foetal ECG patterns which might be of clinical use, but which has previously been impossible to measure. Chapter 7 discusses future research and recommends enhancements to the current system.

Chapter 2

Signal Enhancement

2. *Signal Enhancement*

2.1 Introduction

The poor signal quality of the foetal ECG is a major source of imprecision and uncertainty in foetal ECG analysis. The conditions of the labour ward make good quality data acquisition very difficult, but good quality data is essential for ECG waveform analysis. Much of the clinical observations are difficult to reproduce or fully exploit because of the difficulty of processing and analysing the foetal ECG waveform accurately. The availability of good quality ECG signals or the ability to enhance the data, when necessary, with minimal distortion is a pre-requisite for waveform analysis *(Outram et al. 1995)*. Poor quality signals lead to erroneous ECG features, such as spurious values of the T/QRS ratio and distorted ST waveform shape. This can lead to misclassifications of ECG waveform shape and clinical errors. The approach adopted for this work is therefore to maximise the signal-to-noise ratio (SNR) as much as possible without compromising the important signal content and to reject poor data. *Only good quality data can be used for ST waveform analysis.*

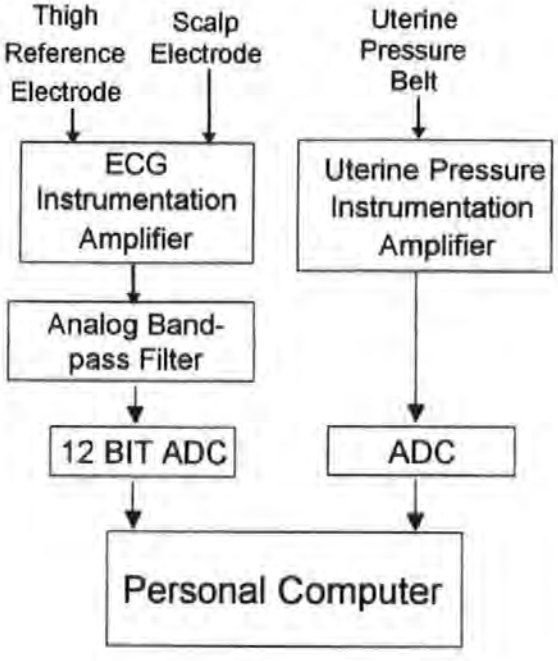

Figure 7 Data acquisition system

The foetal ECG is obtained using a single spiral scalp electrode designed to introduce minimal distortion *(Westgate et al. 1990)* and the signal is band-limited with an analogue filter from 0.05 to 100Hz, as recommended by the *American Heart Association (1975)*, before the signal is digitised to 12 bits accuracy at a sampling rate of 500Hz (see Figure 7). The analogue filter helps to remove some of the high-frequency noise, simplifies the Analogue-to-Digital Conversion (ADC) stages by removing DC offsets and acts as an anti-aliasing filter prior to sampling. The quality of the filtered signal however is still very poor, and still contains relatively high noise and artefact energy. Poor quality ECG signals can often result in an incorrect interpretation of the ECG shape and can lead to an incorrect diagnosis, thus further signal enhancement is absolutely essential for analysing the foetal ECG. Signal enhancement of the foetal ECG with analogue filters is known to introduce distortion due to their non-linear phase response *(American Heart Association 1975)*, therefore digital techniques which do not introduce phase distortion must be employed.

2.2 Sources of noise

There are many sources of noise that degrade the foetal ECG signal quality. The foetal scalp ECG is particularly susceptible to low frequency noise, known as baseline shift, which induces false changes in the ECG waveform shape, especially the ST waveform. Other noise sources are muscle noise, power-line noise, maternal ECG and the foetal electroencephalogram (EEG), although in most cases the maternal ECG and EEG are negligible in the foetal scalp ECG signal.

2.2.1 Baseline shift

Baseline shift is a slow-moving, non-deterministic wave (see Figure 8), which hinders accurate measurement of ECG features. The source of baseline shift is mostly due to scalp electrode movement, a changing impedance of the thigh reference electrode-skin interface and possibly a chemical reaction between the stainless steel in the scalp electrode and the scalp itself. Baseline shift is observed to be most prominent during the first 20-30 minutes after attachment of the electrode and during the last stages of labour when the mother is pushing.

The degree of baseline shift can vary in any one labour from a slowly rising quasi-linear trend as shown in Figure 8(a), a slow quasi-harmonic wave as shown in Figure 8(b) or a sudden transition as shown in Figure 8(c). A major problem with baseline shift is that its spectrum is often wide and overlaps with that of the ECG signal. To design an optimal filter to remove baseline shifts would, by definition, require a-priori knowledge of the ECG signal spectrum. The ECG waveform itself is only quasi-stationary so it is impossible to define a fixed frequency spectrum and how to optimally filter out the baseline shift without removing the important information within the ECG signal. The ECG ST waveform shape, which is of important clinical significance, is particularly sensitive to distortion of the low-frequency signal components of the ECG *(Van Alsté et al. 1985)*. The signal enhancement scheme must therefore be carefully designed so that the important information in the ECG waveform is not lost or distorted. There are periods of very poor quality data when significant baseline shift energy still remains despite the signal enhancement. It is very important that the severity of the remaining baseline shift is known so that sensitive features, such as ST depression, are only measured when there is little or no baseline shift present.

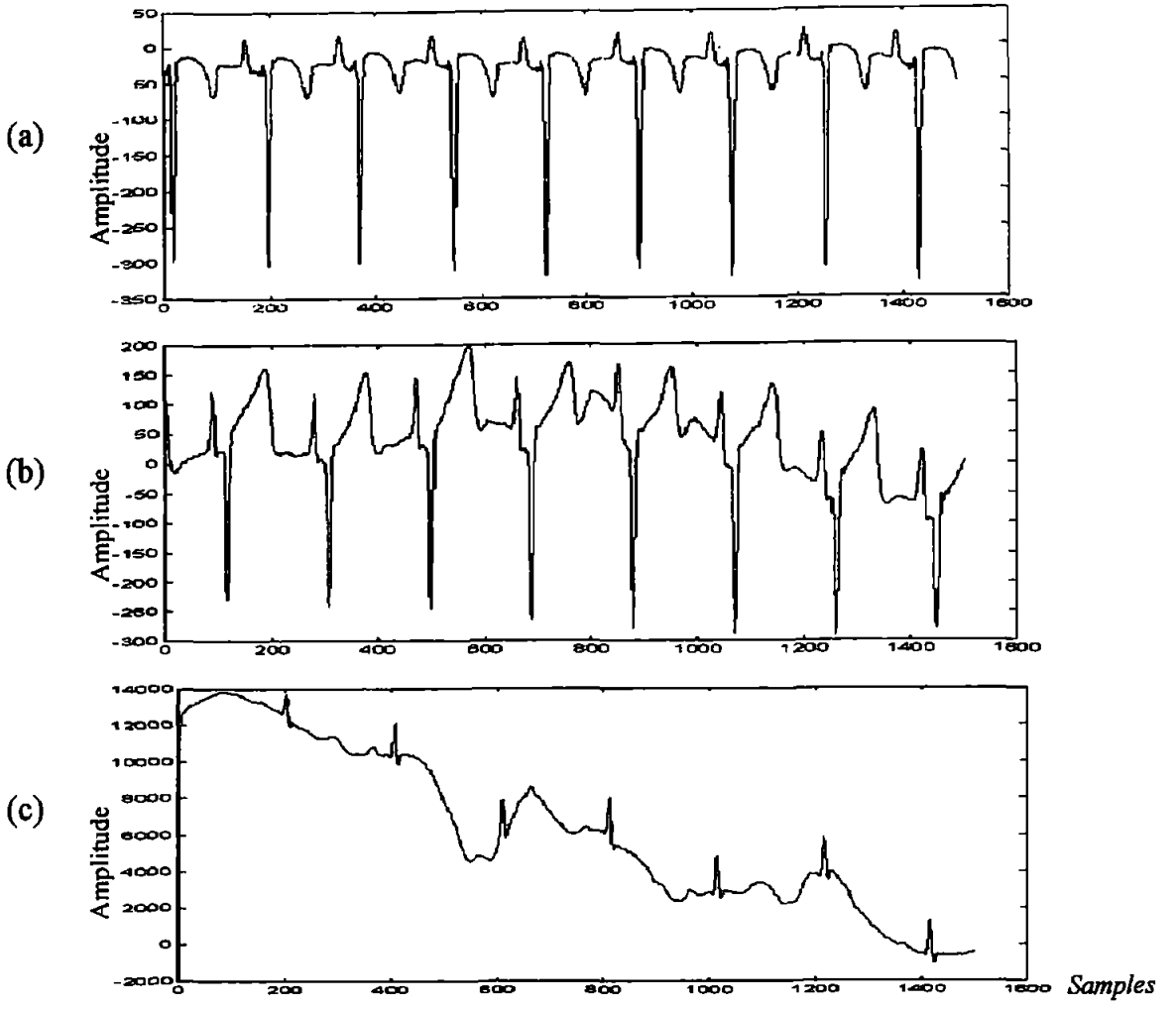

Figure 8 Baseline shift in foetal ECG data. (a) Type 1 - Low baseline shift from a good quality signal , (b) Type 2 - Medium baseline shift and (c) Type 3 - Acute baseline shift which renders the signal unusable for ECG shape analysis

2.2.2 Muscle noise

For muscles to contract, the muscle cells generate chemically induced electrical impulses, and this can be measured from the body surface. Muscle noise is caused by the random firing of muscle fibres. When the mother uses her leg muscles, then the muscle noise is picked up from the reference pad on the maternal thigh. This is most prominent during uterine contractions and while the mother is pushing and tensing her leg muscles. An example of muscle noise is shown in

Figure 9. Muscle noise obscures the important features and timing points, such as the P, Q, R, S and T peaks. Its spectrum spans that of the foetal ECG signal and so it can never be completely removed with linear filtering.

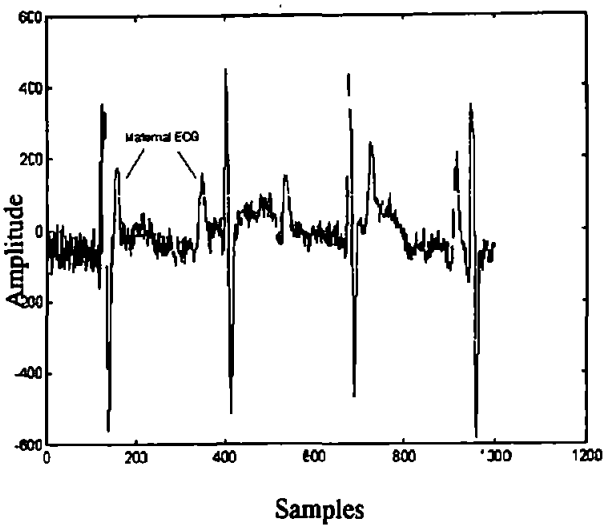

Figure 9 Foetal ECG showing muscle noise and maternal ECG interference

2.2.3 Power-line noise

Power-line noise is often picked up by the scalp-electrode leads from neighbouring equipment such as fluorescent lighting and is amplified by the instrumentation amplifiers (see Figure 7). It is almost periodic (50Hz±1% in the UK) and often high in amplitude with respect to the ECG waveform. Harmonics of 50Hz are observed in the power-spectrum of the ECG signal (see Figure 10). If power-line noise is not suppressed it can obscure the P, Q, R, S and T peaks in the ECG waveform and distort their true amplitudes. The QRS amplitude, which is used throughout the system as a physiological constant, will jitter in the presence of power-line noise and so it is important that is removed. In the UK, the fundamental harmonic is 50Hz which lies within the useful spectrum of the foetal ECG waveform. Care has to be taken in designing a filter to remove unwanted 50Hz power from the signal. The 100Hz peak shown Figure 10 in is outside the useful spectrum of the foetal ECG, so could be removed by low-pass filtering.

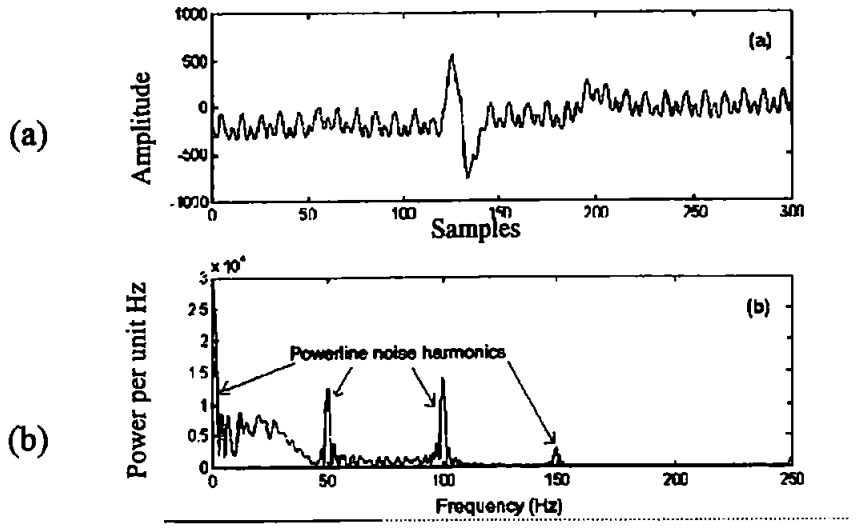

Figure 10 (a) ECG waveform corrupted with power-line noise and (b) the respective power-spectrum

2.3 Signal Enhancement Techniques

The objective of signal enhancement is to maximise the foetal ECG SNR whilst preserving the clinically useful waveform shape information. Describing the ECG shape is achieved by measuring key features such as the P, Q, R, S and T peak heights. Some of the features are more susceptible than others to the effects of noise. For example, the heart-rate is only dependent on the interval between successive R peaks (known as the RR interval) which, incidentally, are usually the largest features in the ECG, and are therefore the easiest features to locate. The RR interval is not affected by the attenuation of low-frequency information and therefore can tolerate more aggressive filter enhancement that other features such as the T/QRS ratio. The ST segment shape is the most sensitive feature because it is easily corrupted by low frequency noise and distortion and is a valuable measure of foetal condition.

An important aspect of this work is to retain as much useful information as possible in the ECG. The first major task is to remove low-frequency noise and power-line noise from the raw ECG signal so that fixed reference timing points, namely the Q, R and S peaks, can be located. This is known as QRS detection (see chapter 3). This uses an "aggressive" filter to simultaneously remove low-frequency and power-line noise. This is known as the *CTG feature signal enhancement scheme* and is

summarised in Figure 11. The details of this are discussed with QRS detection in chapter 3.

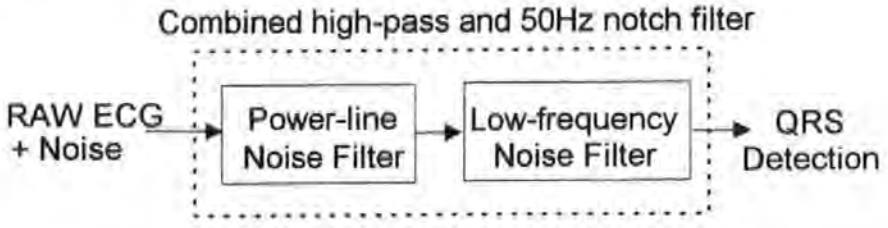

Figure 11 A summary of the CTG feature signal enhancement used to help detect the QRS complex from the raw ECG signal

A less aggressive signal enhancement scheme is used in this work for the analysis of more sensitive features, and is summarised in Figure 12. This is known as the *sensitive feature signal enhancement scheme*. After detecting the R-wave (see chapter 3), linear filters are used to remove some of the power-line noise and baseline shift from the raw data. An approximation of the remaining baseline shift is obtained using a curve fitting technique. This is used to assess the severity of baseline noise corruption and conditionally accept or reject the data. To minimise the effects of muscle noise, an optimal filter is used to maximise the SNR which helps to locate the Q and S peaks in the ECG waveform. A signal average is then used to further suppress random noise. The average waveform is computed from selected good quality raw ECG waveforms. Smooth curves are then evenly fitted to the ST waveform of the current raw and average ECG waveforms. These curves are used to reduce the effects of random noise and to simplify the location and measurement of important features from the ST waveform. This is discussed in chapter 4 (Feature Extraction).

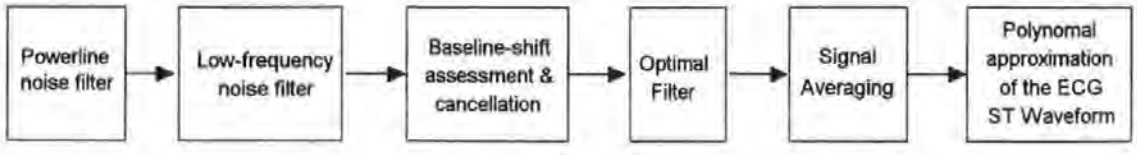

Figure 12 A summary of the sensitive signal enhancement used in this work to minimise the effects of noise in the foetal scalp ECG and preserve the ECG signal shape

Signal quality is assessed before the data is considered for analysis. The signal quality information is used to decide what information can be reliably extracted from the ECG waveform. In the presence of acute baseline shifts for example, only

the most insensitive features, such as RR intervals are considered to be reliable. Waveforms with large baseline shifts are not included in the signal average as baseline shifts tend to be correlated and are not sufficiently removed by the averaging process, thus producing a distorted and potentially misleading waveform shape. The signal-to-noise ratio (SNR) of the signal average waveform is then estimated and this information is used to reject poor quality averaged waveforms distorted by higher frequency noise.

A signal processing scheme is developed to maximise the signal-to-noise ratio without introducing significant signal distortion and compromising the clinical information stored within the signal. The key objective is to maximise the number of good quality waveforms available for sensitive analysis.

2.3.1 Filter Design for Foetal ECG Analysis

Desirable features of noise reduction filters include a linear phase response in the passband to prevent distortion of signal waveshape, and low order to reduce computational overhead. Unfortunately, in this application the noise reduction filters are characterised by narrow transition bands which make them difficult to design. Consider the two filter prototypes shown in figures 13a and b. which are designed to reduce baseline shifts and power-line noise in the foetal ECG waveform respectively.

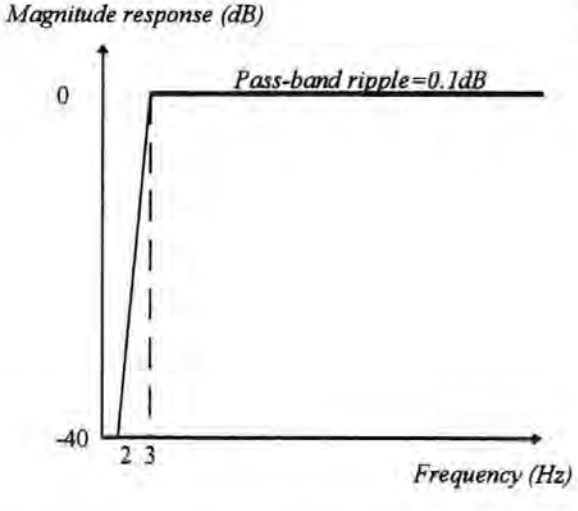

Figure 13a Magnitude response for removing baseline shift energy

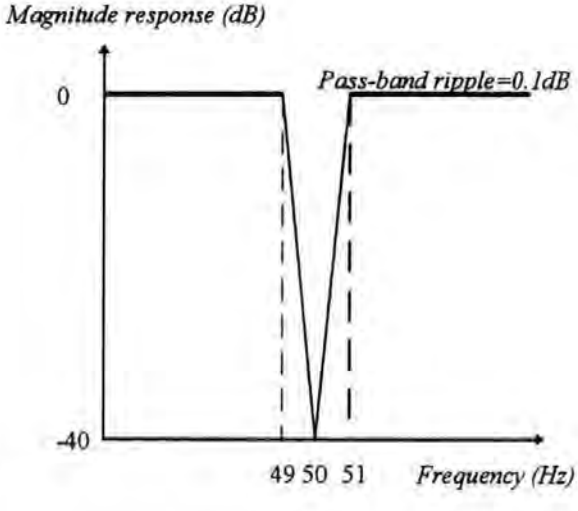

Figure 13b Magnitude response for removing power-line noise

Linear-phase Finite Impulse Response (FIR) filters, designed using the Remez-Exchange algorithm (*Rabiner & Gold 1975*), with 951 and 953 coefficients respectively would be required to meet the specifications.

Infinite impulse response (IIR) filters are attractive as they can have a very good amplitude response for low filter orders. An elliptic filter of 12th order can meet the amplitude response of the 50Hz notch filter, but a major drawback with IIR filters is the non-linear phase response which causes distortion of the foetal ECG shape. This drawback manifests itself as ringing and distortion of ST waveform shape (see Figure 14).

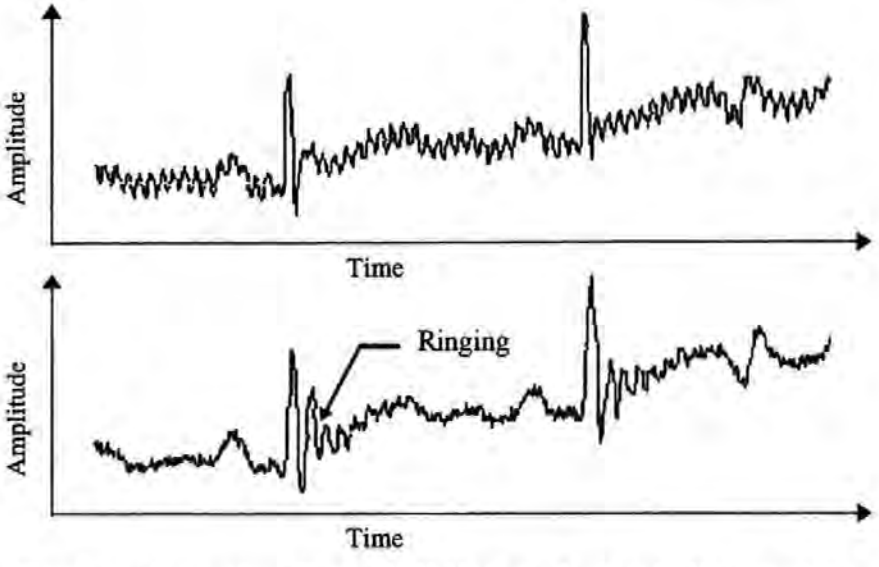

Figure 14 The ringing effects of IIR filters on the foetal ECG waveform

One solution to overcome this is to use a phase-reversal technique (*Proakis & Manolakis 1992*) where the filtered data is fed back in reverse order through the filter. Using this technique the delaying effect of the filter at each frequency is theoretically cancelled out to zero. In practice the data has to be processed in blocks and cannot be run continuously. This is inconvenient as the blocks have to be of sufficient length to allow the filter to settle on each pass. This technique also requires high precision arithmetic to prevent the filter from becoming unstable.

A more practical technique discussed by *Ifeachor and Jervis (1993)* was to design a multi-rate finite impulse response (FIR) filter. This has guaranteed stability, linear phase and does not require very high precision arithmetic. The filter design can often be simplified by first reducing the sampling rate. After filtering at the lower

sampling rate, the sampling rate is then restored. In general, multi-rate filters require the following stages.

1. **Decimation**. Reduce the sampling rate of the data to $Fs'=Fs/K$, where Fs=original sampling rate, Fs' is the new sampling rate, and K is the decimation factor. To do this without introducing aliasing, the following steps are carried out.
   (a) First digitally low-pass filter the data, where that the stop-band edge frequency is less than the new Nyquist frequency ($Fs'/2$).
   (b) Sub-sample the data at the new sampling rate Fs' by extracting *1* in every K samples.
2. **Filter**. Design and implement the desired filter the data at the new lower sampling rate Fs'
3. **Interpolation**. Restore the sampling rate to Fs. To do this without introducing aliasing, the following steps are carried out.
   (a) Pad the filtered data with *(K-1)* zeros between each sample to restore the sampling rate to Fs. This will increase the effective sampling rate but will also create image frequency bands.
   (b) Filter this data using the filter in 1(a) to remove the image frequency bands.

Clearly this method still requires a considerable computational effort, involving additional decimation and interpolation filter stages. This method only works well in filter design problems where it is possible to reduce the sampling rate significantly, which is not always the case. In the case of the filter specification in Figure 13b, the lowest convenient sampling frequency obtainable is to reduce the sampling rate from 500Hz by a factor of $K=4$ to *125Hz*. Even with this reduction, the minimum number of coefficients required to meet the specification is 275.

A much simpler and efficient filter scheme has been developed for ECG analysis *(Outram & Ifeachor 1997)*.

An efficient technique for removing power-line harmonics and low-frequency noise, based on the well known window filter design technique has been proposed *(Van Alsté & Schilder 1985)*. Its main feature is a FIR filter with a repeating frequency

spectrum designed such that a narrow notch occurs at harmonics of the mains frequency of 50Hz (see Figure 15). By allowing the magnitude response of the filter to repeat, the computational effort required to obtain narrow band notches is greatly reduced *(Van Alsté & Schilder 1985)*. This technique requires additional effort in the design phase to achieve the desired band edges because of the difficulties associated with the window method *(Ifeachor and Jervis 1993)*. Further, the window design approach does not allow independent control of the pass-band and stop-band ripples and leads to notches that have the same width, which is inappropriate in some applications, where some of the notches need to be wider than others.

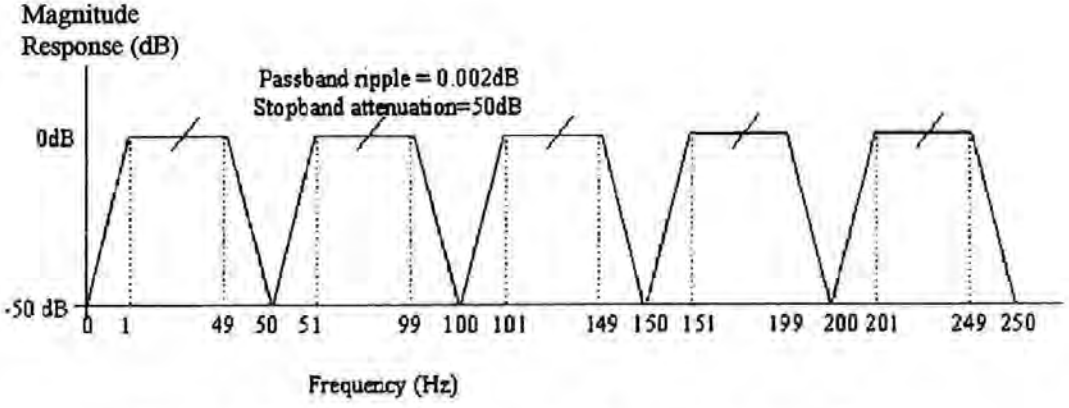

Figure 15 Specification of a repeating frequency spectrum filter.

A novel method has been developed here for designing filters based on the principle of repeating frequency spectrum filters, only the new method allows precise control of the band edge frequencies, pass and stop band ripple and is based on filters designed using the Remez Exchange algorithm. It is also shown how these filters can be combined to obtain useful single or multiple band filters.

2.3.2 New filter design method

The underlying problem to be addressed in this application and many others is the design of an efficient FIR filter with very sharp transition bands. Designing non-recursive digital filters with sharp transition band edges requires many filter coefficients which becomes computationally expensive and inefficient. For illustrative purposes, consider the design specification of the low pass filter in Figure 16.

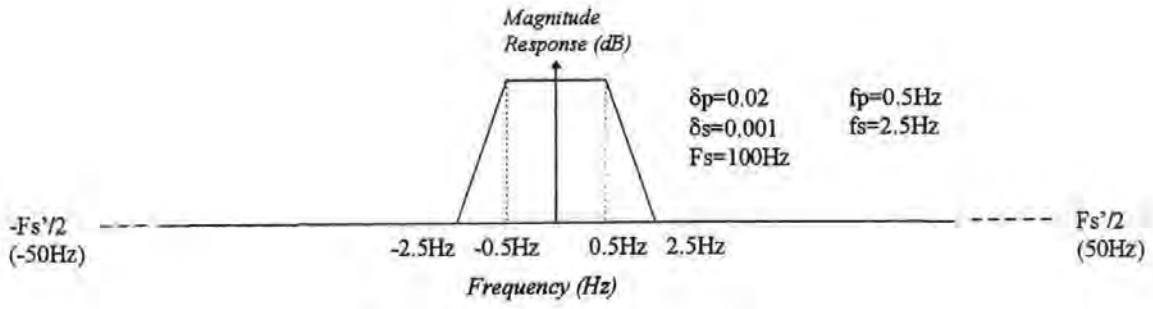

Figure 16 Low-pass filter specification

The number of coefficients N required for a FIR low-pass filter designed with the Remez Exchange algorithm is estimated by

$$N \approx \frac{0.9 \cdot Attenuation(dB)}{20 \cdot \Delta F} \qquad (2.1)$$

where ΔF is the width of the transition band normalised to the sampling frequency Fs given by

$$\Delta F = \frac{|f_s - f_p|}{F_s} \qquad (2.2)$$

Using the expression in (*2.1*), to design this FIR filter directly using the Remez exchange algorithm requires at least $N=675$ filter coefficients. Clearly if the attenuation and band-edge frequencies are fixed, then the only way to reduce N is to reduce the sampling frequency Fs. The filter is therefore re-specified at a lower sampling frequency such that the number of coefficients N is acceptable. The same filter specification as that shown in Figure 16 is now given in Figure 17 but the sampling rate has been reduced by a factor of 5. The new sampling frequency $Fs'=20Hz$.

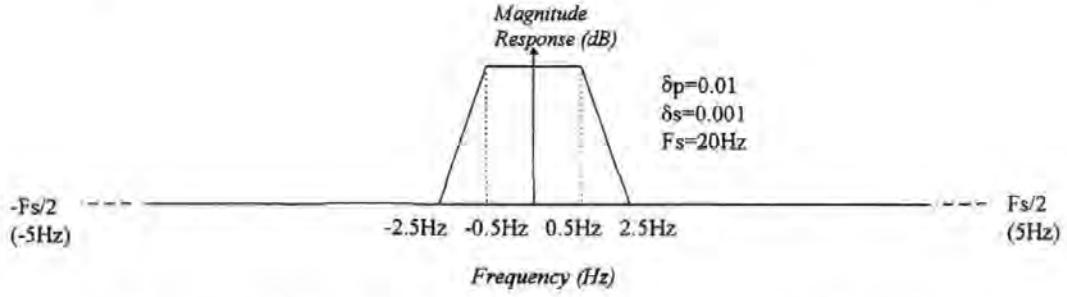

Figure 17 Low pass filter specification at a lower sampling frequency

The actual magnitude response of this filter and the filter coefficients $h1(n)$ of this filter are shown in Figure 18. From (*2.1*), this filter requires at least 27 coefficients,

although 28 have been used here to obtain a magnitude response close to the desired specification[1]. The proto-type filter given in Figure 16 was designed to filter signals at a sampling frequency of *Fs=100Hz*, whereas this filter is specified at a sampling rate of *Fs'=20Hz*. To correct for this, the filter coefficients *h1(n)* are zero-padded by a factor of 5. The effects of this on the magnitude response and filter coefficients are shown in Figure 19.

(a)

(b)

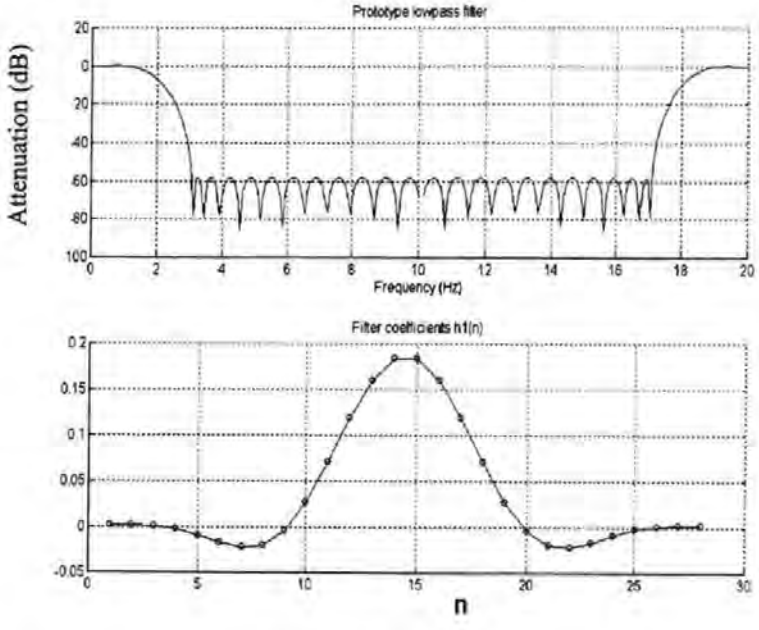

Figure 18 Low-pass filter designed directly with the Remez Exchange algorithm

[1] Note that the expressing in (*2.1*) often under-estimates the true number of coefficients required to meet the specification

(a)

(b)

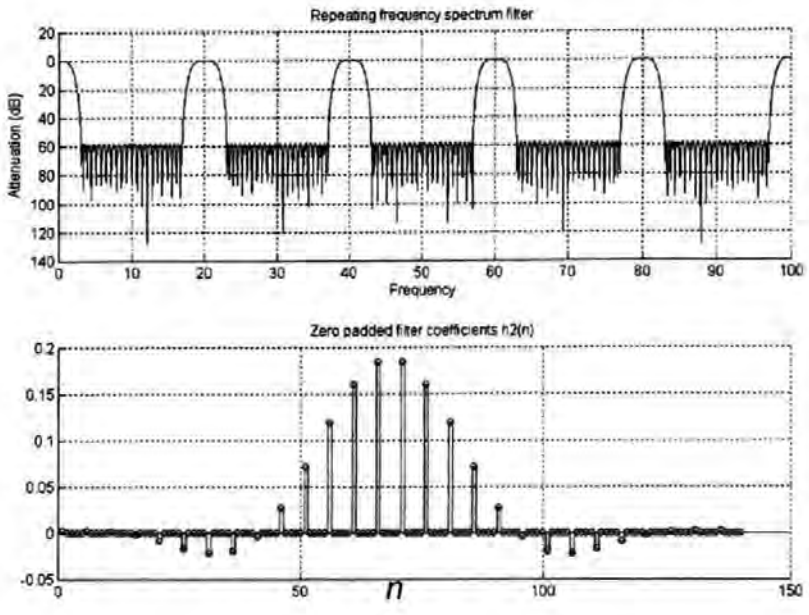

Figure 19 Magnitude response and filter coefficients of a repeating frequency spectrum filter

In general, the effect of zero-padding a time-series by a factor of K is to cause its frequency spectrum to repeat K times, and this is observed in Figure 19. There are three important points to note here. The first is that the magnitude response of the zero-padded filter, over the frequency interval *-Fs'/2...Fs'/2,* is identical to the desired specification in Figure 16. The second point is that although the total length of this filter is now $N'=28*5=280$, the number of non-zero coefficients required to implement this filter is unchanged ($N=28$). This filter is therefore very efficient to implement as there are still only N multiplication operations to execute. The output of the filter is given as

$$y(n) = \sum_{i=0}^{N-1} x(n - i \cdot K) \cdot h1(i) \qquad (2.3)$$

where $x(n)$ is the data sampled at 100Hz, $h1(i)$ are the filter coefficients, and $y(n)$ is the filtered output. The group delay d_{grp} though this filter is given by

$$d_{grp} = \begin{cases} N \cdot K/2 & N \cdot K \text{ is even} \\ (N \cdot K - 1)/2 & N \cdot K \text{ is odd} \end{cases} \qquad (2.4)$$

The third point is that new unwanted pass-bands have been created at 20Hz intervals as a result of zero-padding. The unwanted bands, or images, must be removed by cascading with another low-pass filter, known as the anti-image filter, and this is illustrated in Figure 20.

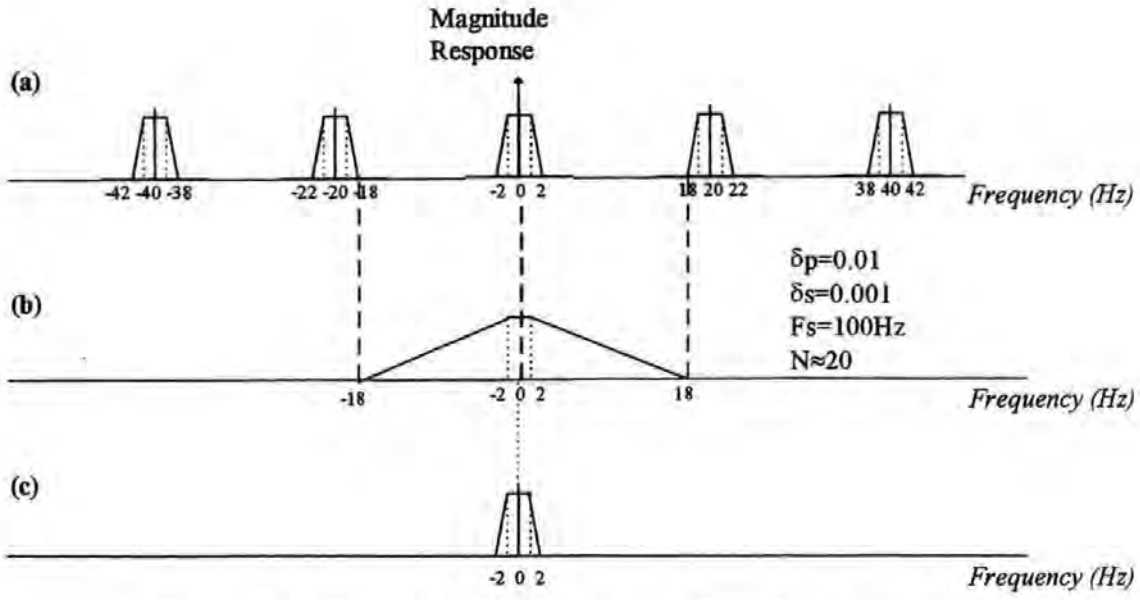

Figure 20 (a) Repeating frequency spectrum filter, (b) anti-image filter & (c) Resulting low-pass filter

The design of this anti-image filter (illustrated in Figure 20b) is straightforward as *the normalised transition width is large because the repeating frequency bands are widely separated.* In this example, the transition width of the anti-image filter $\Delta F=(Fs'-2fp)/Fs=16/100$, where *fp* is the band-edge frequency *(2Hz)*. From *(2.1)* this requires a filter with at least 20 coefficients, although 23 have been used in order to meet the specification. The actual magnitude response and filter coefficients for this filter are shown in Figure 21.

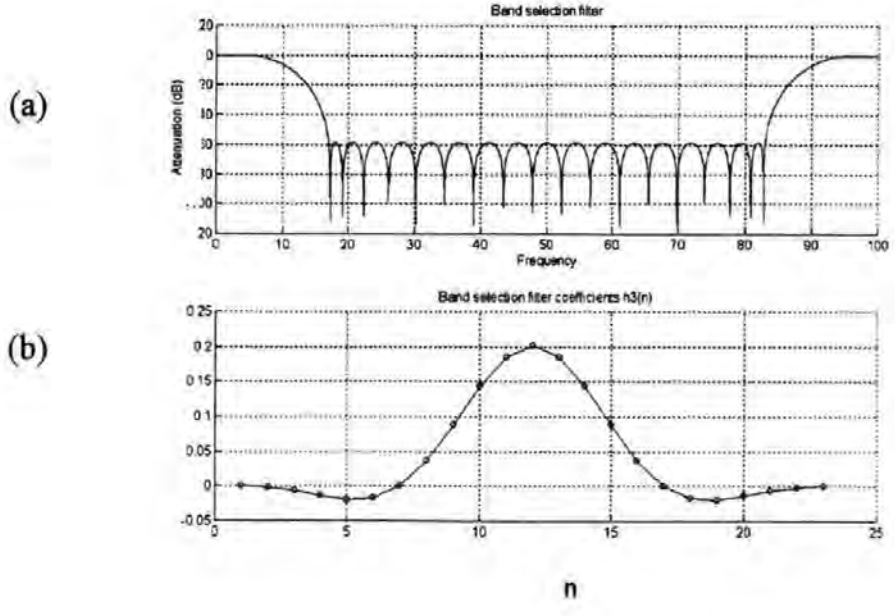

Figure 21 Anti-image filter

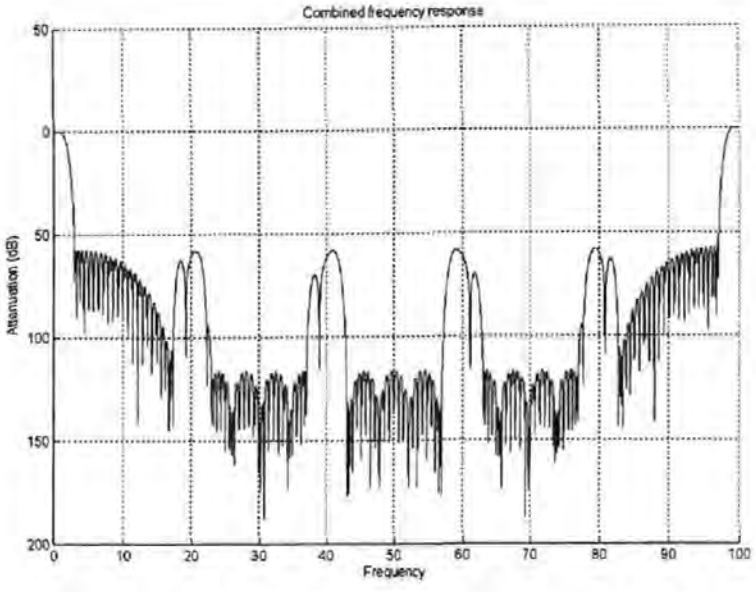

Figure 22 Resulting magnitude response of the cascaded filters

Cascading these two filter gives the overall magnitude response shown in Figure 22. Equally a band-pass filter can be designed by choosing a different anti-image filter as illustrated in Figure 23.

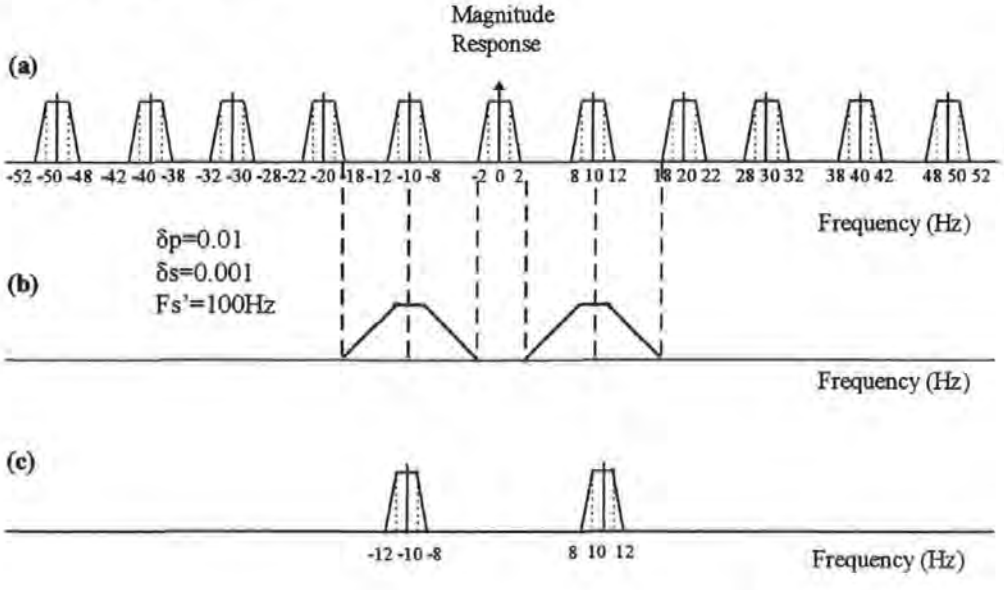

Figure 23(a) Repeating frequency spectrum filter, (b) anti-image filter & (c) Resulting band-pass filter

The anti-image filter requires 28 coefficients. The magnitude response and filter coefficients are shown in Figure 24. The overall magnitude response is shown in Figure 25.

(a)

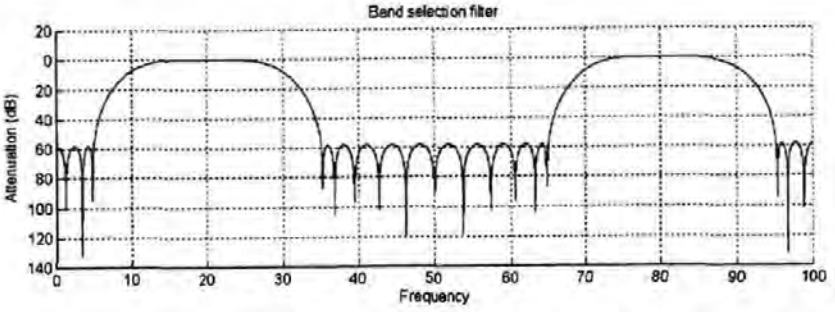

(b)

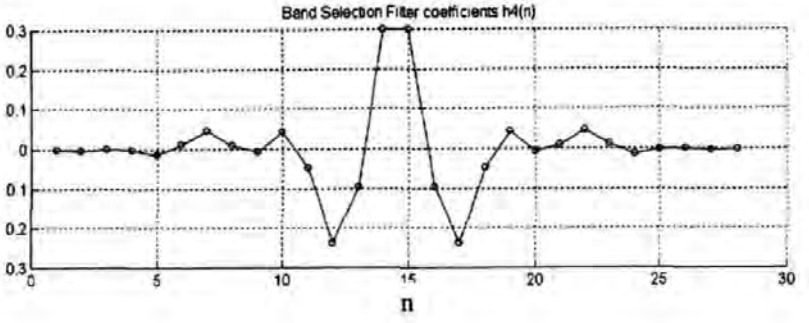

Figure 24 Anti-image filter for the band-pass filter

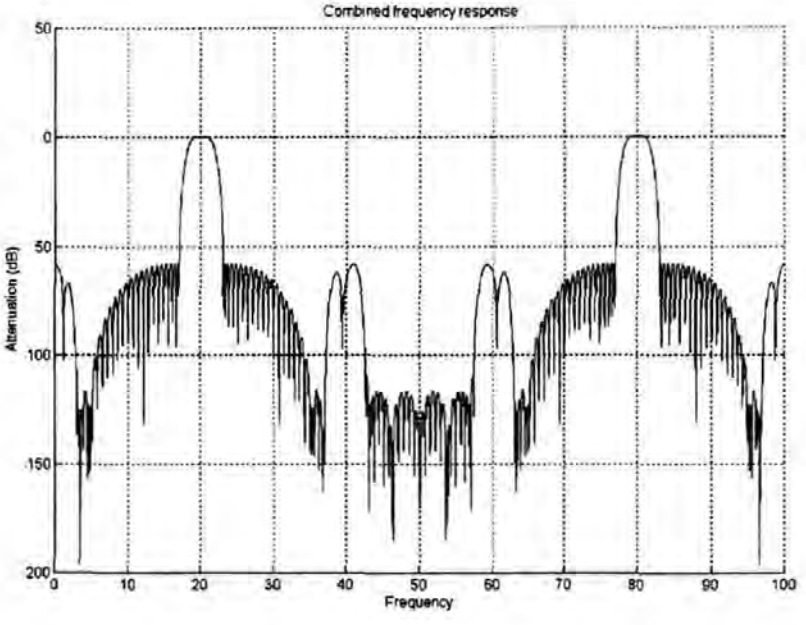

Figure 25 Overall magnitude response of the band-pass filter design

2.3.3 Theory

This technique is closely related to comb filtering *(Proakis et al. 1992)*. A FIR filter is first designed using the well known Remez Exchange algorithm (*Rabiner & Gold 1975*) with coefficients *h(n), n=0..L-1*, where *L* is the filter length and *n* is discrete time. The transfer function of the FIR filter is given by

$$H(Z) = h_0 + h_1 \cdot Z^{-1} + h_2 \cdot Z^{-2} + ... + h_{L-1} \cdot Z^{-(L-1)} \qquad (2.5)$$

and in the frequency domain, substituting $Z = e^{j\omega T}$, this becomes

$$H(e^{j\omega T}) = h_0 + h_1 \cdot e^{-j\omega T} + h_2 \cdot e^{-2j\omega T} + ... + h_{L-1} \cdot e^{-(L-1)j\omega T} \qquad (2.6)$$

where T is the sampling interval and ω is angular frequency (radians per second). Consider the case where the sampling frequency is now increased by a factor of K, such that $\omega_s' = K\ \omega_s$, where ω_s is the original sampling frequency in radians per second, ω_s' is the new sampling frequency. It follows then that the new sampling interval $T' = T/K$. The frequency response now becomes

$$H(e^{j\omega T'}) = h_0 + h_1 \cdot e^{-j\omega T'} + h_2 \cdot e^{-2j\omega T'} + ... + h_{L-1} \cdot e^{-(L-1)j\omega T'} \qquad (2.7)$$

If it is required that the equations *(2.5)* and *(2.7)* are equivalent in the frequency interval - $\omega_s/2 < \omega < \omega_s/2$, then it follows that *(2.7)* must be modified as follows

$$H(e^{j\omega T'}) = h_0 + h_1 \cdot e^{-jK\omega T'} + h_2 \cdot e^{-2Kj\omega T'} + ... + h_{L-1} \cdot e^{-(L-1)Kj\omega T'} \qquad (2.8)$$

The equivalent transfer function then becomes

$$H(Z) = h_0 + h_1 Z^{-K} + h_2 Z^{-2K} + ... + h_{L-1} Z^{(L-1)K} \qquad (2.9)$$

When the frequency response of *(2.9)* is plotted over the interval $-\omega_s'/2 < \omega < \omega_s'/2$, the frequency response over the interval $-\omega_s/2 < \omega < \omega_s/2$ is repeated K times. This is the effect of aliasing and is the cause of the repeating frequency bands. Taking the inverse Z transform of *(2.8)* the new filter has a difference equation of

$$h(n') = h_0 \cdot x(n') + h_1 \cdot x(n' - K) + h_2 \cdot x(n' - 2K) + ... + h_{L-1} \cdot x(n' - (L-1)K) \qquad (2.10)$$

where $n'=n/K$ is discrete time for the new sampling interval T/K. It is important to notice the filter length has increased by a factor of K, but there are still only L non-zero coefficients to be multiplied. The delay through the filter is $KL/2$ for even KL and $(KL-1)/2$ for odd KL. The frequency spectrum of the zero padded filter will contain the desired band and unwanted image bands. These image bands usually need to be removed by cascading other filters. Filters designed using this technique can be cascaded to obtain many other useful filters with very sharp transition bands. High-pass and band-stop filters can equally be designed by subtracting the output of low-pass and band-pass filters respectively from the unfiltered data samples. Two examples of filters applied to foetal monitoring are now discussed.

2.4 Design of a narrow-band notch filter for removing power-line noise.

A linear-phase notch filter with a magnitude response given in Figure 13b is required. The filter is split into two cascaded band-pass filter stages (see Figure 27). This filter can have a repeating frequency spectrum as illustrated in Figure 15 as power-line noise has harmonics at 50Hz and 100Hz (see Figure 10).

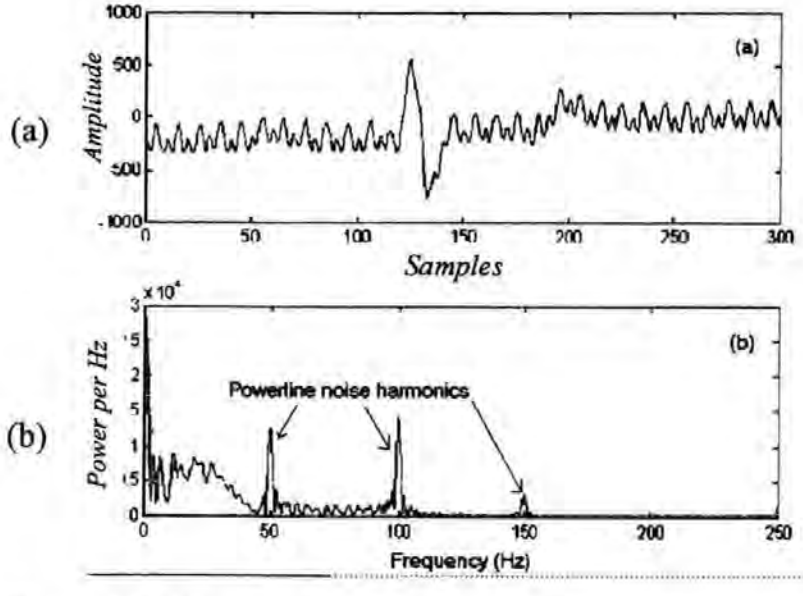

Figure 26 (a) ECG waveform corrupted with power-line noise and (b) the respective power spectrum

The output of the two filters is subtracted from the raw data to produce an enhanced signal, as depicted in Figure 27.

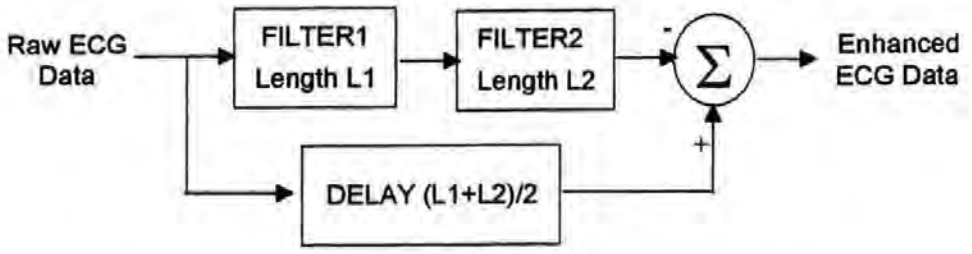

Figure 27 Design of the two stage narrow band notch filter.

The first filter is designed by computing the coefficients *h(n), n=0..24,* of a low-pass filter with a pass band edge at 0.25Hz, a transition width of 0.5Hz and at a sampling frequency of 10Hz using the Remez-Exchange algorithm *(Rabiner et al. 1975).* The magnitude response of this filter is shown in Figure 28a. Using the coefficients *h(n),* another linear FIR low-pass filter with coefficients *h'(n), n=0..249,* is derived by zero padding such that

$$h'(n) = \begin{cases} h(floor(n/50)) & n \bmod 50 = 0 \\ 0 & n \bmod 50 \neq 0 \end{cases} \qquad (2.11)$$

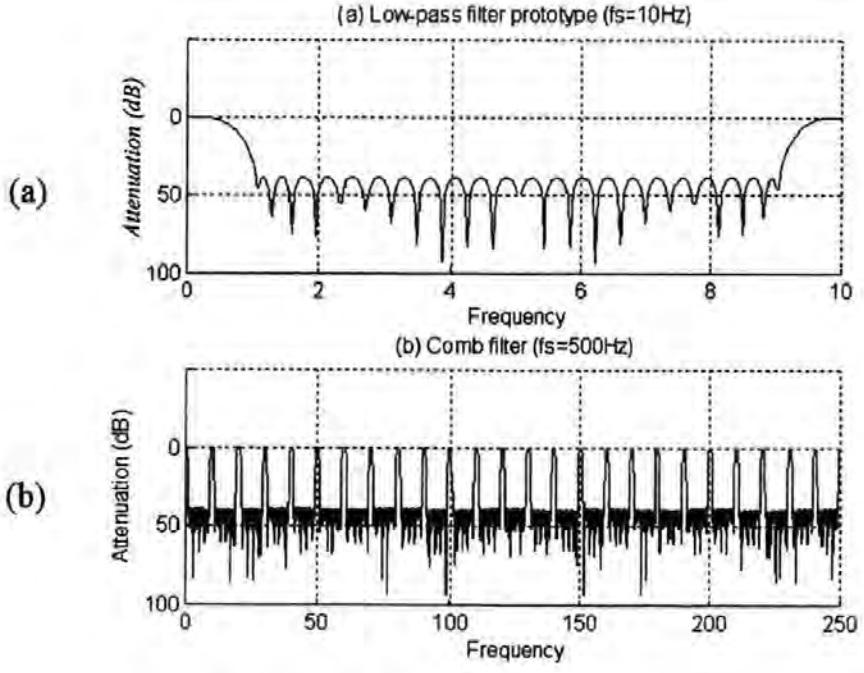

Figure 28Magnitude response of the first multi-band pass filter.

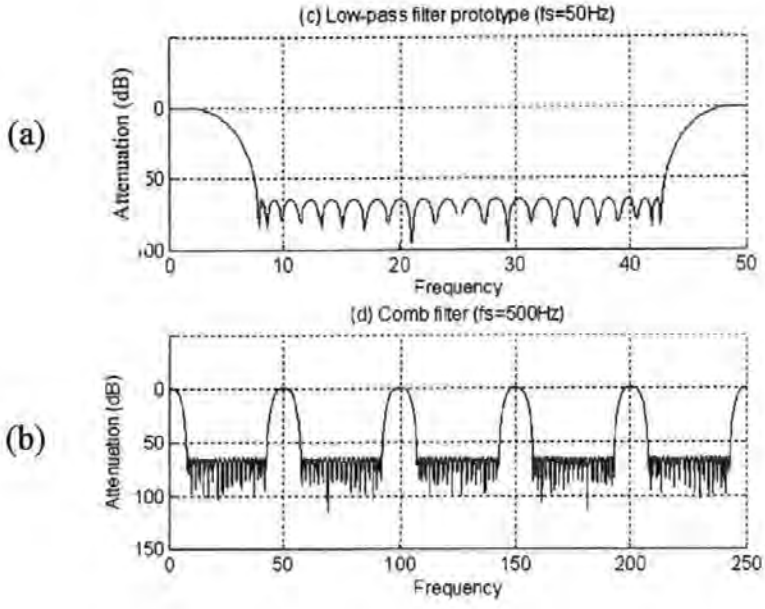

Figure 29 The magnitude response of the second multi-band pass filter.

where *floor(x)* is the integer component of x. The effect of zero padding by a factor of 50 can be considered as effectively increasing the sampling rate of the waveform *h(n)* to 500Hz. As no anti-aliasing is performed prior to this the frequency spectrum repeats every 10Hz. The resulting magnitude response is shown in Figure 28b. This is a multiple band-pass filter with centre frequency peaks at all the harmonics of 10Hz, including 0Hz. Note the narrow transition width is preserved. To meet the final filter specification, only the peaks at the harmonics of 50Hz are required. The purpose of the second filter is to remove all the images other than those at the harmonics of 50Hz. This filter is designed using the same design basic technique. Note a favourable transition width of this second filter is determined by the new sampling rate (500Hz) and the interval between the images. A low-pass filter with a magnitude response shown in Figure 29a is designed using the Remez Exchange algorithm at a sampling rate of 50Hz. The normalised transition width is 8Hz/50Hz which is favourably large. The coefficients are zero-padded by a factor of 10 to increase the sampling rate to 500Hz and the resulting magnitude response is shown in Figure 29b.

The effect of cascading these two filters, viewed in the frequency domain, is shown in Figure 30. All the harmonics of 50Hz (including 0Hz) are selected by this filter. Note that the absolute transition width of each pass-band is the same as it was in the original prototype (1Hz). Implementation of these filters is very efficient. Both

filters have only 27 non-zero coefficients. The difference equation for the first filter is

$$y_1(n) = \sum_{k=0}^{26} h_1(k) \cdot x(n - 50k) \tag{2.12}$$

and the difference equation of the second filter is

$$y_2(n) = \sum_{k=0}^{26} h_2(k) \cdot y_1(n - 10k) \tag{2.13}$$

The final output (shown in) is given by

$$y(n) = x(n - Delay1 - Delay2) - y_2(n)$$

where *Delay1=27*50/2=675 samples* and *Delay2=27*10/2=135 samples*, are the constant delays through filter 1 and 2 respectively, n is discrete time, $x(n)$ are the raw foetal ECG samples, $y_1(n)$ are the output samples of the first filter, $y_2(n)$ is the output of the second filter and $y(n)$ is the overall output. The total delay is 810 samples which is 1.62 seconds for a sampling rate of 500Hz. This technique is suited to this application as the overall filter satisfies the filter specification and the linear-phase constraint.

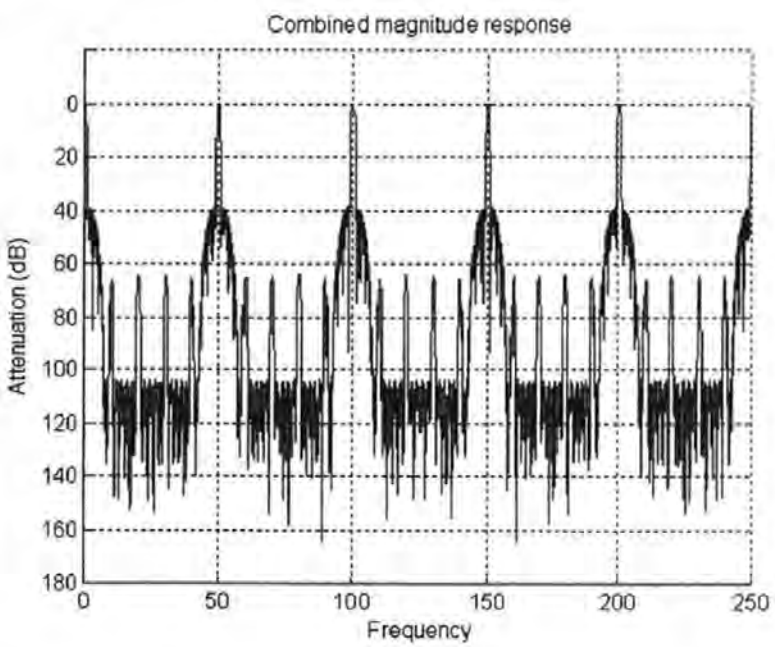

Figure 30 The combined magnitude response for removing narrow band 50Hz harmonics.

2.5 Design of a linear low-pass filter

Baseline shift is a low-frequency noise source and is shown in Figure 8. Some of the baseline shifts are reduced by the filter described above in previous section but it is

desirable to obtain a wider notch about 0Hz as specified in Figure 13b. The same technique is applied to produce a multiple notch filter with the magnitude response shown in Figure 31, but this filter has images with a larger bandwidth of 5Hz. A second anti-image filter in *Figure 32* is used to exclusively select the band between 0 and 2.5Hz. When these filters are cascaded the combined response shown in Figure 33 is produced. This filter will only extract the low-frequency noise and signal components. This way, using two separate filter schemes, the width of the low-frequency notch can differ from that of the power-line notches. Each filter described here only has 27 non-zero coefficients which can easily be implemented on a modern personal computer in real time. Using this technique of cascading comb filters is very efficient and allows accurate narrow-band filters can be designed, only at the expense of delay through the filters.

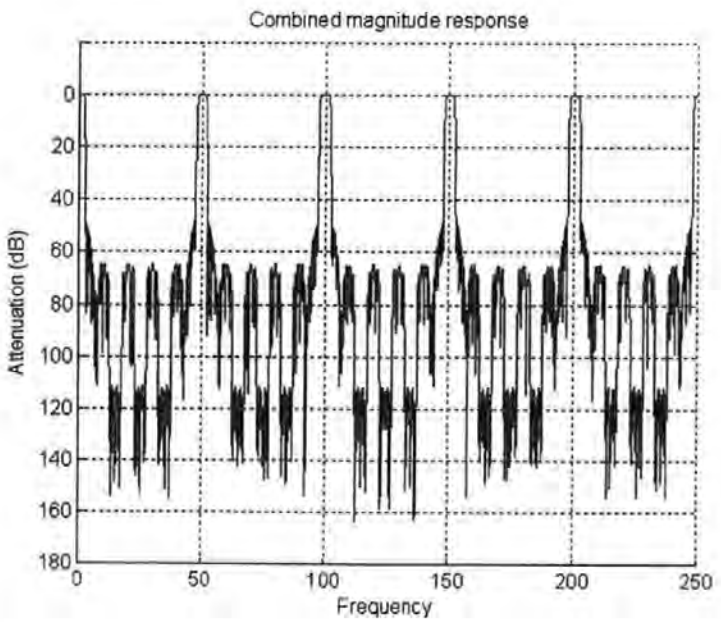

Figure 31 Repeating frequency spectrum filter designed for extracting baseline shift

(a)

(b)

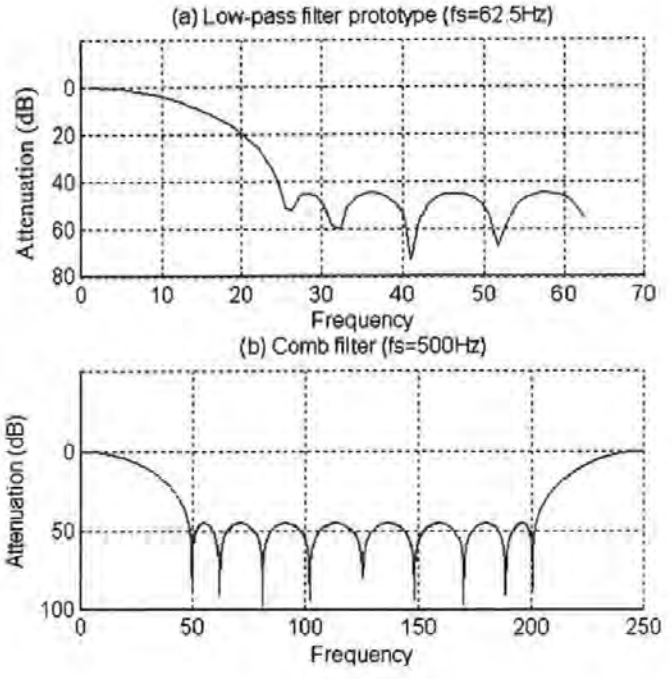

Figure 32 Additional anti-image filter

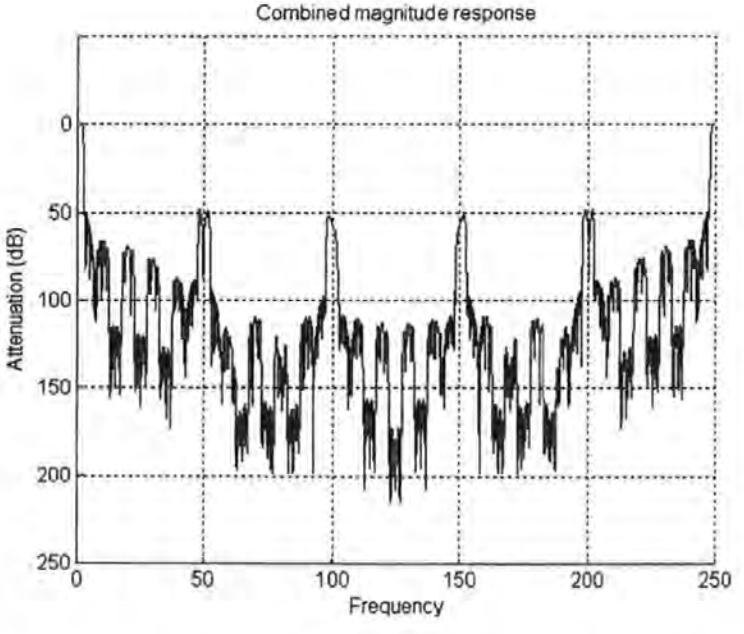

Figure 33 A filter for exclusively removing the low-frequency noise from ECG signals

The output of this filter is finally subtracted from the delayed raw ECG data. Some results are shown in Figure 34.

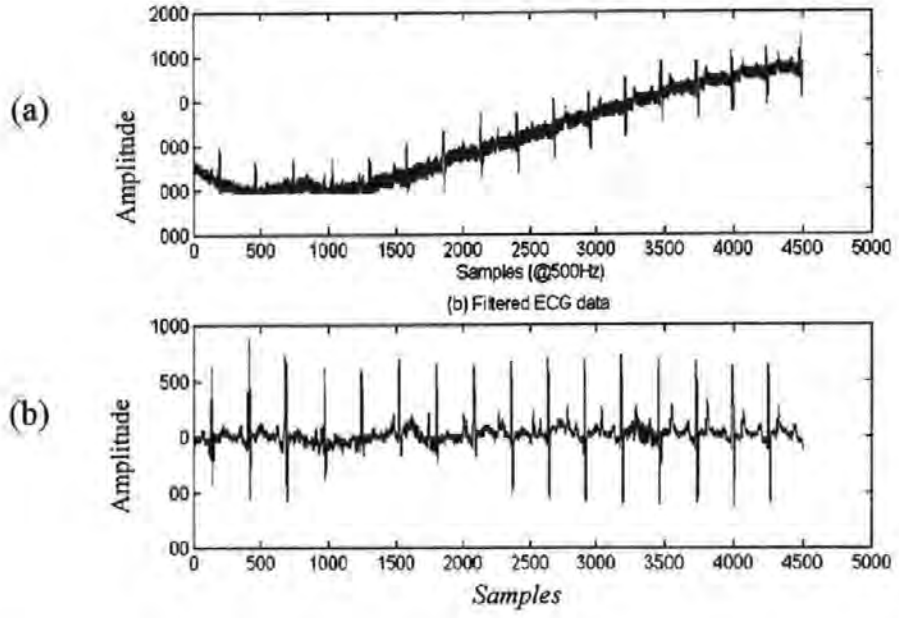

Figure 34 (a) Raw ECG (b) Raw data filtered to remove power-line noise and baseline shifts.

These filters add no significant errors to the features measured from the foetal ECG waveform, and this is discussed in section 2.7

2.5.1 Optimal Filtering

After baseline removal, the SNR may be improved further by averaging and digital low-pass filtering to reduce the effect of muscle and random noise. Muscle noise is due to maternal movement, often from the leg and abdominal muscles, and may be picked up from the reference pad on the maternal thigh. This interference can obscure the Q, R and S reference points especially during uterine contractions and while the mother is pushing. The aim here is to design a filter which maximises the SNR whilst retaining important shape information. The task of reducing the effects of muscle and random noise by filtering is essentially one of optimising the filter characteristics to match closely to the spectrum of the ECG waveform. To preserve wave-shape, an additional constraint on the filter design is that the phase-response is linear over the pass band. A difficulty with this design is that the spectrum of the ECG is not known a priori and will vary with time as the PR and ST waveforms change. A practical method is to infer the "true" spectrum from the average of several ECG complexes (see smooth curve in Figure 35). Using this method, the discrete spectrum $|X(k)|$ is first computed using the fast Fourier transform (FFT) or any other suitable method (see noisy curve in Figure 35), where k is discrete

frequency. This is then smoothed using a Chebyshev polynomial approximation $H(k)$ (See section 2.6.2 for details on Chebyshev polynomials).

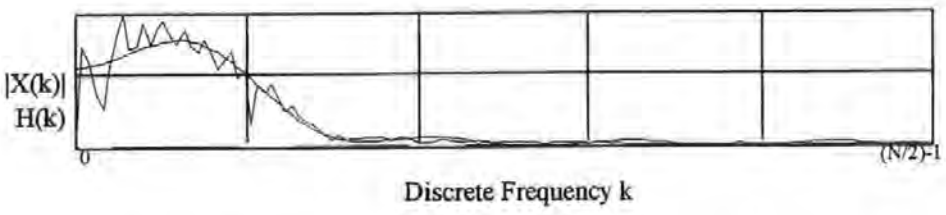

Figure 35 The smooth approximation H(k) of the average signal spectrum |X(k)|

The coefficients of the desired linear filter $h(n)$, $n=0..2m$, that has a smooth frequency spectrum $H(k)$, can be computed directly using the following expression

$$h(n) = \frac{|X(0)|}{N} + \frac{2}{N} \cdot \sum_{k=1}^{N/2-1} |X(k)| \cdot \cos\left(\frac{2\pi k(n-m)}{N}\right) \qquad (2.14)$$

where $2m+1$ is the filter length *(Ifeachor & Jervis 1993)*. To account for the possible changes in the ECG spectrum, the filter coefficients may be repeatedly computed on-line. To reduce computational load, the cosine functions in (2.14) can be pre-calculated or computed recursively using the following relationship.

$$r(k,n) = \cos(2\pi k(n-m)/N) \qquad (2.15)$$

$$s(k,n) = \sin(2\pi k(n-m)/N)$$

$$r(k+1,n) = r(1,n).r(k,n) - s(1,n).s(k,n)$$

$$s(k+1,n) = r(1,n).s(k,n) + s(1,n).r(k,n) \qquad (2.16)$$

For a given value of n, $r(1,n)$ and $s(1,n)$ are first directly evaluated from the definitions in (2.15). The terms $r(k+1,n)$ and $s(k+1,n)$ are then successively computed for $k=1,2...(N/2)-2$, using the recursive relationship (2.16). Finally for $k=1,2,...,(N/2)-1$ the products $|X(k)|$. $r(k,n)$ are formed and summed in the second term of (2.14). This process is repeated for all $n = 0,1,..2m$. This method is similar to the standard frequency sampling method for filter design *(Ifeachor & Jervis 1993)*. The filter coefficients $h(n)$, are symmetric about the centre which ensures a

linear phase response is obtained. The exact number of coefficients $L=2m+1$. An example result is shown in Figure 36a and b.

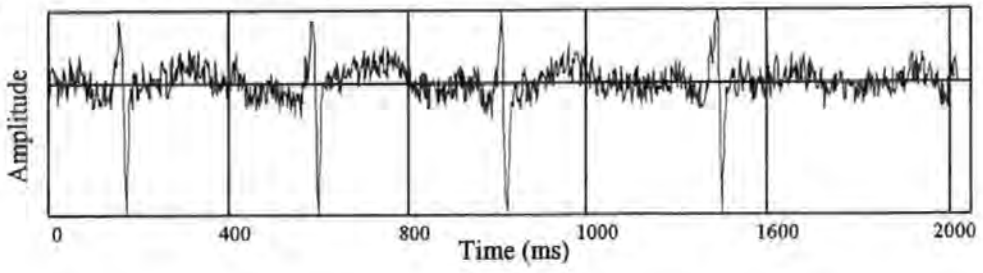

Figure 36a Raw ECG data corrupted with random noise

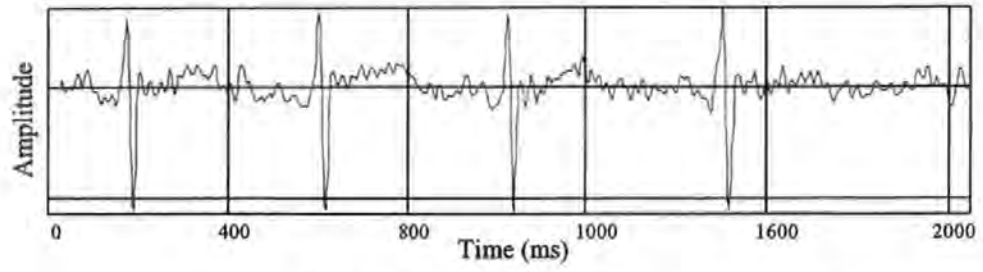

Figure 36b Raw ECG data with noise optimally filtered

The filtered signal in Figure 36b has minimal remaining noise but there is some visible distortion at the onset of the ST segment. The effects of this filter unfortunately can induce a slight ringing just after the J point which is the start of the ST segment. This is not a problem for T/QRS ratio measurement but is a problem for ST segment shape analysis. There are also some real dangers in using this technique in practice. It is essential that a good quality approximation of the signal spectrum is obtained before the filter coefficients are calculated, which is difficult to guarantee without visual inspection. The spectrum can also vary during sudden drops in heart-rate. Since this technique was developed, it was found that a carefully designed fixed linear low-pass filter could achieve very good results without adding any ringing artefact. This is now discussed.

2.5.2 SNR enhancement using fixed linear filtering

A close approximation to the optimal filter is a fixed linear filter with a magnitude response similar to that in Figure 35. The magnitude response is shown in Figure 37a. Given that the signal is pre-filtered with an analogue low-pass filter with a pass-band edge frequency of 100Hz, then the signal energy above 150Hz has

already been attenuated[2]. This is exploited in order to reduce the computational effort of the filter. This is achieved by using the comb-filtering technique as discussed in section 2.3.2. A low pass filter with coefficients *h(n), n=0..36,* is designed with a pass-band edge frequency of 50Hz and a stop-band edge frequency of 65Hz, with at least 40dB attenuation in the stop-band and 0.05dB pass-band ripple. The Remez-exchange algorithm is used to compute the coefficients assuming a sampling rate of 250Hz, the magnitude response of which is shown in Figure 37a. The new filter coefficients *h'(n), n=0..72,* are derived such that

$$h'(n) = \begin{cases} h(floor(n/2)) & n \bmod 2 = 0 \\ 0 & n \bmod 2 \neq 0 \end{cases}$$

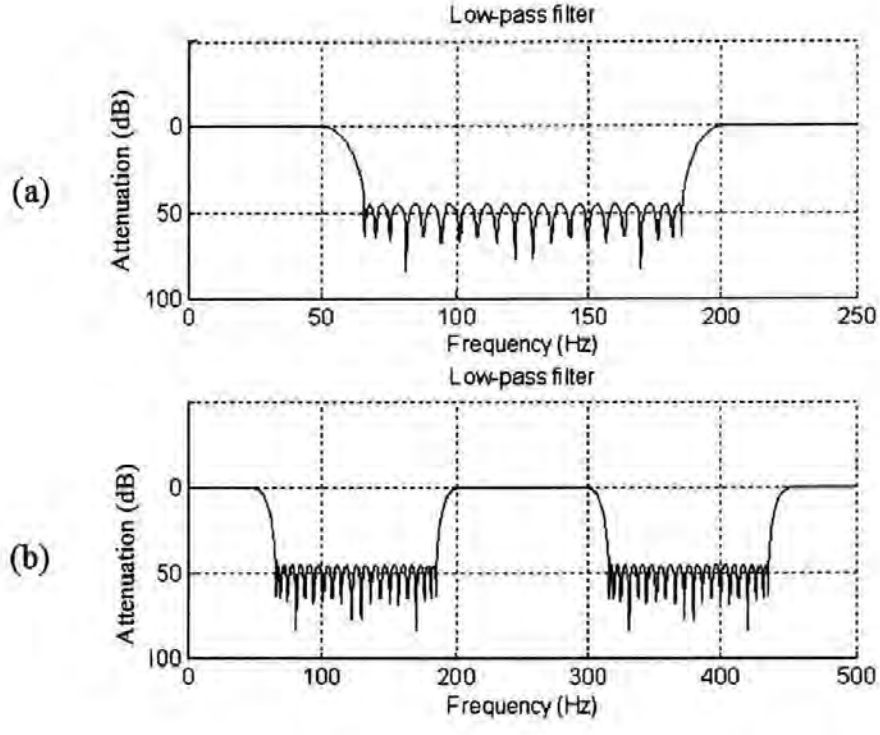

Figure 37 Fixed low-pass filter designed to attenuate muscle noise.

The magnitude response is shown in Figure 37b. There is a strong parallel with conventional multi-rate filter design here. For a multi-rate filter design, the signal would be first pre-filtered to limit the bandwidth to a maximum of 125Hz (which is already performed by an analogue filter in this case), and then every other sample

[2] This may not be the case for adult ECG or for accurate heart-rate analysis.

would be discarded, effectively reducing the sampling rate to 250Hz. The filter design shown in Figure 37a could then be applied and the data would be re-interpolated back up to 500Hz by padding every other sample with zeros. To remove the image frequencies from occurring (*Ifeachor & Jervis 1992*), another low-pass filter would have to be used to limit the bandwidth to 125Hz. Note that each additional digital filter stage will have a finite pass-band ripple, which adds to signal distortion. Using the method described here, only one digital filter stage is required. This way the pass-band ripple is minimised and the decimation and interpolation stages are completely avoided, thus reducing the number of filters and the computational effort.

2.5.3 Signal Averaging

The objective of signal enhancement is to maximise the foetal ECG signal-to-noise ratio (SNR) whilst preserving the useful waveform shape information. The most widely used technique for improving the SNR for repetitive signals, such as the foetal ECG, is signal averaging *(Hon & Lee 1963)*. In general the weighted average signal vector, denoted here as a vector $\boldsymbol{a}$, is computed as

$$\mathbf{a} = \sum_{k=0}^{N-1} x(k) \cdot w(k) \tag{2.17}$$

where $x(k)$, $k=\{0,1,...,N-1\}$, are the individual foetal ECG waveform vectors, $w(k)$ are scalar weightings and N is the number of waveforms in the average. For an arbitrary set of weights $w(k)$, the SNR of the average waveform is theoretically improved by a factor of $\sqrt{\left(\sum_{k=0}^{N-1} w(k)^2\right)}$ over the original raw SNR (See section 2.5.4). For an evenly weighted average, where $w(k)=1/N$, $k=\{0,1,...,N-1\}$, the SNR is theoretically increased by a factor of $\sqrt{N}$. It is shown in section 2.5.4 that this is the theoretical maximum possible improvement that can be obtained for a fixed N, given the assumption that the true signal component is perfectly stationary and the noise is purely random and un-correlated with the signal. This also means the average can be easily updated recursively as shown in (2.18).

$$\mathbf{a}(k+1) = \mathbf{a}(k) + \frac{1}{N}\left(\mathbf{x}(k+1) - \mathbf{x}(k-N+1)\right) \tag{2.18}$$

where $\mathbf{a}(k)$ is the k^{th} average waveform, $\mathbf{x}(k)$ is the k^{th} raw ECG waveform vector and N is the number of waveforms in the average. Unfortunately the foetal ECG signal shape changes over time (non-stationary) and not all the noise sources can be assumed to be random. In particular, the remaining low-frequency noise components in filtered raw signal, such as baseline shifts, tend to be correlated are not completely removed by averaging or filtering. To reduce this effect, one solution is to only include ECG complexes that have low remaining baseline shifts into the average. Despite these limitations, signal averaging is very effective and is very efficient to implement recursively.

In a recent clinical trial (*Westgate et al. 1993*), signal averaging (*N=30*) was used successfully to enhance the ECG signal, it was shown that the T/QRS ratio could be used with the CTG to reduce intervention rates but it was reported that the useable data dropped down to a low 56% in second-stage labour. The current clinical guidelines are based on averaged ECG waveforms, although there is a possibility that clinically significant short term changes might occur near uterine contractions which will be suppressed by the averaging process. Some of the shorter term changes could be preserved by choosing the weighting, *w(k)*, such that the older waveforms have a lesser influence than the more recent, but this in turn would reduce the SNR improvement. To fully understand the problems with averaging, it helps to examine the filtering effect it has on the data.

2.5.4 Averaging and signal-to-noise ratio improvement

It is assumed the corrupted signal vector **y** is the summation of a stationary signal vector **s** and a random noise vector **n**.

$$\mathbf{y} = \mathbf{s} + \mathbf{n} \tag{2.19}$$

The signal power σ^2 is computed as

$$\sigma^2 = \mathbf{y}^T\mathbf{y} = (\mathbf{s}+\mathbf{n})^T(\mathbf{s}+\mathbf{n}) = \mathbf{s}^T\mathbf{s} + 2\mathbf{s}^T\mathbf{n} + \mathbf{n}^T\mathbf{n} \tag{2.20}$$

but as the signal and noise are not correlated,

$$\sigma^2 = \mathbf{s}^T\mathbf{s} + \mathbf{n}^T\mathbf{n} = \sigma_s^2 + \sigma_n^2 \tag{2.21}$$

assuming the noise has constant variance. The signal-to-noise ratio is thus computed as

$$\text{SNR} = \sqrt{\frac{\sigma_s^{\,2}}{\sigma_n^{\,2}}}. \tag{2.22}$$

Now, consider an averaged signal vector

$$\mathbf{a} = \sum_{k=0}^{N-1} w(k) \cdot \mathbf{y}(k) = \sum_{k=0}^{N-1} w(k) \cdot \big(\mathbf{s}(k) + \mathbf{n}(k)\big) \tag{2.23}$$

where *w(k)* are scalar weightings. Splitting this into two summations

$$\mathbf{a} = \sum_{k=0}^{N-1} w(k) \cdot \mathbf{s}(k) + \sum_{k=0}^{N-1} w(k) \cdot \mathbf{n}(k). \tag{2.24}$$

The total signal power $\sigma_{av}^{\,2}$ is

$$\begin{aligned} \sigma_{av}^{\,2} &= \mathbf{a}^{\mathrm{T}}\mathbf{a} \\ &= \left(\sum_{k=0}^{N-1} w(k) \cdot \mathbf{s}(k) + \sum_{k=0}^{N-1} w(k) \cdot \mathbf{n}(k)\right)^{T} \left(\sum_{k=0}^{N-1} w(k) \cdot \mathbf{s}(k) + \sum_{k=0}^{N-1} w(k) \cdot \mathbf{n}(k)\right) \end{aligned} \tag{2.25}$$

The signal component is stationary therefore

$$\sigma_{av}^{\,2} = \mathbf{a}^{\mathrm{T}}\mathbf{a} = \left(\mathbf{s} \cdot \sum_{k=0}^{N-1} w(k) + \sum_{k=0}^{N-1} w(k) \cdot \mathbf{n}(k)\right)^{T} \left(\mathbf{s} \cdot \sum_{k=0}^{N-1} w(k) + \sum_{k=0}^{N-1} w(k) \cdot \mathbf{n}(k)\right) \tag{2.26}$$

and as the weights all sum to unity gives

$$\begin{aligned} \sigma_{av}^{\,2} &= \mathbf{a}^{\mathrm{T}}\mathbf{a} = \left(\mathbf{s} + \sum_{k=0}^{N-1} w(k) \cdot \mathbf{n}(k)\right)^{T} \left(\mathbf{s} + \sum_{k=0}^{N-1} w(k) \cdot \mathbf{n}(k)\right) \\ &= \mathbf{s}^{\mathrm{T}}\mathbf{s} + 2 \cdot \mathbf{s}^{T} \left(\sum_{k=0}^{N-1} w(k) \cdot \mathbf{n}(k)\right) + \left(\sum_{k=0}^{N-1} w(k) \cdot \mathbf{n}(k)\right)^{T} \left(\sum_{k=0}^{N-1} w(k) \cdot \mathbf{n}(k)\right) \\ &= \mathbf{s}^{\mathrm{T}}\mathbf{s} + 0 + \left(\sum_{k=0}^{N-1} w(k) \cdot \mathbf{n}(k)^{T} \cdot w(k) \cdot \mathbf{n}(k)\right) \\ &= \sigma_s^{\,2} + \left(\sum_{k=0}^{N-1} w(k)^2 \mathbf{n}(k)^{T} \mathbf{n}(k)\right) \\ &= \sigma_s^{\,2} + \sum_{k=0}^{N-1} w(k)^2 \cdot \sigma_n^{\,2} = \sigma_s^{\,2} + \sigma_n^{\,2} \cdot \sum_{k=0}^{N-1} w(k)^2 \end{aligned} \tag{2.27}$$

Assuming the noise is random and of constant variance and the signal and noise are statistically independent. Therefore the signal-to-noise ratio

$$SNRav = \sqrt{\frac{\sigma_s^{\,2}}{\sigma_n^{\,2} \cdot \sum_{k=0}^{N-1} w(k)^2}}. \tag{2.28}$$

To maximise the SNR, $w(k)=1/N$ for all k,

$$SNRav = \sqrt{\frac{\sigma_s^2}{\sigma_n^2 \cdot 1/N}} = \sqrt{N} \cdot SNR. \qquad (2.29)$$

This is easily proven by the following

$$SNRav = \sqrt{\frac{\sigma_s^2}{\sigma_n^2 \cdot p}} \; where \; p = \sum_{k=0}^{N-1} w(k)^2 = \mathbf{w}^T \mathbf{w} \qquad (2.30)$$

and where the constraint $\sum_{k=0}^{N-1} w(k) = 1$. The objective is to minimise the noise power of the average, therefore minimise $\sigma_n^2 \cdot p$. Differentiating p with respect to **w** and using lagrange multipliers to constrain the solution.

$$\begin{aligned} &\nabla_w p = \nabla_w \left\{ \mathbf{w}^T \mathbf{w} + \lambda \left(\mathbf{1}^T \mathbf{w} - 1 \right) \right\} = 2\mathbf{w}^T + \lambda \mathbf{1}^T \\ &\therefore w = \frac{\lambda}{2} \cdot \mathbf{1} \end{aligned} \qquad (2.31)$$

Therefore for a maximum SNR all the elements of ***w*** are equal. This means all waveforms in the average waveform have an equal contribution. In this application it would be preferable if the most recent waveforms had greater emphasis than the older waveforms in the average. This would help account for any shape changes in the ECG waveform. An alternative technique, which does not apply an even weighting, is examined in the next section.

2.5.5 Time Coherent Filtering

Averaging is in fact a linear 'time coherent filter'. For an ensemble of N ECG waveforms (vectors) , $\boldsymbol{x}(i)$, $i=\{0,1..N-1\}$, composed of stationary signal vector $\boldsymbol{s}$ added to a random noise vector $\boldsymbol{n}(i)$ then the simplest averaging procedure is to compute the arithmetic mean vector $\mathbf{y} = 1/N \sum_{i=0}^{N-1} \mathbf{x}(i)$.

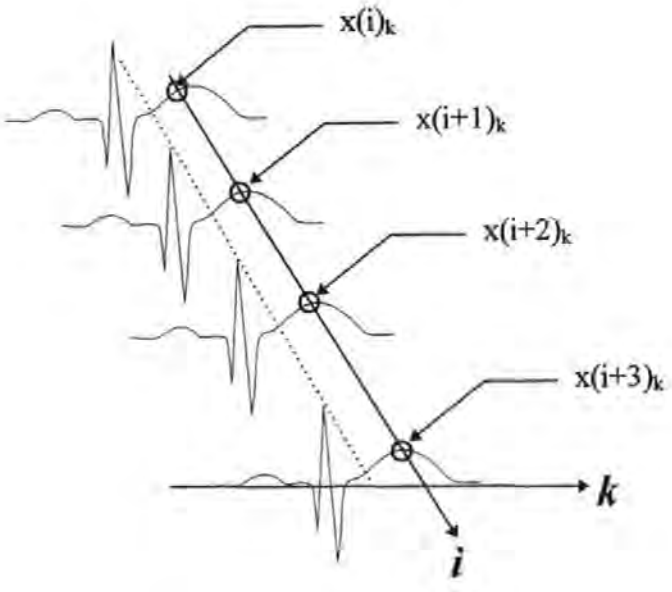

Figure 38 Illustration of time coherent sampling

Considering the k^{th} data point y_k of the average vector y, this can be written as a linear FIR time coherent filter

$$y_k = \sum_{i=0}^{N-1} h_i \cdot \mathrm{x}(n)_k \tag{2.32}$$

where the filter coefficients $h_i = 1/N$ for a simple average where $x(n)_k$ is the k^{th} sample of the n^{th} waveform in the ensemble (see Figure 38). Taking the Z transform, this can be written in the frequency domain as

$$Y(Z) = \sum_{i=0}^{N-1} h_i \cdot Z^{-i} \cdot X(Z)_k \tag{2.33}$$

where N is the number of waveforms in the average, $Z=e^{jwT}$, w is the angular frequency and T is the period between each beat, which is determined by the heart rate. To examine the filtering effect of the averaging process, $x(n)_k$ in (2.32) is assumed to be an impulse, hence $X(Z)=1$ in (2.33). In Figure 39, the amplitude response $|Y(w)|$ of the averaging process for $N=10$, $N=20$, $N=30$ and $N=50$ beats are compared assuming a constant heart-rate. Given the condition that **s** is perfectly stationary and the noise $\mathbf{n}(i)$ is purely random, $h_i=1/N$ is the optimum choice of filter coefficients to maximise the expected SNR. It is observed in Figure 39, that as N is increased from 10 to 50 the frequency of the first zero reduces, but the stop-band attenuation is a constant of approximately 13.5dB. If **s** was perfectly stationary

there would be no limit on N, and every waveform could be averaged in the labour as it is collected. Of course s does change through labour otherwise there would be no changes in the ECG to analyse. Given that it is known that s does change with time then the averaging process is viewed as time-coherent low-pass filtering process, passing the slowest changes and rejecting the more rapid changes (assumed to be caused by noise). Evenly weighted averaging is seemingly an inefficient low pass filter, with $h_i=1/N$, the maximum stop-band attenuation was measured as approximately 13.5 dB for all values of N (see Figure 39). To increase attenuation, N must be increased and the weights $w(i)$ cannot be equal.

An assumption given above was that the heart-rate was constant and therefore the time interval between each sample was also constant. However, a change in heart-rate corresponds to a change in the interval between samples, so doubling the heart-rate (sampling rate) would half the interval between the samples and this has a profound effect on the filtering properties of the filtering process. The time coherent signal $x(n)_k$, $n=\{0,1..N-1\}$, can be considered as a sampled time series, where *the instantaneous sampling rate is the instantaneous heart-rate*. If the heart-rate was constant and the foetal ECG was truly periodic, then time-coherent filtering would be a linear filtering process, but this is certainly not the case with the foetal ECG. For any fixed filter, the band edges are a fixed proportion of the sampling rate. If the heart rate reduces then the effective sampling rate reduces, and hence the absolute filter band-edge frequencies reduce correspondingly. Changes in the ECG are a chemical process which is related to time and not the number of heart beats in time. It can be concluded therefore that by using simple signal averaging, more "information" is removed from the ECG signal at lower heart-rates. This is because ECG changes are chemically induced (time dependant) and independent of the heart-rate.

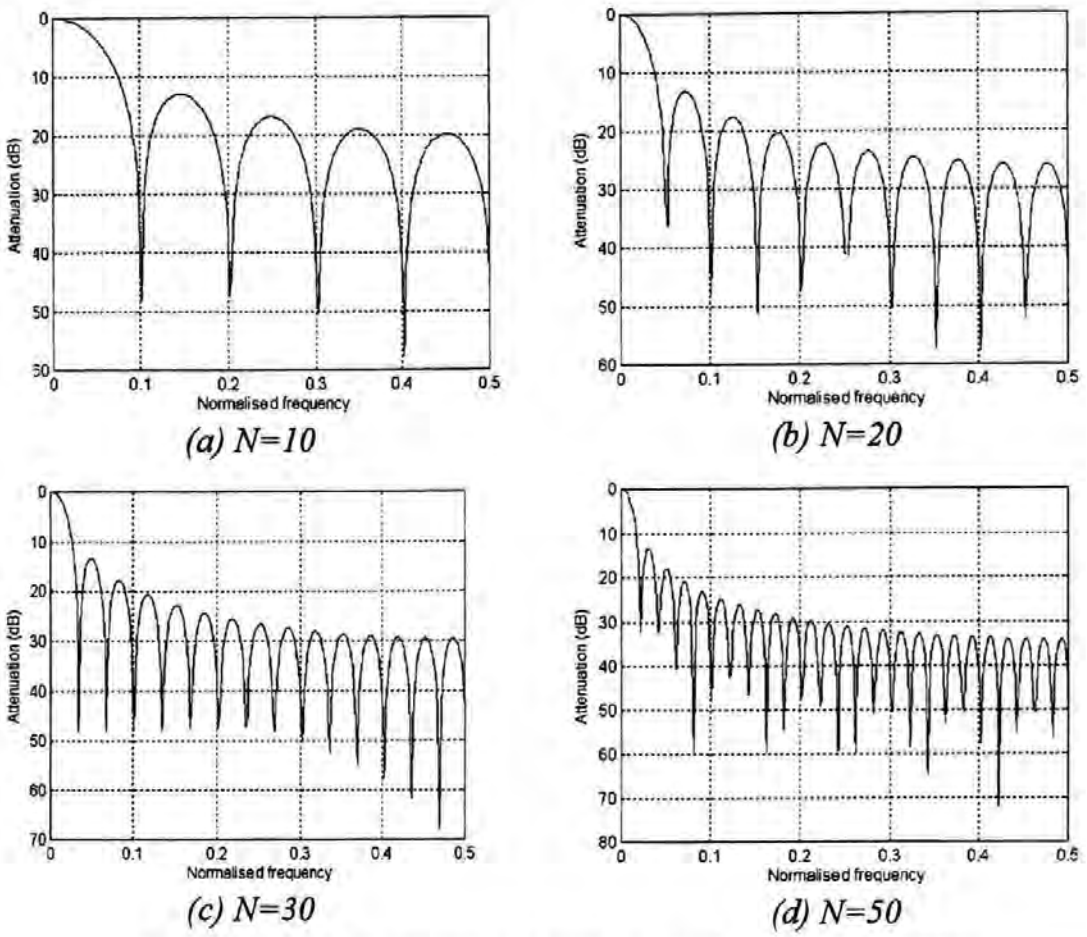

Figure 39 Magnitude response of evenly weighted average (HR=120 bpm) (a) N=10, (b) N=20, (c) N=30 & (d) N=50

Such filtering is an uncontrolled multi-rate filter, where ECG at a lower heart-rate implies a filter with lower band-edge frequencies. In reality the heart rate continuously fluctuates, so the filtering process can be considered as a filter in the Z domain of the form.

$$H(e^{j\omega}) = h_0 + h_1 e^{j\omega T_1} + h_2 e^{j\omega(T_1+T_2)} + h_3 e^{j\omega(T_1+T_2+T_3)} + \ldots + h_m e^{j\omega \sum_{i=1}^{N} T_i} \qquad (2.34)$$

where T_i, $i=\{1..N\}$, are the time intervals between each heart beat as shown in Figure 40 and h_k, $k=1..m$, are the filter coefficients. In the case of a sudden heart-rate deceleration, the results would be very unpredictable.

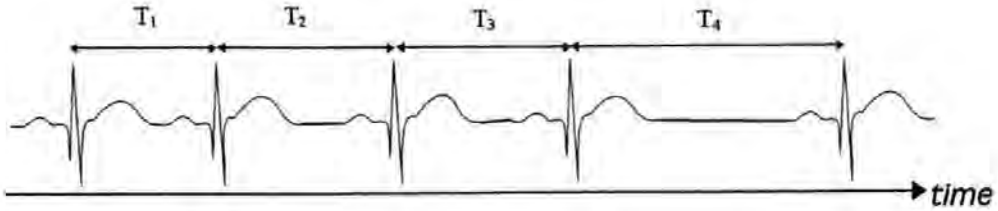

Figure 40 Changing time intervals between consecutive heart beats

To overcome this problem, a practical solution is to re-sample every data point evenly at the highest possible rate that would naturally occur (200 bpm)[3]. Linear interpolation or cubic spline interpolation can be used for this purpose (see Figure 41). In the circles are the m^{th} points of 5 waveforms. These are linearly interpolated and re-sampled at the 200bpm.

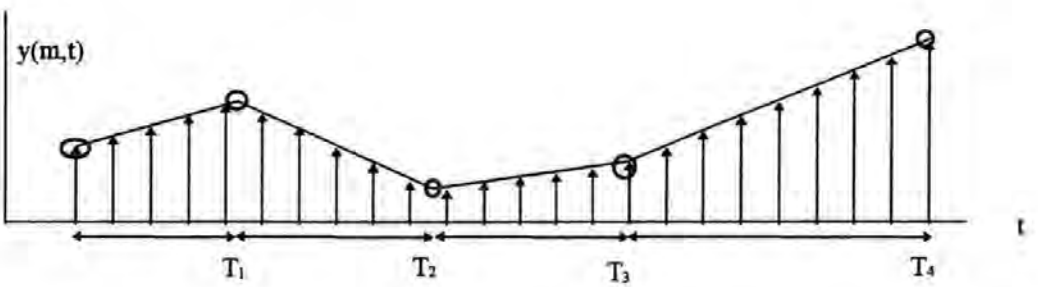

Figure 41 Linear interpolation and re-sampling

Now the data is evenly sampled at the constant sampling rate of 200 bpm (200/60 Hz) any shape changes are filtered consistently by the time-coherent filter. A magnitude response of an evenly weighted 30 beat average process is shown in Figure 42(a) and a time-coherent filter magnitude response with similar band-edge frequencies is shown in Figure 42(b).

[3] Not allowing for ectopic beats which can even overlap another ECG waveform.

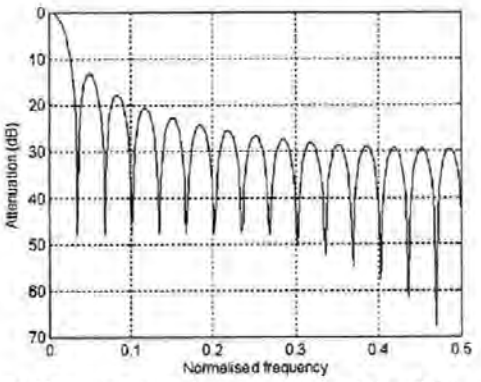

(a) The magnitude response of the 30 beat average

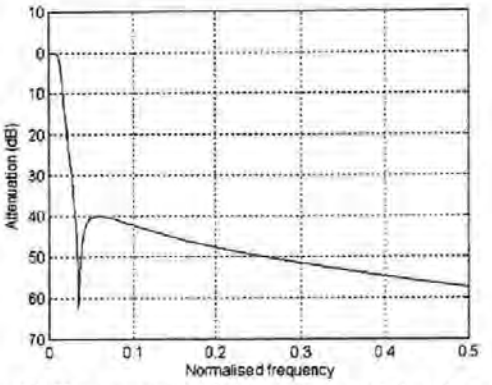

(b) The magnitude response of the time coherent filter

Figure 42 Magnitude response of (a) a 30 beat average and (b) a time-coherent IIR filter

The filter used here is a 4th order recursive elliptic filter which achieves over double the stop-band attenuation (40dB) of the simple average (13.5 dB). With each new ECG waveform vector **x** of length 200, each sample **x**(k), $k=1..200$, is passed into a separate filter (see Figure 43) to produce a new sample **y**(k). A typical result is shown in Figure 44c.

Section 1	a_0=0.01304901795719	a_1=0.013049017957200	a_2=0.00000000000000
	b_0=1.00000000000000	b_1=-0.97390196408560	b_2=0.00000000000000
Section 2	a_3=0.10147437436674	a_4=-0.20181543365985	a_5=0.10147437436675
	b_3=1.00000000000000	b_4=-1.97541693087758	b_5=0.97655024595117

Table 1 Filter coefficients for the time-coherent filter

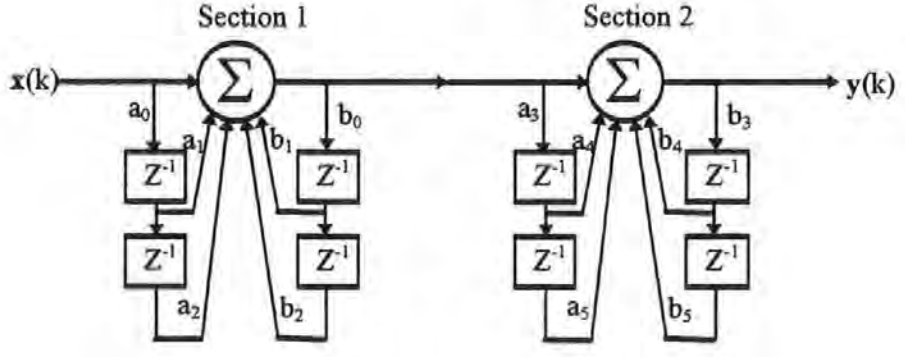

Figure 43 Fourth order recursive filter structure

This structure is convenient to implement as it only requires the previous four ECG waveform vectors to be stored in memory. There is no visible distortion of the ECG waveforms using this technique provided enough numerical accuracy is available. The coefficients given in Table 1 are produced using the MATLAB® Signal Processing Toolbox. The source code is provided in Appendix A. Unlike the simple

averaging algorithm, this technique is not suitable for integer arithmetic and so is computationally more expensive. The result of time coherent filtering is very similar to even weighted signal averaging. An example is given in Figure 44. The non-linear phase response around the transition band of the recursive filter does not appear to induce any signal distortion, so it is assumed that the pass-band edge is beyond the bandwidth of the time-coherent ECG signal. This is a reasonable assumption as *only a very small signal change is expected between each ECG waveform*, whereas the spectrum of the noise is expected to be evenly distributed across the whole spectrum. This technique does not allow for jitter due to incorrect waveform alignment however, which induces a ringing effect over several waveforms. In practice this only occurs near the sharp transitions of the ECG, such as the R-S slope. This can make QRS amplitude measurements unreliable which in turn affects all the measured features. The additional attenuation in the stop-band does not seem to have enough benefit to warrant using recursive time-coherent filtering.

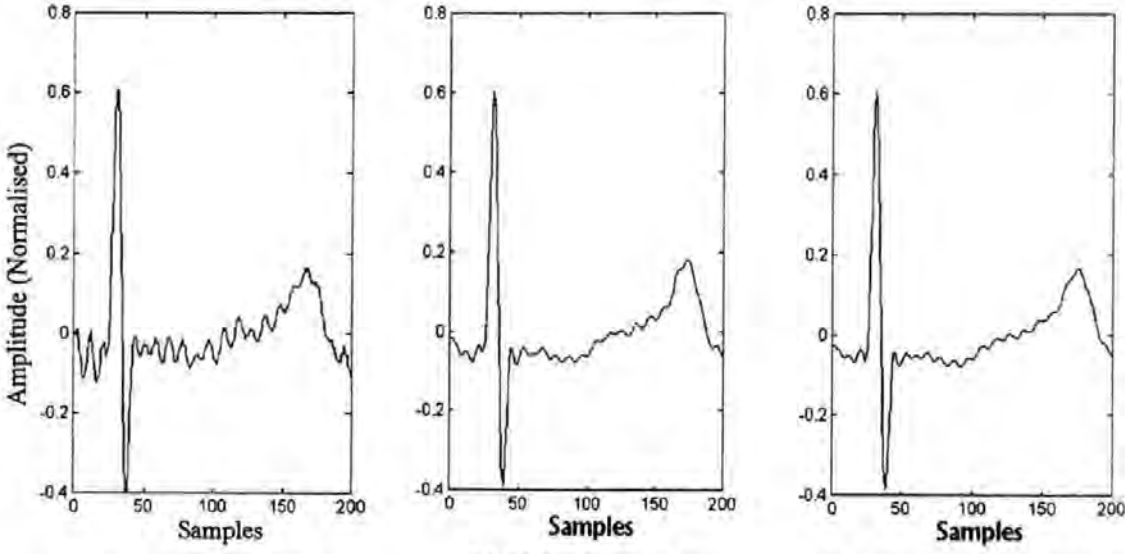

Figure 44 A comparison of the (a)raw, (b) 30-beat-average waveform and (c) time-coherent filtered waveform

2.6 Quality assessment

The signal processing techniques discussed so far are all designed such that the minimum information is lost from the signal. An attempt to enhance and use very poor quality data would require over filtering of the signal and hence produce unreliable measurements. The philosophy of this work has been to keep and

enhance what is safe for analysis, and reject all the bad quality sections of the data. The primary source of error is baseline shift noise. Baseline shift cannot always be completely removed by linear filtering when the signal quality is poor and thus it remains a source or error. Attempts to remove severe baseline shift will distort the important slow moving components of the foetal ECG waveform, such as the ST segment shape, so the data must be rejected. It is essential that the amount of remaining baseline shift energy (after signal enhancement) is quantified and is used as part of the data rejection criteria.

2.6.1 Approximation and Assessment of Baseline Shift Noise

Baseline shift, such as that shown in Figure 45, hinders accurate measurement of ECG features. There are some very real dangers in extracting features from data with high levels of baseline shift.

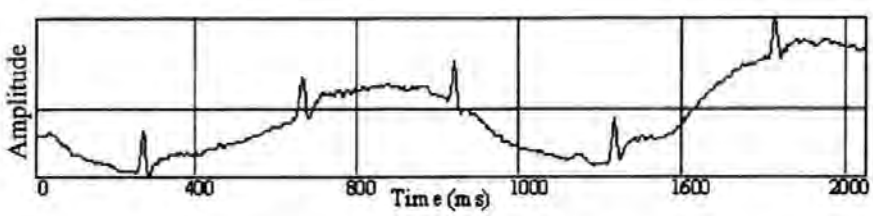

Figure 45 Baseline shift in foetal ECG data

Most of the energy in the baseline shift is low frequency, between 0 and 2Hz, and may be removed by linear filtering. Some baseline shift energy, such as transient shifts caused by the movement of the scalp electrode, extend far beyond the 0-2Hz band. An attempt to remove such noise would require a degree of filtering which would destroy the ST waveform shape. There is also no need to remove such artefact as these episodes are usually only short lasting with enough remaining good data to work with. If there is not, then it is vital that clinicians are made aware of the problem as the electrode is incorrectly attached. It is far more important to have a measure of the data quality so that bad periods of data can be rejected.

A first attempt was made using the Discrete Fourier Transform (DFT) and a Multi-Layered Perceptron (*Ifeachor et al. 1993*). A selection of data were extracted and graded manually. The data was normalised with respect to the average QRS amplitude, and the low frequency magnitude spectrum computed with the DFT. The

resulting vector of 18 values was reduced down to 10 using singular value decomposition (SVD) and passed to a multi-layered-perceptron for training and testing. Performance on the available data was reasonable, details of which are given in a work-shop paper *(Ifeachor et al. 1993)*. This technique has been superseded by a new method.

The new method uses a polynomial approximation of the baseline shift noise from which data quality features can be measured and interpreted. This much more robust and predictable method uses fuzzy logic to interpret the features (the concepts of fuzzy logic are described in chapter 5). The approximation can be used to subtract remaining baseline shift noise from the signal. Approximation of the baseline shift, in the minimax sense, may be closely achieved by curve-fitting methods based on Chebyshev polynomials.

2.6.2 Chebyshev Polynomial Approximation

Any continuous function $x(t)$ may be approximated by a linear combination of a set of polynomial functions $\{\phi_k(t) \mid k=0,1,...,n\}$. The subscript k denotes the degree of the polynomial function $\phi_k(t)$. Thus, we can approximate the baseline $B(t)$ as

$$B(t) = c_0\phi_0(t) + c_1\phi_1(t) + c_2\phi_2(t) + ... + c_n\phi_n(t) \equiv \sum_{k=0}^{n} c_k\phi_k(t) \qquad (2.35)$$

We wish to choose the set of functions $\{\phi_k(t)\}$ and the coefficients $\{c_k\}$ such that $B(t)$ has the smallest maximum deviation from the function $x(t)$. This is none other than the mini-max approximation of degree n, which is unfortunately difficult to compute precisely. However, by choosing the set of functions $\{\phi_k(t)\}$ to be the set of Chebyshev Polynomials $\{T_k(t)\}$ defined over the interval $-1 \le t \le 1$, we can obtain an approximating polynomial $B(t)$ which is almost identical to the true mini-max approximation and is simple to compute. The Chebyshev polynomial *(Burden & Faires 1989)* of degree k is defined as

$$T_k(t) = \cos(k \cdot \cos^{-1}(t)), \quad -1 \le t \le 1 \qquad (2.36)$$

hence we can rewrite (2.37) as

$$x(t) \approx c_0T_0(t) + c_1T_1(t) + c_2T_2(t) + ... + c_nT_n(t) = \sum_{k=0}^{n} c_kT_k(t) = B(t) \qquad (2.37)$$

The problem of baseline approximation then reduces to one of finding the values of the coefficients $\{c_k\}$ and the Chebyshev polynomials $\{T_k(t)\}$. A significant property of the Chebyshev polynomials is that they are orthogonal with respect to the weighting function

$$w(t) = \frac{1}{\sqrt{1-t^2}}, \text{ i.e.}$$

$$\int_{-1}^{+1} T_j(t) \cdot T_k(t) \cdot \frac{1}{\sqrt{1-t^2}} dt = \begin{cases} 0, i \neq j \\ \pi, i = j = 0 \\ \frac{\pi}{2}, i = j \neq 0 \end{cases} \qquad (2.38)$$

This property allows us to compute each coefficient c_k simply as follows. If (2.37) is multiplied throughout by $T_k(t).w(t)$ and both sides are integrated over the interval $-1 \leq t \leq 1$ then from property (2.38) it follows that

$$\int_{-1}^{1} x(t) \cdot T_k(t) \cdot w(t) dt = \int_{-1}^{1} c_k \cdot T_k(t) \cdot T_k(t) \cdot w(t) dt = c_k \cdot \alpha \quad \text{where} \quad \alpha = \begin{cases} \pi & , k = 0 \\ \pi/2 & , k > 0 \end{cases}$$

(2.39)

since all the other integrals vanish identically. Hence

$$c_k = \frac{1}{\alpha} \cdot \int_{-1}^{1} x(t) \cdot T_k(t) \cdot w(t) dt \qquad (2.40)$$

Direct evaluation of (2.39) leads to large numerical errors since $w(t)$ becomes infinite at $t=-1$ and $t=+1$. However this problem is circumvented by the simple substitution of $t=cos(q)$ into which yields the result

$$c_k = \frac{1}{\alpha} \cdot \int_0^{\pi} x(cos(\theta)) \cdot cos(k\theta) d\theta \qquad (2.41)$$

This may be re-written as a sum of integrals over N discrete intervals

$$c_k = \frac{1}{\alpha} \cdot \sum_{m=0}^{N-1} \int_{\frac{m\pi}{N}}^{\frac{(m+1)\pi}{N}} x(cos(\theta)) \cdot cos(k\theta) d\theta \qquad (2.42)$$

and when N is sufficiently large, each integrand may be linearly approximated over its interval of duration p/N. Therefore, each term in the above sum can be approximated using the trapezoidal rule for integration *(Kreyszig E. 1993)* as

$$c_k \approx \frac{1}{\beta} \cdot \left\{ \sum_{m=0}^{N-1} x(y_1(m)) \cdot y_k(m) \right\} \quad , \quad \beta = \begin{cases} \frac{N}{2} & ,k > 0 \\ N & ,k = 0 \end{cases} \tag{2.43}$$

where $y_k(m) = \cos(k \cdot \frac{m}{N} \cdot \pi)$. In practice, the function x is given by a sampled sequence $x_0, x_1, \ldots, x_{N-1}$ therefore to account for this we can re-write (2.42) as

$$c_k \approx \frac{1}{\beta} \cdot \left\{ \sum_{m=0}^{N-1} x[i_m] \cdot y_k(m) \right\} \tag{2.44}$$

where $i_m = round\left\{ \frac{N}{2} \cdot [1 + y_1(m)] \right\}$ and *round(x)* is the nearest integer to x.

Direct on-line evaluation of (2.44) for all k and t is computationally inefficient because of the need to evaluate the trigonometric functions sine and cosine. Whereas these values could be pre-computed off-line and stored in memory, where memory does not permit this the following recursive algorithm can be used.

$$\begin{bmatrix} y_k(m+1) \\ s_k(m+1) \end{bmatrix} = \begin{bmatrix} y_k(1) & -s_k(1) \\ s_k(1) & y_k(1) \end{bmatrix} \cdot \begin{bmatrix} y_k(m) \\ s_k(k,m) \end{bmatrix} \tag{2.45}$$

where $s_k(m) = sin(k \cdot \frac{m}{N} \cdot \pi)$.

which is readily derived from the additive trigonometric identities as follows.

$$\begin{aligned} y_k(m+1) &= \cos\left(\frac{k\pi}{N} \cdot (m+1)\right) = \cos\left(\frac{k\pi}{N}\right) \cdot \cos\left(\frac{k\pi m}{N}\right) - \sin\left(\frac{k\pi}{N}\right) \cdot \sin\left(\frac{k\pi m}{N}\right) \\ &\equiv y_k(1) \cdot y_k(m) - s_k(1) \cdot s_k(m) \\ s_k(m+1) &= \sin\left(\frac{k\pi}{N} \cdot (m+1)\right) = \sin\left(\frac{k\pi}{N}\right) \cdot \cos\left(\frac{k\pi m}{N}\right) + \cos\left(\frac{k\pi}{N}\right) \cdot \sin\left(\frac{k\pi m}{N}\right) \\ &\equiv s_k(1) \cdot y_k(m) + y_k(1) \cdot s_k(m) \end{aligned} \tag{2.46}$$

2.6.3 Evaluation of Chebyshev Polynomials

Direct evaluation of the Chebyshev polynomials $T_k(t) = cos(k \cdot cos^{-1}(t))$ is computationally inefficient since it requires the evaluation of two trigonometric functions. An efficient technique that does not involve direct computation of any trigonometric functions is derived using Clenshaw's Recurrence Formula *(Press et al. 1992, Clenshaw 1962)*. This is an algorithm for evaluating a linear combination of functions $B(t) = \sum_{k=0}^{n} c_k \phi_k(t)$, where the functions $\{f_k(t) \mid k=0,1,\ldots,n\}$ satisfy a

second order recurrence relationship of the form $f_{k+1}(t) = a_k(t).f_k(t) + b_k(t).f_{k-1}(t)$ in which case we can evaluate $B(t)$ directly using the equation:

$$B(t) = b_1(t).f_0(t).p_2 + f_1(t).p_1 + f_0(t)c_0 \qquad (2.47)$$

Where the quantities p_k are recursively computed by

$$p_k = a(k,t).p_{k+1} + b(k+1,t).p_{k+2} + c_k \qquad (2.48)$$

where $k=n,n-1,...,1$ and the initial conditions $p_{n+2}=p_{n+1}=0$. The Chebyshev polynomials satisfy the second order recursive relationship $T_{k+1}(t)=2.t.T_k(t)+(-1).T_{k-1}(t)$ and therefore setting $a(k,t)=2.t$ and $b(k,t) = -1$ it is seen that Clenshaw's algorithm is directly applicable to the approximation $B(t)$ in (2.35).

$$B(t)=-1\cdot T_0(t)\cdot p_2+T_1(t)\cdot p_1+T_0(t)\cdot c_0 \equiv -1\cdot p_2+t\cdot p_1+c_0 \qquad (2.49)$$

where $p_k=2t\cdot p_{k+1}+(-1)\cdot p_{k+2}+c_k$, $k=n,(n-1),...,1$ and where $p_{n+1}=0$ and $p_{n+2}=0$. Typical results of using these techniques to estimate and remove baseline shifts are shown in figure 4a and figure 4b (A 6th order polynomial fit to 1024 sample data points was used).

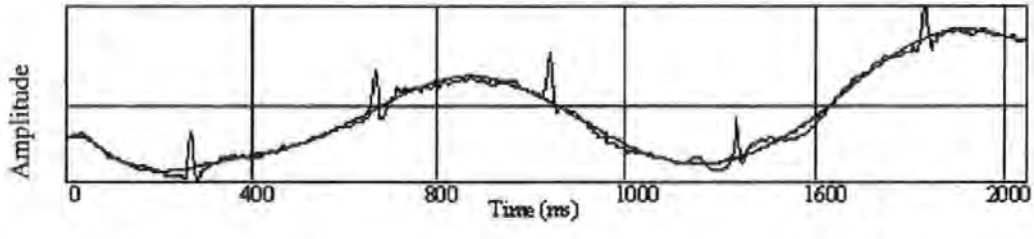

Figure 46a Approximation of the baseline shift in raw foetal ECG data

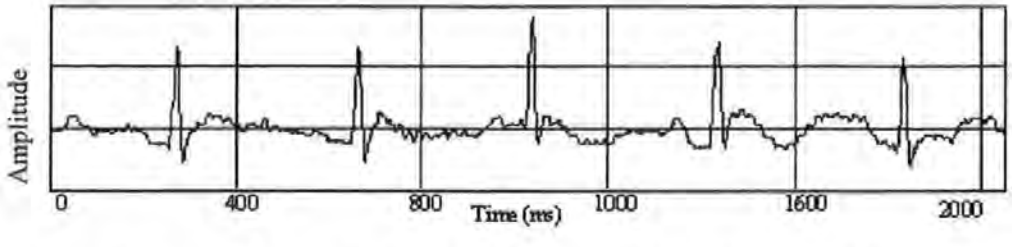

Figure 46b Removal of baseline shift from the raw foetal ECG data

The approximation to the baseline shift can be observed as the smooth curve in Figure 46a. The ECG corrected for baseline shifts is shown in Figure 46b. In this example the baseline shift may be too severe to measure sensitive features such as ST depression.

2.6.4 Determining the degree of approximation

The selection of the degree, n, is important to ensure that only the slow moving components of the data are approximated. If n is too low then the approximation would fail to approximate the baseline shift accurately. If n is too high this results in over-fitting which would tend to approximate the foetal ECG signal itself rather than just the baseline shift. This manifests itself as ringing. A technique is described here to estimate the required degree of approximation, whilst also greatly reducing the computational overhead.

Removing all the energy above 6Hz preserves the baseline shifts removes the Q,R and S peaks which can otherwise introduce errors when approximating the baseline shift. The data is filtered with a low pass filter (see Figure 48) to remove all frequency components above 6Hz. From Shannon's sampling theorem, the sampling rate can therefore be reduced to a minimum of 12Hz without loss of information. The sampling rate is therefore reduced by a factor of 40 from 500Hz down to 12.5Hz. This greatly reduces the number of data points N from 1000 to 25 and thus reduces the computational effort required to compute the approximation. The schematic diagram for this process is summarised in Figure 47. The filter design does not require linear phase and so a recursive filter is used for computational efficiency.

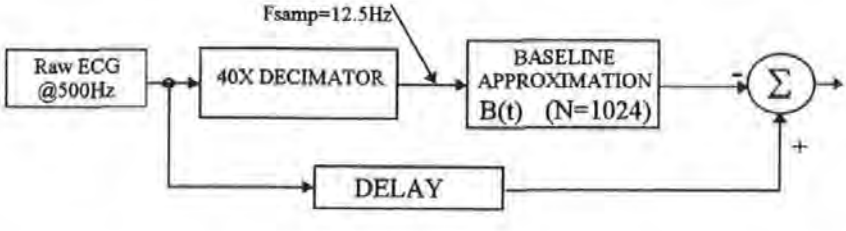

Figure 47 Enhanced baseline approximation using multi-rate filter technique

The filter specification is specified in Table 2. The magnitude and phase response are shown in Figure 48.

Pass band edge=5Hz
Stop Band Edge=6Hz
Pass band ripple=0.5dB
Stop Band Attenuation=40dB

Table 2 Specification for the decimation filter

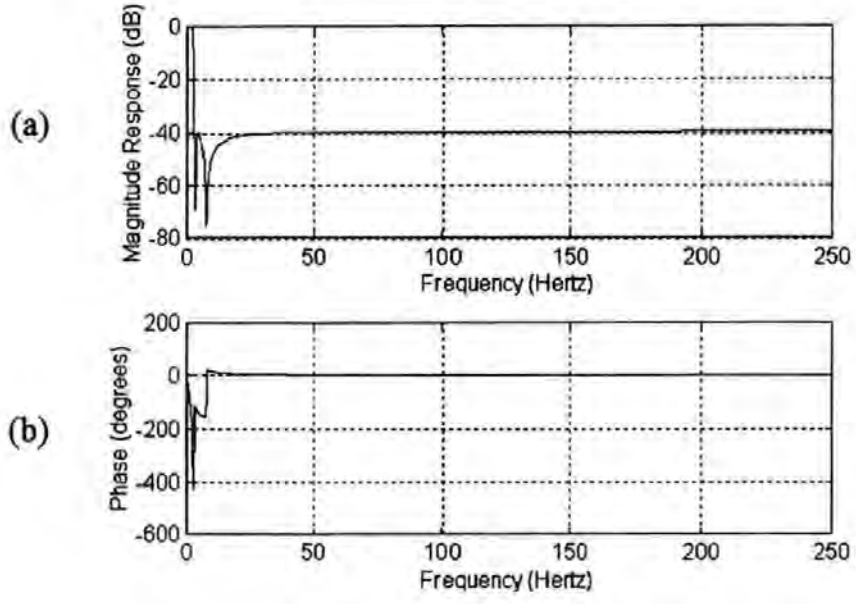

Figure 48 Magnitude and phase response of the sixth order recursive filter used for baseline shift approximation

This filter is a recursive digital filter designed using the MATLAB® Signal Processing Toolbox. This was based on an 6th order elliptic analogue filter prototype. It is implemented using 3 cascaded second order sections. A problem with this design is determining the delay through the filter, and hence the delay of the decimator. The delay, at a given frequency ω, is given by the derivative of the phase with respect to frequency, that is $\tau_g(\omega) = -\frac{d}{d\omega}\phi(\omega)$ where $\tau_g(\omega)$ is known as the group delay, $\phi(\omega)$ is the phase angle at frequency ω (radians per second) (*Proakis 1992*). Clearly from Figure 48 the derivative is not constant, and therefore it follows that the delay at each frequency ω is different, which illustrates the phenomenon known as phase distortion.

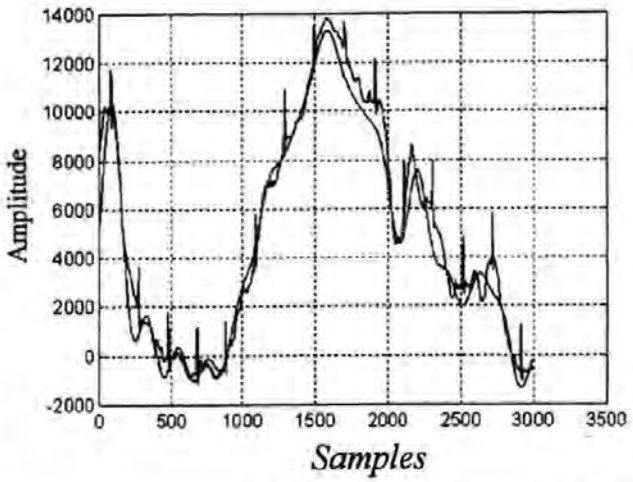

Figure 49 Poor quality raw ECG data and the output of the decimation filter

The estimated delay through the filter is approximately 120 samples, and this is taken to be the delay through the filter. The delayed raw signal and the output of the filter are shown in Figure 49. In summary, the addition of the decimating stage preserves most of the baseline shift information, greatly reduces the influence of the Q, R and S peaks on the approximation and reduces computational overhead at the cost of one extra filter.

The degree of the polynomial can now be calculated as follows.

1. Fit a Chebyshev polynomial of degree n to the decimated data. From experience $n=6$ is adequate.
2. Set $n=0$
3. Truncate and calculate the polynomial degree to degree n, i.e. $B(t) = \sum_{k=0}^{n} c_k \cdot T_k(t)$
4. Measure the approximation error $\varepsilon = \max(|x(m) - B(-1+2*m/(N-1))|)/QRS, m = 0...N$ where N is the number of samples in the data *(typically $N=1000/40=25$)*.
5. If $\varepsilon > 0.1$ and $n < 6$ then increment n and goto 3

The threshold error of 0.1 relates to an error of 0.1*QRS amplitude. This is an empirical value and could be changed to adjust the sensitivity of the algorithm. Fuzzy logic (see chapters 5 and 6) is used to interpret the error term ε.

2.6.5 Assessment of baseline shift using Fuzzy Logic

Given that a curve of degree n is fitted to a window of N filtered ECG samples, a simple measure of remaining baseline severity may be derived from the following parameters.

1. The degree of the polynomial approximation n.
2. The normalised span ε of the baseline approximation, where

$$\varepsilon = \left(\left|\max(B(t)) - \min(B(t))\right| / QRS\right), t = -1..1$$

The normalised span is a measure the baseline shift peak-to-peak amplitude relative to the QRS amplitude. In the presence of a sharp transient shift the degree of the approximation will be high in order to approximate the baseline shift accurately.

Degree n-> / Span ε	LOW	MED	HIGH
LOW	Good	Int.	Int.
MED	Int	Int.	Poor
HIGH	Poor	Poor	Poor

Table 3 Baseline quality decision matrix

Interpretation of these features is based on a set of simple rules which are used to grade this data into one of three categories, *{Good, Intermediate and Poor}*. The rules used are summarised in the Table 3.

The adjectives *High*, *Medium* and *Low* are modelled using "fuzzy sets", with full details given in chapter 6. The fuzzy system returns a single quality index between 0 and 1, where 0 is a complete rejection and 1 is complete acceptance. A low threshold value of 0.3 is used to ensure no poor quality data is accepted any further into the system.

2.6.6 Assessing random noise and short-term transients

The measure of baseline shifts is not sensitive to all types of noise and artefact, such as movement artefact, which often induces a small transient shift in the data and distorts the ECG signal and random noise which adds errors to important features such as the QRS amplitude. Two additional techniques designed to assess these other forms of noise are now discussed and compared.

2.6.7 Estimating the Signal-To-Noise Ratio for an Ensemble of ECG Waveforms Using Eigenvalue Analysis.

Given an ensemble of N ECG waveform vectors $\mathbf{x}(k)$ of length M, $k=0..N-1$, such that $\mathbf{x}(k) = \mathbf{s} + \mathbf{n}(k)$ where $\mathbf{s}$ is the stationary signal vector component and $\mathbf{n}(k)$ is the superimposed noise vector. It is assumed that the noise is random, that is $\mathbf{n}(k)^T\mathbf{n}(j)=0$ for $j \neq k$. All the vectors $\mathbf{x}(k)$ are zero mean and normalised to unit length, that is $\mathbf{x}(k)^T\mathbf{x}(k)=1$. If all the vectors $\mathbf{x}(k)$ are stored in columns of a M by N matrix $\mathbf{X}$, where $N<M$, and where $\mathbf{X}(k)$ is the k^{th} column of the matrix $\mathbf{X}$, then $\mathbf{X}$ is said to lie in a vector sub-space of N dimensions or less. That is, any of the columns of $\mathbf{X}$ need only be represented as a linear combination of no more than N orthonormal linearly independent vectors $\mathbf{u}(k)$.

$$\mathbf{x}(k) = c_0\mathbf{u}(0) + c_1\mathbf{u}(1) + \ldots + c_{N-1}\mathbf{u}(N-1) \qquad (2.50)$$

In matrix notation

$$\mathbf{x}(k)=\mathbf{U}\mathbf{c}$$

Essentially, the ensemble of vectors lie in a hyper-plane of N dimensions (max) within the M dimensional space. We usually assume in Cartesian geometry the data is projected on the "normal basis vectors[4]" which are simply the columns of the identity matrix, $\mathbf{u}(0)=[1\ 0\ 0\ \ldots\ 0]$, $\mathbf{u}(1) = [\ 0\ 1\ 0\ 0\ \ldots\ 0\ ]$, $\mathbf{u}(N-1) = [0\ 0\ 0\ \ldots\ .\ 1]$, i.e. $\mathbf{U}\mathbf{x}(k)=\mathbf{x}(k)$. However, there are good reasons to chose a different set of basis vectors. There are infinite number of possible sets of orthonormal basis vectors, but there is one special set, known as a "natural or principle basis set" which uses the minimum number orthonormal vectors to span the N dimensional column space of $\mathbf{X}$ in a revealing way.

The simplest case is if there was no noise in the ECG data, all columns of $\mathbf{X}$ would be equal to the signal vector $\mathbf{s}$. In this trivial case, $\mathbf{u}(0)$ would be equal to the signal vector $\mathbf{s}$, the remaining basis vectors would represent the null space which make up an orthornomal set such that $\mathbf{U}^T\mathbf{U}=\mathbf{I}$. For all $\mathbf{x}(k)$, c_0 would equal 1 and the others

---

[4] A basis for a vector set is a complete set of vectors that are linearly independent and span the entire space

coefficients **c** would be zero. Essentially, the data in **X** can be represented in one dimension along the axis **s** such that $\mathbf{x}(k) = c_0\mathbf{u}(0) + 0.\mathbf{u}(1) + \ldots + 0.\mathbf{u}(N\text{-}1)$ where $\mathbf{u}(0)=\mathbf{s}$ and $\mathbf{U}^T\mathbf{U}=\mathbf{I}$. In this case, the signal-to-noise ratio is infinity as there is no noise power. In general, the signal vectors will be corrupted with noise. If the signal vector **s** was known or can be estimated, then in general

$$\begin{aligned}\mathbf{x}(k) &= c_0\mathbf{u}(0) + c_1\mathbf{u}(1) + \ldots + c_{N-1}\mathbf{u}(N\text{-}1) \\ &= c_0\mathbf{s} + c_1\mathbf{u}(1) + \ldots + c_{N-1}\mathbf{u}(N\text{-}1)\end{aligned} \tag{2.51}$$

where the basis vectors **u**(i), i=2..N-1, span the noise space. Pre-multiplying (2.51) by $\mathbf{s}^T$ we get the following.

$$\begin{aligned}\mathbf{s}^T\mathbf{x}(k) &= c_0\mathbf{s}^T\mathbf{u}(0) + c_1\mathbf{s}^T\mathbf{u}(1) + \ldots + c_{N-1}\mathbf{s}^T\mathbf{u}(N\text{-}1) \\ &= c_0\mathbf{s}^T\mathbf{s} + c_1 0 + \ldots + c_{N-1}0 \\ &= c_0\mathbf{s}^T\mathbf{s} \\ &= c_0\sigma_s^2\end{aligned} \tag{2.52}$$

where σ_s^2 is the signal power. To obtain an estimate of the signal vector **s** we consider the whole ensemble in the matrix **X**. The objective is to find the principle axis **u**(0) that in some way maximally represents the signal component from the ensemble in **X**. There are different criteria that could be applied. One approach is to assume noise is totally random and **s** to be the average vector of all the columns of **X**. This is not necessarily the best estimate, but is the most computationally convenient and is performs well. Another is to compute the estimate signal power $\sigma_s^2(k)$ for all $\mathbf{x}(k)$, such that the sum of the signal powers (squared) for all k is maximised. A vector **p** is computed, such that $\mathbf{p}_k = \sigma_s^2(k)$, as follows.

$$\mathbf{X}^T\mathbf{s}=\mathbf{p}$$

Squaring both sides

$$\begin{aligned}(\mathbf{X}^T\mathbf{s})^T(\mathbf{X}^T\mathbf{s}) &= \mathbf{p}^T\mathbf{p} \\ \mathbf{s}^T\mathbf{X}^T\mathbf{X}\mathbf{s} &= \mathbf{p}^T\mathbf{p} \\ &= \varepsilon\end{aligned} \tag{2.53}$$

Here the objective is to chose **s** such that ε is maximised. Differentiate (2.53) with respect to **s** and with the constraint that $\mathbf{s}^T\mathbf{s}=1$ by using lagrange multipliers to constrain (*Haykin 1992*), and equate to zero to solve for the maximum.

$$\begin{aligned}\nabla_s \varepsilon &= \nabla_s\left(\mathbf{s}^T\mathbf{X}^T\mathbf{X}\mathbf{s} + \lambda(\mathbf{s}^T\mathbf{s}-1)\right)\\ &= \nabla_s \mathbf{s}^T\mathbf{X}^T\mathbf{X}\mathbf{s} + \nabla_s \lambda(\mathbf{s}^T\mathbf{s}-1)\\ &= 2\mathbf{s}^T\mathbf{X}^T\mathbf{X} + 2\lambda\mathbf{s}^T\end{aligned}$$

Equating to zero gives

$$\mathbf{X}^T\mathbf{X}\mathbf{s} = \lambda\mathbf{s}$$

Therefore **s** is an eigenvector of $\mathbf{X}^T\mathbf{X}$ which corresponds to the largest eigenvalue λ_{max} of $\mathbf{X}^T\mathbf{X}$ *(Haykin 1992)*. It follows then that the noise space **u**(*j*), *j=1..N-1*, are the other eigenvectors. The largest eigenvalue λ_{max} is the relative weight of the signal power. The sum of the other eigenvalues are the relative noise powers. The total power is constant as all the columns of **X** or normal. The signal-to-noise ratio is therefore

$$\begin{aligned}SNR &= \sqrt{\frac{\lambda_{max}}{\sum_{i=1}^{N-1}\lambda_i}}\\ &= \sqrt{\frac{\lambda_{max}}{N-\lambda_{max}}}\end{aligned} \qquad (2.54)$$

This is based on the assumption that **u**(0) is an accurate estimate of the signal vector **s**. A component of noise will still remain in this estimate, so this technique tends to over estimate the true signal-to-noise ratio.

2.6.8 Estimating the signal-to-Noise ratio for an ensemble of ECG waveforms using cross-correlation.

Given the same assumptions stated in 2.6.7, the signal to noise ratio can be estimated by cross correlating two ECG waveform vectors as follows.

$$\begin{aligned}\mathbf{x}(j)^T\mathbf{x}(k) &= (\mathbf{s}+\mathbf{n}(j))^T(\mathbf{s}+\mathbf{n}(k))\\ &= \mathbf{s}^T\mathbf{s} + \mathbf{s}^T\mathbf{n}(j) + \mathbf{s}^T\mathbf{n}(k) + \mathbf{n}(j)^T\mathbf{n}(k)\end{aligned}$$

Given the assumption that the noise is random, and that the signal does not correlate with the noise, then this simplifies to

$$\mathbf{x}(j)^T\mathbf{x}(k)=\begin{cases}\mathbf{s}^T\mathbf{s} & j\neq k\\ \mathbf{s}^T\mathbf{s}+\mathbf{n}(j)^T\mathbf{n}(j) & j=k\end{cases} \tag{2.55}$$

where $\mathbf{s}^T\mathbf{s}$ is the signal power σ_s^2 and $\mathbf{n}(j)^T\mathbf{n}(j)$ is the noise power σ_n^2. Given that all the vectors $\mathbf{x}(j)$, $j=0..N-1$, are normalised to unit length, then it follows that $\mathbf{s}^T\mathbf{s}+\mathbf{n}(j)^T\mathbf{n}(j)=1$, therefore the noise power σ_n^2 is estimated as $1-\mathbf{s}^T\mathbf{s}$ and hence the signal-to-noise ratio (SNR) is computed as follows.

$$\begin{aligned}\sigma_n^2 &= 1-\mathbf{s}^T\mathbf{s}\\ &= 1-\mathbf{x}(j)^T\mathbf{x}(k)\\ \therefore SNR &= \sqrt{\frac{\mathbf{x}(j)^T\mathbf{x}(k)}{1-\mathbf{x}(j)^T\mathbf{x}(k)}}\end{aligned} \tag{2.56}$$

where $j\neq k$

This technique will work assuming the signal is not correlated with the noise and that the noise for $\mathbf{x}(j)$ does not correlate with the noise for $\mathbf{x}(k)$. It is recognised that low-frequency noise, such as baseline shifts, cannot be assumed to be random (*Charayaphan et al. 1989; Charayaphan et al. 1992*). Baseline shifts that correlate will be taken as signal components and therefore artificially increase the SNR estimation. One enhancement of this method is to work with the complete ensemble of ECG waveforms and estimate the root mean squared (RMS) signal power to noise power ratio as follows.

$$\begin{aligned}SNR_{rms} &\approx \sqrt{\frac{S}{1-S}}\\ \text{where } S &= \frac{2}{M(M-1)}\sum_{j=0}^{M-2}\sum_{k=j+1}^{M-1}\mathbf{x}(j)^T\mathbf{x}(k)\end{aligned} \tag{2.57}$$

The parameter S is the mean estimated signal power, and where M is the number of waveforms in the ensemble. This can be further simplified to

$$\begin{aligned}SNR_{rms} &= \frac{r}{(1-r\cdot P^{-1})}\\ &\textit{where}\\ r &= \frac{\mathbf{a}^T\mathbf{a}\cdot M^2-M}{2};\ P=\sum_{i=0}^{M-1}i\end{aligned} \tag{2.58}$$

where **a** is the average waveform. The full proof of this is in Appendix C.

2.6.9 Comparative results for signal-to-noise estimation accuracy

The two techniques are compared using a known signal and a pseudo-random number generator for noise. The MATHCAD® sheet used to evaluate these techniques is given in Appendix C The signal amplitude A is increased from 0.05 to 5, without changing the noise component. Table 4 compares the true signal-to-noise ratio (SNR) with the estimates for the eigen-analysis technique and the cross-correlation technique.

Signal Amplitude A	True SNR (dB)	Eigen-analysis	Cross-correlation
0.05	-32.115	-12.682	-33.157
0.5	-12.115dB	-10.425	-12.164
1	-6.094	-5.586	-6.111
2	-0.073	0.135	-0.057
3	3.449	3.615	3.483
5	7.885	8.038	7.935

Table 4 Comparison of SNR estimation using different techniques

For high SNR, both techniques work acceptably well but with low SNR, the eigen-analysis predictably has poor accuracy. The correlation method is superior because it does not rely on an finding an accurate estimation of the signal component.

The main limitation of both these techniques is that the SNR is over estimated in the presence of slow moving baseline shifts. This is not a problem in practice as most of the baseline shift is removed by the linear filters described in section 2.5. Where there are remaining baseline shifts, this technique is complimented with the baseline assessment technique discussed in section 2.6.5. which rejects waveforms with remaining baselines shifts.

2.7 Validation of different signal enhancement techniques

All the techniques described here contribute to removing noise from the foetal ECG signal or for measuring noise in the signal. For the system to be safe, and to ensure the following properties are maintained.

1. The signal-to-noise ratio is maximised
2. The important signal shape information is not lost
3. False waveform shapes are not created
4. The technique can be practically and safely implemented

Different signal enhancement schemes are employed and the effects of these on the measured features are quantified. Some differences are expected, especially during periods of poor quality data. The following additional signal enhancements are used throughout all the experiments. These

1. The filter described in section 2.5.2 is used to remove high-frequency noise to help reduce QRS amplitude jitter.
2. A simple 30-beat waveform averaging is used.
3. Chebyshev polynomial curves are fitted to the ST waveform prior to feature extraction (see Chapter 4 for more details).
4. The quality test algorithms are disabled to prevent data being rejected. This was so the effects of the signal enhancement could be compared using exactly the same data.

2.8 Assessing the effects of different comb filters on sensitive foetal ECG waveform shapes

Four different filter types are validated. For each the peak and trough T/QRS ratio is measured and visually compared. The most important consideration is the width of the low-frequency notch. These are shown in Figure 50.

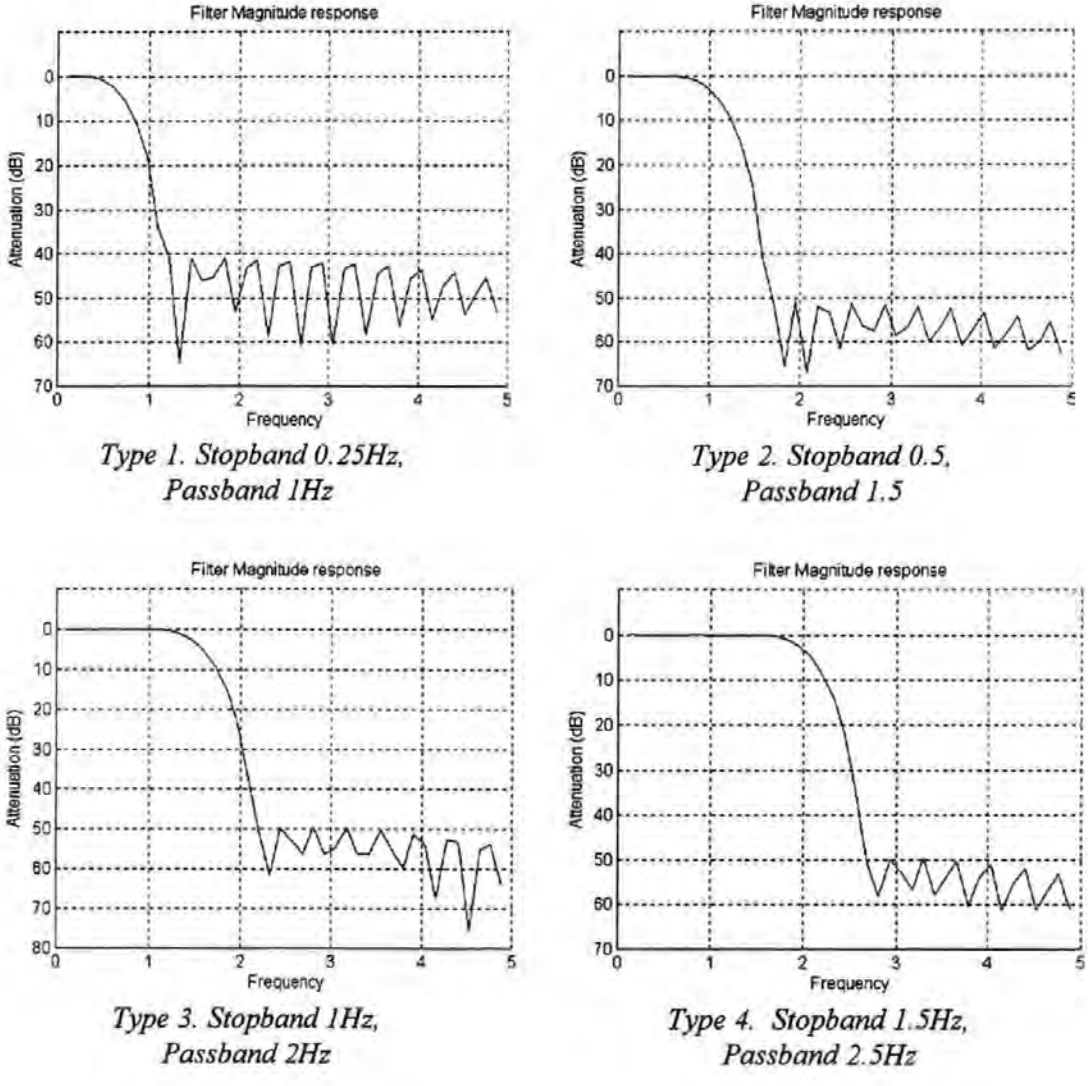

Type 1. Stopband 0.25Hz, Passband 1Hz

Type 2. Stopband 0.5, Passband 1.5

Type 3. Stopband 1Hz, Passband 2Hz

Type 4. Stopband 1.5Hz, Passband 2.5Hz

Figure 50 Different filter specifications for the ECG ST waveform comb filter

Three recordings of foetal ECG are used for this study, cases oe102, oe108 and oe111.

- Case oe102 is a good quality signal but with a very flat T segment. A small bias caused by noise or artefact could make this negative and give misleading results. Some very slightly negative T peaks are observed is the latter half of the labour, but are not significant.

- Case oe108 is of exceptional signal quality, with a few isolated cases of baseline shift and power-line noise. The application of any signal enhancement should not introduce any significant changes into the foetal ECG waveform features. Case oe108 also has some T peak changes at the very end of the labour which should not be attenuated by any signal enhancement technique.

- Case oe111 is of lower signal quality, but demonstrates some very abnormal waveform shapes. Some difference is expected in the features as more noise is removed. The different ST waveform shapes should remain visually detectable. For this case, the features used for automatic classification of the foetal ECG waveform shape (see chapter 6) are also compared. This is to quantify the effects of the filters on abnormal foetal ECG waveform shapes.

2.8.1 Validating the effects of the different comb filters on measured features in the foetal ECG waveform

The three complete cases (listed above and in appendix B) are filtered and the two key features, the T/QRS ratio peak and trough (see chapter 4), are measured. From a visual inspection, there are no significant changes in the foetal ECG waveform shape when any of these filters are used. In comparison to the raw signal however, the quality of the data is significantly improved as the filter bandwidth increases. Plots of the T/QRS ratio peak and trough, which are two key quantifiable ST waveform features (see Chapter 4), are given in appendix A for each filter. These all illustrate the same trends for each filter and did not indicate any bias being

introduced. This is verified by computing the mean, median, standard deviation and range of all the filtered signals. These statistics are summarised in Table 5 and Table 6 for the T/QRS ratio peak and trough respectively.

Case Description	Filter	Mean	Median	Standard Deviation	Range
Case 102	1	0.017	0.0125	0.0174	0.1117
	2	0.018	0.0149	0.0173	0.1114
	3	0.019	0.0177	0.0144	0.0865
	4	0.020	0.0195	0.0144	0.0982
Case 108	1	0.116	0.1187	0.0352	0.2843
	2	0.119	0.1200	0.0395	0.2847
	3	0.1184	0.1192	0.0402	0.2862
	4	0.1145	0.1165	0.0406	0.2881
Case 111	1	0.0556	0.0562	0.0348	0.1865
	2	0.0575	0.0587	0.0315	0.1703
	3	0.0603	0.0603	0.0338	0.172
	4	0.0600	0.0603	0.0322	0.1913

Table 5 Quantifying the effects of different comb filters on the T/QRS ratio peak (shown to 4 significant digits)

Case Description	Filter	Mean	Median	Standard Deviation	Range
Case 102	1	0.0061	0.0028	0.0175	0.1092
	2	0.0075	0.0050	0.0157	0.1110
	3	0.0083	0.0053	0.0120	0.0790
	4	0.0056	0.0036	0.0130	0.0774
Case 108	1	0.0903	0.0972	0.0281	0.1831
	2	0.0888	0.0981	0.0299	0.1859
	3	0.088	0.0981	0.0307	0.2123
	4	0.0846	0.0949	0.0330	0.2336
Case 111	1	0.0099	0.0120	0.0216	0.1082
	2	0.0110	0.0104	0.0192	0.0914
	3	0.0120	0.0127	0.0196	0.0993
	4	0.0089	0.0099	0.0215	0.1078

Table 6 Quantifying the effects of different comb filters on the T/QRS ratio trough (shown to 4 significant digits)

The smallest change in the mean that is considered clinically significant is 0.01. There was no significant difference in the mean T/QRS ratio peak or trough measurement for either the T/QRS ratio peak or trough for any of the cases. This indicates that no significant bias is being introduced. There is no obvious trend in the mean as the filter bandwidth increases. Appendix B shows a plot of all the T/QRS ratio trends for all cases and filters. Some examples are given below in Figure 51 and Figure 52.

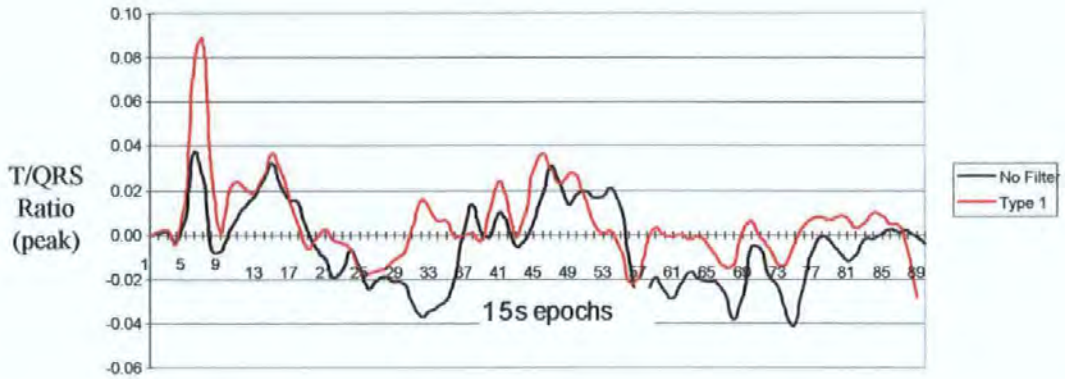

Figure 51 Case oe102: Plot of T/QRS Trough ratio with no filtering and with filter type 1

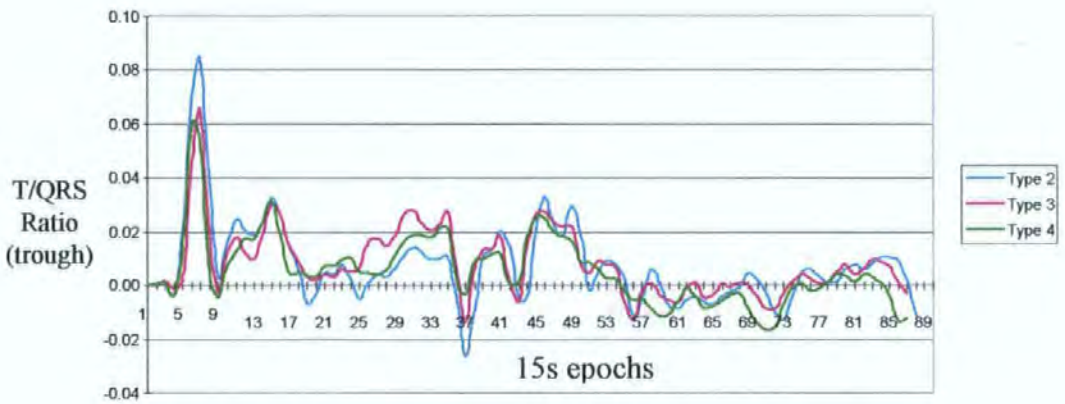

Figure 52 Case oe102: Plot of T/QRS Trough ratio for filters type 2,3 & 4

Note that ST segment changes are not reflected by the T/QRS ratio peaks. The features for quantifying the ST waveform shape (see Chapter 6) are also plotted and compared for case oe111 (which demonstrates the greatest variety of waveform shapes) and for all filter types. Results showed no significant change in the feature trends. Some example plots are shown in Figure 53 and Figure 54.

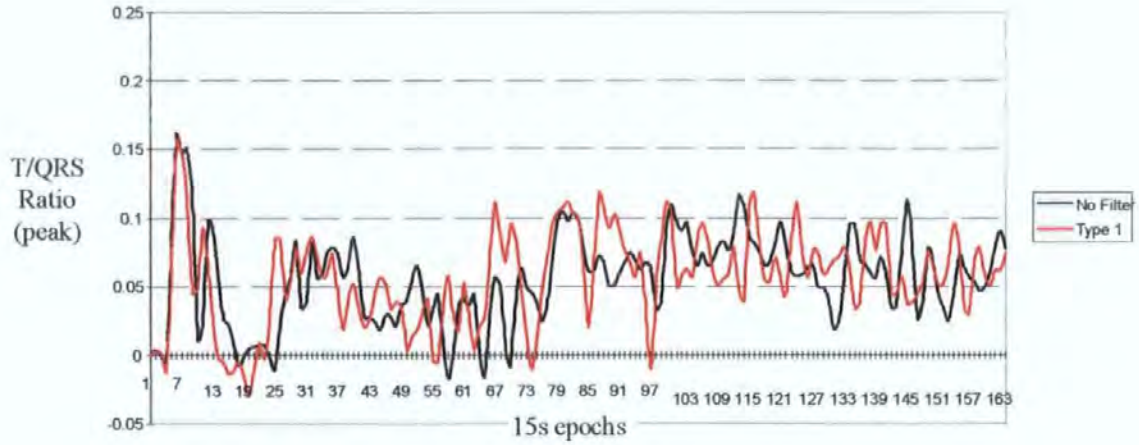

Figure 53 Case oe111: Plot of T/QRS peak ratio with no filtering and with filter type1

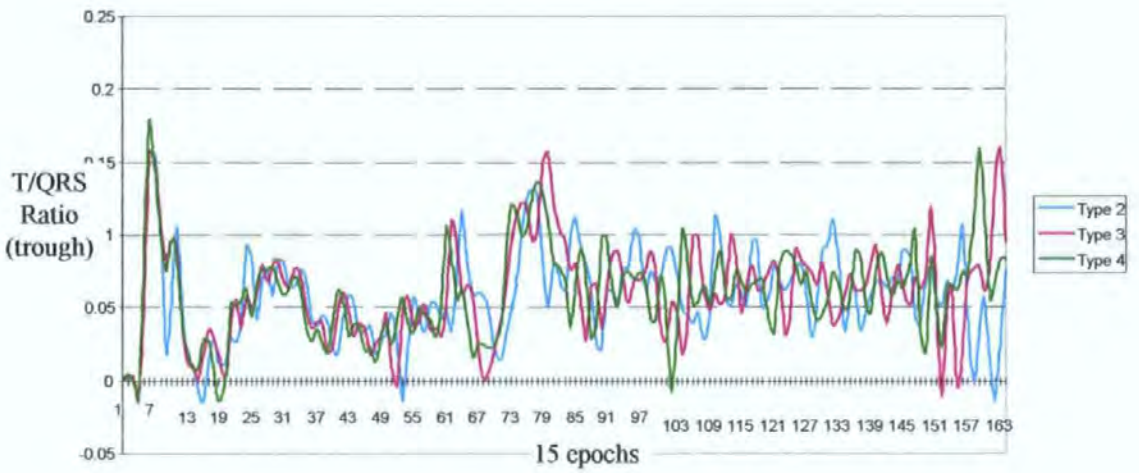

Figure 54 Case oe111: Plot of T/QRS peak ratio for filters type 2,3 & 4

The filter bandwidth could possibly be further widened but there was no obvious signal-to-noise ratio advancement. Filter type 3 was be adopted as the standard filter. Further widening the bandwidth also adds to the risk of removing important information, bearing in mind that the data base available for this study is very limited. There was no significant change in the median, range or the standard deviation of the features in this study either.

In conclusion, all these filter are suitable for T/QRS ratio assessment when used with the quality assessment algorithms and the ST waveform approximation.

2.9 Discussion and Conclusion

The signal quality of the foetal ECG waveforms is very variable and is a major reason why foetal ECG analysis is not widely used. The foetal ECG waveform cannot be analysed unless the data is enhanced and the quality of the resulting data is known as poor quality data can induce artificially abnormal waveform shapes is misleading. The spectrum of the noise overlaps with that of the ECG waveform. By removing noise energy by filtering the signal, then signal components are inevitably removed. The objective of signal enhancement is to maximise the signal-to-noise ratio without compromising the clinical information contained within the signal. If the signal is not of sufficient quality for analysis after enhancement, then it is rejected. In most cases there are enough periods of good quality data to enable meaningful information to be extracted from the foetal ECG signal.

Different techniques have been developed to help remove noise from the signal. Baseline shifts are the most problematic of all the noise sources. The first stage of signal enhancement is an analogue high-pass filter, with a pass-band edge frequency of 0.05Hz as recommended by the *American Heart Association 1975*. This filter removes just enough baseline shift energy to prevent the Analogue-to-Digital-Converters (ADC) from saturating, without significantly distorting the ECG waveform itself, and thus ensures an adequate QRS amplitude can be obtained. If the QRS amplitude is too low, then the resolution of the ECG waveform is too coarse and errors are added. Analogue filters with a higher cut-off frequency were shown to distort the ST waveform, so the standard was set at 0.05Hz. Analogue filters have a non-linear phase response, particularly around the transition band of the filter. It would also be desirable to increase the cut-off frequency of the analogue filter, thus removing more baseline shift noise, and allowing the QRS portion of the ECG waveform to span more bits of the ADC. This way the maximum resolution ECG signal can be obtained.

A novel technique for implementing linear digital notch filters with multiple sharp transition bands was proposed by *VanAlsté & Schilder (1985)*. This technique,

which is based on the window design technique, has been modified and extended, and has now been validated for clinical use under the supervision of our clinical director. This technique exploits the effects of aliasing to achieve a repeating magnitude response with very sharp transition bands. This way the baseline shift and all the power-line harmonics can be simultaneously attenuated. In addition these filters can be cascaded to design very narrow individual or multiple notch and band-pass filters, which would allow independent control over the width of each band. This technique does not require any complex sampling rate conversion and uses the well known Remez-Exchange algorithm to compute the filter coefficients rather than the window method. This has the advantage of providing independent and accurate control over the transition width, pass-band ripple and stop-band attenuation. The resulting filters maintain a linear phase response which is critical to this application. These filters have also been carefully designed and cascaded to derive low-pass and band-pass filters with very sharp transition bands, from which high-pass and band-stop filters can be simply derived. This technique can induce very long signal delays which is not a problem with foetal ECG monitoring but might become a problem if the signal was to be used in a time-critical application, such as de-fibrillation using adult ECG.

Different methods have been proposed in the past to address the problems of baseline shifts. Analogue filters are known to be unsuitable as they have a non-linear phase response which distorts the ST waveform. Recursive filters can be used if a forward/reverse filtering operation is employed to null out the phase response (*Gradwohl et al. 1988*), but this requires processing the data in large blocks which is inconvenient and is sensitive to numerical errors.

Curve fitting techniques such as cubic spline and polynomial approximation *(McManus et al. 1993; Outram et al. 1995)* have been applied to adult ECG. These techniques attempt to approximate the baseline shift with a polynomial curve and subtract it, thus removing the baseline shift. For foetal monitoring the cubic spline is not practical as the iso-electric anchor points (PQ and TP regions) used in the adult ECG cannot always be located. The fixed order polynomial approximation can over

fit the data and ring due to the effects of the R peaks, inducing more artefact than it removes. The preferred baseline approximation technique described here first uses a low-pass filter to remove most of the Q,R and S peak components and a Chebyshev polynomial approximation to approximate the remaining baseline shifts (*Outram et al. 1995*). The Chebyshev polynomial obtains an approximation with an evenly distributed error, unlike the normal polynomial $y(t)=a_0+a_1t+a_2t^2+...+a_nt^n$, which has a good fit in the centre of the data windows and larger errors at the ends (known as end effects). The difficulty with subtracting polynomial approximations is understanding how much information is being removed. Curve fit algorithms work well when the baseline is slow but not otherwise. It is important to have an understanding of how much of the signal is being filtered.

Non recursive linear filters are well understood. A difficulty is that the sharp transition bands required to remove baseline shifts require a very large number of filter coefficients, typically 1000. A technique described by *Sörnmo (1993)*, uses sampling rate conversion to simplify the filter design. A set of linear filters with different band-edge frequencies are pre-designed to extract the baseline shift information and then subtracted from the raw (delayed) signal. An algorithm is used to choose the filter with lowest cut-off frequency such that the baseline is sufficiently removed, and thereby attempting to minimise the degree of filtering. The multi-notch filters described here also used linear filters but to simultaneously remove low frequency energy below 2.5Hz and the power-line noise. This preferred method does not require sampling rate conversion and does not significantly distort the ST segment. Current evidence does not suggest there is any benefit to reduce the band-edge frequencies. A 5Hz wide notch centred at 50Hz does not have any significant effect on the foetal ECG features or the foetal ECG waveform shape. This removes the need for compensation of mains frequency drift. Adaptive filter structures are not necessary within the United Kingdom (UK), although might be required in other countries where the mains frequency has significantly more drift. In such cases a simple adaptive filter structure would be considered as a solution. This would ideally require extra electronics to obtain a digitised sample of the mains power signal.

High levels of muscle noise add errors to the measurement of features. The effects of the muscle noise may be partly removed by averaging, which is the simplest form of time coherent averaging. Evenly weighted averaging of N consecutive ECG waveforms increases the signal-to-noise ratio by a factor of $\sqrt{N}$, assuming the signal is perfectly stationary and the noise is random and not correlated with the signal. In practice the signal is only quasi-stationary and the noise only quasi-random. The foetal ECG shape undergoes normal changes during labour, particularly during heart-rate changes or uterine contractions and so signal averaging may suppress short term information, particularly in the ST segment, might be lost by the averaging process. The noise is not always random, and baseline shifts in different waveform can correlate. A technique to assess the degree of baseline shift in each waveform is therefore essential to prevent poor quality waveforms being included into the average and inducing false shapes. The current clinical knowledge is based on observations on 30 beat average waveforms. Signal averaging is an example of time coherent filtering. The 30 beat average provides a signal of sufficient quality, is very convenient to implement and has become the accepted standard in the commercial STAN® monitor. At this stage of development, using the current clinical guidelines, the normal 30 beat average is recommended. This provides a significant signal-to-noise ratio improvement with no evidence that important information is lost. It is likely that this situation will have to be reviewed in the light of any new clinical findings regarding the interpretation of short-term ECG changes. There is currently no widely accepted knowledge on the clinical implications of short term changes.

In chapter 4, the Chebyshev polynomial is used to approximate the ECG ST segment for the purpose of feature extraction. This technique simplifies the process of feature extraction but also greatly enhances signal-to-noise ratio. The polynomial has a degree m which defines the maximum number of $m-1$ maxima over the interval of the data being approximated. The curve tends to 'fit through' the remaining muscle and power-line noise leaving a clean ST waveform. The principles for computing the polynomial coefficients are the same as described here, with details being given in chapter 4.

When the signal quality is very poor and the enhanced signal is still of insufficient quality for analysis, then the data is rejected. To do this a quantitative measure of signal quality is required. Two quantitative quality measures are used in this work. A estimate of the signal-to-noise ratio of the average waveform is given which considers all the waveforms in the average ensemble. This estimate is limited by the assumptions that the noise is random and that the signal is stationary. The signal is quasi-stationary and can be considered to be stationary over 30 beats because the shape changes are progressive rather than sudden. The muscle noise can reasonably be assumed to be random, but any remaining baseline-shifts cannot. If the baseline shifts correlate between ECG waveform vectors, then the signal-to-noise ratio will be over-estimated. *Charayaphan et al. (1992),* used a technique based on correlating the ECG vector with a shifted version of itself, which is based on the assumption that the ECG component will not correlate but the slower-moving baseline shifts will. Unfortunately this assumption only works for the very slow moving components of the baseline shift which have already been attenuated by the signal enhancement filters. An accurate signal-to-noise measure is not necessarily revealing enough to reject poor data. An example of this is a low-amplitude baseline shift which has a short and sudden shift. The noise power can be relatively low but the distortion to the waveform can still be acute. The preferred method used in this work is to assess the baseline shifts independently from the other sources of noise by pre-filtering the data to remove most of the ECG components and to compute an approximation of the baseline shift itself. From this approximation the power and nature of the noise can be assessed. The filtered data is fit with a high order Chebyshev polynomials (typically 6th order) in order to get a uniform approximation. The approximation degree is truncated, and the degree of fit is increased until a sufficient fit is obtained. The peak-to-peak amplitude and degree of approximation are used to determine the nature of the remaining baseline shifts. A high degree of approximation is indicative of poor quality data as this implies the baseline shift has faster moving components such as sudden jumps caused by movement artefact. Fuzzy logic is used to conveniently derive a measure of baseline quality.

The techniques reported here have applications in other areas of biomedicine where it is required to enhance the data. An example is in the assessment of neonates using evoked potentials where the enhancement and measurement of features are necessary.

2.10 Novelty and contribution to knowledge

The techniques for designing linear multi-band FIR filters with narrow transition bands described by *Val Alsté et al. (1985)* have been extended to allow the design of multi-band or single-band filters. This is based on the well known Remez Exchange algorithm rather than the Window method, thus allowing accurate and independent control over the pass-band ripple, stop-band attenuation and band-edge frequencies. This work has resulted in a journal paper which is currently being prepared *(Outram et al. 1997)*. These filters have been implemented in the STAN® monitor and has resulted in a very noticeable improvement in signal quality. This has contributed to the overall safety and reliability of the system. On the basis of experience so far, when using these filters, it is now possible to demonstrate that the energy below 2.5Hz can be safely removed from the foetal ECG with no significant effect on the ST waveform shape. This now means that the foetal ECG can be analysed with much greater accuracy and confidence.

Two new techniques for estimating the SNR of repetitive signals have been developed and tested. The first is based on eigen-analysis and the second is based on linear correlation. The technique based on correlation has been successfully applied to foetal ECG to ensure unacceptably noisy signals are not presented to clinicians or the expert system. This technique works well but is insensitive to baseline shifts. The concept of curve fitting has been applied to foetal ECG analysis for assessing the severity of baseline shifts in foetal ECG data. Features are extracted from the curves and fuzzy rules are used to derive a single measure of baseline shift severity. The rules are designed such that the system is very sensitive. This work is due be implemented into the STAN® monitor in the near future. The sensitivity of this system has ensured that ECG data can be used for detailed

analysis with far less uncertainty and has contributed to the overall confidence in foetal ECG analysis.

Chapter 3

QRS Detection

3. *QRS Detection*

3.1 Introduction

A critical process in foetal cardiotocogram (CTG) and foetal electrocardiogram (FECG) analysis is to determine the location of each ECG waveform from the raw and often noisy FECG data. There are many problems with detecting the ECG pattern due to the effects of noise and the presence of maternal ECG waveforms. The QRS complex is the only component of the foetal ECG waveform that does not change during labour, unlike the ST and PR waveforms which can change slowly throughout labour. For this reason, only the QRS portion of the foetal ECG waveform is used for detection purposes. Detection of ECG waveforms is therefore commonly known as QRS detection.

The first task is to minimise the effects of noise in the ECG signal, which is known as pre-processing. The QRS complex is a robust element of the ECG waveform (see chapter 2) which enables a relatively aggressive signal enhancement scheme to be employed. The second task is to employ a pattern recognition algorithm to reliably locate each QRS complex.

3.2 Pre-processing : The signal enhancement scheme for QRS detection

Power-line noise and baseline shifts are the most problematic noise sources for QRS detection. The signal processing constraints for QRS detection are much more relaxed than that for ST waveform analysis enabling a much more aggressive signal enhancement scheme to be used. This way, even if the quality of the data is very poor and many of the ECG features cannot be used, the QRS complex can often still be detected and the heart-rate can at least still be measured. The only constraint is that the general shape of the QRS complex should be preserved to the extent that it differs from background noise and can be located reliably.

The primary purpose of pre-processing is to remove all the power-line noise and the low-frequency noise from the signal so that the QRS portion of the ECG waveform can be located accurately and reliably. The filter must attenuate the signal energy in the following frequency bands:

- **0Hz-5Hz**. Mostly DC, baseline shifts PR and ST waveform.
- **49-51Hz**. Mains power-line noise energy.
- **99-101Hz**. Harmonics of the power-line noise produced by neighbouring electrical equipment.

Three different techniques are compared for pre-processing. Differentiation *(Xue Q. et al.)*, linear filtering *(Outram & Ifeachor 1993)* and non-linear prediction filters *(Tompkins et al. 1991)* techniques have been considered for pre-processing.

3.2.1 Differentiation

A simple technique for removing baseline shifts from the QRS complex of the ECG waveform is estimate the first derivative of the FECG data by calculating the first difference. This way, the sharp edges of the QR and RS portions of the ECG complexes are revealed (see Figure 55b). The derivative information is then squared (see Figure 55c) and smoothed using a moving average (see Figure 55d) to enhance the QR or RS derivative peaks. Using this method any remaining baseline shift is almost totally removed because, in the absence of transient shifts, baseline shift has a very small first derivative. The approximate first derivative, $\Delta x(t)$, of the raw data, $x(t)$, is computed as

$$\Delta x(t)=(x(t+1)-x(t-1))/2 \qquad (3.1)$$

The QRS complexes are further revealed by squaring the derivative and smoothing the result with a simple moving average filter.

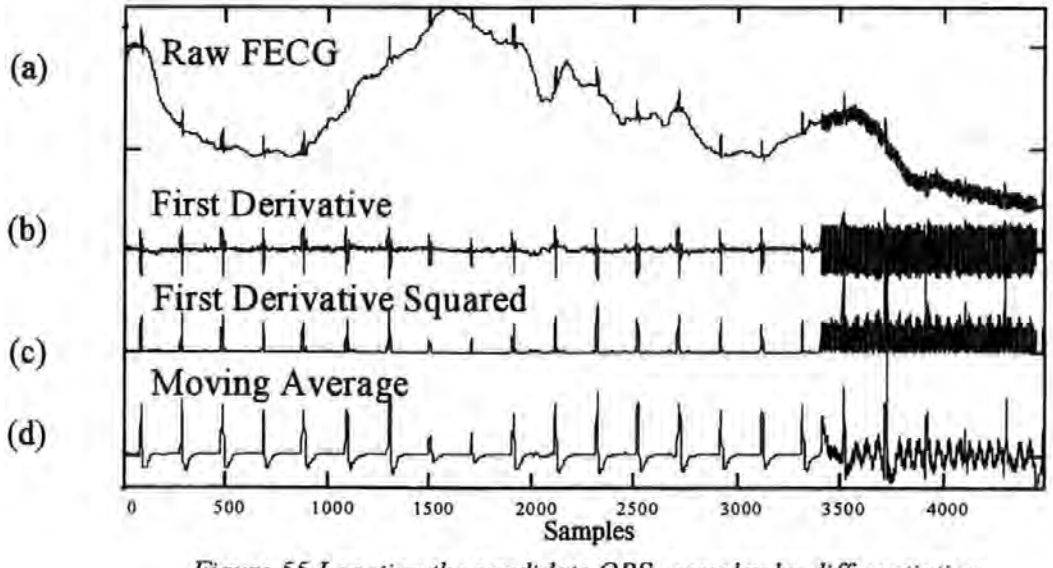

Figure 55 Locating the candidate QRS complex by differentiation

This technique works very well in the absence of high-frequency noise and transient shifts. Differentiation worsens the effects of higher frequency noise because the derivative of a signal is proportional to the frequency. Consider a sinusoidal noise source $n(t)$

$$n(t) = A \sin(\omega t + \theta) \qquad (3.2)$$

where A is the amplitude, ω is the angular frequency and θ is an arbitrary phase shift. Differentiating (3.2) gives

$$dn(t) / dt = A\omega \cos(\omega t + \theta) \qquad (3.3)$$

Note the amplitude of the derivative data is proportional to frequency. Therefore the effects of high frequency noise are increased and this can obscure the important features. This can be observed in Figure 55. Transient shifts produce spikes in the derivative which are detected as candidate QRS complexes. Transient shifts are not a common problem, but can occur during the first 20 minutes of recording, or when the scalp electrode moves. Despite its simplicity, differentiation should be avoided with noisy data.

3.2.2 Non-linear prediction filter

A more complex technique described by *Xue et al. (1992),* acknowledges and circumvents the problems with differentiation. This technique uses a multi-layered perceptron (MLP), with sigmoid activation functions in the hidden layer and a linear output (*Haykin 1994*), as a non-linear prediction filter (see Figure 56). This method claims a better performance than a linear prediction filter, such as that described by *Haykin (1992).* A more detailed description of the MLP and how its parameters are computed is given in later in section 3.5.1 and in *Haykin (1994).*

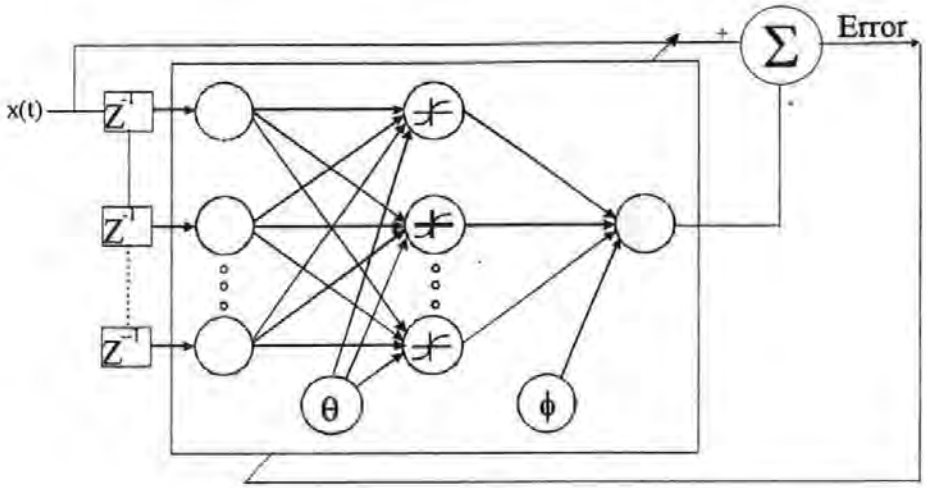

Figure 56 Non-linear prediction filter using a MLP

The MLP parameters are adapted on-line to predict the unwanted lower-frequency components of the signal, such as the baseline shift and PR and ST segments of the ECG waveform. The error between the predicted signal and the actual signal is computed, revealing sharp features, such as the R peak and some of the noise. The output of this is then passed to a pattern recognition algorithm.

The output of the network in Figure 56 approximates to the low-frequency components of the FECG signal (see Figure 57a), including the P wave and T wave. The output error of the filter is the remaining higher-frequency components which include the sharp QRS complex and high frequency noise. The output error is then squared (see Figure 57b) and smoothed using a moving average (see Figure 57c) used to locate the *candidate* QRS complex. For this to work it is important to use the correct training rates for the hidden and output layers. The method described by *Xue et al. (1992),* which computes these parameters automatically is complex and computationally expensive.

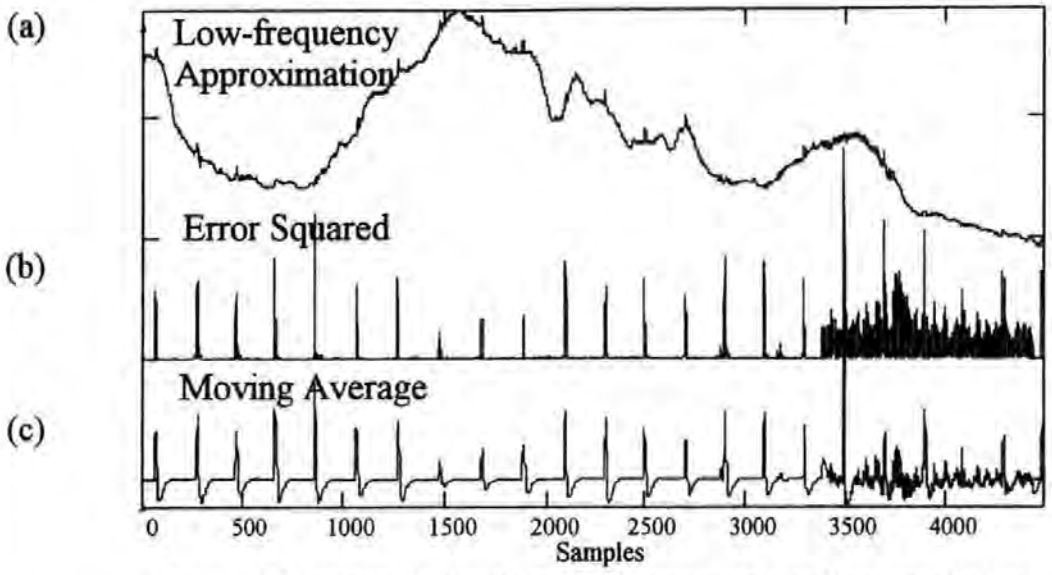

Figure 57 Locating the candidate QRS complex by non-linear prediction

This technique does not suffer from the effects of high frequency noise as much as the differentiation technique, but is difficult to obtain consistent results because the training algorithm for the MLP can become stuck in local minima (*Haykin 1994*) and can produce unpredictable results. The concept behind the non-linear prediction filter however inspired another technique which is far simpler and achieves the same objectives with consistent results *(Outram & Ifeachor 1993)*.

3.2.3 Linear filtering design by least-squares approximation

The technique uses least-squares curve fitting to approximate the slow moving components of the FEGC signal such as the baseline shift, ST and PR segments (see Figure 58). The difference is computed which retains mostly the sharp QRS complex and high frequency noise. A low order curve, of the form

$$f(t)=c_0 + c_1 t + c_2 t^2 + \ldots + c_n t^n \qquad (3.4)$$

where $t=\{-L,-L+1,\ldots,L\}$, is fitted to a window of $2L+1$ raw fetal ECG data points $x(t)$ as shown in Figure 58.

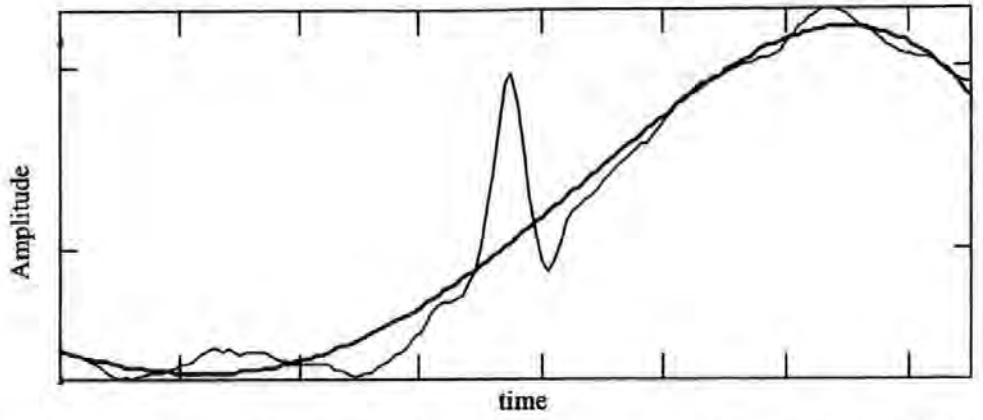

Figure 58 Approximation f(t) of the low-frequency noise content for an individual ECG waveform

The degree of approximation, m, and the window size, $2L+1$, are chosen such that only the slow moving parts of the data (such as baseline shift, PR and ST segments) are accurately approximated but the sharp QRS portions of the data are very poorly approximated. It was found by trial and error that L was typically 15 and m was typically 3. The coefficients **c** in (3.4) are easily computed directly with no need for training algorithms. Equation (3.4) can be written for all t in matrix notation as

$$\mathbf{H}.\mathbf{c} = \mathbf{y} \qquad (3.5)$$

where $\mathbf{H}_{t,k}=t^k$ is a $(2L+1)$ by m rectangular matrix and $y_t=f(t)$, $k=\{0..m\}$, $t=\{0,1,...,2L-1\}$. Pre-multiplying both sides of (3.5) by $\mathbf{H}^+$ gives

$$\mathbf{c}=\mathbf{H}^+\mathbf{y} \qquad (3.6)$$

where $\mathbf{H}^+$ is the pseudo-inverse of $\mathbf{H}$ (m by $(2L+1)$ rectangular matrix) defined as $\mathbf{H}^+\mathbf{H}=\mathbf{I}$, and where $\mathbf{I}$ is the identity matrix. $\mathbf{H}$ is very ill-conditioned, so the most reliable method of computing the pseudo-inverse is by using the singular value decomposition algorithm, whereby $\mathbf{H}$ is factored as $\mathbf{H}=\mathbf{U}\Sigma\mathbf{V}^T$ where $\mathbf{U}$ and $\mathbf{V}$ are orthonormal matrices and Σ is a diagonal *(Press et al. 1992; Jennings & McKeown 1992)*. This can be computed with mathematical computer software such as MATLAB®. The pseudo-inverse is computed from this as

$$\mathbf{H}^+=\mathbf{V}\Sigma^{-1}\mathbf{U}^T \qquad (3.7)$$

In (3.5) $\mathbf{H}$ is a constant matrix, therefore $\mathbf{H}+$ is also a constant matrix. From (3.4), the mid-point of the curve $f(0)$ is taken as the low-frequency approximation, the window is then advanced by one sample, and the process is repeated. From equation (3.4) $f(0)=c_0$, which is simply computed by

$$c_0 = \mathbf{h_0}^+.\mathbf{y} \qquad (3.8)$$

where $\mathbf{h_0}^+$ is the first row of **H+** and is a constant row vector. Given that y is shifted by one sample, then equation (3.8) is simply a convolution operation and can be written as a fixed non-causal fixed FIR filter

$$f(0) = \sum_{n=0}^{2L} \mathbf{h_0}^+(n) \cdot \mathbf{y}_n \qquad (3.9)$$

where $\mathbf{h_0}^+$ are the filter coefficients. This is sometimes referred to as a Savitzky-Golay smoothing filter *(Press et al. 1992)*. For $L=15$ and $m=3$, the magnitude response of this filter is shown below in Figure 59.

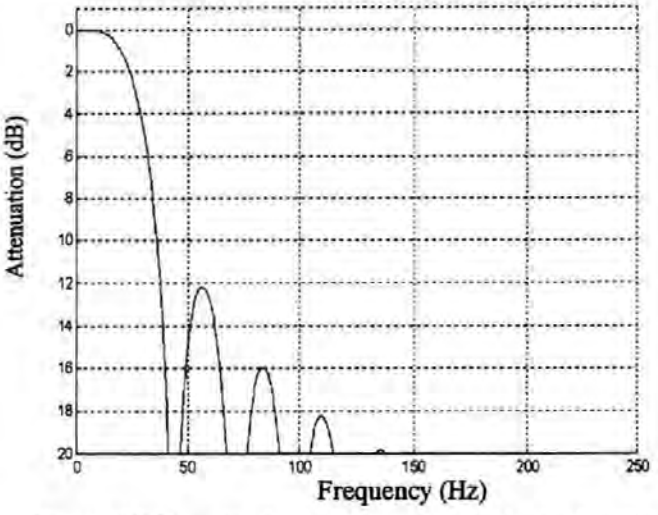

Figure 59 Magnitude response of Savitzky-Golay filter

An example of the low-frequency approximation and the output error is shown in Figure 60. The errors are squared and smoothed with a moving average.

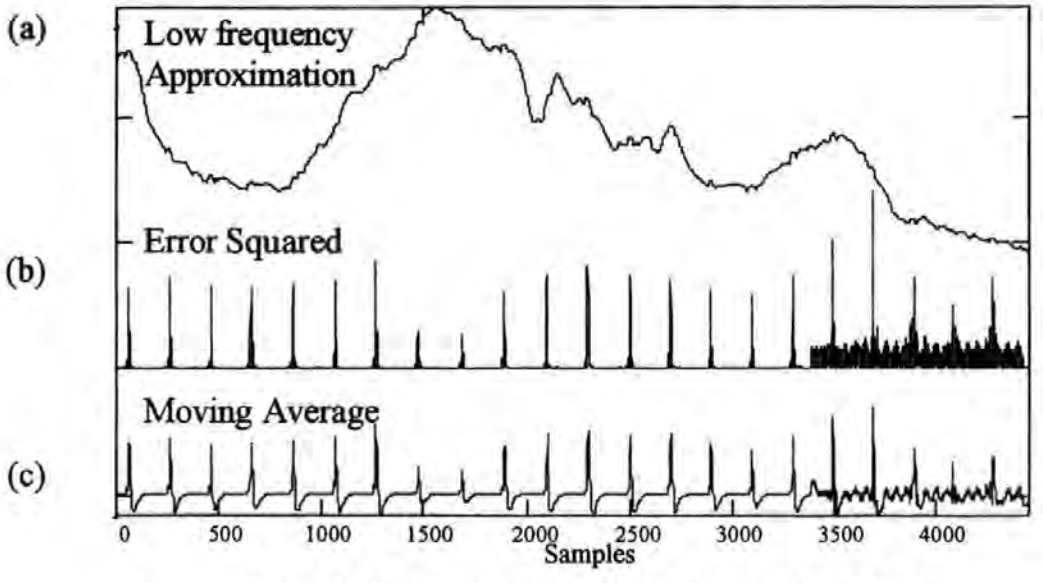

Figure 60 Results of the Savitzky-Golay smoothing filter

From the moving average trace in Figure 60 it is clear that the candidate ECG waveforms can be located by using a threshold detector.

3.2.4 Comb filtering

Most of the foetal ECG spectrum lies approximately between 2.5Hz and 65Hz. The QRS portion of the ECG waveform lies mostly between 10Hz and 40Hz. The magnitude response of a filter, designed to maximise the QRS signal to noise power ratio, would be a band-pass filter with a specification shown in Figure 61.

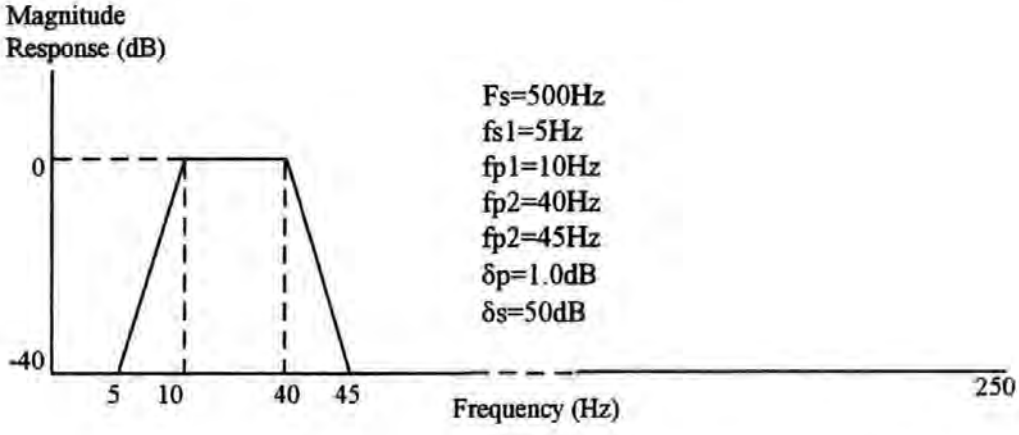

Figure 61 Prototype filter for QRS detection pre-processing

To implement this directly with an optimal FIR filter requires at least 141 coefficients, so it is initially designed at a lower sampling frequency as shown below in Figure 62. The design technique is similar to that descried in chapter 2.

The design starts with the desired filter specification design shown in Figure 62a with an effective sampling frequency of 50Hz. The Remez exchange algorithm is used to design this filter with $L=24$ coefficients h_i, $i=0..L-1$. These coefficients are interpolated with zeros to restore the sampling frequency to 500Hz. This produces a filter with a repeating frequency shown in Figure 63b. The filter can be implemented very efficiently with the following difference equation.

$$y_1(n) = \sum_{i=0}^{23} h_i \cdot x(n-10i) \tag{3.10}$$

$x(n)$ are the raw data samples, h_i are the filter coefficients, and $y_1(t)$ are the filtered output samples.

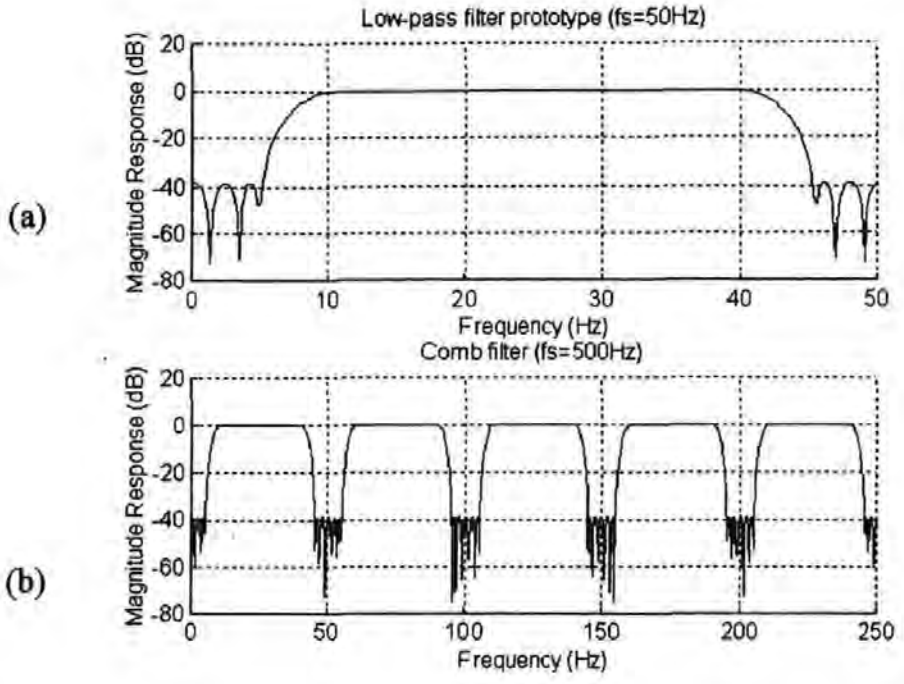

Figure 62 Multiple notch filter for removing baseline shifts and power-line harmonics

The delay through the filter is *24*10/2 = 120* samples. To remove the unwanted frequency bands a second band selection filter is designed at a sampling frequency of 250Hz (see Figure 63a) with coefficients h'_j, $j=0..M$, where $M=23$. The coefficients are again interpolated with zeros to restore the sampling rate to 500Hz which produces a filter with a repeating frequency shown in Figure 63b. The delay through this filter is 24 samples and is implemented using the following difference equation.

$$y_2(n) = \sum_{i=0}^{23} h'_i \cdot y_1(n-2i) \qquad (3.11)$$

where y_1 is the output of the first filter and y_2 is the cascaded filter output. These filters are cascaded to produce a linear band-pass filter of the desired specification (see Figure 64). The overall delay though the filter is 144 samples which equates to 288ms.

(a)

(b)

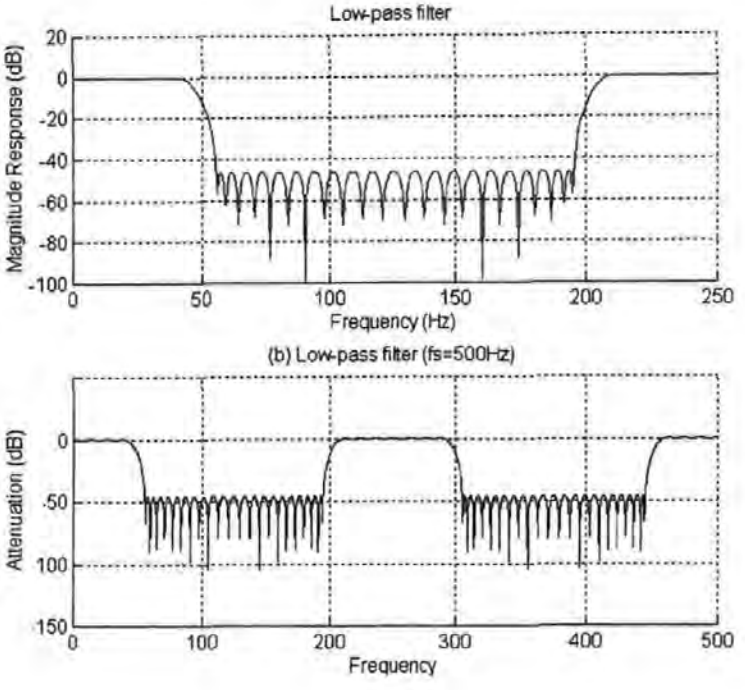

Figure 63 (a)Band selection filter designed at Fs=250Hz and (b) magnitude response after restoring the sampling rate to 500Hz

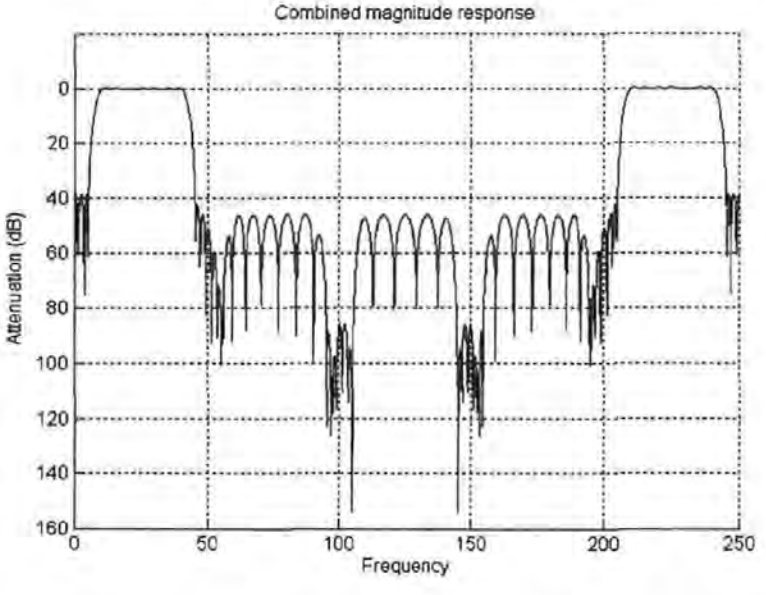

Figure 64 Combined magnitude response for the QRS enhancement filter

Some example results are shown in Figure 65 where baseline shifts and power-line noise and random noise has been added. Note the baseline shift is acute. The MATLAB® source file to implement this is given in Appendix A.

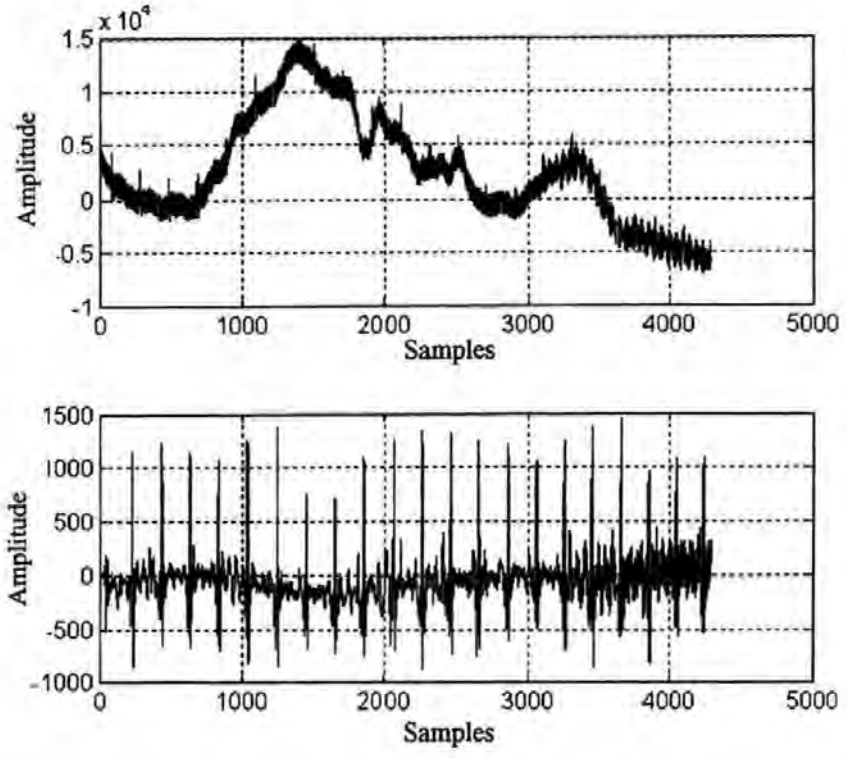

Figure 65 Filtering raw ECG data with high energy baseline shift, power-line and random noise (top) to produce flat ECG data (Bottom) with minimal baseline shift and power-line noise remaining

This technique is very effective and efficient to implement. The delay in the system is 144 samples, which for a 500Hz sampling rate, equates to 288ms, which is very low relative to physiological changes which typically occur over minutes.

3.2.5 Comparison of pre-processing techniques

Pre-processing the foetal ECG data primarily requires the removal of baseline shifts and power-line noise. The QRS complex is the only feature that needs to be preserved so the constraints on the signal enhancement algorithms are more relaxed than that of the signal enhancement for ST analysis. ST waveform analysis and CTG are both dependent on the accurate location of the R peak. Beat-by-beat heart-rate analysis is routinely used, so there is great impetus to measure heart-rate even if the ST waveform cannot be analysed. In this work a separate signal enhancement schemes is used for QRS detection and heart-rate analysis. For removing baseline shifts, differentiation is unsuitable because of the unwanted effect of amplifying higher frequency noise. The non-linear prediction filter is an improvement, but computationally expensive and not always reliable. The use of a Neural Network by *Xue et al. (1992),* although an interesting academic exercise, is also felt to be

unnecessarily complex. It does illustrate the use of Neural Networks and as an extension of linear prediction filter techniques, but is not justified here when much simpler and more robust technique exists. The Savitzky-Golay filter and the multi-band filter both have similar merits in that they perform at least as well as the prediction filter, are both stable and have predictable performance. The multi-band filter does have the added advantage of inherently removing the power-line noise which makes it the preferable choice.

3.3 Design of a pattern recognition technique for QRS detection

Having removed most of the noise from the raw data, each R peak in Figure 65 can now be visually identified, despite the poor quality of the raw signal. Each R peak in the data needs to be accurately located as a reference point for ECG waveform analysis. From the example in Figure 65, a simple threshold detector set at 500 would detect all of the R peaks correctly. In general this is not practical because the signal amplitude of each QRS pattern can vary, requiring the threshold to be adapted on-line. Calculating a threshold adaptively online is very susceptible to problems with rapidly changing amplitudes and noise. It is also difficult to know how many QRS patterns, if any, are expected in any fixed window of data. The simple threshold detector is a very poor solution and leads to many waveforms being missed (false negative detection) and more seriously, false detection (false positives). A more robust scheme is used which employs gain invariant pattern recognition techniques.

The QRS complex, which is the only stationary component of the ECG waveform, is approximately 40ms wide (20 samples for a 500Hz sampling rate). These 20 samples constitute a vector x of 20 elements. The generalised vector pattern classifier shown in Figure 66 is presented with a moving window (vector $\mathbf{x}$) of ECG data which is then classified as either noise, $y(x)=0$, or a QRS pattern, $y(\mathbf{x})=1$.

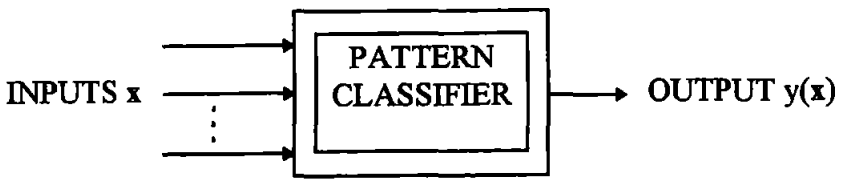

Figure 66 Vector pattern classifier with a simple vector x as an input and a single scalar output y(x)

During the course of labour the gain in the system can vary resulting in a variable signal amplitude. This has the effect of lengthening and shortening the input vector **x** which is undesirable and hinders reliable detection. The pattern information however is represented by the direction of **x** and not the magnitude so the vector **x** can be normalised to unit length as follows

$$\mathbf{x}_{norm} = \frac{\mathbf{x}}{\mathbf{x}^T\mathbf{x}} \qquad (3.12)$$

where $\mathbf{x}_{norm}$ is the new normalised input vector. Normalisation preserves the direction and thus shape of the vector and forces the length to unity. To design a suitable detector, there are some basic properties of the foetal QRS complex that aid understanding of the problem[1].

1. The ECG waveform is 'quasi-periodic'. The heart rate normally varies between 60 and 180 beats per minute, therefore in a one minute block of data there will between 60 and 180 QRS complexes.
2. The R peak or S peak are the largest features in the ECG waveform.
3. The QRS complex will only change shape during a single labour if :
   (i) The electrode is removed and re-cited
   (ii) The foetus is "pre-terminal", that is, almost dead when there is no chance of recovery.

[1] These assumptions are based on a term foetus (38 weeks of gestation or more). This work does not account for a pre-term foetus as the physiological changes are not fully understood.

4. The QRS amplitude is a physiological constant, and varies only due to changes in the gain of the system.[2] The QRS amplitude is used to normalise all other amplitude measurements in the ECG waveform.
5. The width of the QRS complex varies slightly between cases, but is constant throughout a single labour unless there is a chronic heart defect (pre-terminal). Some will be slightly narrower than 40ms samples.
6. The maternal ECG, if present, is usually narrower and smaller in amplitude than the foetal ECG when using a scalp electrode.
7. Random noise is un-correlated with the QRS complex by definition
8. Some noise and artefact such as maternal QRS complexes are not random and partially correlate with the foetal QRS complex. Although they are smaller in amplitude, the normalisation unfortunately removes this discriminating information.

There are two basic approaches for designing a QRS complex detector described here. The first is to learn the shape of the QRS pattern vector w for each individual case at the beginning of recording, during an on-line 'learning phase'. This vector is used as a template for detecting subsequent QRS patterns on-line. The second approach is to have the learning phase off-line and build up a representation or 'memory' of the QRS pattern space from prior examples of QRS complexes from different cases. This representation is used to detect individual QRS patterns on-line.

3.4 Design of a QRS detector using a simple correlation technique

The uncorrupted QRS complex shape differs between cases *(Xue Q. et al.)* due to slight changes in electrode positioning and body weight. This first approach is to obtain an on-line estimate of the QRS pattern vector w for an individual case, which is known as the template vector. This has the advantage of only requiring a simple classifier, such as linear correlation algorithm, to detect ECG waveforms. This is illustrated in the conceptual diagram in Figure 67. Consider Figure 67 as a hyper-

[2]Occasionally small QRS amplitude fluctuations can be observed which are attributed to foetal breathing. The change is small (less than 5% of the QRS amplitude).

sphere in N dimensions, where N is the number of input parameters in the QRS pattern detector (*N=20 for this work*). Assuming the QRS complex pattern to be near stationary, then the QRS complex vector **w** will be expected to lie within a single small region of space, and given that the vector is zero mean and normalised to a fixed length, this region is represented as the small circle on the surface of the hyper-sphere in Figure 67, which is a *N-1* dimensional spherical plane. The detector has to determine if a candidate QRS pattern vector x lies within this plane. The radius of the spherical plane is to allow for slight variability in the QRS shape, errors in the estimate of the QRS complex shape and noise.

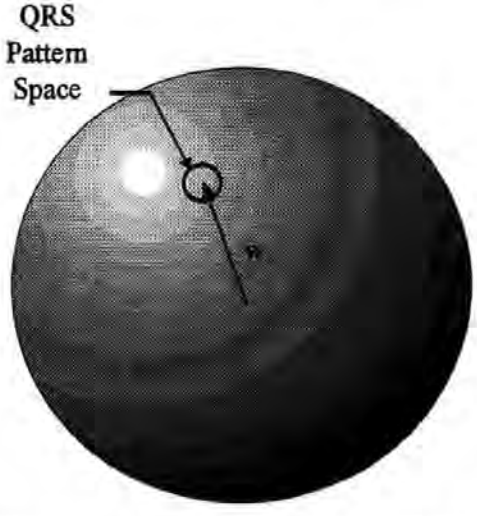

Figure 67 Conceptual diagram illustrating the simple pattern space of the QRS complex & noise

The correlation between the candidate vector x and the template vector w is used to determine whether a candidate vector x lies within the QRS pattern space. The linear correlation r between a presented vector x and the estimate of the QRS pattern vector w is given by

$$\begin{aligned} r &= \mathbf{x}^T \cdot \mathbf{w} \\ &= \cos(\theta) \end{aligned} \qquad (3.13)$$

where w and x have a zero mean and are normalised to unit length and θ is the angle between the vector x and w. In practice, to determine if x is a QRS complex, the correlation r has to exceed a threshold value α. This threshold has to be chosen such that the performance of the detector is optimum in some way. If α is too small noise corrupted QRS patterns will be missed, which will increase the chance of a *false negative*. If α is too large then there is an increased probability that noise will be

classified as a QRS pattern, known as a *false positive*. False positive events are very undesirable because false or highly corrupted ECG waveforms can result in very misleading information for the clinician and an intelligent system. The difficulty with this approach is how to estimate of the QRS pattern vector w, which is now discussed.

3.4.1 Adapting the template vector online

A proposed technique was to optimise the performance of the correlation on-line in order to compensate for the variation in QRS complex shape between patients (*Outram et al. 1993*). Starting with a known QRS template vector w, a simple technique is used for updating the weight vector w

$$w(k+1) = (1-\alpha).w(k) + \alpha.(x(k)-w(k)) \qquad (3.14)$$

where $x(k)$ is the presented input vector, $w(k+1)$ is the next updated template vector, $w(k)$ is the previous template and α is the learning rate $(0.5<\alpha<1)$.

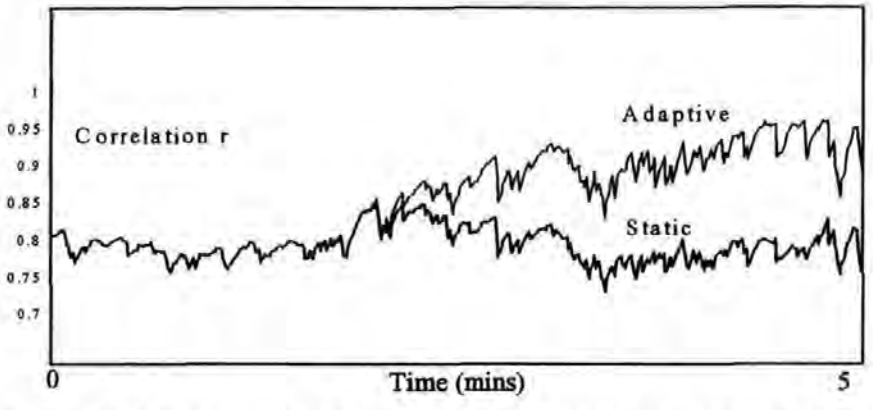

Figure 68 A comparison of the static and adaptive QRS complex detector

Figure 68 illustrates how the adaptive correlation algorithm adapts to the specific ECG complex over a 5 minute period where α=0.9. The mean output increased by approximately 10% over the first 5 minutes giving mean output of approximately 0.95 (95% certainty of detection) for correct hits. A concern here is that this technique depends on good quality data and could fail with persistently noisy data by adapting to the wrong signal.

3.4.2 On-line estimation of the QRS pattern

This technique relies on assumptions 1 & 3 in section 0. A QRS template vector v of length L with high SNR is manually extracted from previous cases is used as an

initial estimate of the QRS pattern. A minute block of data $x(n)$, $n=0..N-1$, where $N=30000$, is correlated with the template vector such that

$$r(n) = v^T x'(n)$$
$$x'(n) = \frac{x(n) - \overline{x(n)}}{\left| x(n) - \overline{x(n)} \right|} \qquad (3.15)$$

where $r(n)$, $n=(L-1)..N-1$, is the linear correlation between the template vector v and the normalised zero-mean data vector x'(n) and where $x(n)$ is a vector of L samples such that $x(n)_k=x(n-k)$, $k=0..L-1$ and $\overline{x(n)}$ is the mean of the vector $x(n)$. The 60 highest correlation coefficients $r(n)$ greater than 0.6 are located and the corresponding data vectors $x(n)$ are extracted, normalised and averaged to compute the estimate QRS pattern vector w_1. If there is periodic noise present and no ECG waveforms then it is possible that the estimate could be just noise. To prevent this the correlation $r(n)$ must exceed 0.6. This process is repeated for the next minute block of data to estimate w_2. If the two vectors are highly correlated such that $w_1^T w_2 \geq 0.98$ then the estimate QRS template is taken as the average $w=(w_1 + w_2)/2$, otherwise the process is repeated. This technique is summarised below.

1. Read in and filter next 60 seconds of raw ECG data.
2. Compute the correlation between the data vectors $x(n)$, $n=L-1..N-1$, with the estimate template vector v
3. Locate the 60 highest correlation coefficients greater that 0.6 and extract the corresponding vectors. If ECG data is present and of good quality, these will correspond to QRS patterns. If 60 cannot be located then go at to 1 and report a "no signal" error.
4. Subtract the mean from each QRS pattern vector and normalise to unit length.
5. Average all the QRS pattern vectors together to compute estimate w_1.
6. Repeat stages 1-5 on next minute of data to compute estimate w_2
7. Compute the correlation $r=w_1^T w_2$
8. If $r<0.98$ then go to stage 1 and report "Noisy data"
9. Compute the QRS pattern template vector $w=[w_1+w_2]/2$.

10. Subtract the mean of and normalise

$w = w - \bar{w}/(w-\bar{w})^T \cdot (w-\bar{w})$ where $\bar{w}$ is the mean of w

11. Compute correlation $r=w^T v$, where v is a manually extracted average QRS pattern vector taken from a previous case.

12. If $r<0.6$ then go to stage 1

Note that in stage 8, the accepted correlation coefficient is very strict. This ensures that the estimate is of very good quality. If more than 5 attempts are made (10 minutes of data), the operator is told to replace the electrodes.

3.4.3 Efficient implementation of the correlation algorithm

Given that an accurate estimate of the QRS pattern vector w has been extracted from the data, with each new sample candidate QRS pattern vector $x(k)$ is updated and correlated with the template vector w as depicted in Figure 69, where k is discrete time and a D in Figure 69 constitutes a delay of one sample.

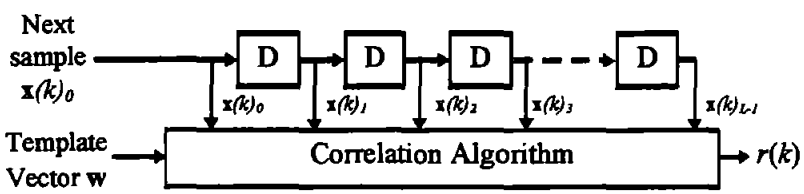

Figure 69 QRS detector based on linear correlation

The output of the correlation algorithm $r(k)$ is given by the following expression

$$r(k) = \frac{\left(x(k) - \bar{x}(k)\right)^T \cdot w}{\left|x(k) - \bar{x}(k)\right|} \qquad (3.16)$$

where $\mathbf{x}(k) = \left[\mathbf{x}(k)_0 \quad \mathbf{x}(k)_1 \quad \ldots \quad \mathbf{x}(k)_{L-1}\right]$ is the k^{th} presented input vector, $\bar{x}(k) = \frac{1}{L}\sum_{i=0}^{L-1} x(k)_i$ is the mean of vector $x(k)$, L is the number of samples in w and x, and where k is discrete time. To implement equation (3.16) directly requires the mean scalar and magnitude scalar $\left|x(k) - \bar{x}(k)\right|$ to be computed for each time k. To reduce the computational overhead, these can be computed recursively as follows. Given a new sample $x(k+1)_0$, the correlation $r(k+1)$ is calculated as follows.

$$r(k+1) = \frac{\left(x(k+1) - \bar{x}(k+1)\right)^T \cdot w}{\left|x(k+1) - \bar{x}(k+1)\right|} \qquad (3.17)$$

where $\mathbf{x}(k+1)=\left[\mathbf{x}(k+1)_0 \quad \mathbf{x}(k+1)_1 \quad \ldots \quad \mathbf{x}(k)_{L-1}\right]=\left[\mathbf{x}(k+1)_0 \quad \mathbf{x}(k)_0 \quad \ldots \quad \mathbf{x}(k)_{L-2}\right]$ is the next input vector, $\bar{x}(k+1)$ is the next mean. The mean $\bar{x}(k+1)$ and the magnitude $\left|x(k)-\bar{x}(k)\right|$ can be computed recursively. The mean $\bar{x}(k+1)$ is computed recursively as follows. Expanding $\bar{x}(k)=\frac{1}{L}\sum_{i=0}^{L-1}x(k)_i$ gives

$$\bar{\mathbf{x}}(k)=\frac{1}{L}\left\{\mathbf{x}(k)_0+\mathbf{x}(k)_1+\ldots+x(k)_{L-1}\right\} \tag{3.18}$$

To compute (3.18) for time $k+1$, we introduce a new sample $x(k+1)_0$ and lose the oldest sample $x(k)_{L-1}$ from the mean. Therefore, it follows that

$$\bar{x}(k+1)=\bar{x}(k)+\frac{1}{L}\left\{x(k+1)_0-x(k)_{L-1}\right\} \tag{3.19}$$

The magnitude scalar $\left|\mathbf{x}(k+1)-\bar{\mathbf{x}}(k+1)\right|$ can also be computed recursively. First expand and simplify $\left|x(k)-\bar{x}(k)\right|$

$$\begin{aligned}
\left|\mathbf{x}(k)-\bar{\mathbf{x}}(k)\right|^2 &= \sum_{i=0}^{L-1}\left(\mathbf{x}(k)_i-\bar{\mathbf{x}}(k)\right)^2 \\
&= \sum_{i=0}^{L-1}x(k)_i^{\,2}-2\bar{\mathbf{x}}(k)\cdot\sum_{i=0}^{L-1}\mathbf{x}(k)_i+\sum_{i=0}^{L-1}\bar{\mathbf{x}}(k)^2 \\
&= \left(\sum_{i=0}^{L-1}x(k)_i^{\,2}\right)-2L\bar{\mathbf{x}}(k)^2+L\bar{\mathbf{x}}(k)^2 \\
&= \left(\sum_{i=0}^{L-1}x(k)_i^{\,2}\right)-L\bar{\mathbf{x}}(k)^2 \\
&= \sigma(k)-L\bar{\mathbf{x}}(k)^2
\end{aligned} \tag{3.20}$$

where $\sigma(k)=\sum_{i=0}^{L-1}x(k)_i^{\,2}$ and $\bar{x}(k)=\frac{1}{L}\sum_{i=0}^{L-1}x(k)_i$. It therefore follows that

$$\left|x(k+1)-\bar{x}(k+1)\right|^2=\sigma(k+1)-L\bar{x}(k+1)^2 \tag{3.21}$$

The term $x(k+1)^2$ is simple the square of 3.19. To recursively compute the magnitude scalar in (3.21), it remains to compute $\sigma(k+1)$.

$$\begin{aligned}
\sigma(k) &= \mathbf{x}(k)_0^{\,2}+\mathbf{x}(k)_1^{\,2}+\ldots+\mathbf{x}(k)_{L-1}^{\,2} \\
\therefore\ \sigma(k+1) &= \sigma(k)+\mathbf{x}(k+1)_0^{\,2}-\mathbf{x}(k)_{L-1}^{\,2}
\end{aligned} \tag{3.22}$$

Using the results in (3.19), (3.21) and (3.22), the expression in (3.17) can be recursively computed as follows.

At start-up k=0

1. Compute the mean $\bar{x}(k) = \frac{1}{L}\sum_{i=0}^{L-1} x(k)_i$
2. Compute $\sigma(k) = \sum_{i=0}^{L-1} x(k)_i^2$
3. Compute the magnitude scalar $\left|x(k) - \bar{x}(k)\right|^2 = \sum_{i=0}^{L-1}\left(x(k)_i - \bar{x}(k)\right)^2$

For each subsequent pass

1. Fetch next sample $x(k+1)_0$
2. Compute $\bar{x}(k+1)$ from (3.19)
3. Compute $\sigma(k+1)$ from (3.22)
4. Compute $\left|x(k+1) - \bar{x}(k+1)\right|^2$ from (3.21)
5. Take the square-root of the result in 4, and compute r(k+1) from (3.17)
6. Increment k and go to 1

3.5 Design of a QRS detector using off-line estimation

The second approach is to compute an off-line estimate of the complete QRS pattern space based on all the previously classified cases. This "complex pattern space" is depicted by the enclosed region on the surface of a hyper-sphere in the conceptual diagram shown in Figure 70.

Figure 70 Conceptual diagram of the complex pattern space of the QRS pattern

If a candidate QRS pattern vector lies within this space, then it is assumed to be a valid QRS pattern. A complex pattern classifier is required to determine when this is

the case. This approach is not dependent on an on-line estimation of the QRS pattern shape, but relies on previous examples to be representative of the total possible QRS pattern space. This technique is more open to the effects of noise as the surface area of the QRS pattern region is inevitably wider in Figure 70 than it is in Figure 67. A random noise vector, normalised to a fixed radius, has a greater chance of "landing" within this region than for the simple correlation technique. Two powerful techniques for representing complex pattern spaces are Multi-Layered Perceptrons (MLP) and Radial Basis Functions (RBF). These both fall under the category of Artificial Neural Networks are now discussed.

3.5.1 Using the Multi-Layered Perceptron to represent a complex pattern space

Artificial Neural Networks (ANN) have become very popular because of their ability to approximate complex functions in multi-dimensions and produce complex mappings. There are many different ANN paradigms, the most popular being the Multi-Layered Perceptron (MLP) which is shown below in Figure 71.

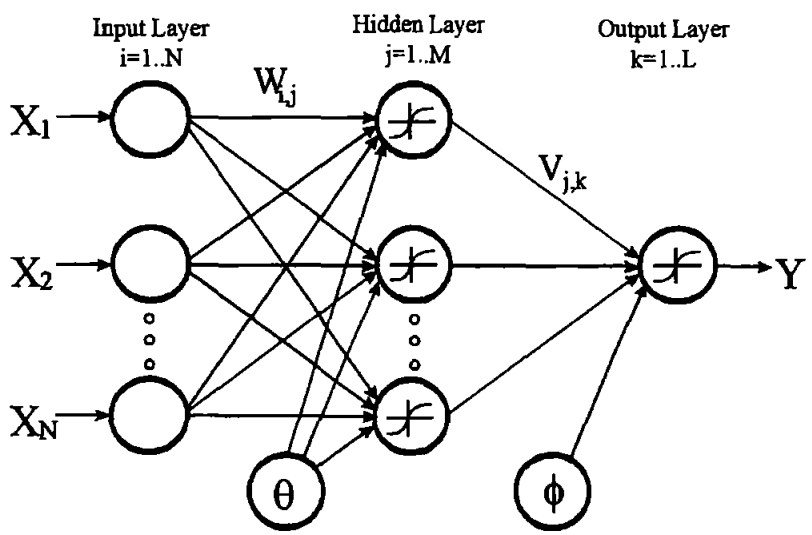

Figure 71 Multi-Layered Perceptron (MLP)

The MLP has a layer of N inputs nodes, at least one 'hidden layer' of M artificial neurons[3] and an output layer of L artificial neurons. Extra inputs with constant values θ and ϕ are added to provide extra degrees of freedom. In the MLP, each layer has full connection from the previous layer such that **Wx=a**, where $\mathbf{W}_{j,i}$ is the weight connecting the i^{th} input node x_i to the j^{th} 'hidden artificial neuron'. The input

to each hidden neuron is a linear combination of the input variables (Figure 72). The artificial neurons in the hidden layer(s) apply a non-linear function $f(\mathbf{a}_i)=\mathbf{h}_i$, where $\mathbf{h}_i$ is the output of the j^{th} hidden neuron. This function is known as the activation function.

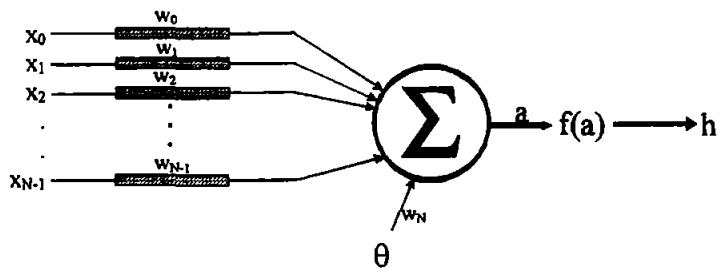

Figure 72 Artificial Neuron

The values at each hidden artificial neuron is computed as

$$h_j = W_{N,j} \cdot \theta + \sum_{i=0}^{N-1} W_{j,i} \cdot x_i \qquad (3.23)$$

where θ is a constant. The output of each hidden neuron is computed as

$$h_j = f(\mathbf{a}_j) \qquad (3.24)$$

The most popular activation function is the sigmoid (see Figure 73) but any non-linear function can be used.

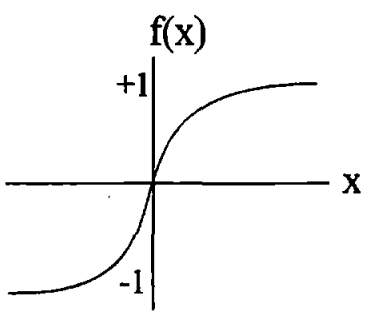

Figure 73 Sigmoidal activation function used at the hidden layer of the MLP

The output neurons $\mathbf{y}_k$ are also connected via weights to the output of each hidden neuron such that $\mathbf{y}=\mathbf{f}(\mathbf{Va})$, where $\mathbf{V}_{k,j}$ is the weight connecting the j^{th} hidden neuron to the k^{th} output neuron. Each output neuron is computed as

$$\mathbf{y}_k = f(\mathbf{V}_{k,M} \cdot \phi + \sum_{j=1}^{M-1} \mathbf{V}_{k,j} \cdot \mathbf{h}_j).$$

---

[3] More than one hidden layer can be used

For this work an ensemble of input vectors, which are a mixture of known QRS pattern vectors and noise vectors, are stored in the rows of a matrix **X** and a corresponding output classification is stored in rows of a vector **Y**. These are presented to the MLP for 'training', which is the process by which the network learns the complex mapping from **X** to **Y**. An output of 1 is assigned to a QRS pattern and an output of 0 to noise. During the learning phase, the weight coefficients **W** and **V** are computed such that each row of **X** maps to each row of **Y** to within an acceptable error. There is unfortunately no known method of directly computing the values in **W** and **V** for the MLP. Gradient descent methods such as the generalised delta rule, with back propagation and momentum, are used to optimise the weight coefficients over many iterations (*Rumelhart & McClelland 1992*). Gradient descent techniques can get stuck in sub-optimal solutions, often known as local minima. Other techniques such as simulated annealing and genetic algorithms (*Masters 1993*) do not suffer as much from local minima, but do take considerably longer to find the desired solution. New QRS and noise vectors are then presented to the MLP and the output is tested against the true classification.

3.5.2 Theoretical discussion of the Multi-Layered Perceptron

The MLP is theoretically capable of approximating any continuous function of any number of variables in a compact form. The accuracy of the approximation greatly depends on the choice of activation function, the number of hidden nodes and the technique used to optimise the weight matrices **W** and **V**. The MLP is essentially an extension of linear algebra to include non-linear terms in the mapping from one vector space to another. The MLP achieves this by forming new variables at the output of the hidden nodes which are non-linear functions of the original variables.

To illustrate how this works, consider a generalised function of two input variables $f(\mathbf{x}_0, \mathbf{x}_1)$. In general, any continuous differentiable function of two variables can be approximated with a infinite Taylor series as

$$f(x_0,x_1) = a_0 + a_1 x_0^{\,1} + a_2 x_1^{\,1} + a_3 x_0^{\,2} + a_4 x_1^{\,2} + \ldots + a_5 x_0^{\,1} x_1^{\,1} + a_6 x_0^{\,3} + a_7 x_1^{\,3} + \ldots + a_m x_0^{\,p} x_1^{\,q} \qquad (3.25)$$

and is represented graphically in Figure 74. Given an ensemble of input vectors $\mathbf{x}(k)=[\mathbf{x}(k)_0\ \mathbf{x}(k)_0]^T$, and a corresponding mapping $\mathbf{y}(\mathbf{x}(k))$, then the coefficients a can

be computed directly to achieve either a perfect mapping (given enough free terms) or a suitable approximation.

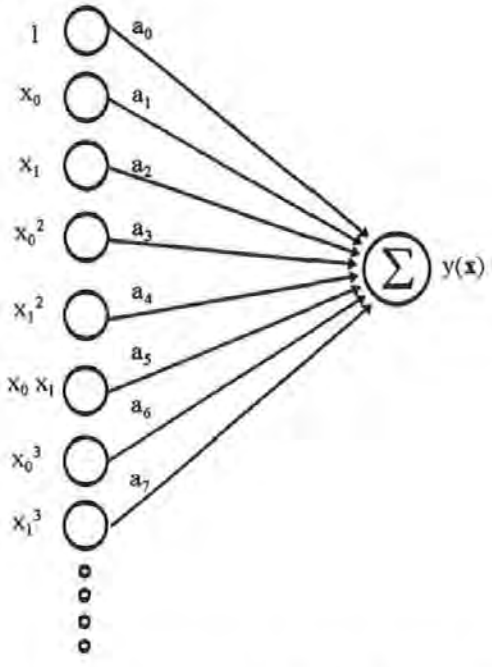

Figure 74 Generalised network structure for a non-linear mapping for two variables

For example, N row vectors $\mathbf{x}(k)=[\mathbf{x}_0(k)\ \mathbf{x}_1(k)]$, stored in rows of a matrix $\mathbf{X}$ are to be mapped to N scalar values $\mathbf{y}(k)$, $k=0..N-1$. For a linear system, this would be solved in a least-squares sense as $\mathbf{Xa}=\mathbf{y}$ where $\mathbf{a}=(\mathbf{X}^T\mathbf{X})^{-1}\mathbf{X}^t\mathbf{y}$. The success of this requires that $\mathbf{y}$ can be formed by a linear combination of the columns in $\mathbf{X}$, that is $\mathbf{y}$ lies within the space spanned by $\mathbf{X}$. Given that $N>2$, this means that there are more equations than free variables in $\mathbf{a}=[\mathbf{a}_0\ \mathbf{a}_1]$, hence this mapping rarely possible without errors (unless the problem is trivial). To reduce this error additional second order non-linear terms $\mathbf{Q}(k)=[\mathbf{x}_0^2(k), \mathbf{x}_1^2(k), \mathbf{x}_0(k)\mathbf{x}_1(k)]$, $k=0..N-1$, are computed and added to form a matrix $\mathbf{M}=[\mathbf{X}|\mathbf{Q}]$ where $\mathbf{Q}$ is a matrix of non-linear terms. For non-trivial problems, the region of space spanned by $\mathbf{M}$ is greater than that of $\mathbf{X}$ and spans some of the null-space[4] of $\mathbf{X}$, although it is directly derived from $\mathbf{X}$ by non-linear functions. The mapping is still maintained as a linear problem, that is $\mathbf{Ma}=\mathbf{y}$ and can be solved directly in a least square sense. This expanded for clarity below in (3.26).

[4] The null-space of $\mathbf{X}$ contains all vectors $\mathbf{a}$ such that $\mathbf{Xa}=0$ (*Strang G., 1988*)

$$\begin{bmatrix} 1 & x_0(0) & x_1(0) & x_0(0)\cdot x_1(0) & x_0^2(0) & x_1^2(0) \\ 1 & x_0(1) & x_1(1) & x_0(1)\cdot x_1(1) & x_0^2(1) & x_1^2(1) \\ : & : & : & : & : & : \\ 1 & x_0(N-1) & x_1(N-1) & x_0(N-1)\cdot x_1(N-1) & x_0^2(N-1) & x_1^2(N-1) \end{bmatrix} \cdot \begin{bmatrix} a_0 \\ a_1 \\ a_2 \\ a_3 \\ a_4 \\ a_5 \end{bmatrix} = \begin{bmatrix} y(0) \\ y(1) \\ : \\ y(N-1) \end{bmatrix} \quad (3.26)$$

Note that the linear terms are still present, as would be for a linear mapping, but in addition non-linear terms are now included. If this does not produce an acceptable approximation, then higher order terms can be added until an acceptable approximation is obtained.

A difficulty with implementing this directly is that the number of terms in **Q** and a soon become unmanageable as the number of input variables increases and/or as the degree of approximation is increased. The MLP however is a much more compact method of performing a non-linear mapping. The MLP structure is a much more efficient representation usually requiring far less free parameters (weights). To illustrate consider a differentiable non-linear activation function *f(a)* at a hidden node of an MLP which expands only to second order (for simplicity sake) such that

$$f(a) = \beta_0 + \beta_1 a^1 + \beta_2 a^2 \quad (3.27)$$

where a is a linear combination of two other variables $a = w_0\mathbf{x}_0 + w_1\mathbf{x}_1$, and β_k, *(k=0..2)*, are real scalar constants which can be computed using the well known Taylor series expansion (*Burden & Faires 1989*). Substituting for a gives

$$f(a) = \beta_0 + \beta_1(w_0\mathbf{x}_0 + w_1\mathbf{x}_1)^1 + \beta_2(w_0\mathbf{x}_0 + w_1\mathbf{x}_1)^2 \quad (3.28)$$

Expanding gives

$$f(a) = \beta_0 + \beta_1 w_0\mathbf{x}_0 + \beta_1 w_1\mathbf{x}_1 + \beta_2 {w_0}^2{\mathbf{x}_0}^2 + \beta_2 w_0\mathbf{x}_0 w_1\mathbf{x}_1 + \beta_2 {w_1}^2{\mathbf{x}_1}^2 \quad (3.29)$$

Equating coefficients in (3.29) and (3.25) gives

$$\begin{aligned} \beta_0 &= a_0 \\ \beta_1\mathbf{w}_0 &= a_1 \\ \beta_1\mathbf{w}_1 &= a_2 \\ \beta_2{\mathbf{w}_0}^2 &= a_3 \\ \beta_2{\mathbf{w}_1}^2 &= a_4 \\ \beta_2\mathbf{w}_0\mathbf{w}_1 &= a_5 \end{aligned}$$

The α and β values are known, with only two unknowns $\mathbf{w}_0$ and $\mathbf{w}_1$ in six equations. Clearly this cannot be solved precisely, but a best fit can often be found. To improve the accuracy more hidden nodes are introduced to add more free

parameters (weights) until a suitable approximation is found. The output of the hidden nodes **H** are linearly combined by the weights **V** to form an output y such that **Hv=y**. Hidden nodes are added until the space spanned by **H** contains y.

In general the non-linear activation functions are not simply second order functions and produce higher order terms when expanded. This gives rise to a good approximation to the ideal mapping often with only a few hidden nodes.

This illustrates that a Neural Network, given enough non-linear hidden nodes with an infinite degree taylor-series expansion, will have enough degrees of freedom to approximate any non-linear mapping.

3.5.3 Novelty detection

There is a real danger with using muli-layered perceptrons when presenting totally new data. The most that can be expected from a non-linear mapping function such as an MLP is that *it will perform well as an interpolator*. Consider Figure 75 where three sets of data {A, B, C} are presented to a pattern classifier. These might be, for example, digitised hand written characters of 'A', 'B' and 'C'. Examples of these are used to train the MLP and define the pattern space for each set Two outputs of the network might be defined as [0 1] for character 'A', [1 0] for character 'B' and [1 1] for character 'C'. If during the testing phase the MLP is given a character 'D', which has similar features to 'B' , it *probably* get classified as such. Presenting with MLP with a totally novel character such as a 'Z' or some random noise, which lie far outside all defined pattern space, *might* also arbitrarily produce a classification of A, B or C. This can be misleading so a form of *novelty detection* is required to detect when a totally novel input pattern is presented.

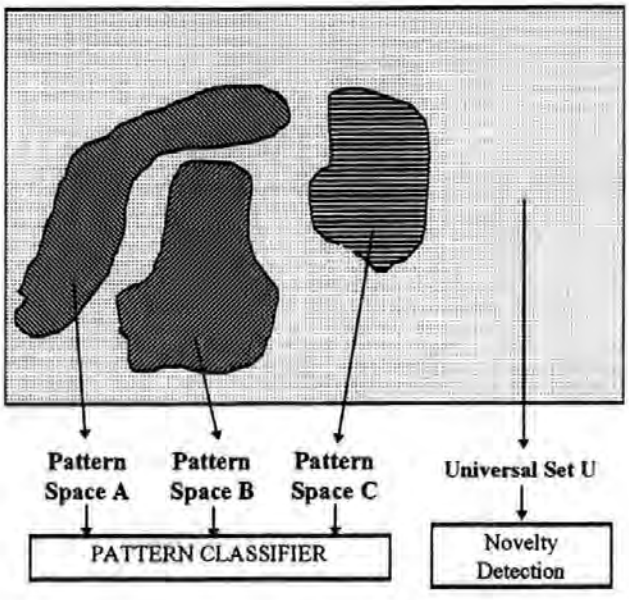

Figure 75 Conceptual diagram illustrating the need for novelty detection

A MLP is particularly powerful at representing and separating data into different complex pattern vector spaces but is poor at novelty detection. The best application for a MLP is where the data is always drawn from a finite set of vector spaces which are represented by the training data. At best the MLP is also able to interpolate between these spaces. In general, the term *generalisation* often attributed to the MLP refers to *interpolation* and *not extrapolation.* If extrapolation will occur, then extra effort is required to perform novelty detection, and unfortunately QRS detection falls into this category. Random noise is regularly presented to the MLP and this can belong to any region within a full 20 dimensional space. Unless the output is defined to be 1 in the small QRS space and constrained to zero at other regions in the 20D space then the MLP will essentially be extrapolating in the presence of random noise and producing erratic behaviour. The training set of vectors consists of QRS pattern vectors and random noise. Producing a representative training set of random noise that sufficiently spans the complete vector space is very time consuming for high dimensional problems.

3.5.4 Supervised training of the Multi-Layered Perceptron for QRS detection

The usual method for training a MLP is to extract a large set of examples from the data and randomly select a sub-set of this for training, leaving the remaining examples for testing. The training examples and desired outputs are presented to the

MLP and the generalised delta rule using back propagation is used to compute the weights.

10 QRS vectors were manually extracted from each of 10 different cases in the database which then define the QRS pattern space and map to a single 1 in the output space. Examples of incorrectly aligned QRS patterns and maternal QRS patterns were manually extracted which map to a 0 in the output space. Random noise was generated using Haltons quasi-random sequences (*Press et al. 1992*). This algorithm evenly fills the vector space, unlike other random number generation sequences which tend to form clusters and leave gaps. To generate M quasi-random N length vectors $v_i(k)$, $i=0..N$, $k=0..M$, where $0<v_i(k)<1$, the following algorithm is employed. To obtain the k^{th} vector $v(k)$ in the Halton sequence,

1. For each element $v_i(k)$ convert k to base b_i, where b_i is the i^{th} prime in an increasing sequence of primes. For example, $b_0=3$, $b_1=5$, $b_2=7$. If k=10, then $v_2(k)=13$ (base 7).
2. Reverse the digits of each element v_i, such that the least-significant digit becomes the most significant digit in base b_i. In the example, $v_2(k)=31$
3. Place a decimal point before all the digits. In the example, $v_2(k)=0.31$
4. Convert to base 10. Finally, $v_2(k)=3*7^{-1}+1*7^{-2}=0.4490$ (4-decimal place accuracy).

This works because the least-significant digit, which varies the most frequently for each k, becomes the most significant digit. Each value of k is unique, therefore it follows the resulting decimal number is always unique, so ensuring the same number is never repeated.

The number of examples used for training relates to the number of weights in the MLP structure. For a MLP with I inputs, J hidden nodes and K outputs, the number of weights w is:

$$w=(I+1).J+(J+1).K \qquad (3.30)$$

As a guideline, the number of examples used for training should be between 2w and 10w. The reason for this is to (hopefully) ensure the problem space is adequately

covered so that network can generalise and to prevent over-training. Training on too few examples will not cover the input space enough and when tested with new examples it's behaviour is not guaranteed causing erratic behaviour at the output. Over-training is another factor which causes erratic behaviour when testing an MLP with new examples. This becomes a problem if the errors at training time are allowed to become too small when there is noise or natural variability in the training data. This phenomena can be explained by considering the MLP as a multi-dimensional curve-fitter or function approximation. To visualise this only 1 dimension for input and output is used, but the same principal holds for higher dimensions. Given that the input values are scalars $\mathbf{x}_k$ ($k=1..20$) and the desired outputs are scalars $\mathbf{d}_k$ it is required to find a function that maps **x** to **d**. In the Figure 76a the crosses are the training data and the continuous line $y(\mathbf{x})$ is the computed approximation. (The underlying function is actually d(x)=sin(x)+error for illustrative purposes). In Figure 76a there is a small finite error for most training examples and large errors for the rogue examples. This results in a satisfactory approximation to the function and is the phenomena known as *generalisation*. In Figure 76b however the approximation has been allowed to fit every point with virtually zero error. This over-fitting or 'over-training' has the effect of losing the general trend in the data. Examining Figure 76a it is clear that presenting a new example of x=0.25 will reproduce the sensible value but in Figure 76b would produce a rogue error due to the over-training.

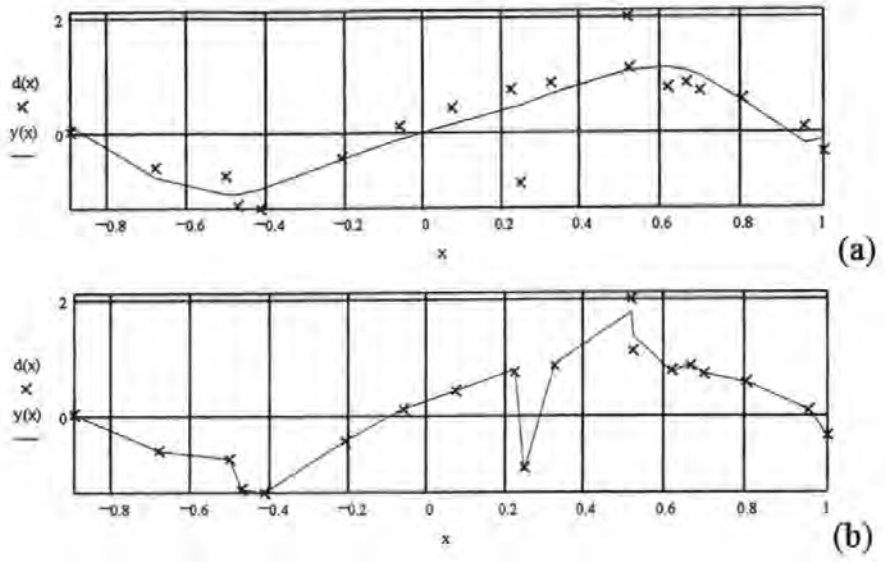

Figure 76 (a) Correct approximation found by fitting to the overall trend in the data and (b) Incorrect approximation found by fitting every point in the data

Plotting the errors in an approximation is a good way to check generalisation but unfortunately for the QRS detection problem with 20 inputs, it is impossible to visualise. Information has to be obtained from looking at how the error decreases during training. In general the error used is the Root Mean Squared error (RMS error) given by

$$RMSerror = \sqrt{\frac{1}{N}\sum_{k=0}^{N-1}(y_k - d_k)^2} \qquad (3.31)$$

A plot of the RMS error for a 20-5-1 MLP is shown below.

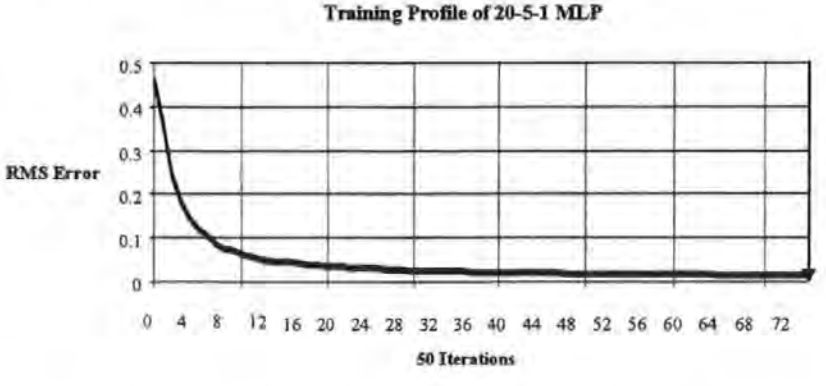

Figure 77 RMS error of 20-5-1 MLP trained on ECG QRS patterns

Training stops when the change in error flattens off and becomes asymptotic. For the above example the training is stopped at 20*50 iterations. The network is now ready for testing and implementation if successful in generalisation.

3.6 Comparing and optimising the performance of the QRS detection techniques

In this work each QRS detector produces a scalar output when presented with a pattern vector. If the output exceeds a given threshold value, then the system has indicated a Positive result. If the output is less than or equal to the threshold value, then the system has indicated a Negative result. The performance of each technique needs to be evaluated for suitability to foetal monitoring. It is inevitable that no single technique is ever perfect. There is always a trade between the number of correctly detected waveforms (true positive events) and the number of false detection's (false positive events). Establishing a balance between the two requires the threshold to be optimised for each technique. The results of the two techniques then need to be compared. A method of achieving this is by Receiver Operator Characteristic (ROC) analysis.

3.6.1 Receiver Operator Characteristic (ROC) Analysis

A technique used to measure how well a given detector can discriminate between two events is known as Receiver Operator Characteristic (ROC) analysis. This was introduced to medical decision making by *Lustard 1991* and has become a popular technique in medical research *(Centor R.M. 1991; Hanley J.A. 1989; McNeil B.J. et al. 1975)*. The four categories of detection are summarised below and in the contingency in Table 7 (*Swets 1988*).

a) *True Positive* : The total number of cases where the pattern classifier correctly detects a real QRS pattern.
b) *False Positive* : The total number of cases where noise is incorrectly classified as a QRS pattern.
c) *False Negative* : The total number of missed QRS patterns.
d) *True Negative* : The total number of cases where noise is correctly classified.

From these measures the Hit Ratio and the False Alarm Ratio are computed as follows.

Event / *System Classification*	**Positive**	**Negative**
Positive	**TP** TRUE POSITIVE (Correct classification)	**FP** FALSE POSITIVE (Missed beat)
Negative	**FN** FALSE NEGATIVE (False alarm)	**FN** TRUE NEGATIVE (Correct noise rejection)

Table 7 Two-by-two contingency table

$$\text{Hit Ratio} = \frac{TP}{TP + FN}$$

$$\text{False Alarm Ratio} = \frac{FP}{FP + TN}$$

where TP is the number of True Positives, FN is the number of False Negatives, FP is the number of false positives and TN is the number of True Negatives. TP+FN is the total number of QRS patterns in the experiment and FP+TN is the total number of non-QRS patterns (noise) used in the experiment. It is important to detect enough ECG complexes in order to extract enough meaningful clinical information, so one objective is to keep the Hit Ratio high. At the same time, this will often be at the expense of increasing number of False Alarm Ratio. For QRS detection, *it is important to keep the False Alarm Ratio very low to avoid adding noise into the signal average and producing misleading waveforms.*

The objective is to find the threshold value that balances the Hit Ratio and False Alarm Ratio in an acceptable way. This is achieved by measuring the Hit Ratio and False Alarm Ratio for different threshold values with each technique. From this a ROC curve can be plotted. From this curve it is possible select a point along the curve and chose the threshold. Equally it provides a means to measure and compare the ability of the different detectors to discriminate between real positive events and false positive events.

To construct a ROC curve for each technique a contingency table is recorded. In the case of the QRS detection problem, the performance characteristics of each detector is recorded for different output threshold values. The Hit-Ratio is plotted against the False Alarm Ratio to produce the ROC curve.

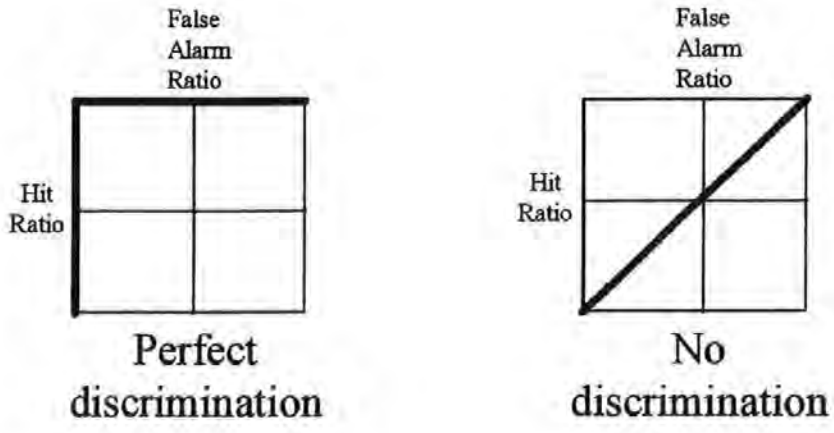

Figure 78 Idealised ROC curves for perfect and no discrimination

Figure 78 shows the ROC curves for a detector with perfect discrimination and no discrimination. An upper-left-diagonal curve indicates perfect ability to discriminate between true and false events, and has an area 1.0 under the curve. A ROC curve for a detector with no ability to discriminate is a straight diagonal line which has an area of 0.5

3.6.2 Validation methodology

Experiments were conducted to optimise the threshold value for each technique and compare their relative performance. Three blocks of 55000 samples, taken from three separate cases, were used to test each technique. These sections of data have variable features, such as large P complexes, muscle and power-line noise and some transient shifts.

The total number of True Positive (TP), False Positive (FP), True Negative (TN) and False Negative (FN) events are counted for each case. Examples of each of the four classes of events are shown in Figure 79.

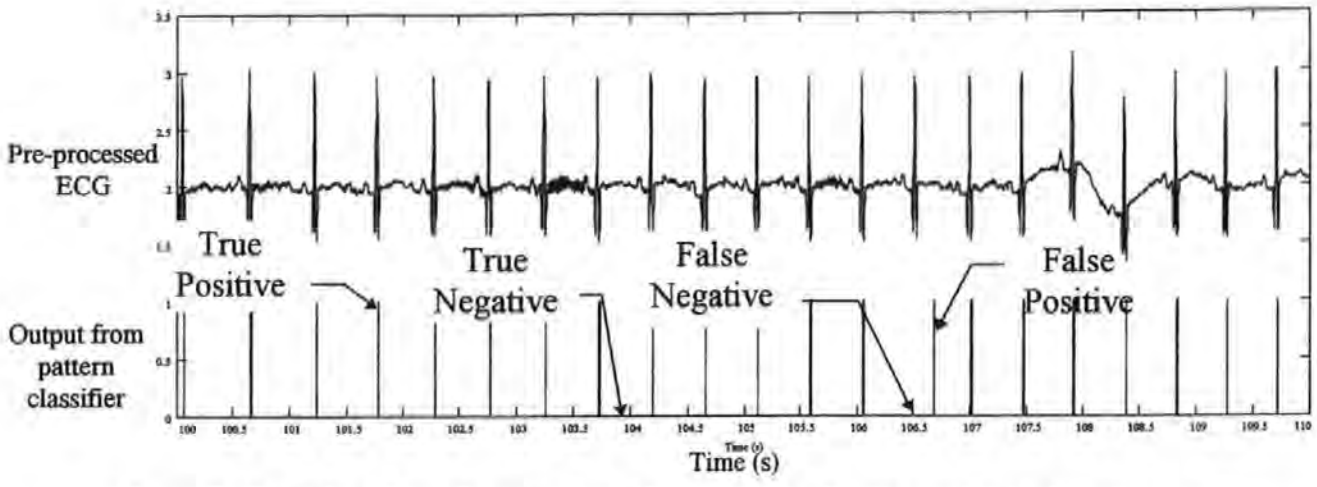

Figure 79 Examples of True Positive, True Negative, False Positive and False Negative events

For each case, there were 55000 data samples sampled at 500Hz. The following procedure was conducted for both the MLP and correlation technique.

1. Set threshold at lowest reasonable value, typically 0.9 for the correlation technique and 0.2 for the MLP.
2. Apply all the **M**=55000*3=165000 candidate QRS data vectors to the pattern classifier. These vectors are a moving window of data samples.
3. Count the number of true QRS complexes (**N**)
4. Count the number of True Positive events (**TP**) and False Positive events (**FP**)
5. Calculate the number of True Negative events **TN=M-N-FP**
6. Calculate the number of False Negative events **FN=N-TP**
7. Increase the threshold by small amount
8. While threshold ≤ 1 Goto 2
9. Record the results in a contingency table.
10. Compute the Hit Ratio and False Alarm Ratio for each threshold value
11. Plot ROC curve and estimate the area for each technique

A larger the area implies a better ability to discriminate. The area under the ROC curve is estimated using the trapezoidal rule.

3.6.3 Results for the correlation algorithm

The results for all three cases are recorded in Table 8 and plotted as an ROC curve in Figure 80a & b. The area under the ROC curve is 0.99873.

A technique for selecting a good compromise threshold value is the point nearest the upper-left corner of the ROC curve, and this point corresponds to a threshold value

between 0.97 and 0.98. For ST analysis however, it is desirable to place an emphasis on reducing the false alarm rate, so a threshold value of 0.98 is chosen. From Table 8 , a value of 0.98 produces a false positive rate corresponding to a 25/164178 probability of producing a false positive. This corresponds to 25 false positive results in approximately 5½ minutes of ECG data, which is slightly less than 5 false positive events per minute. This is considered to be 'reasonable' given that the waveforms are later averaged, although was disappointing. Further increasing the threshold value reduces the False Positive rate but starts to rapidly reduce the True Positive rate. The correlation algorithm, with on-line learning and a high threshold value has good ability to reduce the false positive detection rate. Unfortunately periods of very noisy data was observed to induce too many false negative events.

Threshold	True Positive	False Positive	True Negative	False Negative	False Alarm Ratio	Hit Ratio
0.00	822	164178	0	0	1.0000	1.0000
0.90	820	688	163490	2	0.0042	0.9976
0.95	819	217	163961	3	0.0013	0.9964
0.97	808	76	164102	14	0.0005	0.9830
0.98	781	25	164153	41	0.0002	0.9501
0.99	576	2	164176	246	0.0000	0.7007
1.00	0	0	164178	822	0.0000	0.0000

Table 8 Contingency table for the Correlation algorithm (with on-line learning)

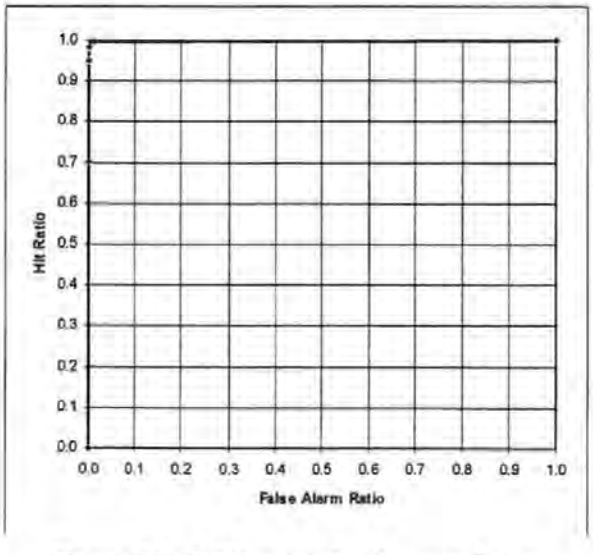

Figure 80a ROC curve for the correlation technique

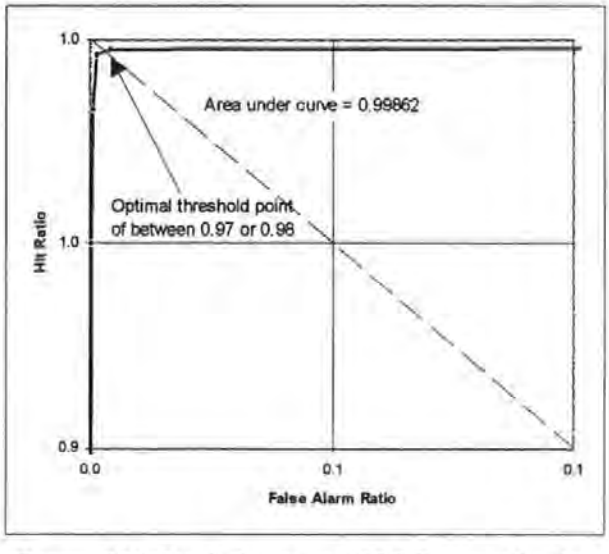

Figure 80b Top left corner of ROC curve for the correlation algorithm showing the optimum threshold point

3.6.4 Results for the MLP

Initial results of the MLP were very variable, depending on the case presented. The MLP has a very high ability to detect QRS complex waveforms, but also initially produced far more false positive events than was acceptable for some of the cases. Case number oe102 in the database was such a case, and the contingency table is given below in Table 9. In this experiment, no single waveform was missed but the false positive rate was unacceptably high.

Threshold	True Positive	False Positive	True Negative	False Negative	False Alarm Ratio	Hit Ratio
0	242	14758	0	0	1.0	1.0
0.2	242	773	13985	0	0.05238	1.0
0.4	242	597	14161	0	0.04045	1.0
0.6	242	484	14274	0	0.03280	1.0
0.8	242	315	14443	0	0.02134	1.0
0.9	242	210	14548	0	0.01423	1.0
0.93	242	151	14607	0	0.01023	1.0
0.95	242	106	14652	0	0.00718	1.0
1	0	0	14758	242	0.0	0.0

Table 9 Contingency table for case oe102 using an MLP

In contrast to this, a much noisier case, oe108, was tested and the results were greatly improved. From the contingency table in Table 10 a threshold value of 0.93 produces only one false positive and 5 false negatives events out of 295 QRS waveforms. Upon examination of the data, the only visual difference was that the *MLP performed far better when the data was noisy.*

Threshold	True Positive	False Positive	True Negative	False Negative	False Alarm Ratio	Hit Ratio
0	295	14705	0	0	1.0	1.0
0.2	295	154	14551	0	0.01047	1.0
0.4	295	89	14616	0	0.00605	1.0
0.6	295	54	14651	0	0.00367	1.0
0.8	295	25	14680	0	0.00170	1.0
0.9	295	12	14693	0	0.00082	1.0
0.93	290	1	14704	5	0.00007	0.98305
0.95	116	0	14705	179	0.0	0.39322
1	0	0	14705	295	0.0	0.00000

Table 10 Contingency table for case oe108 using an MLP

To obtain such good results for such high quality data, a small amount of random noise has to be added to the data if the signal-to-noise ratio was very high.

The reasoning behind this is as follows. During the training phase, the MLP was trained to discriminate QRS complexes and quasi-random noise because the noise was meant to represent the universe of patterns outside the QRS complex pattern space. Clearly this model works very well when random noise is present. There are some cases however where the quality of the data is such that the random noise energy is insignificant. In these cases the true negative data (between QRS complexes) are smooth and slow-moving and it is this data which can induce false positive events. One could argue that these need to be added to the training set and the network should be retrained. Unfortunately it is very difficult to extract a characteristic training set of such data, as the permutations are vast. It is much simpler to ensure the random noise energy is significantly higher than the slow-wave energy. Applying random noise to case oe102 produced the following results.

Threshold	True Positive	False Positive	True Negative	False Negative	False Alarm Ratio	Hit Ratio
0	242	14758	0	0	1.0	1.0
0.2	242	46	14712	0	0.00312	1.0
0.4	242	29	14729	0	0.00197	1.0
0.6	242	19	14739	0	0.00129	1.0
0.8	241	12	14746	1	0.00081	0.99587
0.9	240	7	14751	2	0.00047	0.99174
0.93	240	5	14753	2	0.00034	0.99174
0.95	240	5	14753	2	0.00034	0.99174
1	0	0	14758	242	0.0	0.0

Table 11 Contingency table for case oe102 using an MLP by adding random noise

The results have much improved, for a threshold value of 0.93, with only 5 false positive events and 2 false negative events.

Applying all three cases, and where necessary adding random noise, the MLP produced the following overall results. The contingency table for the MLP is given below in Table 12 and the ROC curve is given in Figure 81a & b. The area under the ROC curve is 0.999957. From Table 12 a threshold value of 0.93 has a very good True Positive rate (799/822) and only 6 False Positive events in 5½ minutes of data, which corresponds to just over 1 False Positive event per minute. This is very satisfactory and a significant improvement over the correlation algorithm.

Threshold	True Positive	False Positive	True Negative	False Negative	False Alarm Ratio	Hit Ratio
0	822	164178	0	0	1.0	1.0
0.2	822	221	163957	0	0.00135	1.0
0.4	822	122	164056	0	0.00074	1.0
0.6	822	73	164105	0	0.00044	1.0
0.8	821	37	164141	1	0.00023	0.99878
0.9	820	19	164159	2	0.00012	0.99757
0.93	799	6	164172	23	0.00004	0.97202
0.95	485	5	164173	337	0.00003	0.59002
1	0	0	164178	822	0.0	0.0

Table 12 Contingency table for the Multi-Layered Perceptron

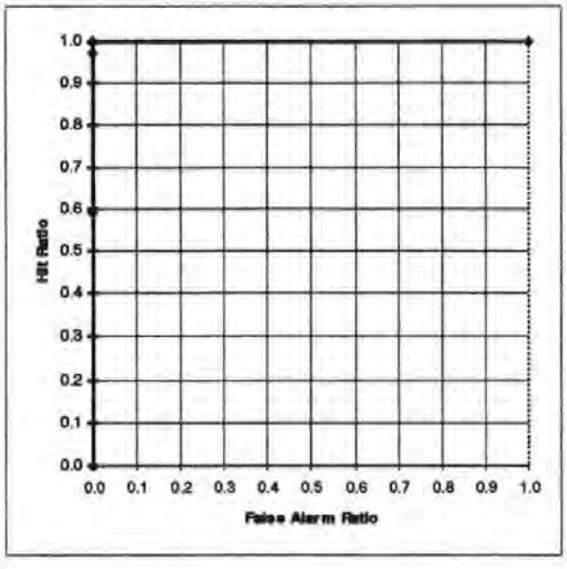

Figure 81a ROC curve for the MLP

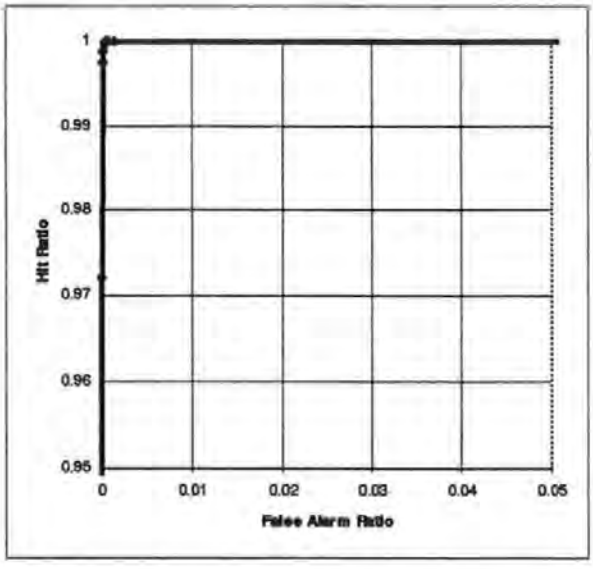

Figure 81b Top left corner of ROC curve for the MLP

1.7 Discussion and conclusion

There are two aspects to QRS detection, pre-processing and pattern recognition. For pre-processing, the differentiation technique was efficient at removing low-frequency noise but worsens the effects of high frequency noise. The MLP prediction filter technique was an improvement as was the least-squares filter. The least-squares technique performed at least as well as the MLP but has the advantage of simplicity and less computational overhead.

It is recognised that an amplitude invariant pattern recognition technique is required to locate each individual QRS complex. The simple correlation technique is restricted to detecting only one pattern, but as the QRS complex does not change

during a single labour, it would seem the theoretically optimal technique given an accurate estimate of the QRS complex can be obtained. The comb filter is the preferred technique as it performs as well as the least-squares filter and obtains a greater attenuation in the stop-band.

A robust novel technique has been developed here to estimate the QRS complex for each particular labour, given that the QRS complex shape does vary between patients. By careful selection of the detection threshold, the correlation algorithm was an acceptable QRS detector. A threshold of 0.93 was suitable. However, this technique suffers from missing too many QRS complexes (False Negatives) during periods of excessive noise.

The on-line estimation of the QRS complex pattern will always have some errors because not all the noise sources can be assumed to be random and will correlate. Small maternal ECG complexes, which get amplified by the normalisation process, remaining power-line noise, transient shifts, baseline noise and mains spikes cannot be assumed to be random noise.

The MLP can represent a much more complex pattern space than simple correlation, and is it shown to be more resistant to the effects of noise. It was found that for this application *the MLP only performs well in the presence of random noise.* Correlation has the theoretical advantage over the MLP in that its output is predictably low in the presence of totally novel inputs, but has less ability to detect every QRS complex. The MLP outperformed the correlation algorithm if random noise was present or artificially added to the data.

Another suitable method might be to use a Radial Basis Function (RBF). This has the advantage of the MLP as it can represent a complex pattern space whilst also maintaining the same predictable performance as correlation in the presence of truly novel inputs. This was not done due to lack of time, however, there might become a need examine the benefits of a RBF.

In conclusion, the combination of linear-filtering to remove noise and artefact and the MLP for pattern recognition perform well in detecting the QRS complex. The MLP out-performs simple linear correlation in the presence of noise as it is capable of representing a complex pattern space and has an improved ability to reject noise.

Chapter 4

Feature Extraction

4.1 Introduction

The interpretation of changes in the foetal ECG is a pattern recognition task. The task of the clinician is to recognise progressive changes in the shape of the ECG waveform, especially changes in the shape of the ST waveform and to assess the clinical significance of these changes. A trained human expert has very good pattern recognition capability, but their performance will reduce with fatigue and boredom, making this task ideally suited to a computer. However, pattern recognition is not so simple for a computer. The pattern recognition task is simplified by dividing the ECG waveform into different component waveforms. The idealised foetal ECG components shown below in Figure 82.

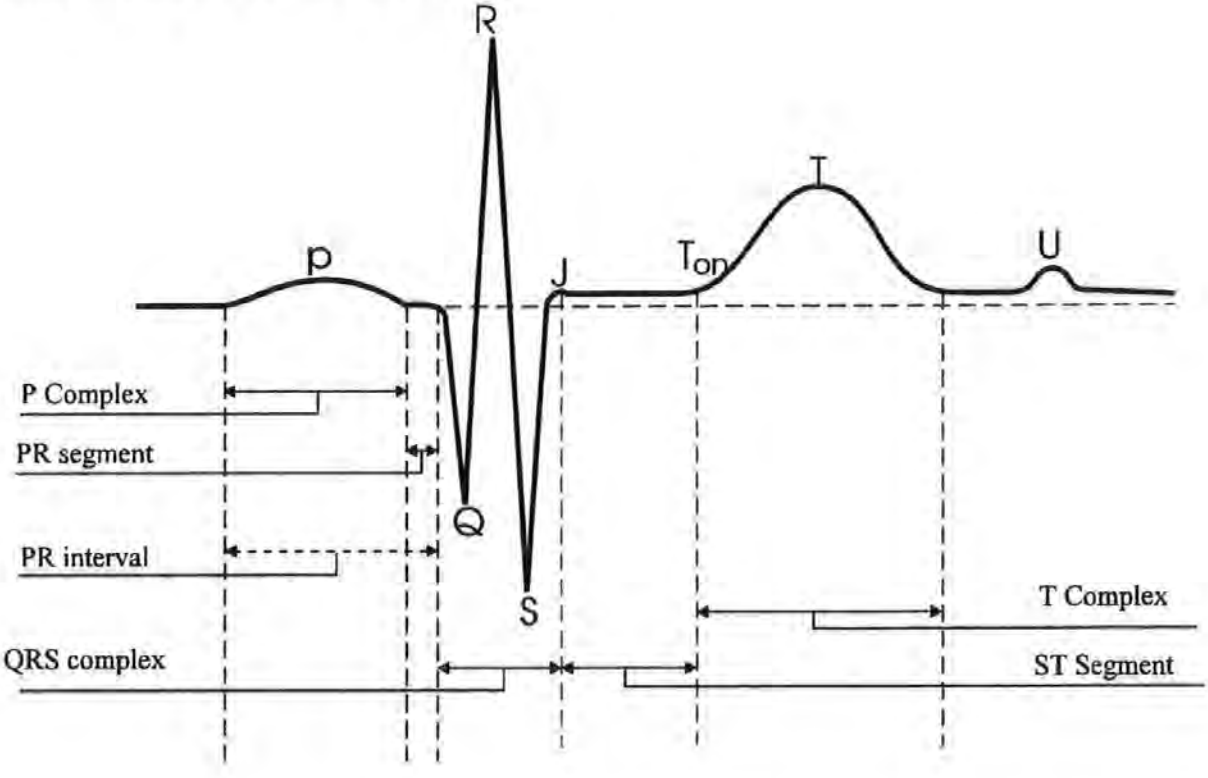

Figure 82 Decomposition of the foetal ECG waveform

Figure 82 is 'decomposed' into component waveforms, namely the P complex, PR segment, QRS complex, ST segment, T complex and sometimes the TU segment and U complex *(Trahanias and Skordalakis 1989)*. The most important components of the foetal ECG waveform for this work are the ST segment and T complex. It is important to be able to identify the shape of these components and determine how they progressively change during labour. To simplify pattern recognition, visible

features are identified and measured in order to quantify the ST segment and T complex shape. For example, from Figure 82 three commonly used features in adult cardiology are the J point, T peak onset (T_{on}) and the T peak amplitude amongst others. These are not the only features of interest however, as alone, they do not describe the ST segment and T complex shape.

To define the start and end of each waveform requires the location and extraction of visible *features* in the waveform, either by a piece-wise search *(Kirk & Smith 1986)* or by self learning techniques *(Akselrod et al. 1987)*. Different methods of decomposing the ECG waveform shape such as pole-zero models *(Murthy & Niranjan 1992)*, neural techniques *(Suzuki & Ono 1992)*, knowledge based search *(Lee & Thakor 1984)* and syntactic pattern recognition *(Trahanias & Skordalakis 1989)* have been reported. Sophisticated techniques such as Neural Networks require large representative sets of ECG data with a wide span of possible ST waveform shapes. A wide span of foetal data are not readily available, but knowledge of abnormal foetal ECG shapes does exist. This work uses simple search algorithms to find key features in the ST waveform using clinical knowledge. Even after signal enhancement, the ECG waveform is usually still contaminated by noise which introduces false peaks and valleys and impedes accurate feature extraction. Locating and measuring peaks, troughs and derivatives of waveforms is difficult in the presence of noise. Further enhancement and simplification of the waveform is clearly required if this method is to be reliable. One solution reported was to fit a series of straight (regression) lines to the foetal ECG complex *(Kirk and Smith 1986)*. This greatly simplifies the process of feature extraction and measurement but inevitably introduces errors when the portions of data cannot be approximated accurately with straight lines (such as bi-phasic waveforms). To solve this problem, this idea has been extended to use higher degree approximations which approximate the data more accurately whilst still simplifying the feature extraction process. Chebyshev polynomial approximations are fitted to the foetal ECG ST and PR waveform (see Figure 83). Chebyshev polynomials are chosen specifically here because the error of the approximation is evenly distributed over the whole approximation. The computation of the polynomial coefficients, as discussed in

chapter 2, is simple and evaluation of the Chebyshev polynomials is less numerically sensitive than ordinary polynomials of the form $c_0 + c_1 t + c_2 t^2 + ... + c_m t^m$.

4.2 Using Chebyshev Polynomials to simplify feature extraction

A smooth curve *f(t)* fitted to the whole ST and PR waveform is shown in Figure 83

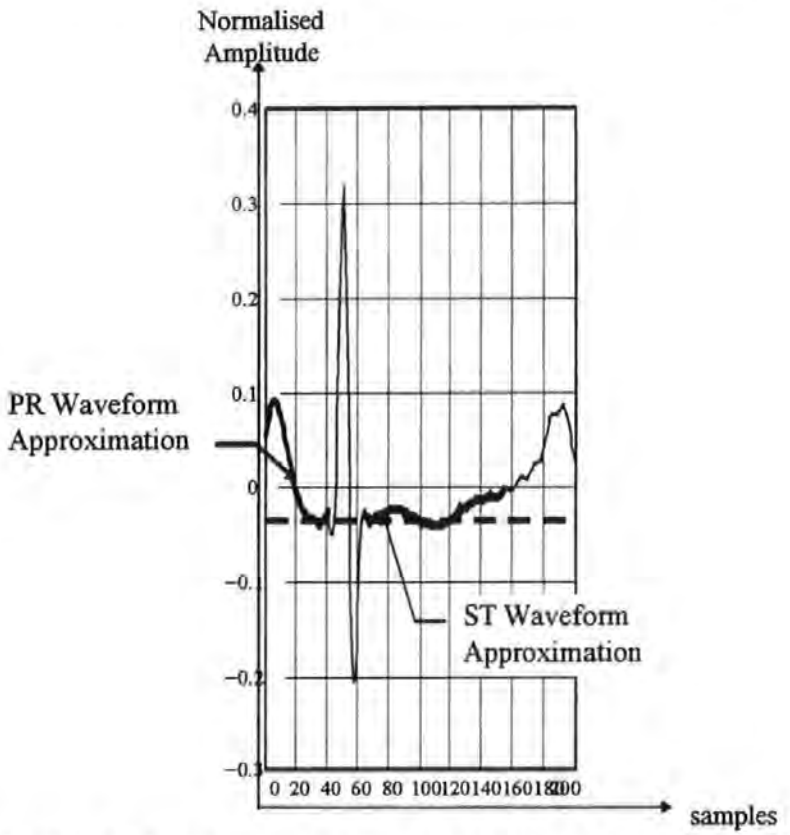

Figure 83. Smooth Chebyshev approximation of the Foetal ECG ST waveform

where $$f(t) = c_0 + c_1 T_1(t) + c_2 T_2(t) + c_3 T_3(t) + ... + c_m T_m(t) \qquad (4.1)$$

and where $T_k(t)$ is the k^{th} degree Chebyshev polynomial $T_k(t)=cos(k.cos^{-1}(t))$, $t=\{-1..+1\}$. This technique has very good signal enhancement properties because the function *f(t)* is continuous and smooth with *a fixed number of extrema* (maxima and minima) determined by the degree of approximation *m*. The approximation tends to fit 'through' any remaining muscle or power-line noise, assuming the noise to have a symmetric distribution, and is a very good approximation to the true foetal ECG waveform itself.

This technique has many advantages when measuring important features from the ST waveform. It allows for convenient and accurate amplitude, derivative and integral measurements to be computed from *f(t)* with great ease. It also inherently

compresses the data as the $m+1$ coefficients are all that is required to reconstruct the whole ST waveform approximation. Using this technique, many of the reported problems associated with feature extraction are greatly reduced. The feature extraction and pattern recognition techniques are now discussed.

4.3 Describing the ST shape by quantitative feature extraction

There are two main patterns that are recognised in the expert-knowledge base. These are T complex configuration *{Negative, Normal, Elevated}* and the ST segment configuration *{Depressed, Normal, Elevated, Bi-Phasic}*. The important shapes recognised by the clinical guidelines are summarised in Figure 84.

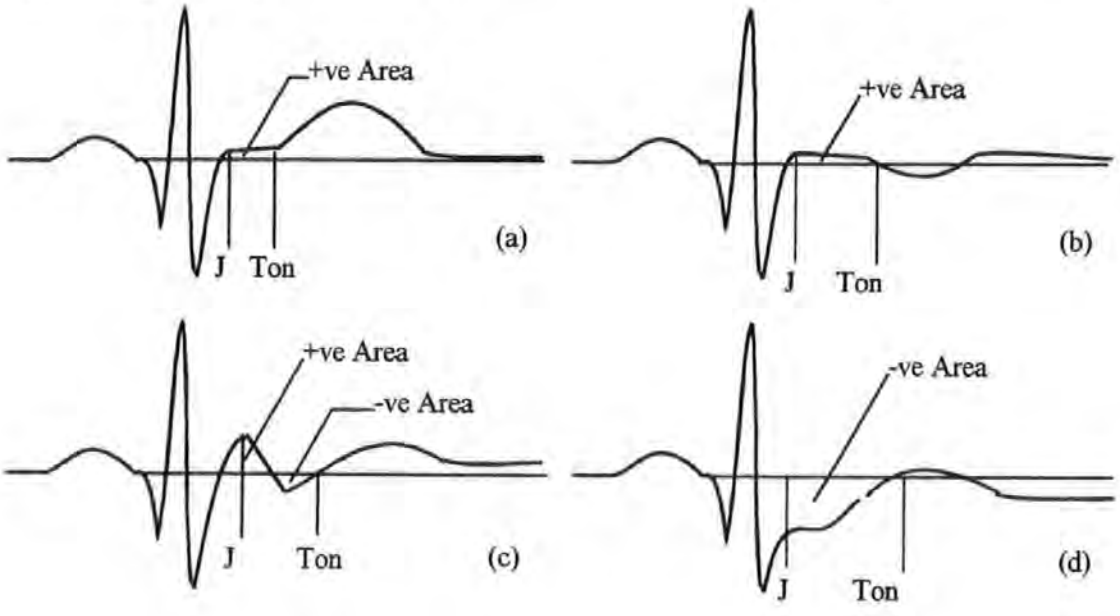

Figure 84 Classification of the ST segment as (a) Normal elevated T, (b) Negative T, (c) Bi-Phasic ST with normal elevated T and (d) Depressed ST with Normal T

Quantifying the shape of the ST waveform is simplified up by extracting features such as the T/QRS ratio and iso-electric level (see Figure 85).

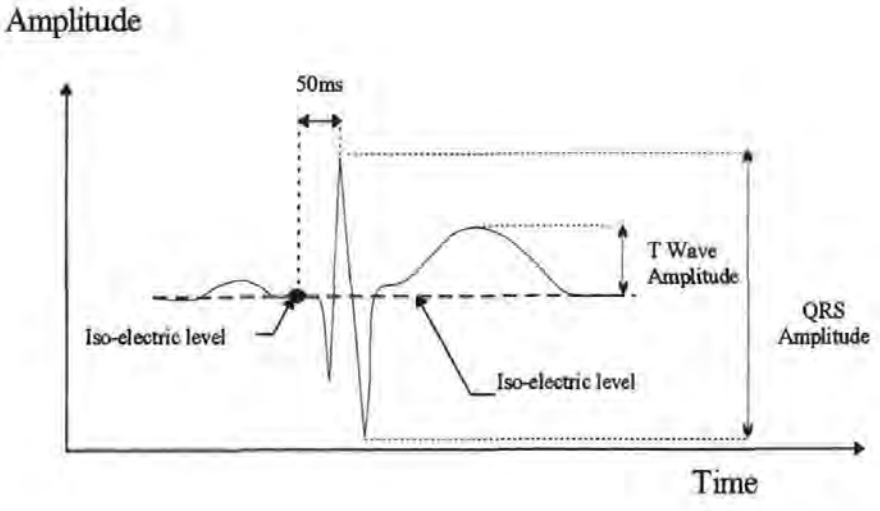

Figure 85 Location of the iso-electric region

One of the most important features of the foetal ECG waveform for discriminating between foetuses coping with normal
stress of labour and those in distress
is the shape of the ST waveform *(Greene 1987; Westgate et al. 1993; Greene & Westgate 1993).*

Significant pattern changes in shape associated with stress or distress include persistently rising T wave amplitude, very high T (Figure 84a), negative T waves (Figure 84b), bi-phasic waveforms (Figure 84c) and depressed ST segments (Figure 84d). In a recent clinical trial (*Westgate et al. 1993*) the ratio of the T wave amplitude to the QRS amplitude (the so-called T/QRS ratio) was successfully used, along with the CTG, to reduce clinical intervention rates with no change in foetal outcome. In general however the T/QRS ratio is not sufficient because the T/QRS ratio is only a crude measure of the ST waveform shape. With the T/QRS ratio alone, important changes in the ST segment, such as ST segment depression and bi-phasic ST waveforms would be missed. The progressive changes in the whole ST waveform must be examined *(Greene & Westgate 1993).* It was proposed that to classify the ST waveform shape, the following features should be measured and used. These are illustrated in
Figure 86.

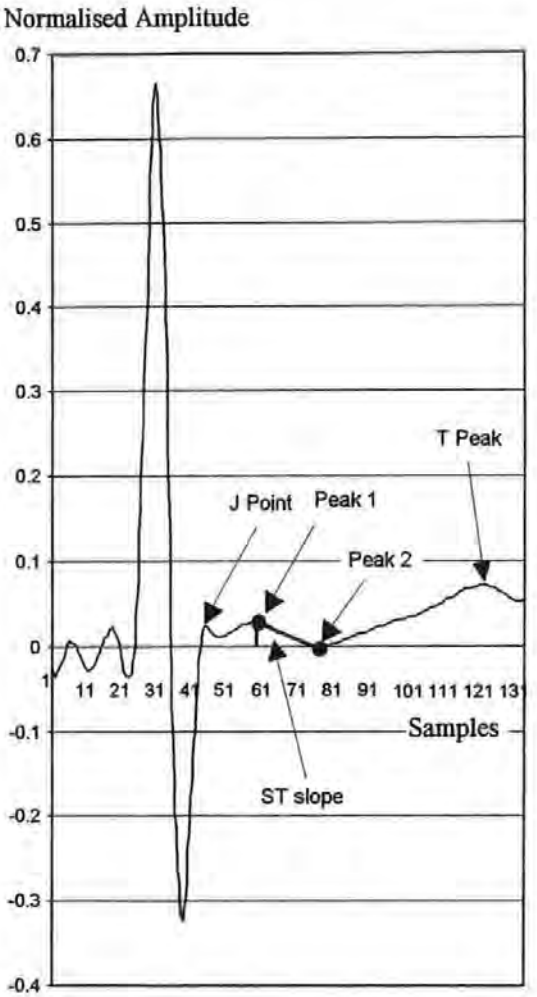

Figure 86 New features used to quantify the ST waveform shape

- **T peak height**. T complex peak amplitude.
- **ST+**. The total positive (+ve) area in the ST segment between J and Ton.
- **ST-**. The total negative (-ve) area in the ST segment between J and Ton.
- **Peak 1** The highest peak amplitude in the ST segment (between the J point and 100ms after the J point)
- **Peak 2** The most negative trough amplitude after peak 1 (equals peak 1 if not trough is found)
- **ΔPeak** The peak difference where ΔPeak=Peak 2- Peak 1
- **ΔT**. The time interval between peak 1 and peak 2

To account for changes in signal amplitude these are all normalised (divided) against the QRS amplitude which is assumed to be a physiological constant[1]. To compute the positive and negative areas ST+ and ST- the region between J and J+100ms is searched for zero-crossings, limits defined for each positive and negative section, and each area (definite integral) is simply computed using the integral expression *I(t)* given later in section 4.4.1. The ST waveform can now be described using the normalised T peak height, T+, T-, Peak 1 and Peak 2 features by a set of 'fuzzy rules', which are discussed in more detail in chapters 5 and 6

4.3.1 Locating the reference points

To decompose the waveform into the different component waveforms requires a rule based search to locate the P,Q,R,S,J,T_{on} and T time-reference features from the function *f(t)* in equation (4.1). Meaningful features are then extracted from these waveforms to build a picture of the ST waveform shape. The different shapes can be defined from amplitudes, first & second derivatives (gradients) and integrals (areas).

4.3.2 Location of the Q and S peaks

Chapter 3 discusses the location of the R wave peak. The expected relative locations of the P,Q,S and T peaks are summarised in

Table 13 *(Kirk & Smith 1986)*. These peaks are normally straightforward to locate if the R wave has been detected correctly. The Q and S wave peaks are taken as the lowest points found within their expected regions, for example, to find the S wave peak, the region from 6ms after the R wave peak to 26 ms after the R wave peak is searched for the lowest point. The offset of the lowest point from the R wave is the S wave peak position.

4.3.3 Locating the J-point

Locating the J point is straight-forward for the normal ECG shown in Figure 87. A short fixed length Chebyshev polynomial is fitted to the ECG waveform starting from the S peak. A search is made, starting from the S wave and moving toward the T wave for 15ms, for one of the following, listed in order of preference.

1. A change in the sign of the gradient

[1] It actually fluctuates slightly - this is attributed to foetal breathing

2. A crossing of the iso-electric level

3. A minimum gradient below 0.1

Should all these criteria fail to be found (as in the case a extreme ST depression) then the S wave peak is taken as the J point. In the case of ST depression, there is no definable J point, but for the purpose of ST pattern recognition, the S peak is suitable.

4.3.4 Iso-electric level

Amplitude and area measurements in the ST waveform are made relative to a zero reference, known as the *iso-electric level*. For the adult ECG it can usually be found between the end of the T wave and the start of the next P wave. Even for the adult this region can often be too short or not present at all at high heart-rates *(Peper et al. 1990)*. For the foetus this true zero reference is extremely difficult to locate reliably because its heart rate is much higher than that of an adult. A much more convenient reference point is 50ms before the R-wave peak, shown as the vertical dotted line in Figure 85. This is theoretically a region of zero potential activity between the end of the P-wave and the QRS complex, but more importantly, it is a region of very low variability. This ensures that the changes in the amplitude features are consistent even if the absolute values become slightly biased. It is changes that are most important in the clinical knowledge base.

4.3.5 Locating the T complex peak

This is a slightly more complex task, because the T wave can vary in amplitude, position and polarity or can be very flat with no defined peak. The expected region is the T peak is 120-210ms after the R-peak. More than one peak can appear in this region and different approaches have been employed to manage this situation. The definition of the T peak location is the peak in the 120-210ms region where the ST waveform deviates the furthest from the iso-electric level. Unfortunately this is was not found to be completely sufficient in practice as important events such as small negative T peaks are sometimes present but are not the dominant peak. A difficulty here is that the T peak is simply a commonly visually identified feature, and it is not necessarily true that there is only one peak. The approach taken is to *consider all peaks as candidates*, the philosophy being that both positive and negative T peaks

can simultaneously exist. This seemingly paradoxical situation is easily handled though fuzzy logic, which is described in chapter 5, by taking the belief that all are possibly T peaks. Fuzzy logic allows the implications of the different T peak values to all be true, but to different degrees of truth.

Reference Point	Offset in samples (at 500Hz)	Timing relative to the R Wave (ms)
Next R Wave	100 +/- 5	200 +/- 10
Q Peak	-8 +/- 5	-16 +/- 10
S Peak	+8 +/- 5	+16 +/- 10
P Peak	-50 +/- 20	-100 +/- 40
T Peak	70 +/- 35	165 +/- 45
Iso-electric point	-25	-50

Table 13 Expected locations of peaks within the fetal ECG relative to the R wave

The algorithm used to locate these peaks is as follows.

```
%Initial values
%First adjust the ST waveform search range for low heart rates
If HeartRate<120 THEN EndOfT=210ms
ELSE EndOfT=190ms
StartOfT=120ms
MaxTPeak=STWAVEFORM[StartOfT]
MinTTrough=MaxTPeak
%Find the highest peak and lowest trough in the search region
FOR t=StartOfT+1 TO EndOfT
        IF STWAVEFORM[t] is a Peak AND STWAVEFORM[t]>MaxTPeak THEN
MaxTPeak=STWAVEFORM[t]
        ELSEIF STWAVEFORM[t] is a Trough AND STWAVEFORM[t]<MinTTrough THEN
MinTTrough=STWAVEFORM[t]
NEXT t
%Subtract the isoelectric
MaxTPeak=MaxTPeak-IsoElectricLevel
MinTTrough= MinTTrough-IsoElectricLevel
%Normalise
MaxTPeak= MaxTPeak/QRSAmplitude
MinTTrough= MinTTrough/QRSAmplitude
```

where MaxTPeak is the maximum peak in the T complex region, MinTTrough is the minimum trough in the T complex region and STWAVEFORM[t] is the amplitude of the ST waveform as measured from the Chebyshev polynomial curve, at time *t ms* from the R peak. A peak is defined as follows.

$$peak(f,t)=\begin{cases}1 & \left(f(t-1)\le f(t)\wedge f(t+1)<f(t)\right)\vee\left(f(t-1)<f(t)\wedge f(t+1)\le f(t)\right)\\ 0 & otherwise\end{cases}$$

(4.2)

where f is a function or vector and t is time. Similarly a trough is defined as follows.

$$trough(f,t)=\begin{cases}1 & \left(f(t-1)\ge f(t)\wedge f(t+1)>f(t)\right)\vee\left(f(t-1)>f(t)\wedge f(t+1)\ge f(t)\right)\\ 0 & otherwise\end{cases}$$

(4.3)

These functions detect corners of plateau's as well as actual peaks. The two features MaxTPeak and MinTTrough are both used to assess the shape of the T complex.

4.3.6 Locating the T-wave onset.

This is the most difficult and ambiguous point to define and find because no strict definition of this point exists, so the simple definition illustrated in Figure 87 is was proposed. Having located the T wave peak, a search is conducted backwards towards the R wave for one the following, which ever is nearer the T peak.

1. A crossing of the iso-electric level.
2. A peak gradient (zero second derivative). From this point, a straight-line tangent to the curve is computed and where this intercepts the iso-electric is used as the T wave onset (Ton). In practice this technique can fail when the T-peak onset has a very low derivative and the Ton point is too near to the J point (see Figure 87).
3. Half way between J and T.

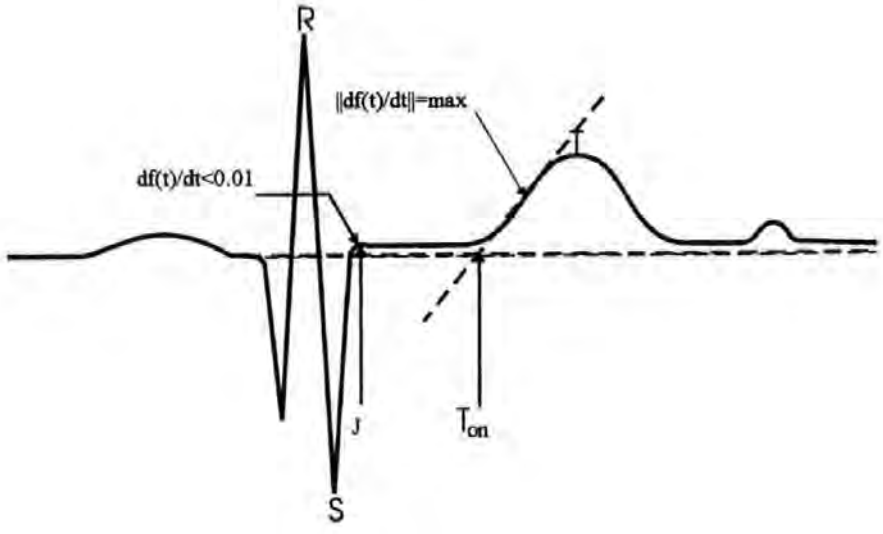

Figure 87 Defining the onset of the T Wave

4.4 Calculating Areas and Derivatives of Chebyshev polymonials

Given that a Chebyshev polynomial curve has been fitted to the ST waveform of the form

$$f(t) = c_0T_0(t) + c_1T_1(t) + c_2T_2(t) + \ldots + c_nT_n(t)$$

then from this it is possible to compute gradient at any point along the curve or the area under any portion of the curve $f(t)$. To compute the area under the curve between time t_1 and t_2 requires the definite integral $\int_{t_1}^{t_2} f(t)dt$ to be calculated. The definite integral $\int f(t)dt = g(t)$ can be precisely written as another Chebyshev polynomial of the form

$$g(t) = d_1T_1(t) + d_2T_2(t) + d_3T_3(t) + \ldots + d_{n+1}T_{n+1}(t).$$

From this the definite integral and hence the area can be computed as $g(t_1)$-$g(t_2)$. Equally any gradient at any point t along the curve is calculated from the first derivative of the polynomial $f'(t) = {}^{df(t)}/_{dt}$. Clearly, as the indefinite integral can be written as another Chebyshev polynomial and derived from another, then the reverse process can be carried out, which is the process of differentiation. It follows that the derivative $f'(t)$ can be written as another Chebyshev polynomial

$$f'(t) = b_0T_0(t) + b_1T_1(t) + b_2T_2(t) + \ldots + b_nT_n(t)$$

The scalar coefficients b and d can all be derived from the coefficients c in the expression for f(t). This requires very little computational effort and is described in the following two sections.

4.4.1 Computing the indefinite integral of the Chebyshev polynomials

Given a n^{th} order Chebyshev polynomial series

$$f(t) = c_0T_0(t) + c_1T_1(t) + c_2T_2(t) + ... + c_nT_n(t) \tag{4.4}$$

and indefinite integral is required of the form

$$g(t) = d_1T_1(t) + d_2T_2(t) + d_3T_3(t) + ... + d_{n+1}T_{n+1}(t) \tag{4.5}$$

That is,

$$\begin{aligned} g(t) &= \int f(t)dt \\ &= \int c_0T_0(t)+c_1T_1(t)+...+c_nT_n(t)\,dt \\ &= c_0\int T_0(t)dt + c_1\int T_1(t)dt + ... + c_n\int T_n(t)dt \end{aligned} \tag{4.6}$$

where $T_k(t) = cos[k.cos^{-1}(t)]$, $-1 \le t \le 1$.

First, the indefinite integral of the function $T_k(t)$ is required. To find this, make the substitution $t=cos(\theta)$ and $\frac{dt}{d\theta} = -\sin(\theta)$.

$$\begin{aligned} let\ I_k(t) &= \int T_k(t)dt \\ &= \int \cos\left[k\cdot\cos^{-1}(t)\right]dt \end{aligned} \tag{4.7}$$

Substituting $t = cos(\theta)$ and hence $dt = -sin(\theta)$ gives

$$\begin{aligned} I_k(\cos(\theta)) &= -\int \cos\left[k\cdot\cos^{-1}\left[\cos(\theta)\right]\right]\cdot\sin(\theta)\,d\theta \\ &= -\int \cos(k\cdot\theta)\cdot\sin(\theta)\cdot d\theta \end{aligned} \tag{4.8}$$

Using the identity

$$2.sin(A).cos(B) = sin(A+B) + sin(A-B) = sin(A+B) - sin(B-A) \tag{4.9}$$

where $A=\theta$ and $B=k\theta$ then re-writing (4.8) using the identity (4.9),

$$\begin{aligned} I_k(\cos(\theta)) &= -\frac{1}{2}\int\{\sin(\theta+k\theta)-\sin(k\theta-\theta)\}d\theta \\ &= -\frac{1}{2}\int\left\{\sin\left[(1+k)\theta\right]-\sin\left[(k-1)\theta\right]\right\}d\theta \\ &= -\frac{1}{2}\int\sin\left[(k+1)\theta\right]d\theta + \frac{1}{2}\int\sin\left[(k-1)\theta\right]d\theta \end{aligned} \tag{4.10}$$

Evaluating (4.10) gives

$$I_k(\cos(\theta)) = \frac{\cos\left[\left((k+1)\theta\right)\right]}{2(k+1)} - \frac{\cos\left[\left((k-1)\theta\right)\right]}{2(k-1)} + q \tag{4.11}$$

where θ is an arbitrary constant and is assumed zero. Given that $t=cos(\theta)$, reverse the substitution , that is substitute $\theta = cos^{-1}(t)$ into (4.11) giving

$$I_k(t)=\frac{\cos\left[\left((k+1)\cos^{-1}(t)\right)\right]}{2(k+1)}-\frac{\cos\left[\left((k-1)\cos^{-1}(t)\right)\right]}{2(k-1)} \qquad (4.12)$$

and from the definition of $T_k(t)$ this simply becomes

$$I_k(t)=\frac{T_{k+1}(t)}{2(k+1)}-\frac{T_{k-1}(t)}{2(k-1)} \qquad (4.13)$$

Each term in (4.6) can now be defined by

$$c_k\int T_k(t)dt=\frac{c_k}{2}\cdot\left\{\frac{T_{k+1}(t)}{(k+1)}-\frac{T_{k-1}(t)}{(k-1)}\right\}$$

Now, substituting into (4.6) and collecting terms of the same order, d_k can be derived

$$\begin{aligned}
g(t) &= c_0\int T_0(t)\,dt + c_1\int T_1(t)\,dt + c_2\int T_1(t)\,dt + c_3\int T_1(t)\,dt + c_4\int T_1(t)\,dt + \ldots + c_n\int T_n(t)\,dt \\
&= \frac{c_0}{2}\left\{\frac{T_1(t)}{0+1}-\frac{T_{-1}(t)}{0-1}\right\}+ \\
&\quad \frac{c_1}{2}\left\{\frac{T_2(t)}{1+1}-\frac{T_0(t)}{1-1}\right\}+ \\
&\quad \frac{c_2}{2}\left\{\frac{T_3(t)}{2+1}-\frac{T_1(t)}{2-1}\right\}+ \\
&\quad \frac{c_3}{2}\left\{\frac{T_4(t)}{3+1}-\frac{T_2(t)}{3-1}\right\}+ \\
&\quad \frac{c_4}{2}\left\{\frac{T_5(t)}{4+1}-\frac{T_3(t)}{4-1}\right\}+ \\
&\quad \vdots \\
&\quad \frac{c_1}{2}\left\{\frac{T_2(t)}{1+1}-\frac{T_{-2}(t)}{1-1}\right\}
\end{aligned} \qquad (4.14)$$

Collecting terms, and noting that $T_{-1}(t) = \cos[-1 \cdot \cos^{-1}(t)] = \cos[1.\cos^{-1}(t)] = T_1(t)$ and that resulting constant terms in the integral expression $g(t)$ are theoretically undefined and therefore neglected. Hence terms of $T_0(t)$ are neglected.

$$
\begin{aligned}
g(t)=&\frac{T_1(t)}{2}\cdot\left\{c_0+c_0-c_2\right\}+\\
&\frac{T_2(t)}{2}\cdot\left\{\frac{c_1}{2}-\frac{c_3}{2}\right\}+\\
&\frac{T_3(t)}{2}\cdot\left\{\frac{c_2}{3}-\frac{c_4}{3}\right\}+\\
&\frac{T_4(t)}{2}\cdot\left\{\frac{c_3}{4}-\frac{c_5}{4}\right\}+\\
&\vdots\\
&\frac{T_k(t)}{2}\cdot\left\{\frac{c_{k-1}}{k}-\frac{c_{k+1}}{k}\right\}+\\
&\vdots\\
&\frac{T_n(t)}{2}\cdot\left\{\frac{c_{n-1}}{n}-\frac{c_{n+1}}{n}\right\}
\end{aligned}
\qquad (4.15)
$$

where $c_{n+1}=0$

therefore by inspection

$$
d_k=\left\{\begin{array}{l}\dfrac{c_{k-1}-c_{k+1}}{2k},k>1\\ \dfrac{2c_0-c_2}{2},k=1\end{array}\right\} \qquad (4.16)
$$

4.4.2 Computing the derivative of Chebyshev polynomials

Seeing as *f(t)* was integrated to get *g(t)*, this process can be reversed by differentiating *g(t)* to get back *f(t)*. Therefore, a solution for the values of c_k, $k=0,1,..,n$, is required in terms of the values of d_k, $k=1,2,..,n+1$. No direct relationship exists but a recursive relationship can be simply found. From (42)

$$
d_{k+1}=\left\{\begin{array}{l}\dfrac{c_k-c_{k+2}}{2(k+1)},k>0\\ \dfrac{2c_0-c_2}{2},k=0\end{array}\right\},k=0,1,..,n+1 \qquad (4.17)
$$

where $c_{n+1}=0 \& c_{n+2}=0$

Solving for c_k gives

$$
c_k=\left\{\begin{array}{c}2(k+1)\cdot d_{k+1}+c_{k+2},k>0\\ \dfrac{2d_1+c_2}{2},k=0\end{array}\right\},k=n,n-1,..,0 \qquad (4.18)
$$

where $c_{n+1}=0 \;\&\; c_{n+2}=0$

4.5 Describing the PR segment shape.

Another feature of interest is the relationship between the PR and the RR intervals *(Murray 1986)*. When there is an abnormal foetal response, the PR interval is said to shorten whilst the RR interval lengthens (i.e. the heart rate decreases), making it potentially useful in discriminating between normal and abnormal heart rate patterns. Recent data have shown this to be a normal response will all episodes of short lasting heart-rate decrease (*Luzietti et al. in press*). Furthermore, when there is a marked bradycardia[2] episode the shape of the P wave changes and becomes negative or disappears. This clinical value of this is still unclear but provision has been provided to measure features from the PR segment should it ever become necessary.

Location of the P wave is still susceptible to similar problems found with the T/QRS ratio so the same techniques as above apply. The difference is that the P complex peak is often notched or missing entirely. The centroid algorithm described in 4.5.1 is used so the effects of a notch would have a minimal effect. The PR interval has had some attention recently (*Marvel & Kirk 1980; Luzietti et al. 1995*) but it is not currently used in the clinical knowledge-base. A facility has been included to locate the P peak for future research purposes only. This uses the well known centroid, or centre of mass.

4.5.1 The centroid

The centre of mass t_c for the P-segment approximation $f(t)$, $t=-1..1$, is located using the well known centroid (centre of mass) formula *(Durkin 1994)* given by

$$t_c = \frac{\int_{-1}^{+1} f(t) \cdot t \, dt}{\int_{-1}^{+1} f(t) \, dt} \tag{4.19}$$

Given $f(t)$ is the form given in equation (4.1), the analytical solution for equation (4.19) is computed as follows. The expression on the numerator cannot be evaluated directly, so integration by parts is used.

$$\int u \, dv = uv - \int v \, du \tag{4.20}$$

Let $dv=f(t)$ and $u=t$. Substituting into (4.20), it follows that the indefinite integral is

[2] Significant drop in baseline heart-rate below 90 bpm

$$\int t \cdot f(t)\,dt = t\int f(t)\,dt - \int\int f(t)\,dt \cdot 1\,dt \\ = t \cdot I_1(t) - I_2(t) \tag{4.21}$$

Using the expression in (4.17), calculate the indefinite integral of $f(t)$, $I_1(t) = \int f(t)\,dt$ such that

$$I_1(t) = d_0 + d_1 T_1(t) + d_2 T_2(t) + \ldots + d_{n+1}(t) \tag{4.22}$$

the second indefinite integral of $I_1(t)$, $I_2(t) = \int I_1(t)\,dt$ such that

$$I_2(t) = e_0 + e_1 T_1(t) + e_2 T_2(t) + \ldots + e_{n+2}(t) \tag{4.23}$$

The definite integral on the numerator of (4.19) is therefore

$$\int_{-1}^{+1} t \cdot f(t)\,dt = \left[t \cdot I_1(t) - I_2(t)\right]_{-1}^{+1} \\ = \left(1 \cdot I_1(1) - I_2(1)\right) - \left(-1 \cdot I_1(-1) - I_2(-1)\right) \tag{4.24}$$

The denominator of (4.19) is simply $I_1(1)$-$I_1(-1)$. Therefore the centroid of $f(t)$ is

$$t_c = \frac{\left(1 \cdot I_1(1) - I_2(1)\right) - \left(-1 \cdot I_1(-1) - I_2(-1)\right)}{I_1(1) - I_1(-1)} \tag{4.25}$$

or in general the centroid of a Chebyshev polynomial over the region $a \le t \le b$ is

$$t_c(a,b) = \frac{\left(b \cdot I_1(b) - I_2(b)\right) - \left(a \cdot I_1(a) - I_2(a)\right)}{I_1(b) - I_1(a)}$$

A hypothesis is that the center of mass is the position that the eye would select as the center of the dominant P peak. With a notched, bi-modal or bi-phasic shaped P peak the centroid position tends to be closer to the center of electrical activity.

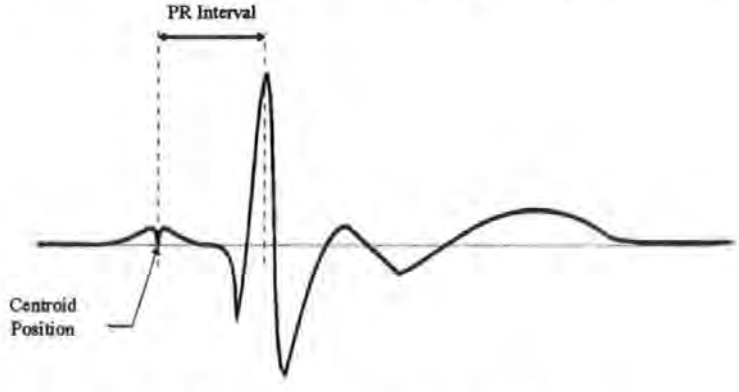

Figure 88 Using the centroid to locate the P wave

The changes in the centroid position may help reveal changes in the PR waveform shape and help understand the changes of heart-rate, but this remains to be investigated fully.

4.6 Extraction of trends in features

Features such as the T/QRS ratio can be very variable and the underlying trends are often visibly obscured. They are also measured from the raw waveforms at uneven sampling times. Linear interpolation is used to evenly (over) sample these features in a similar way to that described in chapter 2. The features can be re-sampled down to a useful rate using multi-rate techniques. A difficulty is knowing the minimum useful sampling rate. The smallest time referenced in the clinical guidelines is "the appearance of negative T waves for less than 5 minutes", which is very vague. After discussions with clinicians it was agreed one measurement every 15 seconds is more than enough required from the guidelines, but also manageable.

Figure 89 shows 20 minutes of raw features, measured on a beat-by-beat basis. To see the trends of the features and for the purpose of illustration, a simple low-pass filter, $y(t)=\alpha.y(t-1) + (1-\alpha).x(t)$, has been used to smooth the results where $0<\alpha<1$, x(t) are the raw features and y(t) are the smoothed features (see Figure 89)

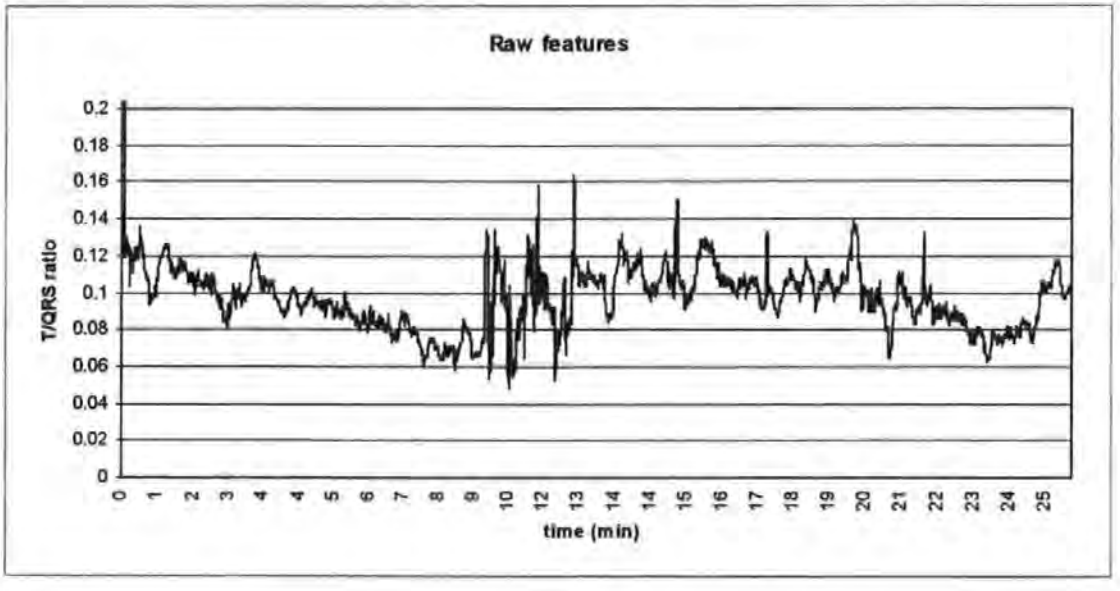

Figure 89 T/QRS ratio measured on a beat-by-beat basis and smoothed.

The problem of analysing the trends in the features still remains. From the expert knowledge, most of the important trends can be categorised as either average values or rates of change over different time periods. Linear regression is used to extract the rate of change of each feature over a given interval. From the gradient of the regression the rate of increase/decrease in a feature can be assessed. A more

complex trend / pattern is the appearance of brief changes in the T/QRS ratio or ST area.

4.7 Decimation techniques to enhance trends in the foetal ECG features

The features, such as those plotted in Figure 89, are unsuitable for direct analysis for the following reasons:

- There is too much sort term variability in the features. This cannot be accounted for in the clinical guidelines, and adds to uncertainty.
- The data is being sampled far more often than is necessary, with only the underlying trends in the data are of clinical interest.
- The data is unevenly sampled, and some cases it is not present because of poor data quality. Regularly sampled data is required for further analysis.

A solution to these problems is to reduce the sampling rate of the data to one which is more manageable and which emphasises the trends in the data more clearly. A common mistake is to just discard data points and only measure the features at 'convenient' times.

To avoid aliasing a sampling rate reduction technique, known as decimation *(Ifeachor & Jervis. 1994)*, is employed. This process involves both filtering and data reduction to pull out the trends and reduce the amount of data to be processed. To simplify this task requires evenly sampled features in time. This is achieved by linear interpolation using straight lines, as illustrated in Figure 90.

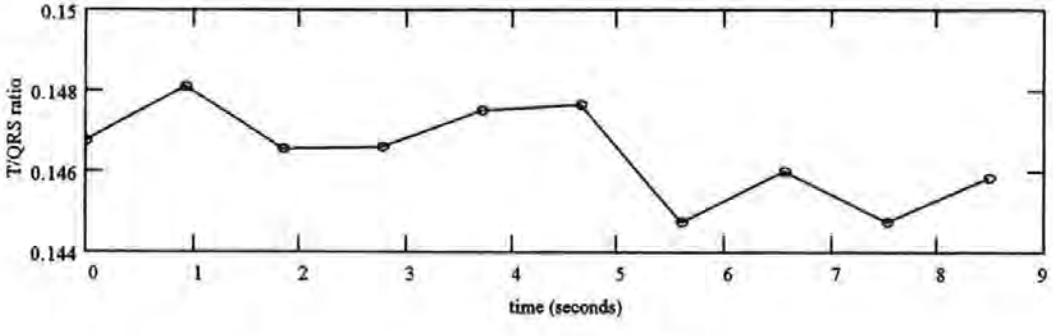

Figure 90 Interpolation of ECG features

The minimum interval between feature data measured from the ECG waveforms is assumed to be $^1/_3$s, which corresponds to a maximum instantaneous heart-rate of

180bpm (3 Hz). The interpolated data is therefore evenly re-sampled at 3Hz as shown in Figure 91.

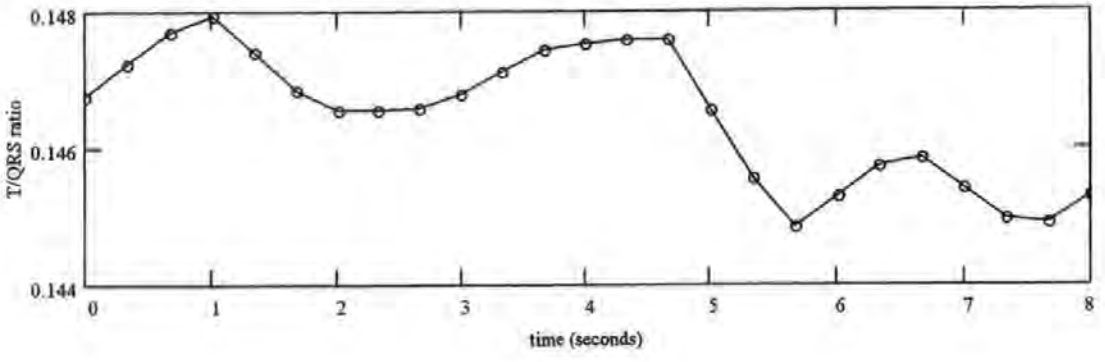

Figure 91 Over-sampling the features at 3Hz

This data can be used for future short-term analysis but is at a higher sampling rate than is actually necessary for practical use with the current guidelines. The current guidelines only account for changes which occur over minutes, and not seconds. With a sampling rate of 3Hz, there are clearly more data samples available than is required. The short term variability also distracts from the more useful longer term trends. To enhance the trends in the data and to reduce the number of samples to a more practical sampling rate requires a sampling rate conversion known as decimation. Reducing the sampling rate too far however will possibly lose important events. An agreed and practical sampling rate was to sample one ST waveform feature on every 15 second time period ($^1/_{15}$Hz). Reducing the sampling rate of the ST waveform features from 3Hz down to $^1/_{15}$Hz is not simply a matter of rejecting data points. Discarding data points without prior filtering introduces a aliasing, which is manifests itself as noise. Sampling a real valued signal in time at a frequency Fs, will have a mirrored spectrum about Fs/2. According to Nyquists theorem, to faithfully represent a signal, it must have a bandwidth below Fs/2, where Fs is the sampling frequency. This is the case with all sampled systems, and has to be carefully considered when converting sampling frequency. To avoid aliasing, frequency components above $^1/_{30}$Hz must be removed by initial filtering. To attempt this directly requires a filter with a very sharp transition band. To design a linear low-pass FIR filter, with a pass-band edge of frequency $^1/_{60}$ Hz and a stop-band edge frequency of $^1/_{30}$Hz (see Figure 92), 0.1dB pass-pand ripple and 40dB

stop-band attenuation, would require at least 346 coefficients for a sampling frequency of 3Hz.

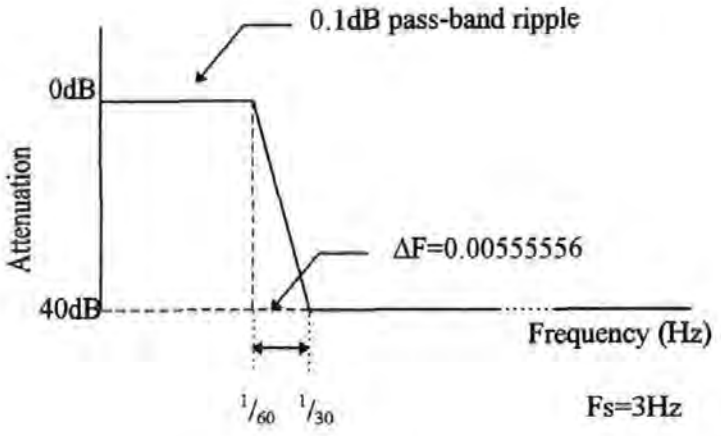

Figure 92 Prototype filter for sampling rate conversion

It is not practical to use a filter with so many coefficients. A more efficient technique is to break the decimation process into stages, as illustrated in Figure 93.

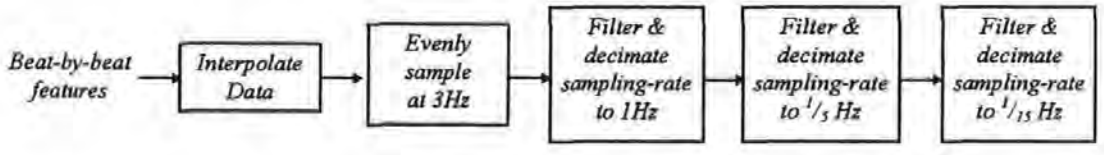

Figure 93 Feature decimation and smoothing scheme

The frequency response of each filter stage is given in Figure 94. Each is 25 coefficients long, making the total filter length 75, which is far more favourable than 346. This process is repeated for each feature measured.

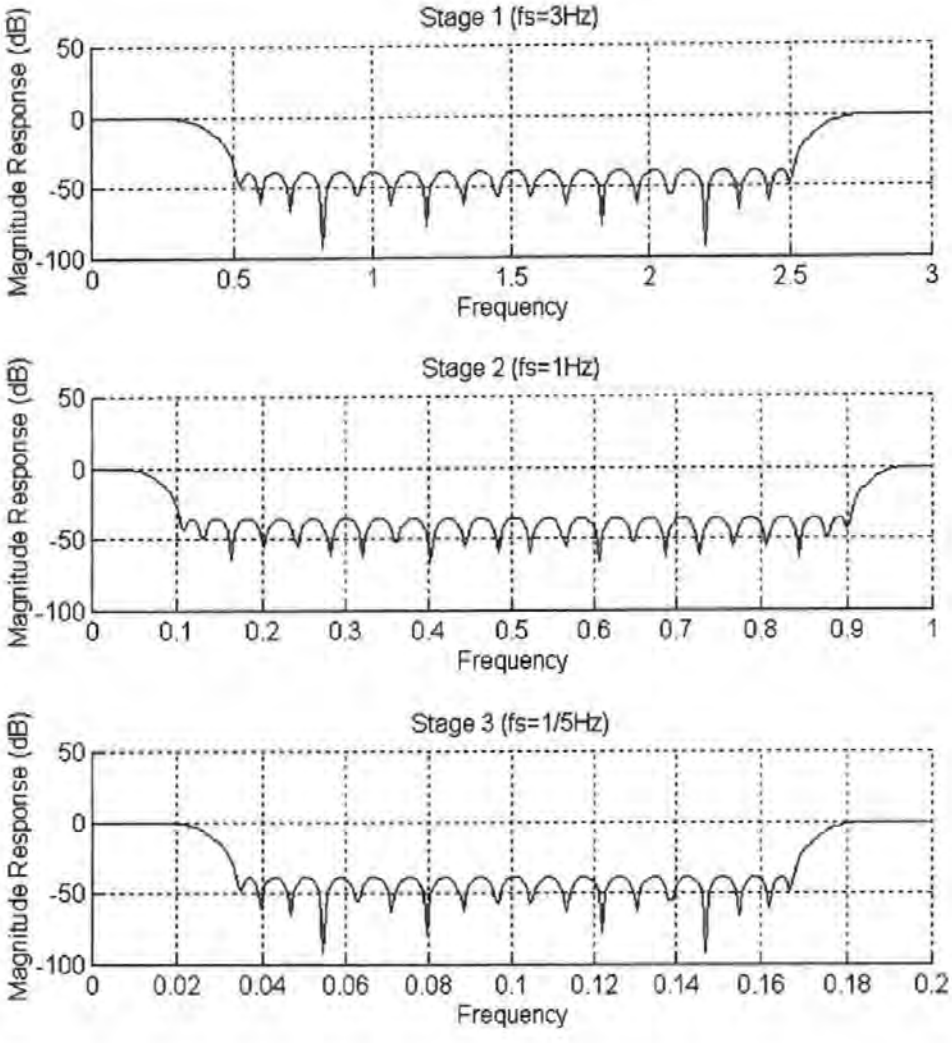

Figure 94 Three filter stages used to decimate the feature sampling rate from 3Hz to 1/15 Hz

An example result is shown in Figure 95. Figure 95a is a plot of the T/QRS ratio which has been interpolated, Figure 95b shows the data after being filtered Figure 95c shows the data after being filtered and decimated to $^{1}/_{15}$Hz. This data is more manageable and retains the useful trends in the data.

Unfortunately this technique has the disadvantage that any transient changes in a features that are relevant will be smoothed. Relevant transient information might occur in the event of a very sudden insult to the foetus. Such changes have been observed in animal data where the umbilical cord is chronically occluded.

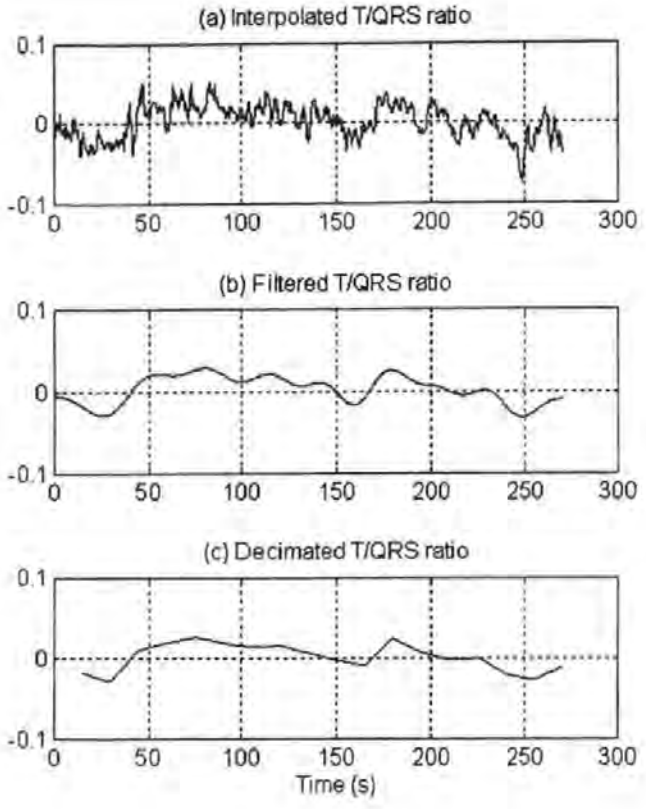

Figure 95 Evenly sampling and decimating the T/QRS ratio features using multi-rate techniques

The second artefact introduced by this technique is to delay the features. The delay in the current system is computed as follows. The delay in each filter stage D = ½LT, where L is the length of the filter and T is the sampling interval.

Filter 1: Delay = ½ 24 $^{1}/_{3}$. = 4s

Filter 2: Delay = ½ 24 $^{1}/_{1}$. = 12s

Filter 3: Delay = ½ 24 $^{5}/_{1}$. = 60s

The total delay in the system is 78s (1min 18s) which is significant in relation to physiological time constants. The decimated data is adequate within the scope of the current clinical guidelines however as changes over 5 minute periods are considered. Recursive IIR filters could be used instead of FIR filters. These have a much shorter delay but suffer from problems of phase-distortion which adds uncertainty. It is also more difficult to compute the delay through IIR filters as the delay is a non-linear function of frequency. A possible solution might be to cascade an additional recursive all-pass filter of the form

$$H_{ap}(z) = \prod_{k=0}^{m} \frac{z^{-1} - a_k^*}{1 - a_k z^{-1}} \qquad (4.26)$$

which can be designed to reduce the phase distortion in the pass-band of the filter. Another technique might be one which can suppress the short-term random variability in the features but preserve the slow trends and sharp defined transient shifts. Such a technique might be one as proposed by *Lu et al. 1992* which uses a filtering technique based on the wavelet-transform.

4.8 Discussion and Conclusion

Feature extraction is a technique used here for quantifying the shape of the foetal ECG waveform. The key to unambiguous feature extraction is to totally remove small peaks and troughs caused by noise. This was achieved using a novel application of Chebyshev polynomial approximation. These polynomials were chosen because they provide a curve with a very uniform approximation across the whole data segment, they are numerically stable and are convenient to manipulate mathematically. This method avoids the need for complex pattern recognition techniques, such as Neural Networks (*Suzuki & Ono 1992*) and Syntactic pattern recognition (*Trahanias & Skordalakis 1989*). These methods have proven to be robust with the data available, but a more exhaustive validation is required to reveal any weakness in these algorithms should they exist. New key features that can be used to quantify the ST waveform shape have been proposed. Algorithms for extracting these features from the polynomial curves have also been successfully developed. These features are extracted from every available waveform, which provides a large quantity of short-term information. However, at present, the clinical guidelines do not use the short-term variability within foetal ECG parameters. Reducing the quantity of data to reveal the underlying trends is a problem in many biomedical applications. Consider a medical device, such as a digital blood-pressure monitor, often only has a single instantaneous display. Blood-pressure is very dynamic function of time, so the measurement very much varies with each instant it is sampled. In practice many readings are taken to allow the clinician to derive a meaningful result. This latter process is a form of conscious or even sub-conscious filtering on behalf of the clinician. Considering the high variability of blood-

pressure, and considering blood pressure as a function of time, then it follows that there are relatively high frequency components in the function. Measuring a few samples of this function at a relatively low frequencies, for example, once every 40s, therefore introduces the effect of aliasing. The data is then being filtering *after* aliasing has occurred. This is far from ideal but is a process enforced by such electronic devices. Had the pressure been regularly plotted over time at a suitable sampling rate, the clinician would be have a chance to filter the data by eye using all the samples and extract meaningful trends. An experienced human eye can naturally perform complex filtering and visualise the trends through the data. To draw an analogy, as with all discrete sampled systems, the correct technique is to first over-sample the data (plot on paper-trace), filter the data to limit the bandwidth (filter by eye) and re-sample (extract trends). To help the clinician, some electronic filtering is often performed. This principal equally applies to any sampled system, including ST waveform analysis. The use of decimation is used to reduce the quantity of data and further enhances the trends within the features. This also contributes towards reducing noise and therefore uncertainty. FIR filters were used for decimation system to avoid any distortion, but these do add a delay in real time. This is adequate for the purpose of the current clinical guidelines, but should the delay in the system become too long, then it will be necessary to validate the use of IIR filters instead. This is more difficult to design as the non-linear phase response of such filters introduces different delays for different frequency components, and this also adds distortion to the data. A limitation of this decimation technique is that any rapid change in the features would be smoothed and delayed. For cases in the current cllinical guidelines there are no rapid physiological changes that would cause such an event. There are investigations into the shorter-term changes on the foetal ECG waveform being carried out (un-published) which might require a different technique to extract the trends. An example might be the use of the wavelet transform. The wavelet transform has the same property of the Fourier transform in that is it a linear transformation on an orthonormal basis. Unlike the Fourier transform it can help to localise signals in both frequency and time. Filtering techniques based on the wavelet transform can preserve different levels of 'detail'.

It is proposed that the slow trends and the transient shifts could be preserved for example, whereas the more chaotic short-term variability could be suppressed. This is an area which requires further research.

Chapter 5

Fuzzy Logic Concepts

5. *Fuzzy Logic Concepts*

5.1 Introduction

Uncertainty and difficulty in interpreting ECG and CTG patterns during labour are the major cause of unnecessary medical intervention (e.g. caesarean section or forceps deliveries), foetal injury or a failure to intervene when needed *(Maeda 1990; Krause et al. 1991)*. The analysis and interpretation of changes in the ECG in association with the CTG are carried out by visual inspection *(Rosén 1994)* which is very subjective.

One aim of this work is to interpret changes in the foetal ECG features, taking into account the uncertainty and imprecision in obstetric data and knowledge, and present the results in a way that will practically aid the busy clinician. The fuzzy logic concepts used in this work are also described elsewhere *(Ifeachor & Outram 1994)*. Fuzzy logic is used here to model a human expert and to take account of uncertainty in the clinical knowledge and in the data.

5.2 Uncertainty and imprecision in management of labour

The qualitative nature of current obstetric knowledge gives rise to a great deal of uncertainty. Figure 96 summarises how the CTG is categorised based on features observed visually in the CTG trace and their perceived significance. Given that features are measured by eye and the normal physiological variations between foetuses, subjective phrases such as *normal*, *intermediate*, *mild-variable* and *abnormal* arise and illustrates the difficulties of interpreting the CTG.

Changes in the ST waveform are assessed qualitatively by analysing its shape (e.g. *elevated*, *negative*, *depressed*, *rapidly rising*, *normal*) and quantitatively by the T/QRS ratio or the ST area. The interpretation of these features, as with the CTG, also suffers from threshold problems. A study of the guidelines for analysing the ST waveform plus the CTG *(Rosén 1994; Rosén et al. 1992)* reveals that the knowledge is highly qualitative. This is due, in part, to the difficulty of drawing valid conclusions based on what is essentially partial information derived from the baby, the dynamic nature of labour, and the normal physiological variations in the measured values between foetuses.

Imprecision in the measured parameters due to the poor quality of data and errors in the feature extraction algorithms are a further source of uncertainty. Artefact from signal enhancement, such as pass-band ripple in digital filters, can contribute to uncertainty. Errors is measurement (e.g. false or missed R-waves, false changes in the features of the CTG, inconsistent T/QRS values) due to poor signal quality are not uncommon *(Westgate et al. 1993)*.

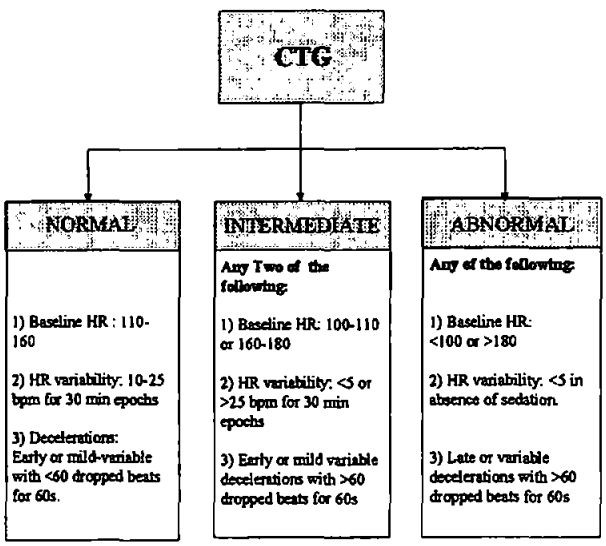

Figure 96 A simplified classification of the CTG into its subtypes

Different techniques for managing uncertainty in the decision making process are available. Fuzzy logic is suited to the problems of imprecision and uncertainty in obstetrics and allows the knowledge to be formalised in a more humanistic rule based form. For example, the terms used to describe changes in the CTG and the ECG features can be represented as linguistic variables. Further, fuzzy logic allowed us to implement a system from the bottom up based on theoretical knowledge and experience. This can later be fine-tuned to get optimum performance as more data and knowledge is collected.

5.3 Development cycle of a fuzzy expert system

The development of a fuzzy expert system is generally less complex than a conventional crisp rule based expert system, usually requiring less rules. A brief summary of the design process is given below in Figure 97.

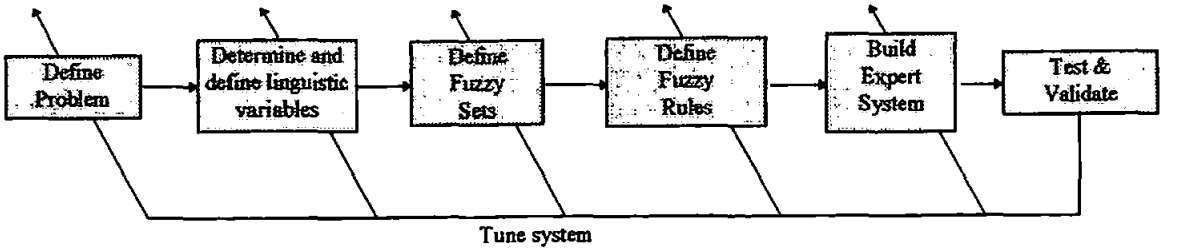

Figure 97 Development of the fuzzy expert system

Each stage is described in more detail.

5.4 Definition of the problem

An understanding of the problem has been build up over several years by talking to the clinicians and by studying the literature. Formal knowledge elicitation sessions were recently carried out by reviewing the literature and conducting interviews with medical experts. The full transcripts of these are too lengthy to include in this report but a tabulated summary of the expert knowledge is given in Appendix D.

5.5 Definition of linguistic and fuzzy variables

The input variables to an intelligent fuzzy system need to be defined and used consistently. When dealing with a medical knowledge base, it is important to understand and use consistent terminology. Some of the variables in this system are the T/QRS ratio, ST waveform shape, CTG and ST segment shape. From the knowledge elicitation, adjectives and adverbs can also be identified which describe these variables. It is important as the knowledge engineer to keep the knowledge base as close to the language of the expert as possible. Examples in foetal monitoring are *increasing T/QRS ratio*, *elevated ST waveform*, *depressed ST waveform* and *reduced heart-rate variability*, where the adjectives are underlined. These linguistic terms will need to be modelled by the fuzzy system.

5.6 Modelling linguistic terms with fuzzy sets

Conventional expert systems use Boolean logic, where a given fact is either true or false. For example, an expert system that estimates car insurance premiums might have a set of rules such as

IF engine_size≤1599cc AND drivers_age<25 THEN risk=LOW
IF engine_size≤1599cc AND (25 ≤ drivers_age < 35) THEN risk=MEDIUM
IF engine_size≤1599cc AND drivers_age>35 THEN risk=LOW
IF engine_size>1599cc AND engine_size≤1999cc AND drivers_age≤35 THEN risk=MEDIUM

With human reasoning, it seems unreasonable for a person to suddenly become a safer driver on his or her 25th birthday and for a 1600cc car to be a higher risk than a 1599cc car. Human reasoning would say that risk reduces with increasing drivers age and increases with increasing engine size. The failing of Boolean systems is that they are a poor model of human reasoning. This same problem exists with interpreting foetal ECG features. For example, in Figure 98 the *T/QRS* ratio 'set' is divided into the 'subsets' {Negative; Normal; Increased; High} which are separated by crisp (discontinuous) boundaries. Given a scalar measurement of *t/qrs*, the fact that this 'object' belongs to the a sub-set A of the set T/QRS can only be TRUE or FALSE. Written formally

$$\mu_A(t/qrs) \in [\text{FALSE, TRUE}]$$

where $\mu_A(t/qrs)$ is known as the membership function which specifies whether the 'object' *t/qrs* belongs to the subset A {Negative; Normal; Increased; High}.

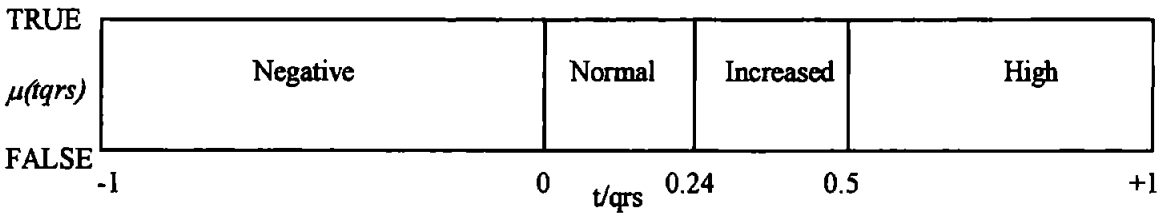

Figure 98 Crisp sub-sets of the T/QRS set

Using the sets in Figure 98 and given the following rules

IF μ(t/qrs) = *normal* AND BaselineHeartRate = *Normal* THEN fetalcondition=*Good*
IF μ (t/qrs) = *Increased* AND BaselineHeartRate =*Normal* THEN fetalcondition =*Intermediate*

It is quite possible that the effects of noise and natural variability would cause the T/QRS ratio to fluctuate about the 0.24 boundary level, causing the outcome (consequence) of these rules to 'jitter' between *Good* and *Intermediate*, which would add uncertainty to diagnosis. When a very small change, which is considered

to tend towards zero, occurs in one or more of the facts in the knowledge and a stepped change in the output results, then this effect is said to be caused by a *discontinuity in the knowledge space.* The problem of jitter can be reduced by introducing hysteresis as shown in Figure 99.

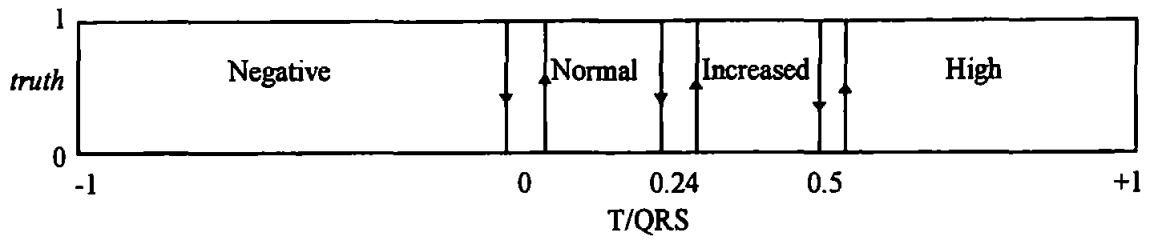

Figure 99 Crisp membership functions for the T/QRS sub-sets with added hysteresis

In this example, for a change in t/qrs membership from a lower sub-set (e.g. Normal) to a higher sub-set (e.g. Increased), the upper threshold is used (denoted by an upwards arrow). For a change in membership from a higher sub-set to a lower sub-set, the lower threshold is used (denoted by an downwards arrow). This helps to reduce jitter caused by noise or natural variability, but has still not solved the fundamental problem of discontinuous jumps at the boundaries of the subsets and may not be satisfactory to human experts. The underlying problem is that a fact (measurement) can only belong to a single set at any one time, and must fully belong to that set i.e. the memberships of each subset of T/QRS in Figure 99 must obey the following conditions

$$\{ \mu_{Negative}(t/qrs) , \mu_{Normal}(t/qrs) , \mu_{Increased}(t/qrs) , \mu_{High}(t/qrs) \} \in [1,0] \quad (5.1)$$

$$\mu_{Negative}(t/qrs) + \mu_{Normal}(t/qrs) + \mu_{Increased}(t/qrs) + \mu_{High}(t/qrs) = 1 \quad (5.2)$$

Fuzzy sets are mathematical models of linguistic terms used by experts. Statements such as "the t/qrs ratio is normal" involves two features, the variable *t/qrs* and the adjective *normal.* The t/qrs variable can take any value between -1.0 and +2.0, which is known as its *Universe of Discourse.* The next question is how do we define the range that the adjective normal applies? Fuzzy logic provides a means of modelling adjectives. Consider a measured value of the t/qrs ratio which can simultaneously be a member of all of the fuzzy sub-sets {Negative; Normal; Increased; High} but with *independent degrees of membership for each sub-set.* The fuzzy membership functions for some of the foetal ECG features are shown in

Figure 100. Fuzzy sets resolve the problem of defining boundaries because their boundaries are continuous, can also over-lap and do not have to obey the constraints given above in 5.1 and 5.2.

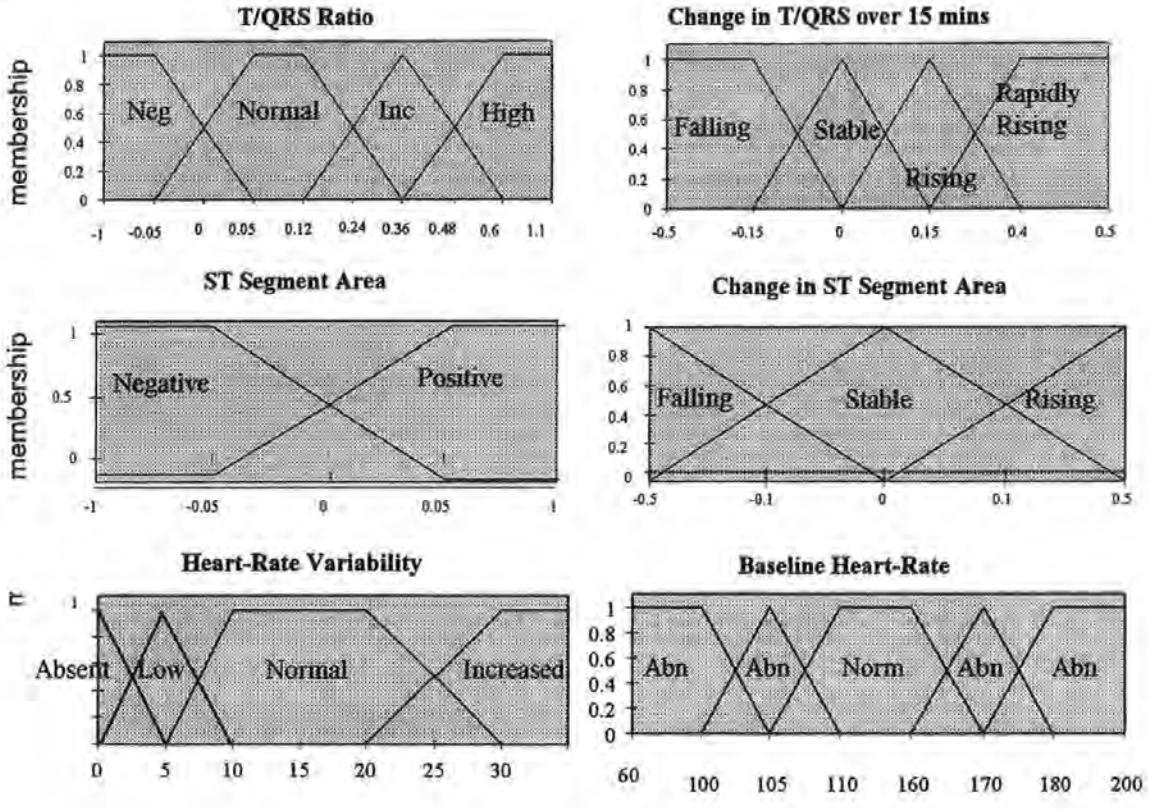

Figure 100 Fuzzy sets

The *degree of membership* of a set is the belief that a given value belongs to that set, and can range anywhere between 0 for least true and 1 to most true. For example, from the fuzzy set T/QRS in Figure 100, a T/QRS ratio measurement of 0.245 would imply the *degree of membership* in the sub-sets *{Negative; Normal; Increased; High}* are {0.0; 0.45; 0.55; 0.0}. This could be interpreted as "*the T/QRS is slightly more Increased than Normal*".

Formally, the definition of a fuzzy set is as follows

Let X be the universe of discourse, with elements of X denoted as x. A fuzzy set A of X is characterised by a membership function $\mu_A(x)$ that associates each element x with a degree of membership values in A (Cox 1994).

The fuzzy membership function is formally written as

$$\mu_A(x)=\text{Degree}(x \in A)\ ,\ 0 \leq \mu_A(x) \leq 1$$

which is the membership that x belongs to sub-set A. Here the universe of discourse X is the range of all possible values {-1..2} of the T/QRS ratio, the element x of X is the specific 'T/QRS' measurement, the fuzzy subset A of X could be any one of *{Negative; Normal; Increased ; High}*. A fuzzy set A (which is a subset of X) is formally defined as

$$A = (\mu_1 / x_1, \mu_2 / x_2, \ldots, \mu_n / x_n)$$

where μ_k / x_k is membership value $\mu_A(x_k)$ of the sub-set A at $x=x_k$. For example, the notation used to represent the fuzzy sub-set *Normal* of the set T/QRS is

Normal = (0.0 / -1.0, 0.0 / -0.05, 0.5 / 0.0, 1.0 / 0.05, 1.0 / 0.12, 0.5 / 0.24, 0.0 / 0.36, 0.0 / 1.0)

5.7 Fuzzy set operators

In Boolean logic, rules are constructed using the fundamental logical operators are AND, OR and NOT. For fuzzy logic, there are many proposed equivalents to these operations. The models of the AND, OR and NOT functions are summarised in (*Klir & Folger 1988*). The most commonly used are the Max-Min operators as they have the most comprehensive theoretical background and are intuitive to understand, although the Product is often used for mathematical simplicity. The Yager class of operators are more general, and introduce an extra scalar constant *k* which controls how hard or soft the logical decision should be.

Operator type	Intersection A AND B $A \wedge B$	Union A OR B $A \vee B$	Complement NOT A $\sim A$
Zadeh	min(A,B)	max(A,B)	1-A
Mean	$\left(\frac{A+B}{2}\right)$	$\left[\frac{(2\cdot\min(A,B)+4\cdot\max(A,B))}{6}\right]$	1-A
Product	$A\cdot B$	$(A+B)-(A\cdot B)$	1-A
Yager	$1-\min\left(1,\left((1-A)^k+(1-B)^k\right)^{\frac{1}{k}}\right)$	$1-\min\left(1,\left(A^k+B^k\right)^{\frac{1}{k}}\right)$	$\left(1-A^k\right)^{\frac{1}{k}}$

Table 14 Logical Operators

It is important to observe some of the fundamental differences between fuzzy operators and Boolean logical operators, and in particular the negation operator. The first is *the law of Non-Contradiction* which states that

"the intersection of a set with its compliment results in an empty or null set"

(Cox 1994).

written formally as $A \cap \sim A \equiv \varnothing$. This assumes sets are exclusive and non-overlapping, This law is frequently broken in fuzzy logic. The second is *the law of the Excluded Middle* which states that

"the union of a set with its compliment results in the universal set of underlying domain"

(Cox 1994).

written formally as $A \cup \sim A \equiv X$. Once again this law can be broken in fuzzy logic. Some fuzzy operators obey the Associative law, $(A \bullet B) \bullet C \equiv A \bullet (B \bullet C)$ and the Commutative law $A \bullet B \equiv B \bullet A$. This is important if there is a need to analysis the functional mapping of the system. An example is logical simplification of an expert system to try and minimise the number of rules by analytical means. Not all operators obey these rules. The properties of different fuzzy operators are compared below.

5.7.1 Zadeh

The Zadeh operators are popular but are not suited to every problem. A good application might be in a safety critical environment where it is important *to limit of a consequent by the minimum truth in the antecedent.* The *min* function used for intersection obeys the Associative law $\min[A, \min[B,C]] \equiv \min[\min[A,B],C]$ and the Commutative law $\min[A,B] \equiv \min[B,A]$. A plot of the *max* and *min* operators is given below in Figure 101.

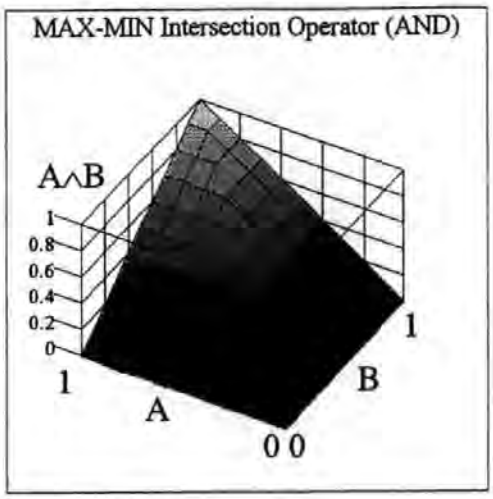

maxminAND

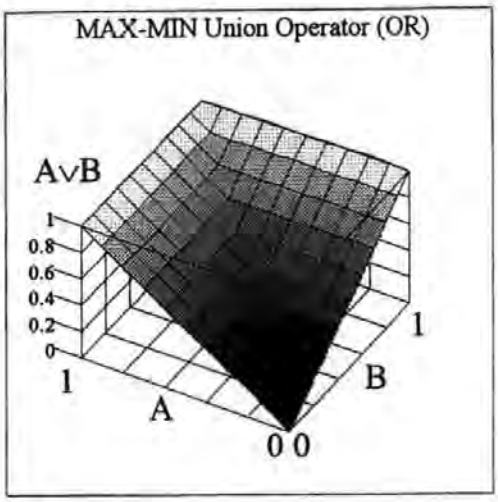

maxminOR

Figure 101 Zaheh's Intersection and fuzzy Union operators

5.7.2 Product

The product operators are a popular choice because of their relative simplicity. The intersection operator, A∩B=AB obeys both the associative law, (AB)C≡A(BC) and the commutative law AB≡BA. The union operator, A∪B≡(A+B)-AB, also obeys and associative law

$$\begin{aligned}(A\cup B)\cup C &\equiv (A+B-A\cdot B)+C-(A+B-A\cdot B)\cdot C\\ &\equiv A+B+C-A\cdot B-A\cdot C-B\cdot C+A\cdot B\cdot C\\ A\cup(B\cup C) &\equiv A+(B+C-B\cdot C)-A\cdot(B+C-B\cdot C)\\ &\equiv A+B+C-A\cdot B-A\cdot C-B\cdot C+A\cdot B\cdot C\\ &\therefore (A\cup B)\cup C\equiv A\cup(B\cup C)\end{aligned} \tag{5.3}$$

and clearly it obeys the commutative law.

$$\begin{aligned}A\cup B &\equiv A+B-A\cdot B\\ B\cup A &\equiv B+A-B\cdot A\\ &\equiv A+B-A\cdot B\\ &\therefore A\cup B\equiv B\cup A\end{aligned} \tag{5.4}$$

The product operator is a 'softer' decision operator. This is a popular choice because of the mathematical simplicity. Unfortunately the produce rule will always produce a truth in the consequent which is lower than the lowest fact in the antecedent of a rule. The truth in the consequent becomes depressed by use of the product operator. It is argued that it is not usually suited to this application or other safety critical expert systems. It can be argued that the same functional mapping

could be created with the product operator, but the adjustments to the rules (to compensate for the truth depressing effect) would render the final rules and sets less meaningful.

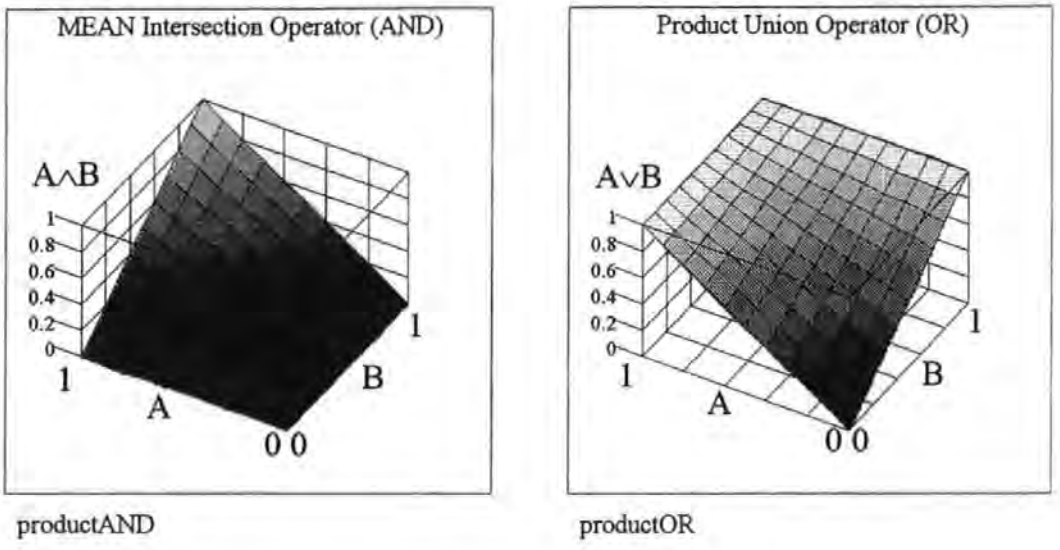

Figure 102 Product Intersection and fuzzy Union operators

5.7.3 Mean

The mean operator is a soft decision operator and has the useful properties that $A \cap \varnothing \neq \varnothing, A \cup \varnothing \neq A$, where $\varnothing$ is the null set. This would seem to be an unusual property for logical operators but there are occasions where this property is suited to model a linguistic rule. The mean intersection operator obeys the commutative law

$$\frac{A+B}{2} \equiv \frac{B+A}{2}$$

but not the associative law

$$\frac{\left(\frac{A+B}{2}\right)+C}{2} \neq \frac{A+\left(\frac{B+C}{2}\right)}{2}$$

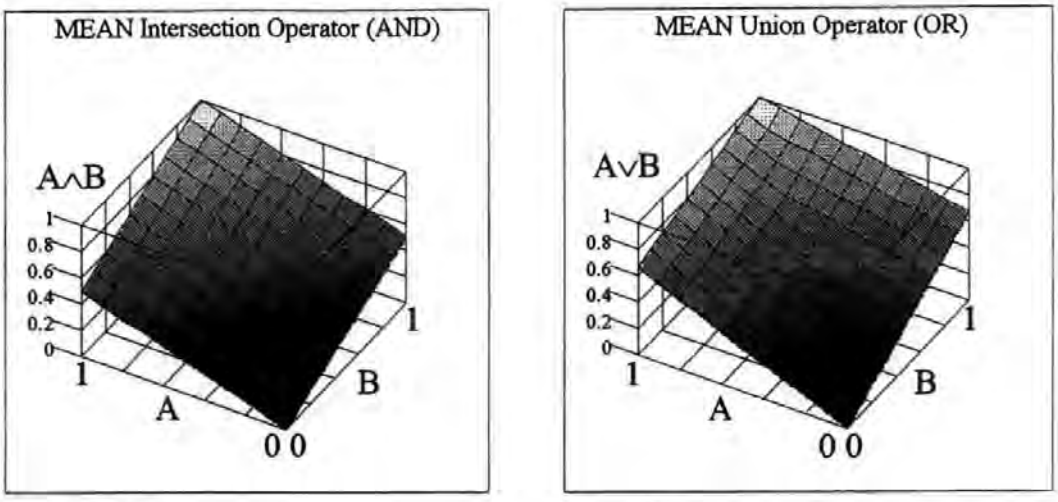

meanAND meanOR

Figure 103 Mean Intersection and fuzzy Union operators

5.7.4 Yager

The fuzzy logic operators developed by Yager (*Yager 1984*) have an extra free parameter k. This parameter defines how strict the rule is.

$$A \wedge B = 1 - \min\left(1, \left((1-A)^k + (1-B)^k\right)^{\frac{1}{k}}\right)$$

$$\lim_{k \to \infty} = \min(A, B)$$

$$A \cup B = \min\left(\left(A^k + B^k\right)^{\frac{1}{k}}, 1\right)$$

$$\lim_{k \to \infty} = \max(A.B)$$

The Yager intersection operator tends to equal the Zadeh min intersection operator as k tends towards infinity (see Figure 105). When $k=1$, it imposes a much harder intersection (see Figure 104). The Yager union operator tends to equal the Zadeh max union operator as k tends to infinity (see Figure 105). When $k=1$, this operator imposes soft union.

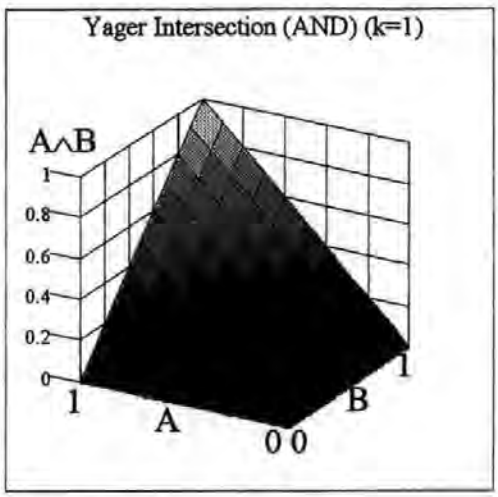

YagerIntersection

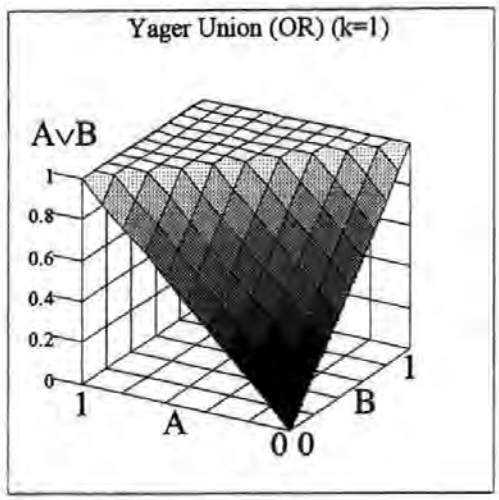

YagerUnion

Figure 104 Yager's Intersection and Union fuzzy operators (k=1)

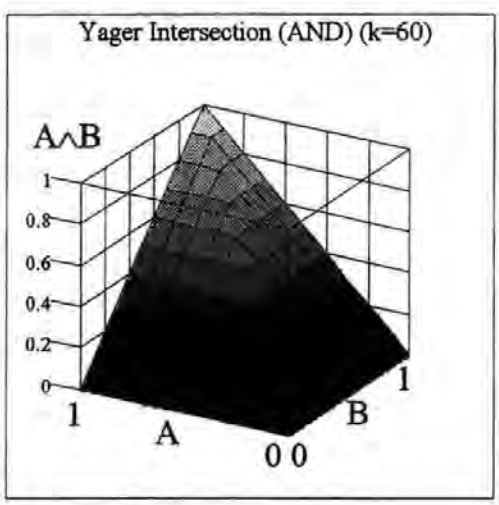

YagerIntersection

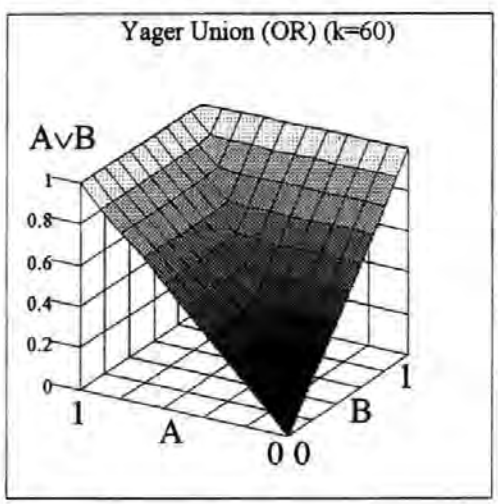

YagerUnion

Figure 105 Yager's Intersection and Union fuzzy operators (k=60)

5.7.5 Comparison of different operators

Consider the following safety critical rule used in a nulear power generation plant.

> IF (core_temperature is Normal) AND (water_pressure is Normal) AND (Background-radiation is LOW) THEN ReactorState is Normal.

Clearly, if the truth in any one of the facts in the antecedent is low then this must be reflected in the consequent (output fact). This rule is modelled well using the Zadeh operator *min* as follows

$$\mu_{Normal}(\mathrm{Re}actorState) = \min\begin{bmatrix}\mu_{Normal}(core\_temperature), \mu_{Normal}(water\_pressure), \ldots \\ \ldots, \mu_{Low}(background\_radiation\end{bmatrix}$$

Another rules might equally state:

IF (core_temperature is High) OR (water_pressure is Low) OR (Background radiation is High)
THEN
ReactorState is Dangerous

If the truth in any one of the facts in the antecedent is high then this must be strongly reflected in the consequent. The *max* function used for union also obey the Associative law max[A, min[B,C]] ≡ max[max[A,B],C] and the Commutative law max[A,B] ≡ max[B,A]. This rule is also modelled well using the Zadeh *max* operator as follows

$$\mu_{Dangerous}(\mathrm{Re}actorState) == \max\begin{bmatrix}\mu_{High}(core\_temperature), \mu_{Low}(water\_pressure),\ldots \\ \ldots, \mu_{High}(background\_radiation\end{bmatrix}$$

Here the maximum truth in the antecedent totally dominates the consequent which is important for this application. In a safety critical system, soft intersection operators such as the mean are unsuitable as the consequent of a rule is not usually sensitive enough to any one fact. For the mean operator, as there are three facts in the antecedent, a single critical event could only induce a maximum change of $^1/_3$ in the output truth.

Consider the another example of assessing the grade of final year degree students. A rule might read:

IF (Paper1 is FIRSTCLASS) AND (paper2 is FIRSTCLASS) AND (Paper3 is FIRSTCLASS) AND (Paper4 is FIRSTCLASS) AND (Paper5 is FIRSTCLASS) THEN FinalMark is FIRSTCLASS

$$\mu_{First} == \left[\mu_{First}(Paper1) \wedge \mu_{First}(Paper2) \wedge \mu_{First}(Paper3) \wedge \mu_{First}(Paper4) \wedge \mu_{First}(Paper5)\right]$$

If a student performs exceptionally well on Papers 1-4 but does not perform quite as well on Paper 5, e.g.

$$\mu_{First}(Paper1) = 1.0; \mu_{First}(Paper2) = 0.99; \mu_{First}(Paper3) = 0.95;$$
$$\mu_{First}(Paper4) = 1.0; \mu_{First}(Paper5) = 0.6$$

1. Using the Zadeh min operator for AND, the final mark $\mu_{First}=0.6$

2. Using the Mean min operator the final mark $\mu_{First}=0.908$

3. Using the Product operator the consequent truth is $\mu_{First}=0.5643$

4. Using the Yager operator ($k=1$) the consequent truth = *0.54 (k=1), 0.6 (k=10)*

The product and Yager *(k=1)* operators used in this way are totally unsuitable as the consequent truth is even lower than the lowest truth in the antecedent. The Zadeh and Yager *(k=10)* operators might still seem a bit harsh by effectively limiting the final mark to the lowest of all the papers. Only the mean seems reasonable, but might be considered to be too lenient. A new operator might be required, such as the mean-squared operator where $A \wedge B=[(A+B)/2]^2$. Using the mean-squared operator, the consequent truth = *0.824464* which might seem more reasonable. It might be possible to add more rules to overcome some of these problems with different operators. This is topic is covered in fuzzy inference and is discussed later.

5.7.6 Compliment operators

There are potentially as many proposed operators for compliment of a set A. The most fundamental one proposed by *Zadeh (1975)* is simply ~A = 1-A.

$$\mu_{\sim A}(x) = 1.0-\mu_A(x)$$

Yager proposed another compliment function in line with the union and intersection operators

$$\sim \mu_A(x) = \left(1-\mu_A(x)^k\right)^{\frac{1}{k}}$$

and Sugeno proposes another

$$\sim \mu_A(x) = \frac{1-\mu_A(x)}{1+k\cdot\mu_A(x)}$$

A comparison is shown below in Figure 106 and Figure 107.

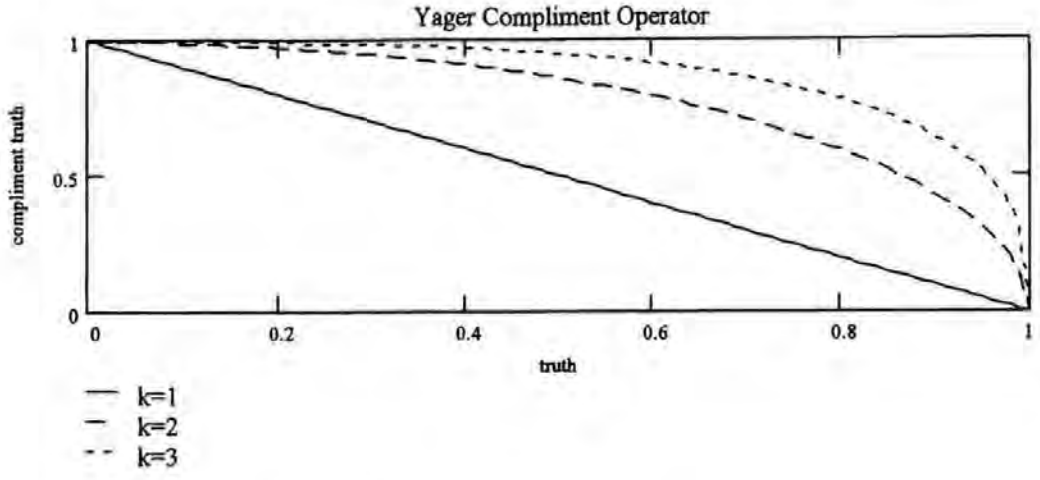

Figure 106 Yager Compliment Operator

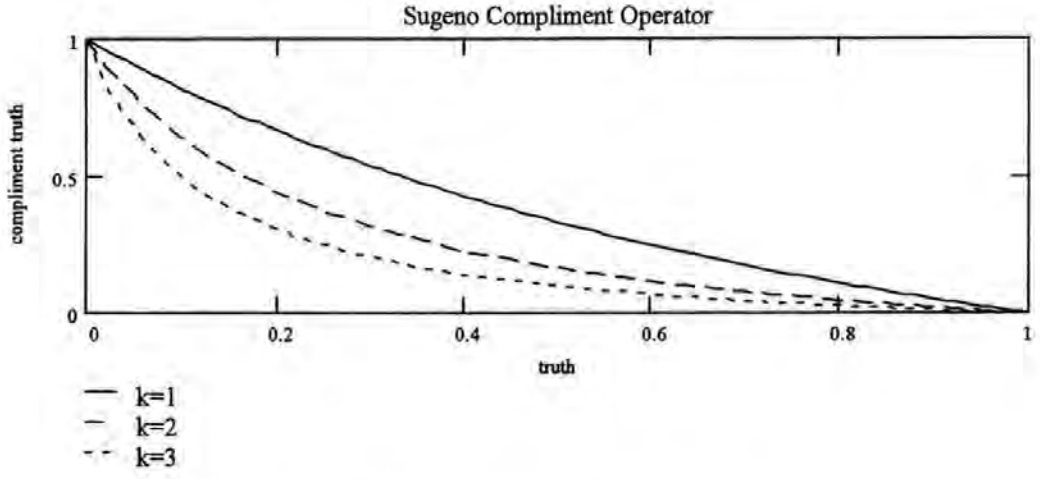

Figure 107 Sugeno Compliment operator

5.8 Hedges

Hedges are the equivalent to adverbs in spoken language, i.e. a word that modifies a verb, an adjective, another adverb or a complete sentence. Words such as *very, somewhat, slightly, definitely* are all hedges. Hedges can be used to modify fuzzy sets to simulate the effect of an adverb. For example, consider Figure 108a,b & c below.

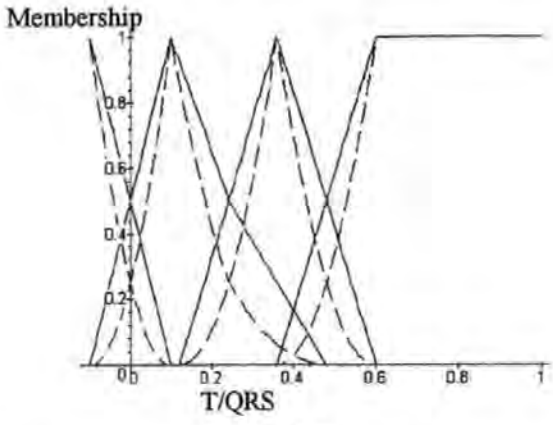

T/QRS

Figure 108a Fuzzy sets for T/QRS modified by the 'very' hedge

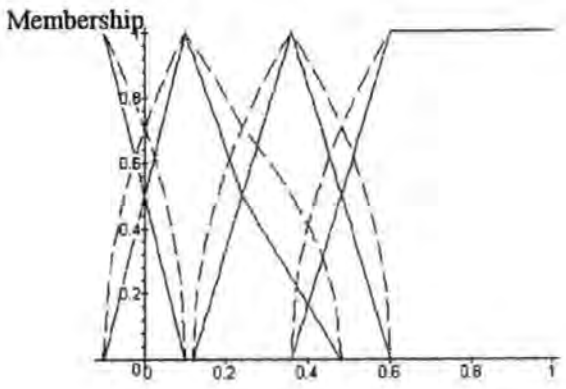

Figure 108b Fuzzy sets for T/QRS modified by 'somewhat' hedge

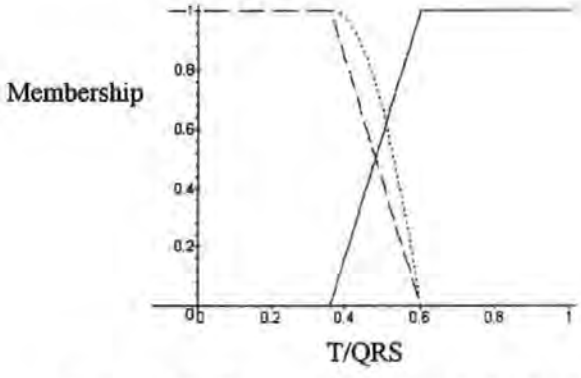

Figure 108c Fuzzy sets for High (solid line), Not High (dashed line) and Not Very High(dotted line)

The solid lines are the original membership functions, and the dashed lines are the modified membership functions. Figure 108a & b illustrate the effect of the hedge *very*, and is defined as

$$\mu_{very(A)}(x) = (\mu_A(x))^2$$

and the hedge for *somewhat* is defined as

$$\mu_{somewhat(A)}(x) = (\mu_A(x))^{1/2}$$

Hedges can be combined with operators. An example is shown in Figure 108c where the member ship function for *High*, *Not High* and *Not Very High* have been plotted.

5.9 Inference

In a conventional rules based system, propositions are constructed in the form

IF A THEN Y

"A" is sometimes referred to as the *antecedent* or condition, and "Y" is referred to as the *consequent*. More complex rules can be constructed using logical operators in the antecedent.

IF (A OR B) THEN Y

Some experts systems use implication such as

IF A THEN X

IF X THEN Y

which implies IF A THEN Y. In practice, if A was asserted as true and the order of these rules were reversed

IF X THEN Y

IF A THEN X

then this would require two sequential passes through the rules to first establish the consequent X from the second rule, and then the consequent Y from the first. More complex systems with many rules test every rule in the knowledge base repeatedly until no more rules fire. This process is often referred to as forward chaining. Medical systems often require the reverse process, where a consequent Y is stated as true, and the clinician is interested in possible causes. If Y is asserted as true, and given the rules above, a search is made for rules which could infer Y, the first of which is "Y is caused by X". The user may wish to search deeper, so the cause of X is searched, with the result "X is caused by A" and therefore by implication, Y is caused by A. This is known as *backward chaining*. For this work it is required that the system interprets facts (foetal ECG features) and produces a conclusion (forward chaining) , whilst also providing the reasoning (backward chaining) behind it's deduction. Forward chaining with fuzzy logic is a natural extension of the techniques used in conventional Boolean systems. Backward chaining is less straightforward, and an equivalent for fuzzy logic has yet to be defined.

Propositional logic and forward chaining in fuzzy expert systems differ slightly from conventional expert systems. In conventional expert systems, some rules are considered to 'fire', that is, their antecedents are true. In fuzzy expert systems, all rules are said to fire because their antecedents are all true, *but to different degrees*.

5.10 Fuzzy compositional rules of inference.

Fuzzy inference differs from conventional propositional logic in that *all* rules are said to fire, but with different degrees of truth. Consider the following fuzzy rule.

IF (T/QRS=NEGATIVE) THEN ST_WAVEFORM=ABNORMAL *[Rule 1]*

The fuzzy sets are defined as follows

T/QRS is Negative = {1.0/-1.0, 1.0/-0.05, 0.5/0.0, 0.0/0.05, 0.0/0.1, 0.0/0.25, 0.0/0.5, 0.0/1.0}
T/QRS is Normal = {0.0/-1.0, 0.0/-0.05, 0.5/0.0, 1.0/0.05, 1.0/0.1, 0.0/0.25, 0.0/0.5, 0.0/1.0}
T/QRS is Increased= {0.0/-1.0, 0.0/-0.05, 0.0/0.0, 0.0/0.05, 0.0/0.1, 1.0/0.25, 0.0/0.5, 0.0/1.0}
T/QRS is High = {0.0/-1.0, 0.0/-0.05, 0.0/0.0, 0.0/0.05, 0.0/0.1, 0.0/0.25, 1.0/0.5, 1.0/1.0}

STWAVEFORM is Abnormal = {1.0/0.0, 1.0/0.2, 0.0/0.4, 0.0/0.6, 0.0/0.8, 0.0/1.0}
STWAVEFORM is Intermediate = {0.0/0.0, 0/0.2, 1.0/0.4, 1.0/0.6, 0.0/0.8, 0.0/1.0}
STWAVEFORM is Normal = {0.0/0.0, 0.0/0.2, 0.0/0.4, 0.0/0.6, 1.0/0.8, 1.0/1.0}

These sets are interpolated and plotted in Figure 109a and Figure 109b. Given that the t/qrs ratio measurement is -0.02 then from Figure 109a the fuzzy membership value $\mu_{Negative}(t/qrs) = 0.7$ and $\mu_{Normal}(t/qrs) = 0.3$.

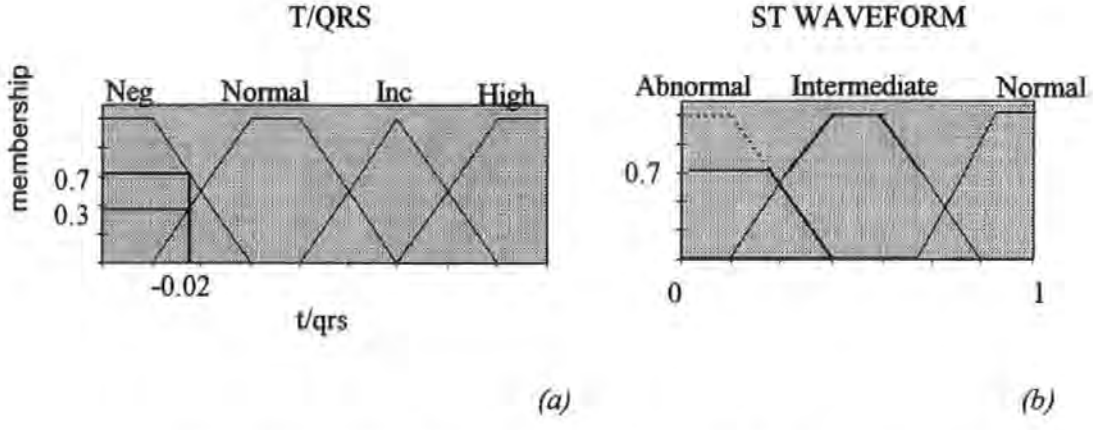

Figure 109(a) T/QRS set and (b) consequent ST Waveform set

The consequent of *Rule 1* $t/qrs \in Abnormal$ can only partially true because $\mu_{Abnormal}(t/qrs)$ can be no greater than 0.7, so the fuzzy set *Abnormal* is truncated, as shown in Figure 109(b). To compute the consequent of *Rule 1* numerically, the following rule of inference is used.

$$\mu_{Abnormal}(i) = \min\left[\mu_{Abnormal}(i), \mu_{Neg}(tqrs)\right], i=\{0..1\} \qquad (5.5)$$

This uses Zadeh's Max/Min operators and inference (known *as Max=Min)* The new fact derived from this inference can be chained using other rules. For example, using a second rule

IF (ST_Waveform=Abnormal) AND (CTG=Abnormal) THEN Fetal_Condirion=ABNORMAL [Rule 2]

Fetal_Condition is Abnormal = {1.0/0.0, 1.0/0.2, 0.0/0.4, 0.0/0.6, 0.0/0.8, 0.0/1.0}
Fetal_Condition is Intermediate = {0.0/0.0, 0/0.2, 1.0/0.4, 1.0/0.6, 0.0/0.8, 0.0/1.0}
Fetal_Condition is Normal = {0.0/0.0, 0.0/0.2, 0.0/0.4, 0.0/0.6, 1.0/0.8, 1.0/1.0}

For this example. Let the CTG be classified as *Abnormal* with membership 0.9 (see Figure 110). Two fuzzy facts are combined by the AND operator. Using Zadeh's min operator, it follows

$$\begin{aligned} \mu_{ABNORMAL}(\text{FetalCondition}) = \; & \mu_{ABNORMAL}(\text{ctg}) \wedge \mu_{ABNORMAL}(\text{st\_waveform}) \\ = \; & \min\left(\mu_{ABNORMAL}(\text{ctg}), \mu_{ABNORMAL}(\text{st\_waveform})\right) \\ = \; & \min(0.9, 0.7) \\ = \; & 0.7 \end{aligned}$$

The output set *Abnormal* for the Foetal Condition is truncated to 0.7 as shown graphically in Figure 110.

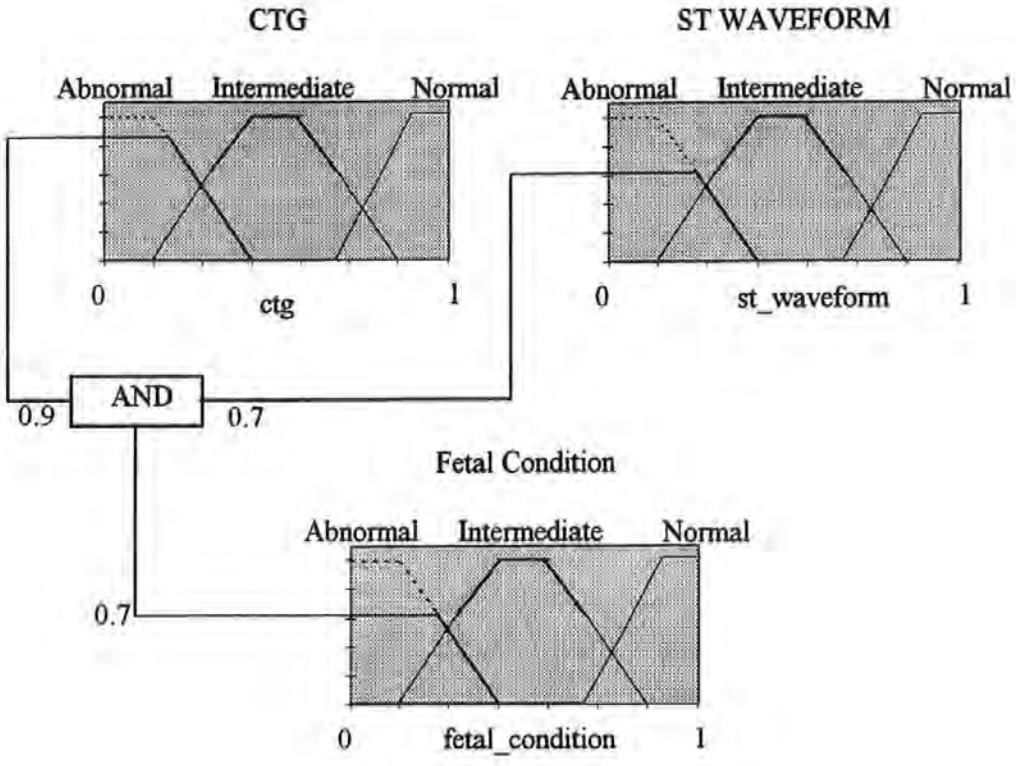

Figure 110 Fuzzy inference using the AND operator

Fuzzy inference also has to manage the situation where two rules map to the same set. For example, given a second rule.

IF (T/QRS=VERY(Negative)) THEN FetalCondition=Abnormal

The membership of *t/qrs* in the set Negative was given previously as 0.7. The hedge modifier *Very* is defined as $Very(x)=x^2$. The membership of *t/qrs* in the set *VeryNegative* is therefore $0.7^2=0.49$. There is now a dilema in that two rules map to the same fuzzy set, but with different truth values of 0.7 and 0.49. This Max-Min inference philosophy is to take the highest truth of all the consequent sets $\mu(x_i)$, $i=\{0..N\}$, where N is the number of rules implicating the same consequent set and $x \in X$ is an element along the universe of discourse X.

$$\mu'(x_i) = \max\left[\mu'(x_i), \mu(x_i)\right] \tag{5.6}$$

where $\mu'_{Normal}(x_i)$, is known as the solution set. In general this can be ambiguous so in practice the rules should be combined explicitly as follows.

IF (T/QRS=VERY(Negative) OR ((ST_Waveform=Abnormal) AND (CTG=Abnormal)))
THEN FetalCondition=Abnormal

In this case the OR is modelled my Zadeh's Max function. From Figure 110 it is observed that each fuzzy set is truncated by a single truth value provided by the antecedent of its respective rule. This is not the only inference mechanism however. An alternative is the additive rule of inference (*Cox 1994*) which uses a bounded sum as follows.

$$\mu'(x_i) = \min\left[1, \mu'(x_i) + \mu(x_i)\right] \tag{5.7}$$

With this model, the truth accumulates for every implication on the same consequent set.

5.11 Interpretation of fuzzy set outputs

Fuzzy inference results in new fuzzy sets or facts, which can be chained using other rules. If the end of the chain is reached, then some meaning has to be derived from its shape and communicated with the user. Consider the consequent set in Figure 110. It would be of little benefit to present an output set to a clinician or midwife in this form unless they have an intimate understanding of the fuzzy system behind it. Interpretation of these sets is a major problem in fuzzy expert systems, and is addressed in the following section.

5.11.1 Interpreting fuzzy sets by de-fuzzification

De-fuzzification attempts to derive a single point x' along the universe of discourse which somehow reflects the information represented in the consequent sets as a single non fuzzy scalar. A commonly used method is the centroid algorithm

$$x' = \frac{\int_{x \in X} \max\left(\left(\mu'_1(x), \mu'_2(x), \ldots, \mu'_m(x)\right)\right) \cdot x \, dx}{\int_{x \in X} \max\left(\left(\mu'_1(x), \mu'_2(x), \ldots, \mu'_m(x)\right)\right) dx} \tag{5.8}$$

where $\mu'_k(x)$ is the k^{th} $(k=1..m)$ consequent solution set. For example, consider the three consequent sets in Figure 110, *Abnormal, Intermediate and Normal*. The consequent solution sets for $\mu'_{Abnormal}(x)$, $\mu'_{Intermediate}(x)$ and $\mu'_{Normal}(x)$ are interpolated and (5.8) is evaluated. The maximum of all the overlapping sets $\mu'_{Abnormal}(x)$, $\mu'_{Intermediate}(x)$ and $\mu'_{Normal}(x)$ is outlined in Figure 111a. The value of x'

is computed as 0.532. Had the membership of *abnormal* been lower, e.g. 0.1 the centroid position would increase to the new centre of mass as x'=0.627 as shown in Figure 111b. As the consequent set *foetal_condition* implies more abnormality, then the centroid position decreases. Conversly, as set *foetal_condition* implies more normality, then the centroid position increases. Unfortunately, this technique fails if a paradoxical situation occurs such as that illustrated in Figure 111c. Here the *Abnormal* and *Normal* linguistic sets have high truth, but the *Intermediate* linguistic set has a low truth. The centroid point x'=0.5 which could equally be derived by having a high truth associated with the *Intermediate* set and a low truth associated with the *Normal* and *Abnormal* sets.

To use the centroid de-fuzzification algorithm, care has to be taken when designing the rule-base to ensure paradoxical situations cannot occur. When used carefully however, it can provide a useful single index for the human operator or outside world. A de-fuzzified output could provide a single index to indicate foetal abnormality if the rule-base is designed sufficiently well. The centroid algorithm is especially useful in control system applications where the centroid position is used to control a device, such as an actuator, a pump or a heater.

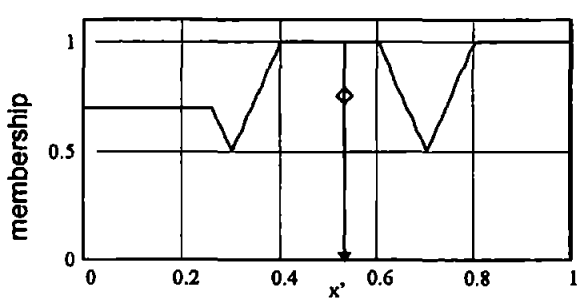

Figure 111a De-fuzzification using the centroid algorithm

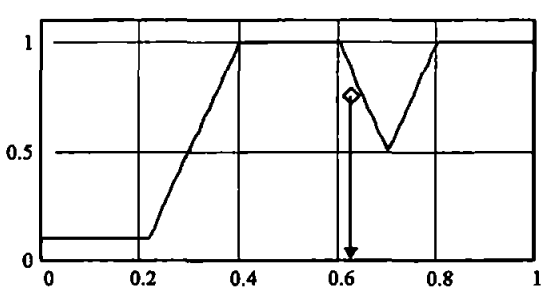

Figure 111b Output set is strongly skewed

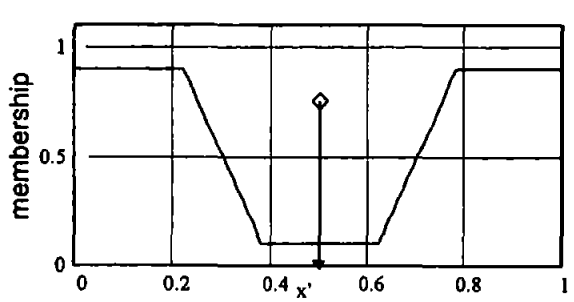

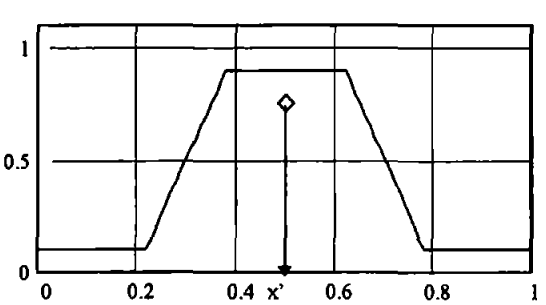

Figure 111c De-fuzzification of two different consequent sets with the same result in centroid position

5.11.2 Interpretation of fuzzy set outputs by linguistic approximation

An alternative to de-fuzzification that is more applicable to expert systems is linguistic approximation. Consider the fuzzy sets *Normal*, *Intermediate* and *Abnormal* in Figure 112a as output fuzzy sets for an expert system.

Normal = {0.0/1, 0.1/1, 0.2/1, 0.3/0.5, 0.4/0, 0.5/0, 0.6/0, 0.7/0, 0.8/0, 0.9/0, 1.0/0}
Intermediate = {0.0/0, 0.1/0, 0.2/0.3333, 0.3/0.6667, 0.4/1, 0.5/1, 0.6/1, 0.7/0.5, 0.8/0, 0.9/0, 1.0/0}
Abnormal = {0.0/0, 0.1/0, 0.2/0, 0.3/0, 0.4/0, 0.5/0, 0.6/0, 0.7/0.5, 0.8/1, 0.9/1, 1.0/1}

Upon chaining some new facts through the system, the consequent set Y becomes

Y = {0.0/0.25, 0.1/0.25, 0.2/0.25, 0.3/0.4, 0.4/0.6, 0.5/0.6, 0.6/0.6, 0.7/0.45, 0.8/0.9, 0.9/0.9, 1.0/0.9}

and is shown in Figure 112b.

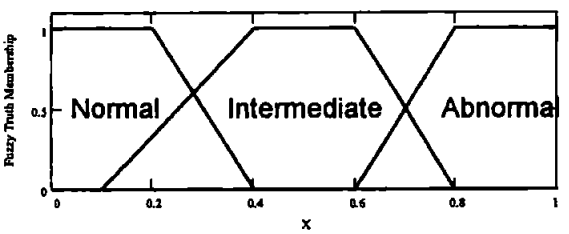

Figure 112a Fuzzy output sets Normal, Intermediate & Abnormal

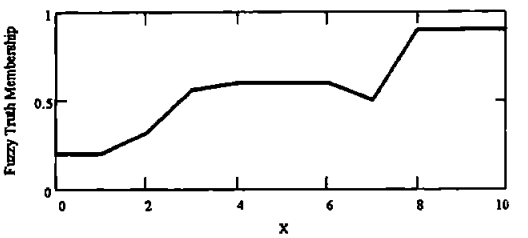

Figure 112b Consequent fuzzy set Y

From the shape of the set *Y* the implication might read :

Y is slightly Normal, possibly Intermediate and most likely Abnormal.

This linguistic explanation is more meaningful to the clinician and more reliable than simply producing a de-fuzzified number. Given the consequent set *Y*, one approach is to approximate the output as $Y=A' \vee B' \vee C'$, where *A*, *B* and *C* represent the sets *Normal*, *Intermediate* and *Abnormal*, *A'*, *B'* and *C'* are hedges of the sets *Normal*, *Intermediate* and *Abnormal* and $\vee$ represents the fuzzy union operator.

A simple technique is resolve the sets *A'*, *B'* and *C'* from the output set *Y*, such that $A'=(A \wedge \mu_{AY})$, $B'=(B \wedge \mu_{BY})$ and $C'=(C \wedge \mu_{CY})$ where $\mu_{AB}=S(A,B)$ is a scalar measure of similarity (*Sugeno & Yasukawa, 1993*) between two fuzzy sets *A* and *B*, defined by

$$S(A,B) = \frac{\|A \cap B\|}{\|A \cup B\|} = \frac{\int_X \mu_A(x) \wedge \mu_B(x)\,dx}{\int_X \mu_A(x) \vee \mu_B(x)\,dx} \tag{5.9}$$

The similarity measures μ_{AY} , μ_{BY} and μ_{CY} might relate to adjective or hedges as shown in Figure 113.

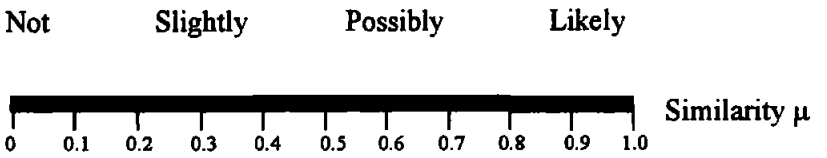

Figure 113 Relating similarity measures to fuzzy hedges

In this example, using the Yager union and intersection operators, the similarity measures μ_{AY}=0.144, μ_{BY}=0.41 and μ_{CY} =0.871 which correspond to *Slightly*, *Possibly* and *Likely* respectively.

This is only one crude method of linguistic approximation. A more satisfactory technique finds the best combination of meaningful fuzzy sets that best fit the output set *Y*. The first task is to pre-determine all the possible and meaningful combinations of fuzzy output sets, and thus attempting to span the whole fuzzy output space for the problem. Some typical examples are given in Figure 114a-o.

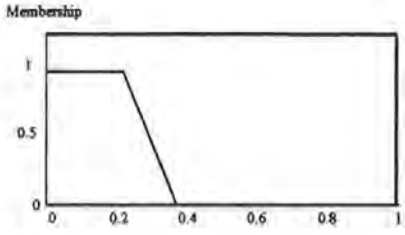

Figure 114a Most likely Normal

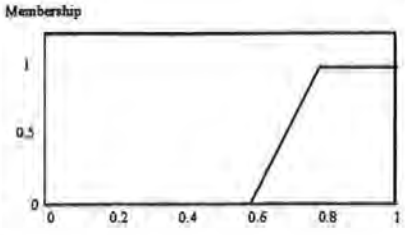

Figure 114b Most likely Abnormal

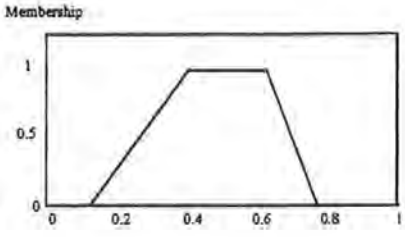

Figure 114c Most likely Intermediate

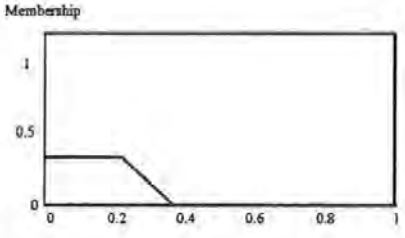

Figure 115d Slightly Normal

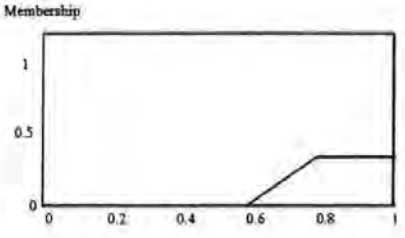

Figure 116e Slightly Abnormal

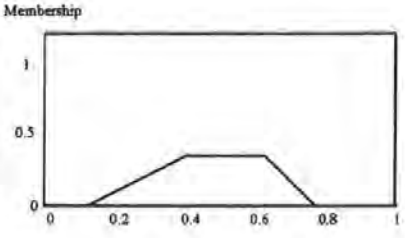

Figure 117f Slightly Intermediate

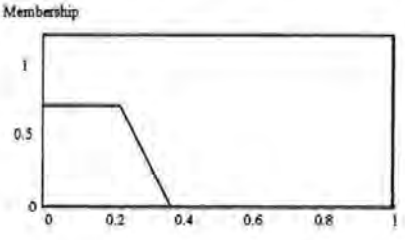

Figure 114g Possibly Normal

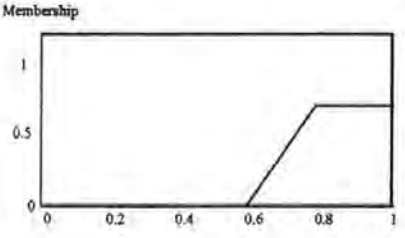

Figure 114h Possibly Abnormal

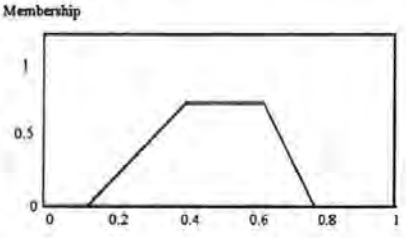

Figure 114i Possibly Intermediate

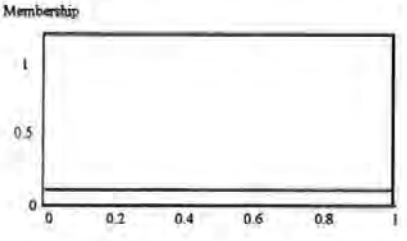

Figure 114j Unknown

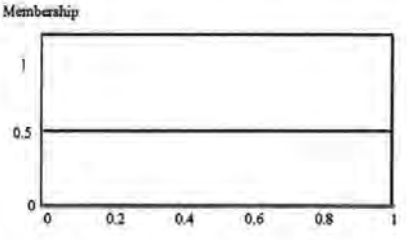

Figure 114k Possible paradox

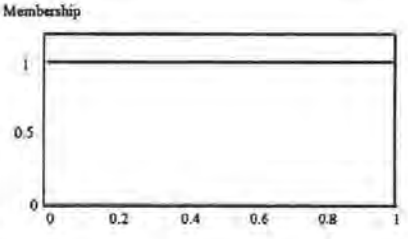

Figure 114l Paradox

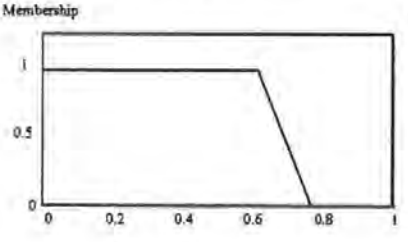

Figure 114m Normal or Intermediate

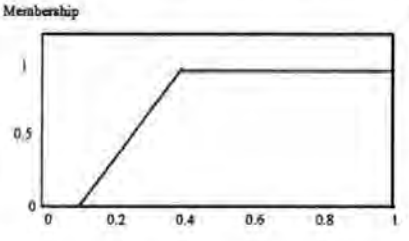

Figure 114n Intermediate or Normal

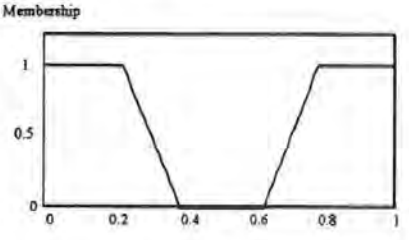

Figure 114o Abnormal and Normal Paradox

To add meaning to the output, extra 'meaningful' fuzzy sets such as *Paradox* and *unknown* are defined. All the hedge sets (not shown) can also be defined, such as *not Normal*, *very possibly Normal*, *not Normal*, *more-or-less Normal*. The objective

is to find the valid combinations of these fuzzy sets that best fit the output set Y whilst minimising the number of terms in the output rule. Given that there are N possible output sets which could be combined in any way, then an exhaustive search would require testing 2^N-1 possible combinations. Clearly this soon becomes unrealistic as N increases. In reality all combinations are not valid or meaningful so the number of terms in the output is restricted to a maximum of M terms. Given that, in general, all possible outputs can be written in the form (all terms connected with AND)

Y is *term1*, *term2*, ..., and *term M*

this would require searching $\sum_{k=1}^{M} {}_N C_k$ possible combinations where ${}_nC_r = n!/(n-r)!r!$ A difficulty with such search techniques is ensuring the result is meaningful and grammatically correct.

An alternative is to extend the number of possible output sets in Figure 114 to *define all possible and meaningful outputs*, that is, complete meaningful sentences. These should be defined by the expert and the knowledge engineer. The task of the system is simply to find the single defined output set which has the greatest similarity to the consequent set Y. In addition, the maximum similarity measure will also indicate the confidence in the output. If no pre-defined interpretation exists for a given consequent set Y, then a low maximum similarity will occur. Conversely, if a high maximum similarity is found then a high confidence is attached to the output. This technique is most suited to this application. It is critical that whatever output the system produces, it is clear, unambiguous and meaningful to the clinician. Attempting to best fit the output consequent set with primitive sets could lead to nonsense or misleading sentences.

Alternative techniques exist which attempt to select the best sets and connectives to approximate the output consequent fuzzy set, whilst keeping the output meaningful. Examples of such techniques are discussed in detail by *Wenstøp F., 1980* and *Eshragh F. & Mamdani H.*

5.12 Discussion and Conclusion

Fuzzy logic uses models of vague linguistic terms, vague rules and human inference to model the complex mapping of raw feature data to linguistic terms performed by the human expert. Constructing this mapping could be attempted using other technologies, such as Neural Networks, but has the advantage over in that the system can be examined and validated by a human expert. Neural Networks on the contrary do not reveal their internal representations and the problem is kept in the domain of the engineer. It is very important to keep the clinicians involved as much as possible. Introducing "black box technology" can distance the clinicians from the knowledge held represented within the system and is potentially dangerous. When new unaccounted scenarios appear, which were not accounted for in the development phase of the intelligent system, the system is essentially being asked to extrapolate. Fuzzy logic defines its behaviour when extrapolating and can be designed to give "all zeros" in such cases. Neural Networks, such as the Multi-Layered-Perceptron often produce an undefined response when asked to extrapolate. A Radial basis function can be used which allows all the outputs to fall to zero when the input vector is outside the span of the training data, but these can be shown to be equivalent to a fuzzy inference mechanism *(Outram & Ifeachor 1995)*.

A limitation with the Mamdani logic adopted here is that it fails to deal with the "unknown" consequent. Other inference schemes might be preferable and might need to be investigated. Although Mamdani in not theoretically rigorous it has been used very successfully in practice. In this application, the limitations of Mamdani can be circumvented by careful design of the rules and fuzzy sets. If this becomes a limitation, then other schemes will be considered.

De-fuzzification is a powerful technique for obtaining a single continuous index that could easily be interpreted by a clinician. Great care has to be exercised to avoid paradoxical situations the consequent output fuzzy sets. Linguistic approximation, which is a technique of mapping a consequent fuzzy set to a meaningful linguistic sentence, is a more suitable technique for expert systems as it provides a direct linguistic interface between the computer and the human operator. Different linguistic methods exist and is an exciting and active research area in Fuzzy logic.

For medical systems such as this one, a pre-defined ensemble of meaningful fuzzy sets are provided and the most similar match to the consequent set is selected. If no suitable match is found, then the output is "don't know". This is safer than trying to produce a good match from more primitive sets which could lead to misleading or nonsense output. The defined output sets can be though of as pre-defined cluster centres in the fuzzy knowledge space and the system as a nearest neighbour classifier.

Chapter 6

Design of the Fuzzy Expert Model

6. *Design of the fuzzy expert model*

6.1 Introduction

This chapter is concerned with the development of a fuzzy logic expert model to help clinicians interpret the changes in the foetal ECG features. The model is intended to present objective and clear information in a simple manner that can be managed in the busy labour-ward environment. The full development process of the fuzzy model is discussed in this chapter.

New features and techniques have been developed for automatically classifying the shape of the foetal ECG ST waveform. This has resolved a major limitation of all previous studies where only a single feature, the T/QRS ratio, was used to crudely quantify the ST waveform shape *(Greene & Westgate 1993; Westgate et al. 1993)*. This technique has allowed, for the first time, the automatic detection of all the ST waveform shapes specified in the clinical guidelines. Furthermore, a new technique based on finite state machines has been proposed to address the problems of modelling the human clinical experts ability to recognise and manage patterns of uncertain events in time. This has addressed the previously unsolved problem of managing uncertain terms in the guidelines which imply time, such as "persistent" and "repeated". To do this, the concept of a finite state machines is extended here to allow for a "soft decision sequential machine" to be designed, known as a "fuzzy state machine". Some of this work is also reported elsewhere in a conference paper *(Outram & Ifeachor 1996)*.

6.2 Development cycle of a fuzzy expert system

The development of a fuzzy expert system is generally less complex than a conventional crisp rule based expert system, usually requiring less rules. A brief summary of the design process is given below. This model was developed with the clinical guidance of Professor Karl Rosén. The development cycle for the expert model is summarised in Figure 118.

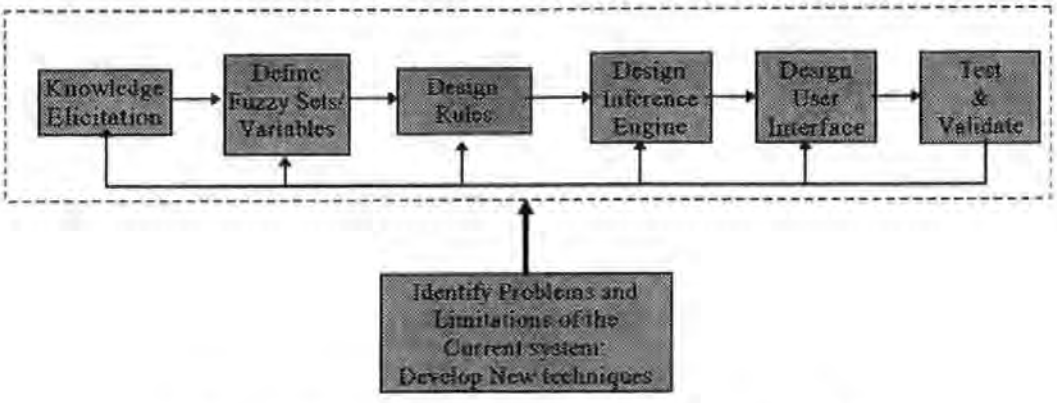

Figure 118 Development cycle of the fuzzy expert model

6.3 Knowledge elicitation

The purpose of Knowledge elicitation is to collate and formalise enough of the expert knowledge to develop a model of the experts approach to foetal ECG monitoring. Knowledge elicitation was continually conducted and reviewed over the duration of this work. Knowledge was collected from different sources and a model for interpreting the foetal ECG waveform was developed. Different elicitation techniques were employed to obtain sufficient knowledge to build the system and is summarised in Figure 119.

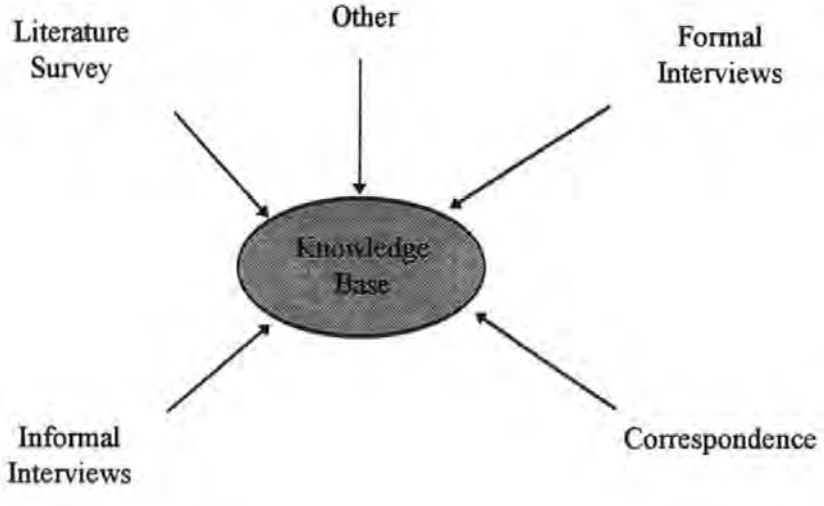

Figure 119 Knowledge elicitation sources

- **Literature Survey**. The initial investigation into electronic foetal monitoring was to conduct a literature survey. All the key publications were collected and examined. Without medical training, reading clinical journals alone with no clinical support would be a very difficult task and project would have been severely compromised without clinical support. Clinical Journals are a very valuable resource however when complimented with clinical support.
- **Formal Interviews**. Formal interviews were conducted to elicit information from Professor Rosén, who is regarded a clinical authority in foetal ECG monitoring. Structured questions were prepared and delivered to Professor Rosén. These interviews were recorded and transcribed. Formal interviews have the advantage that they are structured and disciplined. Their disadvantage is that without prior knowledge it is difficult to design the questions. A major difficulty is that much of the medical knowledge required to interpret foetal ECG is not usually strictly defined, with much of it being 'case based'. An important overview was obtained from the formal interviews, but it was felt at the time that alone they were still restrictive and did not allow for a detailed and relevant discussion. The full transcripts of these are too lengthy to include here but a tabulated summary of the expert knowledge is given in Appendix D.
- **Informal Interviews**. Most of the clinical understanding came from many hours of informal interviews and discussions which were conducted throughout the period of the project over three years. Several major benefits arose from the informal interview approach. The knowledge engineer gains a valuable insight into the clinical details, such as the underlying physiology of the foetal ECG changes & practical design constraints. Equally importantly, this is a way of keeping busy clinicians closely involved in the development of the system. Clinicians do not have the time or the necessary technical expertise to overview the research and development process in detail, but it is important they keep a strong hold on the knowledge itself. This acts as a motivating factor which ensures the development process is continuously improved. Many new ideas evolved and clarified as a result of these discussions.

- **Correspondence**. Increasingly it has become necessary to use electronic correspondence with clinical experts to refine the knowledge in the system. Expert clinicians are rarely easily accessible, but with the easy and low-cost access to electronic mail, fax and peer-to-peer communication, access to clinical expertise has become easier. Fax and electronic mail has become a very useful tool, as has been used extensively to communicate ideas, questions and problems.
- **Other**. Information has been collected from other sources such as engineers, clinicians and conference delegates. During the course of this project seven conferences were attended (one clinical, six engineering), all of which have stimulated new ideas. During the data collection process in the labour wards, there were occasions to discuss the project with clinical personnel, such as mid-wives, obstetricians and hospital physicists.

In conclusion, formal interviews are effective at obtaining overview information such as global aims and objectives, but it is unreasonable to elicit specific details without prior knowledge. Eliciting clinical knowledge was a cumulative process. To design important questions, and appreciate clinical journals, requires a degree of knowledge which is best found through discussions with human clinicians. Attempting a project such as this without clinical support would be very difficult and I believe would severely compromise progress.

6.4 Designing the fuzzy sets and variables.

The input variables to an intelligent fuzzy system need to be defined and used consistently. When dealing with a medical knowledge base, it is important to understand and use consistent terminology. Some variables in this system are the T/QRS ratio, ST waveform shape, CTG and ST segment shape. From the knowledge elicitation, adjectives and adverbs can also be identified which describe these variables. It is important as the knowledge engineer to keep the knowledge base as close to the language of the expert as possible. Some of the important terms used in the clinical guidelines *(Rosén 1994)* are given below. The words in brackets are the different categories.

T/QRS Ratio: *{Constant , Increasing, Rising, Rapidly Increasing, Negative, Positive, High, Normal}*

ST Waveform : *{Normal, Depressed, Negative, Elevated, Raised, Bi-Phasic, Changing, Acute change}*

CTG Pattern: *{Normal reactive, Intermediate, Abnormal, Normal, Pre-terminal}*

Heart Rate Declarations: *{Persistent, Late, Variable, Present, Not Present}*

Baseline Heart Rate: *{Increased, bradycardia, Low, tachycardia, High, Normal, Rapid return}*

Heart-rate Variability: *{Increased, Decreased, Normal, Undulating}*

Some of these terms imply instantaneous events, such as a *High* T/QRS ratio where others imply time, such as a *Rapidly Increasing* T/QRS ratio or *constantly elevated* ST waveform. Others terms, such as *Negative ST waveform shape* are vague and do not refer to any one feature of the foetal ECG, but a visual shape. To manage these problems, new fuzzy variables have been created.

ΔT/QRS(20): *{Low, Medium High}* //Change in T/QRS over 20 minutes

ΔT/QRS(15): *{Low, Medium High}* //Change in T/QRS over 15 minutes

ΔT/QRS(10): *{Low, Medium High}* //Change in T/QRS over 10 minutes

ΔT/QRS(5): *{Low, Medium High}* //Change in T/QRS over 5 minutes

STSegment *{ Normal, Biphasic, Depressed, Elevated}*

Tcomplex *{Negative, Normal, Elevated, Highly Elevated}*

From these terms it was possible to derive the fuzzy variables similar to the linguistic terms used in the rule base.

6.5 Designing the fuzzy sets

Table 15 summarises some of the key fuzzy sets and variables.

CTG	ST Waveform	ST Segment	T-Complex	T/QRS+ Ratio	T/QRS- Ratio	ST Peak 1	ST Peak 2	ΔT/QRS Ratio
Normal	Normal	Depressed	Negative	Negative	Negative	Negative	Negative	Falling
Intermediate	Intermediate	Bi-phasic	Normal	Normal	Nil	Normal	Normal	Stable
Abnormal	Abnormal	Normal	Increased	Increased	Positive	Positive	Positive	Rising
	Changing	Elevated	High	High			Not Present	Rapidly Rising

Table 15 Table of key fuzzy sets.

Note that the measurements to determine the truth values of fuzzy subsets sometimes need to consider time intervals given in the guidelines (see appendix D)

(Rosén 1986). The full plots of these fuzzy sets are given in appendix E. The fuzzy sets are derived partly from the clinical guidelines, but mostly through discussions with a clinical expert. The triangular fuzzy sets are used at this stage of development. Linear interpolation is used to generate a continuous function over the full universe of discourse.

6.5.1 Managing unknown scenarios

An important property of fuzzy logic is that it is possible for all the output consequent sets to have a low truth value when presented with data which is not considered by the rule-base. This implies a "don't know" as an output rather than an attempt to resolve any meaning. This seemingly 'honest' property is a major strength in the favour of fuzzy logic against other technologies. Other scenarios might arise, such as noisy data resulting in unrealistically high input values. It is useful to be able to detect these situations as this provides feedback on data quality. To do this, the universe of discourse for the raw input features are extended to infinity and additional fuzzy sets are added to cater for suspiciously high or low features which extend beyond their expected limits. For example, consider Figure 120. At the extremes of the variable x, outside the expected region of that variable defined in the clinical guidelines, the fuzzy set "Error" is defined.

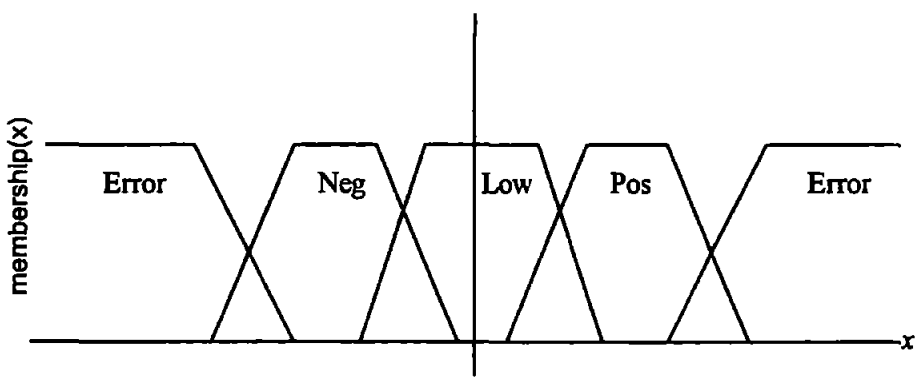

Figure 120 Extending the fuzzy universe of discourse as error checking

Using this approach, additional information on data quality can be inferred. All other intermediate and output sets only span their expected universe of discourse and have a finite area of truth, such as the sets {*Neg, Low, Pos*} in Figure 120. This is a more faithful model of the linguistic terms. Other set functions can be used, but linear interpolation is simple, flexible and easy to modify.

6.6 Designing the fuzzy rules

The rules are derived from the clinical guidelines and through consultation with expert clinicians. They are carefully structured to avoid paradoxical situations and the need for multiple iterations through the rule-base. The full set of rules are given in Appendix F. The structure of the complete rule-base is summarised in Figure 121.

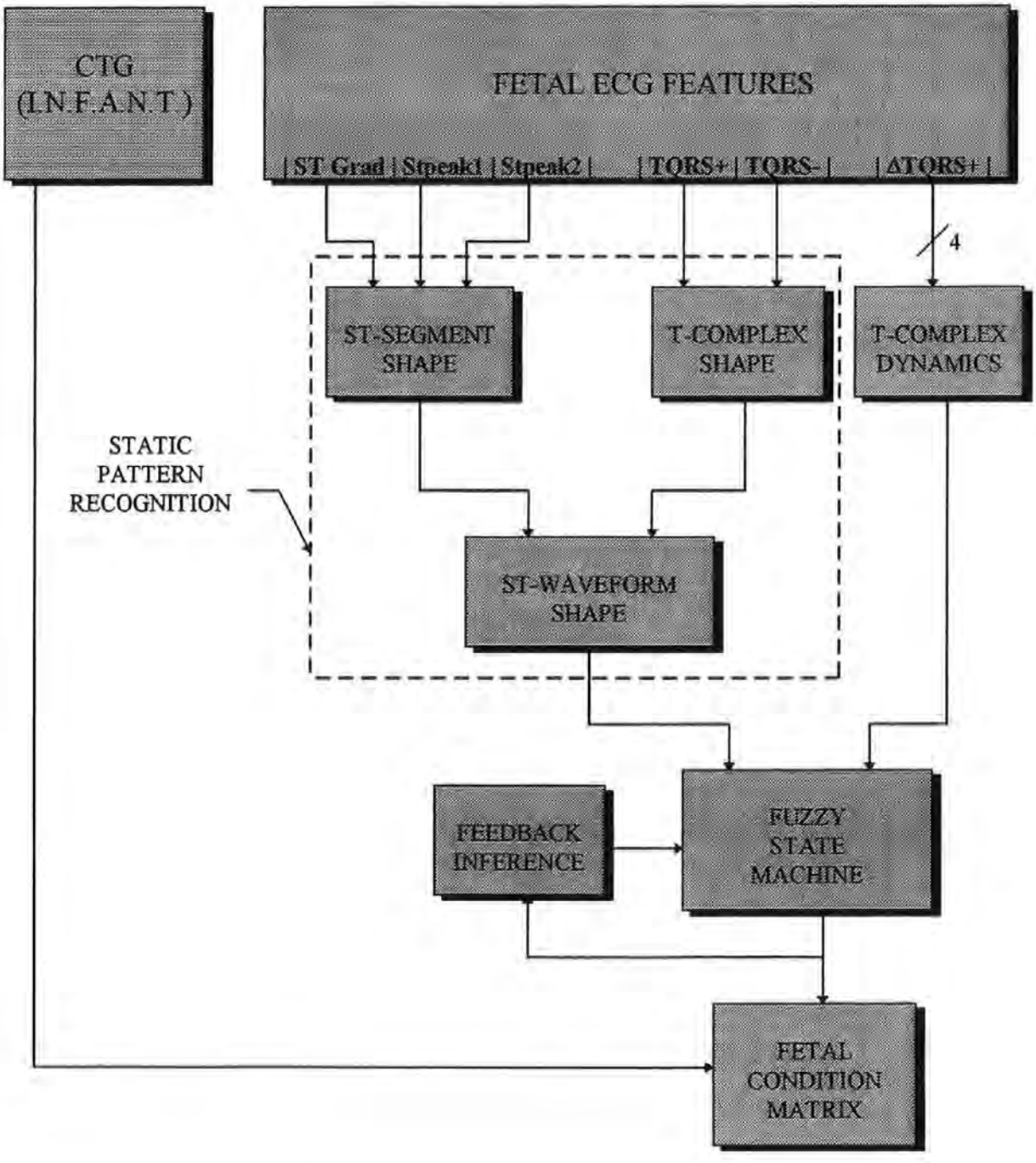

Figure 121 Structure of the fuzzy expert model

The key aspects of this model are

(a) **CTG**

The interpretation of the CTG is to be provided by the INFANT system *(Ifeachor et al., 1991)*.

(b) **Static Pattern Recognition**

The system can classify any given ECG waveform from the extracted features. This breaks into T complex shape and ST segment shape.

(c) **Dynamic Pattern Recognition**

The system manages the progressive change in ECG waveform shape by analysing trends and keeping track of previous events in the labour.

(d) **User Interface**

A means of communicating the output of the intelligent system to the user in a way that is simple and intuitive.

6.7 Rules and fuzzy sets for assessing the quality of ECG data

A simple example of fuzzy logic concepts is demonstrated with the rules for assessing the severity of baseline shifts in the data. The features used for this are discussed in chapter 2. The process of obtaining a single quality measure is as follows.

1. Elicit the rules in normal written language.
2. Define the variables, relevant adjectives and adverbs (hedges) that describe these sets.
3. Define the fuzzy sets to model these adjectives.
4. Define the rules.
5. Measure the features and convert to fuzzy sets (fuzzification process).
6. Apply the rules to determine the shape of the consequent set.
7. De-fuzzify / linguistically approximate the consequent set to produce a meaningful output.

6.7.1 Elicitation of the rules

The initial rules operate on features from the polynomial approximation of the baseline shift. The rules are summarised as follows.

If the baseline order is very low,
then the quality or "usability" of the data is good (irrespective of the peak-to-peak amplitude)

If the baseline order is low, and the peak-to-peak amplitude of the baseline shift is much less than the QRS amplitude,
then the quality of the data is good (can be removed by the curve fit, see Chapter 2)

If the peak-to-peak amplitude of the baseline shift is very much less then the QRS amplitude,
then the data quality is good (irrespective of the order)

If the peak-to-peak amplitude of the baseline shift is high and the order is not low,
then the data quality is poor

Otherwise it is intermediate

6.7.2 Define the linguistic terms, fuzzy variables and relevant adjectives

To recall, there are two features, the span of the baseline shift ε (peak-to-peak amplitude of the baseline shift) and order of the approximation *n*. The adjectives used to describe these are given in Table 16.

Variable	span ε	order *n*
	High	High
	Medium	Medium
	Low	Low

Table 16 Variables and adjectives for baseline quality assessment

The only adverb or "hedge" is *very*, which is assumed to modify a fuzzy set with the function $very(\mu)=\mu^2$

6.7.3 Define the fuzzy sets

The fuzzy sets used for baseline quality assessment are shown in Figure 122a-c. The fuzzy sets were initially designed empirically and later tuned to ensure that the system was highly sensitive. Figure 122a defines the sets for the normalised baseline approximation span ε, where the ε is normalised against the average QRS amplitude.

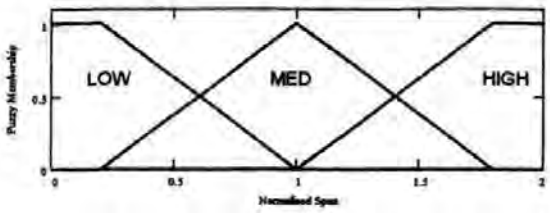

Figure 122a Fuzzy sets for baseline shift span

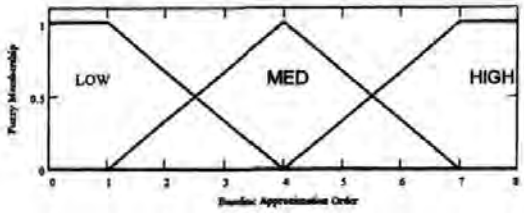

Figure 122b Fuzzy sets for baseline shift degree

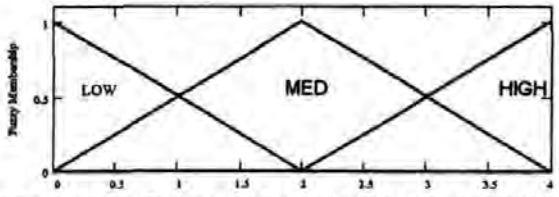

Figure 122c Fuzzy output sets for baseline shift severity

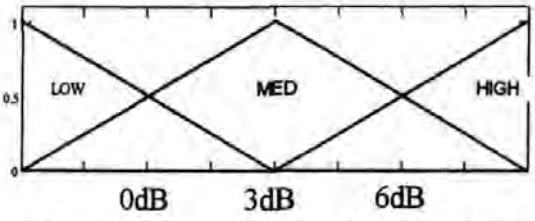

Figure 123 Fuzzy sets for signal-to-noise ratio (dB)

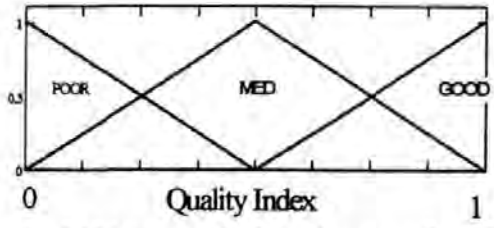

Figure 124 Fuzzy output set for overall quality Index of the data

6.7.4 Define the rules

The following rules are used to assess the severity of the baseline shift.

IF (ε is High) AND ((*n* is High) or (*n* is Medium))
THEN Baseline is *High*

IF ((ε is High) AND (*n* is Low)) OR ((ε is Medium) AND (*n* is High)) OR ((ε is Medium) AND (*n* is Medium))
THEN baseline is *Medium*

IF (ε is Low) OR ((ε is Medium) AND (*n* is Low)) OR ((ε is High) AND (*n* is Very Low))
THEN Baseline is *Low*

The following rules combines the quality measures

IF (Baseline is *High*) OR (snr is *Low*) THEN
Quality is *Poor*

IF (*snr* is *High*) AND (Baseline is *Low*)
THEN Quality is *Good*

IF ((snr is *Medium*) AND (Baseline is *Low*)) OR ((snr is *High*) AND (Baseline is *Medium*))
THEN Quality is *Medium*

Baseline	*Low*	*Medium*	*High*
SNR			
Low	Poor	Poor	Poor
Medium	Medium	"Interpolated"	Poor
High	Good	Medium	Poor

Table 17 Matrix for assessing signal quality

The data is only accepted for ST waveform analysis if the quality is Good or Medium. Note the "interpolated" value is resolved by the fuzzy logic. A rule is not necessary for every explicit case. The fuzzy sets overlap and therefore the quality for *Medium* SNR and *Medium* Baseline will be interpolated somewhere between *Medium* and *Poor* quality.

6.8 Static pattern recognition of the ST segment shape

A important aspect part of the expert model is to determine the shape of the foetal ECG ST waveform. When considering the shape of the ST waveform from any given ECG waveform, there are two levels of detail which are required. The most important question to answer is whether the ST-waveform shape belongs to category Normal, Intermediate or Abnormal. Figure 126(b)-(f) are all classified as abnormal ST waveform shapes (to different degrees). The system can detect most abnormal shapes by looking for any continuously negative area in the ST-waveform. This information might be enough to alert a clinician to take action and potentially prevent some foetal distress. From Figure 121, the ST waveform shape is broken into two sub-classes, *ST Segment Shape* and the *T-Complex Shape*. The simplest rule is as follows

IF (Greatest Negative ST Area is Negative) THEN ST-Waveform is Abnormal

where "Greatest Negative ST Area" is the largest single negative area in the ST waveform which is below the iso-electric level.

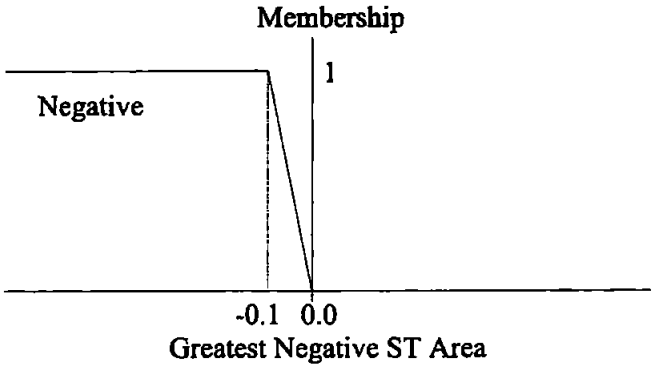

Figure 125 Fuzzy set for ST waveform is Abnormal

From Figure 126, categories (b), (c) and (d) are very abnormal, and usually have negative area. Categories (e) and (f) do not have any negative ST area, but are suspicious waveform shapes which may develop into a more abnormal configuration. It is not satisfactory to solely report an abnormal ST waveform without giving any explanation. There is clearly a need for assessing the instantaneous ST waveform shape as an explanation facility for the clinician and to grade the abnormality of the waveform. The T complex shape is quantified by the T/QRS ratio and has been used successfully in a recent clinical trial (*Westgate et al. 1993*) to reduce unnecessary clinical intervention. It is recognised that the ST segment shape should also be quantified (*Greene K.R & Westgate J. 1993 ; Luzietti R. & Rosén K.G. 1994*) otherwise important shape changes will be missed

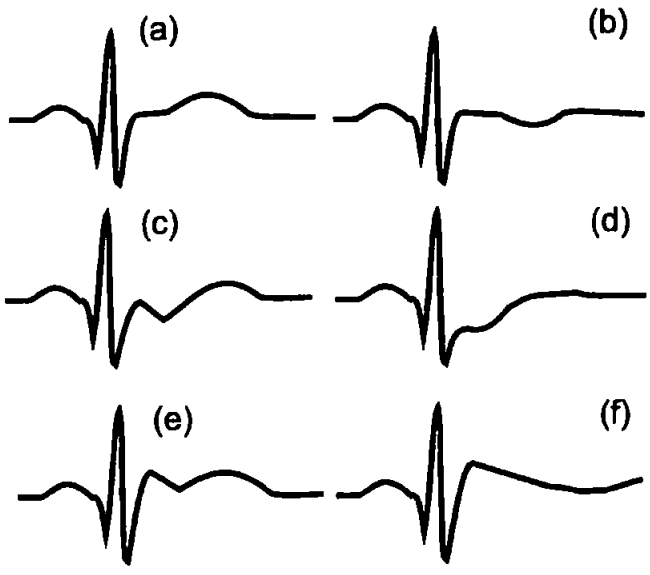

Figure 126 (a) Normal, (b) Abnormal (Negative T), (c) Abnormal (Bi-phasic ST, Positive T), (d) Abnormal (Depressed ST, Normal T), (e) Suspicious (Negative ST slope, Normal T, Positive ST), (f) Suspicious (Negative ST slope, Normal T, Positive ST)

A difficulty in this work is that the majority of the collected data has a normal outcome and only demonstrates normal ST waveform shapes. A single case has been collected however which demonstrates a wide range of ST segment shapes. Using this single case some preliminary fuzzy rules to quantify the ST segment shape have been developed. It must be understood however that *this case is a premature foetus (34 weeks gestation) and would not normally be considered applicable for ST waveform monitoring* as it is believed that the abnormal ST waveform shapes are often normal for the pre-term foetus. It is assumed for the purpose of this study that these are representative of abnormal ST waveforms in the term foetus.

6.8.1 Technique 1: Linear regression

The technique proposed for use in the STAN® monitor to detect bi-phasic waveforms is to fit a linear regression line to a fixed window of data in the ST waveform. The gradient and position of this line is used to assess whether the ST waveform is

(a) Negative sloping and positive (Bi-phasic 1)

(b) Negative sloping crossing the iso-electric level (Bi-phasic 2)

(c) Negative sloping and negative (Bi-phasic 3)

(d) Positive sloping (normal)

A mark of bp1, bp2 or bp3 is placed in the paper trace where each event is deemed to have occurred. A difficulty with this technique is finding where to start and end the linear regression line. This method assumes the negative sloping region of the ST segment can be approximated well by a straight line. This assumption was found to unsatisfactory as the sloping region is of varying length and position, and is not generally well approximated by a straight line. This technique is validated and discussed in section 6.9.2.

6.8.2 Technique 2: Minimum gradient

A similar technique to that described in section 6.8.1 is the minimum gradient technique which tries to overcome the limitations of linear regression by examining the derivative information from the ST waveform polynomial approximation. The minimum derivative in the ST segment is measured and used to detect a negative sloping ST segment in a similar way to section 6.8.1. This technique is particularly prone to false alarms because it is sensitive to short (insignificant) negative sloping regions in the ST segment. Validation of this technique is discussed in section 6.8.3.

6.8.3 Technique 3: New Fuzzy Logic Method.

The third technique for ST segment classification was to use visual features and fuzzy rules to assess the ST segment shape. Consider the case in Figure 127 of a positive ST segment with a significantly sloping ST gradient. Two features, peak 1 and peak 2 are selected from the ST waveform curve fit. Peak 1 is the first peak after the J point and peak 2 is the lowest trough between peak 1 and 100ms after the J point. The features from all good examples of abnormal waveforms were recorded & scatter plots of peak 1 and peak 2 are shown in Figure 128a-d. Considering each graph in turn.

(a) For a significantly sloping ST Segment which is all above the iso-electric level (known as bi-phasic 1), both peak 1 and peak 2 are positive (the upper-right quadrant).

(b) For a significantly sloping ST Segment which crosses the iso-electric level (known as bi-phasic 2), peak 1 is positive and peak 2 is negative (lower-right quadrant).

(c) For an ST Segment which is mostly below iso-electric level (known as bi-phasic 3 or depressed ST segment), peak 1 is a low positive or negative value and peak 2 is always negative (mostly lower-left quadrant overlapping into the lower right).

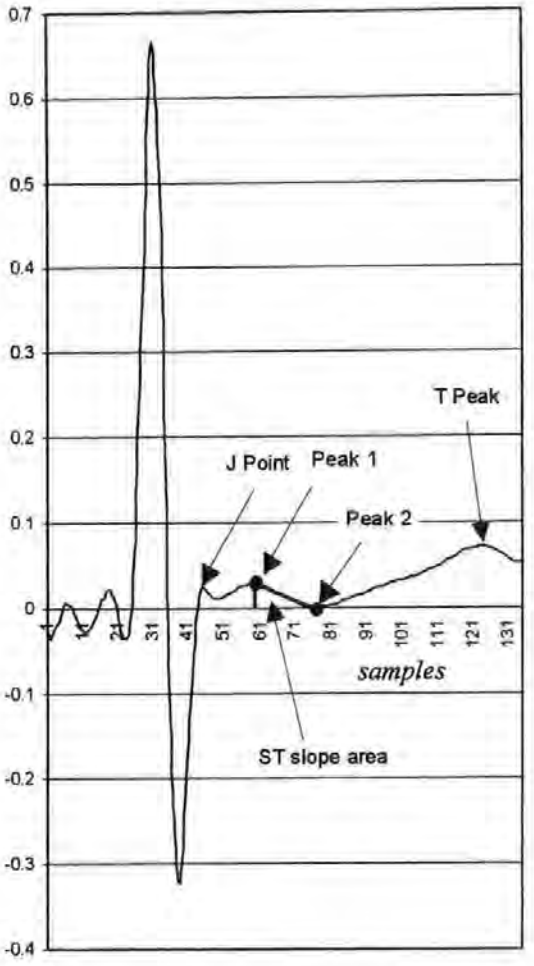

Figure 127 Determining the ST slope

(d) For normal ST waveforms, both peak 1 and peak 2 should be positive (upper right quadrant) and roughly equal, i.e. peak1 ≈ peak2.

Figure 128a-d are visibly clustered. Figure 128a and Figure 128d show a large degree of overlap. For positive ST segments, the relative heights of peak 1 and peak 2 are not always enough to distinguish between a significant negative slope and an insignificant slope (Normal ST segment). A short ST segment slope is relevant if a portion of it is negative, but for the positive ST segment, there is less significance placed upon this shape unless it is of sufficient depth and length. The length and depth of the slope are additional features which need to be considered. A proposed rule to determine if the positive ST segment with a negative slope is significant is

IF peak 2 is lower than peak 1 *AND* peaks 1 and 2 are a significant distance apart THEN
The slope is deep and long enough to be significant.

A scatter plots of the peak difference *Δpeak=(peak2-peak1)* and the distance between the peaks is given in Figure 129a and Figure 129b for both a normal positive ST segment and one with a negative slope. There is an overlap between the two classes, which is to be expected as there is not distinct guideline for the human eye when visually classifying the two classes. It is also important to consider the meaning of the empty regions in the pattern space.

1. There are no waveforms with a high peak differences and a small distance (bottom left quadrant). From general observations, such waveforms are be considered to be artefact rather than genuine and should be left blank or assigned to a "un-recognised waveform" class.
2. There are no waveforms with a low or zero peak difference and a high distance (top right quadrant). These correspond to a normal waveform, although they are not observed in the data.

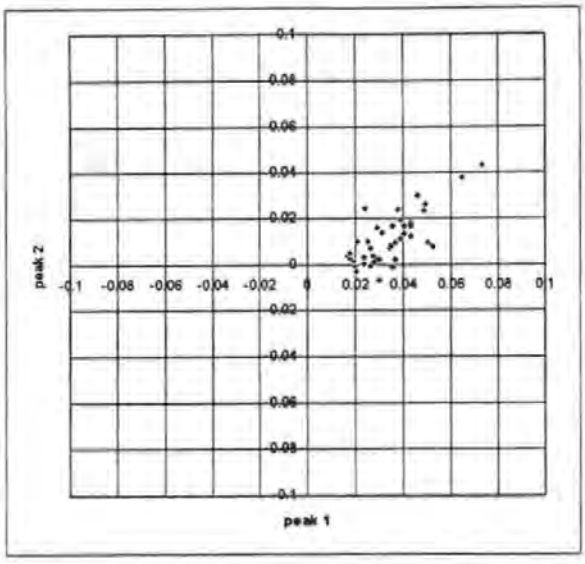

Figure 128a Scatter plot of ST peak 1 and ST peak 2 for a positive ST with a negative ST segment slope

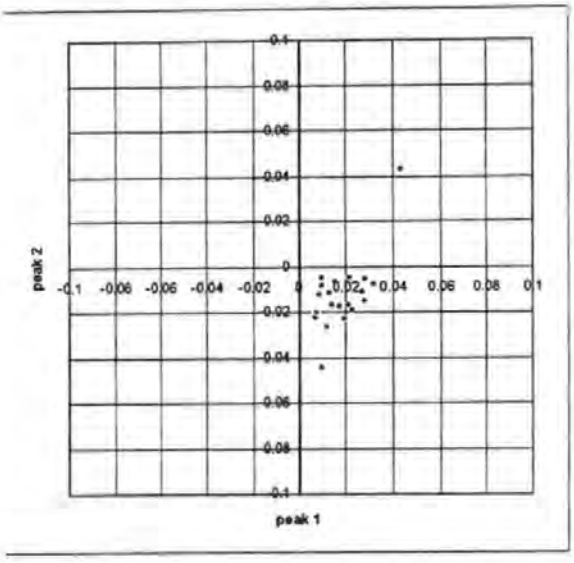

Figure 128b Scatter plot of ST peak 1 and ST peak 2 for a bi-phasic ST segment with a negative ST segment slope

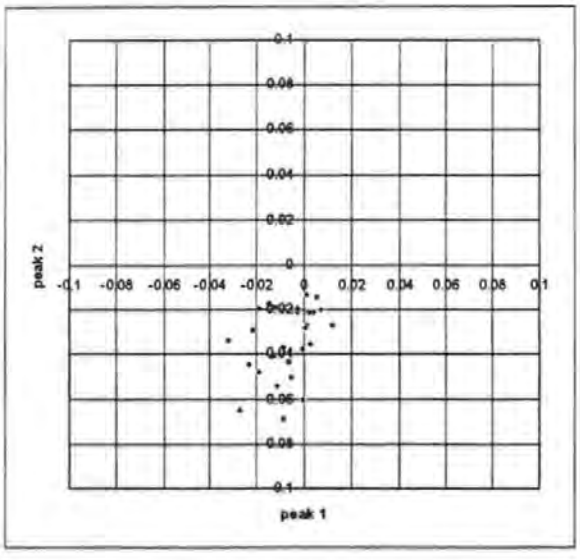

Figure 128c Scatter plot of ST peak 1 and ST peak 2 for a negative ST segment

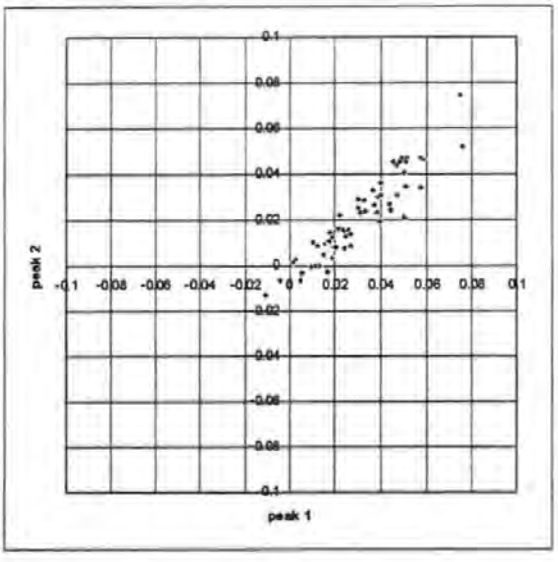

Figure 128d Scatter plot of ST peak 1 and ST peak 2 for a normal ST segment

This illustrates an important advantage of using rule-based systems to construct a pattern space as opposed to other approaches such as neural networks which learn the pattern space. Using a rule based system, such as a fuzzy expert system, each rule is intellectually validated before it is accepted and tested. Rules can also be added or modified to span known areas of space which are not observed in the data base.

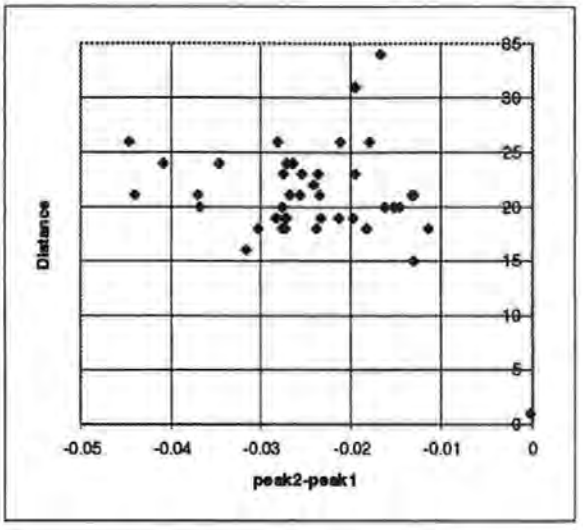

Figure 130a Positive ST with negative slope

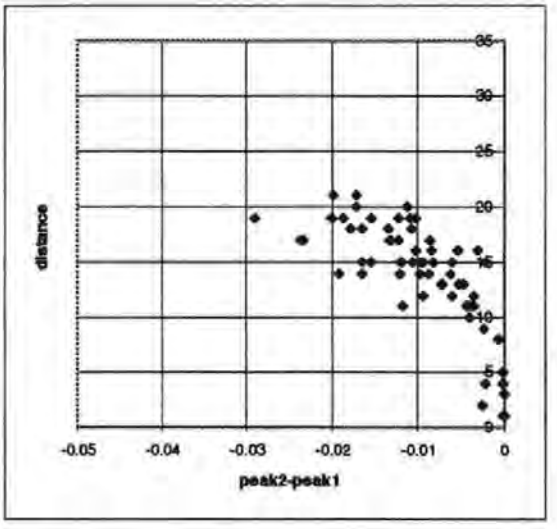

Figure 130b Positive ST with no significant ST slope (Normal ST waveforms)

6.8.4 Designing the rules to classify the ST segment shape

The following rules describe the scatter diagrams and hence the problem space, given that

$\Delta peak=(peak2-peak1)$ and *peakdistance* is the distance between *peak2* and *peak1* in samples (at 500Hz sampling rate).

IF (*peak1* is *positive* OR *peak1* is *zero*) AND (*peak2* is *positive* OR *peak2* is *zero*) AND (Δ*peak* is *zero* OR (Δ*peak* is *small* AND *peakdistance* is *quite_near*)) THEN *stsegment* is *Normal*

IF *peak1* is *positive* AND (*peak2* is *positive* OR *peak2* is *negative*) AND Δ*peak* is *negative* AND *peakdistance* is *significant*
THEN *stsegment* is *biphasic1*

IF *peak1* is *positive* AND *peak2* is *Negative* AND *peakdistance* is *significant* AND Δ*peak* is *negative*
THEN *stsegment* is *biphasic2*

IF (*peak1* is *negative* OR *peak1* is *zero*) AND *peak2* is *negative*
THEN *stsegment* is *biphasic3*

The following rules manage the unaccountable situations.

IF Δ*peak* is *very high* AND *peakdistance* is *close* THEN *stsegment* is *unknown*
IF *peak1* is *negative* AND *peak2* is *positive* THEN *stsegment* is *unknown*

6.8.5 Derivation of the fuzzy sets using frequency distribution data

The frequency distribution of each of the features is shown in Appendix G for each class. This is a useful guideline for designing the fuzzy sets which model the fuzzy terms. From the frequency distributions the fuzzy sets shown in Figure 130 were derived.

6.9 Validating the detection rate of Bi-Phasic waveforms

It is imperative that bi-phasic ST segments are not missed as they are rare, often short-lived and could be highly significant. All bi-phasic ST segments are characterised by a negative slope in the ST segment starting from around the J point and ending 80-100ms afterwards. Shorter regions with negative slope can appear instantaneously in the ST segment, but these are due to noise and artefact.

The output of each technique is computed (using filter type 4) and compared at the end of the experiment. For different values of a the threshold value *Th*, the number of true positive (TP), false positive (FP), true negative (TN) and false negative (FN) events have been counted and tabulated.

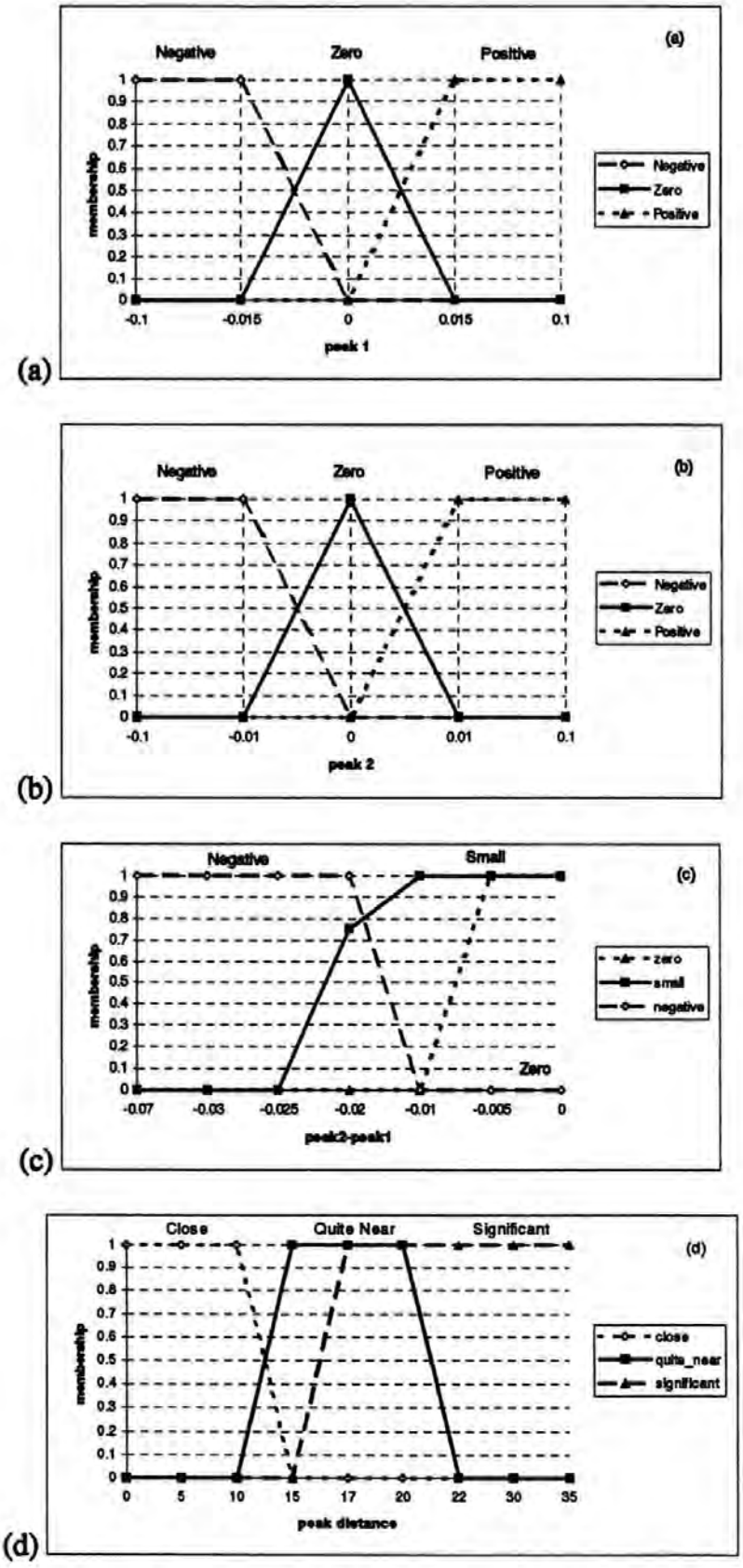

Figure 131 Fuzzy sets used for interpreting the ST segment shape. (a) peak 1, (b) peak 2, (c) Peak difference Δpeak and (d) Distance between the peaks

6.9.1 The minimum gradient technique

Average waveforms are recorded every 15s, stored, plotted and classified as 1 for bi-phasic and 0 for other. For a given threshold, if the minimum gradient in the ST segment (as measured by the system) falls below the threshold, then the system grades the waveform as bi-phasic. The number of true positive (TP), true negative (TN), false positive (FP) and false negative (NF) hits are recorded for different values of the threshold. From these values the hit ratio and false alarm ratio values are computed. A table of results is given in Table 18 and the ROC curve is shown in Figure 131. The area under the ROC curve for this method was 0.7719 which is poor (probability of a correct decision=0.7719).

Threshold	TP	TN	FP	FN	FA	HR
0.1	33	0	119	0	1	1
0	33	1	118	0	0.991597	1
-0.02	33	9	110	0	0.92437	1
-0.04	33	27	92	0	0.773109	1
-0.06	29.5	56.5	62.5	3.5	0.52521	0.893939
-0.08	25	78	41	8	0.344538	0.757576
-0.1	18	95	24	15	0.201681	0.545455
-0.12	12.5	107.5	11.5	20.5	0.096639	0.378788
-0.14	6	115	4	27	0.033613	0.181818
-0.16	1	117	2	32	0.016807	0.030303
-0.18	0	117	2	33	0.016807	0
-0.22	0	119	0	33	0	0

Table 18 Contingency table for the minimum ST gradient method

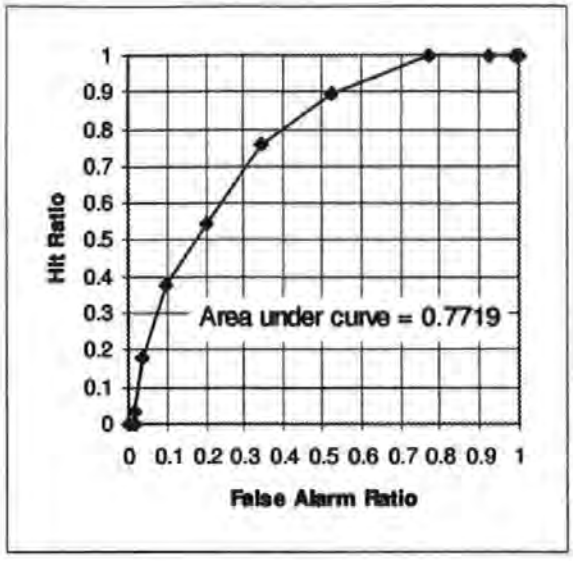

Figure 132 ROC Curve for Bi-Phasic ST detection using the minimum gradient method

Given that it is vital that bi-phasic waveforms are not missed, a threshold value of approximately -0.04 would be required. Clearly this method is unsuitable as the false alarm ratio for this threshold (0.773) is too high. This method has very poor specificity because it is sensitive to small regions of the ST waveform approximation with a significant negative gradient. These regions are caused by noise and artefact which disturbs the curve fit to the extent that an instantaneous gradient is produced which causes a false positive. Too many false positive results in sequence could lead to a miss-interpretation of the ST waveform shape and could result in unnecessary intervention or lack of trust in the system.

6.9.2 The linear-regression technique.

Average waveforms are recorded every 15s, stored, plotted and classified as 1 for bi-phasic and 0 for other. A straight line of 40 samples (80ms) is fitted to the ST waveform curve starting from the J point. For a given threshold, if the gradient of this line falls below a given threshold, then the system grades the waveform as bi-phasic. A table of results is given in Table 19 and the ROC curve is shown in Figure 132. The area under the ROC curve for this method was 0.9615 which is a significant improvement. With a threshold of 0.00033 there is a false alarm ratio of 0.130252 and a hit ratio of 0.984848 which is considered to be acceptable, given that the expert classification is itself ambiguous.

Threshold	TP	TN	FP	FN	FA	HR
-0.25	0	119	0	33		
1.50E-03	33	0	119	0	1	1
0.0005	33	21	98	0	0.823529	1
0	33	74	45	0	0.378151	1
1.00E-04	33	59	60	0	0.504202	1
1.50E-04	33	55	64	0	0.537815	1
-2.00E-04	33	93	26	0	0.218487	1
-0.0003	32.5	103.5	15.5	0.5	0.130252	0.984848
-0.00033	30	106	13	3	0.109244	0.909091
-0.00035	28	107	12	5	0.10084	0.848485
-0.0004	26	111	8	7	0.067227	0.787879
-0.00045	22	113	6	11	0.05042	0.666667
-0.0006	15	117	2	18	0.016807	0.454545
-0.0008	11	119	0	22	0	0.333333
-0.001	8	119	0	25	0	0.242424
-0.0014	3	119	0	30	0	0.090909
-2.50E-03	0	119	0	33	0	0

Table 19 Contingency table for the linear regression method

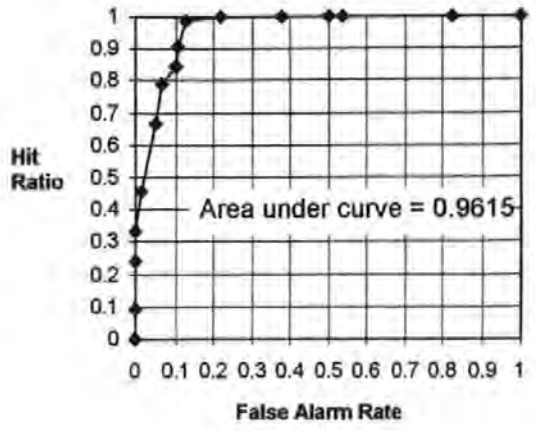

Figure 133 ROC Curve for Bi-Phasic ST detection using the linear regression method

6.9.3 The fuzzy logic technique.

The fuzzy system provides more complex information on the type of bi-phasic waveform. It classifies the data into types normal, bi-phasic type 1,2 and 3. Type 1 is thought of as suspicious rather than normal or abnormal. For the fuzzy system, the contingency tables and ROC curves for each class are given below. All the waveforms on 15s intervals were classified and compared with the expert.

Th	TP	TN	FP	FN	FA	HR
0	64	0	89	0	1	1
0.05	62	65	24	2	0.269663	0.96875
0.1	62	66	23	2	0.258427	0.96875
0.2	60	67	22	4	0.247191	0.9375
0.3	58	70	19	6	0.213483	0.90625
0.4	57	71	18	7	0.202247	0.890625
0.5	55	74	15	9	0.168539	0.859375
0.6	54	76	13	10	0.146067	0.84375
0.7	50	78	11	14	0.123596	0.78125
0.8	41	81	8	23	0.089888	0.640625
0.9	31	84	5	33	0.05618	0.484375
1	0	89	0	64	0	0

Table 20 Contingency table for a Normal ST segment

Th	TP	TN	FP	FN	FA	HR
0	22	0	131	0	1	1
0.05	21	117	14	1	0.10687	0.954545
0.1	21	123	8	1	0.061069	0.954545
0.2	21	128	3	1	0.022901	0.954545
0.3	20	129	2	2	0.015267	0.909091
0.4	20	130	1	2	0.007634	0.909091
0.5	16	130	1	6	0.007634	0.727273
0.6	13	130	1	9	0.007634	0.590909
0.7	10	131	0	12	0	0.454545
0.8	8	131	0	14	0	0.363636
0.9	7	131	0	15	0	0.318182
1	0	131	0	22	0	0

Table 22 Contingency table for a bi-phasic 2 ST segment

Th	TP	TN	FP	FN	FA	HR
0	42	0	111	0	1	1
0.05	40	84	27	2	0.243243	0.952381
0.1	40	88	23	2	0.207207	0.952381
0.2	39	90	21	3	0.189189	0.928571
0.3	38	93	18	4	0.162162	0.904762
0.4	36	96	15	6	0.135135	0.857143
0.5	34	99	12	8	0.108108	0.809524
0.6	33	101	10	9	0.09009	0.785714
0.7	29	102	9	13	0.081081	0.690476
0.8	21	105	6	21	0.054054	0.5
0.9	15	106	5	27	0.045045	0.357143
1	0	111	0	42	0	0

Table 21 Contingency table for a bi-phasic 1 ST segment

Th	TP	TN	FP	FN	FA	HR
0	28	0	126	0	1	1
0.05	28	110	16	0	0.126984	1
0.1	28	114	12	0	0.095238	1
0.2	27	116	10	1	0.079365	0.964286
0.3	26	116	10	2	0.079365	0.928571
0.4	26	120	6	2	0.047619	0.928571
0.5	26	121	5	2	0.039683	0.928571
0.6	22	122	4	6	0.031746	0.785714
0.7	20	124	2	8	0.015873	0.714286
0.8	17	125	1	11	0.007937	0.607143
0.9	13	125	1	15	0.007937	0.464286
1	0	126	0	28	0	0

Table 23 Contingency table for a bi-phasic 3 ST segment

Table 20 applies to the rule "STsegment is Normal", Table 21 applies to the rule "STsegment is bi-phasic 1" (positive ST with negative slope), Table 22 applies to the rule "STsegment is bi-phiasic 2" (Negative slope which crosses the iso-electric level) and Table 23 applies to the rule "STsegment is depressed 3" (Negative ST segment). The hit ratio (HR) and false-alarm ratio (FA) is computed for each threshold value and plotted on the ROC curves shown below.

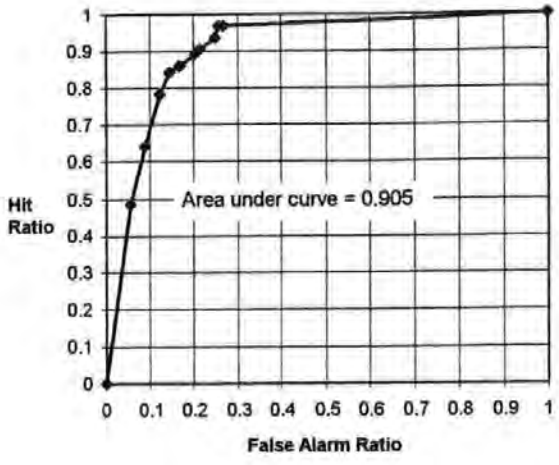

Figure 133 ROC curve for normal

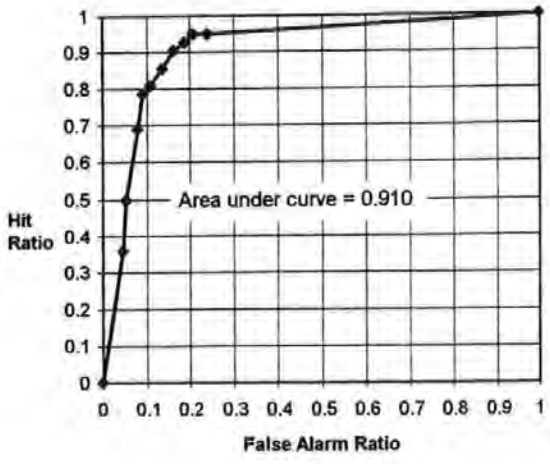

Figure 134 ROC curve for bi-phasic 1

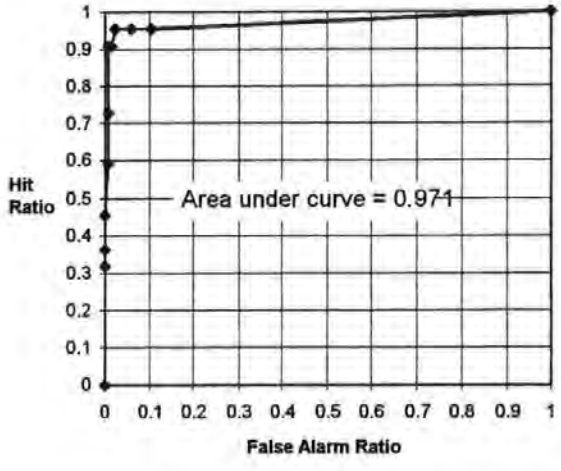

Figure 135 ROC curve for bi-phasic 2

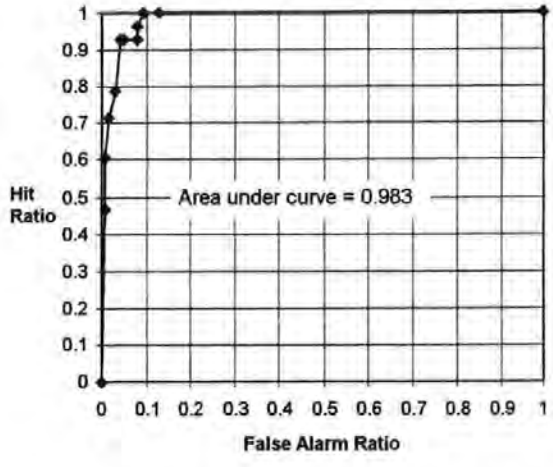

Figure 136 ROC curve for bi-phasic 3

The area under the curve is useful as a comparative performance metric (*Sweats 1988*). The best performance is with the rule to detect bi-phasic 3 (negative) ST waveforms, followed closely by the bi-phasic-2 rule. This is an important achievement as these must not be missed. Differentiating between normal and bi-phasic-1 waveforms is ambiguous and it is no surprise that these are more difficult to separate. The visual classification of bi-phasic-1 waveforms by the expert is sometimes quite uncertain to which some of the errors can be attributed. This is not a critical decision unless the condition is very marked.

The ROC curves are useful, but more important are the contingency tables from which the decision thresholds are determined. A threshold value is required for each

rule. For bi-phasic-2 and 3, this will trigger an alarm and draw the clinicians attention to the patient. Choosing the optimal threshold point depends on the individual problem. Detecting a bi-phasic-3 is of paramount importance, so *there should be an emphasis on the hit-ratio being high*, even at the expense of the false-alarm ratio. Clinicians are accustomed to some false alarms, although too many would disincline them from using the system. A similar criteria applies to bi-phasic-2, although the emphasis on the hit ratio should be less then bi-phasic-3.

6.10 Summary of results

A summary of the results is given in Table 24. The results are stored as *Area Under Curve*; *Sensitivity* (Hit Ratio) / *Specificity* (False Alarm Rate).

Technique / *Bi-phasic Type*	Minimum Gradient	Linear Regression	Fuzzy Logic
Bi-phasic-1	0.7719; 1.0 / 0.77	0.9615; 0.985/ 0.13	0.91; 0.928/0.189
Bi-phasic-2			0.971; 0.954/0.06
Bi-phasic-3			0.983; 1.0/0.095

Table 24 Summary of performance metrics for each bi-phasic waveform classificiation technique.

As a comparative measure for the fuzzy system, the classification of a waveform as abnormal bi-phasic would be bi-phasic-2 OR bi-phasic-3, which is the max(bi-phasic-2, bi-phasic-2). This would result in a sensitivity of 1.0 and a specificity of 0.095. The fuzzy technique is the most successful.

6.11 Pattern recognition of ST waveform shape changes over time.

The instantaneous ST waveform shape alone does not have much meaning. The current clinical guidelines make quite specific references to rates of change in the T/QRS ratio (see Table 26), i.e.

1. T/QRS less than -0.05 for more than 20 minutes.
2. Rising - T/QRS rises more than 0.15 from the baseline level over 15 minutes
3. Rising - T/QRS rises more than 0.4 over 15 minutes
4. Any negative or bi-phasic ST change as well as any T/QRS increase over 5-10 minutes

New fuzzy sets are defined to describe each of these events. The first three categories refer to the dynamics of the T/QRS ratio. The T/QRS ratio dynamics can be considered to be *stable* (category 1), *rising* (category 2) or *rapidly rising* (category 3). Others might be fall into the categories of *falling, rapidly falling,* or just *not stable*. The changes are considered over 20, 15,10 and 5 minute intervals, so time has to be considered. To manage this situation, the trends in features and fuzzy output variables *(*such as *Abnormal ST waveform)* have to be measured and linguistically approximated. Linear regression is used over 5, 10, 15 and 20 minute segments of the T/QRS ratio, and is updated every 15s with all the other features. The gradients of the regressions lines are represented by four new fuzzy variables *ΔTQRS(5), ΔTQRS(10), ΔTQRS(15)* and *ΔTQRS(20)*. Not all changes in the ST waveform can be classified this way however. More complex patterns in time such as "briefly appearing" negative waveforms, "persistently" abnormal waveforms and "re-occurring" abnormal patterns cannot be detected by simple trends in the features. In practice the interpretation of trends and shape changes often depends on previous events in the labour. Some concept of memory is required in the fuzzy system for it to model the human expert and this is now discussed.

6.12 Adding memory

It is important to be able to represent and recognise particular sequences of events in labour, and not just instantaneous events such as an individual abnormal waveform. For example, in the guidelines given in appendix D, with a normal CTG it defines a rising T/QRS if it *rises more than 0.4 from the baseline level over 15 minutes*. In practice, uncertainty may arise because the guidelines cannot span every situation. It is the intermediate cases which a more likely to cause the most uncertainty for the clinician. For example, *a rise in T/QRS of 0.2 over 15 minutes*

is a suspicious change but might not be enough to warrant action. An experienced expert would probably make a note of this event as suspicious, and will act depending on the context of the event. Time and the context in which an event took place is very important when there is a high degree of uncertainty.

There are many factors which could influence the decision of a clinician with the appearance of suspicious and uncertain changes. If the baby is near to the point of delivery, then labour may be allowed to progress naturally. If this was the first abnormal event, and it was short-lasting (<5 mins), then this might be viewed as an anomaly and is not enough evidence to warrant intervention. If other suspicious events had been observed earlier in the labour however, then there would come a point where the evidence has accumulated enough to suggest real abnormality has occurred. The purpose of this work is to expand the fuzzy logic concepts to allow the expert model to 'remember' previous events and manage the accumulation of evidence for foetal distress.

A documented, albeit rare example of this, is the brief appearance of negative or bi-phasic ST waveforms. Each appearance can be considered to be a period where the foetus is unable to compensate for stress in labour, such as a uterine contraction. Repeated exposure to this will lead to damage and possibly death. With a normal CTG, the clinician may not act on the first appearance, but may act on subsequent appearances. The expert model must include the concept of memory and have the ability to include prior events in the reasoning mechanism. Examples of the situations where the expert-model can use memory to reduce uncertainty are summarised as follows.

1. An individual abnormal event is only short lasting, so its validity is in question.
2. An event is only partially true - i.e. suspicious but not marked enough to warrant action
3. An event has occurred before, therefore adding to the belief that it is genuine and not noise.
4. A different but possibly abnormal event had previously occurred.
5. A similar pattern occurred in a previous labour.

The human expert can manage these situations though intelligent reasoning and inference, drawing on experience and knowledge of previous events in the labour, but this is very difficult for a computer. A technique is discussed here to manage these situations using a novel extension to fuzzy logic.

6.13 Using State Machines to add memory to intelligent systems

It is necessary to 'remember' when events have occurred at any time in the past. A technique is needed to recognise sequences in time. In the strictly Boolean domain, this is known as sequential logic design. Digital logic uses a finite state machine, which is made up of some combinational logic, state variables, and feedback logic, as depicted in Figure 137.

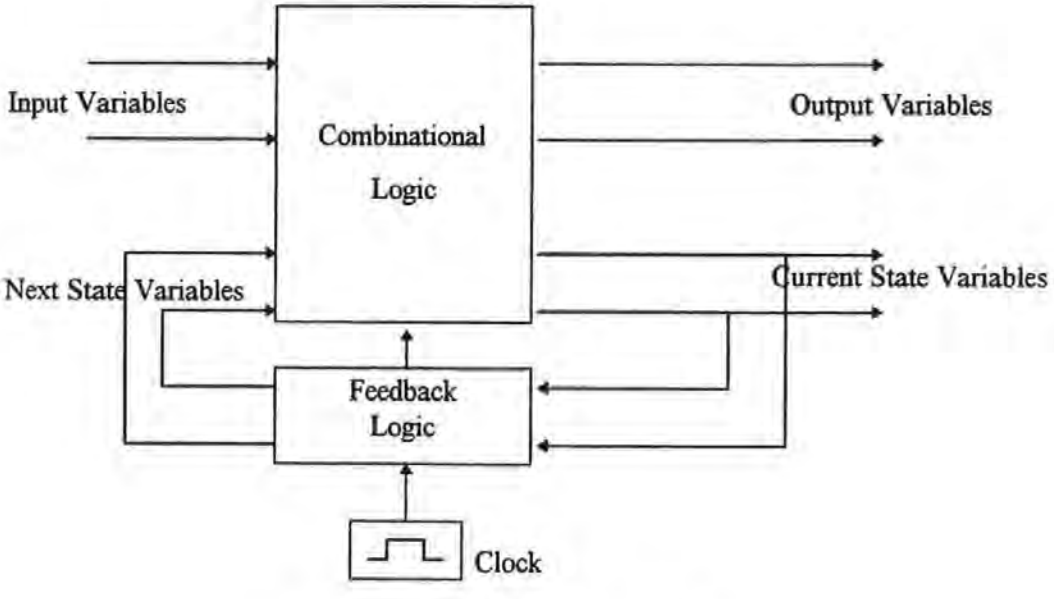

Figure 137 Finite State Machine

The output is dependent on the input variables and the current state variables. The input variables in this context are fuzzified ECG features or fuzzy consequent facts and the current state is an internal fuzzy fact which has some meaning. A state diagram is given below in Figure 138. When the system changes state, *the output is determined either by the state transition and/or the state itself.* For example, the output for a transition from state A to C is independent and possibly different to that of a transition from B to C. Assume the systems starts with state A having been true for at least 20 minutes, which corresponds to a normal T/QRS ratio. The following rules might apply to detect a significant rise and fall in the T/QRS ratio.

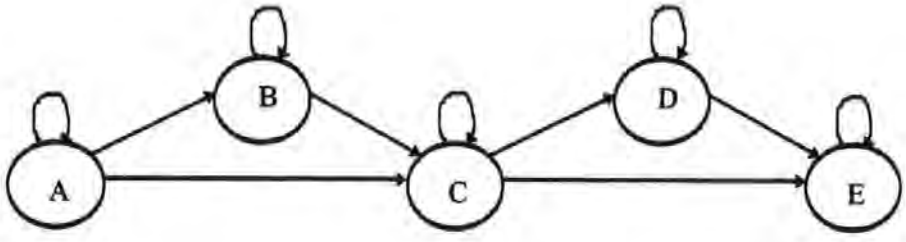

Figure 138 Conceptual state machine

If state A is true and the T/QRS remains at a normal level for 5 minutes, then the state does not change.

IF (State = A) AND TQRS is Normal for 5 minutes THEN State = A

If state A is true, and the T/QRS rises to an intermediate level (approx 0.25) and stays there for at least 5 minutes then this is reflected in a change of state to state B by the following rule.

IF (State = A) AND TQRS is Increased for 5 minutes THEN State = B

If State A is true and the T/QRS rises to an elevated level (>0.4 approx) and stays there for more than 5 minutes then this is reflected in a change of state to state C by the following rule.

IF (State = A) AND (TQRS is Elevated for 5 minutes) THEN State = C

For these two cases, different outputs (consequent facts) can be inferred. Equally important is that the state transition is not reversible. Once state C has been reached, this is a significant event and can never return to state A. This is because the state of the foetus has permanently been affected. From state C, further rules can be chained. If the state remains high for more than 20 minutes then the foetus is thought to be compensating for stress. An example rule might be.

IF (State = C for 20 minutes) THEN Foetal Condition = Compensating

Alternatively, if the T/QRS drops then the state changes again, for example.

IF (State = C) and (TQRS is Normal for 5 minutes) THEN State = E
IF (State = C) and (TQRS is Increased for 5 minutes) THEN State = D
IF (State = D) and (TQRS is Normal for 5 minutes) THEN State = E

The important issue here is that the state is a record of the history of the labour. To get to state E for example, it implies that the T/QRS must have risen for a significant period of time and fallen again for a significant period of time. This model can be extended to manage complex events and modify the output of the fuzzy expert model according to state and state-transition. This model appealed to the expert clinician it provides the freedom to describe significant events in labour in terms of sequences of events or case studies. These case studies can then be modelled. A difficulty with this model is the inference mechanism for state changes. All the rules listed above included time. In the presence of noisy and uncertain data, it is possible to design a filter structure to reduce uncertainty, insisting the event occurred for a significant period of time. The approach here is based on the premise that *the belief that an event is true depends on a function of the time it was observed.* The additive fuzzy inference (*Cox 1994*), as discussed in chapter 5, uses the expression $\mu'(x_i) \leftarrow \min(1, \mu'(x_i) + \mu(x_i))$ to accumulate truth over time where $\mu'(x_i)$ is the solution consequent set. This technique suffers from problems with noise or offset as it is essentially an integrator. The slightest mean offset in the data will cause the consequent truth to grow and eventually saturate.

6.14 Fuzzy State Model for managing complex patterns in time.

A technique is described here for modelling the experts management of complex sequences of events in time, such as those discussed above. This technique is based on the concepts of finite state machines *(Biswas 1993)*, but in this case the states are fuzzy and not discrete. An example of a fuzzy state representation of events in labour is depicted in Figure 139. The states are fuzzy variables that represent the truth that a key event has occurred. The inference mechanism for the fuzzy variables differs from conventional fuzzy systems in that the implied truth value is also dependent on time as well as rules and other fuzzy variables/facts. Consider the example given in Figure 139. Three states are defined.

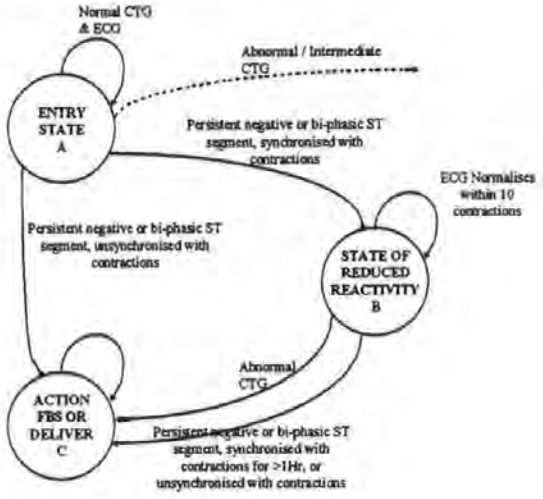

Figure 139 Fuzzy-state machine used to represent and recall events during labour

A. *Entry state*

B. *State of Reduced Reactivity.*

C. *Action State.*

At the entry of monitoring (state A) it is assumed that no prior information is known about the foetal ECG and therefore the *foetal state A is TRUE.* If during labour there are negative or bi-phasic ST waveforms, coupled with an abnormal CTG, then using the following fuzzy rules, the *foetal state C is TRUE.*

IF (STATE=A) and (T/QRS=Negative OR STsegment is Biphasic OR STsegment is Negative) THEN STWAVEFORM=Abnormal
IF (STATE=A) and (STWAVEFORM=Abnormal) and (CTG=Abnormal) THEN STATE=C

These acute changes would normally be routinely detected from the acute CTG changes. A problem arises when the changes are not so acute and the ECG and CTG do not provide such definitive changes. If the negative/bi-phasic ST waveforms only appear briefly (<1min), and are repetitive and synchronised with contractions, then the situation is more uncertain. It would be accurate to say that *state B* is possibly true. It is valid to say that if negative/bi-phasic ST waveforms re-appear within the same 15 minute period, then the belief that *state B* is true should increase. It is also valid to say that if no more negative/ bi-phasic ST waveforms are observed within the next hour then the belief that *state B* is TRUE should reduce or maintain its current level. To manage these uncertain situations, an accumulative model is used to infer each state.

6.15 State transition using an accumulated truth model

As with normal fuzzy variables, all the fuzzy states are true, but to different degrees, and can take on any value between 0 and 1. Any given state is dependent on the other fuzzy states and other fuzzy variables. All the fuzzy states are updated on each time epoch, which, for this work, is a 15s interval. A state is limited by how much it can increase or decrease in each time epoch. In general, the next state is determined by the following expression.

$$NextState(t) = \max\left\{\min\left\{PreviousState(t-1) + GrowthRate \cdot \mu_i(t) - DecayRate \cdot \mu_j(t) - leakage, 1\right\}, 0\right\} \tag{6.1}$$

where $\mu_i(t)$ $(0 \leq \mu_i(t) \leq 1)$ is a fuzzy variable that implies that *NextState* is true, $\mu_j(t)$, $(0 \leq \mu_j(t) \leq 1)$, is a fuzzy variable that infers that *NextState* is *not* true and *leakage* is a constant that reduces the state truth as time progresses. Each state transition has an associated *growth rate*, *decay rate* and *leakage*. This way there is flexibility for the *NextState* truth membership to grow and diminish at different rates. This is the accumulated truth model, which is essentially a leaky integrator of fuzzy truth membership.

6.15.1 Fuzzy filter structures

Consider Figure 140 which shows the truth output of a fuzzy rule for *"ST waveform is abnormal"* from part of a recently recorded case. From the clinical guidelines *(Luzietti & Rosén 1994)*, assuming a normal CTG, there must be a consistently abnormal ST waveform for at least 20 minutes for any change to be consider clinically significant. It is also true that the brief appearance of abnormal ST waveforms is significant if they reoccur. From Figure 140 it is observed that there are some briefly abnormal waveforms and some periods of persistently abnormal waveforms.

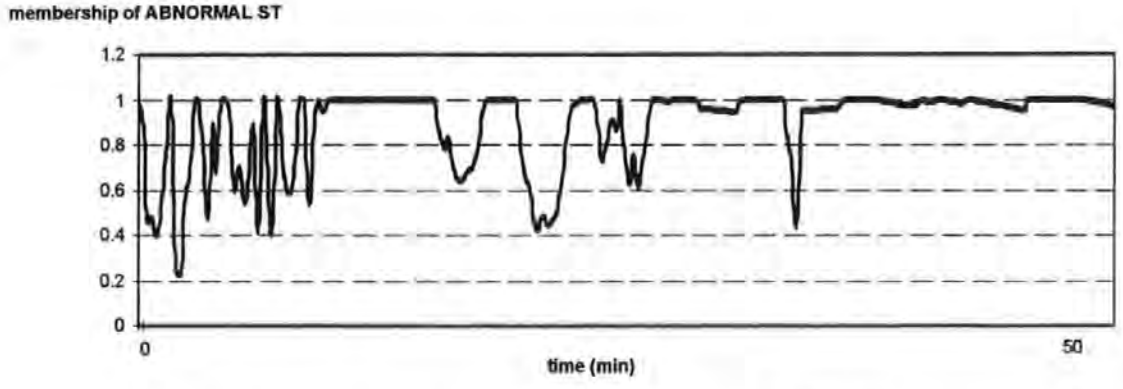

Figure 140 The output truth for "Abnormal ST waveform"

All these events contribute to the evidence that there is some abnormality with this labour, but it is the continuously abnormal waveforms that are of most concern and should contribute the most to the evidence. It is assumed here that the CTG is normal and *STATE A* has been true for 20 minutes. The following rule could be used.

IF (STATE A is consistently true) AND (ST waveform is consistently Abnormal) THEN STATE B

Written formally, using the accumulated truth model, the next state B is calculated as follows.

$$\mu_{STATEB}(\tau+1) = \mu_{STATEB}(\tau) + \gamma \cdot \left(\mu'_{abnormalST}(\tau) \wedge \mu'_{STATEA}(\tau)\right)$$
$$\text{where } \mu'_{abnormalST}(\tau) = \mu_{abnormalST}(\tau) \wedge \mu_{abnormalST}(\tau-1) \wedge \mu_{abnormalST}(\tau-2) \wedge \ldots \wedge \mu_{abnormalST}(\tau-79)$$
$$\text{and } \mu'_{STATEA}(\tau) = \mu_{STATEA}(\tau) \wedge \mu_{STATEA}(\tau-1) \wedge \mu_{STATEA}(\tau-2) \wedge \ldots \wedge \mu_{STATEA}(\tau-79) \quad (6.2)$$

where τ represents a 15s epoch of time, γ is the *growth rate* and $\wedge$ is the fuzzy *intersection* (*AND*) operator. $\mu_{abnormalST}(\tau)$ and $\mu_{STATEA}(\tau)$ are the truth membership values for "the ST waveform is negative" and "*STATE A* is true" respectively. $\mu'_{abnormalST}(\tau)$and $\mu'_{STATEA}(\tau)$ are the truth membership values for "the ST waveform has been consistently abnormal" and "*STATE A* has been consistently true" (respectively) for the 20 minutes previous to time τ.15s. This is represented in the structure shown in Figure 141, where *D* denotes a delay of one epoch (15s).

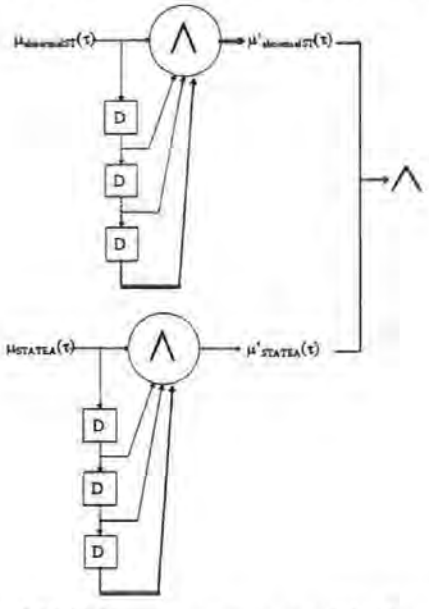

Figure 141 Schematic structure of the fuzzy filter

6.15.2 Fuzzy intersection operator

The fuzzy *intersection* operator $\wedge$ is chosen carefully when computing the accumulated truth. The fuzzy intersection operator used here is defined in equation (6.3) where the variable q is used to modify the characteristics of the fuzzy operator. For $q=1$, this equates to the truncated mean which is a very soft operator. As q increases, the fuzzy rule tends to become increasingly strict, promoting the continuous events and diminishing the intermittent events. This is illustrated in Figure 142.

$$a_0 \wedge a_1 = \max\left(1 - \min\left(\frac{(1-a_0)^{\frac{1}{q}} + (1-a_1)^{\frac{1}{q}}}{2}, 1\right), 0\right) \tag{6.3}$$

$$a_0 \wedge a_1 \wedge \ldots \wedge a_{N-1} = \max\left(1 - \min\left(\frac{1}{N}\sum_{k=0}^{N-1}(1-a_k)^{\frac{1}{q}}, 1\right), 0\right)$$

$$\text{and hence, } \mu'_{abnormalST}(\tau) = \max\left(1 - \min\left(\frac{1}{N}\sum_{k=0}^{N-1}\left(1 - \mu_{abnormalST}(\tau - k)\right)^{\frac{1}{q}}, 1\right), 0\right) \tag{6.4}$$

The growth rate in equation

(6.2) is estimated as follows. Given that the previous state *STATE A* is completely true, and assuming an abnormal waveform to be continuously present for 20 minutes (20x4 epochs), then the growth rate γ for equation

(6.2) is estimated as $\gamma = 1/_{20\times4} = 0.0125$. The leakage rate is small, set at 0.00125, and as there is no rule to reduce the truth of *state B*, the decay rate is zero. Returning to the case in Figure 139, the membership for *state B* is computed as follows.

$$\mu_{stateB}(\tau) = \max\left(\min\left(\mu_{stateB}(\tau - 1) + 0.0125 \cdot \mu'_{abnormalST}(\tau), 1\right) - 0.00125, 0\right) \tag{6.5}$$

The membership truth $\mu'_{abnormalST}(\tau)$ ("ST waveform is consistently abnormal") from equation

(6.4) is shown in Figure 140 for different values of *q*. The accumulated truth is computed using equation (6.5) for different values of *q* and is shown in Figure 143. When *q*=1 or 2, the state accumulates too rapidly as a result of the intermittently abnormal waveforms. When *q*=10 or 100, there is a steady build up of evidence during the intermittent period and a more rapid increase when the waveforms are continuously abnormal. For the remainder of this paper, it is assumed *q*=10.

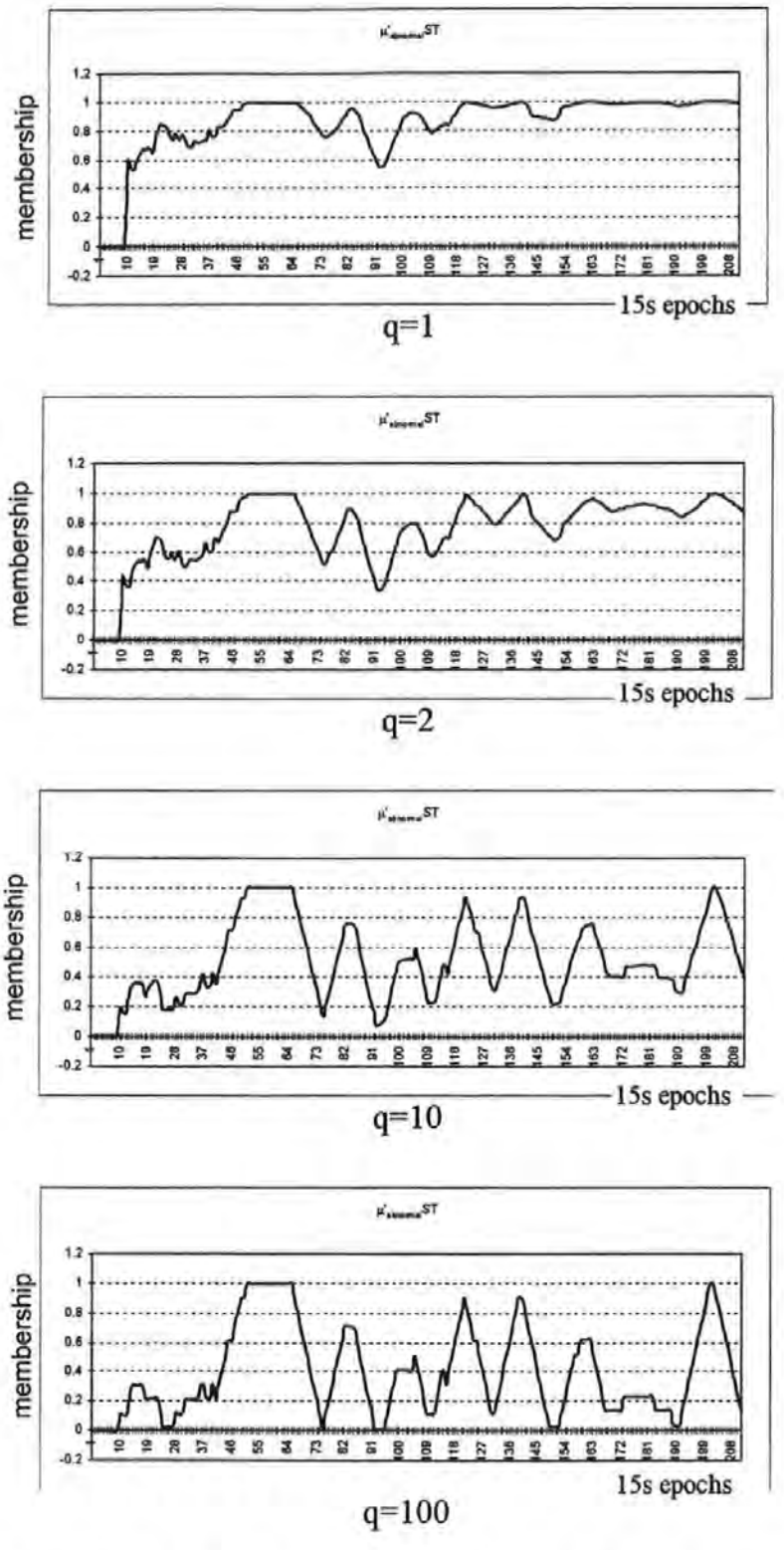

Figure 142 Output truth of the rule "ST waveform is abnormal for 20 minutes or more"

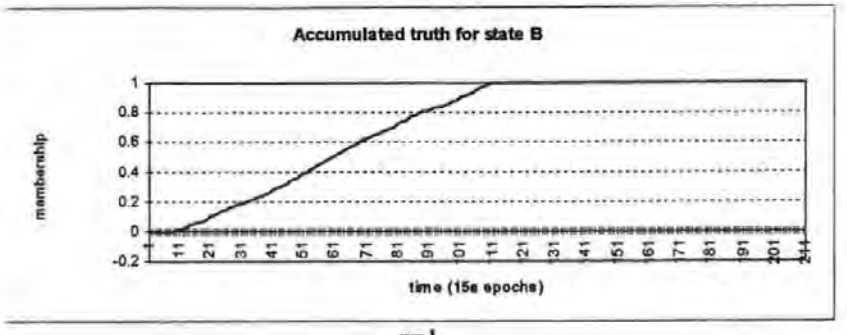

q=1

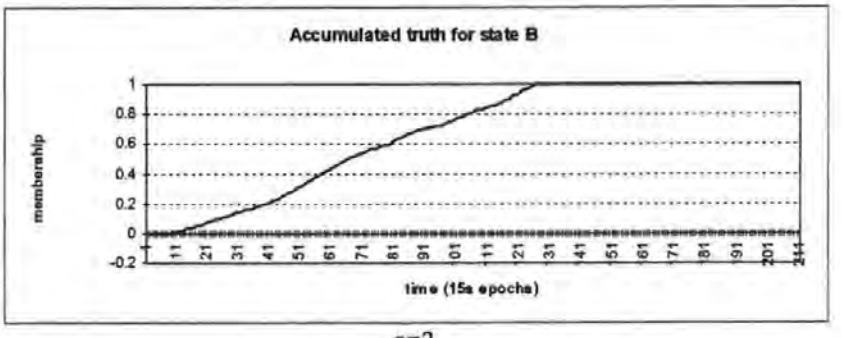

q=2

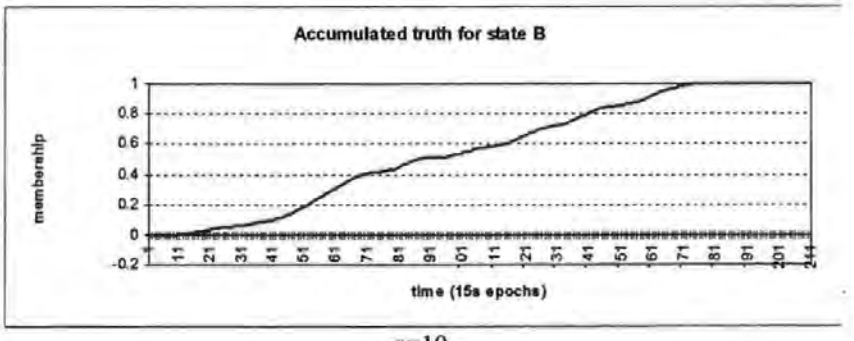

q=10

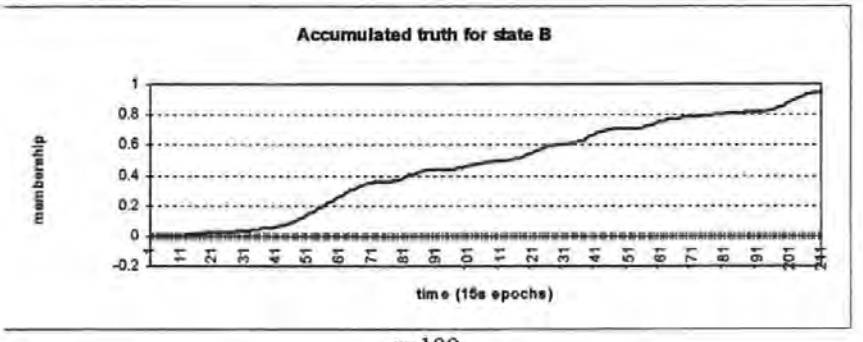

q=100

Figure 143 Accumulated truth for "State B"

6.16 Chaining state transitions

From the example described above, *state B* becomes increasingly true as more evidence accumulates. From Figure 139, for a state transition to occur from *state B* to *state C*, both *state B* must be true and abnormal waveforms must continue (or

reoccur) for more than 10 contractions. For illustrative purposes, 10 contractions equates to 30 minutes, which is 120 epochs. The new state C will be determined using the following rule.

IF (*STATE B* has been true for 30 minutes) AND (*ST Waveform* is Abnormal) THEN *STATE C*

To model this rule, a new fact "*STATE B has been true for 30 minutes*" , with membership $\mu'_{STATEB}(\tau)$, is derived as

$$\mu'_{stateB}(\tau) = \max\left(1 - \min\left(\frac{1}{120}\sum_{k=0}^{119}\left(1-\mu_{stateB}(\tau-k)\right)^{\frac{1}{q}},1\right),0\right) \qquad (6.6)$$

The membership truth for *state C* is accumulated as follows.

$$\mu_{stateC}(\tau) = \max\left(\min\left(\mu_{stateC}(\tau-1) + \frac{1}{120}\cdot\left(\mu'_{stateB}(\tau) \wedge \mu'_{abnormalST}(\tau)\right),1\right) - 0.005,0\right) \qquad (6.7)$$

A plot of the *state C* membership is given in Figure 144. *State C* is observed to grow in truth once *state B* is fully saturated and because the foetal ECG ST waveform remains consistently abnormal. This is a simple illustrative example that has been simplified to demonstrate the concepts of this technique. More complex intermediate state transitions could be added to provide more information to the clinician, such as the repetition of short 5-minute bursts of negatively sloped positive ST waveforms. These are not individually abnormal, but with repeated appearance, then evidence of some abnormality accumulates.

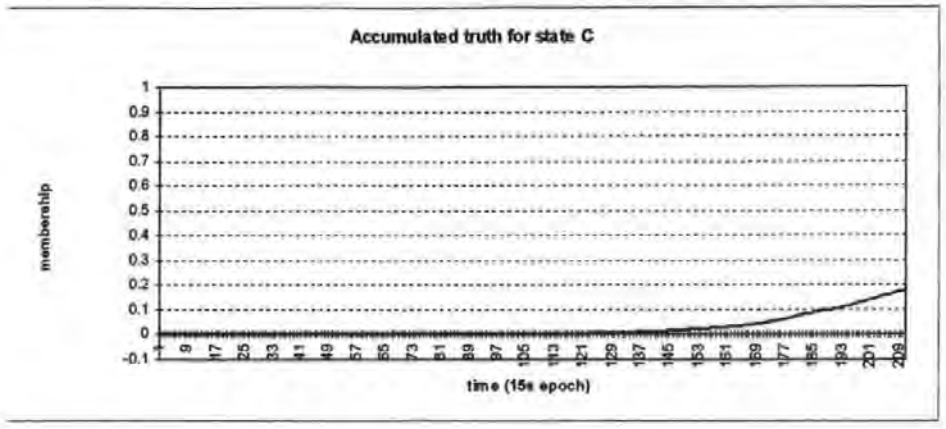

Figure 144 Accumulated truth for state C

6.17 Prototype state model for ST waveform analysis

The first prototype state model for ST waveform analysis is shown in Figure 145. This model does not include CTG parameters and so is not a complete solution. Each state transition has a given growth and leakage rate implied by adjectives such as *briefly* and *persistently*. The actual values are not shown in the diagram for clarity and are subject to change as the system is further developed.

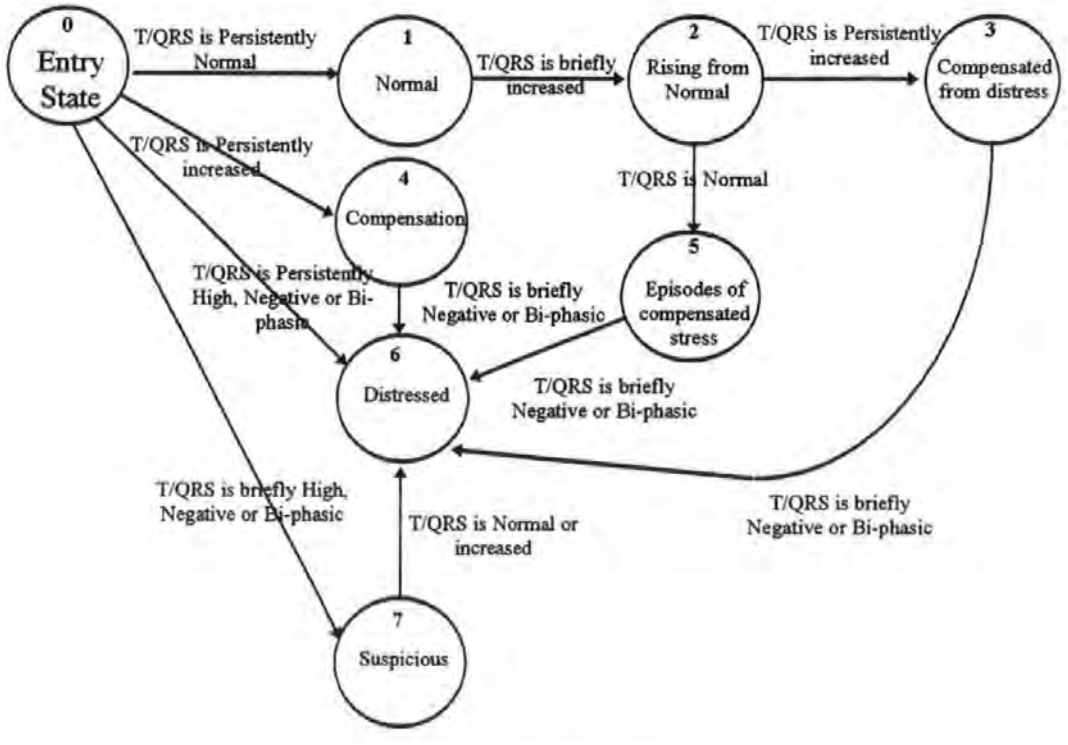

Figure 145 State model for ST waveform analysis

6.18 Foetal Condition Matrix (FCM)

The result of the ECG and CTG analysis and the recommended action are summarised as a foetal condition matrix (see table 2) in line with the clinical guidelines (Rosén 1986). Each element of the matrix (see Table 25) reflects the condition $\{A,B \ldots I\}$of the foetus. Using a set of fuzzy rules, the output of the fuzzy expert system produces a truth value for each of these conditions.

ST Waveform \ CTG	Normal	High and Stable	Negative or Rising
Normal	A **No Action**	B **No Action**	C **FBS[1] or Deliver**
Intermediate	D **No Action**	E **FBS or Deliver[4]**	F **Deliver[2]**
Abnormal	G **FBS or Deliver[4]**	H **Deliver**	I **Deliver[3]**

Table 25 Foetal condition matrix used to guide the clinician.

A fuzzy truth value is computed for each category (A-I) using fuzzy rules, which can be de-fuzzified to a single point on a fuzzy condition map (see Table 25) *(Ifeachor & Outram 1995)*. The following summary of the clinical guidelines accompany this matrix.

STAN® clinical guidelines for action with a mature fetus. (≥36 weeks)
1. Negative/Bi-phasic ST - T/QRS less than -0.05 for more than 20 minutes. Rising - T/QRS rises more than 0.4 over 15 minutes, expediate delivery without FBS 2. Negative/Bi-phasic ST - T/QRS less than -0.05 for more than 20 minutes. Rising - T/QRS rises more than 0.15 from the baseline level over 15 minutes, expediate delivery without FBS. 3. Any negative or bi-phasic ST change as well as any T/QRS increase over 5-10 minutes. 4. FBS should be repeated every hour or earlier. If an FBS is not available, intervention can be delayed until the CTG shows evidence of deterioration. - Loss of short term variability - Progressive tachycardia or bradycardia - Decelerations become wider and deeper - Overshoot accelerations following decelerations If the CTG remains unchanged but the ST waveform shows an acute change, as identified in p.3, delivery should also be expediated. Note: In second stage we recommend these foetuses be delivered within 90 minutes as rapid deterioration can occur after this time. Note: A "pre-terminal" CTG should always cause immediate delivery. No need for additional ST analysis.

Table 26 Summary of the clinical guidelines given to clinicians

Having obtained the truth values for all possible foetal conditions $\{A,B,..,I\}$, the problem of interpreting the results still remains. The truth values for the foetal condition matrix are easy to interpret in cases where one truth value is clearly higher than the others. In such cases the foetal condition can be inferred from the maximum truth value, but this can be unsatisfactory in borderline cases because of jitter. For example, table 3 shows A and D to have very similar truth values. A series of small changes in the features could cause the output to jitter

A=0.50	B=0.30	C=0.10
D=0.49	E=0.30	F=0.10
G=0.10	H=0.05	I=0.00

Table 27 Fuzzy truth values

To avoid this, consider the foetal condition matrix as a 3D solid object. From Table 27, the centre of mass of the solid (centroid) is computed to 'de-fuzzify' the mass and obtain a single point on the foetal condition matrix. In general, for a two dimensional function f(x,y), x={a..b}, y={c..d}, the centre if mass (cx,cy) is computed as

$$cx = \frac{\int_a^b \int_c^d f(x,y) \cdot x \, dxdy}{\int_a^b \int_c^d f(x,y) \cdot dxdy}$$
$$cy = \frac{\int_a^b \int_c^d f(x,y) \cdot y \, dxdy}{\int_a^b \int_c^d f(x,y) \cdot dxdy} \qquad (6.8)$$

and the discrete approximation of this is given by

$$cx = \frac{\sum_{x=a}^{b} \sum_{y=c}^{d} f(x,y) \cdot x}{\sum_{x=a}^{b} \sum_{y=c}^{d} f(x,y)}$$
$$cy = \frac{\sum_{x=a}^{b} \sum_{y=c}^{d} f(x,y) \cdot y}{\sum_{x=a}^{b} \sum_{y=c}^{d} f(x,y)} \qquad (6.9)$$

These techniques avoid the problem of a jittering output on the foetal condition matrix, as there are no discontinuities in the knowledge. For the clinician, it is often the change of position (foetal state) that is of more importance than the absolute position itself. For example, a labour where the foetal state is B throughout the duration of labour has a different interpretation to a progression from A to B. The path or locus of the foetal condition is plotted at 5 minute intervals to display any changes, this gives a simple objective visual display of the history of foetal condition over time.

6.19 Examples

Some example results are given below in Figure 146(a) and (b). Figure 146(a) is a typically normal case where the T/QRS ratio is constantly below 0.24 and the CTG is perfectly normal. Figure 146(b) was a perfectly normal case until the baseline heart-rate dropped and stayed at 60bpm (abnormal CTG).

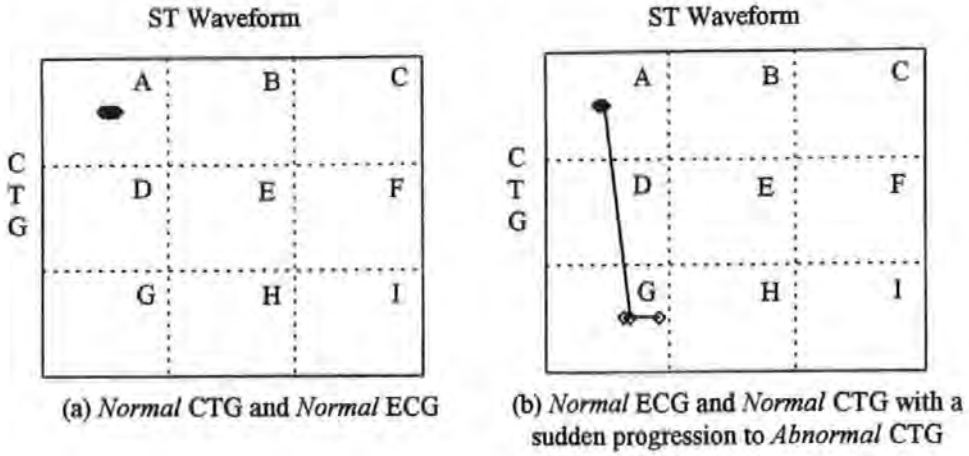

Figure 146 Examples of the foetal condition matrix

The condition of the foetus is shown as a 'moving point' on the foetal condition matrix. The nearer to the bottom right (I) , then the worse the condition of the foetus. The output could have been de-fuzzified onto a single variable of foetal condition but this way the reasoning behind the foetal condition output is lost. The foetal condition can be monitored visually without losing the reasoning behind it.

6.19.1 Current limitations

For testing purposes, the CTG classification is currently provided by the human expert as the automatic interpretation of the CTG is outside the scope of this project. The next phase of this work will combine the rules for CTG interpretation together with the rules for interpreting ST waveform. Currently the system is limited in practice to providing a linguistic description of the ST waveform shape based on current and previous ST waveform shapes. The FCM can only be used once the rules for interpreting the CTG have been converted to a fuzzy system.

6.20 Linguistic approximation

A linguistic description of the fuzzy state and the current ST waveform shape is currently provided. This acts as a guide for clinicians and as an alarm. The current system is limited to simply describing the ST waveform shape and warning the clinician if an abnormal waveform appears.

The output set *STsegment* is spanned by five fuzzy subsets {*Elevated, Normal, Biphasic1, Biphasic2, Biphasic 3*}.

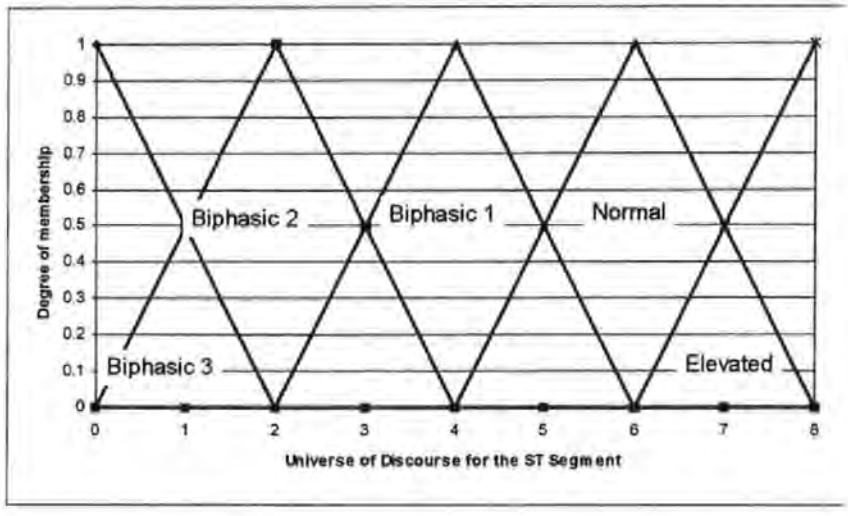

Figure 147 Fuzzy sets describing the ST segment

Given the consequent set *STsegment'*, the similarity measures S(*bipphasic3,STsegment*), S(*bipphasic2,STsegment*), S(*bipphasic1,STsegment*), S(*Normal,STsegment*), S(*Elevated,STsegment*) are calculated. The largest similarity is reported to the clinician alongside the FCM as a simple explanation facility. The similarity measure is discussed in chapter 5, section 2.26.2.

The next stage in the development of this system is to provide a linguistic output describing the changes in the ST waveform *and* the CTG throughout labour. A more comprehensive explanation facility will be developed as a explanation facility for the FCM.

6.21 Discussion and Conclusion

A key achievement of this work is classifying the ST waveform shape using new features and fuzzy rules. It has to be accepted however that any system will produce incorrect classifications, particularly in the presence of noise, but by reporting the

ST waveform shape to the clinician, the clinician can add his or her opinion. The key issue is that no abnormal waveforms are missed. False alarms do not directly create a threat to the patient, and clinicians are used-to a certain level of false alarms in medical devices. Only a very few false negative events can be tolerated however as abnormal patterns are rare and can appear only for a short duration. If there is to be any bias in the system, then it should in favour of sensitivity over specificity to ensure no abnormal waveforms are missed. The use of ROC analysis enables the balance between the hit ratio and the false alarm ratio to be obtained. It also provides a comparative measure for different techniques.

During labour different sequences of events occur which the expert can recognise. Recognising the sequence of events can modify the way the expert interprets the instantaneous data. To enable an expert system to recognise such sequences of events in the same way as human expert, a rule structure based on the principles of finite state machines has been proposed *(Outram et al. 1996).*

The fuzzy state model is a novel technique for representing and modelling sequences of events during the course of labour, and adds memory to the system. This technique is based on finite state machines which are used to design synchronous logic. The finite state machine idea has been modified to make the states *fuzzy*. This introduced the problem that states can only grow in their truth assertion, so a totally new state is required for each transition, with return to old states currently not being allowed for the model to work. Cyclic relationships cannot easily be modelled and this remains a problem. A full fuzzy-state model is currently being developed. The concepts of the fuzzy state model are being developed and tested, the results of which will be submitted for publication in a suitable Journal in the near future. Further work will be needed in order to generalise the model and make it more compact and applicable to other problems.

The Foetal Condition Matrix (FCM) is used to summarise the current foetal state at a glance. This is a copy of the matrix provided in the clinical guidelines and is one which the midwifes are familiar. This is an effective and simple analogue display device. The output of the expert model is continuous and allows the clinician use it in the way that suits them. A useful facility might be to set thresholds and trigger

alarms when the foetal condition moves into a dangerous region in the foetal condition matrix.

Simple linguistic approximation used in addition to the FCM to provide some simple explanation. The most important information, that of the ST waveform shape, is described linguistically as a simple statement.

The fuzzy expert system concepts will be continuously re-examined, refined and developed further to include knowledge on the CTG and a full linguistic explanation facility. Further work is required to interpret changes heart-rate variability, which are critical for useful CTG interpretation. The 'complexity' of the heart-rate is an indication of whether a foetus is reactive. This work, coupled with the ST waveform analysis and current CTG analysis will provide a complete intelligent foetal monitor.

Chapter 7

Discussion, Conclusion and Further Work

7. *Discussion, conclusion and future work*

7.1 Introduction

The long term aim of the initiative, of which this research is a part, is to develop a user friendly, intelligent decision support tool that combines the expertise for CTG based assessment and ECG waveform analysis to assist busy clinicians in making more accurate and timely decisions, thus reduce unnecessary clinical intervention and any permanent damage to a foetus.

The specific aims of this project are to develop techniques to overcome the problems that have hindered the widespread use of foetal ECG pattern analysis and to use these techniques to develop an intelligent decision support tool that models human expert thinking. This will provide non-expert clinicians access to expertise on ECG analysis, which can be combined with routine CTG analysis, to help them make more accurate, objective and timely decisions.

This section discusses the main contributions of this work and highlights novelty, scope and future work.

This work has made contributions in three key areas of electronic foetal ECG analysis, namely signal enhancement of the foetal ECG signal, signal quality assessment and intelligent analysis and interpretation of changes in the foetal ECG waveform.

7.2 Signal enhancement and quality assessment

A major factor that has limited widespread foetal ECG waveform monitoring is the problem of poor signal quality. In many previous studies *(Westgate et al. 1993)*, the enhancement of the foetal ECG waveform has been limited to simple waveform averaging and the use of simple filters as recommended by the American Heart Association *(AHA 1975)*. This often leads to distortion of the ECG waveform making it very difficult to accurately interpret the important ECG shape information, such as the changes in ST waveform shape. A major contribution of this work is to find a solution to this problem by developing and testing new techniques for foetal ECG signal processing which greatly enhance the signal

quality, without introducing significant distortion and compromising the important information.

The specific achievements and contributions to knowledge are :

(i) **New design technique for sharp transition band digital filters for biomedical signal enhancement with minimal distortion.**

This new technique enables the efficient removal of power-line noise and baseline shifts which are a significant problem in foetal ECG analysis using linear FIR filters. These have been shown not to adversely affect the important features of the ECG and have therefore overcome the constraints laid down by the AHA recommendations *(AHA 1975)*. Filters for foetal ECG analysis, designed in this project, are currently being used in a commercially available ECG monitor STAN® (Cinventa AB). The design technique is described in chapter 2 and is the basis for a journal paper currently in preparation *(Outram & Ifeachor et al. 1997)*.

(ii) **Techniques for reliable QRS detection and pre-processing.**

Accurate and reliable detection of the QRS complex is critical for ECG pattern analysis. A high specificity if required in order to prevent misleading artefacts such as artificial ST waveform shapes. An investigation into the problems of QRS detection is described in chapter 3 and has led to the development of a new technique for adaptive automatic template extraction. This provides an accurate estimation of the QRS complex shape at the beginning of monitoring, thus optimising the QRS detection algorithm for each patient. Some of the work related to this is reported in two conference papers *(Outram et al. 1993)*.

(iii) **Novel techniques for reliable foetal ECG enhancement and feature extraction.**

The quantification of the ST waveform shape has hitherto been based on the simple ratio of the T peak and the QRS amplitude, the so called T/QRS ratio *(Greene & Westgate 1993; Westgate 1993; Luzietti & Rosén 1994)*. This is

because of the difficulty in reliably locating and measuring other visually identifiable features which quantify the ST waveform shape. Signal enhancement and the use of novel curve fitting for ST waveform approximation enhances the signal quality and greatly simplifies the problem of feature extraction. New algorithms have been developed to locate key features in the ST and PR waveforms which fully quantify the ST waveform shapes recognised in the clinical guidelines for the first time. This work is discussed in chapter 4 and has been published in an IEE journal paper *(Outram et al. 1995)*.

(iv) **New techniques for quality assessment of the ECG waveform.**

A key issue which is often neglected is the assessment of the quality of the ECG so that subsequent analysis and interpretation of changes in the ECG takes place in the proper context and is not based on false information produced by noisy or corrupted waveforms. This is important as noise and artefact can induce false changes in the ECG waveform which, if unchecked, lead to a false diagnosis. An improved algorithm has been developed to provide a useful estimate of the signal-to-noise ratio for the average ECG waveform. A limitation of this approach is that it is not sensitive to low-frequency noise. Thus, a complimentary technique was developed to independently assess the degree of baseline shift using multi-rate processing and a curve fitting approximation. The two techniques are then combined using fuzzy rules to derive a sensitive technique for assessing signal quality. Thus, if the signal is not of sufficient quality then it is not used for further analysis. This is very important as it provides feedback on the quality of the signal and ensures that no decisions are made based on corrupted waveforms.

These developments remove a major obstacle in electronic foetal monitoring for the first time and make it possible to undertake a reliable detailed waveform analysis. Some of this work has been published in a journal paper *(Outram & Ifeachor 1995)*, a conference paper *(Ifeachor & Outram 1993)* and a second paper in preparation for submission to a reputable journal *(Outram & Ifeachor 1997)*.

7.3 Intelligent foetal ECG interpretation and assessment

A key achievement of this work is the development of a prototype intelligent system to automate the analysis of the progressive changes in the foetal ECG shape. Specific achievements are:

(i) **Development of Fuzzy Logic models of medical expertise for foetal ECG analysis and interpretation.**

A novel technique for fully describing the ST waveform shape, as specified in the clinical guidelines *(Rosén 1994)*, is developed for the first time. This addresses a major limitation of previous studies where only the T/QRS ratio is used to quantify the ST waveform shape *(Greene & Westgate 1993)*. In addition, a new technique is proposed for modelling the expert reasoning over time to mimic the behaviour of an experienced obstetrician.

(ii) **Development of a fuzzy expert system.**

New techniques to capture, for the first time in machine form, the clinical expertise / guidelines for electronic foetal monitoring have been developed. A prototype expert system that embodies the clinical expertise has been developed and tested.

The expert system will form the basis for an advanced system for on-line monitoring. This work represents a significant contribution to foetal monitoring for a number of reasons.

Firstly, the system will facilitate the application of the clinical guidelines to real ECG interpretation. It is not realistic to expect junior doctors and midwifes to know how to accurately interpret all the changes in the ECG waveform as they are not trained in this and only provided with set of guidelines. To become experts, they would need to be motivated and trained, and this will not occur until the ECG waveform has widespread acceptance. The system will facilitate clinicians in learning how to apply the clinical guidelines. This is achieved through experience of

observing and identifying abnormal patterns in the foetal ECG data that are highlighted by the system and described in the guidelines.

7.3.1 Automatic monitoring of the ECG waveform.

Monitoring the ECG waveform requires constant supervision, as the important changes can occur over a spell as short as 5 minutes, and might be missed. Given that only 1% of all child births in the UK have indications of asphyxia at birth, and that monitoring can last up to 5 hours, ECG changes are relatively rare and it would be very difficult, tedious and unreliable to constantly monitor the ECG waveform by constant supervision. Using an intelligent system to supervise and alert clinicians to relevant abnormalities will free the clinician to attend other duties and direct them towards the data when there are unusual patterns. The responsibility for managing labour still lies with the clinician.

7.4 Limitations of the current work

Clearly, much of this work is new and it has not matured to a state where it could be implemented into a real-world product. Some of the work however, such as the signal enhancement filters described in chapter 2, has been implemented in the STAN® monitor as it was thoroughly tested in this project and independently by others. The software developed through the course of this project is currently being used as an off-line research tool to post-process data. It is intended that this work will provide a basis from which to develop a commercial foetal ECG monitor that will demonstrate the full potential of combined foetal ECG waveform and CTG monitoring. To do this however, a number of limitations exist which will have to be addressed and overcome. These are now discussed.

- **Incomplete validation**. A limiting factor in this work is the lack of availability of abnormal case data which prevents full validation. A much larger database of foetal ECG is required which includes examples of foetal distress demonstrating all modes of ECG changes used in the guidelines, i.e. rapidly rising T/QRS, brief and repeated appearance of bi-phasic waveforms, persistently negative T waves, persistently negative / bi-phasic ST waveform and highly elevated T/QRS. An industrial partner in Sweden is currently setting up further data collection of over

1000 cases as part of a clinical trial of the new generation STAN® (Cinventa AB).

- **Measure and optimise performance**. Although individual elements of this work have been validated where possible, it is difficult to define how well the entire fuzzy expert system performs as there are no objective outcome measures for each case. A method is required for objectively determining the outcome of each labour with respect to foetal distress and to use this as feedback to optimise the fuzzy rules in the ECG expert system. There have been some significant developments using blood-gas measures to quantify foetal outcome, and is the subject of another research project *(Garibaldi et al. 1997)*.
- **ECG must be combined with CTG**. The scope of this project is limited to ECG waveform analysis independently from CTG as a fuzzy CTG system has not yet been developed. It is stated in the literature *(Greene & Westgate 1993; Rosén et al. 1992; Westgate et al. 1993)* that it is the combination of ECG and CTG which has the greatest diagnostic potential, and that individually ECG or CTG is not always sufficient. Two independent systems have been produced, the INFANT *(Keith et al. 1994)* and the fuzzy ECG analysis system developed in this project, but they have yet to be combined into one tool. The aim of the initiative of this work is to complete this.
- **User interface**. An effective user interface is important to the success of any interactive software system. Any system with a poor interface is likely to never be used, despite any technical merit. The current user interface is only sufficient for research purposes.

7.5 Future work

This project is part of a larger global project, which aims to combine intelligent ECG, CTG and blood-gas analysis to develop a complete foetal monitoring solution. To achieve this aim, there are many objectives which constitute future work. These are now discussed.

7.5.1 Data collection and archiving

A key problem that limits research into foetal ECG waveform monitoring is the lack of abnormal case data. A new multi-centre clinical ECG trial will establish the

infrastructure of 3-4 centres in Europe to be set up to collect raw data. All centres will collect 12 bit raw ECG data, clinical notes and CTG information. A schematic of the proposed data acquisition system is given in Figure 148. The gain of the ECG instrumentation amplifier is set to stop the baseline shift from saturating the analogue to digital converters (ADC), so at least 12 bit resolution is required in order to get adequate resolution on the foetal ECG itself.

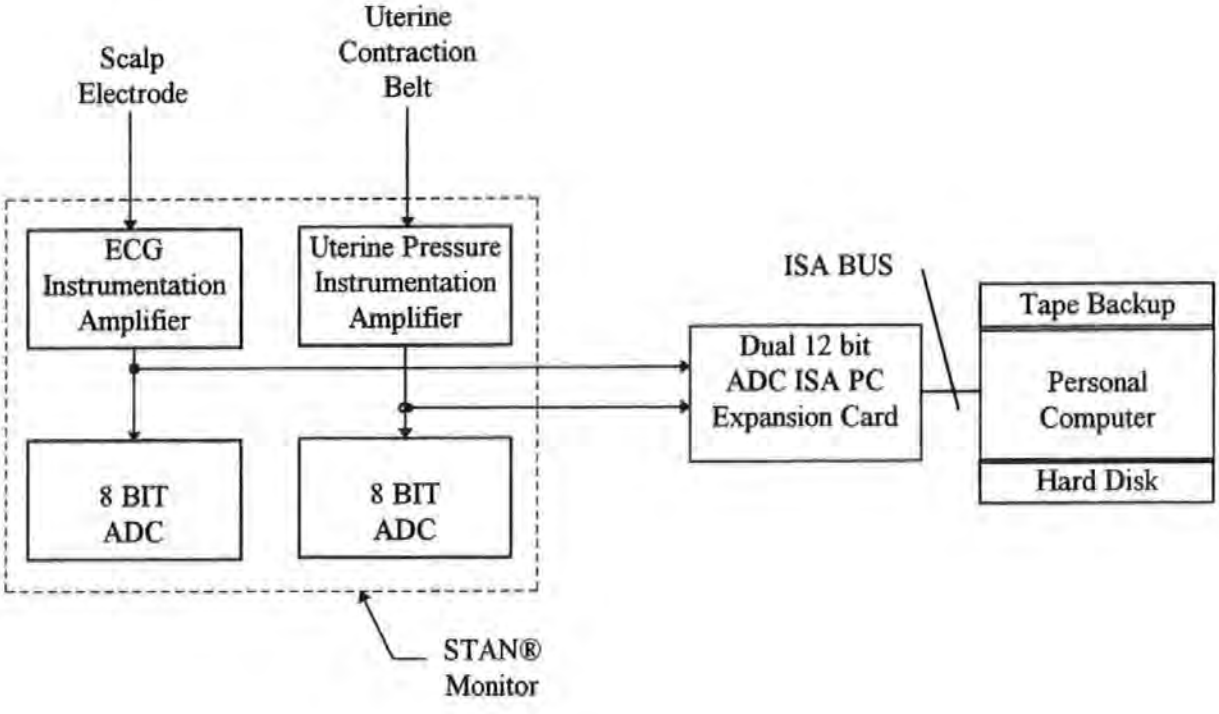

Figure 148 Data acquisition system

The data will be collected on hard disk and backed up onto a portable media such as tape or disk. This data will be used to advance the development of an on-line combined CTG and ECG fuzzy expert system.

7.5.1.1 New analogue signal processing proposal

A common problem with measuring and digitising physiological signals is preventing the signal from saturating the A/D converter. This problem is mostly caused by low-frequency signals, such as baseline shift, which are particularly prevalent in the ECG. To manage this situation, the gain of the signal has to be reduced to prevent saturation, resulting in a relatively low-amplitude ECG signal which only spans a fraction of the potential A/D dynamic range. A solution to this is

to add an analogue high-pass filter prior to the A/D converter stages to remove the baseline shift. Unfortunately, this results in severe distortion in the ECG signal shape due to the non-linear phase characteristics of analogue filters. Two solutions for this are to either (a) design a digital phase compensation filter or (b) produce an accurate inverse digital model of the analogue filter, thus cancelling all the effects of the analogue filter.

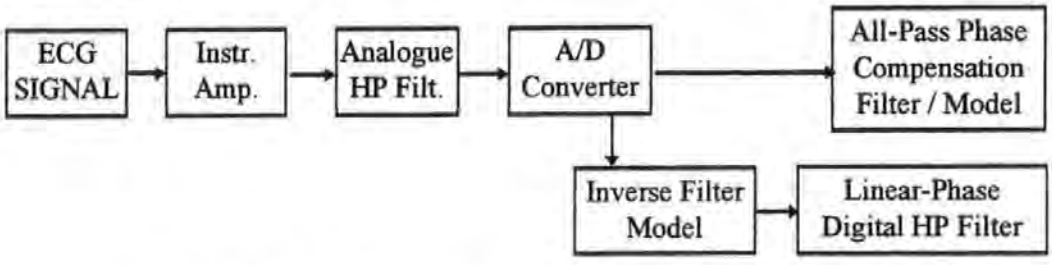

Figure 149 Outline solution for simplifying ECG data aquisition

Task 1. Modify the existing instrumentation amplifier design and add an analogue high pass filter (Stop band 0-2.5Hz).

Task 2. Compare the following two digital techniques for correcting the effects of the filter

1. Design an inverse model of the analogue filter and validate the accuracy. Adaptive filters and/or artificial neural network models will be considered
2. Design an all-pass phase compensation filter to correct phase distortion over the pass-band.
3. Compare results.

A preliminary investigation has been carried out by a final year student at the University of Plymouth.

7.5.2 Develop a medical data database

It is proposed that a central database is created which will hold all the raw ECG data, relevant medical information, the generated features, expert interpretation of the data and auditing information. An outline of the proposed system is illustrated in Figure 150.

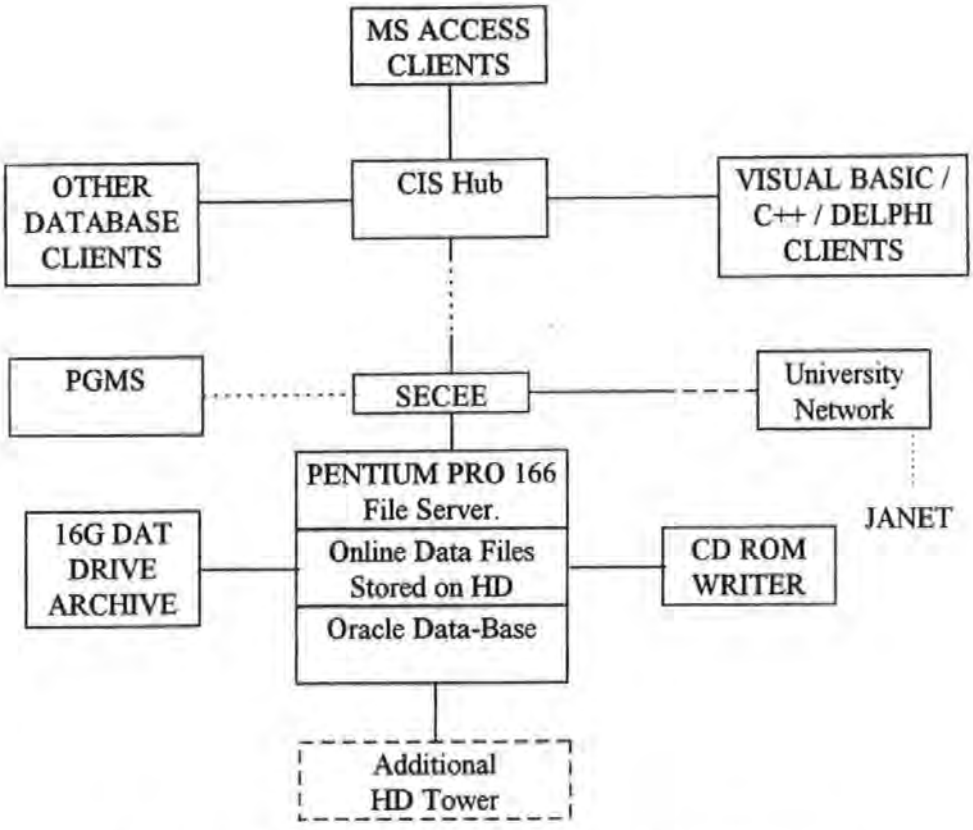

Figure 150 Typical outline for the research data file server

Key.

C.I.S	Centre for Intelligent Systems (University of Plymouth, UK)
S.E.C.E.E.	School of Electronic, Communication and Electrical Engineering.
S.Q.L.	Structured Query Language.
P.G.M.S.	Post Graduate Medical School (University of Plymouth, UK)
J.A.NET.	Joint Academic Network.

This database will also hold and document data for other projects, such as blood gas measurements and EEG.

7.5.2.1 Back-end of the database

The back end of the data base will be a database file stored on the file server or an SQL database server such as Oracle or Microsoft SQL server. The different fields of this file will have the required security to prevent un-authorised modification of the records.

7.5.2.2 Front End

Three options are available.

1. **SQL Client Software**

   This will provide access to the full search facilities of SQL server. This is available through SQL server and Oracle.

2. **Microsoft Access / Other Database Software**

   This is a simple user friendly technique to access the data base, with limited search capability.

3. **MS Visual Basic / Visual C++ / Borland Delphi**

   Custom stand-alone code can be developed for faster and specific access to the data-base. Software with access to the database, such as an ECG data browser is required.

4. **HTML Internet Browsers**

   The database can create dynamic internet pages HTML (Hyper-Text Markup Language) which allow the database to be browsed.

7.5.3 Foetal ECG Simulator

It is very unlikely that examples of all the required abnormal waveforms will be encountered and recorded in the near future. A shorter term solution to this problem is to investigate and develop a technique to electronically model the foetal cardiac cycle. This will enable the engineer and clinician to simulate the abnormal waveform changes which are recognised in the knowledge (see chapter 4). This will then provide a very useful tool for testing and validating future systems.

7.5.4 Further investigation into Fuzzy State Machines

The concept of the fuzzy state machine will be refined and testing in both ECG and CTG fuzzy systems. This will enable the management of complex problems that require the use of cumulative evidence and time information.

7.5.5 Graphical User Interface

A good user interface is essential for the system to be of any benefit to clinicians. Medical devices with a poor interface between the machine and the user will tend to be unused. The interface must be designed carefully, in consultation with end users, such that operation is clear, unambiguous and simple.

7.5.5.1 Archiving

All the raw ECG and CTG data will be collected on the hard disks, compressed & copied to a portable media such as a disk or tape. This will be sent to the research co-ordinator in Plymouth who will document and archive the data. Digital tape storage has been recommended for backup and off-line storage.

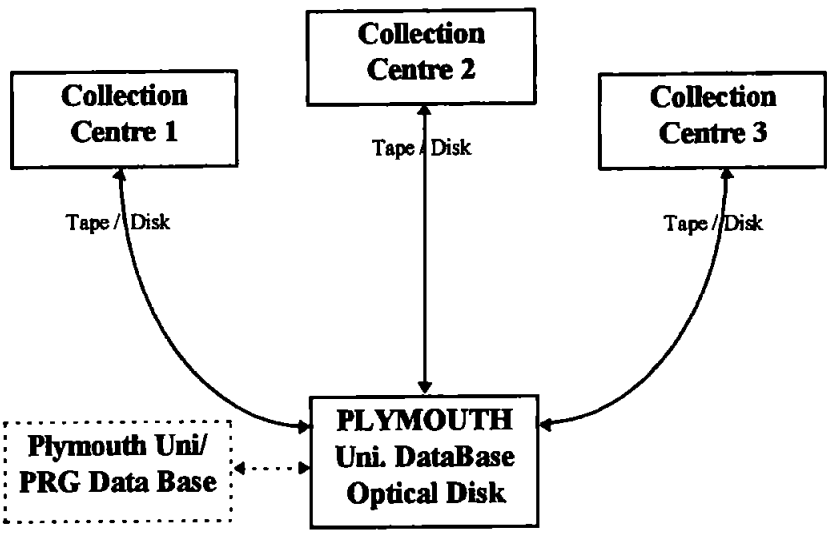

Figure 151 Recommended Multi Centre Data collection

7.5.5.2 Data compression

It is estimated that each centre could probably collect up to one case per day. If the data is sampled at 500Hz using 12 bit accuracy, each hour of data will result in 2.7Mbytes of raw ECG data. Some labours will be recorded for 3-4 hours, often resulting in files over 10Mbytes long. Clearly data compression would be useful, but no data loss must occur as a result of this process. One simple solution is to store the first difference of the data such that it can be recovered perfectly afterwards. Storing the first difference of the data will reduce the number of bits required because the baseline shift, which has a maximum span of 12 bits, has a very low first derivative whereas the foetal ECG has a much smaller span, typically only 6 bits. It is estimated that 50% data compression could be achieved using this technique. A more efficient technique may be used if necessary.

7.5.6 Integrating into the STAN® (Cinventa AB) system

This work is targeted to be integrated within the ST Analyser (STAN), Cinventa AB (Sweden), which is a medical device currently commercially available in the European Community (EC). This device and the operation guidelines underwent a clinical trial in Plymouth (*Westgate et al. 1993*).

The results of this trial was presented as part of an application to a notified body within the EC, as a class 2B medical device, and has successfully obtained a CE certificate as detailed in the European medical device directive MDD93/42/EEC.

7.5.6.1 The clinical role of the system

The realistic aim of an intelligent ECG monitoring system will be to stimulate the development of clinical expertise in foetal ECG analysis. This is achieved by providing an advisory function. The role of the system is to map complex raw information, such as raw ECG, to a humanly manageable form such as text based advisory information. The system has no authority to diagnose, or to even suggest a diagnosis. The system, like many intelligent systems, can be viewed as a filter which extracts the useful trends and patterns from other unwanted information or background noise.

7.5.6.2 Safety and quality standards.

All software should undergo a risk assessment which is documented according to the international standard IEC6601 or European standard EN60601-1-4. The design of a medical device to be used in healthcare must consider the legal implications of a patient becoming injured whilst it is being used as part of the clinical management. To advance this work to a commercial product, design constraints need to be applied to ensure that it is safe and so that it would be accepted by the main regulatory bodies in the European Community and/or the FDA (USA and others).

(i) The European medical device directive MDD93/42/EEC would not allow a technology that is totally automatic. There must always be a clinician present to

make all clinical decisions and intervention. There should always be a active human interface between the system and the patient.

(ii) The system must not provide directly leading information to a clinician. The system must be purely advisory.

The system can only provide the end user with an improved, albeit derived by artificial intelligence, representation of the raw information. The role of the system is not to replace human intelligence but to complement it. It must be possible for the clinician to validate all the information derived and displayed by the system by examining the system output and the raw data.

In clinical practice decisions to intervene, such as perform a caesarean section or a foetal blood sample, are crisp and can only be made by the human monitor, i.e. a clinician either **does** intervene or **does not** intervene. The role of the computer is to interpret all the information available and present an output which alerts/demands the right level of human expertise into the decision making process. The computer is the most basic level of expertise in the chain (see Figure 152) and has no authority in the decision making process. For most labours the mid-wife has the ideal level of authority if she can be alerted to a problem. The more unusual cases should be passed on via the midwife to a more specialist clinician - right up to the Chief consultant. A conceptual diagram is given below.

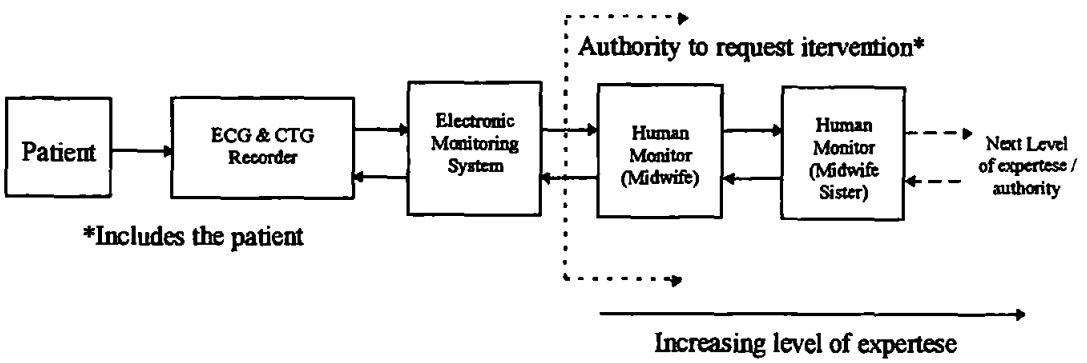

Figure 152 Chain of expertise

A clinician would base the decision on a personalised and highly complex scheme, using the information supplied (CTG+ECG), experience, intuition, patient history and patient handling guidelines. Even if all the useful information could be recorded

and stored, this reasoning could not realistically be done by a computer. It is unreasonable, however, to expect a clinician to perform well with so much extra information, especially within the dynamic labour ward environment. Thus, the role of the system is not to replace the clinician, but to assist them with the task of the analysis of the combined CTG and ECG. This is achieved by *presenting information in an objective and certain form and thus help the clinician to apply the guidelines more effectively*. The clinician can obtain information on important events, and thus make more informed and timely judgements.

For this to be effective, it is necessary to cater for the underlying fuzziness in obstetric data and knowledge. For the cases considered so far, the performance has been predictable and accurate.

7.5.7 Integrating CTG, ECG and Blood-Gas

The INFANT system *(Keith et al. 1994; Ifeachor et al. 1991)* has been designed exclusively to interpret the CTG and provide advice to clinicians. Some of the concepts in INFANT need to be combined with this work to produce a complete foetal monitoring tool. The INFANT system employs a crisp expert system whereas this work uses a fuzzy expert system. Another system being produced in Plymouth, with an industrial collaborator, is a fuzzy expert system to interpret and validate umbilical chord blood gasses *(Garibaldi et al. 1997)*. This provides an objective measure of foetal outcome with respect to foetal distress. A major task will be to produce a combined ECG, CTG and blood-gas fuzzy expert system, with a suitable user interface, which is tested and validated. A plan of how these projects are to be combined is in preparation, and will be reported in a forthcoming paper on fuzzy expert systems in medicine.

7.5.7.1 Heart-rate variability analysis

An element of CTG analysis is the interpretation of the heart-rate variability (HRV). In some centres in the world, a great deal of emphasis is placed on HRV as it is indicative of the reactivity of the foetus. The HRV can be viewed as a deterministic signal plus a chaotic or random process. It is hypothesised that the seemingly chaotic nature of the heart-rate is considered to be a good sign of a reactive foetus and a lack of this pattern is indicative of foetal stress. There has been a large amount

of work on HRV, in particularly the spectral analysis of HRV and the relationship to foetal physiology *(Ferrazzi et al. 1988)*. A literature survey and critical examination of the previous work is required, followed by further investigation into term foetal HRV.

7.6 Publications

Much of the content of this thesis has been published or is being prepared for publication in journals and conference proceedings.

Ifeachor E.C. , Outram N.J. & Greene K.R. Fetal ECG Quality Assessment using Neural Networks., *Workshop on Neural Networks: Techniques and Application of Neural Networks.*, University of Liverpool., 1993

Outram N.J. & Ifeachor E.C., Techniques for detection and classification of the fetal QRS complex., *IEE Coll. Application of neural networks to signal processing.*, iee Digest No. 1994/248, pp 10/1-3, Dec 1993

Ifeachor E.C. & Outram N.J., Fuzzy Logic concepts for pattern analysis and interpretation of changes in the fetal electrocardiogram., *Proc. Int. Conf. on Neural Networks and Expert Systems in Medicine and Healthcare.*, 353-362, University of Plymouth., U.K. 1994

Outram N.J. , Ifeachor E.C. & Van Eetvelt P.W.J., Optimal enhancement of the fetal electrocardiogram during labour., IEE Coll. Signal processing in cardiography., IEE Digest No. 1995/043, 5/1--5/6, 1994

Ifeachor E.C. & Outram N.J. A fuzzy expert system to assist in the management of labour., *Proceedings of the International ICSC Symposium on FUZZY LOGIC.*, ICSC, C97-C102, Zurich, 1995

Outram N.J. & Ifeachor E.C., Neural network and fuzzy logic techniques for classifying patterns in the fetal ECG waveform", Proceedings of the International Workshop on Medical and Biological Signal Processing", University of Plymouth, Plymouth, UK, 91-99, 1995a

Outram N.J. , Ifeachor E.C., Van Eetvelt P.J.W. & Curnow J.S.H., Techniques for optimal enhancement and feature extraction of the fetal electrocardiogram, IEE Proc-Sci. Meas. Technol., 142, 6, Nov. 1995b

Outram N.J. & Ifeachor E.C., Pattern Analysis of Uncertain Changes in the Fetal Electrocardiogram Features during Labour., Proc. 2nd Int. Conf. Neural Networks and Expert Systems in Medicine and Healthcare., pp112-122., 1996

Outram N.J. & Ifeachor E.C., Narrow-Band Digital Filters for Biomedical Signal Enhancement with Application to Fetal ECG., (In preparation.)

Outram N.J. & Ifeachor E.C., A Novel Fuzzy State Machine Concept for Modelling the Human Expert Management of Sequential Events in Labour., (In preparation.)

7.7 Conclusion

An important contribution of this work has been to provide a platform for investigating and demonstrating the validity of the current clinical guidelines for interpreting foetal ECG, which will motivate clinicians to use these guidelines consistently. This has been made possible by the development of signal-processing techniques to enhance the foetal ECG and a fuzzy expert system that can manage the uncertain and qualitative nature of obstetric knowledge. The novelty in this work is in the signal enhancement scheme, the modelling of expert reasoning process in a computer, and in providing a measure of foetal condition in a clear and *objective* form.

Much of the work and effort over the course of this programme of work has gone into understanding the problems in foetal monitoring, developing the signal-enhancement techniques and in developing a real-time fuzzy expert system. A working prototype has been developed which has a basic set of rules. The system needs to be further validated before it is made available for foetal ECG monitoring. This will require a large database to be collected and documented over many years.

References

Akselrod S., Norymberg M., Peled I., Karabelnik E. & Green M.S., Computerised analysis of ST segment changes in ambulatory electrocardiograms., *Med.&Biol.Eng.&Comp.*, 25, pp513-519, 1987

American Heart Association Committee on Electrocardiography 1975 Recommendations for the standardization of leads and specifications for instruments in ECG/VCG Circulation, 52, pp1-25, 1975

Biswas N.N., Logic Design Theory., Prentice Hall International Inc., Englewood Cliffs ., N.J., 1993

Burden R.L. & Faires J.D., Numerical Analysis., fourth edition, PWS-Kent Pub. Co., Boston, 1989

Centor R.M., The Use of ROC Curves and Their Analyses., *Med. Desc. Making.*, 11, pp102-106, 1991

Cox E., The Fuzzy Systems Handbook. A practitioner's guide to building, using and maintaining fuzzy systems., Academic Press Limited., 24-28 Oval Rd, London UK., 1994

Charayaphan, C., Marble, A.E., Nugent, S.T. & Swingler, D., Correlation algorithm and sampling techniques for estimating the signal-to-noise ratio of the electrocardiogram., *J. Bio. Eng.*, 14, pp516-520, 1992

Charayaphan, C., Marble, A.E., Nugent, S.T. & Swingler, D., Estimation of a signal-to-noise ratio of a quasiperiodic cardiovascular signal using coherency and correlation techniques., *Med. & Bio. Eng. & Comp.*, 572579, 1989

Curnow J.S.H., Barron L.B., Westgate J. & Greene K.R., A Four Channel Fetal ECH data collection system., *J. Med. Eng. Phys.*, 17, 2, pp122-125, 1995

Durkin J., Expert Systems, Design & Developments., Maclillan Pub. Co., ch 13, 1994

Garibaldi J., Westgate J., Ifeachor E.C. & Greene K.R., The Development and Implementation of an Expert System for the Analysis of Umbilical Cord Blood., *Artificial Intelligence in Medicine.*, In Press., 1997

Greene K R, The ECG waveform. In *Balliere's clinical obstetrics & Gynaecology*, M. Whittle (ed)., 1, pp131-155, 1987, London.

Greene K.R. & Westgate J., The Fetal ECG with Particular Reference to the ST waveform., In *Intrapartum fetal surveillance.*, Ch. 21., 281-294, Spencer J.A.D. and Ward R.H.T (Ed.), Royal College of Obstetrics and Gynecology, 27 Sussex Place, Regents Park, London., 1993

Hanley J.A., Receiver operator characteristic (ROC) methedology: the state of the art. Crit. Rev. diagn. Imaging., 29, pp307-335, 1989

Haykin S., Adaptive filter theory (second Ed)., Prentice Hall, Englewood Cliffs, NY., 1992

Haykin S., Neural Networks, a comprehensive foundation., Macmillan College Publishing Co., New York., 1994

Hon E.H. & Lee S.T., Noise reduction in fetal electrocardiography II Averaging techniques., *Am. J. Obst. & Gynec.*, 87, 8, pp1086-1096, 1963

Ifeachor E.C. & Jervis B., Digital Signal Processing, a practical approach", Addison Wesley., 1993

Ifeachor E.C., Patel S.R., Westgate J., Curnow J.S. & Greene K.R. Applications of artificial neural networks to fetal monitoring during labour. Techniques and application of neural networks (Ed. Lisboa P.J.G. & Taylor M.J.), Ellis Horwood.

Ifeachor E C, Keith R D F, Westgate J & Greene K R., An expert system to assist in the management of labour. In Liebowitz J (Ed) *World Congress on Expert Systems*, Vol. 4, pp2615-2622, Pergamon Press., 1991

Ifeachor E.C. , Outram N.J. & Greene K.R. Fetal ECG Quality Assessment using Neural Networks., *Workshop on Neural Networks: Techniques and Application of Neural Networks.*, University of Liverpool., 1993

Ifeachor E.C. & Outram N.J., Fuzzy Logic concepts for pattern analysis and interpretation of changes in the fetal electrocardiogram., *Proc. Int. Conf. on Neural Networks and Expert Systems in Medicine and Healthcare.*, 353-362, University of Plymouth., U.K. 1994

Ifeachor E.C. & Outram N.J. A fuzzy expert system to assist in the management of labour., *Proceedings of the International ICSC Symposium on FUZZY LOGIC.*, ICSC, C97-C102, Zurich, 1995

Jennings A. & McKeown J.J., Matrix Computation (Second Edition)., John Wiley & Sons Ltd, Baffins Lane, Chichester, England., 1992.

Keith R., Westgate J., Beckley S., Garibaldi J., Ifeachor E.C. & Greene K.R., A multicentre comparitive study of 17 experts and an intelligent computer system in the management of labour using the cardiotocograph., Submitted *Br. J. Obstet. Gynecol.*

Kirk D.L. & Smith P.R., Techniques for the routine on-line processing of the fetal electrocardiogram., *J. Perinat. Med.*, 14, 1986

Klir G.J. & FolgerT.A., Fuzzy sets, uncertainty and information., Prentice Hall., Englewood Cliffs, NY.,1988

Kosko B., Neural Networks and Fuzzy Systems., Prentice Hall International., Englewood Cliffs., N.J., 1992.

Krause W. Natali by Neiss., A computer-aided monitoring system for supervision of labour. K. Maeda et al (Eds). *Computers and Perinatal Medicine.*, pp103-111, 1990, Elseviere Science Publishers BV Amsterdam.

Lee H.S. & Thakor N.V., Frame-based understanding of ECG signals., *1st Conf. on Artificial Inteligence.*, Denver, pp 624-629, 1984

Lilja H., Greene K.R., Karlsson K. & Rosén K.G., ST waveform changes of the fetal electrocardiogram during labour - a clinical study., *Br. J. Obs. Gynec.*, 92, pp611-617, 1985

Lilja H., Karlsson K., Lindecrantz K. & Rosén K.G., Microprocessor based waveform analysis of the fetal electrocardiogram., *J. Perinat. Med.*, 14, 1986

Lu J., Weaver J.B., Healy D.M. & Xu Y., Noise reduction with multiscale edge representation and perceptual criteria., In. *Proceedings of IEEE-SP International Symposium on Time-Frequency and Time-Scale Analysis.*, 1992

Lusted L.B., Signal delectability and medical decision-making., *Science*, 171, pp1217-1219, 1971

Luzietti R. & Rosén K.G., The fetal electrocardiogram: ST waveform analysis during labour, *J.Perinat.Med.*, 22, pp501-512, 1994.

Masters T., Practical Neural Network Recipes in C++., Academic Press, Inc., 1250 Sixth Ave., San Diego, CA., 1993

Marvel C.J. & Kirk D.L., A simple software routine for the reproducible processing of the fetal electrocardiogram., *J. Biomed. Eng.*, 2, 216-220, 1980

Maeda K., Computerised analysis of cardiotocograms and fetal movements., In *Balliere's Clinical Obstetrics & Gynaecology*., R Lilford. (Ed.), 4, 797-813, 1990

Mamdani E.H. & Assikian S., An experiment in linguistic synthesis with a fuzzy logic controller. *International Journal of Man-Machine Studies.*, 7, pp1-13., 1978.

McNeil B.J., Keeler E. & Adelstein S.J. Primer on certain elements of medical decision making., *N. Engl. J. Med.*, 293, pp211-215., 1975

Murray H.G., The fetal electrocardiogram: current clinical developments in Nottingham., *J.Perinat. Med.*, 14, pp399, 1986

Murthy I.S.N. & Niranjan C., Decompostion of ECG by linear filtering., *Comp.Bio.Med.*, 22, pp13-22, 1992

Newbold S., Wheeler T. & Clewlow F., Comparison of the T/QRS ratio of the fetal electrocardiogram and the fetal heart rate during labour and the relation of these variables to condition at delivery., *British J. Obs. & Gynec.*, 98, pp173-178, 1991

Outram N.J. & Ifeachor E.C., Techniques for detection and classification of the fetal QRS complex., *IEE Coll. Application of neural networks to signal processing.*, IEE Digest No. 1994/248, pp 10/1-3, Dec 1993

Outram N.J. , Ifeachor E.C., Van Eetvelt P.J.W. & Curnow J.S.H., Techniques for optimal enhancement and feature extraction of the fetal electrocardiogram, *IEE Proc-Sci. Meas. Technol.*, 142, 6, Nov. 1995

Outram N.J. & Ifeachor E.C., Neural network and fuzzy logic techniques for classifying patterns in the fetal ECG waveform, *Proceedings of the International Workshop on Medical and Biological Signal Processing*, University of Plymouth, Plymouth, UK, 91-99, 1995a

Outram N.J. & Ifeachor E.C., Narrow-band digital filters for biomedical signal enhancement with application to foetal ECG., In preparation.

Outram N.J. & Ifeachor E.C., A Novel Fuzzy State Machine Concept for Modelling the Humand Expert Management of Sequential Events in Labour., In preparation.

Outram N.J. & Ifeachor E.C., Pattern Analysis of Uncertain Changes in the Fetal Electrocardiogram Features during Labour., *Proc. 2nd Int. Conf. Neural Networks and Expert Systems in Medicine and Healthcare.*, pp112-122., 1996

Peper A., Jonges R., Grimbergen C.A., Losekoot T.G. & Strackee J., Method for the computation of an accurate zero reference for ECG signals., *Med. & Biol. Eng. & Comput.*, 28, pp105-112, 1990

Press W.H., Teukolsky S.A., Vetterling W.T. & Flannery B.P., Numerical recipes in C. (2nd Ed.), Cambridge University Press, Cambridge, UK., 1992

Proakis G.J. & Manolakis D.G., Digital Signal Processing. Principles, Algorithms, and Applications. (Second Edition)., Macmillan pup. Co. , New York., 1992

Rabiner L.R. & Gold B., Theory and Application of Digital Signal Processing., Prentice Hall, Englewood Cliffs, 1975

Rosén K,R., Alterations in the fetal electrocardiogram as a sign of fetal asphyxia - experimental data with a clinical implementation., *J. Perinat. Med.*, 14, 355, 1986

Rosén K G, Arulkumaran S., Greene K R, Lilja H, Lindecrantz K, Seneviratne H, & Widmark C., Clinical validity of fetal ECG waveform analysis. In *Perinatology*, Nestle Nutrition Workshop Series, Vol. 26, Nestec LtD, Vevey/Raven Press, New York,95-110., 1992

Rosén K.G., ST Waveform + CTG clinical guidelines., Internal report, Plymouth Postgraduate Medical School, University of Plymouth, 1994.

Rummelhart D.E. & McClelland J.L., Parallel Distributed Processing, Explorations in Microstructure of Cognition., Volume 1: Foundations., MIT press, Cambridge, England., 1992

Luzietti R. & Rosén K.G., The fetal electrocardiogram: ST waveform analysis during labour., *J.Perinat.Med.*, 22, 501-512, 1994

Sheild J.E.A. & Kirk D.L., The use of digital filters in enhancing the fetal electrocardiogram., 3, *J. Biomed. Eng.*, pp44-48, 1981

Strang G., Linear Algebra and it's applications., third ed., Harcourt Brace Jovanovich, Inc., Orlando, Florida., 1988

Sugeno M. & Yasukawa T., A Fuzzy-Logic-Based Approach to Qualitative Modeling., *IEEE Trans. on Fuzzy Systems.*, 1, 1, 1993

Suzuki Y. & Ono K., Personal computer system for ECG ST-segment recognition based on neural networks., *Med. & Biol. Eng & Comp.*, 30, pp2-8, 1992

Sweats J.A. (1988), Measuring the Accuracy of Diagnostic Systems., *Science.*, 240, 1285-1293

Tompkins W.J.(Ed) Biomedical Digital Signal Processing., Prentice Hall, Inc., Englewood Cliffs, N.J., Ch.13, 1991

Trahanias P. & Skordalakis E., Bottom-up approach to the ECG pattern-recognition problem., *Med.&Biol.Eng.& Comp.*, 27, pp221-229, 1989

VanAlsté J.A. & Schilder T.S., Removal of Base-Line Wander and Power-Line Interference from the ECG by an Efficient FIR Filter with a Reduced Number of Taps., *IEEE Trans. Biomed. Eng*, 32,12,pp1052-1060,1985

Warwick K. (1995)., New Ideas in Fuzzy Clustering and Fuzy Automata., *Proceedings of the International {ICSC} Symposium on FUZZY LOGIC.*, Plenary Session Paper, XXI-XXVII

Wenstøp F., Quantitative Analysis with Linguistic Variables., *Fuzzy Sets and Systems.*, 4, pp99-115, 1980

Westgate J., Harris M., Curnow J. & Greene K.R. Plymouth randomised trial of the cardiotocogram only versus ST waveform plus cardiotocogram for intrapartum monitoring in 2400 cases., *Am. J. Obstet. Gynecol.*, 169, pp1151-1160, 1993

Westgate J., Keith R., Curnow J.S.H., Ifeachor E.C. & Greene K.R., Suitability of fetal scalp electrodes for monitoring the fetal electrocardiogram during labour., *Clin. Phys. Physiol. Meas.*, 11, pp297-306, 1990

Xue Q., Hu Y.H. & Tompkins W.J., Neural-Network-Based Adaptive Matched Filtering for QRS Detection., *IEEE Trans. Biomed. Eng.*, 39, 4, 1992

Yager R., Approximate Reasoning as a Basis for Rule-Based Expert Systems., *IEEE Trans. Sys., Man. & Cyber.*, SMC-14, 4, 1984

Zadeh L. A., The role of fuzzy logic in the management of uncertainty in expert systems., *Fuzzy set and systems.*, 11, pp199-227 , 1983

Zadeh L.A., The Concept of a Linguistic Variable and it's Application to Approximate Reasoning-I., *Information Sciences.*, 8, pp199-249, 1975

Appendix A

MATLAB scripts for signal enhancement

A. Appendices

A.1 The comb filter : main code

```
%Design of multiple linear notch filters
%(c)1996 N.J.Outram, University of Plymouth
%
%
%
%This code is developmental and is to be used for testing
purposes only
%Please note the the usuall disclaimer applies. We give Karl
Rosen
%permission to use this code for research purposes only.
%Neither I or the University of Plymouth accept any
responsibility for
%any adverse outcome as a direct or indirect result of using
this software.
%

f0=figure;
f1=figure;
f2=figure;
f3=figure;
f4=figure;


%This designs the first prototype filter
%Skip every 50 samples
h1=remez(26,[0 0.3 0.5 1],[1 1 0 0],[1 1]);
%This writes the coefficients to disk
%You will need to read these numbers into your code
op=fopen('filter1.fir','wt');
fprintf(op,'%3.10f\n',h1);
fclose(op);

%This is the second stage
%Skip every 10 samples
h2=remez(26,[0 0.04 0.35 1],[1 1 0 0],[1 1]);
%This writes the filter to disk
%Again, you will need these
op=fopen('filter2.fir','wt');
fprintf(op,'%3.10f\n',h2);
fclose(op);


%This is the low-pass filter for removing all noise above
62.5Hz
%Skip every other sample
h3=remez(40,[0 0.4 0.5 1.0],[1 1 0 0],[1 1]);
```

```
%This writes the filter to disk
%Once again, you will need these
op=fopen('filter3.fir','wt');
fprintf(op,'%3.10f\n',h3);
fclose(op);


%Test
%Place RAW ECG in a file called test.raw in the current
directory to see it happen!!!!
%Note - I mean RAW text (not binary)
%i.e. text files you could import into Excel and plot
%Open the file
strm = fopen('poor.raw','rt');
ecg=fscanf(strm,'%f');
fclose(strm);
N=size(ecg,1);
figure(f1);
plot(ecg);

y1=zeros(size(ecg));
y2=zeros(size(ecg));
y3=zeros(size(ecg));
y4=zeros(size(ecg));

filter_length=(26*50+26*10);
for t=1301:N
 %I've added some 50Hz and some 90Hz to demonstrate

ecg(t)=ecg(t)+100.0*cos(2*3.141592654*50*t/500)+100.0*cos(2*3
.141592654*90*t/500);
 y1(t)=0.0;
 y2(t)=0.0;
 for i=1:26
  y1(t)=y1(t)+ecg(t-i*50)*h1(i);
 end
 for i=1:26
  y2(t)=y2(t)+y1(t-i*10)*h2(i);
 end
 y3(t)=ecg(t-filter_length/2)-y2(t);
 y4(t)=0.0;
 for i=1:40
  y4(t)=y4(t)+y3(t-2*i)*h3(i);
 end
end

figure(f2);
plot(y4);


%Display filter characteristics
for i=1:size(h1,2)
 h11(i*50) = h1(i);
end
for i=1:size(h1,2)
 h12(i*10) = h2(i);
end
for i=1:size(h3,2)
 h13(i*2) = h3(i);
end
c1=evfilt(h11,500,'Filter 1',0,250);
```

```
c2=evfilt(h12,500,'Filter 2',0,250);
figure(f3);
plotmag(c1+c2,500,'Magnitude response of the LF / PLN
filter',0,250);
figure(f4);
evalfilt(h13,500,'HF noise filter',0,250);
```

A.2 Time coherent filtering and averaging

```
%Evaluating the effects of time coherent filtering
%The file f6.prn has 291 raw aligned and interpolated (in
time) ECG vectors of 200 elements long
ip=fopen('f6.prn','rt');
X=fscanf(ip,'%f\n',[200,291]);
fclose(ip);
AV=zeros(200,291);
Y=X;
%Data is stored in columns

%Compute the average waveform
for r=1:30
 AV(1:200,30)=AV(1:200,30)+X(1:200,r);
end
AV(1:200,30)=AV(1:200,30)/30.0;
for r=31:291
 AV(1:200,r)=AV(1:200,r-1)+(X(1:200,r)-X(1:200,r-30))/30.0;
end

%Time coherent filtering
clear A;
clear B;
[N,Wn]=ellipord(0.5/60, 2/60, 0.1, 40);
[B,A]=ellip(N,0.1,40,Wn);

for r=1:200
 x=X(r,1:291);
 %y=filtfilt(B,A,x);
 y=filter(B,A,x);
 Y(r,1:291)=y;
end

f1=figure;
f2=figure;
f3=figure;
f4=figure;
f5=figure;

figure(f1);
plot(X(1:200,150))
figure(f2);
plot(Y(1:200,150))
figure(f3);
plot(AV(1:200,150))

for c=1:512
 xx(c,1)=c/512;
end
H=freqz(B,A);
H=abs(H);
figure(f4);
plot(xx(1:256),20*log10(H(1:256)));
xlabel('Normalised frequency');
```

```
ylabel('Attenuation (dB)');
grid on

hh=zeros(512,1);
for c=1:30
 hh(c,1)=1/30;
end
HH=fft(hh);
HH=abs(HH);
figure(f5);
plot(xx(1:256),20*log10(HH(1:256)));
xlabel('Normalised frequency');
ylabel('Attenuation (dB)');
grid on
```

A.3 Pre-processing for QRS detection

```
%CTG signal enhancement scheme

%This is the multi-notch filter
%used to remove baseline and power-line nose
%This filter is unsuitable for ST waveform analysis
h1 = remez(20,[0 0.2 0.4 1.0],[0 0 1 1], [1 1]);
h2=zeros(1,10*size(h1,2));
for i=1:size(h1,2)
 h2(i*10) = h1(i);
end

%This is the lowpass filter for removing HF noise
hlp = remez(36, [0 50/125 65/125 1], [1 1 0 0],[1 2]);
hlp2=zeros(1,size(hlp,2)*2);
for i=1:size(hlp,2)
 hlp2(i*2)=hlp(i);
end

c1=figure;
c2=figure;
c3=figure;

figure(c1);
subplot(2,1,1), evalfilt(h1,50,'Low-pass filter prototype
(fs=50Hz)',0,50); grid on;
subplot(2,1,2), c1=evalfilt(h2,500,'Comb filter
(fs=500Hz)',0,250); grid on;
figure(c2);
subplot(2,1,1); evalfilt(hlp,250,'Low-pass filter',0,250);
grid on;
subplot(2,1,2); evalfilt(hlp2,500,'(b) Low-pass filter
(fs=500Hz)',0,500); grid on;


strm = fopen('d:\ECGdata\poor.raw','rt');
strm2=fopen('ecg111.flt','wt');
ecg=fscanf(strm,'%f');
last = size(ecg,1);

%Add artificial noise
n1=700; n2=500; n3=250;
for i=1:last
```

```
ecg(i)=ecg(i)+n1*sin(50*i*2*3.1415926/500)+n2*sin(100*i*2*3.1
415926/500)+n3*rand-n3/2;
end
%last = 3000;

y=zeros(last,1);
y1=zeros(last,1);

figure(c3);
subplot(2,1,1), plot(ecg(201:last)); grid on;

%Multi-notch filter
for i=201:last
 y(i)=0.0;
 for j=1:20
  y(i)=y(i)+h1(j)*ecg(i-10*j);
 end
end

%Second filter (low-pass)
for i=1+2*size(hlp,2):last
 y1(i)=0.0;
 for j=1:size(hlp,2)
  y1(i)=y1(i)+hlp(j)*y(i-2*j);
 end
end


subplot(2,1,2), plot(y1(201:last)); grid on;
fprintf(strm2,'%3.8f\n',y);
fclose(strm2);
```

A.4 Auxiliary files

PLOTMAG.M

```
function plotmag(magresp, Fsamp, tit, from, to)
%plot mag <mag resp> <fsamp> <title> <from> <to>
%This plots a magnitude response

s=size(magresp,2);
ff = zeros(1,s);
for f=1:s
 ff(f)=f*Fsamp/s;
end
hold on
XLABEL('Frequency');
YLABEL('Attenuation (dB)');
TITLE(tit);
a=1+from*s/Fsamp;
b=to*s/Fsamp;
plot(ff(a:b),magresp(a:b));
hold off
grid on
```

EVFILT.M

```
function HH=evfilt(coeffs, Fsamp, tit, from, to)
%evfilt <coeff file> <Sampling Freq> <Title> <From> <To>
s=size(coeffs,2);
s=ceil(log(s)/log(2));
```

```
s=(2^s);
s=4096;
hh = zeros(1,s);
ff = zeros(1,s);
for f=1:s
 ff(f)=f*Fsamp/s;
end
hh( 1:size(coeffs,2) )=coeffs;
HH=fft(hh);
HH=abs(HH);
HH=20*log10(HH);
hold on
XLABEL('Frequency');
YLABEL('Attenuation (dB)');
TITLE(tit);
a=1+from*s/Fsamp;
b=to*s/Fsamp;
plot(ff(a:b),HH(a:b));
hold off
grid on
```

EVALFILT.M

```
function H=evalfilt(coeffs, Fsamp, tit, from, to)
%evalmyfilter <coeff file> <Sampling Freq> <Title> <From>
<To>
s=size(coeffs,2);
s=ceil(log(s)/log(2));
s=(2^s);
s=s*8;
hh = zeros(1,s);
ff = zeros(1,s);
for f=1:s
 ff(f)=f*Fsamp/s;
end
hh( 1:size(coeffs,2) )=coeffs;
H=fft(hh);
H=abs(H);
H=20*log10(H);
hold on
XLABEL('Frequency');
YLABEL('Magnitude Response (dB)');
TITLE(tit);
a=1+from*s/Fsamp;
b=to*s/Fsamp;
plot(ff(a:b),H(a:b));
hold off
grid on
```

EFILT.M

```
function H=efilt(coeffs, Fsamp, tit, from, to)
%efilt <coeff file> <Sampling Freq> <Title> <From> <To>
s=size(coeffs,2);
s=ceil(log(s)/log(2));
s=(2^s);
s=s*8;
hh = zeros(1,s);
ff = zeros(1,s);
for f=1:s
 ff(f)=f*Fsamp/s;
end
```

```
hh( 1:size(coeffs,2) )=coeffs;
H=fft(hh);
H=abs(H);
H=20*log10(H);
hold on
XLABEL('Frequency');
YLABEL('Attenuation (dB)');
TITLE(tit);
a=1+from*s/Fsamp;
b=to*s/Fsamp;
plot(ff(a:b),H(a:b));
hold off
grid on
```

Appendix B

Validation of the signal enhancement techniques

B. Validation of the signal enhancement techniques

B.1 Assessing the effects of different foetal ECG ST waveform comb-filters

Three cases were used for this study.

Case 1. Oe_00102	ST waveform contains virtually no deviations from the iso-electric level. T/QRS ratio is only just above zero. This case is therefore prone to artificial negative T/QRS ratios due to jitter. The very end of the case has some very slightly negative T peaks, particularly towards the end. The quality of the data is very good, with brief episodes of baseline shift.
Case 2. Oe_00108	This is a case where the T/QRS significantly rises above 0.24 at the end of the labour. Positive ST waveform changes are observed and must not be attenuated.
Case 3. Oe_00111	This is the only case where bi-phasic / netagive ST waveforms are consistently observed. The filters must not visibly remove or attenuate these patterns and must not affect the performance of the pattern recognition algorithms. The quality of the data is mostly good, with some bad episodes.

2.2 Case oe102

From a close visual inspection, there is nothing in this case that is very abnormal. The T/QRS peak value is almost zero throughout the labour, with the appearance of (very slightly) negative T peaks.

2.2.1 Effects on the T/QRS peak ratio

From Figure 153, with no filtering, there are marked episodes of negative T/QRS peaks which are caused by baseline shifts. These are not valid as the peak value of the T/QRS ratio should be zero or more. Filter type 1 visibly improves the feature extraction but negative episodes are still observed.

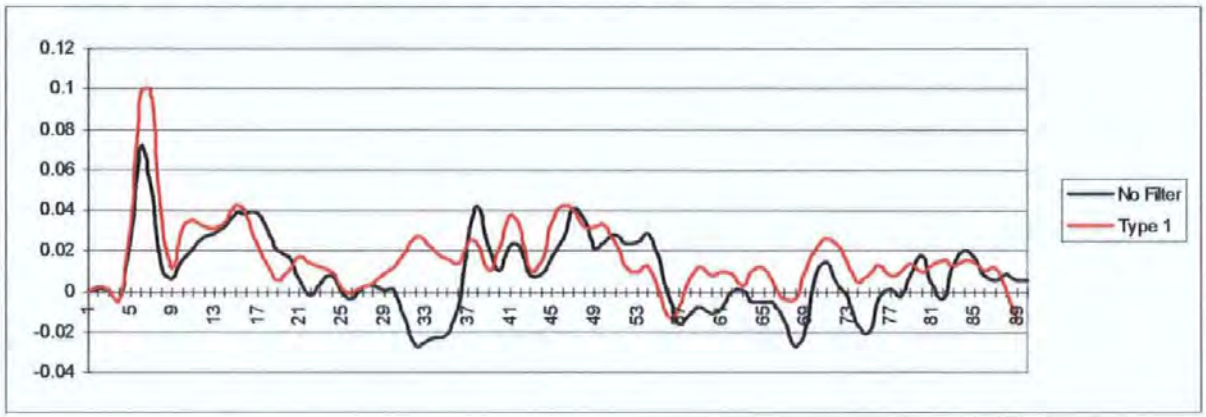

Figure 153Case oe102: Plot of T/QRS Peak ratio with no filtering and with filter type 1

From Figure 154, filters of type 2,3 and 4 have removed the negative T/QRS peak episodes entirely. There is no visibly significant difference in the trends of these features for any of the filters.

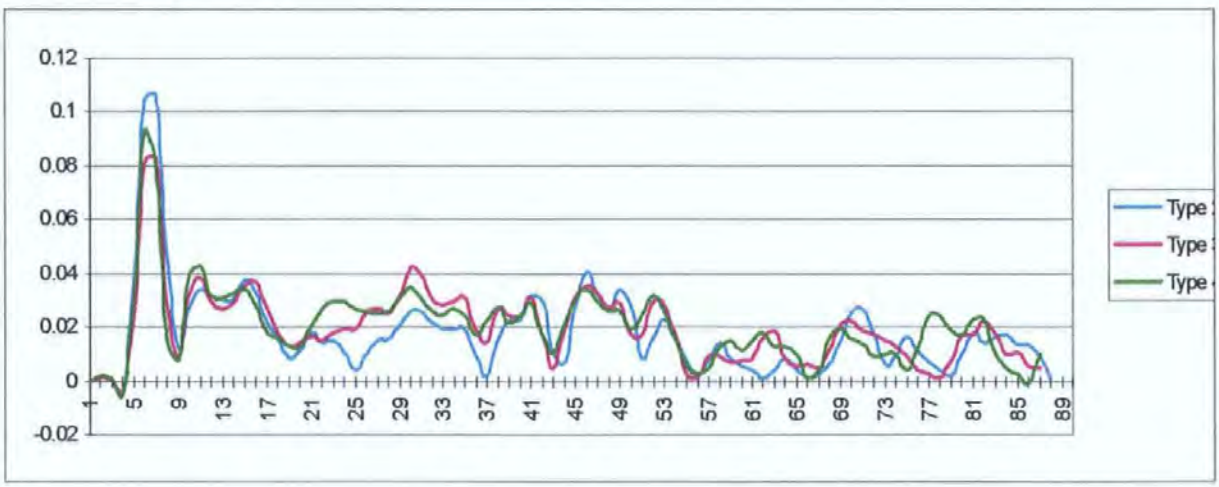

Figure 154 Case oe102: Plot of T/QRS Peak ratio for filters type 2,3 & 4

The correlation matrix for all these cases is given below in Table 29. With no filter, there is a low correlation with any of the filtered features. There is a high degree of correlation between adjacent pairs of filters.

	No Filter	Type 1	Type 2	Type 3	Type 4
No Filter	1				
Type 1	0.675121	1			
Type 2	0.613773	0.923306	1		
Type 3	0.518845	0.822822	0.887473	1	
Type 4	0.522609	0.801827	0.82105	0.90474	1

Table 29 Correlation matrix for different filters using case oe102

From Table 30 there is a very slight increase in mean and median as the filters become more aggressive, but is of no clinical significance.

Type 1		Type 2	
Mean	0.017248621	Mean	0.018110552
Standard Error	0.001876074	Standard Error	0.001855998
Median	0.012561	Median	0.01495
Standard Deviation	0.017498851	Standard Deviation	0.017311599
Sample Variance	0.00030621	Sample Variance	0.000299691
Kurtosis	9.137926367	Kurtosis	13.24595448
Skewness	2.343650794	Skewness	3.013862475
Range	0.111754	Range	0.11149
Minimum	-0.012573	Minimum	-0.005497
Maximum	0.099181	Maximum	0.105993
Confidence Level(95.0%)	0.003729508	Confidence Level(95.0%)	0.003689599
Type 3		Type 4	
Mean	0.019758506	Mean	0.02045777
Standard Error	0.001545528	Standard Error	0.001551193
Median	0.017789	Median	0.019506
Standard Deviation	0.014415723	Standard Deviation	0.014468564
Sample Variance	0.000207813	Sample Variance	0.000209339
Kurtosis	6.181479128	Kurtosis	8.540481539
Skewness	1.74415205	Skewness	1.995288691
Range	0.086583	Range	0.098204
Minimum	-0.00386	Minimum	-0.005351
Maximum	0.082723	Maximum	0.092853
Confidence Level(95.0%)	0.003072405	Confidence Level(95.0%)	0.003083667

Table 30 Descriptive statistics of the T/QRS ratio peak using different filters (case oe102)

B.2.2 Effects on the T/QRS ratio trough

From Figure 155, with no filtering, there are marked episodes of negative T/QRS troughs which are caused by baseline shifts. With no filtering, this trace would be misleading and could indicate an abnormality this was not there. This case highlights

the problems when there is very little T peak or trough. Even with such good quality, the remaining noise is enough to induce false changes, which when accumulated, is misleading.

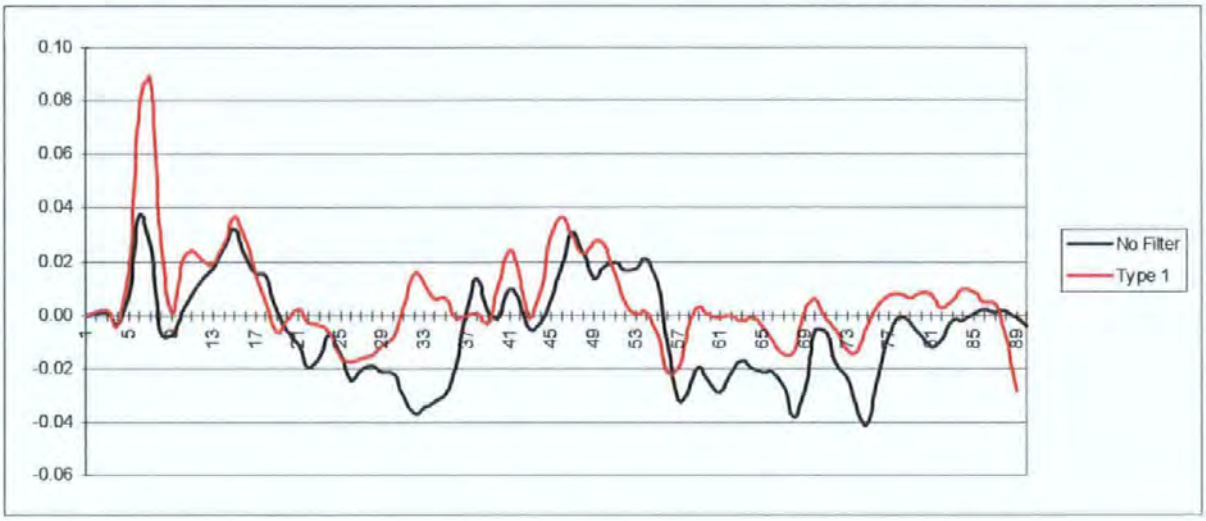

Figure 155 Case oe102: Plot of T/QRS Trough ratio with no filtering and with filter type 1

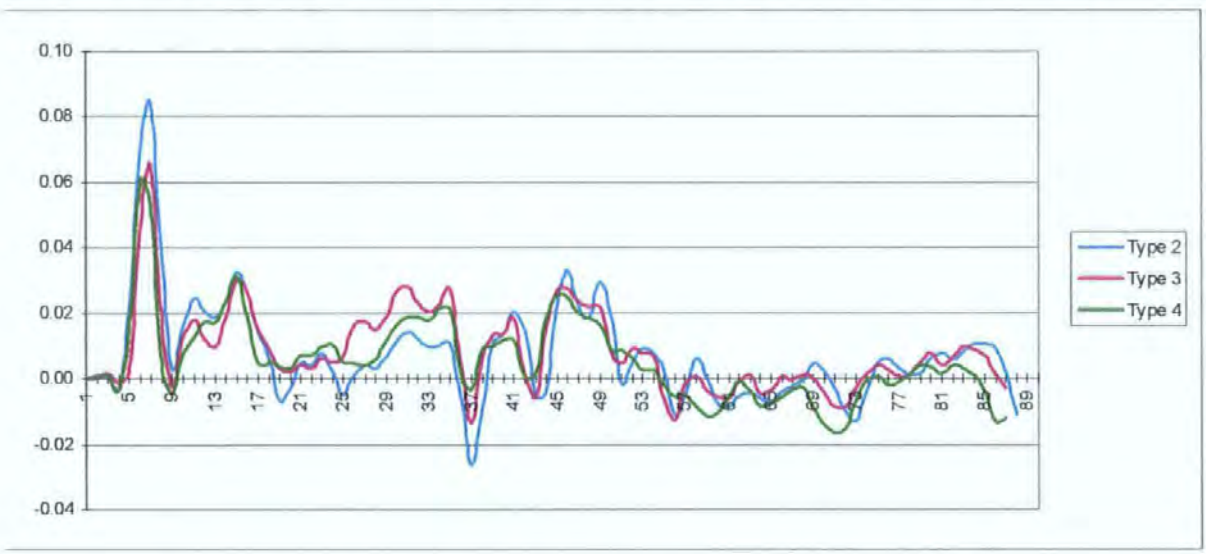

Figure 156 Case oe102: Plot of T/QRS Trough ratio for filters type 2,3 & 4

The correlation matrix in Table 31 illustrates similar relationships to those in Table 29, with a low correlation between the unfiltered and filtered features.

	No Filter	Type 1	Type 2	Type 3	Type 4
No Filter	1				
Type 1	0.659067	1			
Type 2	0.53088	0.88767	1		
Type 3	0.355506	0.721187	0.849335	1	
Type 4	0.465966	0.747707	0.798027	0.903293	1

Table 31 Correlation matrix for filter negative T/QRS trough : case oe102

Again, there is no clinically significant change in any of the feature statistics, which are given in Table 32.

Type 1		Type 2	
Mean	0.006173853	Mean	0.007592905
Standard Error	0.001885699	Standard Error	0.001686151
Median	0.002813	Median	0.005077
Standard Deviation	0.017588626	Standard Deviation	0.015727368
Sample Variance	0.00030936	Sample Variance	0.00024735
Kurtosis	6.715560944	Kurtosis	8.357761836
Skewness	1.957491528	Skewness	2.173749165
Range	0.109298	Range	0.111034
Minimum	-0.021138	Minimum	-0.02618
Maximum	0.08816	Maximum	0.084854
Confidence Level(95.0%)	0.003748642	Confidence Level(95.0%)	0.003351954
Type 3		Type 4	
Mean	0.008342203	Mean	0.005639383
Standard Error	0.001367914	Standard Error	0.001399356
Median	0.005358	Median	0.003646
Standard Deviation	0.01275905	Standard Deviation	0.013052324
Sample Variance	0.000162793	Sample Variance	0.000170363
Kurtosis	3.87419067	Kurtosis	4.074861468
Skewness	1.432463844	Skewness	1.420369416
Range	0.079004	Range	0.077449
Minimum	-0.013855	Minimum	-0.016733
Maximum	0.065149	Maximum	0.060716
Confidence Level(95.0%)	0.00271932	Confidence Level(95.0%)	0.002781825

Table 32 Descriptive statistics of the T/QRS ratio trough using different filters (case oe102)

B.3 Case oe108

Case 108 is a normal labour, but which demonstrates a rapid change in the T/QRS ratio at the very end of the recording. The quality of the data is very high and the foetal ECG waveform shape is normal throughout the duration of the labour.

2.3.1 Effects on the T/QRS ratio peak

A plot of the T/QRS ratio peak for no filter and type 1 filter is shown in Figure 157 and a plot for filter types 1-4 is shown in Figure 158.

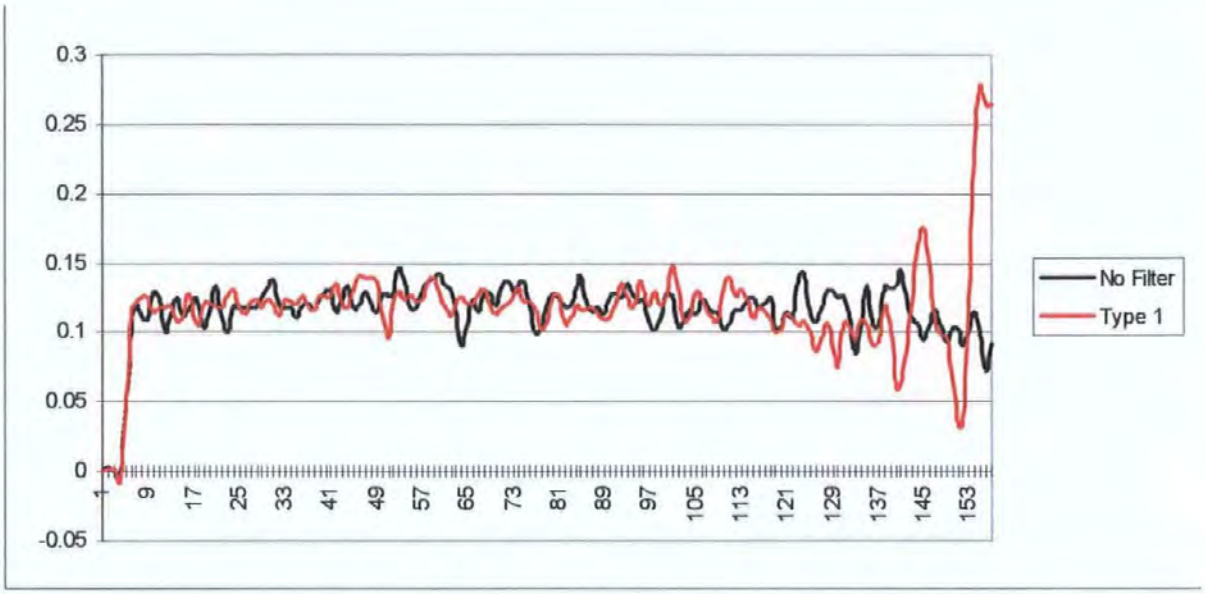

Figure 157 Case oe108: Plot of T/QRS peak ratio with no filtering and with filter type 1

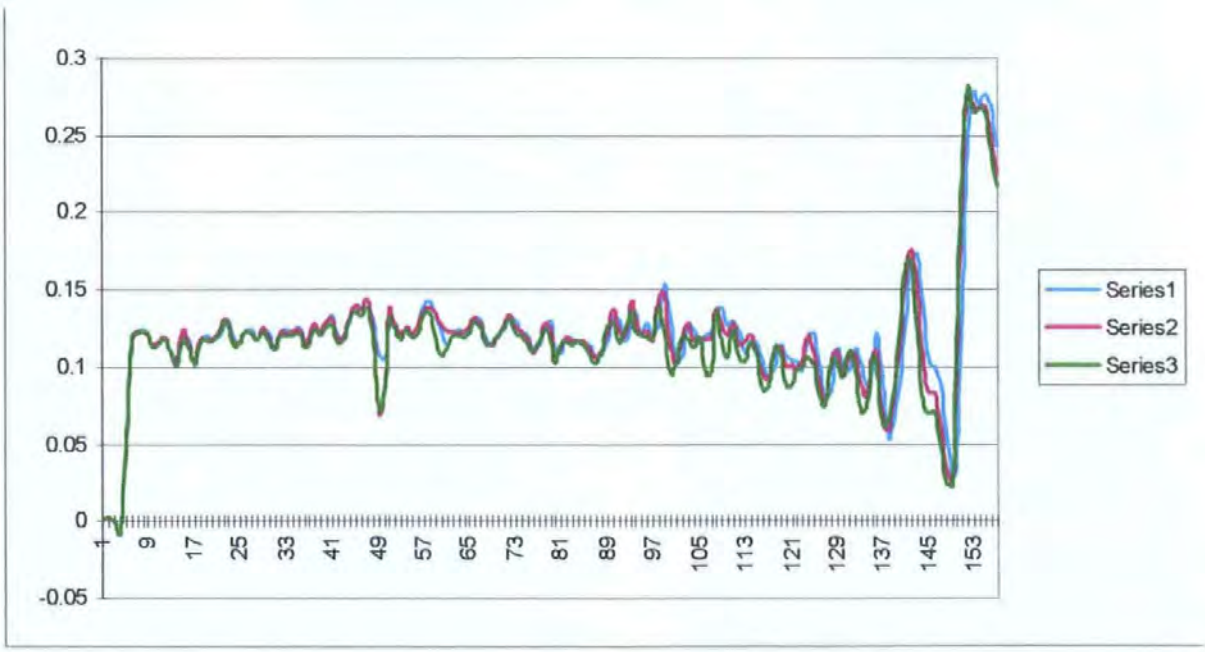

Figure 158 Case oe108: Plot of T/QRS peak ratio for filters type 2,3 & 4

	No Filter	Type 1	Type 2	Type 3	Type 4
No Filter	1				
Type 1	0.398663	1			
Type 2	0.325802	0.672317	1		
Type 3	0.342347	0.546639	0.952927	1	
Type 4	0.334454	0.503622	0.912917	0.986956	1

Table 33 Correlation matrix for filtered T/QRS peak : case oe108

Type 1		Type 2	
Mean	0.116518713	Mean	0.11902549
Standard Error	0.002813734	Standard Error	0.003156242
Median	0.118782	Median	0.120014
Standard Deviation	0.035255982	Standard Deviation	0.039547599
Sample Variance	0.001242984	Sample Variance	0.001564013
Kurtosis	8.749858784	Kurtosis	7.42030433
Skewness	0.559688647	Skewness	1.020350909
Range	0.284352	Range	0.284781
Minimum	-0.007137	Minimum	-0.007056
Maximum	0.277215	Maximum	0.277725
Confidence Level(95.0%)	0.005557929	Confidence Level(95.0%)	0.006234481
Type 3		Type 4	
Mean	0.118457917	Mean	0.114551586
Standard Error	0.003216119	Standard Error	0.003246265
Median	0.119271	Median	0.116592
Standard Deviation	0.040297852	Standard Deviation	0.040675585
Sample Variance	0.001623917	Sample Variance	0.001654503
Kurtosis	6.431116541	Kurtosis	6.394337989
Skewness	0.930757313	Skewness	1.068492393
Range	0.286215	Range	0.288124
Minimum	-0.007038	Minimum	-0.006981
Maximum	0.279177	Maximum	0.281143
Confidence Level(95.0%)	0.006352754	Confidence Level(95.0%)	0.006412302

Table 34 Descriptive statistics of the T/QRS ratio peak using different filters (case oe108)

2.3.2 Effects of the T/QRS ratio trough

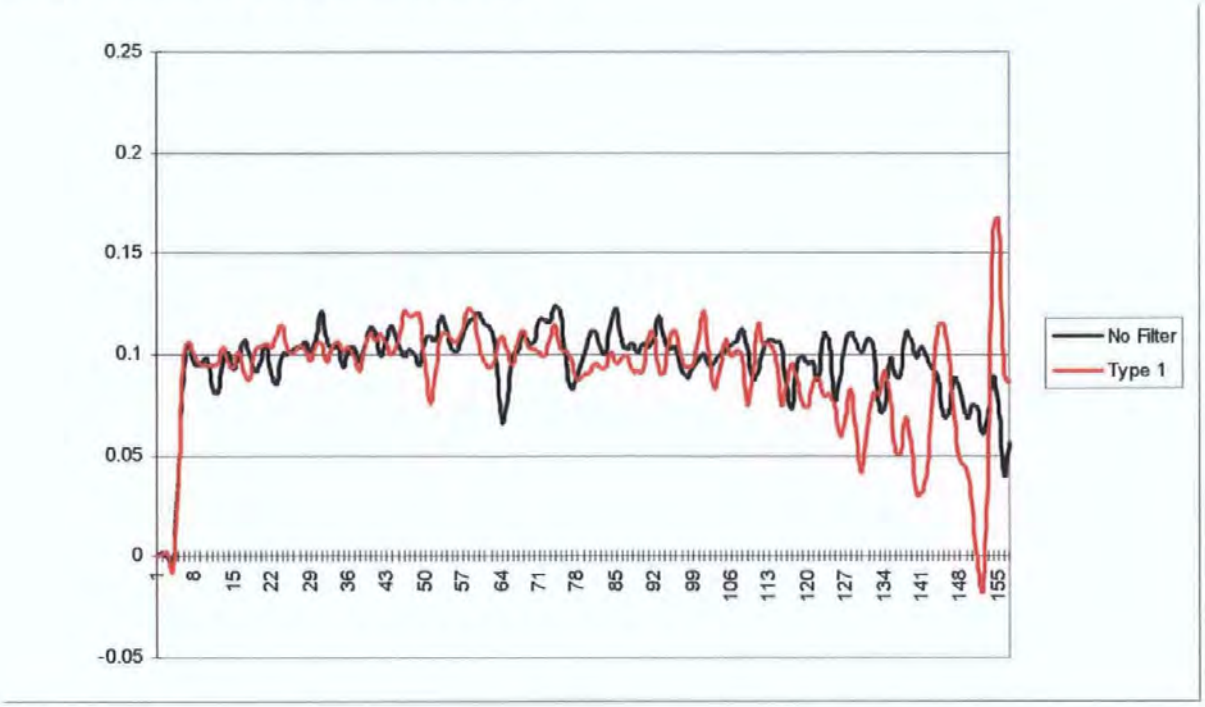

Figure 159 Case oe108: Plot of T/QRS trough ratio with no filtering and with filter type 1

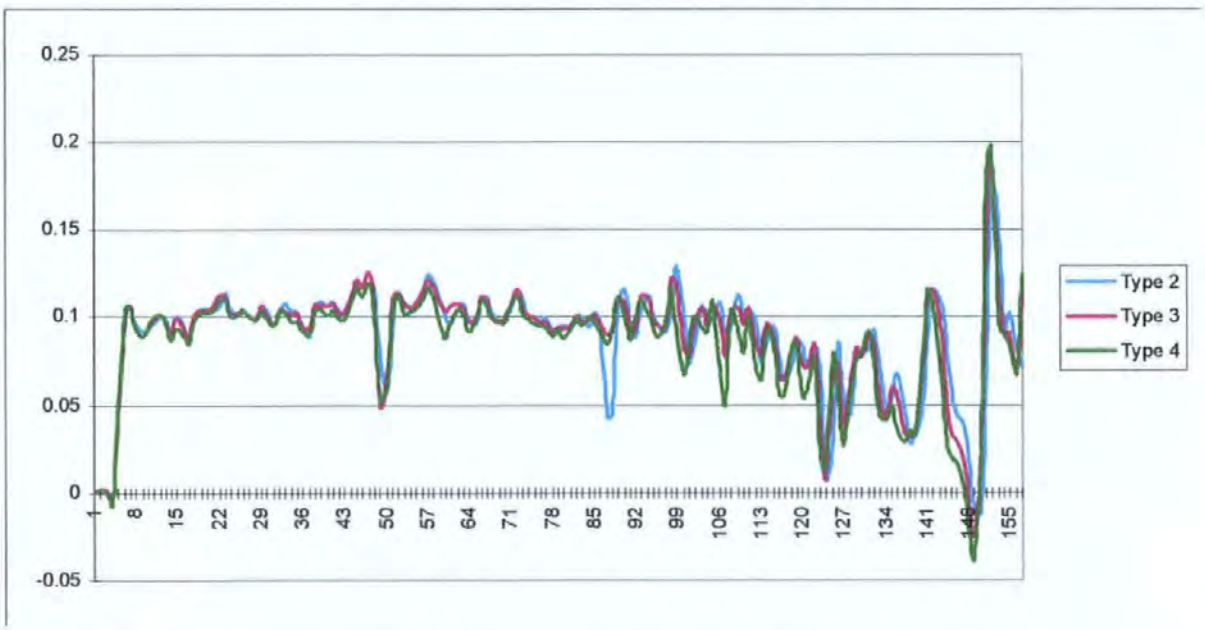

Figure 160 Case oe108: Plot of T/QRS Trough ratio for filters type 2,3 & 4

	No Filter	Type 1	Type 2	Type 3	Type 4
No Filter	1				
Type 1	0.573051	1			
Type 2	0.510451	0.523387	1		
Type 3	0.505498	0.41671	0.898088	1	
Type 4	0.447697	0.351757	0.811824	0.973498	1

Table 35 Correlation matrix for T/QRS trough using different filters : case oe108

Type 1		Type 2	
Mean	0.090352433	Mean	0.088883025
Standard Error	0.002245078	Standard Error	0.002392798
Median	0.097251	Median	0.098153
Standard Deviation	0.028130741	Standard Deviation	0.029981677
Sample Variance	0.000791339	Sample Variance	0.000898901
Kurtosis	3.761371915	Kurtosis	2.654629993
Skewness	-1.576675527	Skewness	-1.408003059
Range	0.183117	Range	0.185989
Minimum	-0.015755	Minimum	-0.011184
Maximum	0.167362	Maximum	0.174805
Confidence Level(95.0%)	0.00443467	Confidence Level(95.0%)	0.004726461
Type 3		Type 4	
Mean	0.08886642	Mean	0.084669401
Standard Error	0.002457715	Standard Error	0.002635573
Median	0.09813	Median	0.094937
Standard Deviation	0.030795076	Standard Deviation	0.033023634
Sample Variance	0.000948337	Sample Variance	0.00109056
Kurtosis	2.849487064	Kurtosis	2.71843099
Skewness	-1.369183609	Skewness	-1.023219364
Range	0.212304	Range	0.233654
Minimum	-0.02443	Minimum	-0.036949
Maximum	0.187874	Maximum	0.196705
Confidence Level(95.0%)	0.004854689	Confidence Level(95.0%)	0.00520601

Table 36 Descriptive statistics of the T/QRS ratio trough using different filters (case oe108)

B.4 Case oe111

OE111 is an important case as it demonstrates short and long periods of abnormal ST waveforms.

2.4.1 Assessing the effects on the T/QRS peak

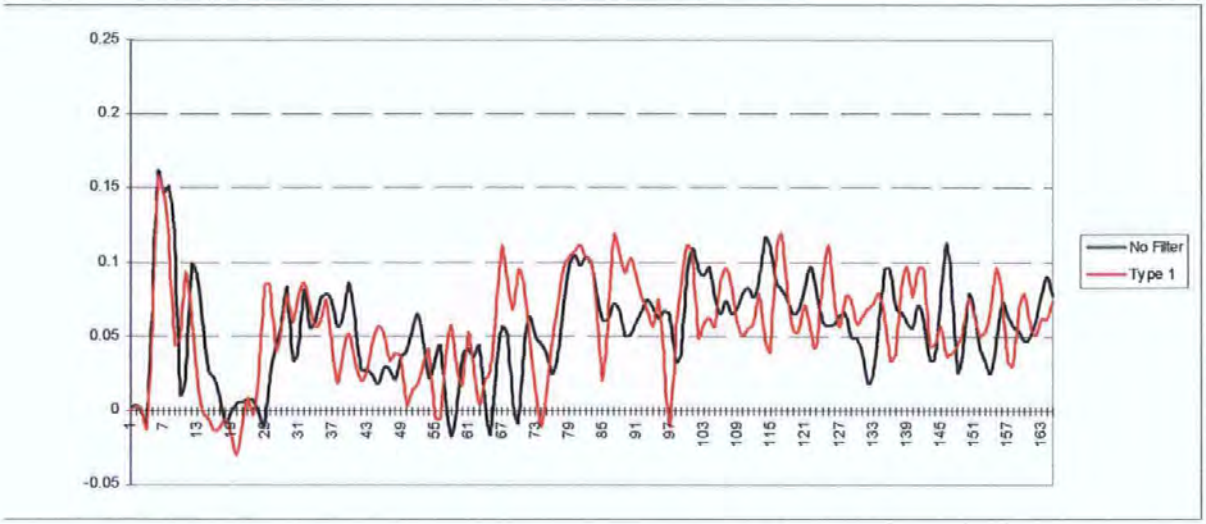

Figure 161 Case oe111: Plot of T/QRS peak ratio with no filtering and with filter type 1

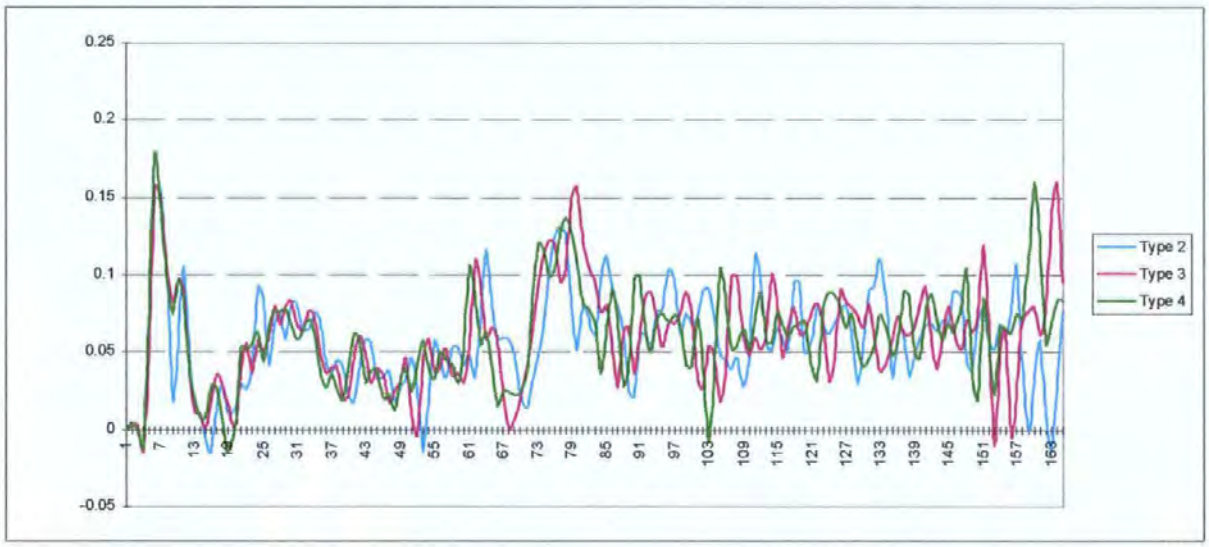

Figure 162 Case oe111: Plot of T/QRS peak ratio for filters type 2,3 & 4

	No Filter	Type 1	Type 2	Type 3	Type 4
No Filter	1				
Type 1	0.516495	1			
Type 2	0.328681	0.400913	1		
Type 3	0.445739	0.405298	0.443924	1	
Type 4	0.399778	0.429416	0.489854	0.647735	1

Table 37 Correlation matrix for T/QRS peak using different filters : case oe111

Type 1		Type 2	
Mean	0.055693127	Mean	0.057521848
Standard Error	0.002712783	Standard Error	0.002452365
Median	0.056289	Median	0.058773
Standard Deviation	0.034846325	Standard Deviation	0.031501204
Sample Variance	0.001214266	Sample Variance	0.000992326
Kurtosis	-0.091224307	Kurtosis	0.507044644
Skewness	-0.091609983	Skewness	0.20168774
Range	0.186595	Range	0.170311
Minimum	-0.029737	Minimum	-0.014452
Maximum	0.156858	Maximum	0.155859
Confidence Level(95.0%)	0.005356486	Confidence Level(95.0%)	0.004842283
Type 3		Type 4	
Mean	0.060318477	Mean	0.060055079
Standard Error	0.002634825	Standard Error	0.002513499
Median	0.060374	Median	0.060398
Standard Deviation	0.033844936	Standard Deviation	0.032286484
Sample Variance	0.00114548	Sample Variance	0.001042417
Kurtosis	0.663900007	Kurtosis	0.9750011
Skewness	0.439577645	Skewness	0.462593828
Range	0.17223	Range	0.191327
Minimum	-0.012956	Minimum	-0.014477
Maximum	0.159274	Maximum	0.17685
Confidence Level(95.0%)	0.005202555	Confidence Level(95.0%)	0.004962994

Table 38 Oe0111: Descriptive statistics of the T/QRS ratio peak using different filters

(case oe111)

B.4.2 Assessing the effects on the T/QRS trough

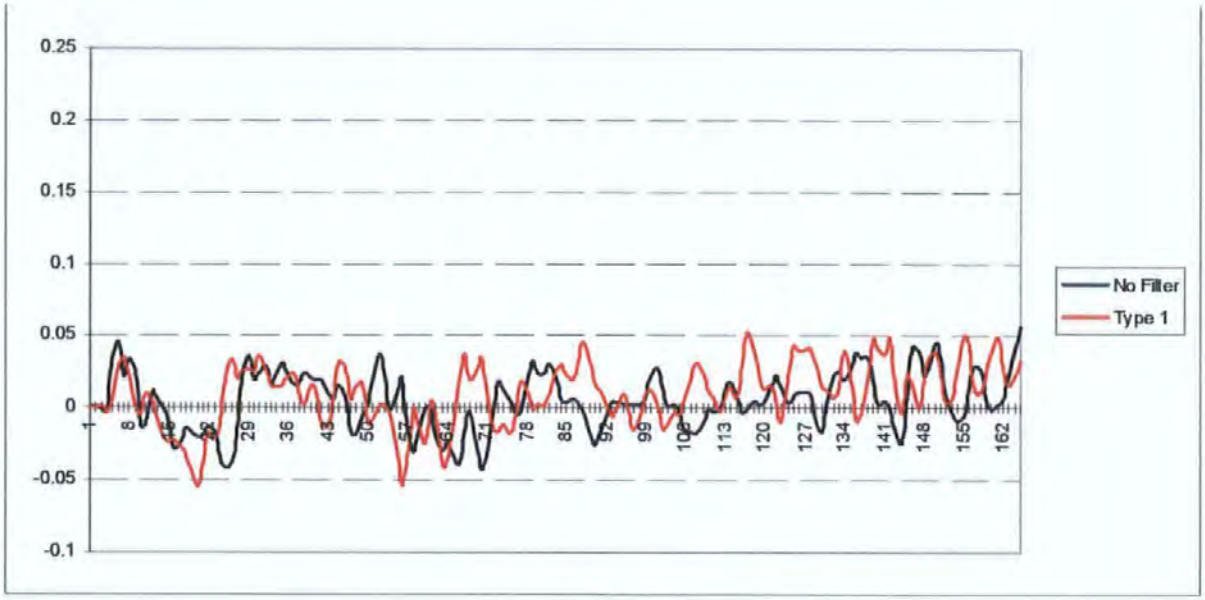

Figure 163 Case oe111: Plot of T/QRS trough ratio with no filtering and with filter type 1

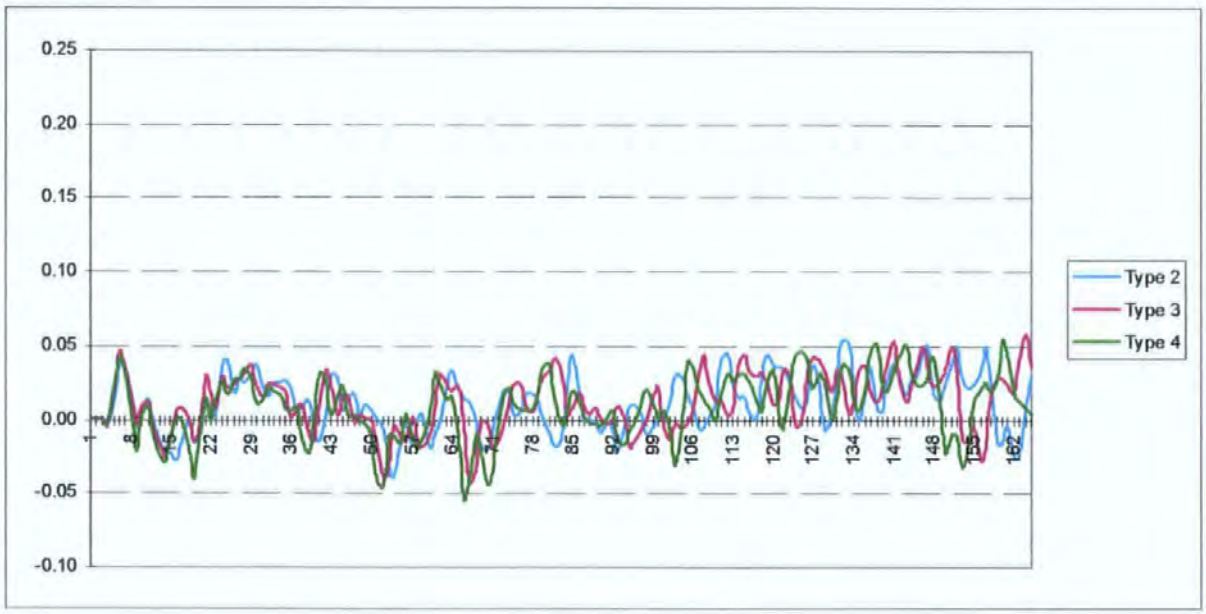

Figure 164 Case oe111: Plot of T/QRS trough ratio for filters type 2,3 & 4

	No Filter	Type 1	Type 2	Type 3	Type 4
No Filter	1				
Type 1	0.203923	1			
Type 2	0.250903	0.244768	1		
Type 3	0.26196	0.319688	0.334783	1	
Type 4	0.250567	0.292167	0.353329	0.55487	1

Table 39 Correlation matrix forT/QRS trough using different filters : case oe111

Type 1		Type 2	
Mean	0.009964298	Mean	0.011013845
Standard Error	0.001684585	Standard Error	0.001498521
Median	0.012046	Median	0.010456
Standard Deviation	0.021638887	Standard Deviation	0.019248848
Sample Variance	0.000468241	Sample Variance	0.000370518
Kurtosis	0.150374009	Kurtosis	-0.520799599
Skewness	-0.474495874	Skewness	-0.015881218
Range	0.108299	Range	0.091423
Minimum	-0.054885	Minimum	-0.038602
Maximum	0.053414	Maximum	0.052821
Confidence Level(95.0%)	0.003326273	Confidence Level(95.0%)	0.002958883
Type 3		Type 4	
Mean	0.012033214	Mean	0.008967278
Standard Error	0.001528621	Standard Error	0.001674083
Median	0.012714	Median	0.009932
Standard Deviation	0.019635495	Standard Deviation	0.021503979
Sample Variance	0.000385553	Sample Variance	0.000462421
Kurtosis	-0.334565491	Kurtosis	0.038809912
Skewness	-0.221611041	Skewness	-0.398884021
Range	0.099348	Range	0.107841
Minimum	-0.040916	Minimum	-0.053747
Maximum	0.058432	Maximum	0.054094
Confidence Level(95.0%)	0.003018317	Confidence Level(95.0%)	0.003305536

Table 40 Descriptive statistics of the T/QRS ratio trough using different filters (case oe111)

B.4.3 Effects on the ST segment peaks

The ST segment peaks are critical for quantifying the ST segment shape. Some variability is expected as the baseline noise is removed. With different filters, it is inevitable that the peak location algorithms select different points in the ST segment. A plot of these peak values for filters type 1-4 are shown below in Figure 165-Figure 168. This is for the whole of case oe00111. The trends in the data are very similar for all the different filters, although there are instantaneous differences. In Figure 167 and Figure 168, at times 59 and 65, and 68 minutes filter type 1 would imply there are negative components in peak 2. These are all induced by baseline noise and are removed with the more aggressive filtering. Figure 169 shows the average waveforms at 59 minutes. For filter type 1, the ST segment has dropped completely below the iso-electric level, which is enough to imply a negative ST segment (bi-phasic 3). At 80 minutes, all the waveforms demonstrate a negative peak 1 and peak2, which is verified as a depressed ST waveform (see Figure 170).

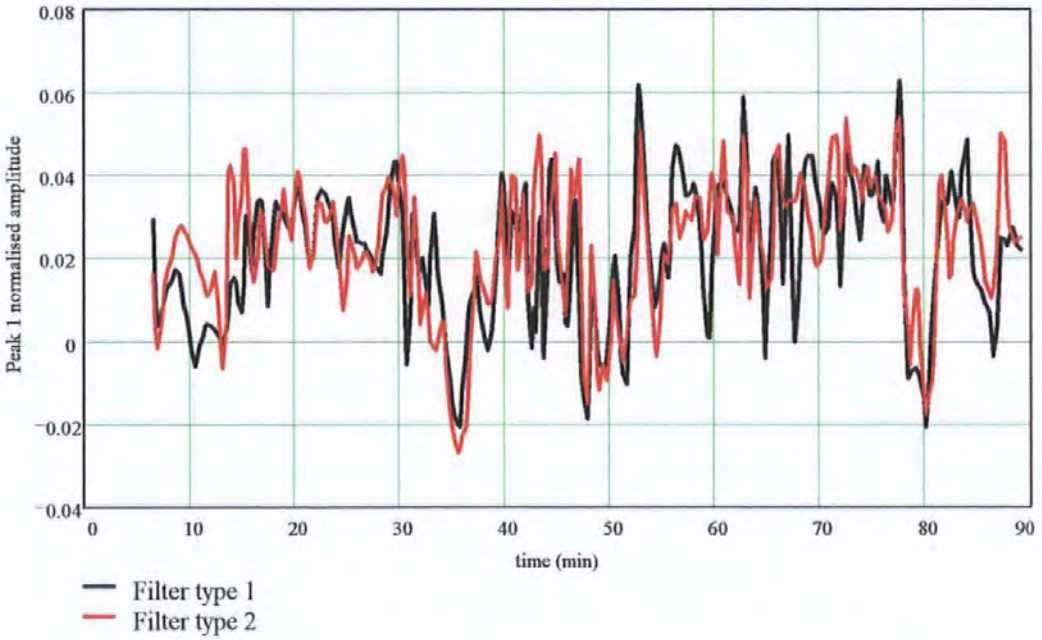

Figure 165 oe00111: ST segment peak 1 (Filter type 1 & 2)

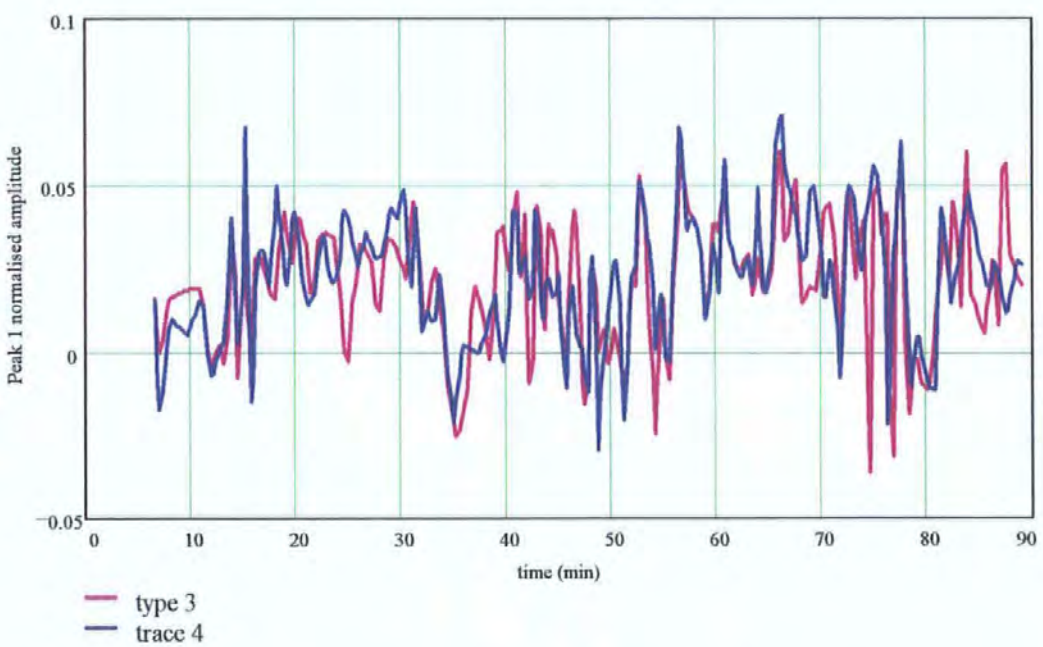

2.4.4

Figure 166 oe00111: ST segment peak 1 (filter type 3 & 4)

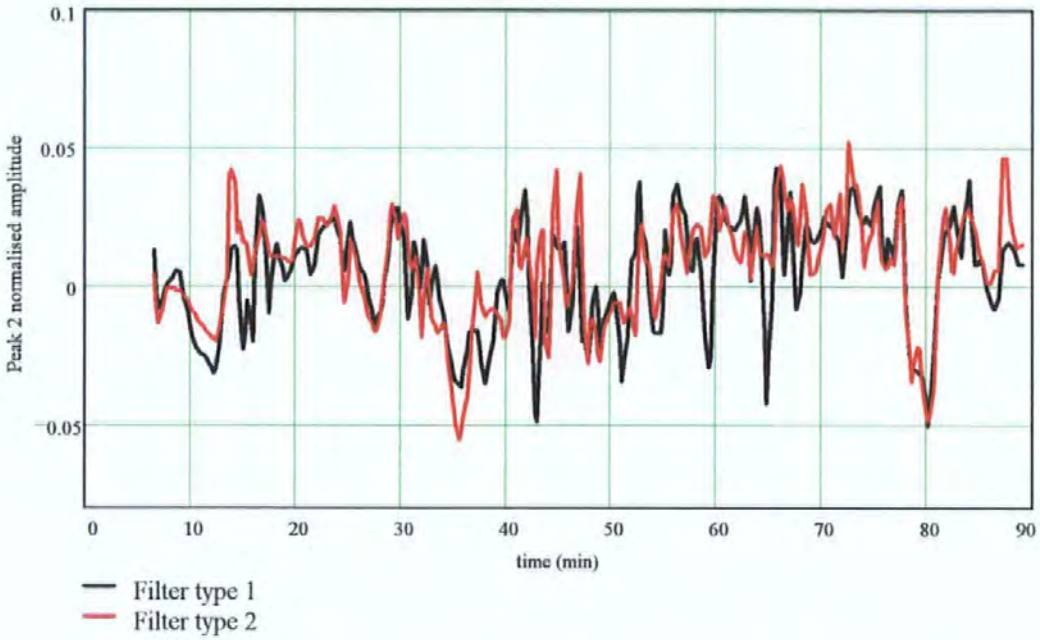

Figure 167 oe00111: ST segment peak 2 (Filter type 1 & 2)

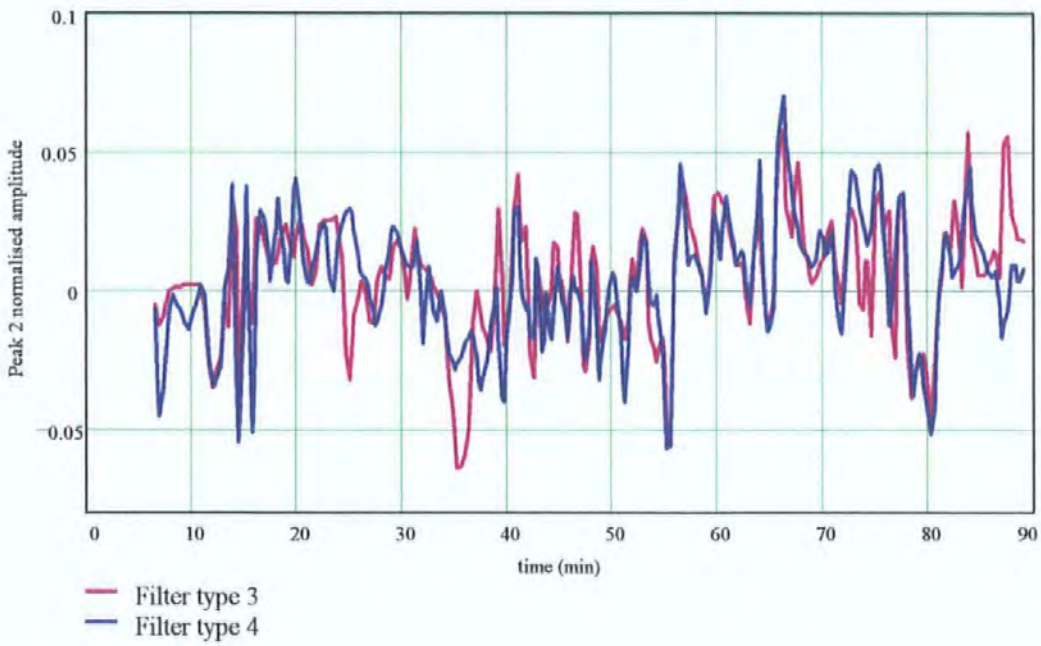

Figure 168 oe00111: ST segment peak 2 (Filter type 3 & 4)

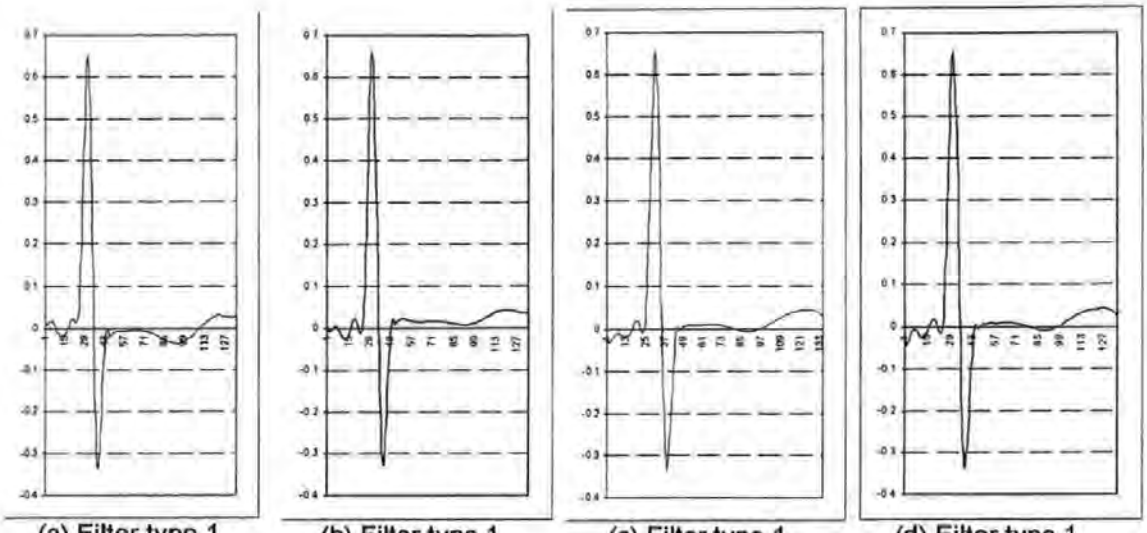

(a) Filter type 1 (b) Filter type 1 (c) Filter type 1 (d) Filter type 1

Figure 169

Table 41 and Table 42 show no significant bias being introduced into the features as the filters are made for aggressive. A change of 0.1 would in the mean and median would be considered significant, but is not observed. For these filters to suppress ST segment changes, a significant reduction in the standard deviation and range would be expected, which is not the case here. There is no clear trend in any of the statistics as the filters become more aggressive.

ST peak 1	Mean	Median	Standard Deviation	Range
Type 1	0.0172008	0.0177193	0.0142575	0.0835063
Type 2	0.0200725	0.0217115	0.0153863	0.0975796
Type 3	0.0184548	0.0192179	0.015613	0.0732048
Type 4	0.017585	0.0171409	0.016369	0.0882422

Table 41 Statistics for ST peak 1 with filter type 1-4

ST peak 2	Mean	Median	Standard Deviation	Range
Type 1	0.00067	0.0019571	0.0175995	0.0835063
Type 2	0.0022447	0.0038615	0.018615	0.0975796
Type 3	0.00002	0.0019748	0.0200506	0.1060827
Type 4	0.0021018	0.001369	0.0196616	0.094884

Table 42 Statistics for ST peak 2 with filter type 1-4

From a visual inspection of the filtered data, there is benefit in using the most aggressive possible.

There is no evidence to suggest that these filters suppress any ST waveform changes. It is important to note that this is based on the only currently available recorded case with depressed ST waveforms, and so should not be regarded as conclusive

evidence. More data with abnormal ST waveform changes will be required to suggest these filters are totally safe.

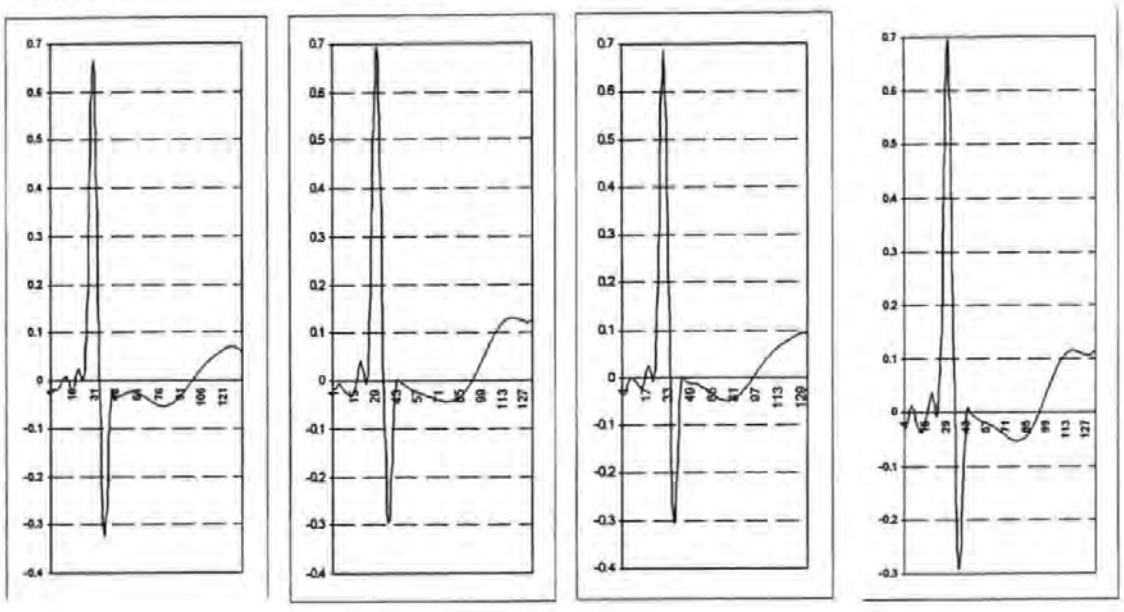

Figure 170 Depressed ST segment (and negativeT)

Appendix C

Comparison of techniques for assessing the signal-to-noise ratio

---

C. Signal to noise estimation

C.1 Computing and updating the average waveform

The individual ECG waveforms x(k) are detected by the QRS detection algorithm and extracted from the filtered data, where k is the number of waveforms detected. These waveforms are usually corrupted with noise cannot be used for detailed analysis. The standard used in the STAN® system to minimise the effects of random noise is to use a 30 beat average a(k), such that

$$a(k) = [\, x(k) + x(k-1) + \ldots + x(k-29) \,]/30 \qquad (C.1)$$

This algorithm is does not need to be re-computed each time a new ECG vector waveform is presented. Upon detecting the next R-peak, a signal vector x(k+1) is extracted from the filtered data and the average waveform is updated as follows.

$$a(k+1) = a(k) + [\, x(k+1)-x(0) \,] / 30 \qquad (C.2)$$

where x(k+1) is the next raw ECG waveform vector, a(k) is the current average ECG vector and a(k+1) is the next updated average ECG waveform vector. For the purpose of this work, each raw ECG waveform vector must have a zero mean and unit length such that

$$x(k)^T x(k)=1$$

$$\Sigma x(k)=0$$

C.2 Estimating the Signal-to-Noise Ratio of the ECG waveform

Given two sequential noise corrupted ECG waveform vectors $\mathbf{x}(k)$ and $\mathbf{x}(k+1)$, then it follows that

$$\mathbf{x}(k) = \mathbf{s} + \mathbf{n}(k)$$
$$\mathbf{x}(k+1) = \mathbf{s} + \mathbf{n}(k+1)$$

where $\mathbf{s}$ is the pure signal vector, $\mathbf{n}(k)$ and $\mathbf{n}(k+1)$ are two noise signals. The following assumptions are made.

1. *The signal is stationary*

   The signal vector does not change with time, such that $\mathbf{s}(k) = \mathbf{s}(k+1) = \mathbf{s}$

2. *The noise is random*

   The noise is zero mean and uncorrelated in time, such that $\mathbf{n}(k)^T\mathbf{n}(k+1)=0$, which based on the assumption that the noise is random.

3. *The noise is uncorrelated with the signal.*

   $\mathbf{s}^T\mathbf{n}(k)=0$. This assumes that the noise is random. This assumption would not necessarily hold for very low-frequency noise.

Given these assumptions above it follows that the inner product of each ECG waveform vector equals the signal power plus the noise power, that is

$$\begin{aligned}\mathbf{x}(k)^T\mathbf{x}(k) &= (\mathbf{s} + \mathbf{n}(k))^T(\mathbf{s} + \mathbf{n}(k)) \\ &= \mathbf{s}^T\mathbf{s} + 2\mathbf{s}^T\mathbf{n}(k) + \mathbf{n}(k)^T\mathbf{n}(k) \\ &= \sigma_s^2 + \quad 0 \quad + \sigma_n^2(k) \qquad\qquad (C.3)\end{aligned}$$

where σ_s^2 is the signal power and σ_n^2 is the noise power. Similarly, $\mathbf{x}(k+1)^T\mathbf{x}(k+1) = \sigma_s^2 + \sigma_n^2(k+1)$. Given that each ECG signal vector $\mathbf{x}$ is normalised to unit length, then it follows that

$$\sigma_s^2 + \sigma_n^2(k) = 1$$

and

$$\sigma_s^2 + \sigma_n^2(k+1)=1$$

It also follows that the inner-product of x(k) and x(k+1) equals the signal power, that is

$$\begin{aligned} \mathbf{x}(k)^T\mathbf{x}(k+1) &= (\mathbf{s} + \mathbf{n}(k))^T(\mathbf{s} + \mathbf{n}(k+1)) \\ &= \mathbf{s}^T\mathbf{s} + \mathbf{s}^T\mathbf{n}(k) + \mathbf{s}^T\mathbf{n}(k+1) + \mathbf{n}(k)^T\mathbf{n}(k+1) \\ &= \sigma_s^2 + 0 + 0 + 0 \end{aligned} \qquad \text{(C.4)}$$

From (C.C.3) and (C.C.4) it follows that

$$\begin{aligned} \sigma_n^2(k) &= \mathbf{x}(k)^T\mathbf{x}(k) - \mathbf{x}(k)^T\mathbf{x}(k+1) \\ &= 1 - \mathbf{x}(k)^T\mathbf{x}(k+1) \end{aligned}$$

therefore

$$\begin{aligned} SNR &= \sigma_s^2 / \sigma_n^2(k) \\ &= \mathbf{x}(k)^T\mathbf{x}(k+1) / [\,1 - \mathbf{x}(k)^T\mathbf{x}(k+1)\,] \end{aligned} \qquad \text{(C.5)}$$

For this work, it is the signal-to-noise ratio of the average waveform a(k) that is most important and not any constituent pair of waveforms. For an ensemble of waveforms x(k), *k=0..29*, that constitute the average waveform in (C.C.1), all combinations of the inner-product pairs can be computed as follows to give the average signal-to-noise ratio (SNR_{av}) as follows.

$$SNR_{av} = r / (1-r/M) \qquad \text{(C.6)}$$

where $r = \Sigma_{i=1..29}\,\Sigma_{j=0..i-1}\,\mathbf{x}(i)^T\mathbf{x}(j)$ and $M = \sum_{i=0}^{N-1} i$, *where* $N = 30$

To compute (C.C.6) directly is time consuming, but can easily be derived from the average waveform a(k) itself as follows. Taking the inner product of the average waveform $\mathbf{a(k)}^T\mathbf{a(k)}$

$$\begin{aligned}\mathbf{a(k)}^T\mathbf{a(k)} &= (1/30) \cdot (1/30) \cdot [\mathbf{x}(0)+\mathbf{x}(1)+ \ldots +\mathbf{x}(29)] \cdot [\mathbf{x}(0)+\mathbf{x}(1)+ \ldots +\mathbf{x}(29)]^T \\ &= (1/30) \cdot (1/30) \cdot \Sigma_{i=0..29}\, \Sigma_{j=0..29}\, \mathbf{x}(i)^T\mathbf{x}(j) \\ &= (1/30) \cdot (1/30) \cdot [\, 2r + \Sigma_{i=0..29}\, \mathbf{x}(i)^T\mathbf{x}(i)\,] \\ &= (1/30) \cdot (1/30) \cdot [\, 2r + 30]\end{aligned}$$

Solving for r gives

$$r = [\, [\, \mathbf{a(k)}^T\mathbf{a(k)} \cdot 30^2\,]-30\,] / 2$$

Therefore $\quad SNRav = r / (1-r/M) \qquad (C.7)$

$$M = \sum_{i=0}^{N-1} i, \; where \; N = 30$$

The following is a MathCad Script used to demonstrate and test the two different signal-to-noise ratio estimation techniques.

C.3 MATHCAD SCRIPTS

Estimation of the Signal-to-Noise Ratio (SNR)

Number of vectors in the Ensemble $N := 50$

Length of the vectors $M := 100$

$j := 0..N-1 \quad i := 0..M-1$

Signal Amplitude $A := \frac{1}{20}$

The Signal $s_i := \mathrm{mod}(i, 20) \cdot A$

The noise $n_{i,j} := rnd(2) - 1 \qquad sbar := mean(s)$

The true signal power $\sigma_s := \left| \frac{(s - sbar)^T \cdot (s - sbar)}{M} \right|$ $\sigma_s = 0.083$

The true noise power $\sigma_n := \left| \frac{1}{N \cdot M} \cdot \left(\sum_j n^{\langle j \rangle T} \cdot n^{\langle j \rangle} \right) \right|$ $\sigma_n = 0.338$

The true signal-to-noise ratio (SNR) in dB

$10 \cdot \log\left(\frac{|\sigma_s|}{|\sigma_n|} \right) = -6.094$

Superposition of the noise and signal $X^{\langle j \rangle} := s + n^{\langle j \rangle}$

Subtract the mean from each vector $X^{\langle j \rangle} := X^{\langle j \rangle} - \text{mean}\left(X^{\langle j \rangle}\right)$

Normalise each vector to unit length $X^{\langle j \rangle} := \frac{X^{\langle j \rangle}}{|X^{\langle j \rangle}|}$

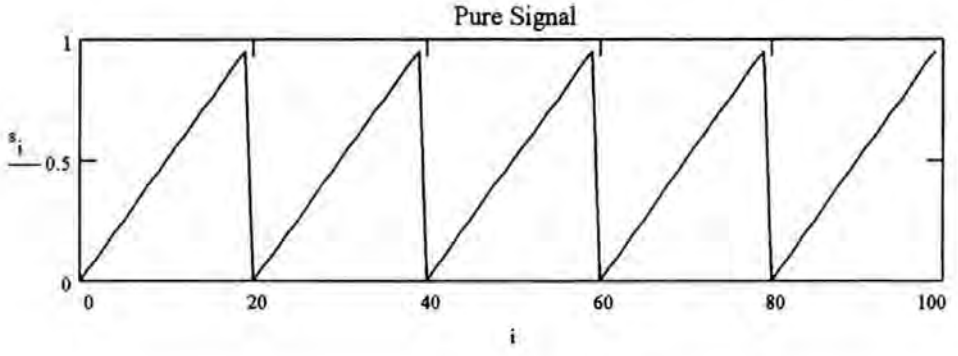

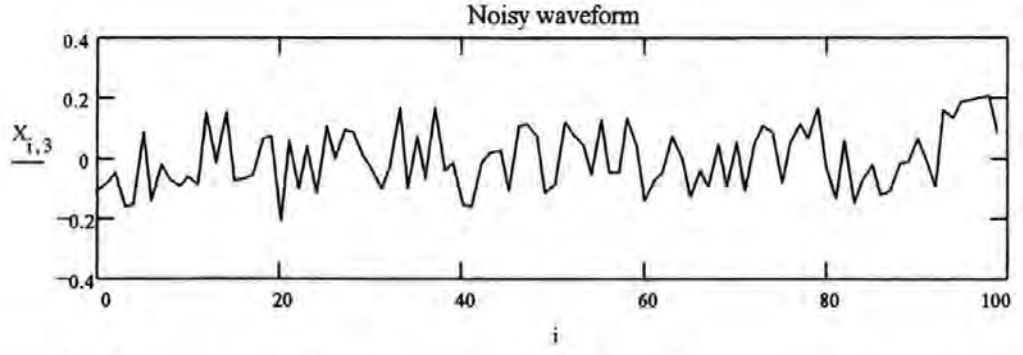

$\lambda := \text{reverse}\left(\text{sort}\left(\text{eigenvals}\left(X^T \cdot X\right)\right)\right)$ $ev := \text{eigenvec}\left(X \cdot X^T, \lambda_0\right)$

$\lambda^T =$

	0	1	2	3	4	5	6	7	8
0	10.825	2.072	2.007	1.965	1.806	1.659	1.56	1.54	1.431

$\sum \lambda = 50$ $\frac{\lambda_0}{\sum \lambda} = 0.217$ $1 - \frac{\lambda_0}{\sum \lambda} = 0.783$

$10 \cdot \log\left(\frac{\lambda_0}{N - \lambda_0} \right) = -5.586$ **dB**

Estimate signal-to-noise ratio $\sqrt{\frac{\lambda_0}{N-\lambda_0}} = 0.526$ $10\log\left(\frac{\sigma_s}{\sigma_n}\right) = -6.094$ dB

Actual signal-to-noise ratio $\sqrt{\frac{\sigma_s}{\sigma_n}} = 0.496$

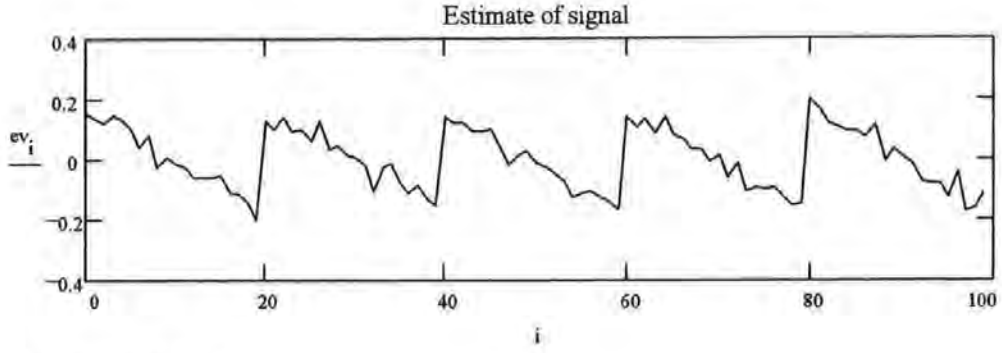

Correlation method

$R := X^T \cdot X$ $\sum_j R_{j,j} = 50$

$$Sall := \left(\sum_{r=0}^{N-1} \sum_{c=0}^{N-1} R_{r,c} - N \right) \cdot \frac{1}{N \cdot N - N} \quad Sall = 0.197$$

Estimated signal-to-noise ratio $\sqrt{\frac{Sall}{1-Sall}} = 0.495$ $10\log\left(\frac{Sall}{1-Sall}\right) = -6.111$ dB

C.3.1 Results

The signal amplitude A, as shown above, is increased from 0.05 to 5, without changing the noise component. Table 43 compares the true signal-to-noise ratio (SNR) with the estimates for the eigen-analysis technique and the cross-correlation technique.

Signal Amplitude A	True SNR (dB)	Eigen-analysis	Cross-correlation
0.05	-32.115	-12.682	-33.157
0.5	-12.115dB	-10.425	-12.164
1	-6.094	-5.586	-6.111
2	-0.073	0.135	-0.057
3	3.449	3.615	3.483
5	7.885	8.038	7.935

Table 43 Comparison of SNR estimation using different techniques

For high SNR, both techniques work acceptably well but with low SNR, the eigen-analysis predictably has poor accuracy.

Appendix D

Clinical Guidelines

D. Clinical guidelines

ST pattern verified from ECG complexes.	Physiological background	Clinical Implication
T/QRS 0-0.24	Unstressed heart- no need for additional energy from stored glycogen.	The fetus is capable of handling the strain of labour.
T/QRS > 0.24 Constant level	The fetal heart is stimulated by adrenaline released due to the general arousal caused by labour or by hypoxia.	Normal when combined with a reactive CTG non reactive CTG - a sign of fetal distress.
Increasing T/QRS >0.24 for < 5 min.	Hypoxic episode where the degree of change in T/QRS and duration inform about severity. Note that glycogen has been utilized and the ability to handle another episode of hypoxemia may be less.	An episode of compensated fetal stress.
Increasing T/QRS >0.24 and maintain	Acute hypoxia where the fetus uses its defence systems e.g. myocardial glycogenolysis.	A sign of compensated fetal distress. Intervention will depend on FHR pattern
Increasing T/QRS >0.5.	Acute severe hypoxia where the fetus is compensating maximally	Immediate action is needed regardless of FHR.
bi-phasic or negative waves. Constant pattern > 20 min.	The fetal heart is unable to fully respond hypoxia. Risk for myocardial depression decreased pumping capacity. Note this pattern may be seem more frequently in the immature fetus which does not react as vigorously with high T waves.	These are term fetuses that may very easily become asphyxiated if the strain of labour persists.
Appearance of negative T/QRS .	This could be an acute hypoxia where the fetus is unable to activate its defence systems. The fetus does not react with arousal in response to hypoxemia.	If appearing during a bradycardia - a sign of threatening cardiovascular collapse .

Table 44 Summary of guidelines for ST waveform analysis in the term fetus

CTG pattern	Physiological background	Clinical implication
Normal reactive	Optimal reflex control of the cardiovascular system.	The impression of a normal FHR is reinforced by a normal ST waveform.
Intermediate	Unclean pattern where different reflex systems starts to be activated.	If normal ST waveform - no intrapartum asphyxia
Abnormal	This group contains FHR patterns which originate from the activation of different reflex pathways. These situations are exemplified below.	The FHR pattern as such does not allow quantification of degree of hypoxemia. Additional information from ST analysis or fetal blood samples is needed. If both FHR and ST changes - more substantial hypoxia with development of metabolic acidosis.
Persistent declarations	Persistent declarations are problematic as they usually are harmless but occasionally appear pre-terminal. If a bradycardia persists there will also be a secondary hypoxemia due to decreased cardiac output and placental blood flow. A physiologic bradycardia may thus develop into a pathologic.	If normal ST - no myocardial hypoxia and clinical action should be directed towards eliminating posture related decrease in maternal placental blood flow. If ST changes develop the type of change will guide clinical management.
Late declarations	Late declarations are a sign of contraction-induced hypoxemia and chemoreceptor activation. An increase in fetal blood pressure may also play an important part. Usually the hypoxemic phase is short lasting and of a magnitude which does not affect the fetal heart or the brain.	If normal ST - the degree of hypoxia is not affecting the high priority organs. Acidosis may develop if an abnormal CTG pattern like this persists over hours. If ST changes - more substantial hypoxia with development of met. acidosis.
Variable declarations	A sign of cardiovascular adaptation to cord compression. Any such reflex bradycardia will also have a decrease in cardiac output and reduced peripheral blood-flow. This will lead to the accumulation of C02 but also to some lactic acid generation by the peripheral tissues. The rate of change in FHR may indicate the capacity of the cardiovascular system to adjust.	Provided cord blood flow is restored as identified by a rapid return of FHR these episodes should be of little significance. The additive effect of repeated declarations during 2nd stage will cause a mixed acidosis. If declarations with ST changes - more significant hypoxia.
Increased baseline fetal heart rate variability	An increased variability should be a sign of a general activation of different reflexes. This can be seen during the initial phase of hypoxaemia.	May not be that significant on its own.
Decreased baseline fetal heart rate variability or an undulating (saltatory) pattern	A reduced variability may appear normally due to sedation or low activity sleep state. If persistent loss of variability especially with ST waveform changes hypoxemia is affecting the ability of the fetus to modulate the cardiovascular system. A silent pattern may be the only sign of chronic hypoxia. An undulating (saltatory) pattern may occur in a situation where the cardiovascular control is markedly reduced.	Persistently reduced variability should mean asphyxia unless otherwise proven. Chronic hypoxemia may cause a very shallow reaction not only from FHR but also from ST. Look for trends of increasing T/QRS over hours. Use scalp acid base sampling. Watch for ST depression

Table 45 Summary of guidelines for CTG

STwaveform / CTG	Changing ST Waveform T/QRS > 0.24, constant pattern with no ST Depression.	T/QRS > 0.24, constant pattern.	Changing ST waveform T/QRS > 0.24 and maintained	Changing ST waveform T/QRS >0.24 for limited period	Changing ST waveform T/QRS >0.5 and increasing.	Neg. T/QRS with ST depression and/or neg. T. Constant Pattern.	Acute change with neg. T/QRS, ST depression and/or neg. T
Normal	No hypoxia. Cont vag delivery	Fetal arousal. Cont. vag delivery	Compensated moderate hypoxia. Cont. vag delivery	Compensated moderate hypoxia. Cont. vag delivery	Marked acute hypoxia. immediate delivery	Hypoxia with inadequate response. FBS or delivery	Risk for hypoxia with inadequate fetal response.
Intermediate	No hypoxia. Cont. vag delivery	Compensated moderate hypoxia. FBS or op delivery.	Compensated mode rate hypoxia. FBS or op delivery	Compensated moderate hypoxia. Cont. vag delivery	Marked acute hypoxia. immediate delivery	Hypoxia with inadequate response. FBS or delivery	Hypoxia with inadequate response. FBS or delivery
Abnormal	If > 60 min. - FBS.	Compensated moderate hypoxia. FBS or op delivery.	Compensated moderate hypoxia. FBS or op delivery.	If both ST and FHR improve - cont. vag delivery	Marked acute hypoxia. Immediate delivery	Hypoxia with inadequate response. Immediate delivery	Hypoxia with inadequate response. Immediate delivery
Persistent decel.	No initial hypoxia. Watch closely	Decompensate d hypoxia. Immediate delivery	Compensated moderate hypoxia. FBS or op delivery.	If both ST and FHR improve - cont. vag delivery	Marked acute hypoxia. immediate delivery	Decompensated hypoxia. Immediate delivery	Decompensated hypoxia. Immediate delivery
Late decel.	If > 60 min. - FBS.	Compensated moderate hypoxia. FBS or deliver	Compensated moderate hypoxia. FBS or, delivery	If both ST and FHR improve - cont. vag delivery else FBS.	Marked acute hypoxia. immediate delivery	Hypoxia with inadequate response. Immediate delivery	Hypoxia with inadequate response. Immediate delivery
Variable decel.	If > 60 min. - FBS.	Compensated moderate hypoxia. FBS or op delivery.	Compensated moderate hypoxia. FBS or op delivery.	If both ST and FHR improve - cont. vag delivery else FBS.	Marked acute hypoxia. Immediate delivery	Hypoxia with inadequate response. Immediate delivery	Risk for hypoxia with inadequate fetal response.
Increased variability	No hypoxia. Cont. vag delivery	Fetal arousal. Cont. vag delivery	Compensated moderate hypoxia. Cont. vag delivery	Compensated moderate hypoxia. Cont. vag delivery	Marked acute hypoxia. Immediate delivery	Hypoxia with inadequate response. FBS or delivery	Risk for hypoxia with inadequate fetal response.
Decr. Variability or undulating (saltatory) FHR	Watch for chron hypoxia -FBS	Decompensate d hypoxia. immediate delivery	Decompensated hypoxia. I mediate delivery	Risk for chron hypoxia. FBS.	Marked acute hypoxia. Immediate delivery	Decompensated hypoxia. Immediate delivery	Decompensated hypoxia. Immediate delivery

Table 46 Summary of guidelines for combined ECG and CTG interpretation

Appendix E

Fuzzy Sets

E. Fuzzy Sets

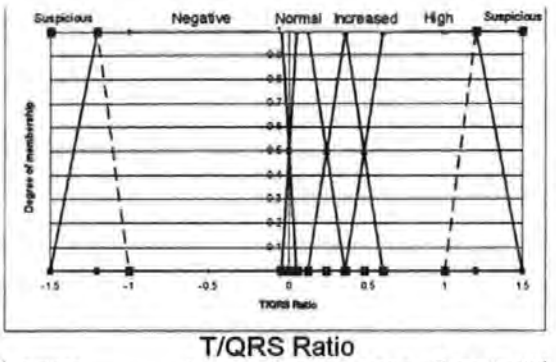

T/QRS Ratio

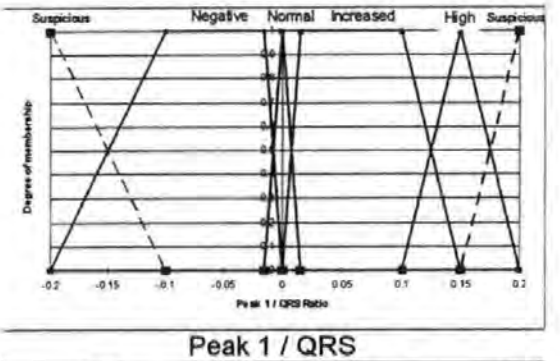

Peak 1 / QRS

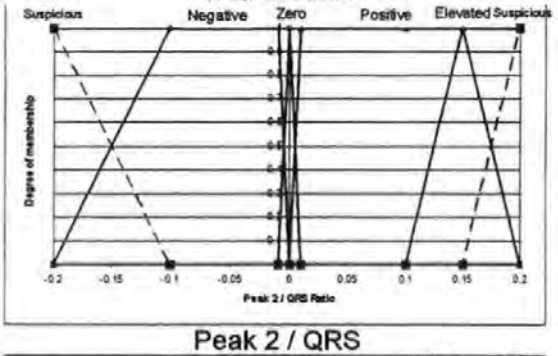

Peak 2 / QRS

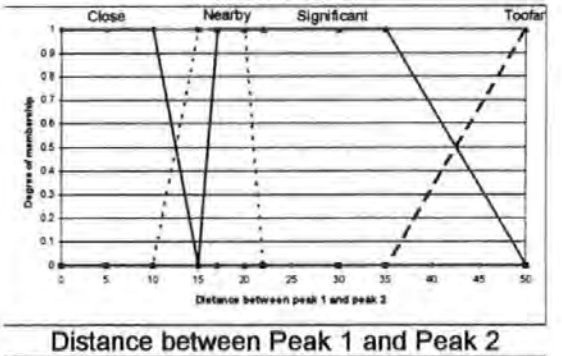

Distance between Peak 1 and Peak 2

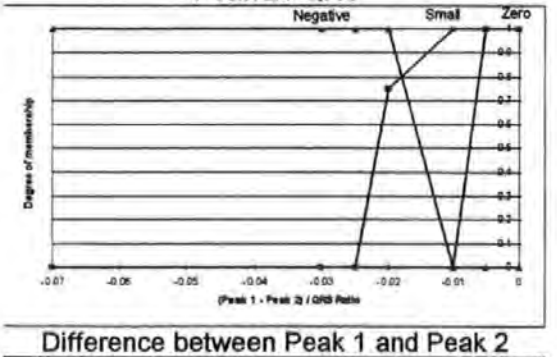

Difference between Peak 1 and Peak 2

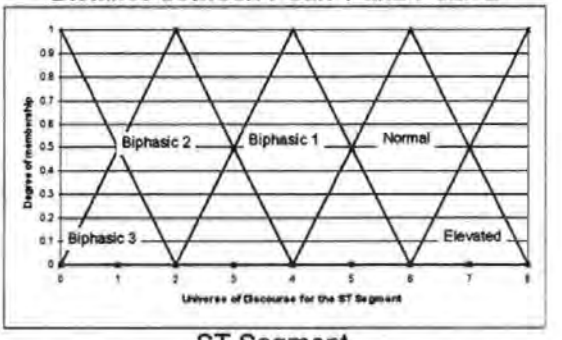

ST Segment

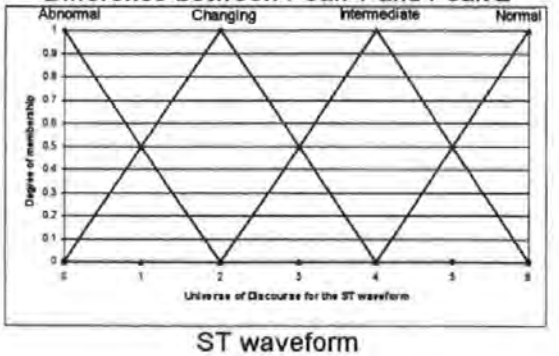

ST waveform

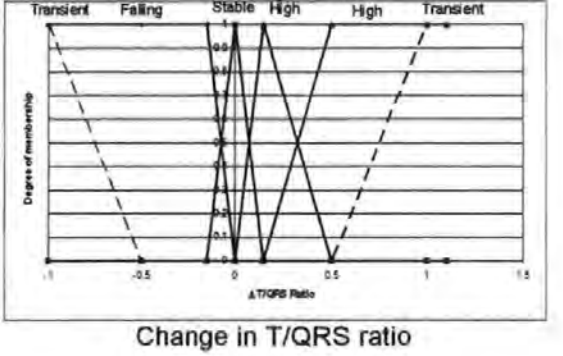

Change in T/QRS ratio

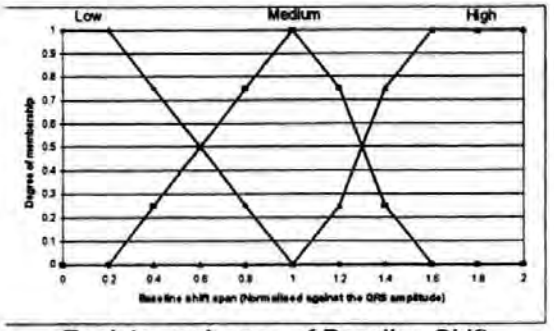

Peak to peak span of Baseline Shift

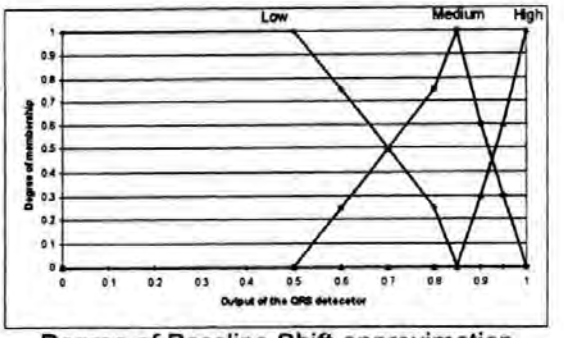

Degree of Baseline Shift approximation

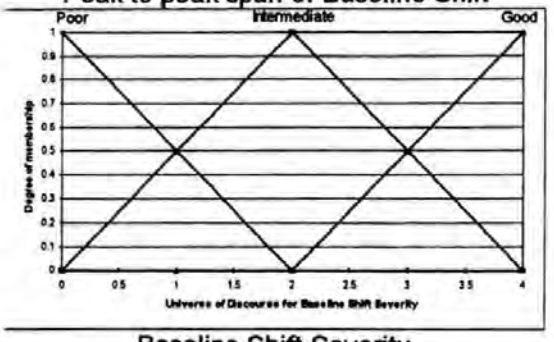

Baseline Shift Severity

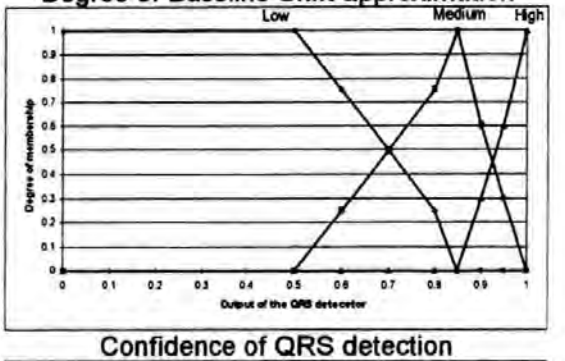

Confidence of QRS detection

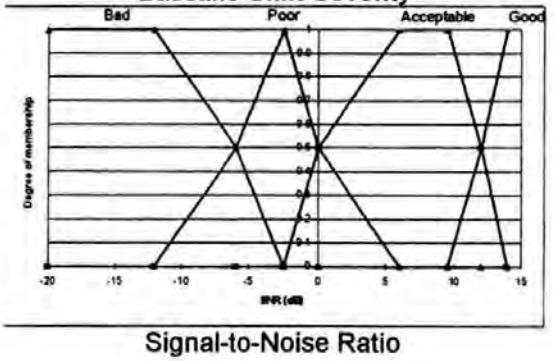

Signal-to-Noise Ratio

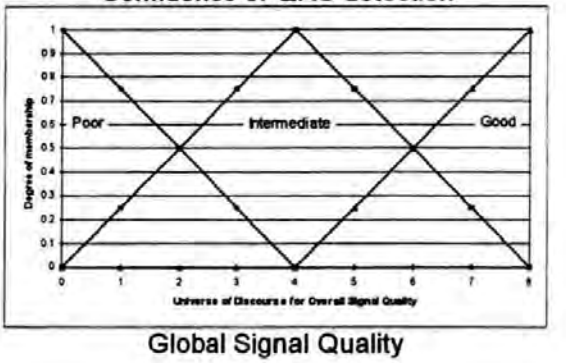

Global Signal Quality

Appendix F

Fuzzy rules

F. Fuzzy rules

An example of the fuzzy rules are given below. These rules for are for assessing the ST waveform shape (as described in chapter 6) and are implemented in C^{++} . The full source code is published in a separate complimentary volume.

```
void fes::rules()
{
      //Apply rules to get truth values for (A..I)
      //Assess CTG
      CTG.Normal<=(BLHR.Normal && HRVAR.Normal);
      CTG.Intermediate<=
            (BLHR.Intermediate && (HRVAR.Normal || HRVAR.High));
            CTG.Abnormal<=(BLHR.Abnormal || HRVAR.High.verytrue() ||
            HRVAR.Low);

      //This line is used because ECG complexes merge at very high Heart
      Rate (normally applies to sheep data only)
      if (blhr4 > 200) return;

      //Assess instantaneous ST Segment shape
      STSHAPE.Normal<=
            ((STPEAK1.Positive || STPEAK1.Zero) &&
            (STPEAK1.Positive || STPEAK1.Zero) &&
            (STPEAKDIFF.Zero  || (STPEAKDIFF.Small &&
            STPEAKDIST.Quite_Near)));

      STSHAPE.Elevated<=(STPEAK1.Elevated && STPEAK2.Elevated );

      STSHAPE.Bip1<=
            (STPEAK1.Positive &&(STPEAK2.Positive || STPEAK2.Zero) &&
            STPEAKDIFF.Negative && STPEAKDIST.Significant );

      STSHAPE.Bip2<=
            (STPEAK1.Positive && STPEAK2.Negative &&
            STPEAKDIST.Significant && STPEAKDIFF.Negative );

      STSHAPE.Bip3<=
            ((STPEAK1.Negative || STPEAK1.Zero) &&
            STPEAK2.Negative );

      //Construct continuous set of stsegment shape
      stshape = STSHAPE.Normal;
      stshape|= STSHAPE.Elevated;
      stshape|= STSHAPE.Bip3;
      stshape|= STSHAPE.Bip2;
      stshape|= STSHAPE.Bip1;

      //Assess ST waveform trends
      STWAVEFORM.Normal<=
      (     D_TQRS15.Stable &&
```

```
      D_TQRS20.Stable &&
      D_TQRS10.Stable &&
      D_TQRS5.Stable &&
      STSHAPE.Normal &&
      TQRS.Normal
);

STWAVEFORM.Intermediate<=
(     (TQRS.High || TQRS5.High || TQRS10.High
      || TQRS.Increased || TQRS5.Increased || TQRS10.Increased) &&
      D_TQRS5.Stable && D_TQRS10.Stable &&
      (STSHAPE.Normal || STSHAPE.Elevated || STSHAPE.Bip1)
);

STWAVEFORM.Changing<=
      (!D_TQRS15.Stable || !D_TQRS20.Stable ||
      !D_TQRS10.Stable || !D_TQRS5.Stable);

STWAVEFORM.Abnormal<=
      (TQRS20.Negative || TQRS15.Negative || TQRS10.Negative ||
      TQRS5.Negative || TQRS.Negative || STSHAPE.Bip3 ||
      STSHAPE.Bip2 || STWAVEFORM.Changing );


//Construct continuous set of STWAVEFORM
stwaveform=STWAVEFORM.Normal;
stwaveform|=STWAVEFORM.Intermediate;
stwaveform|=STWAVEFORM.Changing;
stwaveform|=STWAVEFORM.Abnormal;

//Truth values for A-I
FETALCOND.A<=(CTG.Normal && STWAVEFORM.Normal);
FETALCOND.B<=(CTG.Normal && STWAVEFORM.Intermediate);
FETALCOND.C<=(CTG.Normal && STWAVEFORM.Abnormal);
FETALCOND.D<=(CTG.Intermediate && STWAVEFORM.Normal);
FETALCOND.E<=(CTG.Intermediate && STWAVEFORM.Intermediate);
FETALCOND.F<=(CTG.Intermediate && STWAVEFORM.Abnormal);
FETALCOND.G<=(CTG.Abnormal && STWAVEFORM.Normal);
FETALCOND.H<=(CTG.Abnormal && STWAVEFORM.Intermediate);
FETALCOND.I<=(CTG.Abnormal && STWAVEFORM.Abnormal);

//Compute center of gravity
A=FETALCOND.A.truth;
B=FETALCOND.B.truth;
C=FETALCOND.C.truth;
D=FETALCOND.D.truth;
E=FETALCOND.E.truth;
F=FETALCOND.F.truth;
G=FETALCOND.G.truth;
H=FETALCOND.H.truth;
I=FETALCOND.I.truth;
totalvol=A+B+C+D+E+F+G+H+I;
//If no rules fire, the total truth is zero
if (totalvol>0.01) {
      ybar=(0.0*(A+B+C)+1.0*(D+E+F)+2.0*(G+H+I))/totalvol;
      xbar=(0.0*(A+D+G)+1.0*(B+E+H)+2.0*(C+F+I))/totalvol;
}

summary="Summary @";
summary+=(long)patient_rec.hrs;
summary+=":";
summary+=(long)patient_rec.min;
summary+=":";
summary+=(long)patient_rec.sec;
summary+=" ST Segment is ";

STdescript.reset();
STdescript << 0;
```

```
        STdescript << STSHAPE.Bip3.truth;
        STdescript << 1;
        STdescript << STSHAPE.Bip2.truth;
        STdescript << 2;
        STdescript << STSHAPE.Bip1.truth;
        STdescript << 3;
        STdescript << STSHAPE.Normal.truth;
        STdescript << 4;
        STdescript << STSHAPE.Elevated.truth;

        switch (STdescript.overall_max_pos)
        {
              case  0:    summary+="Biphasic 3";
                          break;
              case  1:    summary+="Biphasic 2";
                          break;
              case  2:    summary+="Biphasic 1";
                          break;
              case  3:    summary+="Normal";
                          break;
              case  4:    summary+="Elevated";
                          break;
        } ;
}
```

Appendix G

Histogram plots of ST waveform features

G. Histogram plots

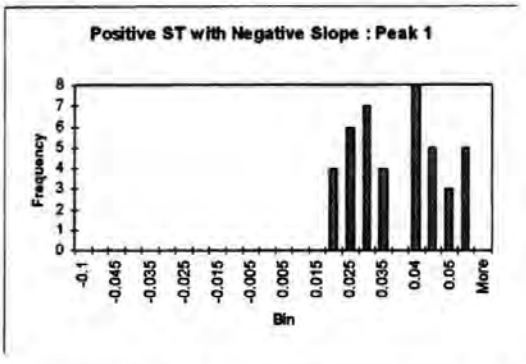

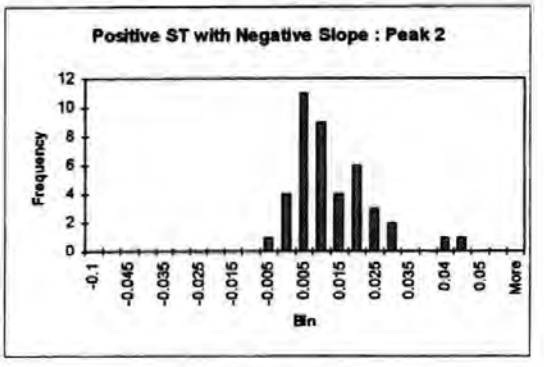

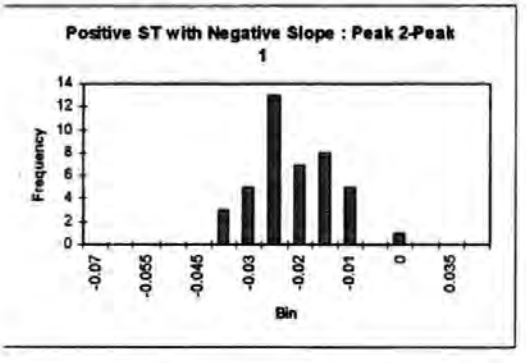

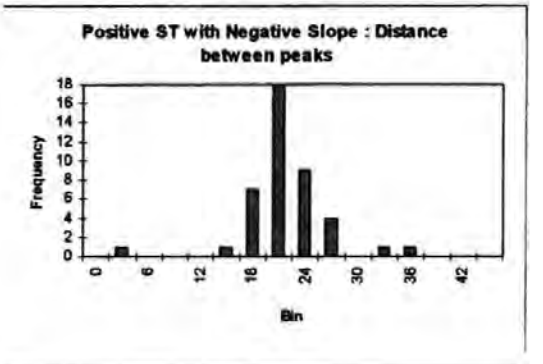

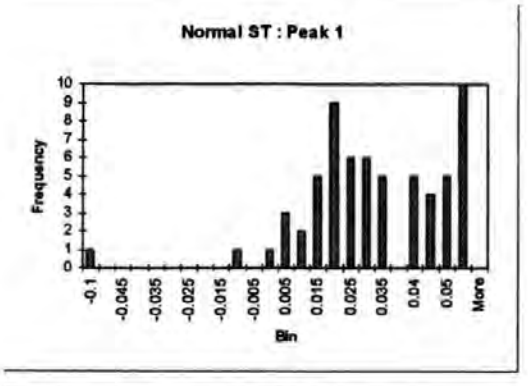

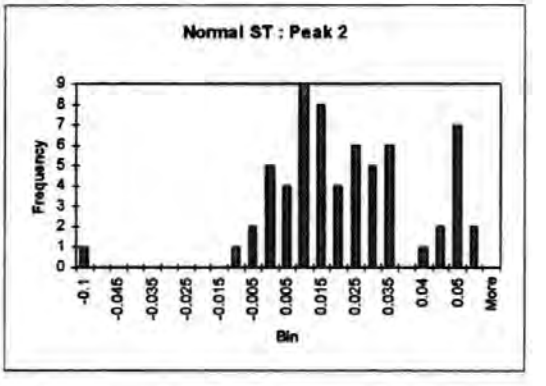

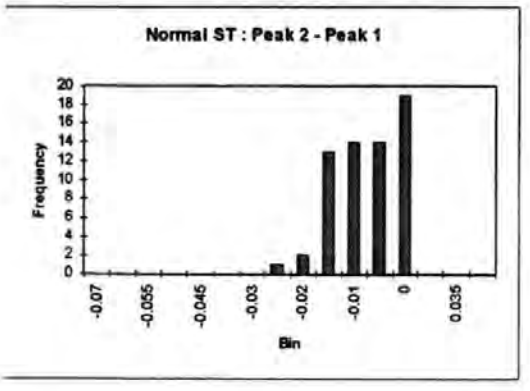

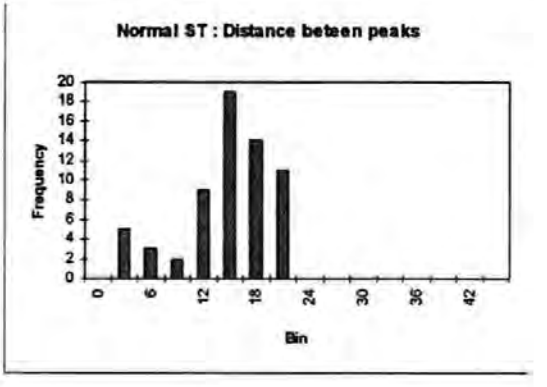

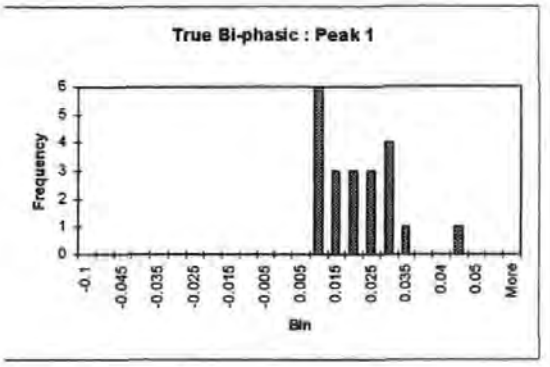
True Bi-phasic : Peak 1
Frequency
Bin
-0.1
-0.045
-0.035
-0.025
-0.015
-0.005
0.005
0.015
0.025
0.035
0.04
0.05
More

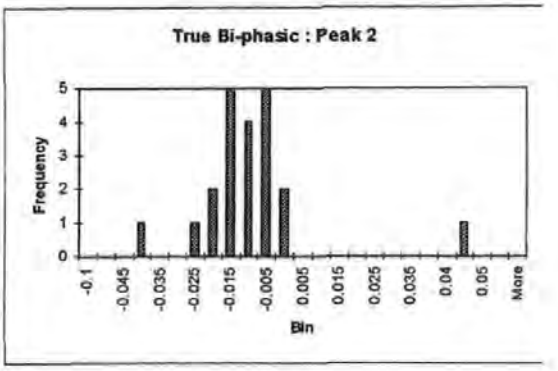
True Bi-phasic : Peak 2
Frequency
Bin
-0.1
-0.045
-0.035
-0.025
-0.015
-0.005
0.005
0.015
0.025
0.035
0.04
0.05
More

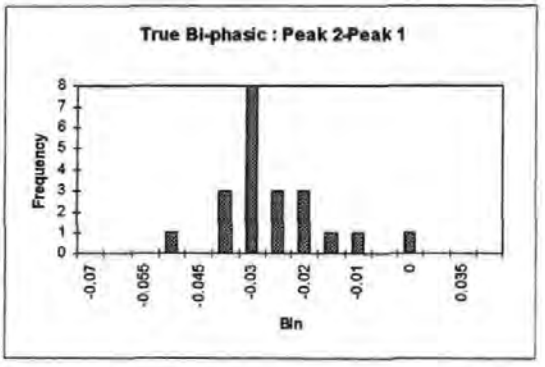
True Bi-phasic : Peak 2-Peak 1
Frequency
Bin
-0.07
-0.055
-0.045
-0.03
-0.02
-0.01
0
0.035

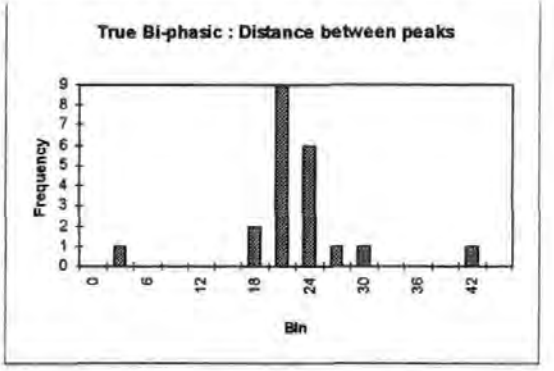
True Bi-phasic : Distance between peaks
Frequency
Bin
0
6
12
18
24
30
36
42

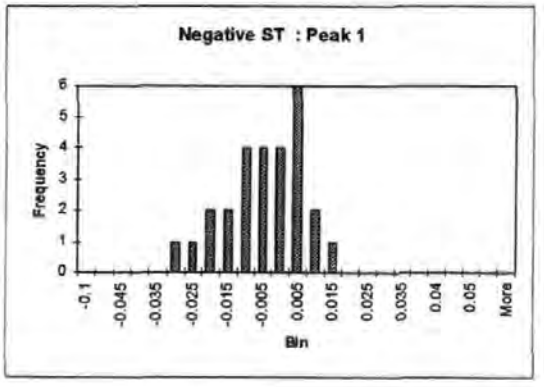
Negative ST : Peak 1
Frequency
Bin
-0.1
-0.045
-0.035
-0.025
-0.015
-0.005
0.005
0.015
0.025
0.035
0.04
0.05
More

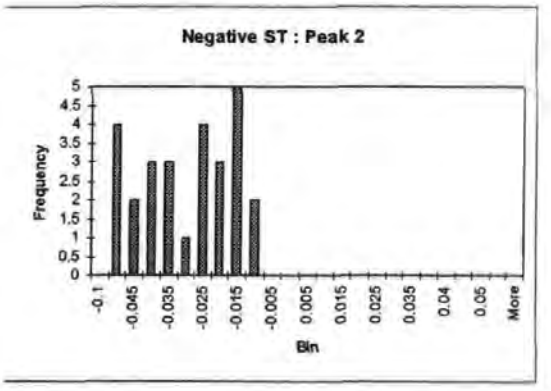
Negative ST : Peak 2
Frequency
Bin
-0.1
-0.045
-0.035
-0.025
-0.015
-0.005
0.005
0.015
0.025
0.035
0.04
0.05
More

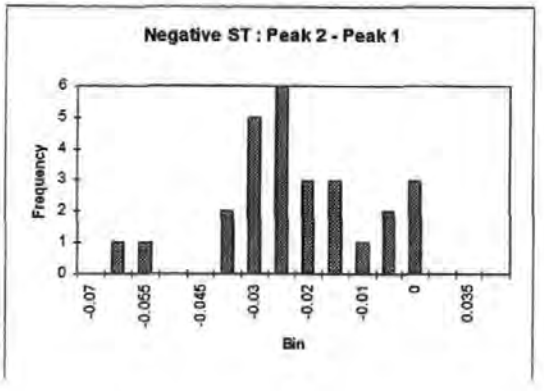
Negative ST : Peak 2 - Peak 1
Frequency
Bin
-0.07
-0.055
-0.045
-0.03
-0.02
-0.01
0
0.035

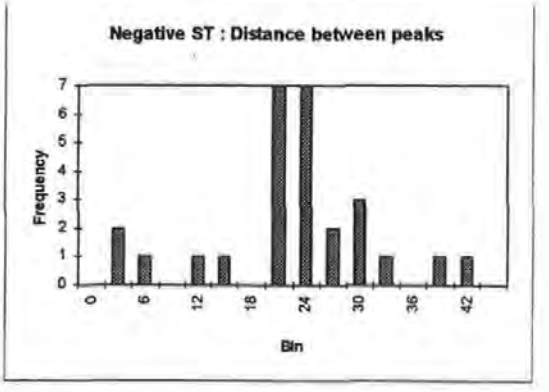
Negative ST : Distance between peaks
Frequency
Bin
0
6
12
18
24
30
36
42

Publications

ABSTRACT 2

FETAL ECG QUALITY ASSESSMENT USING NEURAL NETWORKS

E.C. Ifeachor, N.J. Outram and K.R. Greene
University of Plymouth and
Plymouth Postgraduate Medical School.

Introduction

The need for computer-assistance in the management of labour to reduce incidents of unnecessary medical intervention and fetal injury at birth is widely recognised [1-3]. We have recently developed an expert system, the INFANT [3], to analyse and interpret changes in fetal heart rate (FHR) patterns and to provide advice to clinicians during labour. The significance of the INFANT has been demonstrated in a number of studies [3], but the FHR does not provide the information needed, in all cases, for accurate assessment of the condition of the fetus. Additional information may be obtained by proper analysis of progressive changes in the fetal ECG (electrocardiogram)[4], but the quality of the fetal ECG is extremely variable, making it difficult to distinguish between genuine changes and changes induced by noise or the measurement system.

In this paper, we present preliminary results of a novel approach, based on multi-layer neural networks and conventional signal processing, that automatically assesses and grades the ECGs so that subsequent interpretation in the INFANT takes place in the proper context.

The ECG data used in the work were taken from our perinatal research data base. Each ECG record was obtained from a scalp electrode attached to the fetus during labour and digitised to 12-bits at a sampling frequency of 500 Hz.

Artefacts and Noise in the fetal ECG

The fetal ECG is prone to degradation by noise and artefacts of which the most prominent are baseline shifts, noise spikes and high frequency noise. Baseline shifts are low frequency activity superimposed on the fetal ECG and depend, among other factors, on the connection made by the scalp clip. For accurate analysis of the ECG waveform, it is essential to remove the base line shift if it is present, typically by filtering, or at least take it into account. However, over filtering may obscure or destroy important shape information in the ECG waveform. Knowledge of the severity of baseline shift is important for 'optimum' filtering of the ECG.

The fetal heart rate (FHR) pattern is perhaps the most important feature obtained from the ECG at the present. Typically, the FHR is obtained by detecting successive QRS complexes (or R-waves) in the ECG and computing the reciprocals of the R-R intervals. Noise spikes can lead to false or missed QRS complexes, leading to artificial changes in the FHR patterns.

High frequency noise (~50 Hz) tends to obscure the components of the ECG waveform and is often dealt with by filtering, although some care should be exercised as filtering may cause the noise spikes to look even more like genuine QRS complexes making QRS detection more difficult. There are other noise or artefact problems in ECG analysis, e.g ADC (analogue-to-digital converter) saturation, dropout, and filtering effects, but these may be dealt by a proper choice of system parameters (e.g ADC resolution, anti-aliasing filters, programmable gain control, and sampling frequency).

Previously, the quality of the ECG was assessed visually, although a limited quantitative assessment has been attempted before using conventional algorithms. For the information to be useful in the INFANT quality assessment must be automated. We are primarily concerned here with the assessment of the effects of noise spikes and baseline shifts. The effects of high frequency noise was carried out using numerical methods and will be reported elsewhere.

In our study, the quality of the ECG with respect to each of the major noise or artefact was assessed seperately. Eventually, the various quality indices would be combined to give an overall quality index.

Quality assessment of noise spikes

Quality assessment with respect to noise spikes involve two considerations: (i) discriminating between noise spikes and genuine QRS complexes, and (ii) assessing the significance of the noise spikes in terms of their densities and positions relative to important ECG features. The first requires a form of pattern recognition and was thought to be more suited to neural network approach. The second aspect was tackled using conventional methods and will be reported elsewhere.

The raw ECG data is pre-processed to extract meaningful information prior to using the neural network. First, the data is differenced to minimise the effects of the baseline on the analysis and to help identify the locations of the spikes or QRS complexes. A possible noise spike or QRS complex exists where the differenced data exceeds a prescribed threshold (currently 1024). For each possible spike or QRS complex, 44 data points (21 before the peak + the peak + 22 after the peak) are extracted, normalized to a unit length vector and presented to a 44-3-2 neural network for classification as either a noise spike or a QRS complex. For computational speed and reliability, another threshold is set at 2048. Peaks exceeding the second threshold is normally a spike. The network used is a fully connected, feedforward multi-layer perceptron, with the learning algorithm and the output threshold function modified slightly to yield a near linear function between 0 and 1.

Difficulties in the network size, training and generalisation led us to investigate other methods of pre-processing. In particular, the singular value decomposition (S.V.D.) method was used to reduce the newtwork size to 5-3-2.

Quality assessment of baseline shifts

The assessment of the baseline shift is a subjective problem. The task here is to classify the raw ECGs into three categories: grades 1, 2 and 3, where in grade 1, the baseline shift is hardly evident and in grade 3 the baseline shift is severe. Grade 2 is any ECG data that does not fit either grade 1 or 3. Features which discriminate the grades are not immediately obvious and so the grading is subjective. In the training set a '0' output was assigned to grade 1, a '1' output to grade 3 and '0.5' to grade 2. With this assignement, it was intended that the network would map all the cases onto a continuous output reflecting the severity of baseline shift.

The data was pre-processed before being applied to the neural network by removing the mean (allowing for the spikes), and computing the low frequency components (6 values) and the amplitude distribution (11 values) of the ECG data. The two resulting vectors were each normalised to give a unit length vector, and passed to a 17x5x1 neural network for classification. The output threshold function was modified from the usual S-shaped

sigmoid to a 'lazy-S' giving a continuous near linear output in the range 0 to 1. A training set of 60 examples, containing equal number of grades 1, 2 and 3 was created. A test set of 328 (including the 60) was also created - 136 for grades 1, 103 grade 2, and 89 grade 3.

To deal with the problem of long training times, the SVD was applied to the training and test data leading to a reduction in the network input size from 17 to 10.

Results and discussions

For the noise spikes, 215 test cases were presented to the trained networks, 117 QRS complexes and 98 Spikes. An RMS Error greater than 0.5 was considered a miss. The network with the simple data pre-processing outperformed that using the SVD, 98.6% compared to 93.5%. However, an analysis of the results for the SVD suggested that the noise spike problem may be linearly separable with the exception of three cases. This may explain why the SVD results are inferior. For the baseline grading, the use of the SVD led to improved training times and slightly better performance than without SVD (96.1% versus 95.2%).

Work is in progress to optimise the pre-processing operations to improve accuracy and the training speed, and to integrate the various quality assessment and optimal filtering schemes already developed. We see the use of the SVD as of potential value in pre-processing the data, especially in reducing the dimension of the network and training times. An attempt to reduce the training times by using GA to train the network was successful for the QRS/spike discrimination. In the case of the baseline, the network failed to converge.

The results reported here are preliminary findings of our attempt to automate the quality assessment of fetal ECG which is important for computer-assisted interpretation of the fetal ECG during labour. Knowledge of the signal quality would allow us to enhance the fetal ECG signal when necessary using the most appropriate technique to achieve minimal distortion of information of clinical interest and to ensure that the parameters extracted from the ECG are of adequate quality for subsequent interpretation by the INFANT. It would also enable us to determine when it is best to reject the data or to decide what features of the ECG waveform that can be reliably extracted at any given stage during labour.

References

[1] Maeda, K. Computersed analysis of cardiotocograms and fetal movements. R. Lilford (ed.) Balliere's Clinical Obstetrics & Gynaecology, London, 4, 797-813, 1990.

[2] Krause, W. Natali by Neiss, A computer-aided monitoring system for supervision of labour. K. Maeda et al (eds). Computers and Perinatal Medicine, 103-11, Elsevier Science Publishers, BV Amsterdam, 1990.

[3] Ifeachor, E.C., Keith, R.D.F., Westgate, J. and Greene, K.R. An expert system to assist in the management of labour. J. Liebowitz, (ed.) Proc. World Congress on Expert Systems, 4, 2615-22, Pergamon Press, 1991.

[4] Greene, K.R. The ECG waveform. Balliere's clinical obstetrics & Gynaecology, M. Whittle (ed.), 1, 131-55, London, 1987.

OPTIMAL ENHANCEMENT OF THE FETAL ELECTROCARDIOGRAM DURING LABOUR.

Outram N J, Ifeachor E C and Van Eetvelt P W J

Introduction

The assessment of the condition of the fetus during labour is based on visual analysis and interpretation of the fetal heart rate pattern, together with the uterine contractions (known as the cardiotocogram or CTG), but this requires a great deal of experience which is not always available to all labour wards day and night. Difficulty in interpreting CTG patterns during labour leads to unnecessary medical intervention, fetal injury or a failure to intervene when needed [1]. The impetus for investigating the value of the fetal electrocardiogram (ECG) waveform comes from extensive experimental research, clinical observations and studies which suggest that the assessment of fetal condition based on the combination of one or more ECG variables plus the CTG can improve the quality of care [2-3]. The availability of good quality fetal ECG signals, or the ability to enhance the data with minimal distortion, is a essential for ECG waveform analysis. There are many potential sources of signal contamination, notably mains noise, baseline shifts, muscle noise and random noise which may induce false changes in the ECG waveform. Many of the clinical observations are difficult to reproduce or fully exploit because of the immense difficulty of processing and analysing the fetal ECG waveform. This paper presents novel techniques for processing the fetal ECG to improve the signal-to-noise ratio (SNR) and for assessing signal quality. This ensures the subsequent feature extraction, analysis and interpretation of the fetal ECG features is reliable. The fetal ECG is normally obtained from a fetal scalp electrode and is band-limited to 0.05 - 100Hz before it is digitised [4]. An important aspect of our work is the need to retain as much useful information from the ECG as possible. Thus our methods allow measurements to be made on every raw ECG complex where possible, allowing analysis of short term as well as long term variations in the fetal ECG shape.

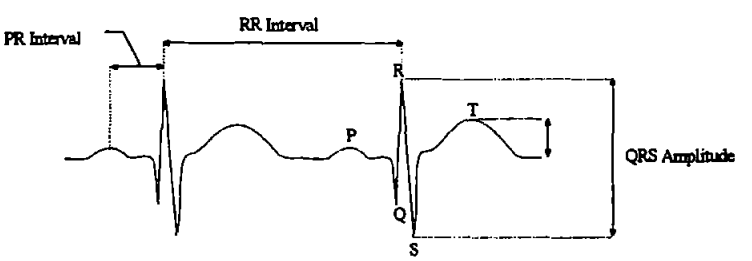

Figure 1. The fetal ECG features showing R-to-R and P-to-R intervals and the T and QRS amplitudes.

Fetal ECG signal enhancement

The most widely used technique for improving the signal-to-noise (SNR) ratio for repetitive signals, such as the fetal ECG, is averaging [5-6]. In general the weighted average signal vector a is computed as

$\mathbf{a} = \sum_{k=0}^{N-1} \mathbf{x}(k) \cdot w(k)$, where x(k) are the individual fetal ECG waveforms (vectors), w(k) are scalar weightings and N is the number of waveforms in the average. For an evenly weighted average, w(k)=1/N, k={0,1,...,N-1}, the SNR is increased by a factor of up to $\sqrt{N}$. This assumes that the true signal component is perfectly stationary and the noise is purely random and un-correlated with the signal. Unfortunately this is not always the case with the fetal ECG as the signal shape changes over time and not all the noise sources can be assumed to be random or un-correlated. In particular the low-frequency noise components in the raw signal, such as baseline shifts, tend to be correlated and are therefore not removed by averaging. To reduce this effect, one solution is to only include ECG complexes that have low baseline shifts into the average. A major drawback of

School of Electronic, Communication and Electrical Engineering, University of Plymouth.

signal averaging is that it suppresses the short term changes in the ECG waveform which may be of clinical interest. This can be improved by choosing the weighting, w(k), such that the older waveforms have a lesser influence than the more recent, but this in turn reduces the SNR improvement. The optimum solution to the problem of fetal ECG enhancement would require the complete removal of the baseline shifts and other noise using digital filters. A summary of our fetal ECG signal processing scheme is depicted in figure 2.

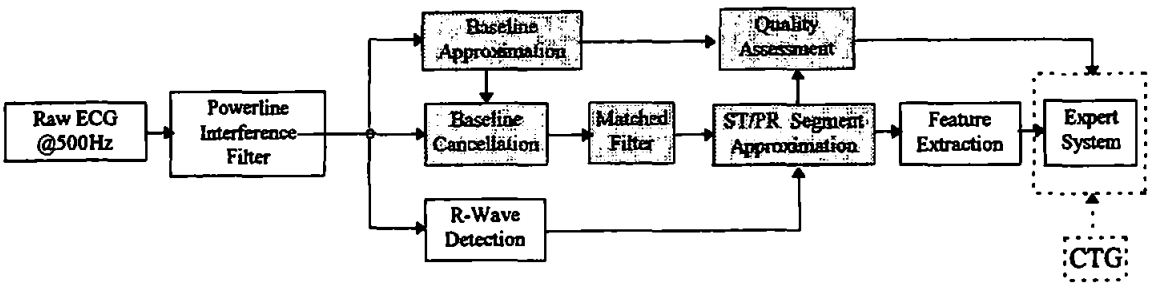

Figure 2. Summary of the fetal ECG signal processing scheme for enhancement and feature extraction

The 50Hz power line interference is removed by a linear band-stop filter centred at 50Hz using multi-rate techniques to simplify the design. Low frequency noise such as baseline shifts are approximated and removed by curve fitting techniques. To maximise the SNR the remaining noise, such as muscle noise, random noise and 100Hz power line interference, is removed with a matched filter. The R wave detection identifies the location of the next ECG complex and then smooth curves are fitted to the ST and PR segments. From these curves the important features can be extracted. Signal quality information is measured from the baseline, ST segment and PR segment curves. This is used to determine which features can then be reliably interpreted by the expert system.

This paper is primarily concerned with the techniques for enhancing the SNR of the raw ECG data and assessing the quality of the signal (shaded boxes in figure 2).Techniques for R wave detection [7-8], feature extraction [9] and interpretation [10] are discussed elsewhere.

Baseline approximation, assessment and removal

Baseline shift is due to excessive movement artefact in labour and greatly hinders accurate measurement of ECG features. Over filtering the information in the low frequency spectrum of the ECG distorts useful information in the ST segment[4]. For the adult ECG, it been shown that the low frequency energy below 1Hz can be removed using linear filters [11-13] with minimal distortion to the ST segment. Unfortunately the spectrum of the fetal and adult ECG differ so it is uncertain how much can be filtered from the fetal ECG without compromising important information in the ST segment.

To avoid these problems we use a curve fitting technique to obtain an accurate approximation b(t) of the baseline shift as shown in figure 3a. This approximation is then subtracted from the raw signal to remove the baseline shift as shown in figure 3b. The advantage of this technique over conventional filtering is that it only removes what is actually required to cancel out the baseline shift. For example, when there is no baseline shift present nothing other than DC is (theoretically) removed from the signal. In such cases, sensitive features such as the ST segment shape can be analysed with confidence. Thus it is very important to measure the severity of the baseline shift to identify when features can be reliably extracted and interpreted. This is derived from the approximation b(t) using the following

$$v_1 = \max\left\{\frac{|b[t]-x[t]|}{QRS}\right\} \quad , \quad v_2 = \max\left\{\frac{|b[t]-b|}{QRS}\right\}$$

where QRS is the peak-to-peak amplitude of the fetal ECG complex, x[t], t={0,1,...,N-1}, are the raw data samples, b[t] is the approximation and b is the mean. v_1 is the maximum deviation between the baseline approximation and the raw ECG data and is a measure of goodness of fit. This is used to detect occasions where the baseline approximation cannot fit to the raw ECG data (e.g. transient shifts). v_2 is the maximum deviation between the baseline approximation and its mean (DC) which is used to detect large baseline shift swings. These measures are interpreted by the expert system.

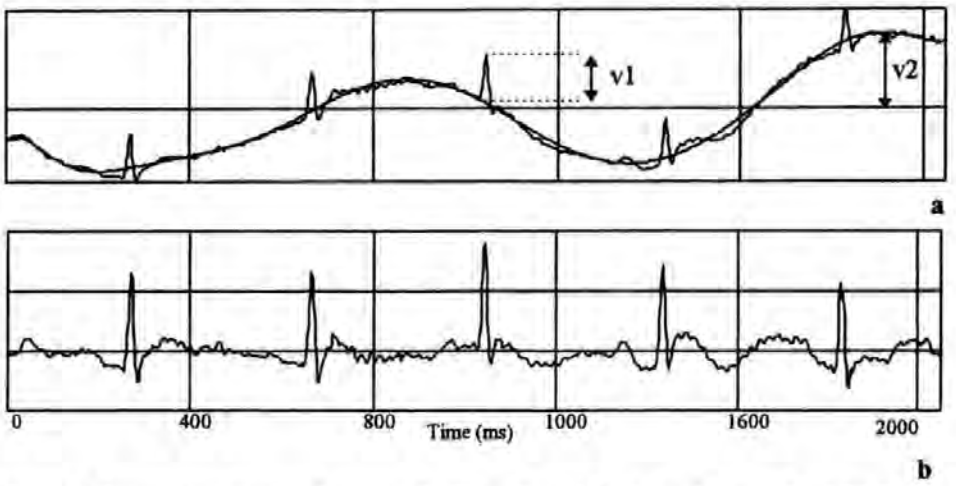

Figure 3 Approximation and removal of baseline shift from the raw fetal ECG data

To obtain the approximation b(t) we use a Chebyshev polynomial approximation of the form

$$b(t) = c_0 T_0(t) + c_1 T_1(t) + c_2 T_2(t) + \ldots + c_m T_m(t)$$

where $T_k(t)=\cos(k.\cos^{-1}(t))$ is the Chebyshev polynomial of degree k and $c_0, c_1,\ldots,c_m$ are scalar coefficients. Chebyshev polynomial approximations have the advantage over other polynomial approximations such as cubic spline and least-squares [14] that they give an evenly distributed error over the whole approximation. This is important so a bias is not introduced into the equations for v1 and v2. Chebyshev approximations also have the advantage of being numerically stable to compute and they can be truncated [15]. This is useful as approximations of different degrees are required for quality assessment (high degree) and baseline removal (low degree). Computing the coefficients c_k for the Chebyshev polynomials and evaluating the curves of different degree is discussed in more detail elsewhere [9].

One problem is the undesirable effect of the R-wave peaks on the approximation. To obtain greater accuracy, a refinement of this method is to decimate the sampling rate from 500Hz down to a much lower rate,

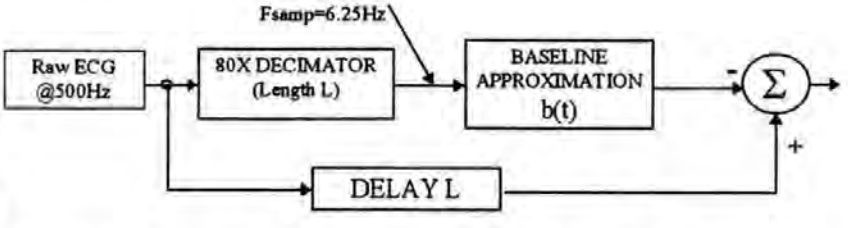

Figure 4. Enhanced baseline approximation using multi-rate technique

e.g. 6.25Hz (see figure 4). This preserves all the baseline shift information, greatly reduces the influence of the R wave peaks on the approximation and reduces computational overhead. Interpolation is very simple as b(t) is continuous and can be re-sampled at 500Hz.

Optimal matched filtering

After baseline removal the SNR is further improved by matched filtering to reduce the effect of unwanted higher frequency noise such as muscle and random noise. This uses a filter with characteristics matched to the spectrum of the ECG waveform. The difficulty is that the spectrum of the ECG is not known appriori and is not fixed. A practical method is to infer the "true" spectrum from the average of several ECG complexes. In this method, the spectrum of the average ECG waveform $|X(w)|$ is first computed using the fast Fourier transform (FFT) or any other suitable method (ARMA). A smooth ECG spectrum is obtained by fitting a cosine series through the coarse magnitude spectrum (see figure 5).

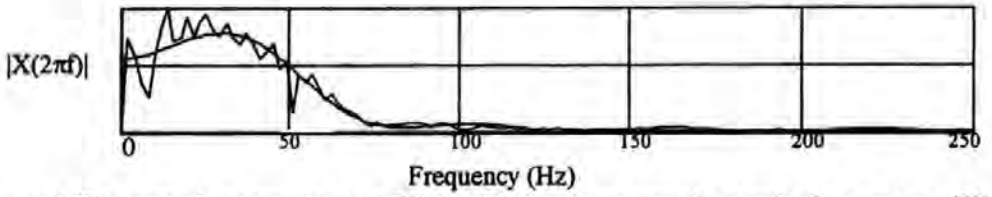

Figure 5 The smooth approximation H(ω) of the average signal magnitude spectrum |X(ω)|

From the smooth cosine series the coefficients of a FIR filter with the same impulse response can easily be computed[9]. Because the coefficients are guaranteed to be symmetric, the difference equation of the filter is $y(t) = h\left(\frac{L-3}{2}+1\right)\cdot x\left(t-\left(\frac{L-3}{2}+1\right)\right) + \sum_{n=0}^{(L-3)/2} h(n)\cdot\{x(t-n)+x(t-L-1+n)\}$ where x(t) is the raw fetal ECG signal, y(t) is the output signal, L is the filter length (odd integer) and h(n) are the filter coefficients. It can be shown that the coefficients h(n) of a linear phase FIR filter with an equivalent frequency response H(ω) is given by $h(n) = \frac{2}{\beta}\cdot\sum_{k=0}^{N/2}|X(k)|\cdot\cos\left(\frac{2\cdot\pi\cdot k\cdot n}{N}\right)$ where $\beta = \begin{cases} N, n=0 \\ N/2, n\neq 0 \end{cases}$ where N is the total number of frequency samples (e.g. N=500 in figure 6).

PR and ST segment enhancement and approximation

The presence of false peaks and valleys in the ECG waveform, even after signal enhancement, greatly impedes accurate measurement and location of features such as the T peak[16]. A possible solution is to locate features by fitting a series of regression lines to portions the fetal ECG complex[6]. A more accurate alternative is to fit smooth continuous curves to the ST and PR segments (see figure 6). Fitting these smooth curves greatly enhances the signal and clearly defines the features without ambiguity. These curves also provide an analytical expression of the ECG waveform, making it possible to compute amplitudes and derivatives at any point and integrals over any interval. Extracting features such as the

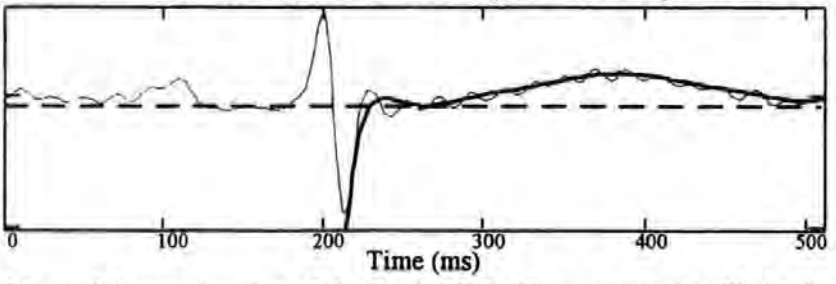

Figure 6 Approximation of the Fetal ECG ST segment using Chebyshev polynomials

T/QRS ratio, ST area (for assessing ST depression) and gradient information is made very simple. Chebyshev polynomials are used for the reasons stated earlier.
Spurious low frequency noise, which is too short to be removed by the baseline shift algorithm, can sometimes corrupt small segments of an individual ECG waveform. To verify that an individual waveform is not corrupted we can correlate it with the average waveform. This assumes that the average waveform is a good estimate of the expected fetal ECG shape and any raw complex that greatly differs from it is of poor quality. As the Chebyshev polynomial approximations of the ST and PR segments are of most interest then they are computed for both the individual and the average waveforms. The linear correlation r is conveniently computed as $r = \frac{1}{C \cdot A} \cdot \sum_{k=1}^{m} c_k \cdot a_k$ where $A = \sqrt{\sum_{k=1}^{m} a_k^{\,2}}$ and $C = \sqrt{\sum_{k=1}^{m} c_k^{\,2}}$, where a_k and c_k are the scalar coefficients for the average and individual waveform approximations. By computing r for both the ST and PR approximations separately we gain the advantage of not rejecting the ST segment if only the PR is corrupted and vice-versa.

Measuring high frequency noise.
Sometimes it is useful to measure the high frequency (HF) noise power content of the signal (e.g. remaining mains and muscle noise). The Chebyshev curves are a good approximation of the signal minus the noise, assuming the noise to be of zero mean. The levels of high frequency noise power for both the PR and ST segments are obtained as

$$\text{Average Noise Power (dB)} = 10 \cdot \log_{10}\left\{\frac{1}{(N-1)} \cdot \sum_{m=0}^{N-1}\left(\frac{x[t]-f[t]}{QRS}\right)^2\right\}$$ where f[t], t={0,1,...,N-1}, is the discrete Chebyshev approximation of the ST or PR segment, x[t] is the raw data of the ST or PR segment, QRS is the peak-to-peak amplitude of the fetal ECG complex and N is the number of samples.

Example results

Some features extracted from the fetal ECG measured on a beat-by-beat are illustrated in figure 7. This data was obtained from a patient during the second stage of labour with a normal outcome. Some of these features have been smoothed to show up the trends.

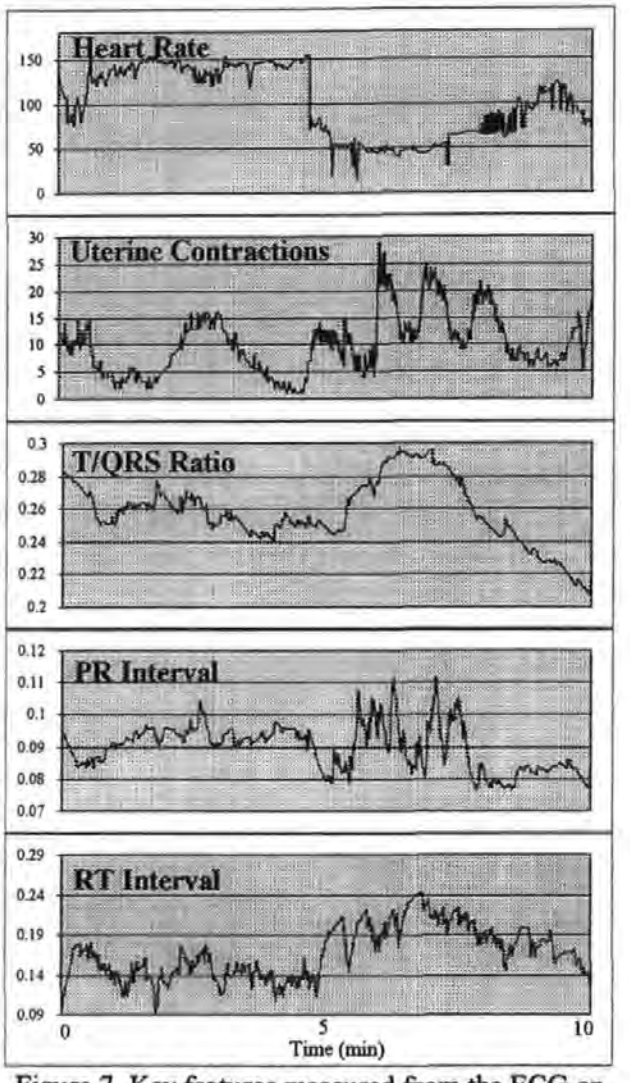

Figure 7. Key features measured from the ECG on a beat-by-beat basis

Discussion and Conclusion

An important objective of this work is to make it possible to measure features from the fetal ECG on a beat-by-beat basis and so retain as much clinical information as possible. This has not previously been possible because quality of the raw fetal ECG data is often very poor. Baseline shift is the major cause of poor quality data but because it is usually caused by maternal movement, it is also only short lasting.

Important features such as the ST segment shape can only be measured from good quality data and with minimal signal processing as attempts to enhance poor data can distort the ST shape. Other features, such as the RR and PR intervals are more robust and can tolerate higher degrees of signal processing.

We feel it is very important that the quality of the raw data, as well as the features themselves, are measured on a beat-by-beat basis. This is made possible by use of curve fitting techniques which provide specific signal quality measures, as well as enhance the signal with minimal distortion. We are developing as part of a fuzzy expert system [10] rules to decide what features are reliable based on these signal quality measures. Using this approach we believe our system can be robust enough to cope with the dynamic nature of labour and prevent the clinician from being mislead with false measurements.

The techniques reported here also have applications in other areas of biomedicine where it is required to enhance and assess the quality of the data. An example is in the assessment of neonates using evoked potentials where the enhancement and measurement of features are necessary.

Further work

The next stage of our work is to carry out a thorough analysis of the change in the ECG features, investigate their relationships to other events in labour and evaluate their clinical value in fetal monitoring. At the present, work is in progress at our units and other centres, as part of the European Community concerted action on new methods of fetal monitoring to collect data from various categories of patients. This will provide data for the next stage of the research which will be published in due course.

School of Electronic, Communication and Electrical Engineering, University of Plymouth.

Acknowledgements

The authors gratefully acknowledge the assistance of John Curnow, Peter VanEetvelt, Dr Mark Davies, Dr Roberto Luzietti, Prof Karl Rosén and Dr Keith Greene for helpful comments and support for this work. We thank the labour ward staff at Plymouth General Hospital for their help and co-operation. The financial support of the P.C.F.C. , EPSRC and South-West Regional Health Authority for this work is gratefully acknowledged.

References

[1] Ifeachor E.C., Keith R.D.F., Westgate J. and Greene K.R., An expert system to assist in the management of labour. In Liebowitz J.(Ed) World Congress on Expert Systems, Pergamon Press. ,4, pp2615-2622, 1991

[2] Murray H.G., The fetal electrocardiogram: current clinical developments in Nottingham., J.Perinat. Med., 14, pp399-404, 1986

[3] Westgate J., Harris M., Curnow J. and Greene K.R., Plymouth randomised trial of the cardiotocogram only versus ST waveform plus cardiotocogram for intrapartum monitoring in 2400 cases., Am. J. Obstet. Gynecol., 169, pp1151-1160, 1993

[4] American Heart Association Committee on Electrocardiography 1975 Recommendations for the standardization of leads and of specifications for instruments in ECG/VCG Circulation, 52, pp1-25

[5] Sheild J.E.A. and Kirk D.L., The use of digital filters in enhancing the fetal electrocardiogram., J. Biomed. Eng., 3, pp44-48, 1981

[6] Kirk D.L. and Smith P.R., Techniques for the routine on-line processing of the fetal electrocardiogram., J. Perinat. Med., 14, pp391-397, 1986

[7] Xue Q., Hu Y.H. and Tompkins W.J., Neural-Network-Based Adaptive Matched Filtering for QRS Detection., IEEE Trans. Biomed. End., 39,4, pp317-329, 1992

[8] Outram N.J. and Ifeachor E.C., Techniques for detection and classification of the fetal QRS complex., IEE Coll. Applications of neural networks to signal processing., Digest No. 1994/248., pp 10/1-3, Dec 1994

[9] Outram N.J., Ifeachor E.C., VanEetvelt P.W.J. and Curnow J.S.H., Techniques for optimal enhancement and feature extraction of the fetal electrocardiogram., (Submitted) IEE Proc A., 1994

[10] Ifeachor E.C. and Outram N.J., A fuzzy expert system to assist in the management of labour., (Accepted), International Symposium on FUZZY LOGIC, Zurich, Switzerland, May 1995

[11] Van Alsté J.A. and Schilder T.S., Removal of Base-Line Wander and Power-Line Interference from the ECG by an Efficient FIR Filter with a Reduced Number of Taps., IEEE Trans. Biomed. Eng., 32,12, pp 1052-1060, 1985

[12] Pottala E.W., Bailey J.J., Horton M.R. and Gradwohl J.R., Suppression of Baseline Wander in the ECG Using a Bilinearly Transformed, Null-phase Filter., J. of Electrocardiology., 22, pp243-247

[13] Sörnmo L., Time-varying digital filtering of ECG baseline wander., Med. & Biol. Eng., 31, pp503-508, 1993

[14] McManus C.D., Teppner U. and Neubert D. Estimation and Removal of Baseline Drift in the Electrocardiogram., Comp. and Biomed. Research., 18, pp1-9, Nov. 1993

[15] Strang G., Linear algebra and its applications (2nd ed.)., New York : Academic Press, 1980.

[16] Tompkins W.J. (Ed.), Biomedical Digital Signal Processing., Prentice Hall., Englewood Cliffs, NJ 07632, Ch 13, 1994

School of Electronic, Communication and Electrical Engineering, University of Plymouth.

Techniques for optimal enhancement and feature extraction of fetal electrocardiogram

N.J.Outram, BEng
E.C.Ifeachor, MSc, PhD, CEng, MIEE
P.W.J.Van Eetvelt, MSc, CEng, MIEE
J.S.H.Curnow, CEng, MIEE

Indexing terms: ECG distortions, Digital filtering, Curve fitting, Fetal monitoring

Abstract: Detailed analysis of the fetal electrocardiogram (ECG) during labour could provide valuable additional information to assist clinicians in reducing incidents of unnecessary medical intervention without altering current patient handling routines, but poor signal quality and difficulty of processing the ECG without significant distortion have impeded such analysis. The paper presents novel optimum curve fitting and digital filtering techniques that make it possible to enhance the quality of the ECG with minimal distortion and to measure, on a beat-by-beat basis, almost any feature (e.g. time constants, amplitudes, areas, maxima and minima) from the fetal ECG waveform accurately. This development removes a major obstacle in the use of fetal ECG and creates a basis for a thorough analysis of the changes in the key fetal ECG features and for evaluating their clinical value in fetal monitoring.

1 Introduction

The fetal electrocardiogram (ECG) contains potentially valuable information that could assist clinicians in making more appropriate and timely decisions during labour, but the signal is susceptible to noise and difficulty of processing it without significant distortion has impeded its use [1–4]. This paper presents novel techniques for processing the fetal ECG to improve the signal-to-noise ratio (SNR), accurate feature extraction, and for assessing signal quality to ensure that the analysis and interpretation of the ECG features take place in the proper context. The assessment of the condition of the fetus during labour is based on visual analysis and interpretation of the fetal heart rate (FHR) pattern and uterine contractions, known as the cardiotocogram (CTG), but this requires a great deal of experience which is not always available to all labour wards day and night. Difficulty in interpreting CTG patterns during labour leads to unnecessary medical intervention (e.g. Caesarean section or forceps deliveries), fetal injury or a failure to intervene when needed [5, 6]. However, the CTG alone does not provide all the information needed in all cases for accurate assessment of fetal condition. Additional information may be obtained by a proper analysis of progressive changes in the fetal ECG without altering current patient handling routines as the ECG is the source of the FHR [1, 4].

1.1 Key features of ECG waveform

One of the potentially important features of the fetal ECG waveform for discriminating between fetuses coping with normal stress of labour and those in distress is the shape of the ST segment (Fig. 1) [7]. Significant pattern changes in shape associated with stress or distress include persistently rising T-wave amplitude, negative T-waves and depressed ST segments. Changes in the ST waveform may be quantified as a ratio of the amplitude of the T-wave to that of the QRS (the so-called T/QRS ratio); see Fig. 1.

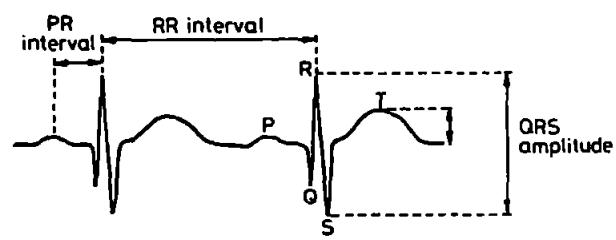

Fig. 1 *Fetal ECG features showing R-to-R and P-to-R intervals and T and QRS amplitudes*

The T/QRS ratio is a crude measure of the ST waveform shape. With the T/QRS ratio, some important changes in the ST segment, such as ST segment depression, may be missed unless the progressive changes in the whole waveform is examined [7]. The need remains for a detailed study of the ECG waveform to make the most of the information contained therein. Other features of the ECG of potential interest, such as the ST area, the variability in the RR intervals, the correlation between the PR and RR intervals [2] and other time constants, such as the duration of the P-wave and the width of the QRS complex.

The impetus for investigating the value of the ECG waveform comes from extensive experimental research, clinical observations and studies which suggest that the assessment of fetal condition based on the combination

IEE Proceedings online no. 19952074

Paper first received 7th November 1994 and in revised form 10th May 1995

The authors are with Plymouth Postgraduate Medical School, University of Plymouth, Derriford Hospital, Plymouth PI6 8DH, UK

N.J. Outram and E.C. Ifeachor are also with the School of Electronic, Communication and Electrical Engineering, University of Plymouth, Plymouth PL4 8AA, UK

of one or more ECG variables plus the CTG can improve the quality of care [1, 2, 4, 7]. However, much of the clinical observations are difficult to reproduce or fully exploit because of the immense difficulty of processing and analysing the fetal ECG waveform. The availability of good quality ECG signals or the ability to enhance the data, when necessary, with minimal distortion is a prerequisite for waveform analysis [1, 3, 8–10]. Poor quality signals lead to erroneous ECG features, such as spurious values of the T/QRS ratio. There are many potential sources of signal contamination, notably mains noise, baseline shifts, muscle artefacts and random noise which may induce false changes in the ECG waveform, especially in the low-frequency components such as the ST waveform. Others include the maternal ECG and the fetal electroencephalogram (EEG), although in most cases these have negligible effects in the fetal scalp ECG. The measurement of the ECG features with minimal distortion remains a major challenge.

In practice, the fetal ECG is obtained from a fetal scalp electrode, not the maternal abdomen, to achieve a better signal-to-noise ratio and from this the FHR is derived. The fetal ECG is normally bandlimited to 0.05 – 100Hz before it is digitised to 12 bits accuracy at a rate of 500Hz in line with the recommendations of the American Heart Foundation [11].

2 Fetal ECG signal enhancement

The most widely used technique for improving the signal-to-noise ratio for repetitive signals, such as the fetal ECG, is averaging [8, 9]. A major flaw in signal averaging is that it tends to remove short term changes in the ECG waveform. Further, a single ECG complex of poor quality may have an undue influence or indeed distort the resulting ECG average. To avoid this, only ECG complexes that satisfy a suitable quality criterion are included in the averaging process. However, this may distort the 'time of occurrence' information and makes it difficult to correlate changes in the ECG waveform to those in the CTG or other events in labour which is important for a proper assessment of the fetal condition. Further, the existence of significantly large low-frequency noise components which are correlated, such as baseline shifts, serve to reduce the effectiveness of averaging.

The optimum solution to the problem of fetal ECG enhancement for feature extraction would require the removal of the baseline shifts as well as matching the digital filter spectrum to that of the fetal ECG. This way the distortion of the features of the ECG is kept to a minimum by the signal processing.

2.1 The new approach

An important aspect of our work is the need to retain as much useful information as possible in the ECG. Thus our method allows measurements to be made on every raw ECG complex where possible allowing analysis of short term variations in the fetal ECG shape to be made. A summary of our fetal ECG signal processing scheme is depicted in Fig. 2. The first major task is to accurately locate a fixed reference timing point, normally the R-wave, within the often noisy fetal ECG signal. The problem of reliable R-wave detection using various methods, including the multilayer perceptron, cross correlation and matched filtering, is reported elsewhere [12].

After detecting the R-wave, an estimate of the baseline shift is obtained using a curve fitting technique and is then subtracted from the raw ECG signal. Signal quality is assessed to decide what information can be reliably extracted from the waveform. In the presence of severe baseline shift for example, only the most insensitive features, such as RR intervals, are measured.

2.2 Baseline shift

Baseline shift, Fig. 3, hinders accurate measurement of ECG features. Most of the energy in the baseline shift is low frequency, between 0 and 3Hz, and may be removed by high-pass filtering. However, overfiltering will distort the low-frequency components such as the ST-segment shape [11]. To preserve waveshape, we have developed a method that allows us to compute an approximation to the baseline shift, assess its severity, and then subtract it from the signal. The main advantage of this method is that when there is little or no baseline shift present, then nothing is removed from the ECG signal and in these cases sensitive morphological features such as ST segment depression can be measured.

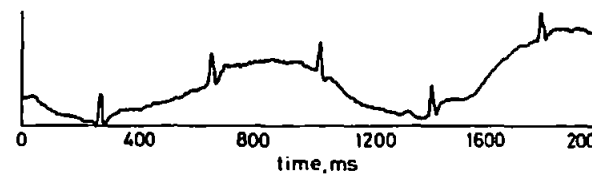

Fig.3 *Baseline shift in fetal ECG data*

Optimal approximation of the baseline shift may be achieved by curve-fitting methods based on Chebyshev polynomials. These allow us to estimate, remove and assess the severity of baseline shift with minimal distortion of the signal component.

2.3 Chebyshev polynomial approximation

Any continuous function $x(t)$ may be approximated by a linear combination of a set of polynomial functions $\{\phi_k(t)|\ k = 0, 1, \ldots, n\}$. The subscript k denotes the degree of the polynomial function $\phi_k(t)$. Thus, one can approximate the baseline $B(t)$ as

$$B(t) = c_0\phi_0(t) + c_1\phi_1(t) + c_2\phi_2(t) + \ldots + c_n\phi_n(t) \equiv \sum_{k=0}^{n} c_k\phi_k(t) \quad (1)$$

We wish to choose the set of functions $\{\phi_k(t)\}$ and the coefficients $\{c_k\}$ such that $B(t)$ has the smallest maximum deviation from the function $x(t)$. This is none other than the minimax approximation of degree n, which is unfortunately difficult to compute. However, by choosing the set of functions $\{\phi_k(t)\}$ to be the set of Chebyshev polynomials $\{T_k(t)\}$ defined over the interval $-1 \le t \le 1$, one can obtain an approximating polynomial $B(t)$ which is almost identical to the true minimax approximation and is simple to compute. The Chebyshev polynomial [13, 14] of degree k is defined as

$$T_k(t) = \cos(k\cos^{-1}(t)), \qquad -1 \le t \le 1 \quad (2)$$

hence we rewrite eqn. 1 as

$$x(t) \simeq c_0T_0(t) + c_1T_1(t) + c_2T_2(t) + \ldots + c_nT_n(t) = \sum_{k=0}^{n} c_kT_k(t) = B(t) \quad (3)$$

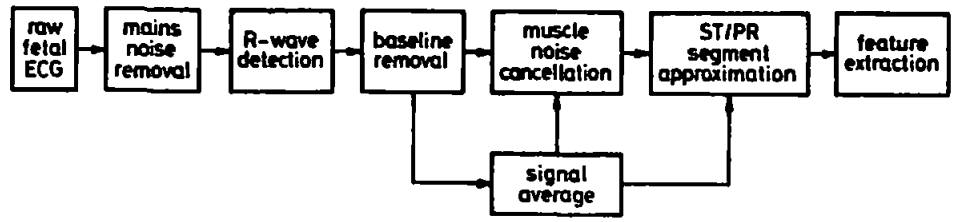

Fig. 2 *Summary of fetal ECG signal processing scheme for enhancement and feature extraction*

The problem of baseline approximation then reduces to one of finding the optimal values of the coefficients $\{c_k\}$ and the Chebyshev polynomials $\{T_k(t)\}$. A significant property of the Chebyshev polynomials is that they are orthogonal with respect to the weighting function $w(t) = 1/\sqrt{1-t^2}$, i.e.

$$\int_{-1}^{1} T_j(t)T_k(t)\frac{1}{\sqrt{1-t^2}}dt = \begin{cases} 0, & i \neq j \\ \pi, & i = j = 0 \\ \frac{\pi}{2}, & i = j \neq 0 \end{cases} \quad (4)$$

This property allows us to compute each coefficient c_k simply as follows. If eqn. 3 is multiplied throughout by $T_k(t)$ $w(t)$ and both sides are integrated over the interval $-1 \leq t \leq 1$ from eqn. 4 it follows that

$$\int_{-1}^{1} x(t)T_k(t)w(t)dt = \int_{-1}^{1} c_k(t)T_k(t)T_k(t)w(t)dt = c_k\alpha$$

$$\text{where } \alpha = \begin{cases} \pi, & k = 0 \\ \frac{\pi}{2}, & k > 0 \end{cases}$$

since all the other integrals vanish identically. Hence

$$c_k = \frac{1}{\alpha}\int_{-1}^{1} x(t)T_k(t)w(t)dt \quad (5)$$

Direct evaluation of eqn. 5 leads to large numerical errors since $w(t)$ becomes infinite at $t = -1$ and $t = +1$. However this problem is circumvented by the simple substitution of $t = \cos\theta$ into eqn. 5 which yields the result

$$c_k = \frac{1}{\alpha}\int_0^{\pi} x\cos(\theta)\cos(k\theta)d\theta \quad (6)$$

This may be rewritten as a sum of integrals over N discrete intervals

$$c_k = \frac{1}{\alpha}\sum_{m=0}^{N-1}\int_{\frac{m\pi}{N}}^{\frac{(m+1)\pi}{N}} x\cos(\theta)\cos(k\theta)d\theta \quad (7)$$

and when N is sufficiently large, each integrand may be linearly approximated over its interval of duration π/N. Therefore, each term in the sum can be approximated using the trapezoidal rule for integration [14]

$$c_k \simeq \frac{1}{\beta}\left\{\sum_{m=0}^{N-1} xy_1(m)y_k(m)\right\}, \quad \beta = \begin{cases} \frac{N}{2}, & k > 0 \\ N, & k = 0 \end{cases} \quad (8)$$

where $y_k(m) = \cos(km\pi/N)$. In practice, the function x is given by a sampled sequence $x_0, x_1, \ldots, x_{N-1}$ therefore to account for this we rewrite eqn. 8 as

$$c_k \simeq \frac{1}{\beta}\left\{\sum_{m=0}^{N-1} x[i_m]y_k(m)\right\} \quad (9)$$

where $i_m = \text{round}\{[1+y_1(m)N/2]\}$ and round(x) is the nearest integer to x. Direct online evaluation of eqn. 9 for all k and t is computationally inefficient because of the need to evaluate the trigonometric functions sine and cosine. Whereas these values could be precomputed offline and stored in memory, where memory does not permit this the following recursive algorithm can be used:

$$\begin{bmatrix} y_k(m+1) \\ s_k(m+1) \end{bmatrix} = \begin{bmatrix} y_k(1) & -s_k(1) \\ s_k(1) & y_k(1) \end{bmatrix}\begin{bmatrix} y_k(m) \\ s_k(k,m) \end{bmatrix} \quad (10)$$

which is readily derived from the additive trigonometric identities as follows:

$$\begin{aligned} y_k(m+1) &= \cos\left(\frac{k\pi}{N}(m+1)\right) \\ &= \cos\left(\frac{k\pi}{N}\right)\cos\left(\frac{k\pi m}{N}\right) - \sin\left(\frac{k\pi}{N}\right)\sin\left(\frac{k\pi m}{N}\right) \\ &\equiv y_k(1)y_k(m) - s_k(1)s_k(m) \\ s_k(m+1) &= \sin\left(\frac{k\pi}{N}(m+1)\right) \\ &= \sin\left(\frac{k\pi}{N}\right)\cos\left(\frac{k\pi m}{N}\right) + \cos\left(\frac{k\pi}{N}\right)\sin\left(\frac{k\pi m}{N}\right) \\ &\equiv s_k(1)y_k(m) + y_k(1)s_k(m) \end{aligned}$$

2.3.1 Evaluation of Chebyshev polynomials:

Direct evaluation of the Chebyshev polynomials $T_k(t) = \cos(k\cos^{-1}(t))$ is computationally inefficient since it requires the evaluation of two trigonometric functions. An efficient technique that does not involve direct computation of any trigonometric functions is derived using Clenshaw's recurrence formula [14, 15]. This is an algorithm for evaluating a linear combination of functions $B(t) = \Sigma_{k=0}^{n} c_k\phi_k(t)$, where the functions $\{\phi_k(t) | k = 0, 1, \ldots, n\}$ satisfy a second-order recurrence relationship of the form $\phi_{k+1}(t) = \alpha_k(t)\phi_k(t) + \beta_k(t)\phi_{k-1}(t)$, in which case we evaluate $B(t)$ directly using the equation

$$B(t) = \beta_1(t)\phi_0(t)p_2 + \phi_1(t)p_1 + \phi_0(t)c_0 \quad (11)$$

where the quantities p_k are recursively computed by $p_k = \alpha(k,t)p_{k+1} + \beta(k+1,t)p_{k+2} + c_k$ where $k = n, n-1, \ldots, 1$ and the initial conditions $p_{n+2} = p_{n+1} = 0$. The Chebyshev polynomials satisfy the second-order recursive relationship $T_{k+1}(t) = 2tT_k(t) + (-1)T_{k-1}(t)$ and therefore setting $\alpha(k,t) = 2t$ and $\beta(k,t) = -1$ it is seen that Clenshaw's algorithm is directly applicable to the approximation $B(t)$ in eqn. 1.

$$\begin{aligned} B(t) &= -1T_0(t)p_2 + T_1(t)p_1 + T_0(t)c_0 \\ &\equiv -1p_2 + tp_1 + c_0 \end{aligned} \quad (12)$$

where $p_k = 2tp_{k+1} + (-1)p_{k+2} + c_k$, $k = n, (n-1), \ldots, 1$ given $p_{n+1} = 0$ and $p_{n+2} = 0$. The selection of the order n is important to ensure that only the slow moving parts of the waveform are approximated. Using an order that is too high would result in overfitting which would tend to approximate the fetal ECG signal itself rather than just the baseline shift. Using an order that is too low would fail to remove the baseline shift enough for feature extraction.

2.4 Typical results

Typical results of using these techniques to estimate and remove baseline shifts are shown in Figs. 4 and 5 (a sixth order polynomial fit to 1024 sample data points was used). The approximation to the baseline shift can be observed as the smooth curve in Fig. 4. The ECG corrected for baseline shifts is shown in Fig. 5. In this example the baseline shift may be too severe to measure sensitive features such as ST depression as detailed in Section 4.1.

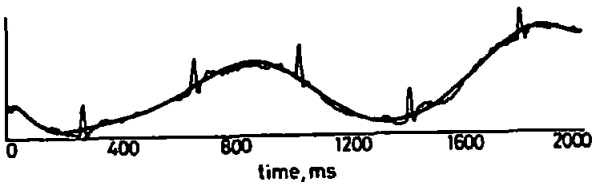

Fig.4 *Approximation of baseline shift in raw fetal ECG data*

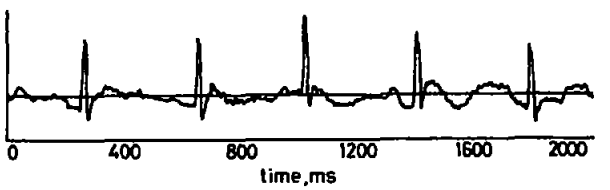

Fig.5 *Removal of baseline shift from raw fetal ECG data*

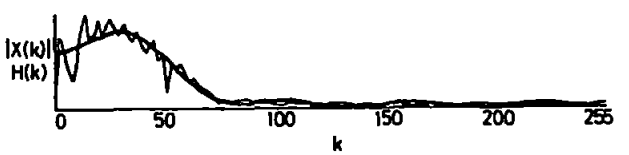

Fig.6 *Smooth approximation H(k) of avarage signal spectrum |X(k)|, where N = 512 and m = 10*

2.5 Muscle noise

After baseline removal, the *SNR* may be improved further by averaging and digital low-pass filtering to reduce the effect of muscle and random noise. Muscle noise is due to maternal movement, often from the leg and abdominal muscles, and may be picked up from the reference pad on the maternal thigh. This interference can obscure the Q, R and S reference points especially during uterine contractions and while the mother is pushing. The task of reducing the effects of muscle and random noise by filtering is essentially one of optimising the filter characteristics to match closely to the spectrum of the ECG waveform. The aim is to filter the data to obtain the maximum SNR while retaining important shape information. The difficulty is that the spectrum of the ECG is not known *a priori* and may not be fixed. An approach is to employ an adaptive noise cancelling technique, but this would require an additional reference pad which would alter current patient handling routines.

A practical method is to infer the 'true' spectrum from the average of several ECG complexes (see smooth curve in Fig. 6). In this method, the discrete spectrum $|X(k)|$, $k = 0, 1, ..., N-1$, of the average ECG waveform is first computed using the fast Fourier transform (FFT) or any other suitable method (see noisy curve in Fig. 6), where k is discrete frequency and N is the number of samples in the average waveform. The coefficients $h(n)$, $n = 0 \ldots 2m$, of the desired linear filter that has a smooth frequency spectrum $H(k)$ can be computed directly using the following expression:

$$h(n) = \frac{|X(0)|}{N} + \frac{2}{N}\sum_{k=1}^{N/2-1} |X(k)|\cos\left(\frac{2\pi k(n-m)}{N}\right) \quad (13)$$

where $2m+1$ is the chosen filter length [16]. To account for the possible changes in the ECG spectrum, the filter coefficients may be repeatedly computed online. To reduce computational load, the cosine functions in eqn. 13 can be computed recursively using the following relationship:

$$\begin{aligned} r(k,n) &= \cos(2\pi k(n-m)/N) \\ s(k,n) &= \sin(2\pi k(n-m)/N) \end{aligned} \quad (14)$$

$$\begin{aligned} r(k+l,n) &= r(l,n)r(k,n) - s(l,n)s(k,n) \\ s(k+l,n) &= r(l,n)s(k,n) + s(l,n)r(k,n) \end{aligned} \quad (15)$$

For a given value of n, $r(l,n)$ and $s(l,n)$ are first evaluated directly from the definitions in eqn. 14. The terms $r(k+l,n)$ and $s(k+l,n)$ are then successively computed for $k = 1, 2 \ldots (N/2)-2$, using the recursive relationship of eqn. 15. Finally for $k = 1, 2, ..., N/2-1$ the products $|X(k)|r(k,n)$ are formed and summed in the second term of eqn. 13. This process is repeated for all $n = 0, 1, \ldots 2m$. This method is similar to the standard frequency sampling method for filter design [16]. The filter coefficients $h(n)$, are symmetric about the centre which implies a linear phase response. The exact number of coefficients $L = 2m+1$. An example result is shown in Figs. 7 and 8. The filtered signal in Fig. 8 has minimal remaining noise and no visible distortion to the underlying waveshape.

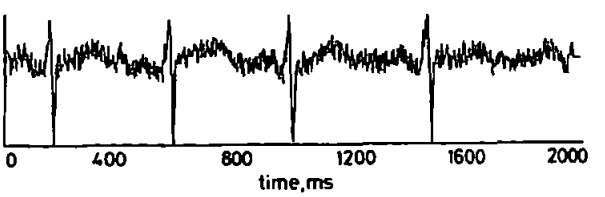

Fig.7 *Raw ECG data corrupted with random noise*

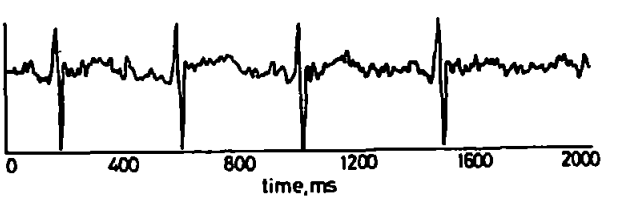

Fig.8 *Raw ECG data with noise optimally filtered*

3 Feature extraction

The presence of false peaks and valleys in the ECG waveform, even after signal enhancement, impedes accurate feature extraction. One solution to the problem is to fit a series of straight (regression) lines to the fetal ECG complex [3]. Using modern signal processing techniques this idea can be taken a stage further by fitting smooth continuous curves to the data.

An elegant technique is to fit Chebyshev curves to portions of the raw or average fetal ECG, such as the ST and PR segments in a similar manner to the baseline approximation. A smooth curve fitted to the ST segment is shown in Fig. 9. Such curves make feature extraction much easier and less ambiguous, as the measurements can be made on the smooth curves. Amplitude measurements in the fetal ECG are made relative to a reference. The true zero reference of the

fetal electrocardiogram, known as the isoelectric level, is extremely difficult to locate reliably. A convenient reference point is 50ms before the R-wave peak. This is theoretically a region of zero potential activity between the P-wave and the *QRS* complex. This reference is illustrated in Fig. 9 by the dotted line.

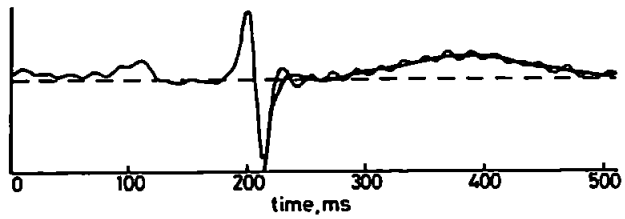

Fig. 9 *Location of isoelectric level and smooth approximation of fetal ECG ST segment*

3.1 Measurement of the T/QRS ratio

The T/QRS ratio is a feature of special interest [7] and is given by the T-wave amplitude normalised against the QRS amplitude. The QRS amplitude is taken to be a physiological constant, in theory not changing with time or fetal condition. To preserve short-term changes in the waveform, measurements of the T/QRS ratios should be made on a beat-by-beat basis from the raw rather than average data. There can be major difficulties in doing this as the location of the T-wave can become difficult. When a T-wave is present (Fig. 10) locating the T-peak is a simple exercise of peak detection, but unfortunately this is not always the case (Fig. 11). Further, when there is severe baseline shift a false ST segment depression may be introduced Fig. 12.

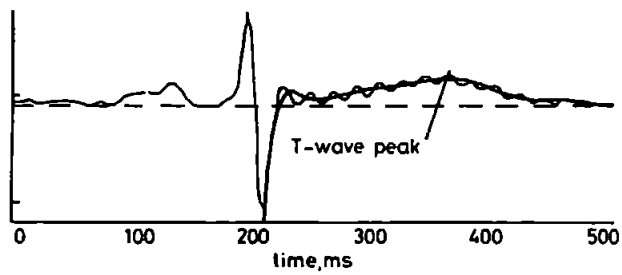

Fig. 10 *Raw fetal ECG with prominent T-wave*

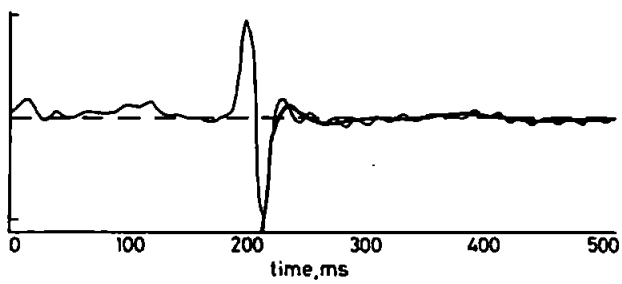

Fig. 11 *Raw fetal ECG with flat or absent T-wave*

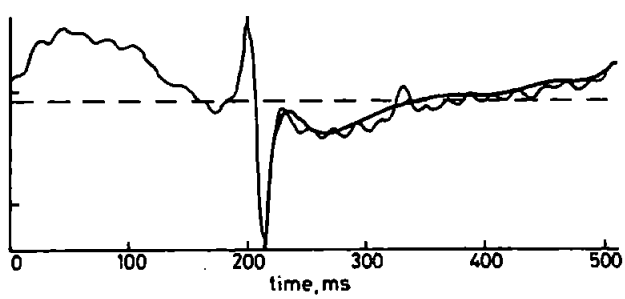

Fig. 12 *Raw fetal ECG with false ST depression caused by remaining baseline shift*

To minimise these problems, the average ECG waveform may be used to locate the expected time region of the T-wave peak. Using this additional information, the nearest peak to this in the filtered ST segment is taken to be the T-wave. This allows direct beat-by-beat measurement of the T/QRS ratio from the filtered data to preserve short-term changes in the waveform. For reliable measurement of the T/QRS ratio it is important for the data to be of good quality. A way of inferring the quality of data is discussed in Section 4.2.

3.2 PR/RR ratio

The ratio PR/RR = (time interval between the P-wave peak to the R-wave peak)/(time interval between the previous R-wave and the current R-wave) has been found to be of clinical interest [2]. Location of the P-wave is still susceptible to similar problems found with the T/QRS ratio so the same techniques apply. Again, knowledge of signal quality is essential.

3.3 Measurement of ST and PR area and gradient

Accurate measurement of ECG features such as the ST area (for assessing ST depression) and gradient information (e.g. for location of extrema and defining the starting point of features) require the computation of the definite integrals and derivatives of the Chebyshev curves fitted to the ST and the PR segments. Given the equation of the Chebyshev curve for the ST or PR segment $f(t)$,

$$f(t) = c_0T_0(t) + c_1T_1(t) + c_2T_2(t) + \ldots + c_nT_n(t) \quad (16)$$

its indefinite integral $g(t)$ may be expressed as another Chebyshev polynomial series of degree $n+1$:

$$\begin{aligned} g(t) &= c_0 \int T_0(t)dt + c_1 \int T_1(t)dt + c_2 \int T_1(t)dt + \\ &\quad c_3 \int T_1(t)dt + c_4 \int T_1(t)dt + \ldots + c_n \int T_n(t)dt \\ &= \frac{c_0}{2}\left\{\frac{T_1(t)}{0+1} - \frac{T_{-1}(t)}{0-1}\right\} + \frac{c_1}{2}\left\{\frac{T_2(t)}{1+1} - 0\right\} + \\ &\quad \frac{c_2}{2}\left\{\frac{T_3(t)}{2+1} - \frac{T_1(t)}{2-1}\right\} + \ldots + \frac{c_n}{2}\left\{\frac{T_{n+1}(t)}{n+1} - \frac{T_{n-1}(t)}{n-1}\right\} \end{aligned}$$

Noting that $T_{-1}(t) = \cos[-1 \cos^{-1}t] = \cos[1 \cos^{-1}t] = T_1(t)$, collect for functions of the same degree we now write this as

$$\begin{aligned} g(t) &= \frac{T_1(t)}{2}\{c_0 + c_1 + c_0\} + \frac{T_2(t)}{2}\left\{\frac{c_1}{2} - \frac{c_3}{2}\right\} + \\ &\quad \frac{T_3(t)}{2}\left\{\frac{c_2}{3} - \frac{c_4}{3}\right\} + \ldots + \frac{T_n(t)}{2}\left\{\frac{c_{n-1}}{n} - \frac{c_{n+1}}{n}\right\} \end{aligned}$$

where $c_{n+1} = 0$. We can therefore see by inspection that

$$d_k = \begin{cases} \dfrac{c_{k-1} - c_{k+1}}{2k}, & k > 1 \\ \dfrac{2c_0 - c_2}{2}, & k = 1 \end{cases} \quad (17)$$

Using this we can compute the area (definite integral) for any section of the curve. For example, to compute the area between the ST segment curve $f(t)$ and the isoelectric level in the time interval $0.1 \leq t \leq 0.5$ we first subtract the DC isoelectric reference level, I, and then compute the indefinite integral $g(t)$ as above. The desired area is simply computed as $\{g(0.5) - g(0.1)\}$. The derivative of the Chebyshev curve for the ST or PR segment can be readily obtained by exploiting the

relationship between c_k and d_k. Thus, given $g(t)$ in eqn. 17, we find $f(t)$ in eqn. 16 by computing the coefficients c_k from d_k:

$$\frac{d}{dt}T_{k-1}(t) = \frac{k-1}{k+1}T_{k+1}(t) - (k-1)\frac{d}{dt}T_k(t), \quad k > 0 \quad (18)$$

which is a two-term recurrence relationship for evaluation of the derivatives, where from eqn. 17 it is clear that

$$d_{k+1} = \begin{cases} \dfrac{c_k - c_{k+2}}{2(k+1)}, & k > 0 \\ \dfrac{2c_0 - c_2}{2}, & k = 0 \end{cases}$$

and solving for c_k we get the recursive relationship

$$c_k = \begin{cases} 2(k+1)d_{k+1} + c_{k+2}, & k > 0 \\ \dfrac{2d_1 + c_2}{2}, & k = 0 \end{cases} \quad (19)$$

for $k = n, n-1, \ldots, 0$. By definition, $c_{n+1} = 0$ and $c_{n+2} = 0$. We are effectively remapping an integral expression back to the original, where the coefficients d_k are the coefficients of the $(n+1)$th-order approximation and c_k are the coefficients of the derivative. Eqns. 17 and 19 are very useful for reliable feature extraction and for evaluating new features from the fetal ECG, such as ST area and shape, which have hither to not been possible.

Fig. 13 *Fetal heart rate measured on beat-by-beat basis over period of 10min*

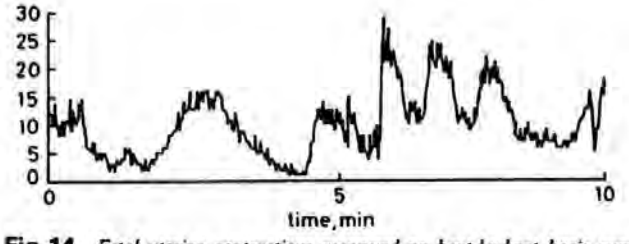

Fig. 14 *Fetal uterine contractions measured on beat-by-beat basis over period of 10min*

Fig. 15 *Fetal ECG T/QRS ratio measured on beat-by-beat basis over period of 10min*

3.4 Example results

Some of the important features which are continuously measured from the fetus and mother are shown in figs. 13–17. The fetal heart-rate and uterine contraction plots, which together are known as the CTG, are usually the only information continuously available to the clinician. The T/QRS ratio, PR interval and RT interval (see Fig. 1) are all extracted and plotted here on a beat-by-beat basis and this enables the short-term trends in the fetal ECG to be analysed. For example, the sharp fall in heart rate shown in Fig. 13 is known as a bradycardia and is an abnormal CTG pattern. Using the techniques described it is possible to display and investigate the simultaneous changes in the ECG features, which has not previously been possible. The features in Figs. 13–17 have all been smoothed to clarify their short-term trends. These data were obtained from a patient during the second stage of labour. The baby was delivered with a normal outcome. Only 0.5% of these data were rejected, with over 80% being of very good quality.

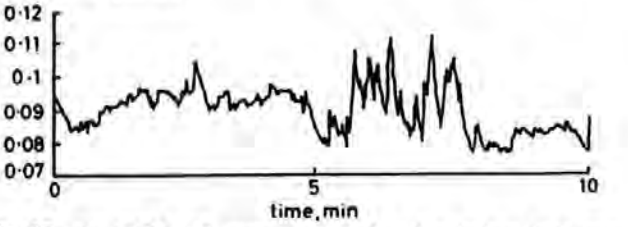

Fig. 16 *Fetal ECG PR interval measured on beat-by-beat basis over period of 10min*

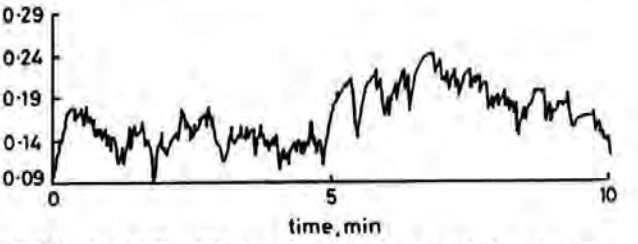

Fig. 17 *Fetal ECG RT interval measured on beat-by-beat basis over period of 10 min*

4 Quality assessment

There are some very real dangers in extracting features from poor quality data. The signal processing techniques discussed so far are all designed such that the minimum information is lost from the signal, but this is obviously dependent on the quality of the data. An attempt to enhance very poor quality data may result in over filtering of the signal and hence unreliable measurements. Many of the techniques described in this paper inherently provide quality measures which may be used to determine which features can be reliably measured. Due to the complexity of this problem, a full treatment of the subject cannot be given here but will be published separately. A brief summary is described here.

4.1 Baseline shift quality index

For a given ECG, a simple measure of baseline severity may be derived from

$$v_1 = \frac{1}{N-2}\sum_{m=0}^{N-1}\left(\frac{B[m] - x[m]}{\text{QRS}}\right)^2$$
$$v_2 = \frac{1}{N-2}\sum_{m=0}^{N-1}\left(\frac{B[m] - \bar{B}}{\text{QRS}}\right)^2 \quad (20)$$

where QRS is the peak amplitude of the fetal ECG complex. v_1 is the mean square deviation between the baseline approximation and the raw ECG data and is a measure of goodness of fit. This is used to detect occasions where the baseline approximation cannot fit to

the raw ECG data. This is caused by events such as transient shifts in baseline. v_2 is the mean square deviation between the baseline approximation and its mean (or DC). This is a measure of the energy in the baseline. All of these measures are normalised against the QRS amplitude to compensate for any change in signal amplification.

Interpretation of these measures is based on a set of simple rules which are used to grade this data into one of three categories. These are excessive baseline (reject the data), minimal baseline (restricted use) and little or no baseline (unrestricted use). The full details of this will be published separately.

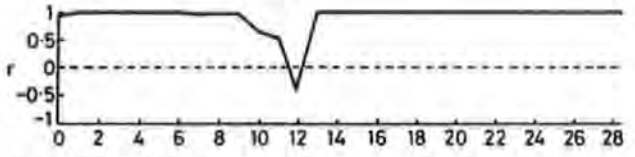

Fig. 18 *Correlation r between coefficient vectors of 30 ST segment approximations and average coefficient vector*

4.2 PR and ST segment quality

Assessment of the ST and PR segment quality is based on the correlation r of the average ECG complex and each individual raw ECG complex. Assuming that the average waveform is a good estimate of the expected fetal ECG shape, then any raw complex that differs greatly from this indicates that its quality is suspicious. As polynomial approximations are computed for the ST and PR segments for both raw and average data, then the linear correlation coefficient r is computed using the coefficients of the raw and the average polynomial approximations. The correlation r is computed as follows:

$$r = \frac{1}{CA} \sum_{k=1}^{m} c_k a_k \tag{21}$$

where $A = [\Sigma_{k=1}^{m} a_k^2]^{1/2}$ and $C = [\Sigma_{k=1}^{m} c_k^2]^{1/2}$. An example is shown in Fig. 18, where 30 complexes are correlated to their average waveform. Vectors 11 and 12 in this example have a correlation coefficient r of only 0.5 and −0.4, respectively. This implies their shape differs significantly from that of the average waveform and so these are assumed to be corrupted by noise and would be rejected. On inspection of the data, these examples were distorted owing to remaining baseline shift. This method works well with detecting distortions due to baseline shift. However, this method is insensitive to high frequency noise such as muscle and mains noise. This is because the curves tend to fit through the noise, effectively filtering it out. The levels of high-frequency noise for both the PR and ST segments are obtained as follows.

average noise power (dB) =

$$10 \log_{10} \left\{ \frac{1}{(N-1)} \sum_{m=0}^{N-1} \left(\frac{x[m] - f[m]}{\text{QRS}} \right)^2 \right\} \tag{22}$$

where $f[m]$, $m = 0, 1, ..., N-1$, is the discrete Chebyshev approximation of the ST or PR segment, $x[m]$ is the raw data of the ST or PR segment, and QRS is the peak-to-peak amplitude of the fetal ECG complex. Interpretation of these measures is again performed by a set of simple rules and will be published separately.

5 Discussion and conclusion

An important objective of this work is to make it possible to measure features from the fetal ECG on a beat-by-beat basis to retain as much clinical information as possible. Measurement of features on a beat-by-beat basis has not previously been possible because of the poor quality of the raw data. To ensure that the features are measured accurately it is necessary to enhance the SNR of the ECG, e.g. by filtering. However, over filtering the data also removes potentially useful clinical information from the signal, although it is unclear how much filtering can be tolerated before a significant amount of useful information is lost. Thus, our approach is to keep filtering to a minimum. For some of the more sensitive features such as ST depression which may not change very rapidly, unlike RR values for example, it may be sufficient to take measurements intermittently only when good quality data is available. Thus it is important that the quality of the raw data is measured on a beat-by-beat basis so that the good data can be identified. An advantage of our approach is that it provides quality information automatically.

The baseline shift is a major cause of poor quality data. For adult ECG, different fixed filtering techniques have been applied to remove baseline shift caused by breathing artefact. It has been shown that low-frequency energy can be removed using either fixed filter [18, 19] or a time-varying [20] filter with minimal distortion to the ST segment. In all these cases provision was made to avoid phase distortion avoid distortion of the ST segment. Curve-fitting techniques such as cubic spline and polynomial approximation have also been successfully applied to adult ECG without introducing significant distortion to any one complex [21]. However, due to movement atrefact in labour the baseline shift found in the fetal ECG signal has a wider spectrum to the adult and can typically range up to and sometimes beyond 2hz. We can only justify using minimal linear filtering (−3dB < 1Hz) as it is not clear at this stage how much of the low-frequency energy can be filtered from the fetal ECG before sensitive shape changes in the ST segment are suppressed. For fetal monitoring the cubic spline is also not practical as the isoelectric anchor points [21] (PQ and TP regions) used in the adult ECG cannot always be located.

Our preferred method was polynomial approximation. This way we minimise the information being removed while also minimising distortion to any one complex [21]. Using this approach, the effects of baseline shift on the signal quality can be assessed and if it is too severe, measurement of sensitive features such as ST segment shape may be avoided. Where there is minimal baseline shift, this technique takes very little away from the signal enabling ST segment shape to be analysed with more confidence. McManus found a sixth-order polynomial approximation sufficient for adult ECG. We modified the technique to use higher order Chebyshev polynomials (typically 10th order) to get a more uniform approximation and better computational stability. Where the quality of the data is deemed good, the Chebyshev approximation can then easily be truncated to a much lower order (typically sixth) and the baseline shift removed.

High levels of muscle noise add uncertainty to the measurement of features. Measurement and assessment of mains and muscle noise is again important and

allows feature extraction to be selective or interpreted in the correct context. The effects of the muscle noise may be removed by averaging, but the optimum number of ECG complexes to average without the loss of important clinical information may change between patients. Further, the fetal ECG shape undergoes normal changes during labour, particularly during heart-rate changes or uterine contractions and so signal averaging may suppress short term information, particularly in the ST segment. Measurement on a beat-by-beat basis remains the attractive approach.

Fitting smooth curves to ECG segments greatly enhances the signal and defines clearly the features in the waveform without ambiguity. The smooth curve provides an analytical expression of the ECG waveform, making it possible to compute time, amplitude, integrals and gradients, etc. Thus, we can potentially measure any features (time constants, amplitude, area, zero crossings, maxima and minima) from the waveform very accurately.

Different curve-fitting techniques have been tried using normal polynomials, cubic splines and rational functions for adult ECG [21] to provide a least-squares fit to data. We have found Chebyshev polynomials to be superior giving a more satisfactory representation for both baseline approximation and feature extraction. This is because Chebyshev polynomials can produce a curve where the maximum error of the approximation is kept to a minimum. As a result, the error of the approximation is evenly distributed over the whole waveform. This is not the case for least-squares techniques where the errors are usually large at the ends of the data and very small at the centre. Chebyshev polynomials are numerically stable even when the order is high. Curve fitting also provides inherent data compression as the approximation coefficients represent the useful data. This may be exploited for efficient data storage and subsequent analysis.

The techniques reported here have applications in other areas of biomedicine where it is required to enhance the data. An example is in the assessment of neonates using evoked potentials where the enhancement and measurement of features are necessary.

5.1 Further work

The next stage of our work is to carry out a thorough analysis of the change in the ECG features, investigate their relationships to other events in labour and evaluate their clinical value in fetal monitoring. This would include spectrum analysis of heart rate variability and the ECG complex itself. At present, work is in progress at our units and other centres, as part of the European Community concerted action on new methods of fetal monitoring to collect data from various categories of patients. This will provide data for the next stage of the research, which will be published in due course.

6 Acknowledgments

The authors acknowledge the assistance of Dr Jenny Westgate and Dr Sarah Beckley for clinical assistance. They are indebted to Professor Karl Rosén for helpful comments and support for this work. They also thank the labour ward staff at Plymouth General Hospital for their help and cooperation. The financial support of the PCFC and South-West Regional Health Authority for this work is acknowledged.

7 References

1 GREENE, K.R.: 'The ECG waveform' *in* WHITTLE, M. (Ed.): 'Balliere's clinical obstetrics and gynaecology', (London, 1987), 1, 2, pp. 131–155
2 MURRAY, H.G.: 'The fetal electrocardiogram: current clinical developments', *J. Perinat. Med.*, 1986, **14**, pp. 399–404
3 KIRK, D.L., and SMITH, P.R.: 'Techniques for the routine on-line processing of the fetal electrocardiogram', *J. Perinat. Med.*, 1986, **14**, pp. 391–397
4 LILJA, H., KARLSSON, K., LINDECRANTZ, K., and ROSEN, K.G.: 'Microprocessor based waveform analysis of the fetal electrocardiogram during labour', *Int. J. Gynecol. Obstet.*, 1989, **30**, pp. 109–116
5 KRAUSE, W.: 'A computer-aided monitoring system for supervision of labour', *in* MAEDA, K., *et al.* (Eds.): 'Computers and perinatal medicine', (Elsevier, Amsterdam, 1990), pp. 103–111
6 IFEACHOR, E.C., KEITH, R.D.F., WESTGATE, J. and GREENE, K.R.: 'An expert system to assist in the management of labour' *in* LIEBOWITZ, J. (Ed): 'World congress on expert systems. Vol. 4. (Pergamon, 1991), pp. 2615–2622
7 WESTGATE, J., HARRIS, M., CURNOW, J., and GREENE, K.R.: 'Plymouth randomised trial of the cardiotocogram only versus ST waveform plus cardiotocogram for intrapartum monitoring in 2400 cases', *Am. J. Obstet. Gynecol.*, 1993, **169**, (5), pp. 1151–1160
8 SHEILD, J.E.A., and KIRK, D.L.: 'The use of digital filters in enhancing the fetal electrocardiogram', *J. Biomed. Eng.*, 1981, **44**, (3), pp. 44–48
9 HON, E.H., and LEE, S.T.: 'Noise reduction in fetal electrocardography, II Averaging techniques', *Am. J. Obstet. Gynecol.*, 1963, **87**, (8), pp. 1086–1096
10 WESTGATE, J., KEITH, R., CURNOW, J.S.H., IFEACHOR, E.C., and GREENE, K.R.: 'Suitability of fetal scalp electrodes for monitoring the fetal electrocardiogram during labour', *Clin. Phys. Physiol. Meas.*, 1990, **11**, (4), pp. 297–306
11 'Electrocardiography recommendations for the standardization of leads and of specifications for instruments in ECG/VCG circulation'. American Heart Association Committee, 1975, pp. 1–25
12 OUTRAM, N.J., and IFEACHOR, E.C.: 'Techniques for detection and classification of the fetal QRS complex'. IEE colloquium on *Applications of neural networks to signal processing*, digest 1994/248, pp. 10/1–3
13 AMBARDAR, A.: 'Analogue and digital signal processing' (PWS, Boston, USA, 1995)
14 KREYSZIG, E.: 'Advanced engineering mathematics' (Wiley, New York, USA, 1993, 7th edn.)
15 CLENSHAW, C.W.: 'Mathematical tables, Vol. 5'. National Physical Laboratory, (London, H.M. Stationary Office, 1962)
16 IFEACHOR, E.C., and JERVIS, B.: 'Digital signal processing, a practical approach' (Addison–Wesley, Wokingham, UK, 1993)
17 XUE, Q., HU, Y.H., and TOMPKINS, W.J.: 'Neural-network-based adaptive matched filtering for QRS detection', *IEEE Trans.*, 1992, **BE–39**, (4), pp. 317–329
18 VAN ALSTE, J.A., and SCHILDER, T.S.: 'Removal of base-line wander and power-line interference from the ECG by an efficient FIR filter with a reduced number of taps', *IEEE Trans.*, 1985, **BE–32**, (12), pp. 1052–1060
19 POTTALA, E.W., BAILEY, J.J., HORTON, M.R., and GRADWOHL, J.R.: 'Suppression of base-line wander in the ECG using a bilinearly transformed, null-phase filter', *J. Electrocardiol.*, **22**, pp. 243–247
20 SÖRNMO, L.: 'Time-varying digital filtering of ECG baseline wander', *Med. Biol. Eng. Comput.*, 1993, **31**, pp. 503–508
21 MCMANUS, C.D., TEPPNER, U., and NEUBERT, D.: 'Estimation and removal of base-line drift in the electrocardiogram', *Comput. Biomed. Res.*, 1993, **18**, pp. 1–9

TECHNIQUES FOR DETECTION AND CLASSIFICATION OF THE FETAL QRS COMPLEX.

Outram N.J.[1] and Ifeachor E.C.[1]

INTRODUCTION

A critical process in both the fetal cardiotocogram (CTG) and fetal electrocardiogram (FECG) analysis is to determine the location of the QRS complex from the raw FECG data. Difficulties arise because the FECG signal is degraded and sometimes totally obscured by noise. Thus, to determine the location of the QRS complexes is a two stage process: pre-processing of the noisy FECG to detect candidate QRS complexes, and pattern recognition to classify these as genuine QRS complexes or noise. In this paper, we have compared an ANN technique with conventional techniques for both pre-processing and pattern recognition of the FECG.

PRE-PROCESSING

Initially an optimal filter[1] and a 50Hz notch filter is used to improve the signal-to-noise ratio, but low frequency baseline shifts and mains noise often still remain. Three different techniques for baseline shift removal are compared. In the first technique we detect the sharp gradients of the QR and RS portions of a candidate QRS complex by differentiating the FECG data. The candidate ECG complexes are then located by a simple threshold detector. The baseline shift is almost totally removed because it has a very small first derivative[2]. The approximate first derivative, $\Delta x(t)$, of the raw data, $x(t)$, is computed as

$\Delta x(t)=(x(t+1)-x(t-1))/2$. The threshold detector is aided further by squaring the derivative and smoothing the result with a simple band-pass filter. Unfortunately differentiation worsens the effects of higher frequency noise and this can be very problematic.

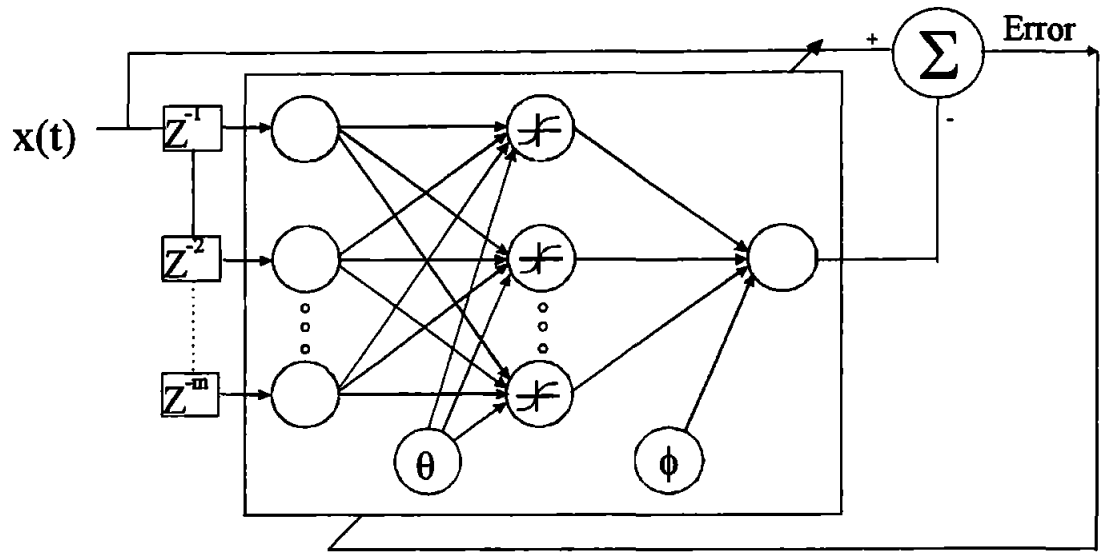

Figure 1 Non-linear prediction filter using a MLP

The second technique avoids differentiation and some of its problems. This technique uses a multi-layered perceptron, with sigmoid activation functions in the hidden layer and a linear output, as a non-linear prediction filter[2] (see figure 1). The network is trained on-line to predict the unwanted low-frequency components of the corrupted FECG signal. The output error is mostly high-frequency noise and the QRS complex. It is important to obtain the correct training rates for the hidden and output layers. The method described in [2] computes these rates automatically but it is quite complex and computationally expensive.

The third technique uses least-squares fitting to approximate the unwanted low-frequency components of the corrupted FEGC signal. A low order curve, of the form $f(t)=c_0 + c_1t + c_2t^2 + ... + c_nt^n$; $t=\{-L,-L+1,...,L\}$, is fitted to a window of 2L+1 raw FECG data points x(t). The degree of approximation, n, and the window size, 2L+1, are chosen such that only the slow moving parts of the data (such as baseline shift) are accurately approximated but the sharp QRS portions of the data are very poorly approximated. L was typically between 10 and 15 and n typically 2 or 3. The mid-point of the curve, $f(0)=c_0$, is then

taken as the low-frequency approximation. The window is then advanced by one sample and the process is repeated. Note we only need to compute the coefficient c_0 and examining the expression for computing c_0 it can be shown that this is simply a fixed non-causal fixed FIR filter. This is sometimes referred to as a Savitzky-Golay smoothing filter[3].

Some example results are of the three techniques are shown in figures 2,3 and 4.

[1]School of Electronic, Communication and Electrical Engineering, University of Plymouth, Devon, UK.

PATTERN RECOGNITION

Having located the candidate QRS complexes a pattern recognition technique is used to discriminate the QRS complex pattern from all other possible patterns such as noise. The results of Principal Component Analysis (PCA) suggest that 25 samples of the FECG are sufficient for the pattern classifier input vector $\mathbf{x}$ 10 samples before and including the R wave peak and 14 after the R wave were used as the input vector $\mathbf{x}$. This is normalized ,i.e. $\mathbf{x}_{norm} = \mathbf{x} / \mathbf{x}^T\mathbf{x}$, before being presented to the classifier. Two techniques are compared. The first is a correlation algorithm $r=\mathbf{x}^T\mathbf{w}$, where r is the correlation coefficient and $\mathbf{w}$ is the template vector. The second is a Multi-Layered Perceptron (MLP). 250 actual QRS examples and 250 false examples (noise) were extracted from the data. The MLP was trained on a subset of 50 correct (QRS) and 50 false cases using the generalized delta rule with back-propagation. For the correlation technique, the template $\mathbf{w}$ was computed from the 50 examples of QRS complexes as follows. Each example QRS complex is stored in a column of a matrix $\mathbf{X}$. The correlation matrix $\mathbf{R} = \mathbf{X}.\mathbf{X}^T$ is calculated, and it can easily be shown that the optimum solution for $\mathbf{w}$ is an eigen-vector of $\mathbf{R}$, such that $\mathbf{R}.\mathbf{w} = \lambda_{max}.\mathbf{w}$, where λ_{max} is the largest eigen-value of $\mathbf{R}$. Both these techniques were then tested on the full set of examples.

A summary of the results are given below. The accuracy of the two methods are measured according to $\%accuracy=100\%.(N-F_p-F_n)/N$, where N is the total number of examples in

the test, F_p is the number of false positives and F_n is the number of false negatives. For this experiment N was 500.

Technique	Dimensions	False Positives	False Negatives	Accuracy
Correlation	25-1	1	0	99.8
Multi-Layer Perceptron 25_2_1	25-2-1	3	0	99.4
Multi-Layer Perceptron 25_3_1	25-3-1	4	0	99.2
Multi-Layer Perceptron 25_4_1	25-4-1	3	0	99.4

DISCUSSION AND CONCLUSION

For baseline removal the differentiation technique was prone to the effects of high frequency noise. The MLP technique was an improvement but the preferred method was the least-squares technique. The least-squares technique performed at least as well as the MLP but has the advantage of simplicity and less computational overhead.

Correlation was the most reliable pattern recognition technique. Although the MLP can represent a much more complex pattern space, it fails because its behavior can never be guaranteed when presented with random noise. The result of the correlation algorithm however is a predictable linear function of the angle θ between the 'weight vector **w**' and the presented vector **x**. i.e. $r = |\mathbf{x}|\,|\mathbf{w}| \cos\theta$. The output of a MLP is a non-linear function of θ and is therefore not predictable in the presence of noise. Unlike the MLP, the correlation technique is limited when dealing with more than one pattern. Since the QRS complex can change shape between patients and even during a single labour[4], the performance of the correlation technique can diminish. To overcome this we update the template vector on-line. If a positive detection is made ($r>0.9$) and the features (such as QRS width and QR,RR,RS intervals) are within acceptable limits then the template is modified towards the presented example. This way the system tracks the changes in the

FECG and certainty of detection is maintained or improved. The improvement in performance at the start of a previously unseen patient data is illustrated in figure 5. These findings have suggested another suitable method might be to use a Radial Basis Function. This has the advantage of the MLP as it can represent a complex pattern space whilst also maintaining the same predictable performance as correlation in the presence of noise.

FIGURES

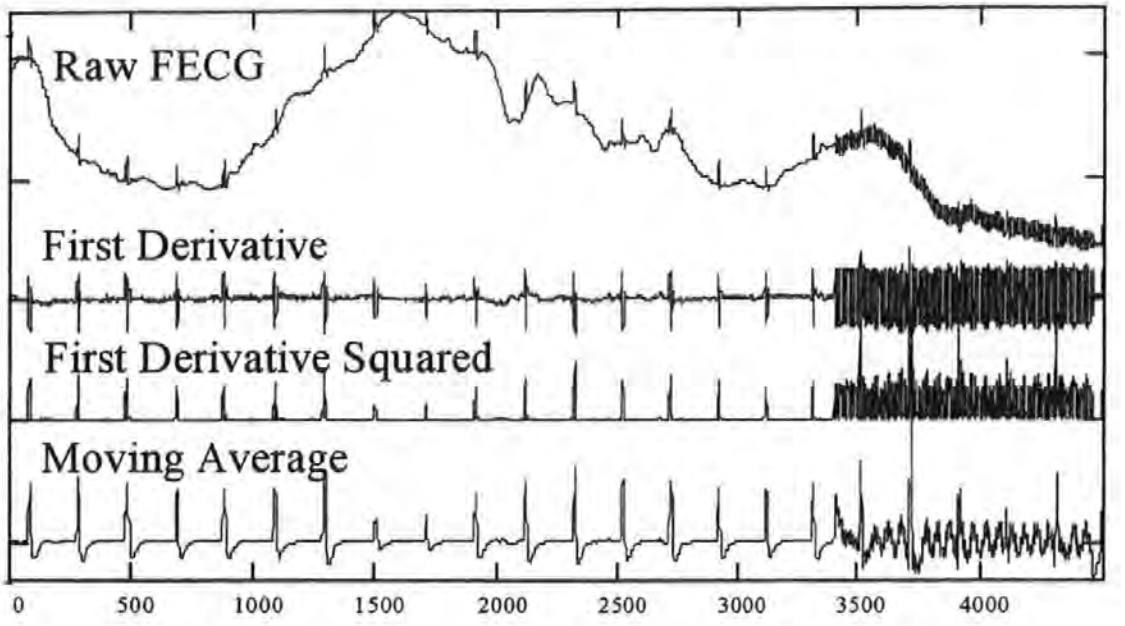

Figure 2. Results of Differentiation

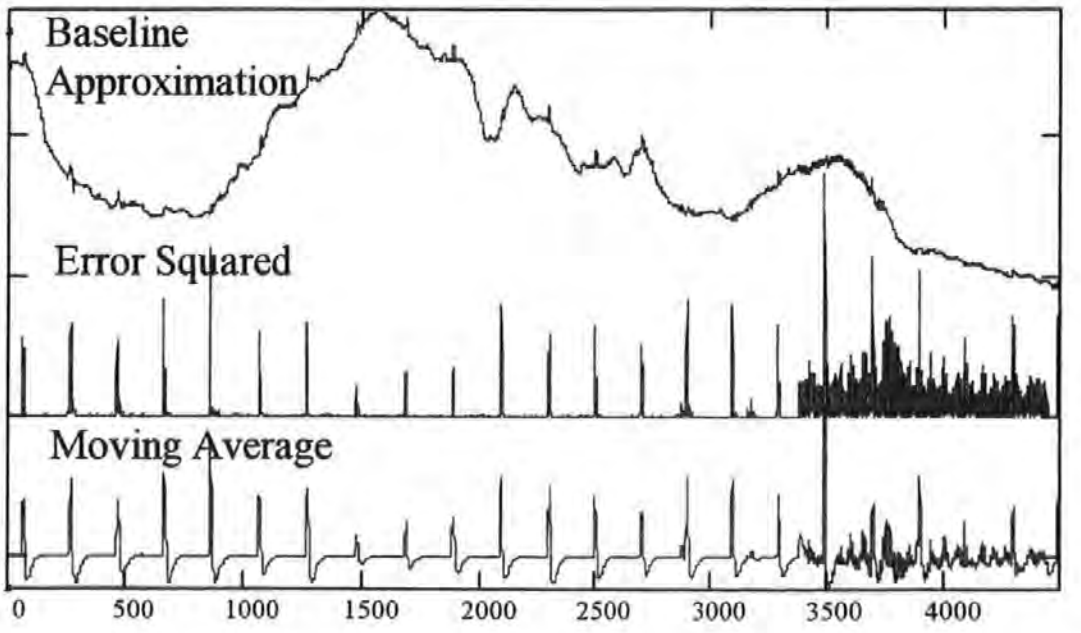

Figure 3. Results of MLP non-linear prediction filter

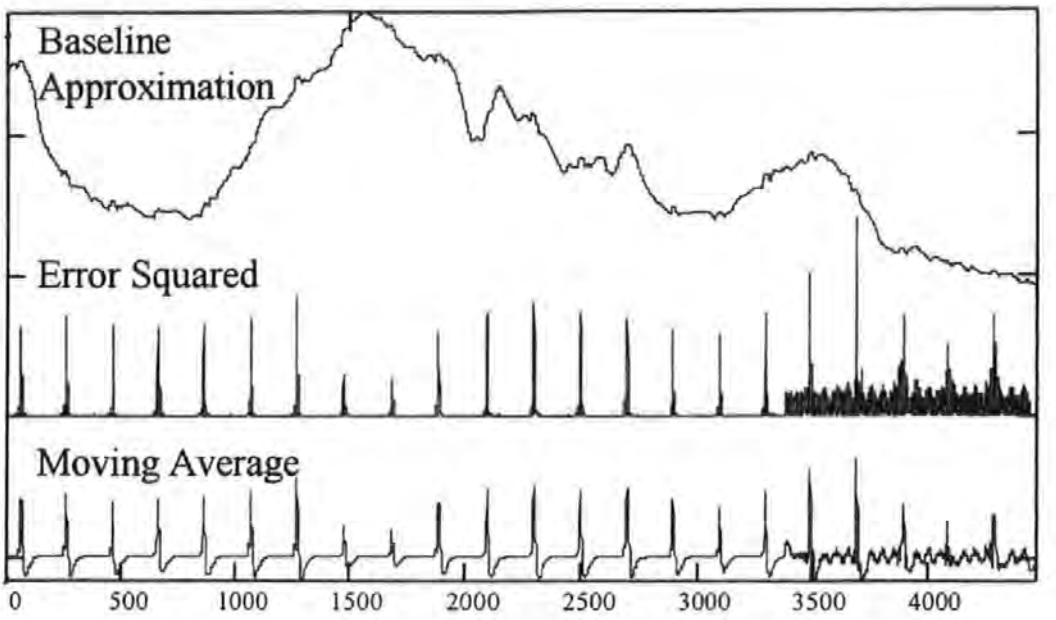

Figure 4. Results of fixed Filter

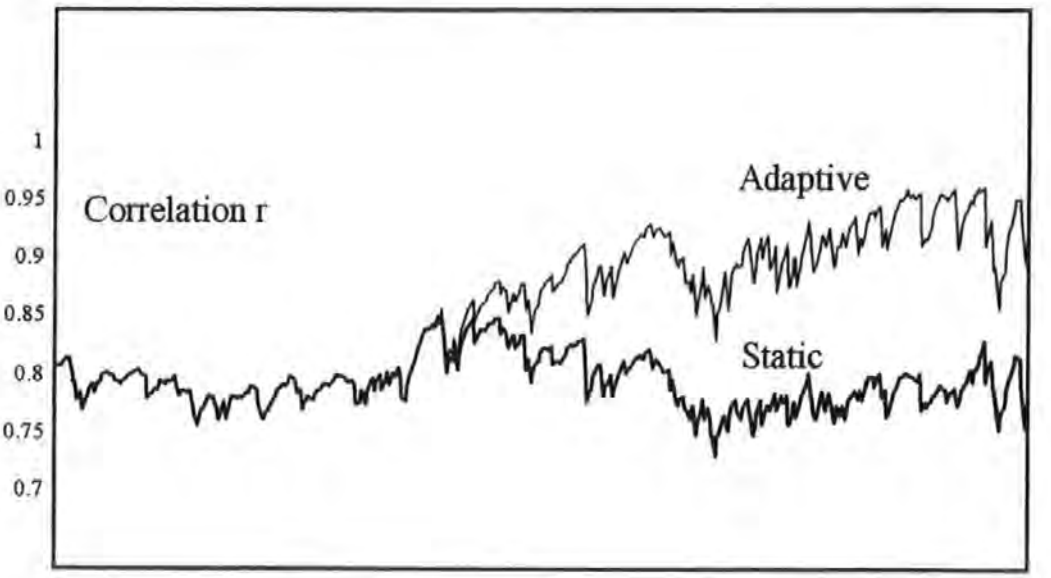

Figure 5. Comparison of static and adaptive correlation algorithm.

REFERENCES

[1] Outram N.J., Ifeachor E.C., VanEetvelt P., Curnow J.S.H & Greene K.R., Techniques for optimal enhancement of the fetal electrocardiogram, submitted to IEE, 1994

[2] Xue Q., Hu Y.H. and Tompkins W.J., Neural-Network-Based Adaptive Matched Filtering for QRS Detection., IEEE Trans. Biomed. Eng., 39, 4, (1992)

[3] Press W.H., Teukolsky S.A., Vetterling W.T. & Flannery B.P., Numerical recipes in C. (2nd Ed.), Cambridge University Press, Cambridge, UK., 1992

[4] Murray H.G., The fetal electrocardiogram: current clinical developments in Nottingham., J. Perinat. Med., 14, 1986, pp399-403

FUZZY LOGIC CONCEPTS FOR PATTERN ANALYSIS AND INTERPRETATION OF CHANGES IN THE FETAL ELECTROCARDIOGRAM

Outram N J , Ifeachor E C

School of Electronic, Communication and Electrical Engineering, University of Plymouth, PLYMOUTH, Devon, UK, PL4 8AA

Abstract

The need for computer-assistance in the management of labour to improve the quality of obstetric care is widely recognised. Uncertainty and difficulty in visually interpreting cardiotocogram (CTG) patterns can lead to unnecessary medical intervention or fetal injury. The CTG does not provide all the information needed in all cases, but the fetal electrocardiogram (ECG) could contain the extra information required by clinicians. Because interpretation of the ECG requires a great deal of experience, which is not always available, we are working to extend the capability of the INFANT expert system to include the fetal ECG features. In this paper we examine the process of representing imprecise and uncertain expert knowledge such that it can be built into a fuzzy expert system. To achieve this, the sources of uncertainty and imprecision in both knowledge and data are identified and the concepts of linguistic variables and fuzzy membership functions are defined. Finally we consider a rule structure based on finite state machines that can model the experts ability to recognise pattern changes in time from the CTG and ECG features.

1. Introduction

The fetal electrocardiogram (FECG) waveform represents the electrical activity of the baby's heart as measured from the body surface, see figure 1. Like the adult ECG, the normal fetal ECG is characterised by five peaks and valleys labelled P, Q, R, S, and T. From the fetal ECG the instantaneous fetal heart rate (FHR) can be derived

in beats per minute (bpm). A plot of successive instantaneous heart rates gives the FHR pattern. A continuous display of the FHR pattern together with the contraction of the womb (uterine activity) is known as the cardiotocogram (CTG). The fetal ECG contains potentially valuable information that could assist clinicians in making more appropriate and timely decisions during labour[1]. This has not been widely put into practice because the current knowledge and expertise required to interpret the changes the fetal ECG is rare and has been restricted to a few centres in the world. The many years of research has never been collated and implemented such that clinicians can make full use of it. This has also been hindered by the difficulty of processing the often noisy fetal ECG without significant distortion[10].

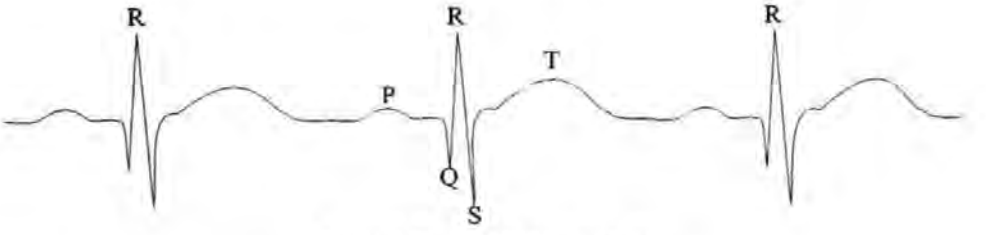

Figure 1 The fetal ECG waveform

Currently, the assessment of the condition of the fetus during labour is based on visual analysis and interpretation of the CTG, but this requires a great deal of experience which is not always available to all labour wards day and night. Uncertainty and difficulty in interpreting CTG patterns during labour leads to unnecessary medical intervention (e.g. caesarean section or forceps deliveries), fetal injury or a failure to intervene when needed [2-3]. In the UK alone, over £350M is spent each year in birth related medical negligence claims. The need for computer-assistance in the management of labour to improve the quality of obstetric care is widely recognised [2-7].

The INFANT expert system[6] has been sucessfully developed to analyse and interpret changes in the CTG, taking into account important events in labour, and to provide advice to clinicians during labour. However, the CTG alone does not provide all the information needed, in all cases, for accurate assessment of fetal condition. Additional information may be obtained by a proper analysis of progressive changes in the fetal ECG without having to alter current patient handling routines. The impetus for investigating the value of the ECG waveform comes from extensive experimental research, clinical observations and studies which suggest that the assessment of fetal condition based on the ECG pattern changes plus the CTG can improve the quality of care [1],[7-9]. In a recent clinical study, the use of the combination of the ST waveform plus CTG analysis led to a significant reduction in caesarean section and forceps delivery for fetal distress with no adverse effect on neonatal outcome[7].

1.1 Key features of the ECG waveform

One of the potentially important features of the fetal ECG waveform for discriminating between a fetus coping with normal stress of labour and those in distress is the shape of the ST segment (see figure 1) [1][7]. Significant pattern changes in shape associated with stress or distress include persistently rising T wave amplitude, negative T waves and depressed ST segments. Some of the changes in the ST waveform may be quantified as a ratio of the amplitude of the T wave to that of the QRS , known as the T/QRS see Figure 2.

However, the T/QRS ratio alone is a crude measure of the ST waveform shape[7-8]. There are other features in the ECG of potential interest including the ST area , the variability of the RR intervals, and other time constants, such as the duration of the P-wave and the width of the QRS complex (see
Figure 2) [10].

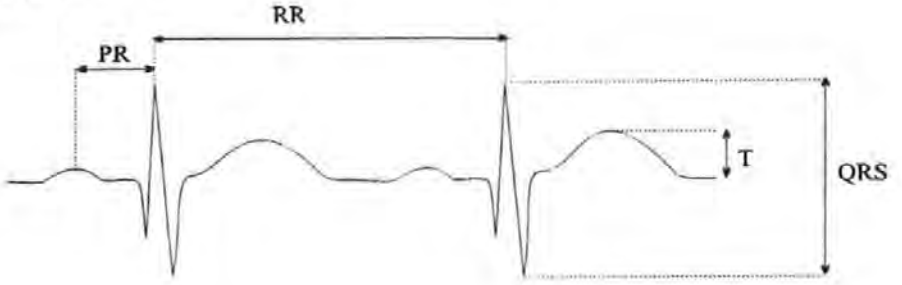

Figure 2 The fetal ECG features showing R-to-R and P-to-R intervals and the T and QRS amplitudes

These can all be used to build up a picture of the important changes in the fetal ECG shape at any stage during labour.

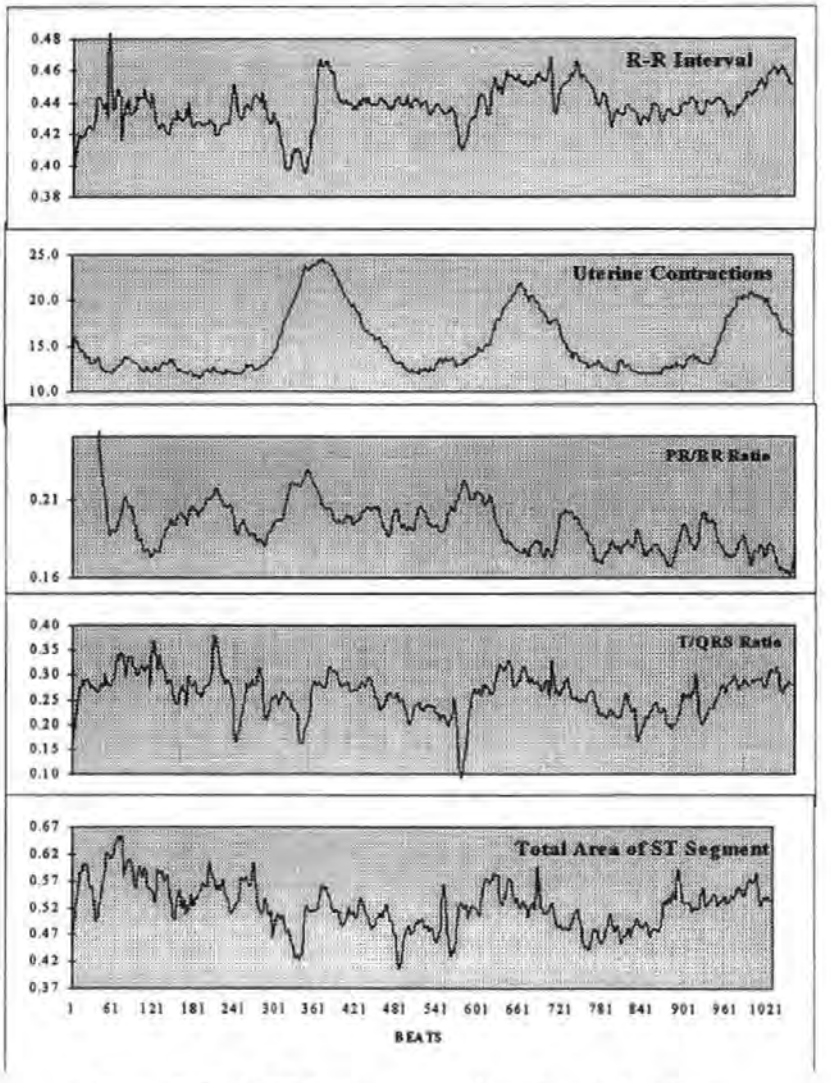

Figure 3. Fetal ECG features measured on a beat-by-beat basis

It has been shown in the past that it is hard enough for a clinician to interpret the changes in the CTG as it requires a great deal of expert knowledge and experience. Supplying further information, such as the features shown in Figure 3, would further increase the demands on expertise and possibly create more problems for the clinician. The additional problems of uncertainty and imprecision in both the obstetric data and knowledge further complicates the situation. An important the aim of our current work is to extend the capability of the INFANT expert system to include analysis and interpretation of changes in the fetal ECG features. This will provide the clinician with clear additional information that will improve the management of labour.

In this paper we discuss the problems of uncertainty and imprecision in the obstetric data and knowledge, and develop fuzzy logic concepts that best handle them. The sources of uncertainty in both the knowledge and the data are identified and discussed in section 2. The concepts that allow fuzzy logic to handle the uncertainty are discussed in section 2.2. Finally in section 3 we need to consider the process of formalising the obstetric knowledge such that it follows the experts thinking.

2. Fuzzy Logic concepts for Decision Making

We need to examine the concepts involved in developing a fuzzy expert. This will include identifying the sources of uncertainty and imprecision, defining the linguistic variables and fuzzy membership curves.

2.1 Sources of uncertainty and imprecision

The noise in the raw fetal ECG signal is a notorious source of imprecision and a major contributor to uncertainty. The fetal ECG features can become corrupted and give misleading information due to the presence of maternal ECG complexes, baseline shift , muscle noise and mains noise. Some ECG features are more sensitive than others to the effects of noise. For example, the RR interval is a very robust feature which can tolerate a great deal of signal enhancement without loss of information, and hence is very reliable. However, the shape of the ST waveform is very sensitive to signal enhancement and therefore far less can be done to remove the noise [10][17]. We have developed a signal enhancement scheme for the fetal ECG [10] which greatly improves the signal quality, and is capable of extracting fuzzy quality information from the data. From this, an assessment can be made to determine which features can be measured reliably. This is a source to uncertainty, particularly with borderline cases.

The feature extraction process can introduce imprecision and levels of uncertainty. Location of the P,Q,R,S and T peaks in the fetal ECG can be difficult in the presence of noise and certain ECG configurations. Problems such as notched P,R or T waves make it difficult to define the peak of the wave. Imprecision in the zero reference in the fetal ECG (known as the iso-electric line) will adversly effect other features such as the T/QRS ratio.

Even when the quality of the data seems acceptable, the natural variability of some of the features can be misinterpreted and lead to imprecision. For example, if the change in the RR interval is greater than 28bpm then this is regarded as an error (a false QRS detection), whether it is a genuine change or not. This is beause the knowledge does not account for such large changes and assuming such changes to be errors. The amplitude of the QRS complex is assumed to be a physiological constant and is used as a reference to normalise other features against changes in amplifier gain.

In reality, there is some natural variability in the QRS amplitude which causes the features such as the T/QRS ratio to fluctuate. This might explain the variability in the T/QRS and ST area features shown in Figure 3. Another problem is the variability in the shape of the fetal ECG. On rare occasions, the fetal ECG QRS complex can noticibly change shape, with a tendency for small R-waves and very deep S-waves. These can vary between patients or even within a signle labour. The means of identifying such cases is uncertain as there is a continuum of possible shapes. Fetal ectopic beats, although rare, can also add uncertainty, giving misleading RR intervals and very unusuall ST segment shapes.

Other sources of uncertainty and imprecision derive from the knowledge itself. Some of the existing knowledge is purely qualitative, based on observations, experience or theory which cannot easily be reproduced experimentally for often practical reasons. Sometimes the expert is not aware of all the rules he or she uses. When the knowledge is elicited and formalised, there might appear to be omissions, contradictions and imprecision within the knowledge. A significant problem is the process of converting what is often imprecise knowledge and data into a precise form that can be interpreted by a computerised expert system.

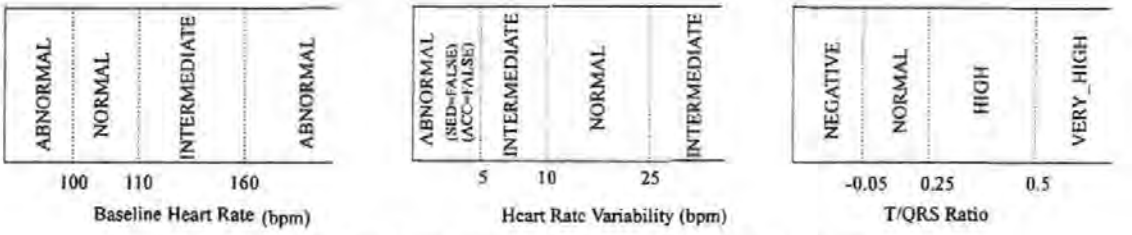

Figure 4 Classifying the features using a crisp decision boundary

A typical example shown in Figure 4, which is intended to classify fetal ECG features into meaningful categories. If 100 bpm was chosen as the 'crisp cut-off point' between Normal and Abnormal for the baseline heart rate (See Figure 4), then is it reasonable that 99.9 is Abnormal and 100.0 is Normal? This dilemma cannot be resolved because crisp decision boundaries such as this are abstract to human reasoning. Since human reasoning works with imprecision, dilemmas such as this are common and are illustrated below in a simplified knowledge-base, based on guidelines given to clinicians for interpretation of changes in the CTG and the T/QRS ratio.

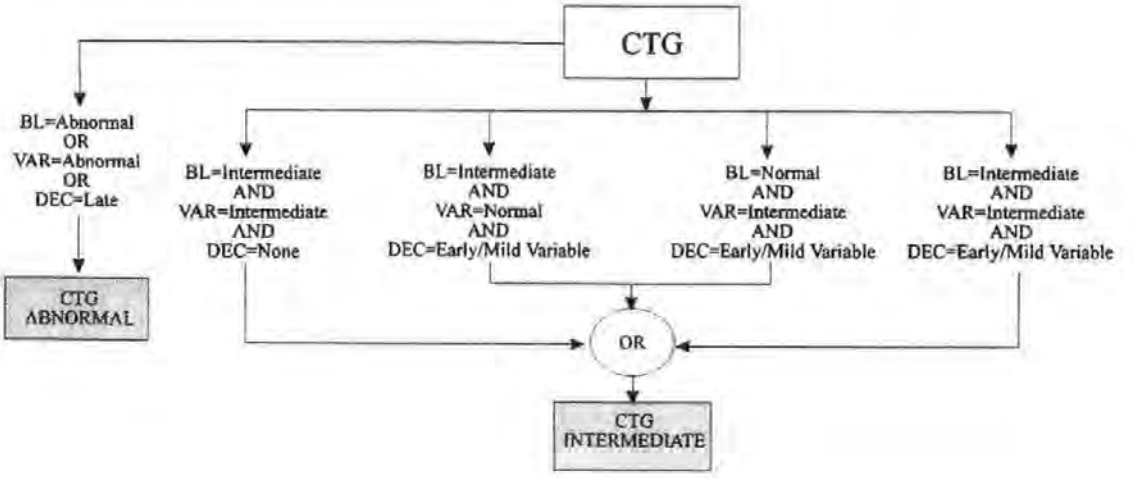

TOP LEVEL RULES		
IF	(TQRS = VERY_HIGH OR TQRS=NEGATIVE & DURATION>20MIN)	THEN FBS/DELIVER
IF	(CTG=INTERMEDIATE & TQRS=NORMAL)	THEN NO_ACTION
IF	(CTG=INTERMEDIATE & TQRS=HIGH & TQRS=STEADY & DURATION>30MIN)	THEN FBS
IF	(CTG=INTERMEDIATE & TQRS=NEGATIVE)	THEN FBS/DELIVER
IF	(CTG=ABNORMAL & TQRS=NORMAL & DURATION>60MIN)	THEN FBS
IF	(CTG=ABNORMAL & TQRS=HIGH & ΔTQRS=ZERO)	THEN FBS/DELIVER
IF	(CTG=ABNORMAL & ((TQRS=HIGH & ΔTQRS=POS) OR TQRS=NEGATIVE)	THEN DELIVER

BL= measured baseline heart-rate ; VAR = measured heart-rate variability ; ACC = existence of heart-rate accelerations ; DEC = existence of heart-rate deceleration's (This is already classified for us); FBS=Fetal Blood Sample ; SED=presence of sedation ; ΔTQRS=trend in TQRS ratio, POSitive, negative or zero.

The crisp rules in this rule-base are undesirable because scenarios will arise when a very small change in one fact/rule can drastically affect many others. For example, when the baseline is about 100 bpm small changes due to noise or variability will cause very large changes in CTG classification.

Fuzzy logic [12-13] is a technique of defining rules that have no sudden decision thresholds, thus avoiding the dilemma of the crisp boundaries in Figure 4 and enabling the expert to formalise the knowledge in a more humanistic form. This is achieved by using the actual imprecise linguistic reasoning used by the expert, rather than the more abstract (computer orientated) concept of crisp rules. Fuzzy logic makes the system less sensitive to noise, errors and natural variability in the data and can often reduce the size of the rule-base. To implement this we need to extract linguistic concepts from the knowledge that will become the basis for thye fuzzy logic expert system.

2.2 Managing uncertainty with fuzzy logic

There are two primary fuzzy logic concepts to be addressed. The first is to describe all the features and facts using linguistic variables. This has already been done to a certain extent in the example above. e.g. The T/QRS is classified by one of the set of the following set of linguistic labels:

TQRS ∈ { NEGATIVE, NORMAL, STEADY_HIGH, RISING_HIGH, VERY_HIGH}

Similarly the heart-rate baseline can be one of the following.

BASLINE ∈ { NORMAL, INTERMEDIATE, ABNORMAL}

However, with crisp rules each feature/fact can only have a single classification at any one time. The second concept is to fuzzify the classification or membership of each feature such that there are no crisp boundaries and also to make it possible for a feature to be classified by more than one linguistic variable at a time. The crisp sets then become overlapping fuzzy sets. This is achieved by creating membership curves for each feature/fact. See Figure 5a,b and c.

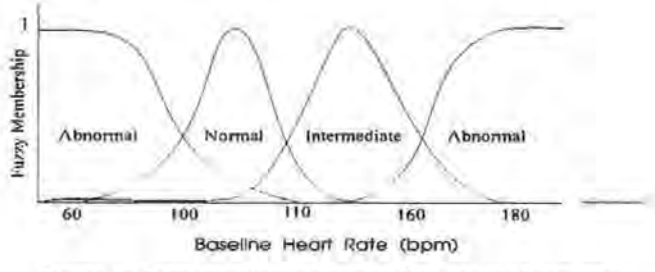

Figure 5a Fuzzy membership curves for baseline heart rate

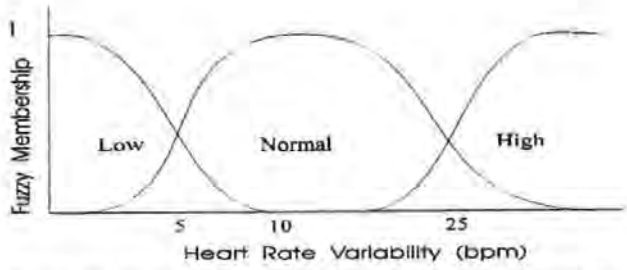

Figure 5b Fuzzy membership curves for heart rate variability.

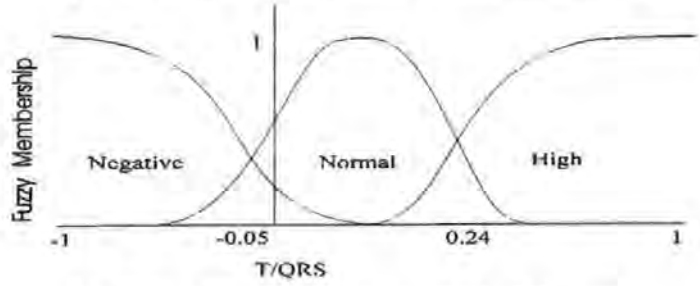

Figure 5c Fuzzy membership curves for the T/QRS ratio.

Take the example of Figure 5a. Note the different categories overlap, therefore given a measure of baseline heart-rate in bpm, the baseline could simultaneously be classified as a member of the Normal, Abnormal and Intermediate categories, but to different degrees of certainty/membership. This is more like the behaviour of an expert or a consensus of experts.

For example, given these rules:

IF (BASELINE=ABNORMAL OR VARIABILITY=ABNORMAL OR DEC=LATE OR DEC=SEVERE VARIABLE)
THEN CTG=ABNORMAL

IF ((BASELINE=INTERMEDIATE & VARIABILITY=INTERMEDIATE & DEC=NONE
THEN CTG=INTERMEDIATE

If baseline heart rate is 150 bpm, heart rate variability is 24 bpm and there are no deceleration's, we then have the case where both these rules would be activated and the CTG would be classed as both Intermediate and Abnormal. We say that both are true - the CTG is Intermediate AND Abnormal, but to different degrees of certainty.

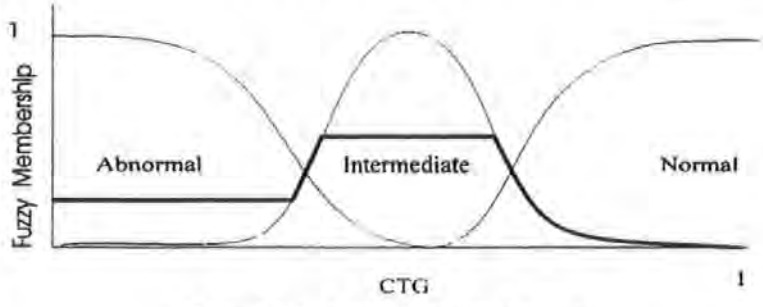

Figure 6 CTG fuzzy classification curves

This is not as paradoxical as it might first seem. Using the AND operator we have created is a 'new fuzzy fact about the CTG' which will have a new membership curve (the thick line in Figure 6). In this case the CTG will be part Intermediate and part Abnormal. This is used as a fact to other rules and so the procedure continues until end rule is reached. This might be a rule that advises to just keep watching the data, or to

advise the clinician to take a fetal blood sample, or even suggest the imminent injury to the fetus unless it is delivered. We have so far discussed how to manage the rules and uncertainty in expert knowledge which leads on to the problem of knowledge representation in a fuzzy expert system.

3. Formalising the knowledge

Translating expert knowledge into a fuzzy expert system is not just a matter of compiling IF THEN rules because human reasoning is rarely that simple. Rules can change as more facts are collected, and this can lead to a very complex rulebase unless an efficient rule structure is found that models the experts thinking. During labour different sequences of events are recognised by the expert as patterns which resemble a theoretical or previous case. Each case recognised in labour can modify the way the expert interprets the presented facts. This can change the rules and liguistic variables or possibly introduce new ones into the decision process. This case-based reasoning needs to be built into the expert system. To enable the expert system to recognise sequences of events in the same way as an expert, we propose a rule structure that is based on finite state machines. As new patterns are established then the fetal 'state' will change. For example, during the first stages of monitoring (the Entry State) a labour could seem normal as there is no knowledge available to suggest otherwise. After some time, the system might obtain extra information and change state accordingly. Therefore a modified set of rules will apply. For example, if the ECG should produce negative T waves for 2 minutes then this will change the rules regarding the assessment of the CTG.

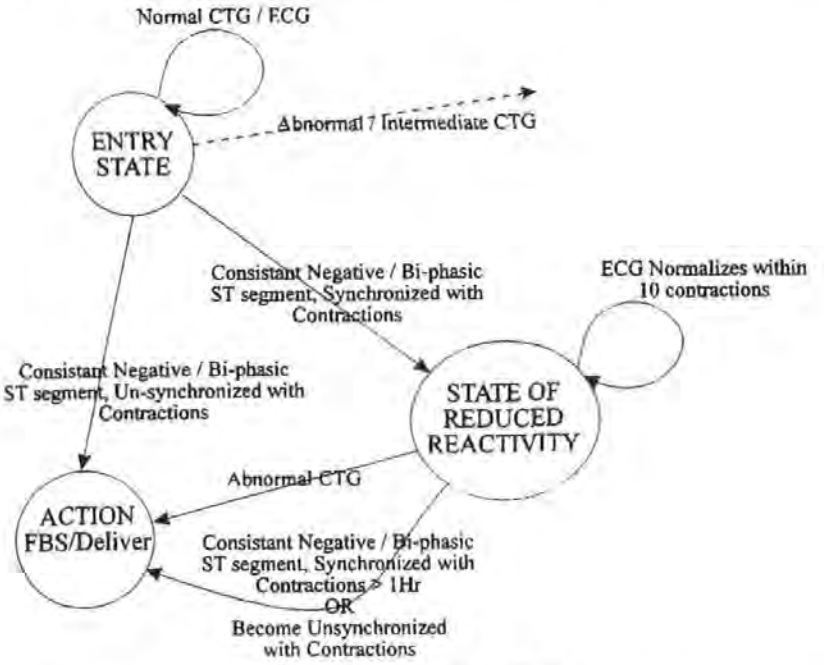

Figure 7 Simplified state diagram

It is possible in this (rare) case that the fetal heart rate is less capable of reacting to any abnormalities that might occur and therefore there will be a reduced indication of any abnormalities from the CTG. What is regarded as a normal, intermediate and abnormal CTG may have to change, even if the ECG becomes normal again. We say that the (fetal) state has changed to one of 'Reduced Reactivity' (See Figure 7). Any future

state depends on its previous state. This example is formalised in Figure 7. Each state is represented by a circle and has a full set of rules associated with it. Using this approach the knowledge can be formalized in a way that decisions are be based on previously recognized events during labour.

4. Discussion and Conclusion

In our research, the role of the computer in fetal monitoring is to maximise the knowledge of an expert in the labour ward. By supplying a busy clinician with expert knowledge will help to make confident and accurate decisions and without upsetting normal patient handling routines. Expert systems are suited to this where the rules and knowledge governing the data can be elicited and defined explicitly. The fuzzy expert systems can also manage uncertainty in the knowledge or the data (noise). This technology is becoming mature and well tested. Fuzzy logic has the advantage that its behaviour is well understood by humans, who after all are being asked to use the system and to trust in it's advice. This is important as instigating change into medical practice by introducing technology is a very subject.

Our approach is not to relieve responsibility on human decision making (which would be unrealistic and rightly rejected), but to motivate and enhance it. Knowledge and information that is sometimes overlooked by even the most expert clinician, particularly when under stress in a busy labour ward, can hopefully be brought to his or her attention via the human-computer interface. The computer needs only to be artificially intelligent so that it can alert a clinician, who is truly intelligent, to information within the data.

4.1 Further work

The next stage of our work is to continue with a thorough knowledge elicitation programme to identify the changes in the ECG features and their relationships to other events in labour. At the present, work is in progress at our units and other centres, as part of the European Community concerted action on new methods of fetal monitoring to collect data from various categories of patients. This will provide data for the next stage of the research which will be published in due course.

5. Acknowledgements

The authors gratefully acknowledge the assistance of Dr. Jenny Westgate and Dr. Sarah Beckley for clinical assistance and we thank Keith Greene and Karl Rosén for their expert advice and knowledge. We thank the labour ward staff at Plymouth General Hospital for their help and co-operation. The financial support of the P.C.F.C. and South-West Regional Health Authority for this work is gratefully acknowledged. We also thank and acknowledge the constructive help, advice and expertise of John Curnow and Peter Van Eetvelt.

6. References

[1] Rosen K G, Arulkumaran S, Greene K R, Lilja H, Lindecrantz K, Seneviratne H, and Widmark C. Clinical validity of fetal ECG waveform analysis. in Perinatology, Nestle Nutrition Workshop Series, Vol. 26, Nestec LtD, Vevey/Raven Press, New York, 1992, 95-110.

[2] Maeda K, Computerised analysis of cardiotocograms and fetal movements. R Lilford (Ed). Balliere's Clinical Obstetrics & Gynaecology, London 4, pp797-813, 1990
[3] Krause W. Natali by Neiss., A computer-aided monitoring system for supervision of labour. K. Maeda et al (Eds). Computers and Perinatal Medicine., pp103-111, 1990, Elseviere Science Publishers BV Amsterdam.
[4] Ifeachor E C, Keith R D F, Westgate J and Greene K R., An expert system to assist in the management of labour. In Liebowitz J (Ed) World Congress on Expert Systems, Vol. 4, pp2615-2622, 1991, Pergamon Press.
[5] Westgate J., Keith R., Curnow J.S.H., Ifeachor E.C. and Greene K.R., Suitability of fetal scalp electrodes for monitoring the fetal electrocardiogram during labour., Clin. Phys. Physiol. Meas., 11, pp297-306, 1990
[6] Keith R., Westgate J., Beckley S., Garibaldi J., Ifeachor E.C. and Greene K.R., A multicentre comparitive study of 17 experts and an intelligent computer system in the management of labour using the cardiotocograph., Submitted Br. J. Obstet. Gynecol., 1994
[7] Westgate J., Harris M., Curnow J. and Greene K.R., Plymouth randomised trial of the cardiotocogram only versus ST waveform plus cardiotocogram for intrapartum monitoring in 2400 cases., Am. J. Obstet. Gynecol., 169, pp1151-1160, 1993
[8] Greene K.R. and Westgate J. The Fetal ECG with Particular Reference to the ST waveform.. In Spencer J.A.D. and Ward R.H.T (Ed.), Intrapartum fetal surveillance., Ch 21, pp281-294, 1993, Royal College of Obstetrics and Gynecology, 27 Sussex Place, Regents Park, London.
[9] Rosén K,R., Alterations in the fetal electrocardiogram as a sign of fetal asphyxia - experimental data with a clinical implementation., J. Perinat. Med., 14, pp355, 1986
[10] Outram N.J., Ifeachor E.C., Van Eetvelt P.W.J., Curnow J.S.H and GreeneK.R., Techniques for optimal enhancement and feature extraction of the fetal electrocardiogram., Submitted, Press, 1994
[11] Ifeachor E.C. and Jervis B., Digital Signal Processing , a practical approach, Addison Wesley., 1993
[12] Kosko B., Fuzzy Thinking, the new science of fuzzy logic., Harper Collins, Glasgow., 1994
[13] Yager R.R., Approximate Reasoning as a Basis for Rule-Based Expert Systems., IEEE Trans Sys., Man. and Cyber., Vol. SMC-14,4, 1984
[14] Zadeh L.A., The Concept of a Linguistic Variable and it's Application to Approximate Reasoning-I, Information Sciences 8, pp199-249, 1975
[15] Archer N.P., Wang S., Fuzzy Set Representation of Neural Network Classicication Boundaries., IEEE Trans Sys., Man. and Cyber., Vol. 21,4, 1991
[16] Ifeachor E.C., Patel S.R., Westgate J., Curnow J.S. and Greene K.R., Applications of Artificial Neural Networks to Fetal Monitoring During Labour., Techniques and Application of Neural Networks., Ed. Taylor M. and Lisboa P. Ch 6, 1993, Ellis Horwood workshops.
[17] Ifeachor E.C., Outram N.J. and Greene K.R., Fetal ECG Quality Assessment Using Neural Networks, Workshop on Neural Networks: Techniques and Applications., University of Liverpool., 1993
[18] Press W.H., Teukolsky S.A., Vetterling W.T. & Flannery B.P., Numerical Recipes in C. The Art of Scientific Computing. Second Edition., Cambridge University Press, Cambridge UK, 1992

A fuzzy expert system to assist in the management of labour

Emmanuel C Ifeachor and Nicholas J Outram
School of Electronic, Communication and Electrical Engineering, University of Plymouth, PLYMOUTH, Devon, UK, PL4 8AA. Fax: +44 1752 232583
e-mail:nicko@uk.ac.plym.cis

Abstract - This paper presents the development of a natural rule set for an obstetric expert system using fuzzy logic. During labour, uncertainty and difficulty in assesing the condition of the fetus, based on visual analysis of the fetal heart rate and uterine contractions known as the cardiotocogram (CTG), can lead to unnecessary medical intervention or failure to intervene when needed. Computer-assisted interpretation of the CTG can improve the quality of obstetric care, but the CTG alone does not provide all the information needed in all cases. The fetal electrocardiogram (ECG) provides extra information that could aid clinicians in decision making. In our new system, fuzzy logic is used to assist in the analysis and interpretation of changes in the fetal ECG, in association with the CTG, taking into account uncertainty and imprecision which are pervasive in both the obstetric data and knowledge. The output of the fuzzy expert system is displayed as a map of the fetal condition and this serves as an objective visual aid to decision making by the clinician. The implementation and retrospective application of the fuzzy expert system on real cases are discussed.

Keywords - Labour, Fetal heart rate, Cardiotocogram, Electrocardiogram, Expert system, Fuzzy Logic, Fetal Condition Matrix.

Introduction

The fetal electrocardiogram (ECG) waveform represents the electrical activity of the baby's heart as measured from the body surface. Figure 1 illustrates some of its important features. The fetal heart rate (FHR) is derived from the R-to-R intervals. A visual analysis of the continuous display of the FHR together with the uterine activity, known as the cardiotocogram (CTG), is normally used to assess the condition of the fetus, but this requires a great deal of experience which is not always available. Uncertainty and difficulty in interpreting CTG patterns during labour can lead to unnecessary medical intervention (e.g. caesarean section or forceps deliveries), fetal injury or a failure to intervene when needed [1,2]. Computer assisted interpretation of the CTG can improve the quality of obstectric care and a system for doing this, the INFANT, has been successfully developed[3,4]. However, the CTG alone does not provide all the information needed, in all cases, for accurate assessment of fetal condition. The fetal ECG contains potentially valuable information that could assist clinicians in making more appropriate and timely decisions during labour without having to alter current patient handling routines [5-8].

A potentially important feature of the fetal ECG waveform is the shape of the ST segment [5-8]. Significant pattern changes in shape associated with stress or distress include persistently rising T wave amplitude, negative T waves and depressed ST segments. Some of the changes in the ST waveform may be quantified as a ratio of the amplitude of the T wave to that of the QRS, known as the T/QRS ratio, see figure 1.

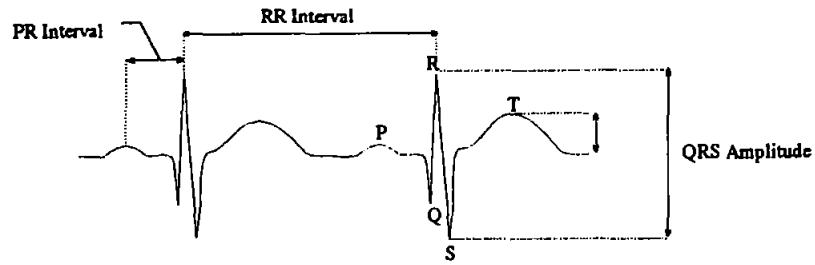

Figure 1 The fetal ECG waveform showing some of the important features: R-to-R and P-to-R intervals and the T, and QRS amplitudes

Other features of potential interest include the ST area, the variability of the R-to-R intervals, the duration of the P-wave and the width of the QRS complex (see figure 1)[9].

As yet, the fetal ECG is not in widespread clinical use. The expertise required to interpret changes in the fetal ECG is not widely available and is yet to be implemented in a form that can be fully utilised by clinicians without constant expert supervision. The analysis and interpretation of changes in the ECG in association with the CTG are carried out by visual inspection[10] which is very subjective.

An aim of our work is to extend the capability of the INFANT to include the analysis and interpretation of changes in the fetal ECG features, taking into account the uncertainty and imprecision in obstetric data and knowledge, and present the result in a way that will practically aid the busy clinician. The fuzzy logic concepts used in the system presented in this paper are described in more detail elsewhere[11].

Uncertainty and imprecision in managing labour

The qualitative nature of current obstetric knowledge gives rise to a great deal of uncertainty. Figure 2 summarises how the CTG is categorised based on features observed visually in the CTG and their perceived significance[10]. Given that features are measured by eye and the normal physiological variations between fetuses, phrases such as *normal*, *intermediate* and *abnormal* in figure 2 are subjective, and illustrates the difficulties of interpreting the CTG. An experienced clinician would take adequate care in interpreting CTGs that are near the boundaries.

Changes in the ST waveform are assessed qualitatively by analysing its shape (described as e.g elevated, negative, depressed, rapidly rising, normal) and quantitatively by the ratio of the T/QRS or the area. The interpretation of the T/QRS ratio, as with the CTG, also suffers from threshold problems. A study of the guidelines for analysing the ST waveform plus the CTG [6, 7, 10] reveals that the knowledge is highly qualitative and full of hedges. This is due, in part, to the difficulty of drawing valid conclusions based on what is essentially partial information derived from the baby, the dynamic nature of labour, and the normal physiological variations in the measured values between fetuses. Imprecision in the measured parameters due to the poor quality of data and errors in the feature extraction algorithms are a further source of uncertainty[9,11]. Errors in measurements (e.g false or missed R-waves, false changes in the features of the CTG, inconsistent T/QRS values) due to poor signal quality are not uncommon[7,9].

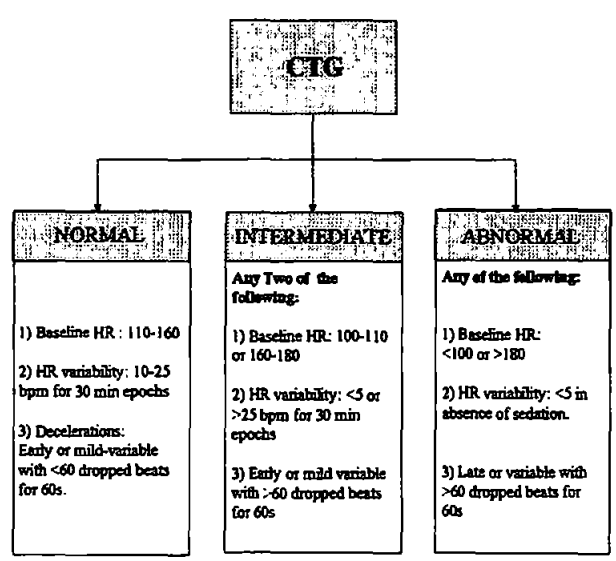

Figure 2 A simplified classification of the CTG into its subtypes

Different techniques for managing uncertainty in the decision making process are available. We have used fuzzy logic because it is well suited to the problems of imprecision and uncertainty in obstetrics and allows the knowledge to be formalised in a more humanistic form. For example, the terms used to describe changes in the CTG and the ECG features can be viewed as linguistic variables. Further, fuzzy logic allowed us to implement a system from the bottom up based on theoretical knowledge and experience. This can later be fine-tuned to get optimum performance as more data is collected.

Fuzzy expert system design

The development of a fuzzy expert system is generally less complex than a conventional crisp rule based expert system, but it is important to keep all fuzzy variables and rules consistent. Some of the important terms used in the clinical guidelines[10] are given below. The words in brackets are the different categories.

T/QRS Ratio: {Constant , Increasing, Rising, Rapidly Increasing, Negative, Positive, High, Normal}
ST Waveform : {Normal, Depressed, Negative, Elevated, Raised, Bi-Phasic, Changing, Acute change}
CTG Pattern: {Normal reactive, Intermediate, Abnormal, Normal, Pre-terminal}
Heart Rate Decelerations: {Persistent, Late, Variable, Present, Not Present}
Baseline Heart Rate: {Increased, bradycardia, Low, tachycardia, High, Normal, Rapid return}
Heartrate Variability: {Increased, Decreased, Normal, Undulating}

From these terms we were able to derive the fuzzy sets used in the rule base after several sessions of knowledge elicitation. It is important to choose meaningful linguistic variables which are close to the real language of the clinical expert and keep them consistent. Table 1 summarises the key fuzzy sets and their subsets. The fuzzy membership functions are shown in figure 3. These membership functions are derived from the way the clinical guidelines are used, although they may require slight modification at a later date when the system is optimized.

At the present, the fuzzy rule base contains about 20 rules for interpreting changes in the ECG. The result of the ECG and CTG analysis and the recommended action are summarised as a fetal condition matrix (see table 2) in line with the clinical guidelines[10]. The analysis is carried out over a sufficient time interval before the recommendations are made. Each element of the matrix (see table 2) reflects the condition $\{A,B..I\}$of the fetus. The output of the fuzzy expert system produces a truth value for each of these conditions.

T/QRS Ratio	ΔT/QRS Ratio	ST Segment Area	ΔST Segment Area	HR Variability	Baseline Heart-Rate	CTG
Negative	Falling	Negative	Falling	Absent	Abnormal	Normal
Normal	Stable	Positive	Stable	Low	Normal	Intermediate
Increased	Rising		Rising	Normal	Intermediate	Abnormal
High	Rapidly Rising			Increased		

Table 1 Table of key fuzzy sets and subsets.

N.B. The measurements to determine the truth values of fuzzy subsets are made over time intervals given in the guidelines (not shown) [10].

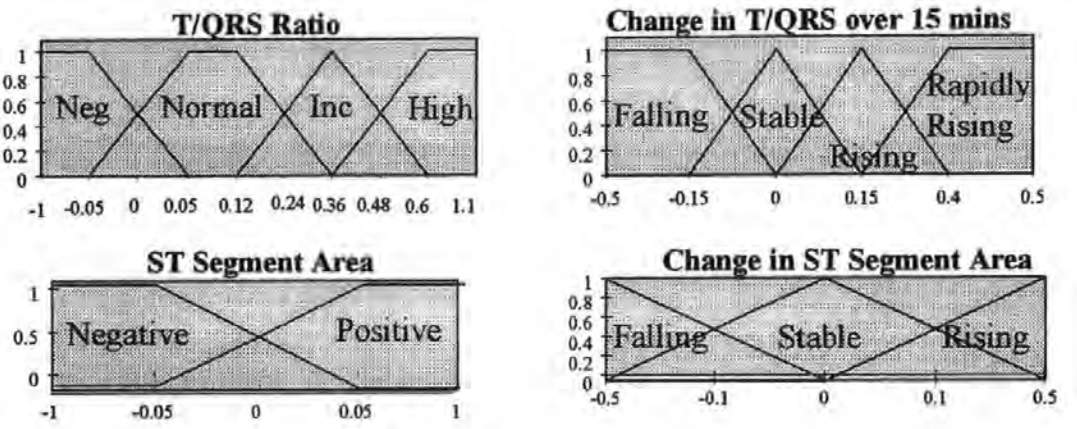

Figure 3. Examples of fuzzy membership functions

ST Waveform \ CTG	Normal	High and Stable	Negative or Rising
Normal	A **No Action**	B **No Action**	C **FBS[1] or Deliver**
Intermediate	D **No Action**	E **FBS or Deliver**	F **Deliver**
Abnormal	G **FBS or Deliver**	H **Deliver**	I **Deliver**

Table 2 Fetal condition matrix used to guide the clinician.

1. Fetal Blood Sample

These truth values are derived from a set of fuzzy rules, such as
IF (TQRS(20)=*NEGATIVE*) OR (STAREA(20)=*NEGATIVE*) THEN ST_WAVEFORM=*NEGATIVE*
IF (CTG=*NORMAL*) AND (ST_WAVEFORM=*NORMAL*) THEN A
IF (CTG=*ABNORMAL*) AND ((ST_WAVEFORM=*CHANGING*) OR (ST_WAVEFORM=*NEGATIVE*)) THEN I
The numbers in brackets indicate the time these measurements are measured over.

Interpretation of the output matrix

Having obtained the truth values for all possible fetal conditions $\{A,B,..,I\}$, we are faced with the problem of interpreting the results. The truth values for the fetal condition matrix are easy to interpret in cases where the outcome is unambigious. In such cases the fetal condition can be inferred from the maximum truth value, but this can be unsatisfactory in borderline cases because of jitter. For example, table 3 shows A and D to have very similar truth values. A series of small changes in the features could cause the output to jitter between A and D.

A=0.5	B=0.3	C=0.1
D=0.49	E=0.3	F=0.1
G=0.1	H=0.05	I=0.0

Table 3

To avoid this ,we consider the fetal condition matrix as a 3D solid object. From this, we compute the centroid of the solid to 'de-fuzzify' and obtain a single point on the fetal condition matrix. This avoids the problem of a jittering output on the fetal condition matrix. For the clinician, it is often the change of position (fetal state) that is of more importance than the absolute position itself. For example, a labour where the fetal state is B throughout the duration of labour has a different interpretation to a progression from A to B. We display the path or locus of the fetal condition at 5 minute intervals to display any changes, this gives a simple objective visual display of the history of fetal condition over time.

Results

Some example results are given below in figures 5(a) and (b). Figure 5(a) is a typically normal case where the T/QRS ratio is constantly below 0.24 and the CTG is perfectly normal. Figure 5(b) was a perfectly normal case until the baseline heart-rate dropped and stayed at 60bpm (abnormal CTG).

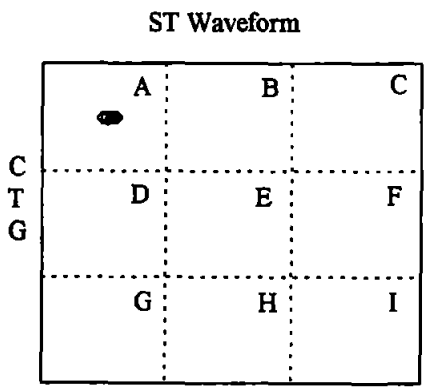

Figure 5(a) *Normal* CTG and *Normal* ECG

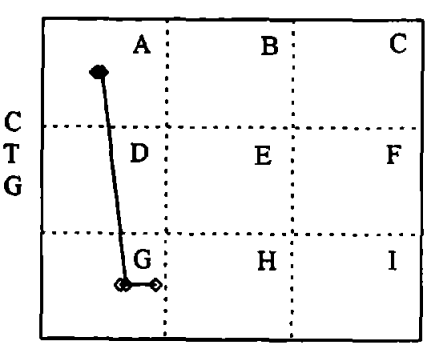

(b) *Normal* ECG and *Normal* CTG with a sudden progression to *Abnormal* CTG

The condition of the fetus is shown as a 'moving point' on the fetal condition matrix. The nearer to the bottom right (I) , then the worse the condition of the fetus. We could have linearised the output onto a single line but this way the reason for the fetal condition output is lost. The fetal condition can be monitored visually without losing the reasoning behind it.

Conclusions

Clinical decisions are ultimately crisp, i.e. a clinicial either **does** intervene or **does not** intervene. A clinician would base the decision on a personalised and highly complex scheme, using the information supplied (CTG+ECG) , experience, intuition, patient history and patient handling guidelines. Even if all the useful information could be recorded and stored, this reasoning could not realistically be done by a computer. It is unreasonable, however, to expect a clinician to perform well with so much extra information, especially within the labour ward environment. Thus, the role of the system is not to replace the clinician, but to assist them with the task of the analysis of the combined CTG and ECG. By presenting the information in a more meaningful and humanistic form, it can draw the clinician's attention to important events, and help them to make more informed judgments.

For this to be effective, it is necessary to cater for the underlying fuzziness in obstetric data and knowledge. For the cases we have considered, the performance has been predicatable and accurate. A more comprehensive rule base will be required for the rarer cases of genuine fetal distress.

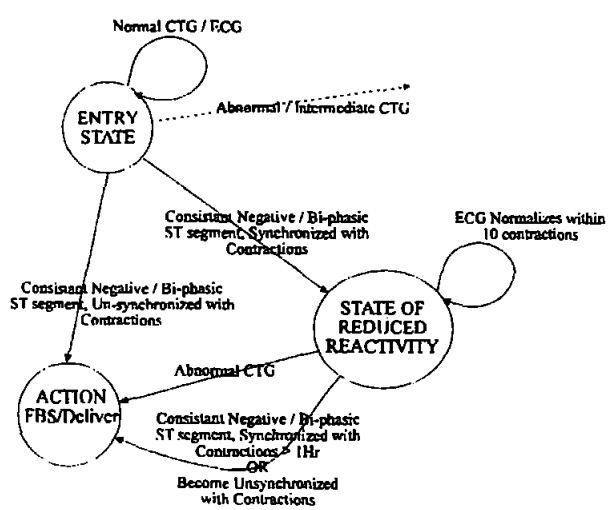

Figure 6 Example state diagram

During labour different sequences of events occur which the expert can recognize. Recognising the sequence of events can modify the way the expert interprets the instantaneous data. To enable an expert system to recognise such sequences of events in the same way as human expert, a rule structure based on the principles of finite state machines has been proposed[11]. Each state has a full set of rules associated with it.In this approach, the recognised changes in the fetal condition can be represented as 'states'. In figure 6 each state is represented by a circle.

For example, during the first stages of monitoring (the Entry State) a labour may be regarded as normal unless there is a prior knowledge to suggest otherwise. When a new piece of information becomes available, such as brief negative T-waves (condition C), a change of state will occur (see figure 6.) and the rules change.

Acknowledgements

The authors gratefully acknowledge the assistance and contribution of John Curnow, Mark Davies, Peter VanEetvelt, Jenny Westgate, Keith Greene, Roberto Luzietti and Karl Rosen to aspects of this work and to our understanding of the problems in fetal monitoring. We thank the labour ward staff at Plymouth General Hospital for their help and co-operation. The financial support of the P.C.F.C., EPSRC and the South-West Regional Health Authority for this work is gratefully acknowledged.

References

1 Maeda K (1990) Computerised analysis of cardiotocograms and fetal movements. R Lilford (Ed). Balliere's Clinical Obstetrics & Gynaecology, 4:797-813.

2 Krause W. Natali by Niess (1991) A computer-aided monitoring system for supervision of labour. In K. Maeda et al (Eds). Computers in Perinatal Medicine, 103-111, Elsevier Science Publishers BV Amsterdam.

3 Ifeachor E C, Keith R D F, Westgate J and Greene K R. (1991), An expert system to assist in the management of labour. In Liebowitz J (Ed) World Congress on Expert Systems, Vol. 4: 2615-2622, Pergamon Press.

4 Keith R., Westgate J., Beckley S., Garibaldi J., Ifeachor E.C. and Greene K.R. (In press), A multicentre comparative study of 17 experts and an intelligent computer system in the management of labour using the cardiotocograph., Br. J. Obstet. Gynecol.

5 Rosen K G, Arulkumaran S, Greene K R, Lilja H, Lindecrantz K, Seneviratne H, and Widmark C (1992). Clinical validity of fetal ECG waveform analysis. in Perinatology, Nestle Nutrition Workshop Series, 26:95-110, Nestec Ltd, Vevey/Raven Press, New York.

6 Westgate J., Harris M., Curnow J. and Greene K.R. (1993), Plymouth randomised trial of the cardiotocogram only versus ST waveform plus cardiotocogram for intrapartum monitoring in 2400 cases., Am. J. Obstet. Gynecol., 169:1151-1160.

7 Greene K.R. and Westgate J.(1993) The Fetal ECG with Particular Reference to the ST waveform.. In Spencer J.A.D. and Ward R.H.T (Ed.), Intrapartum fetal surveillance., Ch 21, 281-294, Royal College of Obstetrics and Gynecology, 27 Sussex Place, Regents Park, London.

8 Rosen K,R. (1986), Alterations in the fetal electrocardiogram as a sign of fetal asphyxia - experimental data with a clinical implementation., J. Perinat. Med., 14:355

9 Outram N.J., Ifeachor E.C., Van Eetvelt P.W.J., Curnow J.S.H and GreeneK.R. (submitted) Techniques for optimal enhancement and feature extraction of the fetal electrocardiogram. IEE Proc. A.

10 Rosen K. G. (1994) ST waveform + CTG clinical guidelines. Internal report, Plymouth Postgraduate Medical School, University of Plymouth.

11 Ifeachor E.C. and Outram N.J., (1994), Fuzzy Logic concepts for pattern analysis and interpretation of changes in the fetal electrocardiogram., Proc. Neural Networks and Expert Systems in Medicine and Healthcare., Uni. Plymouth., U.K., Aug.

12 Zadeh L.A., (1975) The Concept of a Linguistic Variable and it's Application to Approximate Reasoning-I, Information Sciences 8:199-249

13. Zadeh L. A. (1983) The role of fuzzy logic in the management of uncertainty in expert systems. Fuzzy set and systems, 11:199-227.

Neural network and fuzzy logic techniques for classifying patterns in the fetal ECG waveform

Outram N.J.[1] & Ifeachor E.C.[1]

1 School of Electronic, Communication and Electrical Engineering
University of Plymouth, UK
email: njoutram@plymouth.ac.uk, eifeachor@plymouth.ac.uk & pveetvelt@plymouth.ac.uk

Abstract

There is a need to provide clinicians with computer assistance for making a more objective and accurate assessment the condition of the fetus during labour. It is important to exploit all the useful information contained within the fetal electrocardiogram (ECG) to help reduce uncertainty, unnecessary clinical intervention [1] and clinical errors during labour. This can be achieved by automatically assessing the changes in the fetal ECG waveform shape during labour using a fuzzy expert system [2]. The expert knowledge required to correctly interpret the ECG exists as a set of written guidelines, some of which are quantitative and explicit while others are still qualitative and rely on subjective visual interpretation [3]. We have investigated methods combining the strengths of Radial Basis Functions (RBF) and Fuzzy Logic to automatically classify the different shapes of ECG waveforms where explicit rules do not exist. In this paper we demonstrate the relative merits of these techniques by classifying the fetal ECG ST-waveform shape. We discuss the problems of computing the accuracy of the pattern classifier and some preliminary results are given in the paper.

1 Introduction

The fetal electrocardiogram (ECG) waveform represents the electrical activity of the baby's heart as measured from the body surface (see figure 1). The fetal heart rate (FHR) is derived from the R-to-R intervals. A visual analysis of the continuous display of the FHR together with the uterine activity, known as the cardiotocogram (CTG), is normally used to assess the condition of the fetus, but this requires a great deal of experience which is not always available. Uncertainty and difficulty in interpreting CTG patterns during labour can lead to fetal injury, unnecessary medical intervention such as caesarean section or forceps deliveries or a failure to intervene when needed [1]. Computer assisted interpretation of the CTG can improve the quality of obstetric care and a system for doing this, the INFANT, has been successfully developed [4]. However, the CTG alone does not provide all the information needed, in all cases, for accurate assessment of fetal condition. The fetal ECG contains potentially valuable information that could assist clinicians in making more appropriate and timely decisions during labour without having

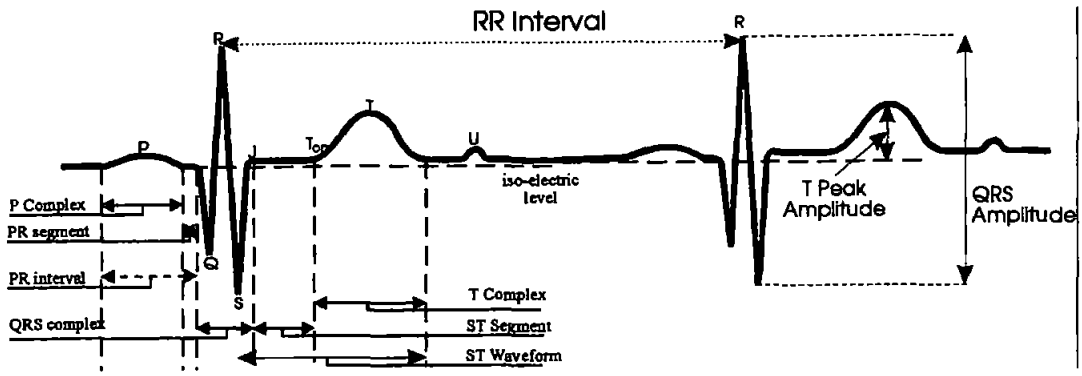

Figure 1: Decomposition of the the fetal ECG waveform into its different wave components

to alter current patient handling routines [5]. The impetus for using the fetal ECG comes from many years of research, observation and physiological reasoning. Furthermore ST analysis has been successfully used in a recent randomised trial [5] to reduce the need for clinical intervention without any change in outcome. Unfortunately the use of the ECG is limited to a few centres in the world because it has not been widely accepted or proven to be of clinical value. The proper use of the fetal ECG by clinicians requires training, but even with training, it is still difficult not to miss important and rare ECG patterns without constant supervision. Our aim is develop a bed-side intelligent system which will automate the continuous monitoring of the fetal ECG and alert clinicians towards any abnormalities that may develop.

Physiology of the ST waveform

The shape of the fetal ECG reflects the super-position of the electrical signals within the heart as seen from the body surface [6]. The ST waveform (see figure 1) of the ECG is routinely used in adult cardiology during stress tests to detect heart damage. The ST waveform, which represents the re-polarization of the heart muscle cells, is very sensitive to coronary insufficiency such as ischemia in the adult ECG [6]. A hypothesis which has been undergoing investigation for more than 20 years is that the fetal heart should also show changes in the ST waveform as a response to stresses in labour, such as the natural squeezing effect of uterine contractions, temporary occlusions of the umbilical cord, maternal hypotension or placental haemorrhaging. These stresses can be intermittent, resulting in slow and subtle changes in the fetal CTG and ECG. In extreme cases, these stresses can also be chronic and potentially fatal for the fetus, and show up as rapid changes in the CTG and ECG. The fully developed term fetus however is equipped to cope with the normal stresses of labour. Stresses such as uterine contractions can reduce blood-flow from the placenta and restrict oxygen supply. If there is is an imbalance between oxygen consumption and supply, the fetus is normally able to compensate by diverting blood flow away from non-vital to the vital organs. It also has rich glycogen supplies which can be consumed to anaerobically maintain heart function. This latter process,

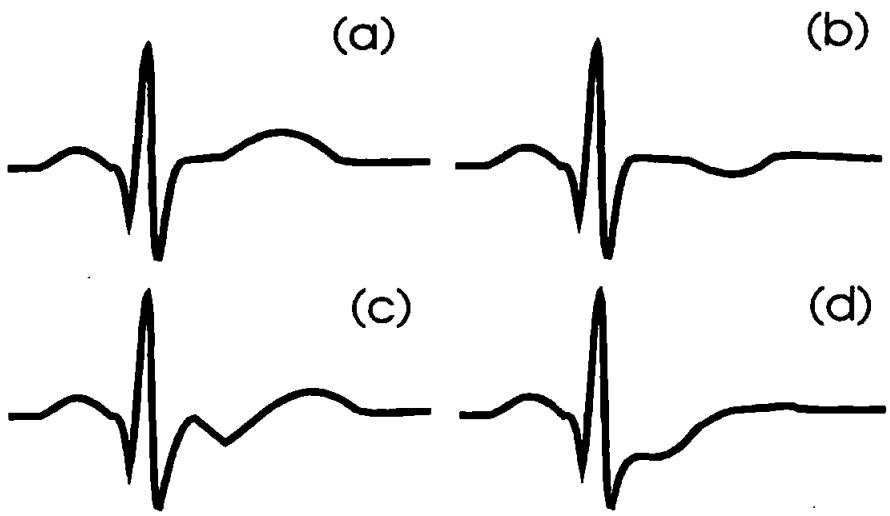

Figure 2: Different configurations of the ST waveform. (a) Normal with elevated T complex, (b) Abnormal with Negative T complex, (c) Abnormal bi-Phasic ST waveform & (d) Abnormal depressed ST segment .

known as anaerobic metabolism, produces lactic acid and potassium ions (K^+). The extra potassium ions are responsible for a change in heart muscle cell potentials, which in turn results in a change in ST waveform shape [3]. This can can be continuously monitored by examining the ECG and has been observed to show up abnormalities before any tissue damage has occurred [6] . A compensating fetus will typically show an ST waveform with a permanently elevated T complex and an elevated ST segment (See figure 2(a)). A fetus which is not fully compensating will show a changing T complex, negative T complex, bi-phasic ST waveform or depressed ST segment (see figures 2(b),(c) and (d)).

2 Feature extraction

The T complex height, normalised against the QRS amplitude (see figure 1) is known as the T/QRS ratio. This is a robust feature of the ST waveform and is simple to quantify. We elicited the knowledge required to interpret the changes in the T/QRS ratio from interviews with experts and from printed guidelines. We have developed a system to enhance the fetal ECG signal quality with minimal information loss [7] and to interpret the changes in the T/QRS ratio using a fuzzy expert system [2]. Fuzzy logic was used to model expert thinking and to reduce the effects of uncertainty, details of which are given elsewhere [2, 8]. It is accepted however that too much emphasis has been put on the T/QRS in the past because it cannot be used alone to detect significant waveforms such as bi-phasic and depressed ST waveforms [6]. Detection of other waveforms such as those shown in figures 2(c) and (d) has never been automated because the expert knowledge required is still subjective and has yet to be quantified.

An aim of this work is to expand the fuzzy-logic model to automatically recognise all

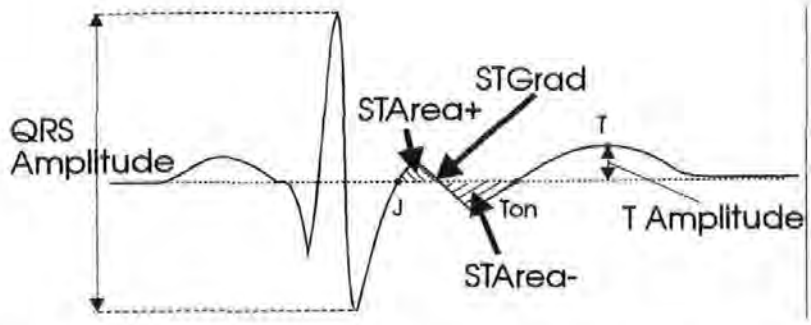

Figure 3: The important features required for pattern recognition

the known classes of ST waveform shape by extracting new fuzzy-rules from data which has been classified by experts. For the new rules to be robust and meaningful we have identified a set of visually identifiable key features in the ST waveform which can be used to represent the ST waveform shape. The key features are :

ST Area+ Total area above the iso-electric level in the ST segment

ST Area- Total area below the iso-electric level in the ST segment

ST Grad Maximum negative slope between 40ms and 90ms after the R-wave peak

T/QRS The T wave peak amplitude.

All these features (see figure 3) are normalised against the QRS amplitude to correct for changes in signal gain. We digitised a set of examples of normal and abnormal fetal ECG waveforms and had them re-classified by an expert to check their validity. The ST waveform of each fetal ECG waveform was approximated and smoothed by fitting a Chebyshev polynomial curve of the form

$$f(t) = c_0 + c_1 T_1(t) + \ldots + c_m T_m(t) \ , t = -1 \ldots + 1$$

to the raw data, where $T_k(t) = cos(k.arccos(t))$ and m is the degree of approximation [7]. An example is shown in figure 4. Using the polynomial approximation *f(t)* rather than the raw data to extract the features greatly enhances the waveform and reduces ambiguity when locating and measuring the features. This is because the approximation is defined to have a maximum of m-1 extrema. Computing the areas, derivatives and amplitudes can all be performed analytically from *f(t)*.

3 Fuzzy rule induction

Artificial Neural Networks and Fuzzy Logic are both powerful techniques in pattern recognition. Multi-Layered Perceptron (MLP) neural networks have the useful property of

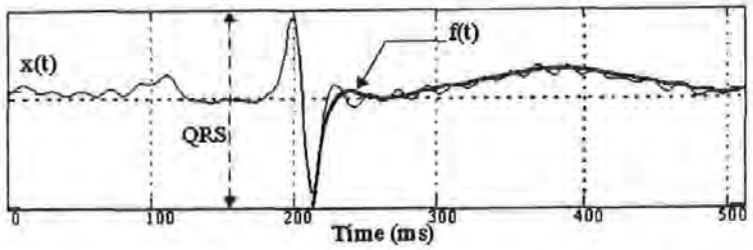

Figure 4: Approximation of the fetal ECG ST waveform using Chebyshev polynomials

learning new knowledge by utilising a supervised learning algorithm, but difficulties arise in analysing and predicting the behavior of the trained network. Fuzzy inference systems are easy to analyse once the knowledge is acquired, but with incomplete knowledge, a large number of input parameters and possible permutations of input parameters, this becomes a very difficult and time-consuming task. Other research has now demonstrated that neural networks and fuzzy inference systems can be made to be interchangeable [9, 10, 11] such that fuzzy inference systems can be trained like a MLP to extract rules from data [10] and can be easily analysed. Most of these techniques use the *max-product* fuzzy logic scheme where

$$\{AandB\} = A.B \quad (1)$$

$$\{AorB\} = max(A, B) \quad (2)$$

as this simplifies the training algorithm. However, we prefer the *max-min* fuzzy logic [12] scheme given by

$$\{AandB\} = min(A, B) \quad (3)$$

$$\{AorB\} = max(A, B) \quad (4)$$

as this has a better theoretical foundation but unfortunately makes the training algorithm more complex. We are currently investigating techniques for extracting new fuzzy rules from the data using the *max-min* fuzzy logic scheme. We aim to extract a set of rules from the data that will classify the ST waveform as {*Normal, Normal with elevated ST, Abnormal with depressed ST, Abnormal with bi-phasic ST*} in accordance with human experts.

3.1 Representing fuzzy rules in a radial basis function neural network

A radial basis function, as shown in figure 6, can be considered to be functionally equivalent to a fuzzy inference system [9]. The input nodes are fully connected (via unit weights) to all the hidden nodes which in turn *fuzzify* each input variable [8] and combine them all with an *and* function. The expression for the j^{th} hidden node $r_j(\overline{x})$ is

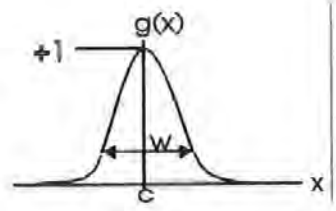

Figure 5: Each fuzzy set is a gaussian function g(x) with centre c and width w

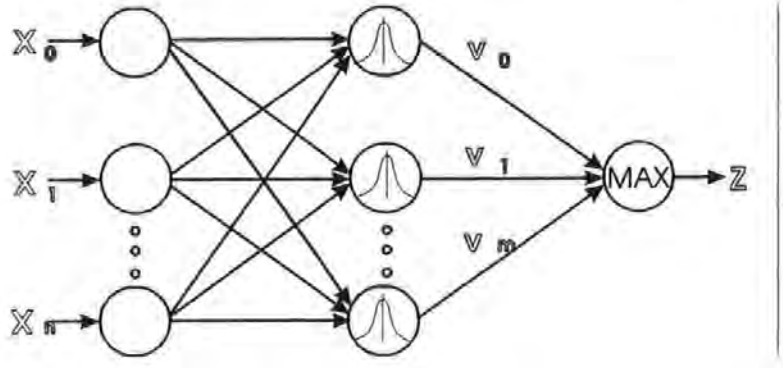

Figure 6: Fuzzy Radial Basis Function

$$r_j(\overline{x}) = min\{g(x_0), g(x_1), \ldots, g(x_n), v_j\} \quad (5)$$

where (6)

$$g(x_i) = e^{-(x_i - c_i)^2 w_i^2} \quad (7)$$

$g(x_i)$ is a gaussian function which fuzzifies an input variable x_i. c_i is the centre of the fuzzy set and w_i controls the set width (see figure 5). Each hidden node is considered to be a single rule, with the output of each rule being truncated by a value v_j which is considered as the confidence in the rule. These rules are all combined at the output y with an *or* function as follows.

$$y = max\{r_j(x), j = 0 \ldots m\} \quad (8)$$

where m+1 is the number of rules. To train the network, the centres c, width parameters w and confidence values v have to be computed. To initially find the centres a number of techniques such as cluster analysis and random selection can be used [13]. We used the K-means clustering algorithm, although better techinques such as fuzzy-clustering [11] will be investigated later. The parameters w and the confidence values v are initially set to 1.

3.2 Tuning the centres, widths and confidence

Our initial investigation was to extract a set of rules to classify the ST waveform as either *Normal* or *Abnormal* using the features listed in section 2. Given a complete set of features stored in the colombs of matrix x and their respective classification stored in the vector $\overline{Y}$, the centres, width parameters and confidence values in the network are optimised to obtain the 'best' desired mapping from the inputs to the output. In this investigation we firsrt define the error ϵ as

$$\epsilon = \sum_{p=1}^{N} \{y_p - Y_p\}^{2.a} \tag{9}$$

where (10)

$$y_p = max\left\{min\left\{v_j,\ e^{-(x_{i,p}-c_{j,i})^2.w_{j,i}^2},\ i=0\ldots n\right\},\ j=0\ldots m\right\} \tag{11}$$

where a is a positive integer. To minimise the error, equation 9 is differentiated with respect to each of the parameters $w_{j,i}$, $c_{j,i}$ and v_j. Each parameter is repeatedly updated using the following equations until the error ϵ is falls below a pre-defined level.

$$w_{j,i} = w_{j,i} - \alpha.2.a.\sum_{p=1}^{N}\{y_p - Y_p\}^{2.a-1}.\frac{\partial y_p}{\partial w_{j,i}} \tag{12}$$

$$c_{j,i} = c_{j,i} - \beta.2.a.\sum_{p=1}^{N}\{y_p - Y_p\}^{2.a-1}.\frac{\partial y_p}{\partial c_{j,i}} \tag{13}$$

$$v_j = v_j - \gamma.2.a.\sum_{p=1}^{N}\{y_p - Y_p\}^{2.a-1}.\frac{\partial y_p}{\partial v_j} \tag{14}$$

where (15)

$$\frac{\partial y_p}{\partial w_{j,i}} = \begin{cases} -2.(x_{i,p} - c_{j,i}).w_{j,i}.e^{-(x_{i,p}-c_{j,i})^2.w_{j,i}^2} & \text{if} y_p = e^{-(x_{i,p}-c_{j,i})^2.w_{j,i}^2} \\ 0 & \text{otherwise} \end{cases} \tag{16}$$

$$\frac{\partial y_p}{\partial c_{j,i}} = \begin{cases} 2.w_{j,i}^2.(x_{i,p} - c_{j,i}).e^{-(x_{i,p}-c_{j,i})^2.w_{j,i}^2} & \text{if} y_p = e^{-(x_{i,p}-c_{j,i})^2.w_{j,i}^2} \\ 0 & \text{otherwise} \end{cases} \tag{17}$$

$$\frac{\partial y_p}{\partial v_j} = \begin{cases} 1 & \text{if} y_p = v_j \\ 0 & \text{otherwise} \end{cases} \tag{18}$$

α, *beta* and γ are small constants (< 1) which determine the training rates and N is the number of examples in the training data. The parameter a is used to control the distribution of the errors in the final solution. Setting a=1 will guide the training algorithm towards the least-squares solution. A high value for a will guide the training algorithm towards the optimal or 'minimax' solution.

4 Results

At the time of writing a very limited set of abnormal waveforms was available because abnormal waveform are very rare. In an initial study using 30 abnormal example waveforms and 30 normals, we were able to train a small network to correctly distinguish all the abnormal waveforms from the normals with no wrong classifications error. We are currently working to produce a more comprehensive set of test cases from new data and hope to extract rules to classify the ST waveform. The results will be published elsewhere in the near future.

5 Discussion and Conclusion

The fetal ECG ST waveform can be used to automatically assess if the fetus is coping with stresses in labour. Assessing the shape of the ST waveform is simplified by approximating the ST waveform with a Chebyshev polynomial and extracting robust features. Not all the rules required to interpret these features have been quantified. We have started to address this by combining the advantages of supervised neural networks and fuzzy inference systems to derive new rules for interpreting these features from the features and a human experts qualitative classification. The training algorithm, which is based on gradient descent, allows a max-min fuzzy inference system to trained. A limitation of this system are that the rules produced are not guaranteed to be intuitive to a clinician. One possible modification to this technique could be to optimise currently known rules as well as attempt to create new rules. Currently the system does not exploit known knowledge, although this important feature should not be overlooked will be added in future. The work so far shows promise and some useful results should be available in the near future.

6 Acknowledgments

We would like to acknowledge Prof. Karl Rosén, Dr. Roberto Luzietti and Dr. Mark Davies for their clinical assistance, Peter VanEetvelt John Curnow and Dr. Shaohua Tan for their valuable help and advice and the PCFC for assistance with funding.

References

[1] Maeda K. Computerised analysis of cardiotocograms and fetal movements. In R Lilford., editor, *Balliere's Clinical Obstetrics & Gynaecology*, volume 4, pages 797–813. 1990.

[2] Ifeachor E.C. and Outram N.J. A fuzzy expert system to assist in the management of labour. In *Proceedings of the International ICSC Symposium on FUZZY LOGIC*, pages C97–C102. ICSC, 1995.

[3] Rosén K. G. ST waveform + CTG clinical guidelines. Internal report, Plymouth Postgraduate Medical School, University of Plymouth., 1994.

[4] Westgate J Ifeachor E C, Keith R D F and Greene K R. An expert system to assist in the management of labour. In Liebowitz J, editor, *World Congress on Expert Systems*, volume 4, pages 2615–2622. Pergamon Press, 1991.

[5] Curnow J. Westgate J., Harris M. and Greene K.R. Randomised trial of the cardiotocogram only versus ST waveform plus cardiotocogram for intrapartum monitoring in 2400 cases. *Am. J. Obstet. Gynecol.*, 169:1151–1160, 1993.

[6] Rosén K.G. and Luzietti R. The fetal electrocardiogram: ST waveform analysis during labour. *J.Perinat.Med.*, 22:501–512, 1994.

[7] Van Eetvelt P.W.J. Outram N.J., Ifeachor E.C. and Curnow J.S.H. Techniques for optimal enhancement and feature extraction of the fetal electrocardiogram. Accepted for publication in IEE Proc. A.

[8] Ifeachor E.C. and Outram N.J. Fuzzy logic concepts for pattern analysis and interpretation of changes in the fetal electrocardiogram. In *Proc. Int. Conf. on Neural Networks and Expert Systems in Medicine and Healthcare*, pages 353–362. University of Plymouth., U.K., 1994.

[9] C-T Sun J-S Roger Jang. Functional equivalence between radial basis function networks and fuzzy inference systems. *IEEE Transactions on Neural Networks*, 4(1):156–158, 1993.

[10] Shigeo Abe & Ming-Shong Lan. A method for fuzzy rules extraction directly from numerical data and its application to pattern classification. *IEEE Trans. Fuzzy Systems*, 3(1):18–28, 1995.

[11] Warwick K. New ideas in fuzzy clustering and fuzy automata. In *Proceedings of the International ICSC Symposium on FUZZY LOGIC*, pages XXI–XXVII, 1995. Plenary Session Paper.

[12] Zadeh L.A. The concept of a linguistic variable and it's application to approximate reasoning-I. *Information Sciences*, 8:199–249, 1975.

[13] Haykin S. *Neural Networks, A Comprehensive Foundation.* Macmillan College Publishing Co. Inc., New York, 1994. ISBN 0-02-352761-7.

PATTERN ANALYSIS OF UNCERTAIN CHANGES IN THE FETAL ELECTROCARDIOGRAM FEATURES DURING LABOUR.

Outram N.J. and Ifeachor E.C.

School of Electronic, Communication and Electrical Engineering, University of Plymouth,

Plymouth, UK, PL4 8AA.

ABSTRACT

A fuzzy system has been developed to recognise abnormal ST waveforms shapes during labour [*Ifeachor & Outram, 1995*]. It is shown that both intermittent and persistently abnormal ST waveforms are observed during labour. The events are regarded as cumulative evidence for fetal distress, although more weight should be placed on persistently abnormal waveforms. The fuzzy system has been extended to model the clinician's management strategy in the face of fetal ST waveform changes using a technique based on finite state machines. In the new system "fuzzy states" rather than "finite states" are used. The truth of a state depends on previous states and fuzzy facts. A specific filter-type structure is used in the fuzzy inference mechanism to determine if events are continuous or if previous fuzzy states have settled. This process is illustrated with a real case measured from a foetus taken from our data-base.

Introduction

The fetal electrocardiogram (ECG) waveform represents the electrical activity of the baby's heart as measured from the body surface, which for this work, is measured from the fetal scalp (see Figure 1). Like the adult ECG, the normal fetal ECG is characterised by five peaks and valleys labelled P, Q, R, S, and T (see Figure 2). From the fetal ECG the instantaneous fetal heart rate (FHR) can be derived in beats per minute (bpm). A plot of successive instantaneous heart rates gives the FHR pattern. A continuous display of

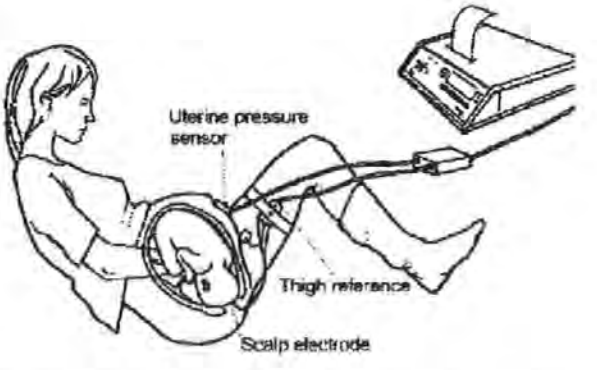

Figure 1 Internal fetal ECG monitoring

the FHR pattern together with the contraction of the womb (uterine activity) is known as the cardiotocogram (CTG), and is illustrated in Figure 3. The fetal ECG contains potentially valuable information that could assist clinicians in making more appropriate and timely decisions during labour [*Luzietti & Rosén, 1994*]. This has not been widely put into practice because the current knowledge and expertise required to interpret the changes the fetal ECG is rare and has been restricted to a few centres in the world. This has also been hindered by problems with noise and the difficulty of processing noisy fetal ECG without introducing significant distortion [*Kirk and Smith, 1986; Outram et. al., 1995*].

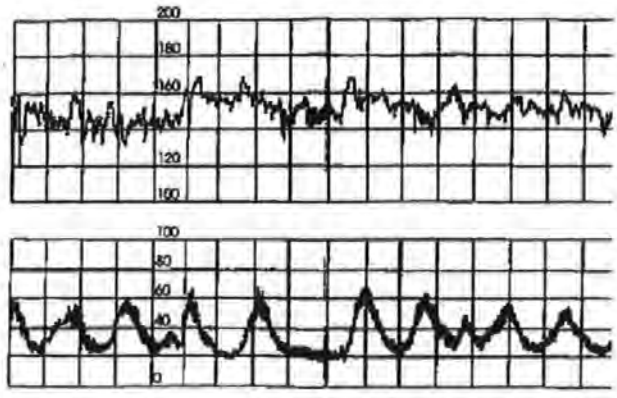

Figure 3 The cardiotocogram (CTG)

Currently, the assessment of the condition of the foetus during labour is based on visual analysis and interpretation of the CTG. Unfortunately this requires a great deal of experience which is not always available to all labour wards day and night [*Ifeachor et. al., 1991*]. Uncertainty and difficulty in interpreting CTG patterns during labour lead to unnecessary medical intervention (e.g. caesarean section or forceps deliveries), fetal injury or a failure to intervene when needed. In the UK alone, over £100M is spent each year in birth related medical negligence claims. The need for computer-assistance in the management of labour to improve the quality of obstetric care is widely recognised [*Keith et. al. 1994, Ifeachor et. al. 1991*].

The INFANT expert system [*Ifeachor et. al., 1991*] has been successfully developed to analyse and interpret changes in the CTG, taking into account important events in labour,

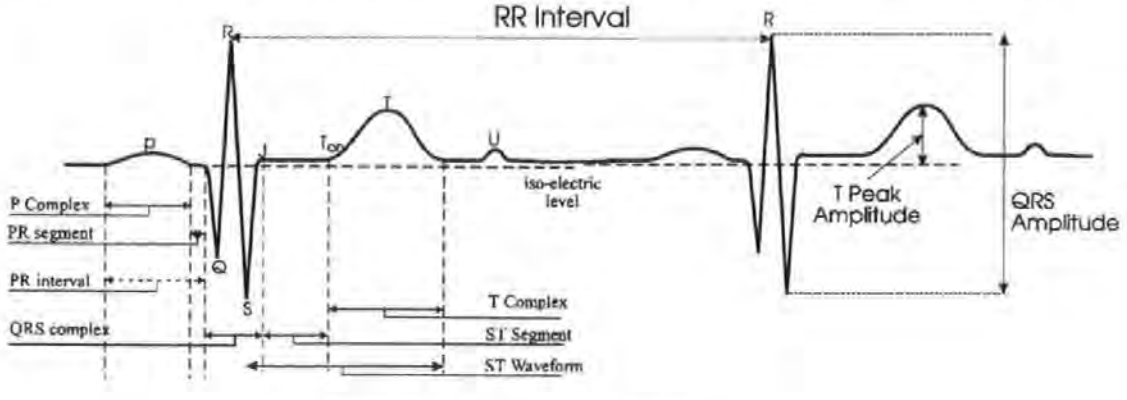

Figure 2 The fetal ECG waveform

and to provide advice to clinicians during labour. However, the CTG alone is difficult to interpret and does not provide all the information needed, in all cases, for accurate assessment of fetal condition. *Additional information may be obtained by a proper analysis of progressive changes in the fetal ECG without having to alter current patient handling routines.* The impetus for investigating the value of the ECG waveform comes from extensive experimental research, clinical observations and studies which suggest that the assessment of fetal condition based on the ECG ST waveform pattern changes (see Figure 2) plus the CTG can improve the quality of care [*Luzietti and Rosén., 1994; Rosén et. al., 1992.; Murray, 1986*]. In a recent clinical study, the use of the combination of the ST waveform plus CTG analysis led to a significant reduction in caesarean section and forceps delivery for fetal distress with no adverse effect on neonatal outcome [*Westgate et. al., 1993*]. In this study, the ratio of the T peak amplitude to the QRS amplitude (see Figure 2), known as the T/QRS ratio, was used to quantify ST waveform shape. It is recognised that there has been too much emphasis on the T/QRS ratio as it is only a crude quantification of the ST-waveform shape [*Rosén & Luzietti 1994; Greene & Westgate, 1993*]. The T/QRS ratio does not help to identify all of the important ST waveform shapes illustrated in Figure 4. Bi-phasic and negative ST waveforms are abnormal patterns but would be missed if only the T/QRS ratio is considered.

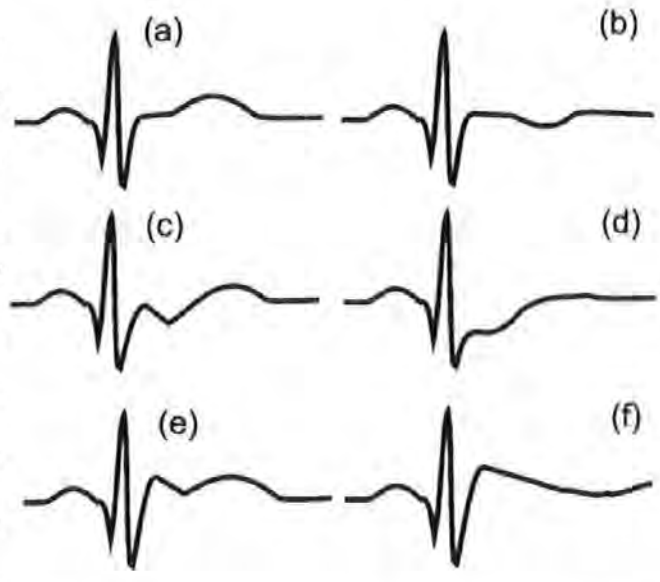

Figure 4 A summary of all the important ST waveform shapes

(a) Normal, (b) Abnormal (Negative T), (c) Abnormal (Bi-phasic ST, Positive T), (d) Abnormal (Depressed ST, Normal T), (e) Suspicious (Negative ST slope, Normal T), (f) Suspicious (Negative ST slope, Normal T)

An intelligent fuzzy system has been developed to classify the ST waveform shape and interpret the shape changes [*Ifeachor & Outram, 1995*]. A simplified block diagram of the system is illustrated in Figure 5. The raw ECG signal is enhanced and if the quality of the data is sufficient, then key features such as the T/QRS ratio and ST-segment slope are measured from a moving average of ECG waveform. Key quantitative features are

measured from the fetal ECG waveform, decimated to a lower sampling rate using multi-rate signal processing techniques, and passed to the fuzzy expert model for interpretation.

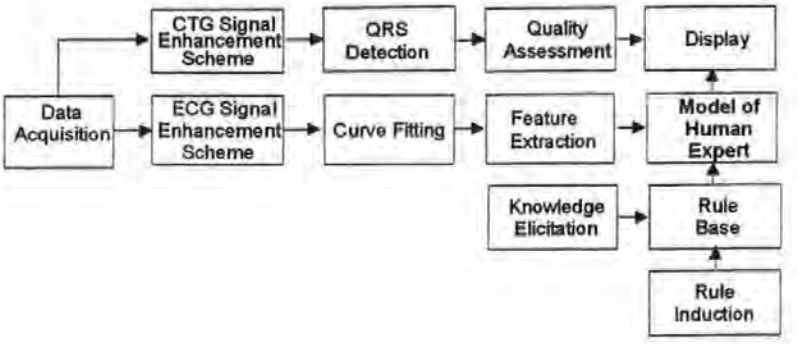

STAN® Clinical guidelines for action with a mature fetus. (≥36 weeks)
1. Negative/Biphasic ST - T/QRS less than -0.05 for more than 20 minutes. Rising - T/QRS rises more than 0.4 over 15 minutes, expediate delivery without FBS 2. Negative/Biphasic ST - T/QRS less than -0.05 for more than 20 minutes. Rising - T/QRS rises more than 0.15 from the baseline level over 15 minutes, expediate delivery without FBS. 3. Any negative or biphasic ST change as well as any T/QRS increase over 5-10 minutes. 4. FBS should be repeated every hour or earlier. If an FBS is not available, intervention can be delayed until the CTG shows evidence of deterioration. - Loss of short term variability - Progressive tachycardia or bradycardia - Decelerations become wider and deeper - Overshoot accelerations following decelerations If the CTG remains unchanged but the ST waveform shows an acute change, as identified in p.3, delivery should also be expediated. Note: In second stage we recommend these foetuses be delivered within 90 minutes as rapid deterioration can occur after this time. Note: A "pre-terminal" CTG should always cause immediate delivery. No need for additional ST analysis.

Table 1 A summary of the clinical guidelines used to accompany the Fetal condition matrix

Figure 5 Simplified block diagram of the fetal ECG fuzzy intelligent system

Modelling the human expert strategy using fuzzy logic

The knowledge concerning how to interpret the changes in the fetal ECG during labour has been acquired from experimental findings and clinical observations over many years. From this knowledge a set of clinical guidelines has evolved for fetal ECG monitoring. The guidelines are summarised in Table 1 and the recommended clinical action is summarised in Table 2. The guidelines form the basis for the fuzzy expert model which provides a linguistic description of the instantaneous ECG waveform shape and the sequence of changes in the shape during labour. The shape information is then mapped

ST Waveform / CTG	Normal	High and Stable	Negative or Rising
Normal	**A**:No Action	**B**:No Action	**C**:FBS or Deliver see note 1
Intermediate	**D**:No Action	**E**: see note 4	**F**:Deliver see note 2
Abnormal	**G**: see note 4	**H**:Deliver see note 3	**I**:Deliver see note 4

Table 2 Fetal condition matrix(see Table 1 for notes)

onto a "fetal condition matrix" (see Table 2) and is displayed to the clinician (*Ifeachor E.C. & Outram N.J., 1995*).

A fuzzy truth value is computed for each category (A-I) using fuzzy rules, which can be de-fuzzified to a single point on a fuzzy condition map (see Figure 6) (*Ifeachor E.C. & Outram N.J., 1995*). The clinical guidelines that accompany this matrix are given in Table 1. The basic concepts of fuzzy logic in this application are discussed by *Ifeachor & Outram, (1994).*

Managing complex patterns in time

This paper is concerned with the techniques required to represent and interpret the ECG feature changes throughout labour. For proper management of labour it is important to be able to represent and recognise particular sequences of events in labour, and not just instantaneous events such as isolated abnormal waveforms. For example, in the guidelines given above, with a normal CTG, a T/QRS ratio is said to be rising if it *rises more than 0.4 from the baseline level over 15 minutes*. In practice, uncertainty may arise because the guidelines cannot span every situation.

It is the intermediate cases which a more likely to cause the most uncertainty for the clinician. For example, *a rise in T/QRS of 0.25 over 15 minutes* is a suspicious change but might not be enough to warrant action. An experienced clinician would probably make a note of this event as suspicious, and will act depending on the context of the event. Time and the context in which an event took place are very important when there is a high degree of uncertainty.

There are many factors that could influence the decision of a clinician with the appearance of suspicious and uncertain changes. If the baby is near to the point of delivery, then labour may be allowed to progress naturally. If this was the first abnormal

event, and it was short-lasting (<5 mins), then this might be viewed as an anomaly and not enough evidence to warrant intervention. If other suspicious events had been observed earlier in the labour however, then there would come a point where the evidence has accumulated enough to suggest intervention is required. The purpose of this work is to expand the fuzzy logic concepts to allow the expert model to 'remember' previous events and manage the accumulation of evidence for fetal distress.

A documented example of this is the brief appearance of negative or bi-phasic ST waveforms (see Figure 4). Each appearance can be considered to be a period where the foetus is unable to compensate for a stress in labour, such as a uterine contraction.

Repeated exposure to stress may lead to distress, damage and possibly death. With a normal CTG, the clinician may not act on the first appearance of abnormal waveforms, but may act on subsequent appearances. The expert model must include the concept of memory and have the ability to include prior events in the reasoning mechanism. Examples of the situations where the expert-model can use memory to reduce uncertainty are summarised as follows.

1. An individual abnormal event is only short lasting, so its validity is in question.
2. An event is only partially true - i.e. suspicious but not marked enough to warrant action
3. An event has occurred before, therefore adding to the belief that it is genuine and not noise.
4. A different but possibly abnormal event had previously occurred.
5. A similar pattern occurred in a previous labour.

The human expert can manage these situations though intelligent reasoning and inference, drawing on experience and knowledge of previous events in the labour, but this is very difficult for a computer. We propose a technique to manage these situations using a novel extension to fuzzy logic.

Fuzzy State Model for managing complex patterns in time.

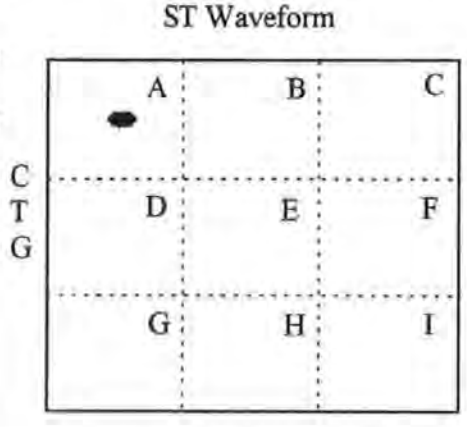

Figure 6 Fetal condition map

Fuzzy logic is used to model an expert clinician, the concepts of which are published elsewhere [*Ifeachor & Outram, 1994*]. We have extended these concepts and developed a technique for modelling the expert's management of complex sequences of events in time, such as those discussed above. This technique is based on the concepts of finite state machines [*Biswas, 1993*], but in our case the states are fuzzy and not discrete. An example of a fuzzy state representation of events in labour is depicted in Figure 7. The states are fuzzy variables that represent the truth that an event has occurred. The inference mechanism for the fuzzy variables differs from conventional fuzzy systems in that the implied truth value is also dependent on time as well as rules and other fuzzy variables/facts. Consider the example given in Figure 7. Three states are defined.

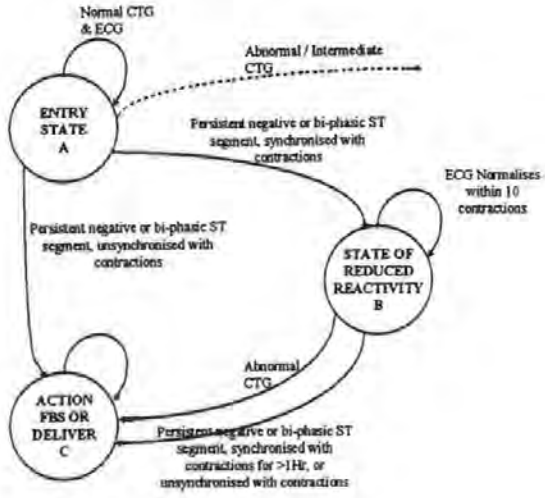

Figure 7 Fuzzy-state machine used to represent and recall events during labour

A. *Entry state*

B. *State of Reduced Reactivity.*

C. *Action State.*

At the entry of monitoring (state A) it is assumed that no prior information is known about the fetal ECG. We say that the *fetal state A is TRUE*. If during labour there are negative or bi-phasic ST waveforms, coupled with an abnormal CTG, then using the following fuzzy rules, the *fetal state C is TRUE*.

IF (STATE=A) and (T/QRS=Negative OR STsegment is Biphasic OR STsegment is Negative) THEN STWAVEFORM=Abnormal
IF (STATE=A) and (STWAVEFORM=Abnormal) and (CTG=Abnormal) THEN STATE=C

These acute changes would normally be routinely detected from the acute CTG changes. A problem arises when the changes are not so acute and the ECG and CTG do not provide such definitive changes. If the negative/bi-phasic ST waveforms only appear briefly (<1min), and are repetitive and synchronised with contractions, then the situation is more uncertain. It would be accurate to say that *state B* is possibly true. It is valid to say that if negative/bi-phasic ST waveforms re-appear within the same 15 minute period,

then the belief that *state B* is true should increase. It is also valid to say that if no more negative/ bi-phasic ST waveforms are observed within the next hour then the belief that *state B* is TRUE should reduce or maintain it's current level. To manage these uncertain situations, an accumulative model is used infer each state.

State transition using an accumulated truth model

As with normal fuzzy variables, all the fuzzy states are true, but to different degrees, and can take on any value between 0 and 1. Any given state is dependent on the other fuzzy states and other fuzzy variables. All the fuzzy states are updated on each time epoch, which, for this work, is a 15s interval. A state is limited by how much it can increase or decrease in each time epoch. In general, the next state is determined by the following.

$$NextState(t) = \max\left\{\min\left\{PreviousState(t-1) + GrowthRate \cdot \mu_i(t) - DecayRate \cdot \mu_j(t) - leakage, 1\right\}, 0\right\} \quad (1)$$

where $\mu_i(t)$ $(0 \leq \mu_i(t) \leq 1)$ is a fuzzy variable that implies that *NextState* is true, $\mu_j(t)$, $(0 \leq \mu_j(t) \leq 1)$, is a fuzzy variable that infers that *NextState* is *not* true and *leakage* is a constant that reduces the state truth as time progresses. Each state transition has an associated *growth rate*, *decay rate* and *leakage*. This way there is flexibility for the *NextState* truth membership to grow and diminish at different rates. This is the accumulated truth model, which is essentially a leaky integrator of fuzzy truth membership.

Fuzzy filter structures

Consider Figure 8 which shows the truth output of a fuzzy rule for *"ST waveform is abnormal"* from part of a recently recorded case. From the clinical guidelines [*Luzietti & Rosén 1994*], assuming a normal CTG, there must be a consistently abnormal ST waveform for at least 20 minutes for any change to be consider clinically significant. It is

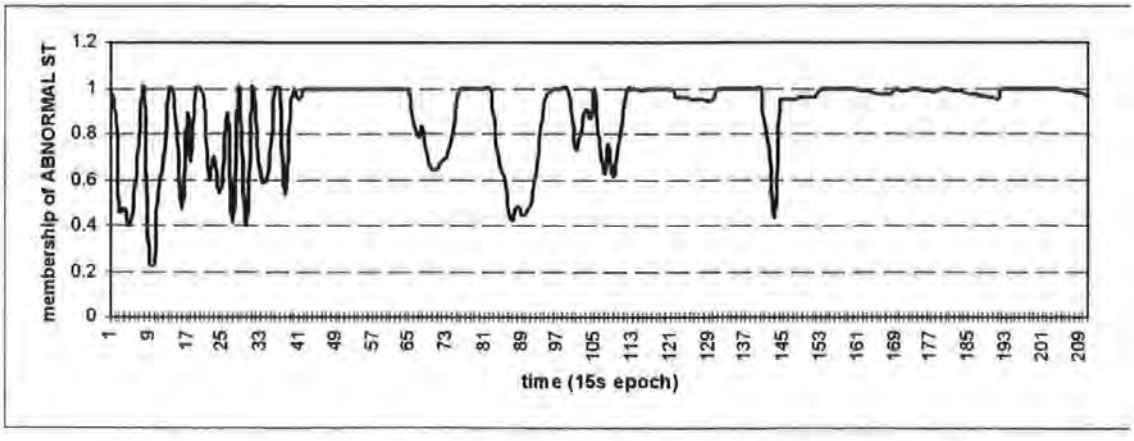

Figure 8 The output truth for "Abnormal ST waveform"

also true that the brief appearance of abnormal ST waveforms is significant if they reoccur. From Figure 8 it is observed that there are some briefly abnormal waveforms and some periods of persistently abnormal waveforms.

All these events contribute to the evidence that there is some abnormality with this labour, but it is the continuously abnormal waveforms that are of most concern and should contribute the most to the evidence. It is assumed here that the CTG is normal and *STATE A* has been true for 20 minutes. The following rule could be used.

IF (STATE A is consistently true) AND (ST waveform is consistently Abnormal) THEN STATE B

Written formally, using the accumulated truth model, the next state B is calculated as follows.

$$\mu_{STATEB}(\tau+1) = \mu_{STATEB}(\tau) + \gamma \cdot \left(\mu'_{abnormalST}(\tau) \wedge \mu'_{STATEA}(\tau)\right)$$

where $\mu'_{abnormalST}(\tau) = \mu_{abnormalST}(\tau) \wedge \mu_{abnormalST}(\tau-1) \wedge \mu_{abnormalST}(\tau-2) \wedge \ldots \wedge \mu_{abnormalST}(\tau-79)$

and $\mu'_{STATEA}(\tau) = \mu_{STATEA}(\tau) \wedge \mu_{STATEA}(\tau-1) \wedge \mu_{STATEA}(\tau-2) \wedge \ldots \wedge \mu_{STATEA}(\tau-79)$

(2)

where τ represents a 15s epoch of time, γ is the *growth rate* and $\wedge$ is the fuzzy *intersection* (*AND*) operator. $\mu_{abnormalST}(\tau)$ and $\mu_{STATEA}(\tau)$ are the truth membership values for "the ST waveform is negative" and "*STATE A* is true" respectively. $\mu'_{abnormalST}(\tau)$and $\mu'_{STATEA}(\tau)$ are the truth membership values for "the ST waveform has been consistently abnormal" and "*STATE A* has been consistently true" (respectively) for the 20 minutes previous to time τ.15s. This is represented in the structure shown in Figure 9, where *D* denotes a delay of one epoch (15s).

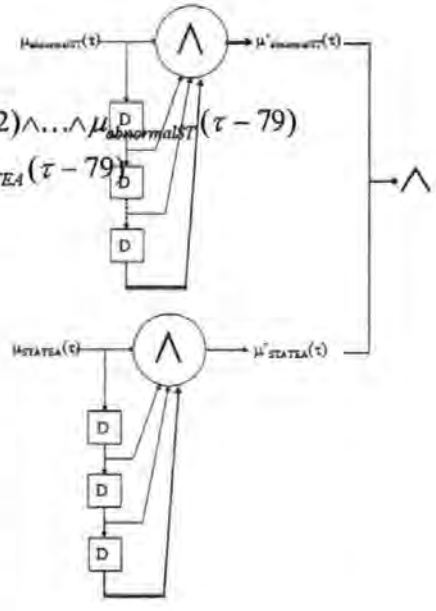

Figure 9 Schematic structure of the fuzzy filter

Fuzzy intersection operator

The fuzzy *intersection* operator $\wedge$ is chosen carefully when computing the accumulated truth. The fuzzy intersection operator used here is defined in equation (3) where the variable q is used to modify the characteristics of the fuzzy operator. For $q=1$, this equates to the truncated mean which is a very soft operator. As q increases, the fuzzy rule tends to become increasingly strict, promoting the continuous events and diminishing the intermittent events. This is illustrated in Figure 10.

$$a_0 \wedge a_1 = \max\left(1 - \min\left(\frac{(1-a_0)^{\frac{1}{q}} + (1-a_1)^{\frac{1}{q}}}{2}, 1\right), 0\right)$$

$$a_0 \wedge a_1 \wedge \ldots \wedge a_{N-1} = \max\left(1 - \min\left(\frac{1}{N}\sum_{k=0}^{N-1}(1-a_k)^{\frac{1}{q}}, 1\right), 0\right) \quad \textbf{(3)}$$

$$\text{and hence, } \mu'_{abnormalST}(\tau) = \max\left(1 - \min\left(\frac{1}{N}\sum_{k=0}^{N-1}(1-\mu_{abnormalST}(\tau-k))^{\frac{1}{q}}, 1\right), 0\right)$$

The growth rate in equation (2) is estimated as follows. Given that the previous state *STATE A* is completely true, and assuming an abnormal waveform to be continuously present for 20 minutes (20x4 epochs), then the growth rate γ for equation (2) is estimated as $\gamma = 1/_{20\times4} = 0.0125$. The leakage rate is small, set at 0.00125, and as there is no rule to reduce the truth of *state B*, the decay rate is zero. Returning to the case in Figure 7, the membership for *state B* is computed as follows.

$$\mu_{stateB}(\tau) = \max\left(\min\left(\mu_{stateB}(\tau-1) + 0.0125 \cdot \mu'_{abnormalST}(\tau), 1\right) - 0.00125, 0\right) \quad \textbf{(4)}$$

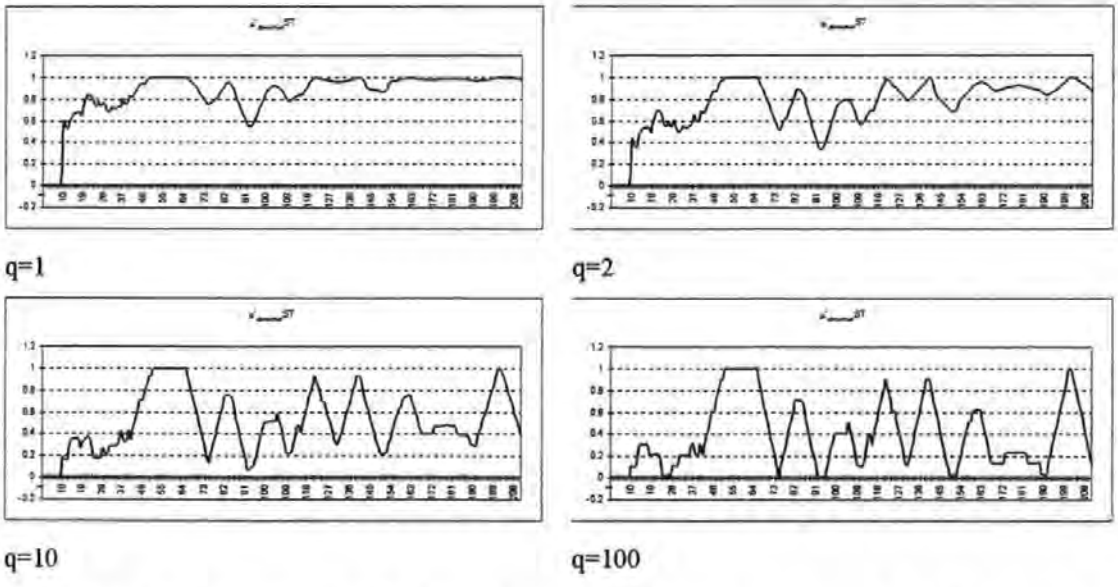

Figure 10 Output truth of the rule "ST waveform is abnormal for 20 minutes or more"

The membership truth $\mu'_{abnormalST}(\tau)$ ("ST waveform is consistently abnormal") from equation 3 is shown in Figure 8 for different values of q. The accumulated truth is computed using equation (4) for different values of q and is shown in Figure 11.

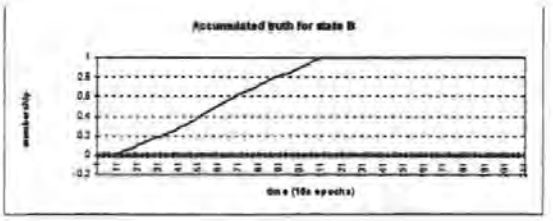

q=1

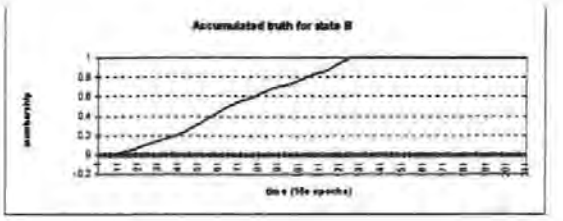

q=2

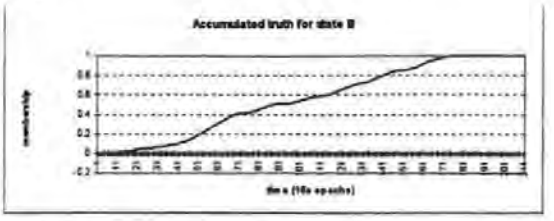

q=10

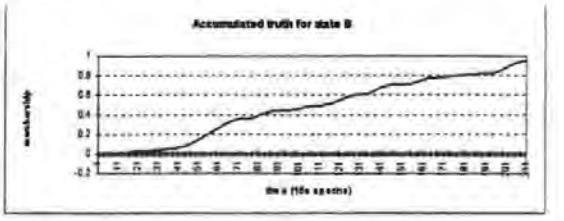

q=100

Figure 11 Accumulated truth for "State B"

When q=1 or 2, the state accumulates too rapidly as a result of the intermittently abnormal waveforms. When q=10 or 100, there is a steady build up of evidence during the intermittent period and a more rapid increase when the waveforms are continuously abnormal. For the remainder of this paper, it is assumed q=10.

Chaining state transitions

From the example described above, *state B* becomes increasingly true as more evidence accumulates. From Figure 7, for a state transition to occur from *state B* to *state C*, both *state B* must be true and abnormal waveforms must continue (or reoccur) for more than 10 contractions. For illustrative purposes, 10 contractions equates to 30 minutes, which is 120 epochs. The new state C will be determined using the following rule.

IF (*STATE B* has been true for 30 minutes) AND (*ST Waveform* is Abnormal) THEN *STATE C*

To model this rule, a new fact "*STATE B has been true for 30 minutes*" , with membership $\mu'_{STATEB}(\tau)$, is derived as

$\mu'_{stateB}(\tau) = \max\left(1 - \min\left(\frac{1}{120}\sum_{k=0}^{119}\left(1-\mu_{stateB}(\tau-k)\right)^{\frac{1}{q}},1\right),0\right)$. The membership truth for *state C* is accumulated as follows.

$$\mu_{stateC}(\tau) = \max\left(\min\left(\mu_{stateC}(\tau-1) + \frac{1}{120}\cdot\left(\mu'_{stateB}(\tau)\wedge\mu'_{abnormalST}(\tau)\right),1\right) - 0.005,0\right) \quad \textbf{(5)}$$

A plot of the *state C* membership is given in Figure 12.

State C is observed to grow in truth once *state B* is fully saturated and because the fetal ECG ST waveform remains consistently abnormal. This is a simple illustrative example that has been simplified to demonstrate the concepts of this technique. More complex intermediate state transitions could be added to provide more information to the clinician, such as the repetition of short 5-minute bursts of negatively sloped positive ST waveforms. These are not individually abnormal, but with repeated appearance, then evidence of some abnormality accumulates.

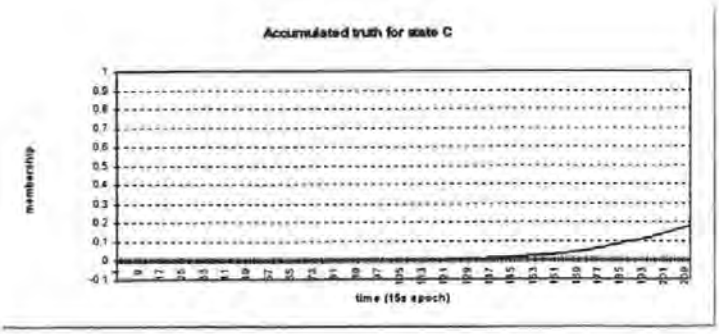

Figure 12 Accumulated truth for state C

Discussion and Conclusion

Fuzzy logic has been successfully used to model expert clinical knowledge for interpreting fetal ECG waveforms during labour. A weakness in this system was that time was not accounted for in the model. The fuzzy logic concepts have been successfully extended to model the management of time by accumulating evidence over time and defining fuzzy states, using a technique based on finite state machines. Transition between fuzzy states cannot happen immediately as their truth membership has to first accumulate over time. Complex models can be built which define many intermediate states in order to reach a final state, thus allowing the recognition of complex patterns in time. This uses same concept as sequential state machines used to detect a series of binary transitions. Future work will apply the model to more cases and complex scenarios in fetal ECG waveform monitoring.

Acknowledgements

The authors gratefully acknowledge the assistance and contribution of Karl Rosén, John Curnow, Peter VanEetvelt, Jenny Westgate, Roberto Luzietti, Mark Davies and Keith Greene for their contribution to our understanding of the problems in fetal monitoring and for sharing with us their expertise and knowledge in this difficult area. The financial support of the P.C.F.C. and the South-West Regional Health Authority for this work is gratefully acknowledged.

References

[1] Biswas N.N., Logic Design Theory., Prentice Hall International Inc., Englewood Cliffs ., N.J., 1993

[2] Greene K.R. and Westgate J. The Fetal ECG with Particular Reference to the ST waveform. In Spencer J.A.D. and Ward R.H.T (Ed.), Intrapartum fetal surveillance., Ch 21, pp281-294, 1993, Royal College of Obstetrics and Gynecology, 27 Sussex Place, Regents Park, London.

[3] Ifeachor E C, Keith R D F, Westgate J and Greene K R., An expert system to assist in the management of labour. In Liebowitz J (Ed) World Congress on Expert Systems, Vol. 4, pp2615-2622, Pergamon Press., 1991

[4] Ifeachor E.C. and Outram N.J, Fuzzy Logic concepts for pattern analysis and interpretation of changes in the fetal electrocardiogram, Proc. Int. Conf. on Neural Networks and Expert Systems in Medicine and Healthcare, University of Plymouth., U.K., pp353-362, 1994.

[5] Ifeachor E.C. and Outram N.J., A fuzzy expert system to assist in the management of labour, Proceedings of the International ICSC Symposium on FUZZY LOGIC, Zurich, ppC97-C102, 1995.

[6] Keith R., Westgate J., Beckley S., Garibaldi J., Ifeachor E.C. and Greene K.R., A multicentre comparitive study of 17 experts and an intelligent computer system in the management of labour using the cardiotocograph., Br. J. Obstet. Gynecol., 1994

[7] Kirk D.L. & Smith P.R., Techniques for the routine on-line processing of the fetal electrocardiogram., J. Perinat. Med., 14, pp391-397, 1986.

[8] Luzietti R. and Rosén K.G., The fetal electrocardiogram: ST waveform analysis during labour, J.Perinat.Med., 22, pp501-512, 1994.

[9] Murray H.G., The fetal electrocardiogram: current clinical developments in Nottingham., J. Perinat. Med., 14, pp399-403, 1986.

[10] Outram N.J. and Ifeachor E.C. and Van Eetvelt P.J.W. and Curnow J.S.H., Techniques for optimal enhancement and feature extraction of the fetal electrocardiogram, IEE Proc. A, 1995

[11] Rosén K G, Arulkumaran S, Greene K R, Lilja H, Lindecrantz K, Seneviratne H, and Widmark C. Clinical validity of fetal ECG waveform analysis. in Perinatology, Nestle Nutrition Workshop Series, Vol. 26, Nestec LtD, Vevey/Raven Press, New York, 1992, 95-110.

[12] Westgate J., Harris M., Curnow J. and Greene K.R., Plymouth randomised trial of the cardiotocogram only versus ST waveform plus cardiotocogram for intrapartum monitoring in 2400 cases., Am. J. Obstet. Gynecol., 169, pp1151-1160, 1993